LOWER MANTLE DIAMONDS FROM THE RIO SORISO (JUINA, BRAZIL)

by

PATRICK HAYMAN

B.Eng., Queen's University, 1999

A THESIS SUBMITTED IN PARTIAL FULFILLMENT OF
THE REQUIREMENTS FOR THE DEGREE OF

MASTER OF SCIENCE

in

THE FACULTY OF GRADUATE STUDIES
(Department of Earth and Ocean Sciences)

We accept this thesis as conforming to the required standard

THE UNIVERSITY OF BRITISH COLUMBIA

March, 2004

Library Authorization

In presenting this thesis in partial fulfillment of the requirements for an advanced degree at the University of British Columbia, I agree that the Library shall make it freely available for reference and study. I further agree that permission for extensive copying of this thesis for scholarly purposes may be granted by the head of my department or by his or her representatives. It is understood that copying or publication of this thesis for financial gain shall not be allowed without my written permission.

PATRICK HAYMAN
Name of Author *(please print)*

01/04/2004
Date (dd/mm/yyyy)

Title of Thesis: LOWER MANTLE DIAMONDS FROM THE RIO SORISO

Degree: MSc   Year: 2004

Department of EARTH & OCEAN SCIENCES
The University of British Columbia
Vancouver, BC   Canada

Abstract

The morphology, colour, fluorescence (FL), cathodoluminescence (CL), nitrogen content and aggregation state, internal morphology and mineral inclusion chemistry have been studied for sixty-nine alluvial diamonds recovered from the Rio Soriso, Juina area, Brazil.

The majority of the Rio Soriso diamonds are colourless, but grey, yellow, brown and non-uniform colours are also observed. Diamonds fluoresce and cathodoluminesce a variety of shades and intensities of blue, turquoise and green. There is a correlation between FL and body colour, with most brown diamonds fluorescing turquoise or green. In general, diamonds with brighter CL have higher nitrogen concentrations. Diamond crystals are generally well resorbed, fragmented and plastically deformed, all of which contributed to the obscuration of the primary crystal habit. Most diamonds are classified as either tetrahexahedroids or dodecahedroids, but crystals of undetermined morphology are abundant. CL examination of polished diamond surfaces and plates indicate that some crystals developed through intermittent episodes of octahedral growth and resorption.

Infrared spectroscopic studies show that the diamonds contain trace amounts of both nitrogen (0-541 ppm, averaging 72 ppm) and hydrogen. There is strong positive correlation between nitrogen and hydrogen concentrations. Nitrogen in most diamonds is fully aggregated as B centres (type IaB, 54%), but there is also a large proportion of nitrogen free stones (type IIa, 38%). A small population of diamonds contain nitrogen in the form of A centres (type IaA, 1.5% and IaAB, 7%), which is indicative of residence in the upper mantle. Nitrogen contents typically decrease from crystal core to rim.

Mineral inclusions recovered and analysed from 30 diamonds include: ferropericlase, MgSi-perovskite, CaSi-perovskite, 'olivine', tetragonal-almandine-pyrope-phase,

pyrrhotite, magnetite, pyrope-almandine-grossular garnet and perovskite. Based on the mineralogy of diamond inclusions and diamond morphology, CL, FL, nitrogen content and aggregation state, the Rio Soriso suite was subdivided into six paragenetic groups which formed in the lower mantle, transition zone and upper mantle. These paragenetic groups are: 1) ultramafic lower mantle diamonds, 2) ultramafic diamonds sourced from the boundary between the upper and lower mantle, 3) mafic diamonds sourced from 580-660 km, 4) mafic diamonds sourced from any sub-lithospheric depths, 5) eclogitic diamonds sourced from the upper mantle, and 6) peridotitic diamonds sourced from the upper mantle. The preferred explanation for the sampling of such a large depth interval within the mantle (~200 to >660 km) is that the diamonds were entrained in a plume that originated at the core-mantle boundary.

Table of Contents

List of Figures

xi

List of Tables

Acknowledgements

First and foremost, I want to thank my mother, father and brother who have always supported me during my time at UBC. Although contact with them has become increasingly sporadic and they know little about my thesis, they certainly deserve most of my thanks.

There are many people who I am indebted to for help in all aspects of completing my thesis while at UBC. The guidance, patience and generosity of my supervisor, Maya Kopylova, have helped me immensely towards completing my thesis. Mati Rudsuepp deserves thanks for teaching me to use much of the analytical equipment in the department – and although I didn't initially appreciate his constant heckling, I soon came to accept it, and, strangely, now appreciate his humour! I would also like to thank people in the EOS building that help with the general efficiency of the running of the department. In particular, I would like to thank Bryon Cranston, for his ability to find any equipment with little notice, and Ray and Doug for their expert construction of gadgets that became vital for the collection of data for my thesis. I would also like to thank Mark Hutchison for his eagerness and willingness to help and to answer questions regarding Juina diamonds.

There are many people that have kept me sane and helped me see and enjoy many of the wonderful things that Vancouver has to offer. As my project came closer to completion, I worked more days and longer hours, and I am grateful to Heidi for putting up with my ridiculous schedule and being such a great girlfriend. Chad and Alastair have been my housemates for over two years and have become great friends over that time. People that deserve thanks are too numerous to list individually, so I offer a general thank you to all the graduate students that I have met while studying here, most of which I now consider as friends.

1.0 Introduction

1.1 Motivation for the project

There are two main motivations for this thesis. The first is to study the rare mineral inclusions in the diamonds and the second is to characterise the suite for exploration purposes.

Diamonds recovered from the Juina area of Brazil contain a rare set of mineral inclusions which suggests that the diamonds crystallised in the lower mantle (e.g. Harte and Harris (1994); Wilding (1990); Hutchison (1997); Kaminsky *et al.*, (2001a)). The mineral inclusions found are extremely rare and are recovered from less than 1% of diamonds worldwide (Stachel, 2001). These rare inclusions have also been recovered from diamonds from other continents, e.g. Australia (Scott-Smith *et al.*, 1984), South Africa (Scott-Smith *et al.*, 1984), Western Africa (Stachel *et al.*, 2000b), central USA (Otter and Gurney, 1989) and the Northwest Territories, Canada (Davies *et al.*, 1999a), but are generally rare. There are three localities where these rare inclusions make up a significant proportion of the diamond population: DO-27, NWT, where they make up ~25% of the total population (Davies *et al.*, 1999a); Kankan, Guniea, where the proportion is unreported but significant (Stachel *et al.*, 2000b); and Juina, where most diamonds are considered to be from the lower mantle (Hutchison, 1997). This study will examine 69 diamonds from the region that has historically produced the highest proportion of diamonds containing these rare inclusions.

Many rocks found on the Earth's surface have origins in the deep Earth (e.g. xenoliths, orogenic massifs, and diamonds, among others). Of these materials available for study, diamonds are unique in that they are the only medium that can preserve a pristine sample of deep mantle at the Earth's surface. Diamond is a relatively inert mineral and may act as an impermeable seal around mineral inclusions that were accidentally trapped during

1

diamond crystallisation. Thus, diamonds have the ability to preserve an uncontaminated part of the mantle, albeit very small. Material from all other sources do not have the benefit of having been isolated for their existence outside of the mantle and may have their chemistry changed through mixing or alteration. Pristine diamond inclusions are truly our only samples from the deep Earth that geologists can collect for study, and for this reason, they are extremely valuable. Many of the inclusions found in diamonds from Juina are interpreted as having origins at depths >660 km, which is considerably deeper than where most diamonds are sourced (~200-250 km). These diamonds are indeed rare and are of extreme importance in terms of scientific study. Because of the rarity of these inclusions, the published database is very limited. This study will increase the size of the current database for further interpretation.

The diamonds for this study were recovered from the Rio Soriso, located in the diamond mining district of Juina. Juina is the largest producer of diamonds in Brazil, at roughly 10 million carats per year (Teixeira, N. (RTZ Mineracao), 1997 personal communication to M.T. Hutchison). All economic operations recover diamonds from channels, paleo-channels, flats and terraces in the region. Large amount of diamonds are being mined out of this drainage system and yet geologists cannot pinpoint the source for the abundant diamond deposits. There are a number of kimberlites in the region, which are an obvious source, but they are generally poorly studied. Another candidate for the diamond source is that of local secondary collectors.

Characterisation of diamond suites is a necessary step towards determining if the alluvial diamonds are indeed sourced from the local kimberlites, the secondary collectors or some other, yet undiscovered, source. Characterisation of diamond suites (also referred to as a diamond *fingerprinting*) can involve any of a number of techniques. This study will characterise the Rio Soriso diamonds in terms of morphology, colour, fluorescence, cathodoluminescence, internal morphology, impurities and inclusions. Through these studies, it was possible to subdivide the suite into subpopulations.

2

1.2 Location map

Rio Soriso is located in the Juina Province, Mato Grosso State, Brazil, which is approximately in the centre of South America at the west-central margin of Brazil (Fig. 1.1). The river is located approximately 550 kilometres northwest of Cuiaba (by air) or 724 km by ground transit.

Fig. 1.1. Location map of the Juina area.

1.3 Geology

1.3.1 Continental scale geology

In 2001, Brazil was the 11th largest diamond producer in the world in terms of volume (14th in terms of value) (Mining Journal, London, Aug 23, 2003). All economic quantities are recovered from placer deposits and other secondary collectors. Four cratons are recognised in Brazil (Fig. 1.2), with most diamond deposits occurring on or slightly off either the Amazonica (Amazonian) or Sao Francisco cratons. There are two large continental scale lineaments defined by aeromagnetics surveys and aerial photography: lineament 125°AZ, which
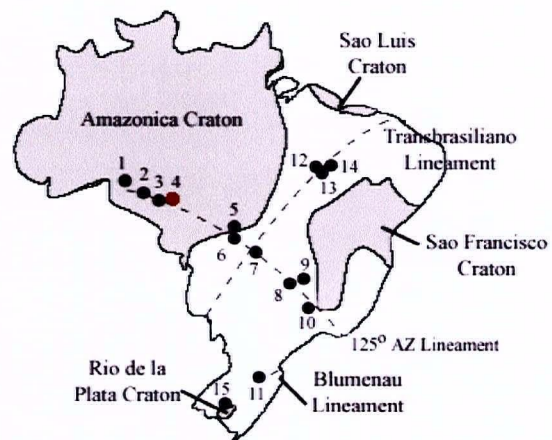
Fig. 1.2. Location of cratons, major lineaments and kimberlite provinces (numbered) in Brazil. 1 - Ariquemes, 2 - Pimenta Bueno, 3 - Vilheno, 4 - Juina (Aripuana), 5 - Paranatinga (Batovi), 6 - Poxoreu, 7 - Amorinopolis, 8 - Alto Paranaiba, 9 - Presidente Olegario, 10 - Bambui, 11 - Lajes, 12 - Redondao, 13 - Santa Filomena-Bom Jesus (Gilbues), 14 - Picos, and 15 - Jaguari-Rosario do Sul. Modified from Tompkins (1992) and Hutchison (1997).

trends NW-SE (Bardet, 1977), and the Transbrasiliano lineament, which trends SW-NE and continues into Africa (Schobbenhaus and Campos, 1984). The Blumenau lineament, although much smaller in scale, is also recognised (Hartman *et al.*, 1980). All lineaments were reactivated during the opening of the South Atlantic, which resulted in the emplacement of numerous alkaline intrusions along these lineaments (Tompkins, 1992). Lineament 125°AZ has been interpreted as a continental extension of oceanic fractures in the South Atlantic (Bardet, 1977).

The Amazonian craton is surrounded by Neoproterozoic orogenic belts and is divided into six geochronological provinces (Fig. 1.3). Juina is situated in the Rio Negro-Juruena Province (1.8-1.55 Ga) and is bounded by the older Ventuari-Tapajos Province (1.95-1.80 Ga) to the north, northeast, and the younger Sunsas Province (1.25-1.0 Ga) to the southwest (Tassinari *et al.*, 1999). The basement rocks of the Rio Negro-Juruena Province are mostly composed of granitic gneisses and granitoids of tonalitic and granodioritic composition (Tassinari *et al.*, 1999).

There are fifteen recognised kimberlite or alkaline rock provinces in Brazil and each falls along one of the three lineaments previously introduced (Fig. 1.2) (Tompkins, 1992; Svisero, 1995). Diamonds are recovered from two main districts, Mato Grosso (includes numbers 1-4, although most diamonds are recovered from Juina, Fig. 1.2) and Minas Gerais (numbers 8-10, Fig. 1.2).

1.3.2 Local geology

The Junia mining district lies between 59° and 60° West and 11° and 12° South (Fig. 1.4). Lineament AZ°125 does not have a topographic expression in the Juina area but forms a basement feature that passes just to the south of the mining district. Diamonds are recovered from streams that lie in the more rugged terrain to the north, as well as the less rugged areas to the south that are mostly obscured by Phanerozoic cover.

Geochronological Provinces

- Central Amazonian >2.3 Ga
- Maroni-Itacaiunas 2.2-1.95 Ga
- Ventuari-Tapajos 1.95-1.8 Ga
- Rio Negro-Juruena 1.8-1.55 Ga
- Rondonian-San Ignacio 1.5-1.3 Ga
- Sunsas 1.25-1.0 Ga

Geological Units

- Phanerazoic covers
- Granitoids
- Precambrian Sedimentary covers
- Acid-Int. Volcanic covers
- Basic Volcanism
- Greenstone Belts
- Granulitic complex
- Neoproterozoic mobile belt
- Basement Structural high

Fig. 1.3. Geochronological provinces and the main lithological associations of the Amazonian craton (reproduced from Tassinari *et al.*, 1999). The star indicates the location of the Juina mining district.

Rio Soriso is the second northernmost river in the Juina mining district. It is fed by the Chicoria Creek and in turn feeds into the Aripuana River, which flows into the Madera River and eventually drains out through the Amazon river. The coordinates of the junction between Rio Soriso and Chicoria Creek are approximately 59° 10′ West and 11°20′ South. Diamonds have been recovered from most streams in the area, particularly from many of the small streams that feed into the Rio Cintra Larga. Diamonds from many of these streams have been the focus of several studies. The largest collection of data is for diamonds recovered from Rio Sao Luiz (Wilding *et al.*, 1991; Hutchison, 1997; Harte and Harris, 1994). A more recent publication by Kaminsky *et al.* (2001a) reports data from Rio Sao Luiz, Rio Mutum, Corrigo Chicoria and Rio Vermelho. Diamonds from several rivers (Sao Luiz, Porcao, Duas Barras, Cinta Larga) as well as diamonds from three local kimberlites, are the focus of an ongoing study by Araujo *et al.* (2003).
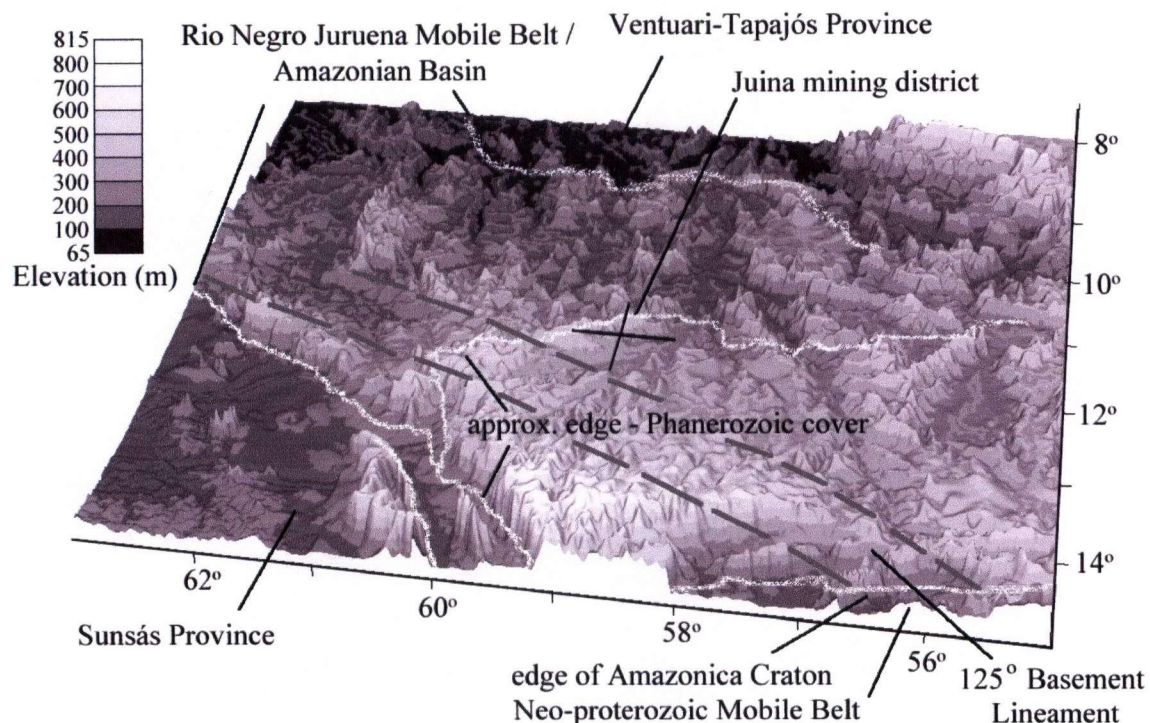
Fig. 1.4. Topographic map of Juina mining district and surroundings. Three geochrolological provinces are visible: the Rio Negro Juruena mobile belt, in which Juina sits; the Ventuari-Tapajos Province to the north; and the Sunsas Province to the south.

There are a number of kimberlites in the area (Fig. 1.5) two of which have been dated at 92-95 Ma (U/Pb dating of zircons from kimberlitic breccia) (Heaman *et al.*, 1998). Kimberlites are located near the southwestern margin of the Amazonian craton and are mostly emplaced in the Permo-Carboniferous sedimentary rocks of the Fazenda da Casa Branca Formation. Other kimberlites have intruded the older Rio Negro-Juruena Province (Tassinari *et al.*, 1999). It is speculated that the Chicoria Creek diamonds are sourced from at least four local kimberlite pipes (M. Tremblay, personal communication, 2004).
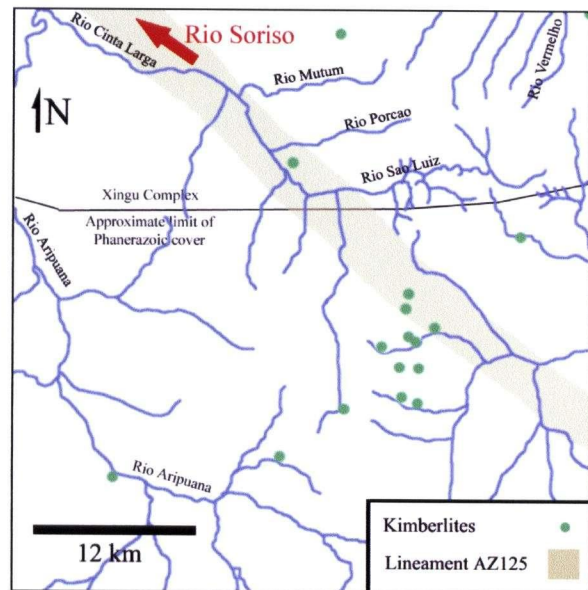
Fig. 1.5. Detailed location map of Juina diamond mining district. Included are the local drainage, kimberlite locations, and several rivers that have been the focus of previous studies. Reproduced from Juina Mining website. Rio Soriso is located just off the map and drains into Rio Aripuana.

No kimberlites are currently being mined and it is unclear whether or not they contain economic quantities of diamonds. It is also unclear if they are indeed the source for all the diamonds recovered from local rivers. The Chapadao sediments (Cretaceous-Tertiary sandstones of the Parecis Formation, Heaman *et al.*, 1998) located at the headwaters of the Rio Sao Luiz, are thought to be a possible source for alluvial diamonds.

2.0 Diamond Morphology

2.1 Introduction

Morphological studies are considered essential for fingerprinting diamond populations (e.g. Harris *et al.*, 1975; Robinson, 1979; Orlov, 1977; Gurney *et al.*, in print), and is of particular importance for the suite represented here as the primary source is unknown. Through coupling morphological studies with previous experimental work, much can be determined about a diamond's history (e.g. Robinson *et al.*, 1989). This study documents features described by others together with experimental findings to develop a history for the population, and to determine if there is any basis for considering if this suite comprises two or more population sub-sets, each with unique histories.

2.1.1 Crystal habit

The variety of primary crystal habits in diamond has been the focus of numerous studies (e.g. Orlov, 1977; Sunagawa, 1984b). Orlov (1977) divided single crystal forms into five types: 1) octahedral, 2) cubic, 3) certain cubes and combinations of cubes, octahedra, and dodecahedra, 4) coated stones and 5) black or dark stones (due to the presence of inclusions of graphite). Orlov (1977) also divided the polycrystalline habits of diamond into five categories. They are: 1) ballas, 2) aggregates, 3) bort comprised of small euhedral crystals, 4) bort characterized by irregular granular crystals and 5) carbonado. It is unclear why Orlov created some classes based on properties seemingly irrelevant to crystal habit, such as the presence of graphite inclusions.

Crystal habit is a product of numerous factors, such as growth rate of crystal faces, temperature and pressure conditions, and the chemistry of parental fluid (Klein and Hurlbut, 1985). Sunagawa (1984b) states that primary diamond morphology is strongly controlled by the level of carbon supersaturation (σ) between the liquid and solid phase.

Although Sunagawa's (1984b) classification scheme for diamond is similar to Orlov (1977), he bases divisions on the level of supersaturation. Above a critical supersaturation value (σ^{**}), unstable and abnormal growth conditions prevail which are favourable to the formation of radiating, granular and concentric habits. Under these conditions, polycrystalline aggregates of cryptocrystalline diamond such as bort, carbonado, framesite and ballas, develop. Below a critical supersaturation level (σ^*), stable conditions prevail in which single crystals develop through layer-by-layer growth (discussed in greater detail in chapter 7.0 on growth studies). Aggregates of euhedral crystals also form under these stable conditions. Between these critical supersaturation levels, hopper crystals (hollow crystals that have a skeletal texture by failing to grow faces) are expected. Most natural cubes exhibit a radiating structure (Lang and Moore, 1972) and are thus believed to form under conditions near but slightly below σ^{**} (Sunagawa, 1984b).

Growth experiments on synthetic diamond in controlled environments have demonstrated that crystal habit is in part controlled by pressure and temperature (Clausing, 1997) (Fig. 2.1A). Cubes crystallize at lower temperatures while octahedra crystallize at greater temperatures. There is a transition zone between these forms where cubo-octahedra are stable. These experimental observations are likely the basis for Haggerty's (1986) model of crystal form stratification within the lithospheric root, where octahedral forms crystallise in the lowest reaches of the root, cubes form at the most shallow depths possible for diamond stability and transitional forms are found between these extremes. However, Sunagawa (1984a) cautions application of experimental results from synthetic diamonds to natural systems as there are still properties of the mantle that remain poorly understood. The stability fields for diamond and graphite are shown in Fig. 2.1B.
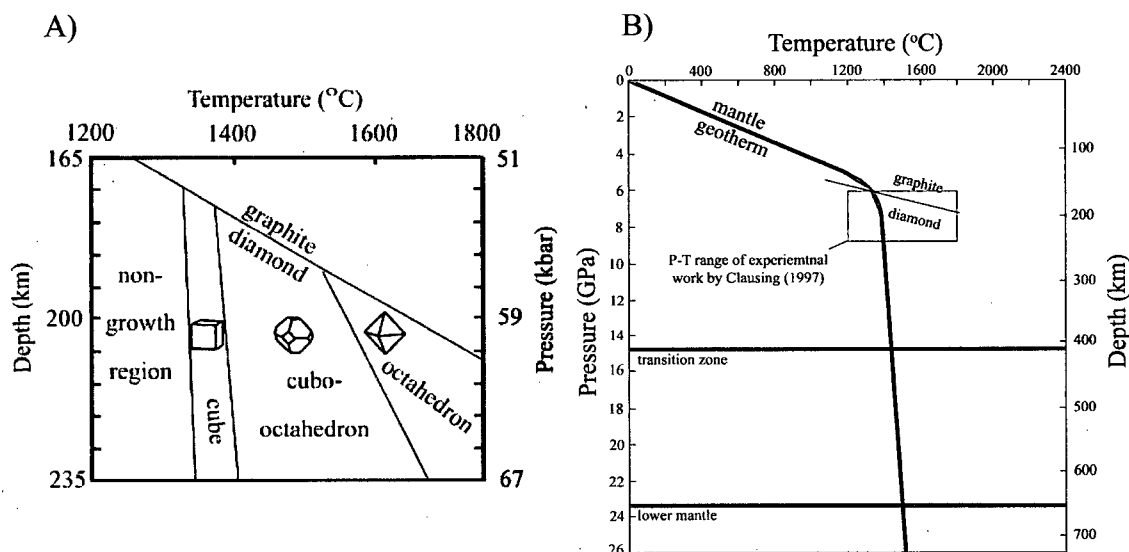
Fig. 2.1. Pressure-temperature plot of primary diamond crystal form and diamond-graphite stability. A) After Clausing (1997). B) Diamond-graphite field after Kennedy *et al.* (1976). Horizontal lines at ~14.5 GPa and 23.5 GPa mark the approximate upper limits of the transition zone and lower mantle respectively and the thick bent curve indicates an approximate geothermal gradient (from Joswig *et al.*, 1999)

2.1.1.1 Monocrystalline diamond

The three primary single crystal forms described here (octahedron, cube, and cubo-octahedron) are the result of growth. The external morphology of diamond, however, does not reflect just growth; it also reflects the post crystallization history, including resorption, brittle fracturing and deformation. As well, there are cases involving multiple stages of growth, fracturing and dissolution. Nevertheless, some background on the crystal structure of diamond is warranted.

The octahedron is the most common primary form of diamond observed in nature (Orlov, 1977). Octahedra comprise eight triangular faces or three-point surfaces with three-point symmetry (Fig. 2.2). In diamond literature, these faces are often described using Miller indices. The surface labelled (111) (Fig. 2.2) is the growth face that intersects the imaginary axes at
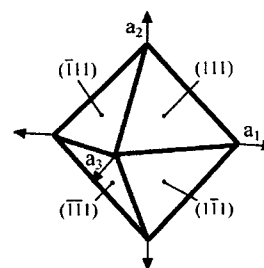
Fig. 2.2. Octahedral crystal form.

10

coordinates (1,0,0), (0,1,0) and (0,0,1). Because every face intersects the a_1-a_2-a_3-axes at either positive or negative 1, all faces belong to the {111} form. Throughout this report when discussing octahedral growth surfaces or features that form on these surfaces, the term '(111) surface' will be used for brevity to describe all eight surfaces. A similar convention will be adopted to describe cubic faces (belonging to the {100} form), which will be referred to as (100) surfaces.

In terms of growth mechanics, a diamond is bound by the crystal faces that take the longest time to grow; the face that nucleates and grows quickly, grows to extinction (Clausing, 1997). Under most conditions where diamonds form, the cubic face (100) grows to extinction, thus letting the octahedral faces develop and control the morphology of the stone. Octahedral faces may be flat and smooth (Fig. 2.2) or they may have stepped development.

Although not as common as octahedral crystals, cubic crystals often make up a significant proportion of total diamond populations. They are characterized by six square faces or four-point surfaces with four-fold symmetry (Fig. 2.3). Cubic crystals rarely exhibit smooth faces, rather, their surfaces are usually undulating and rough. Phaal (1965) attributes this roughness to the tendency for dissolution to concentrate on (100) faces.
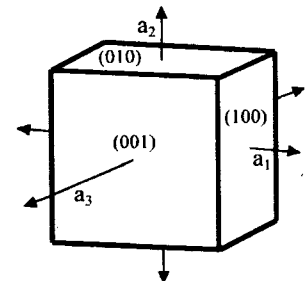
Fig. 2.3. Cubic crystal form.

The cubo-octahedron is a combination of forms. It exhibits eight triangular faces and six square faces, for a total of 14 (Fig. 2.4). The ratio of size of octahedral to
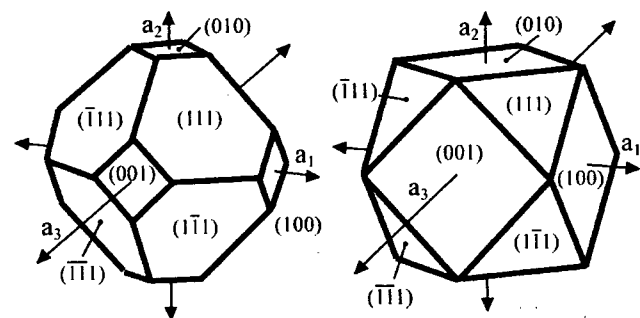
Fig. 2.4. Cubo-octahrdron, a combination form of cube and octahedron. Crystal morphology varies by relative size between (111) and (100) faces.

cubic faces can vary so that the crystal appears from *nearly* cubic to *nearly* octahedral. Laboratory experiments have shown that there is a full transition from octahedron to cubo-octahedron to cube and that a combination form with a large (111):(100) ratio likely formed at higher temperatures than a crystal with a lower (111):(100) ratio.

2.1.1.2 Polycrystalline diamond

Polycrystalline diamonds can be broadly divided into two classes, twins and aggregates. Aggregates, or what Orlov (1977) refers to as variety VII diamond, are the coalescence of multiple octahedral crystals (Fig. 2.5). Harris *et al.* (1975) describe aggregates as being composed of two or more diamonds in some form of conjunction. This includes a diamond entirely enclosed within another, a diamond embedded within the surface of another, or multiple stones unconformably aggregated together. A twin, however, is the symmetrical intergrowth of two or more crystals of the same substance (Klein and Hurlbut, 1985). Unlike aggregations, twinning is crystallographically controlled. The most common diamond twin observed has a triangular morphology and is called a *macle* (Fig. 2.6). The classification of an aggregate in this study essentially follows that of Harris *et al.* (1975); any stone containing two or more crystals that do not share the same crystallographic axis is considered an aggregate. When possible, the individual crystals that make up an aggregate are described in terms of single crystals.

0.5 mm
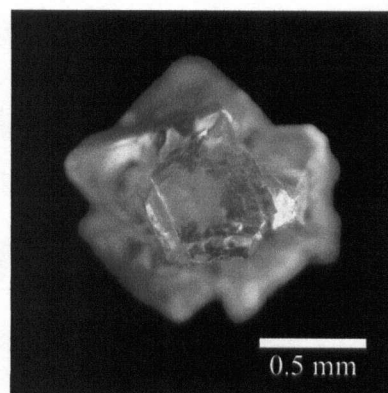
Fig. 2.5. Photograph of diamond aggregate (this study).

2 mm
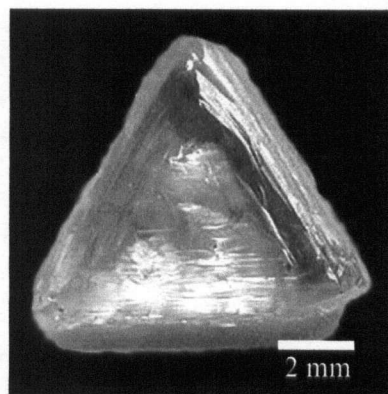
Fig. 2.6. Photograph of a diamond macle twin. The flattened triangular shape is characteristic of macles. The shared crystallographic axis is parallel to the plane of the page, and hence the reason why the second crystal is not visible.

Other forms of polycrystalline diamond, such as ballas, bort, framesite, stewartite and carbonado (Orlov, 1977; Sunagawa, 1984b) and yakutite (Kaminsky, 1992) were not observed in this study.

2.1.2 Resorption

Rounded crystals are common to most diamond suites and, as such, led many to believe that rounded morphology was a primary crystallographic form of diamond. The failure of modern experiments to crystallize rounded diamond (e.g. Bovenkerk, 1961; Clausing, 1997) has weakened the growth argument. The ability of experiments to reproduce rounded crystals through diamond dissolution (e.g. Kanda *et al.*, 1977) strongly suggests that rounded diamonds are a product of resorption. The development of cathodoluminescence as a tool to examine the internal growth habit of diamond has shown conclusively that all rounded diamonds are a result of dissolution (see Moore and Lang (1974) for a more comprehensive history of this debate).

It is generally accepted that rounded diamonds are the result of dissolution. However, there is still no consensus on the corrosive agent responsible for the resorption of diamond. Examples of diamonds partially exposed in mantle xenoliths often exhibit non-uniform resorption, with the exposed part of the diamond more resorbed than the portion enclosed by the xenolith. This observation is cited as evidence that kimberlite magma dissolves diamond. Robinson *et al.* (1989) proposed that the wide variation of resorption observed in one kimberlite reflects the time at which each diamond was liberated from its hosting xenolith. Diamonds released at great depths during magmatic ascent are more resorbed than diamonds that are liberated near the Earth's surface. However, Haggerty (1986) and Pattison and Levinson (1995), among others, have observed euhedral microdiamonds in some diamond suites. They suggest that these diamonds are much younger than macrodiamonds from the same kimberlite. It is unclear why microdiamonds, which one would expect to be most resorbed due to their small surface to

volume ratio, lack signs of dissolution. Pattison and Levinson (1995) propose that microdiamonds crystallise from kimberlite magma. In any case, it is likely that kimberlite magma is corrosive to diamond when specific conditions are met (perhaps when oxygen fugacity levels are conducive for carbon dissolution), however, other corrosive agents (i.e. carbon dioxide, steam, and oxygen, among others) may play a role in diamond dissolution. Cathodoluminescence (CL) studies of polished diamond surfaces reveal that many crystals have experienced numerous periods of growth and dissolution, indicating that kimberlitic magma is not the only possible corrosive agent, and that dissolution can occur in the mantle where diamonds reside.

Because the rounded shape of diamond was once believed by many to be a product of growth, we are left with confusing terminology to describe these rounded grains. It was recognized that unlike true crystal faces, the surfaces on rounded diamonds are curved. As such, it was agreed that any crystallographic term used should end in the suffix 'oid', to signify that the form lacks flat faces. Robinson (1979) and many others use the term tetrahexahedroid (THH), which has 24 trigonal faces, to describe rounded crystals of initially octahedral habit. Others, such as Kaminsky *et al.* (2000) and Moore and Lang (1974), use the term dodecahedroid (12 rhombic faces) to describe these rounded crystals. The term 'combination O-D' is used by Kaminsky *et al.*, (2000) to describe transitional crystals between the dodecahedroid and the octahedron. There is no consensus as to which terms should be used to describe rounded and partially rounded diamonds, and there likely never will be if resorbed shapes are to be described using crystallographic terminology. However, it is recognized that most published data includes these terms and for the purposes of comparison, they are included in this study.

Otter and Gurney (1989) developed a classification scheme, first proposed by D. Robinson, which avoids the problem of describing shapes unrelated to crystal growth with crystallographic terms. They divided the degree of resorption based on percent preservation into 5 classes, with class 1 describing diamonds that have between 1-55% of
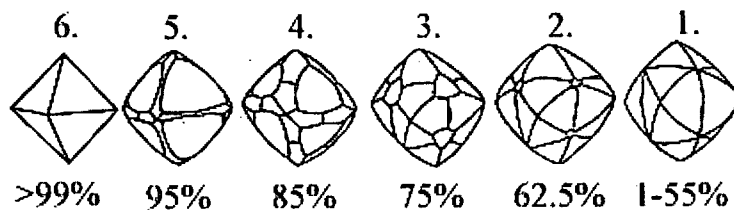
Fig. 2.7. Semi-quantitative resorption classification scheme for crystals that initially grew as octahedrons. Numbers on top refer to the resorption class while the percent values on bottom represent the amount of crystal preservation (after McCallum *et al.*, 1994).

their initial crystal preserved and class 5 greater than 95% preserved. McCallum *et al.* (1994) further developed this classification to include a sixth class, which includes forms with greater than 99% preservation. Fig. 2.7, from McCallum *et al.* (1994) illustrates the percent preservation for each class. Although no such classification scheme exists for cubic or cubo-octahedral forms, certainly a similar scheme could be developed.

It is suggested here that the terms dodecahedroid and tetrahexahedroid be dropped from scientific papers as descriptive terms for diamond morphology. The lack of consistency in terminology, coupled with what is deemed an incorrect usage of a crystallographic term, makes these terms confusing and unscientific. Crystallographic terms say something intrinsic about a crystal and should not be used to describe a secondary, superficial modification of a crystal. The resorption class scale suggested by McCallum *et al.* (1994) avoids confusion and is semi-quantitative. Similar resorption classification

Table 2.1. Conversion between various terminology classification schemes

Resorption Class (McCallum *et al.*, 1994)	Percent Preservation	McCallum *et al.*'s, (1994) suggested terminology	Terms used in this study
1	1-55	Tetrahexahedroid	Tetrahexahedroid
2	55-70	Octahedral tetrahexahedroid	Dodecahedroid
3	70-80	Transitional octa-THH	Transitional O-D
4	80-90	Transitional THH-octa	Transitional O-D
5	90-99	Tetrahexahedroidal octahedron	Transitional O-D
6	>99	Octahedron	Octahedron

Semi-quantitative resorption classification and their equivalent qualitative terms, from McCallum *et al.*, (1994) and terminology used in this study.

15

schemes should be developed for the other primary, single crystal forms of diamond; namely, for cubic and cubo-octahedral forms.

2.1.3 Crystal regularity

Crystal regularity is a measurement based on comparison of the lengths of three orthogonal axes. Following terminology used by Robinson (1979), equidimensional grains have three axes of equal lengths, slightly distorted grains have axes of similar length, flat grains have two axes of equal length and one that is less than 1/3 of the others, elongate grains have two axes that are less than 1/3 the length of the third axis, and irregular grains are those that fall outside of any of the above classes.

2.1.4 Crystal intactness

Intactness is a term used to describe the amount of the original crystal lost to brittle fracturing. It does not consider the loss of diamond to etching or resorption. The four divisions used in this classification are: intact, broken, fragment, and fraction (after F.V. Kaminsky, personal communication). An intact crystal retains all growth and/or resorption surfaces, a broken grain retains greater than 2/3's of the original crystal, a fragment comprises between 1/3 and 2/3's of the initial crystal, and a fraction represents less than a third of the initial crystal. Although this classification scheme is subjective, the divisions convey a general idea of crystal intactness.

2.1.5 Surface features

Numerous surface features of diamond have been documented most thoroughly by Robinson (1979). Many features reveal significant events in a diamonds history while others appear to be manifestations of one event affecting another. For example, shield-shaped laminae are the result of partial resorption of stepped growth on octahedral faces.

16

As such, the presence of shield-shaped laminae are not recorded, instead, the growth and resorption events are documented. Features which were deemed important in terms of *adding more to the story* were documented, while those that were deemed superfluous were not recorded. For this reason many of the 41 pristine surface features described in Robinson (1979) are not mentioned here. In this study, surface features examined for include: etch pits (trigons, hexagons, and quadrons); etch channels; corrosion sculptures; frosting; deformation laminations; hillocks; green spots; fracturing; and mechanical wear.

There is no obvious way to divide surface features. Some clearly form earlier than others, some are produced by chemical dissolution while others form as a result of mechanical wear, and some are restricted to growth faces while others form only on resorbed surfaces. The approach adopted here was to divide surface features into two categories, those that formed as a result of etching, and all other features.

2.1.5.1 Surfaces features associated with etching

Etching is a common event that affects the vast majority of diamonds. Common features observed are etch pits, etch channels, and frosting. Some features occur during residence in the mantle, others occur immediately after magma emplacement, some features are restricted to particular faces while others show no preferential development on particular faces. The coupling of detailed examination of diamonds and laboratory experiments has led to the establishment of constraints on some environmental conditions. For this reason, etching observations may be considered important in terms of piecing together the history of the diamonds.

Trigons and hexagons are found on (111) faces while tetragons are restricted to (100) faces. Most other features associated with etching are found on resorbed surfaces. Trigons and tetragons may be flat-bottomed or point-bottomed (pyramidal) while only flat-bottomed hexagons exist (Robinson, 1979). Trigons exhibit either positive

orientation, whereby the apices of the trigon points in the same direction as the apices of the (111) face, or more commonly, they exhibit negative orientation, whereby the apices of the trigon point to the long edges of the octahedral face (Fig. 2.8). In a similar manner, tetragons display both positive and negative orientations.

Positive orientation   **Negative orientation**

Cubic {100} faces

Octahedral {111} faces
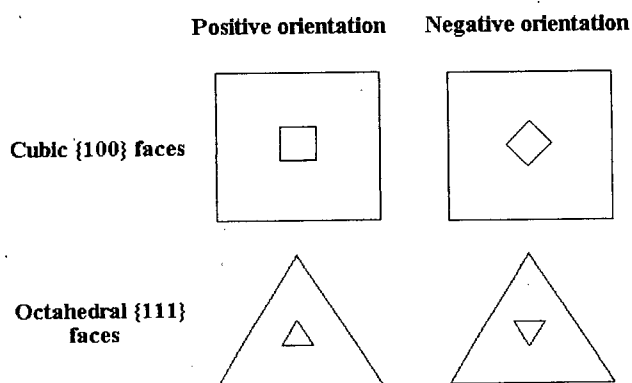
Fig. 2.8. Etch pit orientation on cubic and octahedral faces.

Tolansky (1955) proposed that trigons, hexagons and tetragons are growth features, or more precisely, a result of growth failure. However, experiments by Sunagawa *et al.* (1984) have demonstrated quite conclusively that these features are products of etching and that they are focused on the outcrop of screw dislocations in the crystal structure. The direct cause of this attack on the structure of diamond is unclear, but there have been numerous proposals as to the corrosive agent(s) responsible. Some hypotheses are kimberlite magma, steam, carbon dioxide, oxygen, chlorine, bromine, hydrogen, hydrogen fluoride and hydrogen bromide (Robinson, 1979).

Various experiments have been done to induce etch features on diamond (Harris and Vance, 1974; Robinson, 1979). Results vary considerably depending on etchant used and temperature and pressure conditions. Robinson (1979) summarises the results of many of these experiments. Two of these points are considered pertinent to this study and are reproduced here: 1) negatively oriented features require temperature in excess of 950°C and etchants are likely carbon dioxide and steam, and 2) at low pressures, oxygen gas and strong oxidizing agents are the only etchants capable of creating positively oriented etch features at temperatures between 450 and 1000°C. From these observations, Robinson *et*

al. (1989) concluded that negatively oriented etch features form earlier than positively oriented ones and that different etchants and temperatures may explain different orientations. Experiments by Phaal (1965) demonstrate that the orientation of etch features is controlled by the same conditions for diamonds of both cubic and octahedral habit. As well, it was noted that cubic faces are more easily etched and that when both tetragons and trigons occurred on the same diamond, tetragons were more pronounced and better developed (this point was mentioned in section 2.1.1.1 on the roughness of natural cubic forms).

The formation of hexagons is interpreted by Phaal (1965) to be the product of two etchants acting simultaneously. Oxygen gas is responsible for the positively oriented component while steam or wet carbon dioxide is responsible for the negative component. Hexagons have been produced in etching experiments under low pressure at temperatures between 950 and 1000°C (Evans and Sauter, 1961), although Robinson (1979) states that they can be formed at temperatures above 1000°C.

Etch channels, also referred to as ruts, are straight or, more commonly, sinuous grooves that penetrate the diamond as a result of etching (Orlov, 1977; Robinson, 1979). Ruts postdate resorption and typically: 1) trace octahedral to subconchoidal planes on resorbed surfaces, 2) radiate from inclusion pits, or 3) develop along seams between interpenetrantly-twinned crystals (Robinson, 1979). Orlov (1977) attributes the formation of ruts to oxidizing fluids coming in contact with diamond. He proposes that these fluids penetrate cracks within a xenolith hosting diamond, thus locally etching the diamond.

Frosting is another common surface feature, and is described as a clouding or *frosting* of the diamond's appearance. It typically forms on rounded (resorbed) diamonds and roughens smooth surfaces; in the process, an otherwise transparent crystal becomes semi-transparent. Etching experiments by Robinson (1979) demonstrate that frosting can be

reproduced by chemical dissolution of diamond. Although frosting preferentially forms on rounded diamond, it is not restricted to resorbed faces and is sometimes observed on flat faces and fracture surfaces. Robinson's (1979) experiments produced two types of frosting, 1) coarse frosting, which results from rapid etching by either wet carbon dioxide or steam with subordinate free oxygen at temperatures between 950 and 1000°C, and 2) fine frosting, which results from rapid etching by oxygen gas at temperatures at or below ~950°C. Based on cross-cutting relationships, Robinson (1979) and Robinson et al. (1989) interpret frosting as a late-stage etch feature that occurs at a similar time to positively oriented etch pits.

2.1.5.2 Other surface features

Surface features not associated with etching are described here. These are: deformation laminations, hillocks, fracture surfaces and mechanical wear.

Deformation laminations (also called deformation lamellae) are lines or striations that form as a result of plastic deformation of diamond (Urusovskaya and Orlov, 1964) and are usually visible only after resorption (Robinson et al., 1989). Laminations form as the crystal structure glides along the (111) plane, and thus are crystallographically controlled. Striations are more resistant to dissolution than the rest of the diamond (due to work hardening), and become positive features after resorption (De Vries, 1975). They may form as one, two or even three sets of parallel lines on a resorption surface. Experiments by De Vries (1975) have shown that ductile deformation of diamond begins at temperatures between 900 and 1100°C and pressures between 10 and 60 kbars.

Hillocks are a loosely defined surface feature. Orlov (1977) describes hillocks as pyramidal and drop-shaped features of positive-relief which are controlled by crystal habit but are visible only on rounded faces. Robinson (1979) divided hillocks into five subcategories: 1) elongate hillocks, 2) ellipsoidal hillocks, 3) semi-cylindrical hillocks

with hexagonal pits, 4) transverse hillocks, and 5) pyramidal hillocks. Robinson (1977) states that the first four types are controlled by the same factors as suggested by Orlov (1977), but asserts that some pyramidal hillocks are associated with deformation laminations and may form at the intersection of two sets of lines. Other workers associate elongate hillocks with deformation laminations (e.g. McCallum et al., 1994; McKenna, 2001).

At one time diamond was believed to be so strong that it could not be broken (Krajick, 2001). We now know this not to be true; most diamonds have experienced at least partial brittle fracturing in the mantle, during kimberlite ascent or during residence in the surficial environment. In this study two types of brittle fractures were observed: 1) 'pre-eruption' fracture surfaces, those formed during residence in the mantle that appear to pre-date at least some resorption; 2) and late-stage fractures, which are formed either during magma ascent or in the surficial environment and are characterised by conchoidial surfaces. The latter category is somewhat related to the degree of intactness and this study aims to be consistent between the two classifications.

Mechanical wear, like dissolution, preferentially attacks the corners and edges of diamond. However, unlike dissolution, mechanical wear produces a rough texture on these surfaces and is clearly distinguishable from the chemical wear of diamond. Abrasion occurs during residence in the surficial environment and is a common feature on alluvial and paleo-alluvial diamonds that have been transported over long distances (i.e., diamonds found off the west coast of Namibia).

2.1.6 Sequence of events

A summary of a diamond's history can be determined by placing all the features documented in this chapter in order of occurrence, mainly based on cross-cutting relationships. The sequence of events (Fig. 2.9) is reported by Robinson et al. (1989): 1)

diamond growth, 2) plastic deformation, 3) etching in the form of negatively oriented features, 4) resorption and 5) etching in the form of positively oriented features and the development of frosting. However, this 'sequence of events' is clearly an oversimplification as cathodoluminescence studies on

Fig. 2.9. The relative timing of common features observed on diamond. The number refers to the relative timing of each feature. Features are discussed in detail in this chapter. Growth faces (section 2.3.3), lamination lines (section 2.3.7.2a), negatively oriented etching (section 2.3.7.1a), resorption (section 2.3.4) and positively oriented etching (section 2.3.7.1a). (after Robinson et al., 1989).

polished diamond surfaces often reveal that the diamond experienced numerous alternating episodes of growth and dissolution.

2.2 Analytical techniques

Diamonds were analysed using a transmitted light optical microscope and a scanning electron microscope (SEM).

A Leica MZ FLIII optical microscope with a 10x zoom lens and 1x objective lens was used for macroscopic examination of diamonds. Observations were made in both transmitted and reflected light mode. Digital images were collected using a Spot Insight Colour 3.2.0 digital camera and when required, were enhanced using Adobe Photoshop 6.0.

Detailed examination of small surface features on diamond was done using a SEM. Diamonds were placed on standard aluminium stubs without being carbon coated (for fear of creating future complications during infrared analysis). Without a carbon coat, it was uncertain whether or not the stones would charge up. The fraction of small stones

(those less than 0.5 carats or ~4 mm in size) generally did not charge up on the instrument, thus permitting detailed examination. The fraction of larger stones, however, frequently charged up and are thus poorly represented in SEM images. The SEM was operated in back-scattered electron (BSE) mode using an accelerating voltage of 15 kV and an estimated beam current of 1 nA.

2.3 Results

The results for the morphological characterization of the Rio Soriso diamonds are summarised in Appendix B. A more detailed description of the features catalogued is presented below.

2.3.1 Size

The diamonds studied range considerably in weight, from 0.003 to 0.404 grams (0.015-2.02 carats). A plot of diamond weight against normalized frequency (Fig. 2.10) demonstrates the bimodal character of the diamond suite and that it does not fit a lognormal distribution, as would be expected for a randomly selected suite of one population
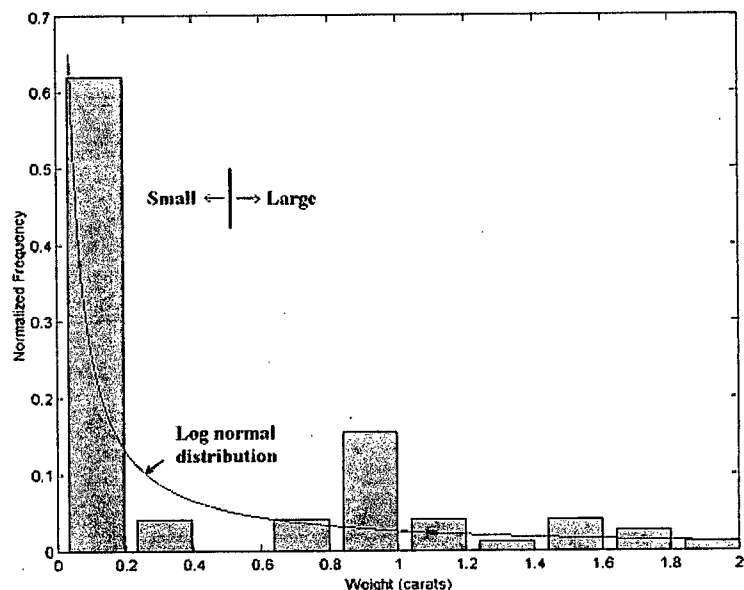
Fig. 2.10. Weight in carats versus normalized frequency. A log normal distribution is superimposed on the graph to illustrate that the data does not fit. For some correlations the population is divided into two halves, large (>0.5 carats) and small (<0.5 carats).

(Boggs, S., 1987). The size distribution of the samples does not reflect the diamond population as a whole, but is an artefact of sampling bias. Large diamonds were preferentially selected for study as there is a greater probability that they contain more and larger inclusions than small diamonds.

2.3.2 Crystal habit

Of the 69 diamonds available for study, 64 were monocrystalline and 5 were polycrystalline. None of the monocrystalline diamonds exhibits well-formed primary crystal morphology, as described in section 2.1.1. Octahedral

Fig. 2.11. Images of an octahedral crystal (Diamond 4-18). A) SEM image of flat-faced crystal growth. Step development is minor and resoprtion is absent. B) Photograph of same diamond showing the complex nature of the crystal.

(111) faces are rare or obscured and cubic (100) faces are absent. Diamond 4-18 is the closest crystal to an octahedron (Fig. 2.11A and B), but has a somewhat more complex morphology than for a perfect octahedron (e.g. Fig. 2.2). It should be stressed here that this does *not* imply that octahedral growth did not occur. The results of this work will show that most crystals likely grew as octahedrons (or at least grew octahedral faces) but that these faces have since been rounded by dissolution, broken by brittle fracturing, and/or deformed by plastic deformation. The five

Fig. 2.12. SEM image of aggregate of octahedral crystals (Diamond 6-8).

polycrystalline stones are classified as aggregates (e.g. Fig. 2.12). Two aggregates are comprised of only two crystals (diamonds 2-1 and 4-11) while the other three are comprised of more than five individual crystals (diamonds 4-15, 5-8 and 6-8). No crystals appear to share a common crystallographic axis and are thus aggregates and not twins.

2.3.3 Resorption

The degree of resorption of monocrystalline and polycrystalline stones was estimated using Fig 2.7 as a guide. Data is presented in Table 2.2 under the heading 'resorption category' and the population distribution is graphically presented in Fig. 2.13. Some crystals,
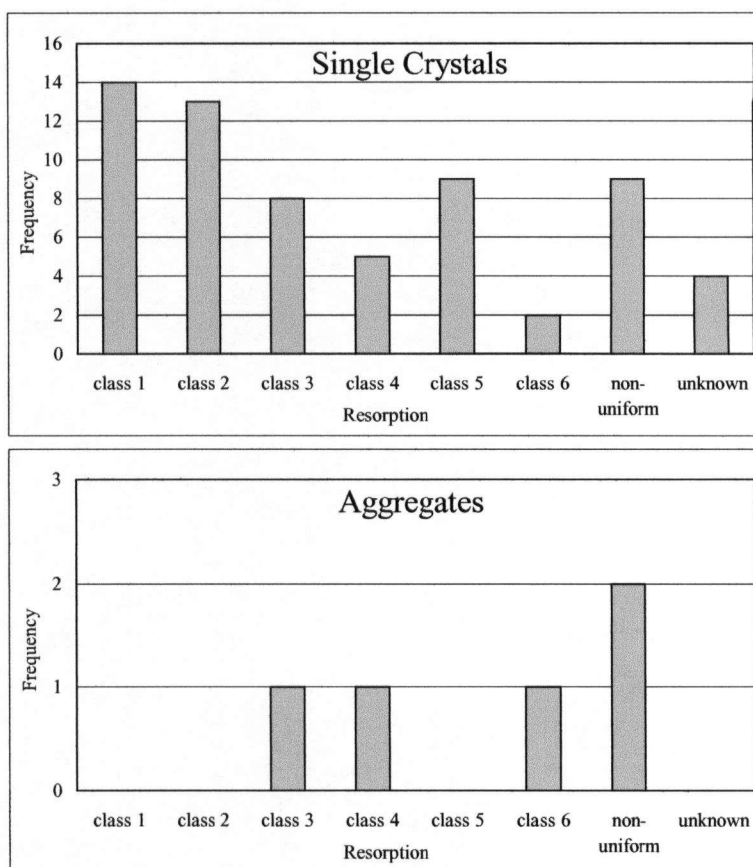
Fig. 2.13. Frequency versus resorption class. Top graph is for single crystals (n=64) and bottom graph is for aggregates (n=5). Non-uniform stones possess two resorption classes. Resorption classes are from McCallum *et al.* (1994).
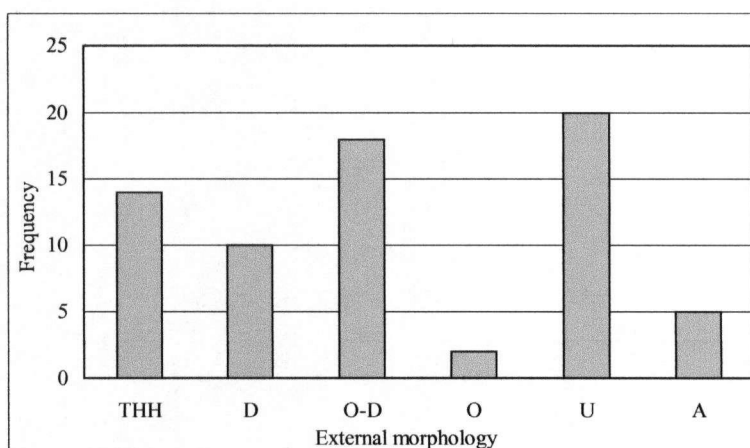
Fig. 2.14. Frequency versus external morphology. The abbreviations used are: THH - tetrahexahedroid; D – dodecahedroid; O-D – transitional octahedron-dodecahedroid; O – octahedron; U – unknown; and A – aggregate. Table 2.1 explains the conversion between these terms and the resorption scale used in Fig. 2.9.

typically those which are considered fractions (see section 2.3.5), could not be classified and are labelled 'unknown'. Some crystals possess non-uniform resorption and are classified as such. Stones were also described using morphological terms (described in section 2.1.2) so that the data can be compared with other data sets (Fig. 2.14). Consistency between the two classification schemes was retained whenever possible, although many more crystals were classified as having an unknown morphology using the descriptive classification. (See Table 2.1 for conversion between the McCallum *et al.*, 1994 semi-quantitative classification scheme and the qualitative descriptive classification scheme). Diamonds in this study are strongly resorbed, with the average degree of dissolution falling between classes 2 and 3 for single crystals while aggregates tend to be less resorbed. SEM images of typical examples of rounded forms can be seen in Fig. 2.15.
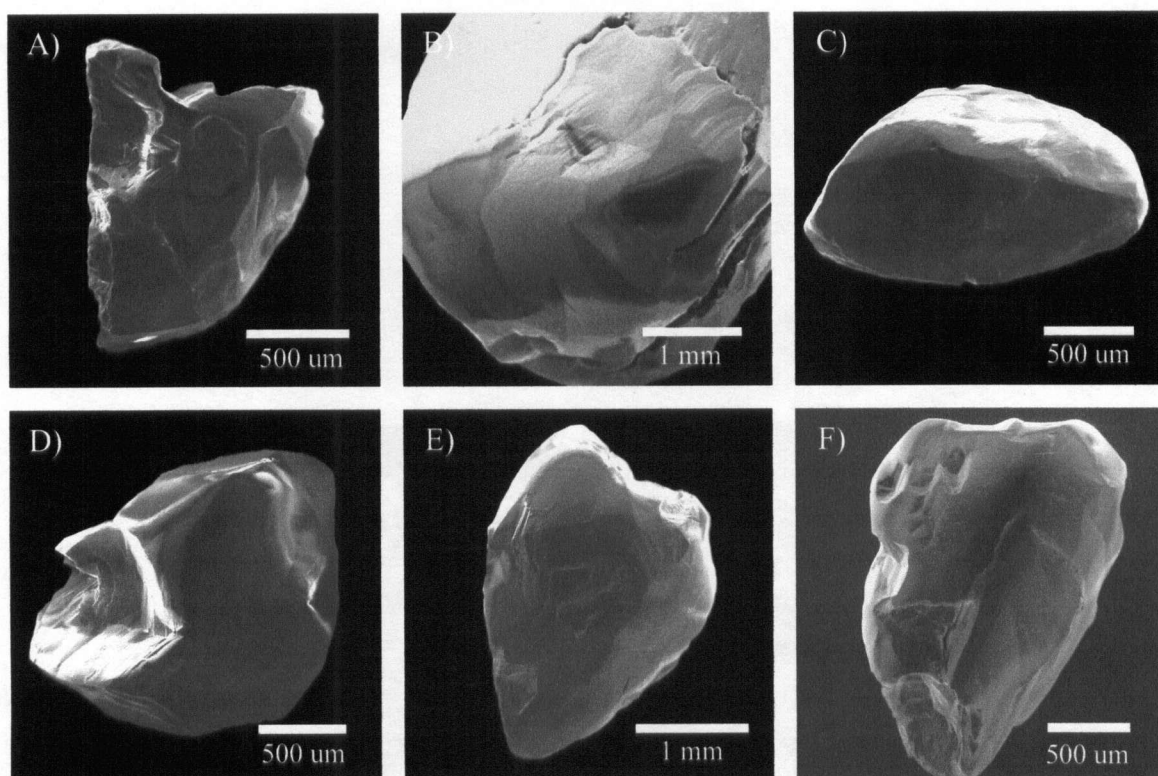
Fig. 2.15. SEM images of diamond resorption. A) resorption class 3, etch features on flat crystal face, resorbed corners on right (diamond 6-4); B) resorption class 3, black surface in middle of photograph is crystal face (diamond 2-1); C) resorption class 1, no flat crystal faces (diamond 4-12); D) resorption class 1 (diamond 4-16); E) resorption class 1 (diamond 5-2) and; F) resorption class 1 (diamond 4-13). Resorption scale is from McCallum *et al.*, (1994) and is reproduced in Fig. 2.9.

2.3.4 Crystal regularity

Twenty-nine percent of grains studied are either equidimensional or slightly distorted, 67% are considered irregular and only 4% are considered flat. There are no elongate grains. However, note that the irregular forms are not necessarily products of growth but may be a manifestation of other processes such as non-uniform dissolution, plastic deformation and brittle fracturing.

2.3.5 Crystal intactness

Most crystals are considered to be either broken (45%) or fragments (29%), with fraction and fully intact crystals making up the remainder of the population (11% and 14% respectively) (Fig. 2.16). Examples of each degree of intactness can be seen in Fig. 2.17. Brittle fracturing, either during residence in the mantle, residence in the surficial environment or during mining are the reason(s) for the small percentage of fully intact crystals (see section 2.3.9).
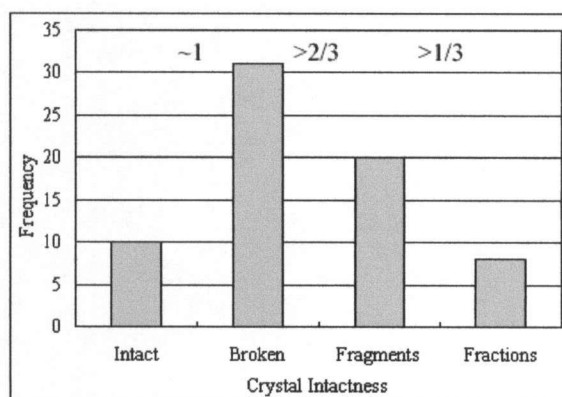
Fig. 2.16. Frequency versus degree of intactness for all diamonds in study. Numbers 1, 2/3, and 1/3 represent the estimated amount of the original diamond crystal preserved.
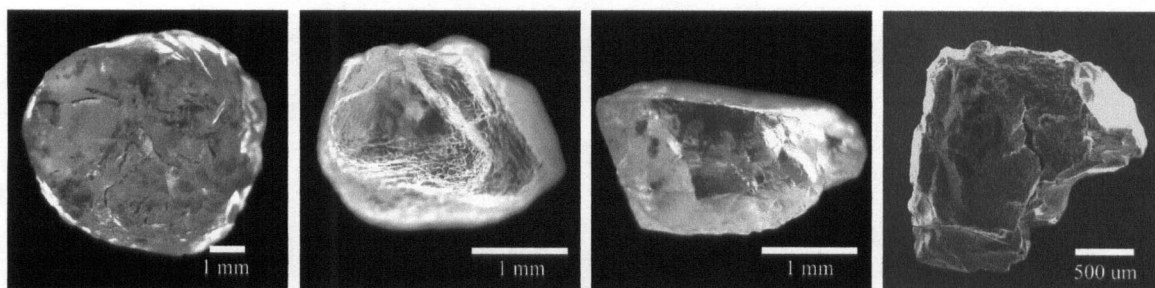
Fig. 2.17. Photos and SEM image of examples from this study for the four classes of 'intactness'. From left to right: Intact crystal (diamond 3-1); broken crystal (diamond 4-1); fragment (diamond 6-6); and fraction (diamond 6-5).

27

2.3.6 Etching

For the diamonds in this study, trigons, hexagons, tetragons and etch channels are abundant, and found on 80% of the stones.

2.3.6.1 Trigons

Fifty-four percent of the population exhibits trigonal pits (Fig. 2.18). Pits are mostly small (on the order of 10-100 μm) however some are as large as 0.5 mm. Flat-bottomed trigons are predominant but there
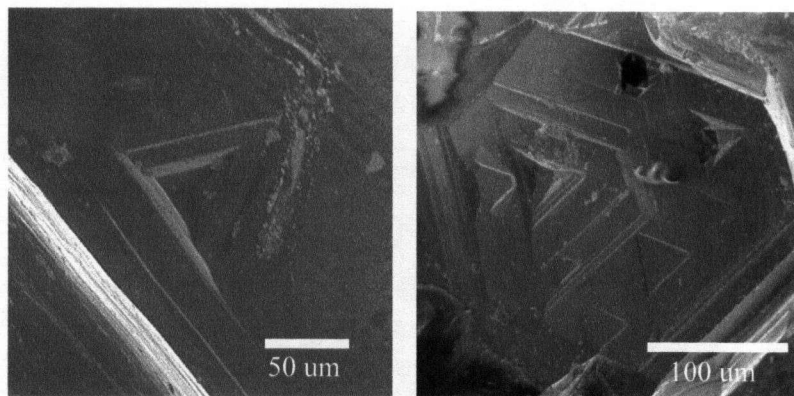
Fig. 2.18. SEM photo of trigonal pits. Left image is single trigonal pit (diamond 5-9) and image on right shows several trigonal pits, some super-imposed on one another (diamond 6-4).

are several instances of point-bottomed trigons. Positively oriented trigons were verified on only 3 diamonds while negatively oriented trigons were confirmed on 24 diamonds. Roughly 1/3 of the diamonds examined lack adequate crystal faces to confirm trigon orientation.

2.3.6.2 Hexagons

Hexagons are found on 54% of diamonds examined (Fig. 2.19). All hexagons observed are flat-bottomed and
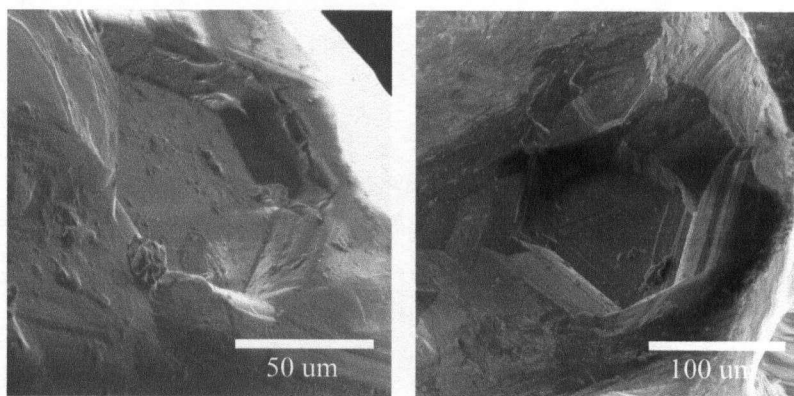
Fig. 2.19. SEM photo of hexagonal pits. Left image is from diamond 4-15 and right image from diamond 5-3.

relatively large compared to trigons, some measuring up to 0.75 mm. Although some inclusion pits resemble hexagons, they invariably lack flat bottoms and are thus easily differentiated. Trigons of both positive and negative orientations are observed in the bases of hexagons.

2.3.6.3 Tetragons

Thirty-six percent of diamonds examined exhibit tetragonal pits (Fig. 2.20). The largest pits measure ~0.25 mm across while the average size measures less than 20 μm. As discussed in section 2.3.2, cubic or
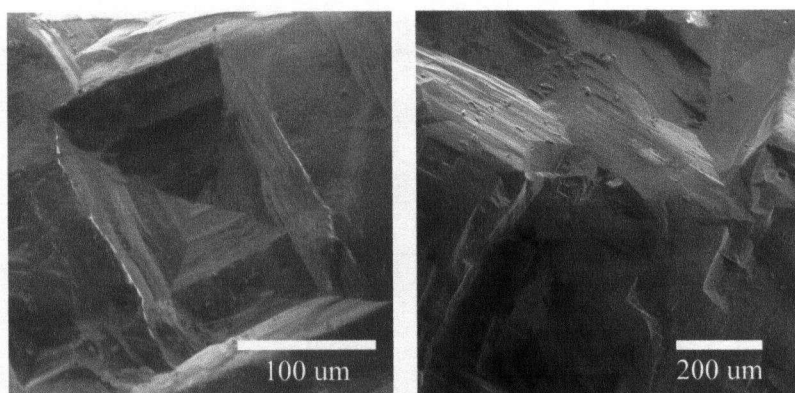
Fig. 2.20. SEM photo of tetragons (sometimes referred to as quadrons). Photo on left is from diamond 4-3 and photo on right from diamond 3-8.

(100) faces were not observed, thus determining the orientation of the tetragons was difficult. Pit orientations are determined based on their relationship to (111) faces. In the rare case where (111) faces are not detectable, tetragon orientation is not possible to discern. All tetragons observed have positive orientation with the exception of tetragons on two grains. The presence of tetragonal pits is not sufficient evidence for a cubic growth face. CL examination of polished diamond surfaces (chapter 7.0) as well as discussion with J. Harris, has led to a more reasonable and consistent interpretation. The abundant brittle fracturing of stones during residence in the mantle (cross-cutting relationships require that fracturing occurred before dissolution in many cases) has created surfaces that are sub-parallel to (100) surfaces; subsequent etching likely formed tetragonal pits on these paleo-fracture surfaces.

2.3.6.4 Etch channels

Etch channels occur in 28% of the diamonds and are commonly associated with inclusion pits (Fig. 2.21).
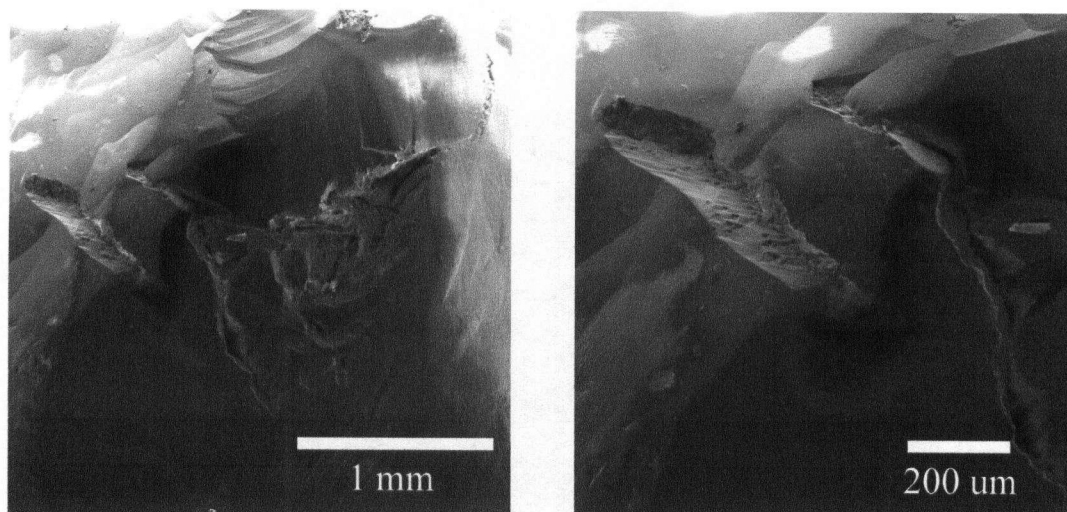
Fig. 2.21. SEM photo of ruts or etch channels. Photo on left is a more macroscopic view of etch channels emanating from what is likely an inclusion pit (diamond 3-1). The photo on the right is a close-up of two typical sinuous etch channels (diamond 3-1).

2.3.6.5 Frosting

Frosting is observed on 19% of the diamonds and is recognised by its 'rough' appearance on the diamond surface under the optical microscope. Robinson (1979) provides no quantitative divide between coarse and fine frosting, and as such, no distinction was made in this study. SEM examination of some frosted surfaces reveal a very fine 'roughness' to the diamond surface (e.g. Fig. 2.22). Frosting most commonly occurs on rounded surfaces of heavily resorbed diamonds (classes 1 or 2).
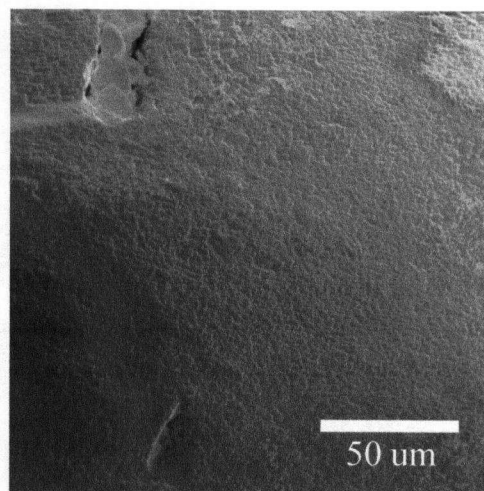
Fig. 2.22. SEM image of fine frosting (diamond 4-13).

2.3.7 Deformation Laminations

Twenty percent of the diamonds examined in this study display deformation lamellae. In some cases they occur as two sets of pronounced laminations (e.g. Fig. 2.23) while in other cases they are quite obscure. There is ambiguity as some features look like both hillocks (see section 2.3.8) and deformation laminations. There may be an argument for grouping these features into one category.
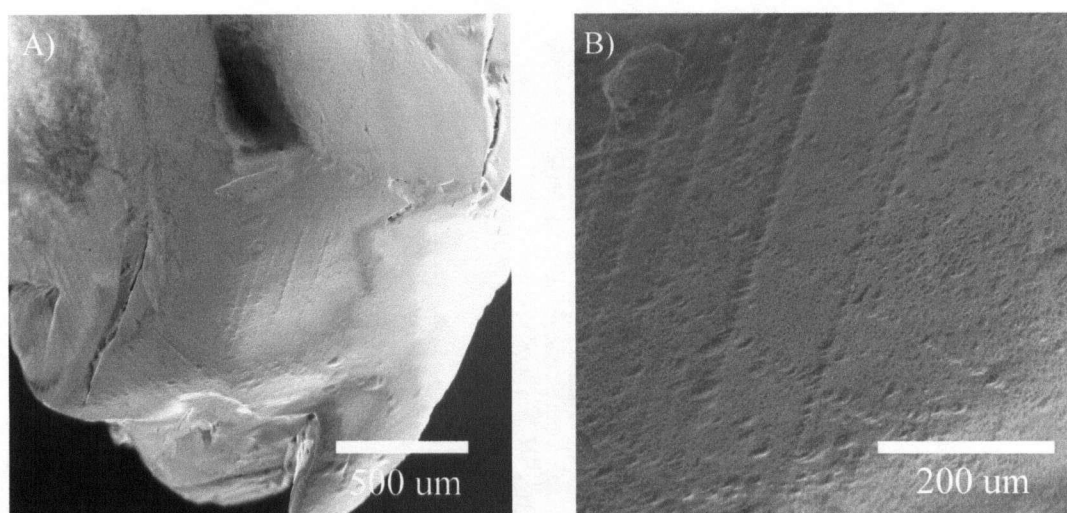
Fig. 2.23. SEM image of deformation laminations. A) Macroscopic view of laminations on diamond 1-3. B) Close-up of laminations on same diamond.

2.3.8 Hillocks

Ellipsoidal and elongate hillocks were observed on 17% of diamonds examined. However, it was generally difficult to differentiate between poorly developed deformation laminations and hillocks. Figures 2.24D-F show three views of successively magnified digital images of the same diamond, illustrating that deformation laminations can be made up of elongate hillocks. Macroscopically, many of the features observed in Fig. 2.24 look
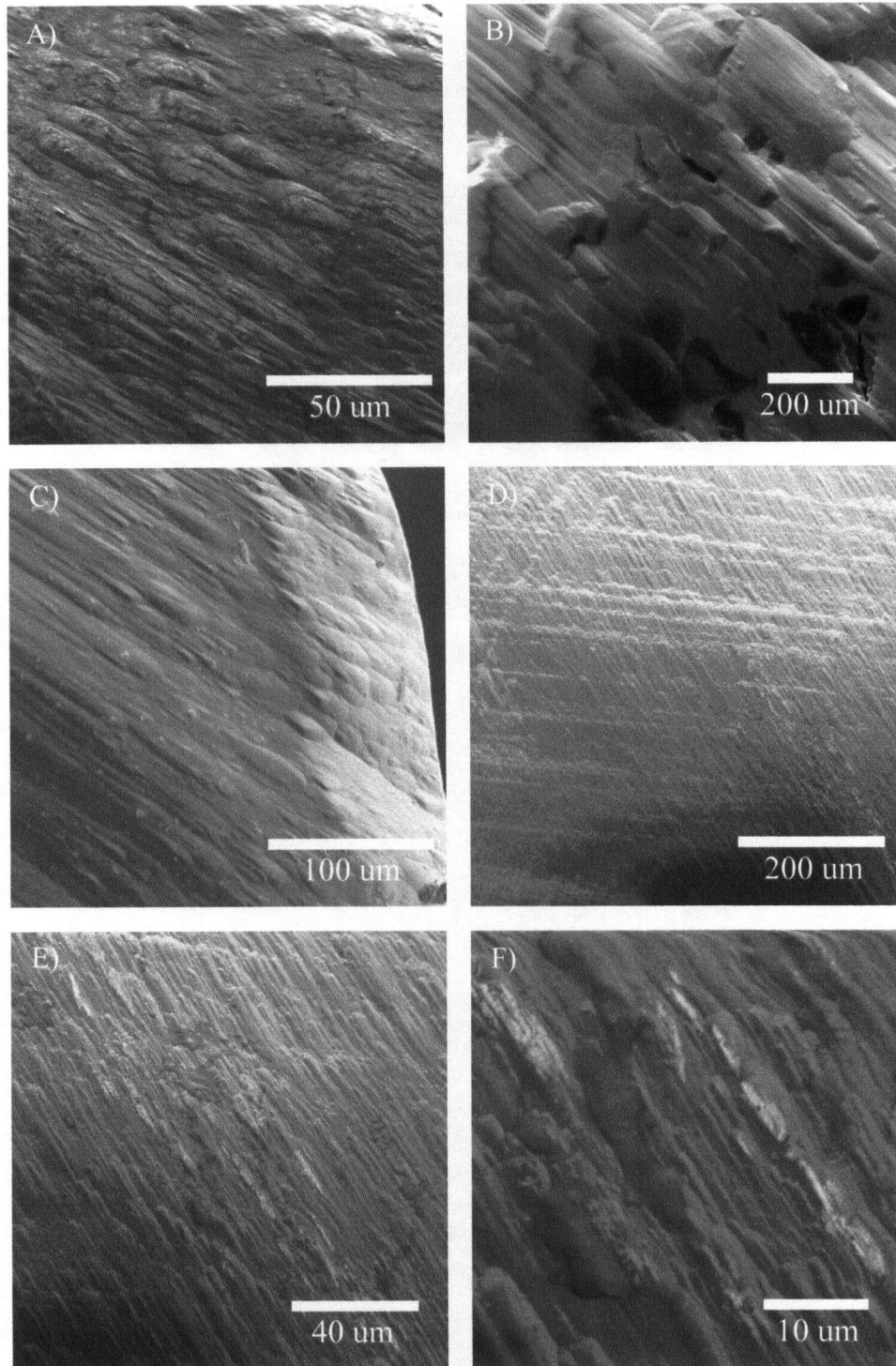
Fig. 2.24. SEM images of hillocks. Photos illustrate the association between hillocks and deformation laminations. A) ellipsoidal hillocks are observed in the top half of photo while elongate hillocks are seen in bottom left (diamond 4-8), B) elongate hillocks or deformation laminations? (diamond 1-4), C) elongate hillocks that grade into ellipsoidal hillocks as the face angle changes (diamond 3-2), D-F) the last three images show successively higher magnifications of the same features (diamond 2-9). In the first image deformation laminations are clearly visible, however, on closer examination, these lamination lines look more like what could be called 'elongate hillocks'.

32

like typical deformation laminations. Fig. 2.24C illustrates how the morphology of hillocks is dependent on which part of the rounded form of diamond that it is being viewed on. For planes that closely parallel (111) faces, hillocks take on a more elongate morphology, while on surfaces that do not parallel (111) faces hillocks tend to take on a more rounded or ellipsoidal morphology. There appears to be an association between deformation laminations and both ellipsoidal and elongate hillocks. The morphology the hillock exhibits is controlled by the orientation relative to the (111) face on which the feature develops. Certainly, a case can be made for grouping these two surface features, however, for historical reasons (e.g. Robinson, 1979; Orlov, 1977), they are catalogued here separately.

2.3.9 Fracturing

'Pre-eruptive' fracture surfaces are observed on 86% of the diamonds and late stage conchoidial fractures are observed on 49% of the diamonds in this study. Fifty-two percent of stones have both 'pre-eruptive' and late stage fractures. In the case of late stage fractures, it is unclear whether these formed during magma ascent, transport in the surficial environment, or mining. However, the scarcity of etching features on these faces suggests they formed sometime after the final stages of magma ascent. The high percentage of fracturing has resulted in significant loss of diamond.
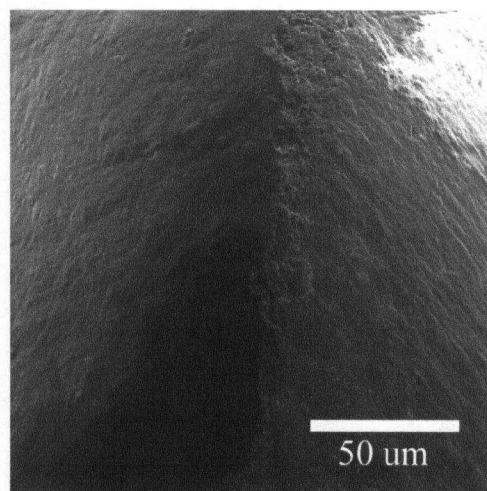
Fig. 2.25. SEM image of mechanical wear on an edge of a diamond (Diamond 5-9).

The diamonds examined seldom exhibit any signs of mechanical abrasion. Fig. 2.25 shows faint mechanical wear along one edge of a diamond. The relative absence of this feature is consistent with diamonds that have not been transported far from their source.

2.4 Discussion

2.4.1 Summary of the physical characteristics

The morphological characterization of these diamonds has provided much insight into their history from initial growth to deposition in Rio Soriso. A more comprehensive story will emerge when all studies, including studies of impurities, diamond growth and inclusions are combined.

The morphology of the diamonds is difficult to describe. Crystals are rarely intact and possess only remnant primary growth faces. The diamonds are strongly resorbed, with 52% of stones falling between classes 1 to 3 on the resorption scale of McCallum et al. (1994) while 13% exhibit non-uniform resorption. Following Kaminsky et al. (2001a), most diamonds are considered dodecahedroids. Single crystals make up 87% of the population while aggregates (7%) and unknown crystals (6%) make up the remainder of the suite. Features that are a product of local etching are observed on most diamonds in the form of trigonal, hexagonal, or tetragonal pits, as well as in the form of etch channels. Deformation laminations are visible on at least 20% of the diamonds. Frosting and hillocks are present on less than half of the stones, while signs of mechanical abrasion are weak and observed on one grain. Based on the studies reported in this chapter, there is not sufficient evidence to suggest that more than one population of stones is being represented.

2.4.2 Comparison with other diamond studies from the Juina area

Detailed studies by Hutchison (1997) and Kaminsky et al. (2001a) on Juina diamonds warrant comparison with studies from this chapter. In terms of morphology, the results from the three studies of Juina diamonds (including this study) are different (compare Fig. 2.26, previous studies, with Fig. 2.14 from this study). However, the lack of
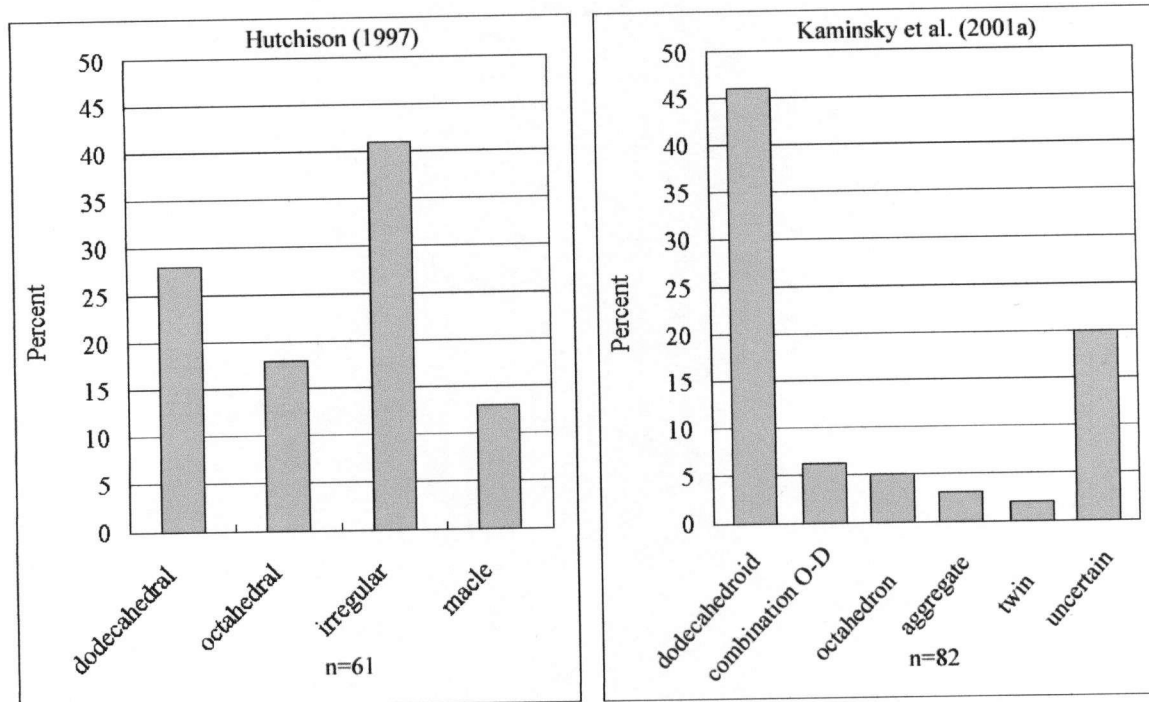
Fig. 2.26. Morphology distribution from two previous studies on Juina diamonds. For data from Hutchison (1997), it is unclear if the term macle is being used according to its strict definition to describe twins (when two or more crystals share a common crystallographic axis) or whether this category makes no distinction between aggregates (no shared crystallographic axis) and twins.

consistency in describing diamond morphology (discussed in detail in section 2.1.2) is a possible reason for many of the differences. All three studies indicate that the diamonds exhibit complex and irregular forms thus making morphological classification difficult. All studies indicate the presence of a small proportion of multiple crystal stones, be they aggregates or macles. Another important point is that no cubes or cubo-octahedral stones were found in any of the Juina area diamond suites studied.

Hutchison (1997) reports that 77% of diamonds display plastic deformation laminations while Kaminsky et al. (2001a) also indicates that plastic deformation laminations are abundant. If diamonds from this study containing either lamination lines or hillocks are combined (the reasons and defence of such a grouping are discussed in section 2.3.7) then ~30% of diamonds from this study may exhibit signs of plastic deformation. Although this number is still considerably low, deformation laminations are often subtle.

Kaminsky *et al.* (2001a) and Hutchison (1997) record other surface features, such as etch channels, etch pits and frosting, but describe these only in qualitative terms.

3.0 Colour

3.1 Introduction

Colouration in diamond is a result of full, partial or the lack of, white light absorption (Fritsch, 1998). Factors which control whether diamond will absorb light or not include: impurities, crystal defects, and inclusions (Orlov, 1977). The colour classification of diamond is based on the body colour; any colouration due to mineral inclusions, if visible, is ignored.

The colour of gem quality diamond is typically classified using colour charts, such as the Gemological Institute of America (GIA) colour grading scheme. Using this chart, diamond colour can be ranked from colourless (D) to yellow (Z). Other 'fancy' colours are classified using different schemes. Colours of rough stones, however, are usually described in more qualitative terms, such as colourless, brown, or yellow (see Harris *et al.*, 1975; Kaminsky *et al.*, 2001a; Gurney *et al.*, in print).

3.1.1 Causes of colouration in natural diamond

Colouration in natural diamond is the result of impurity defects, dislocations and irradiation. Many impurities have been found in diamond. Bibby (1982) found fifty-five non-substitutional impurities in diamonds from some South African kimberlite pipes; however, most colouration from impurities is a result of two elements that substitute for carbon in the crystal structure: nitrogen and boron (Harris, 1987). Plastic deformation of diamond creates dislocations at which amorphous carbon precipitates. This amorphous carbon results in a variety of colours. Colouration due to irradiation is unlike colouration due to impurities and dislocations. Irradiation typically forms only on the diamond surface and usually only as round spots. More detailed descriptions for the causes of colouration in diamond relevant to this study are discussed below.

Colourless diamonds are generally considered the most pure in terms of lacking impurities and crystal defects. In a perfectly colourless diamond, no wavelengths are absorbed and white light remains unaffected as it passes through the stone, thus emitting a colourless hue (Fritsch, 1998). Some diamonds with nitrogen impurities arranged in platelet form are also colourless (Brunton, 1978). Although some colourless diamonds have been referred to in literature as 'white', this term is discouraged here and will refer only to 'cloudy' or 'milky' stones which are semi-opaque to opaque.

Grey colouration in diamond is thought to be a result of microscopic dark inclusions, most likely graphite (Orlov, 1977; Robinson, 1979). Grey colouration is not believed to be a true body colour, however, even microscopic examination of diamonds sometimes does not resolve these inclusions. Robinson (1979) suggests that grey colouration may be a result of crystallisation at lower temperatures. Recent work by Titkov et al. (2003) has found that magnetite is the source of grey colouration in some Siberian diamonds.

Numerous studies have linked brown colouration in diamond to plastic deformation (Urusovskaya and Orlov, 1964; Orlov, 1977; Robinson, 1979). Plastic deformation likely occurs in the mantle where pressures and temperatures are sufficient so that diamond deforms in a ductile manner. Deformation results in the destruction of valency bonds and the creation of defect centres (Orlov, 1977). Harris (1987) proposes that atomic sized graphite or amorphous carbon precipitates in these defect centres and imparts a brown colour

Pink colouration has been linked to the same processes that impart brown colouration in diamond (Harris, 1992; Orlov, 1977). Harris (1987, 1992) suggests that plastic deformation produces a continuum of colours between pink and brown diamonds.

Two types of yellow stones are commonly recognised in literature: canary yellow and Cape yellow. Colouration in the former is a result of paramagnetic substitution of

nitrogen into the crystal structure (also referred to as type Ib diamond (section 6.1.1)) while colouration in the latter is a result of aggregation of nitrogen into N3 centres (IR-inactive forms comprised of three aggregated nitrogen atoms) (Harris, 1987; Fritsch, 1998). Orlov (1977) also recognises two main yellow hues. The first one he terms 'straw-yellow', which is analogous to Cape yellows, and the second term is 'amber yellow', which is analogous to canary yellows although he considers this colour as being restricted to cubic diamonds. Two less common yellow hues are recognised in the literature and are interpreted to be the result of annealing of green pigmentation patches (Orlov, 1977) and hydrogen defects (Fritsch, 1998).

Milky, white or cloudy colouration in diamond is interpreted by Orlov (1977) to be the result of microscopic internal defects in the crystal structure. More specifically, Navon et al. (1988) suggest that numerous small fluid inclusions are responsible for milky colouration in diamond.

Green colouration is caused either by impurities in the lattice structure or by alpha-particle damage (Fritsch, 1998). Green colouration due to impurities is a true body colour, while colouration due to alpha-particle damage manifests itself in three ways: as green spots on the surface, as a homogenous green coat on diamond (Vance et al., 1973), and as a green halo around a mineral included in diamond (Kopylova et al., 1997). Alpha particles are emitted from unstable isotopes that, if near to or in contact with diamond and in sufficient abundance, may cause green colouration. The length of time for colouration to occur depends on the radiogenic element, its abundance, and distance from the diamond. Green surface spots arise when an isolated radiogenic element is the source for alpha-particles, while a uniform green coat requires a relatively even distribution of radiogenic elements surrounding the diamond, most likely as a dissolved component in ground waters. Green spots on diamond could form in alluvial deposits or in kimberlite, however intense green spot colouration is likely to be a product of irradiation in an alluvial environment (Vance et al., 1973). Experiments have also demonstrated that

diamonds with green colouration due to alpha-particle damage turn brown on heating to temperatures greater than 500 to 600 ^{o}C (Vance and Milledge, 1972). This heat in nature could be generated by a variety of different sources, such as a later injection of kimberlite magma or any other proximal intrusive event, or due to intense burial in a sedimentary basin.

3.2 Analytical techniques

Diamonds were analysed using a Leica MZ FLIII binocular optical microscope with a 10x zoom lens and 1x objective lens. Observations were made in both transmitted and reflected light mode. Digital images were collected using a Spot Insight Colour 3.2.0 digital camera and enhanced using Adobe Photoshop 6.0.

3.3 Results

The majority of diamonds were classified as uniform (93%) while the remainder of grains contain domains of both coloured and colourless diamond. Fig. 3.1 graphically illustrates the colour distribution in this diamond suite. One faint green pigmentation spot was observed on a colourless diamond. Appendix A contains photos of every diamond in this study. Note that in several cases, the apparent diamond colours seen in the photographs are a result of mineral inclusions and/or secondary material in grooves and pits, and thus do not reflect the true diamond body colour. Every attempt was made to ignore effects of these obscuring features.

Brown ■	(7)
Colourless □	(30)
Grey ▣	(14)
Yellow ▢	(9)
Pink ▩	(2)
Milky ▢	(2)
Non-uniform ▨	(5)
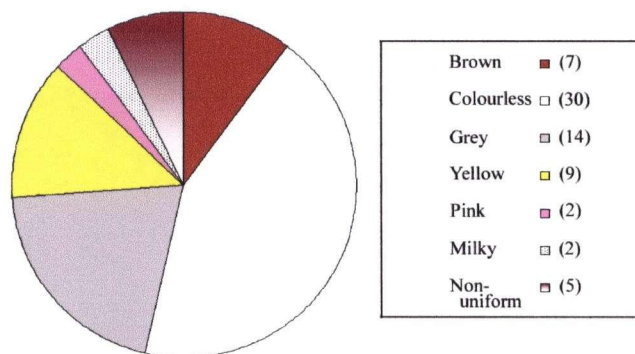
Fig. 3.1. Distribution of diamond colours. Number in parentheses indicates sample size.

3.3.1 Uniform body colours

In order of decreasing abundance, the six colours observed in this diamond suite are colourless (43%), grey (20%), yellow (13%), brown (10%), pink (3%) and milky (3%). Representative photographs of each colour are presented in Fig. 3.2

Colourless diamonds make up almost half of the diamond suite and are generally the most transparent stones. Grey diamonds make up a significant percentage of this population. However, it will be shown in section 9.1 that the grey diamonds likely contain graphite in an otherwise colourless stone. For this reason, 43% is a minimum for the percentage of colourless diamonds and 20% is a maximum proportion for grey diamonds. Many of the brown stones have surface features that are consistent with
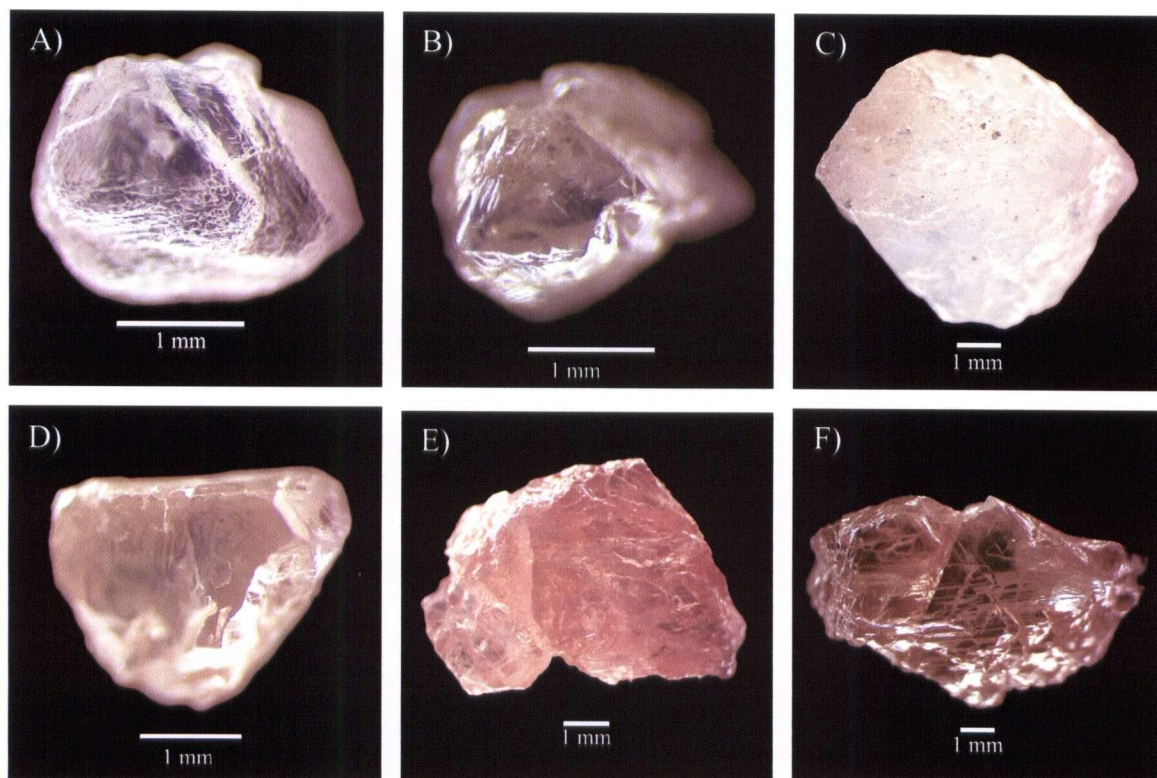
Fig. 3.2. Photographs of representative diamonds colours observed. A) colourless (diamond 4-1), B) grey (diamond 5-8), C) milky (diamond 1-5), D) brown (diamond 5-4), E) pink (diamond 2-4), and F) yellow (diamond 2-3).

plastic deformation. There are nine yellow stones, all with weak colouration except diamond 2-3, which exhibits an intense yellow hue (Fig. 3.2F). It is not clear whether these stones represent Cape or canary yellows. Because these yellow hues are a result of impurity content (section 3.1.1), further classification of yellow stones will be considered only in conjunction with impurity data obtained from studies of infrared spectra (section 9.1). The two milky diamonds observed were the closest grains to being considered opaque.

3.3.2 Non-uniform colours

Five colourless diamonds contained portions of either brown diamond (3 stones) or grey diamond (2 stones).

One diamond examined displays fairly weak green colouration that occurs as a spot approximately 0.25 mm in diamond and is a result of radiation damage. It is uncertain whether colouration occurred in the host rock, in a secondary collector or in the alluvial environment from where the diamond was recovered.
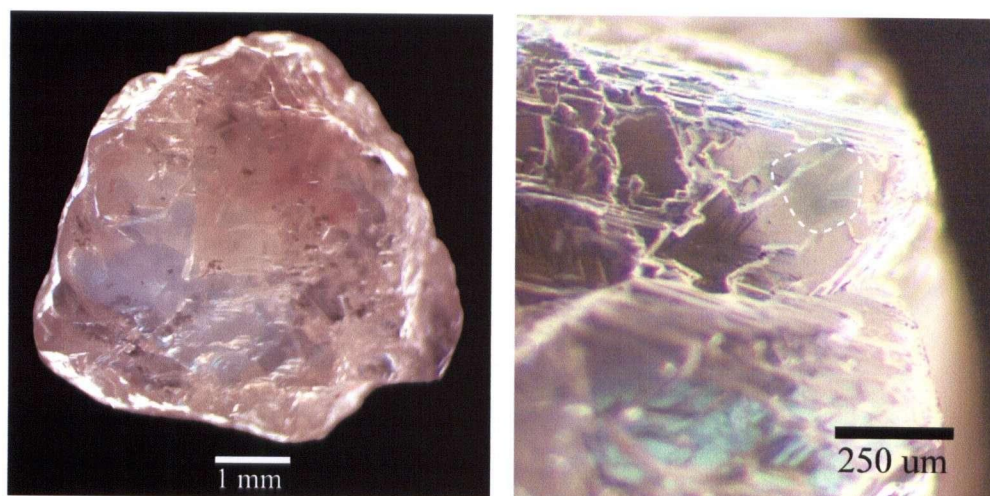
Fig. 3.3. Photograph of non-uniform colour. On left, non-uniform brown and colourless diamond (diamond 1-4), on right, alpha-particle damage (circled by white dashed line) on diamond surface (diamond 4-18).

42

3.4 Discussion

3.4.1 Comparison with other studies

Other studies on Juina diamonds report similar colour distributions. Hutchison (1997) divides the suite into only three categories, colourless (41% of the population), brown (57%), and cloudy (2%). Kaminsky *et al.* (2001a) does not include a detailed description of diamond colour, but indicates that most stones exhibit shades of brown colouration (from pale to dark brown) and are semi-transparent with a silky lustre. This study includes more colour subdivision: colourless, grey, yellow, brown, pink, cloudy and non-uniform. Faint yellow and brown colourations are similar and there may be evidence for grouping these two colours for the purpose of comparison. Grey stones are not mentioned in either of the previous work. In section 9.1 it will be shown that many grey stones are likely colourless diamonds with abundant graphite inclusions (or some other dark inclusions). There is evidence for grouping grey and colourless stones for the purpose of comparison. Also for the purpose of comparison, non-uniformly coloured diamond can be re-distributed into either brown (3 diamonds) or colourless (2 diamonds) stones. The two pink stones found in the study are quite remarkable in colour (Fig. 3.2E) and may not be represented in the other suites. Under the new grouping described, this suite comprises colourless (64%), brown (30%), cloudy (2%) and pink (3%) diamonds. The sampling bias mentioned in section 2.3.1 may be responsible for differences in colour distribution.

4.0 Fluorescence of Diamonds

4.1 Introduction

The fluorescence (FL) of diamond is a property that has been recognised for many decades and is used in some sorting plants to separate diamonds from other heavy minerals extracted from mines. FL is caused by the excitation of electrons by exposure to ultraviolet (UV) light. UV light 'excites' valence electrons in optical centers to higher energy states. When these 'excited' valence electrons fall back to their original energy state they emit light, referred to as FL. The FL of diamond can be used as a preliminary method to determine qualitatively the relative concentrations of optical centers as well as distinguish between different types of optical centers. Its usefulness in grouping diamonds when used in conjunction with other studies, such as diamond morphology and colour (chapters 2 and 3 respectively) or infrared (chapter 6) is greatly improved.

The specific defects responsible for FL colours in diamond are surprisingly poorly documented. Blue FL is generally considered to be a result of nitrogen impurities in diamond, with the relative FL intensity reflecting the relative concentration of nitrogen impurities. Fritch (1998) reports that 1/3 of gem-quality diamonds fluoresce blue. Clark et al., (1992) finds that diamonds graded as 'brown' that are exposed to UV-light often fluoresce bright yellow. Other FL colours have been reported but their specific causes are generally unknown.

4.2 Analytical methods

Diamond fluorescence was examined using a 100 watt ultraviolet bulb attached to a Leica MZ FLIII optical microscope and powered by an EBQ Netz power source. A Spot Insight Colour 3.2.0 digital camera was used to record images of diamond fluorescence. A steel skeleton frame fitted with a 'skirt' was designed by the in-house machine shop to

fit over the microscope stage to block out any contaminating light. Two images were collected for each diamond; the first one using an exposure time of twenty seconds while the second one was dependant on the FL intensity of the particular stone being examined and varied from 1 to 60 seconds. By maintaining a constant exposure time for at least one image for each diamond, the relative FL intensity between stones could be examined. The objective of the second photo was to match the exposure time to the relative FL intensity so as to best capture the luminescent features for that particular stone.

Through comparison of FL digital photographs for each diamond, stones are described in terms of three variables: colour, homogeneity, and intensity. Each diamond is grouped into one of the four FL colours (or none), classified as either uniform or non-uniform, and is qualitatively rated in terms of relative intensity (strong, moderate, weak or very weak), determined by comparing images of all diamonds collected using a constant exposure time.

4.3 Results

Sixty-nine diamonds were examined under ultraviolet light. A summary of the results is presented in Appendix B under the column heading 'Fluorescence'. Photographs of diamond fluorescence for all stones, using variable exposure times, are presented in Appendix A.
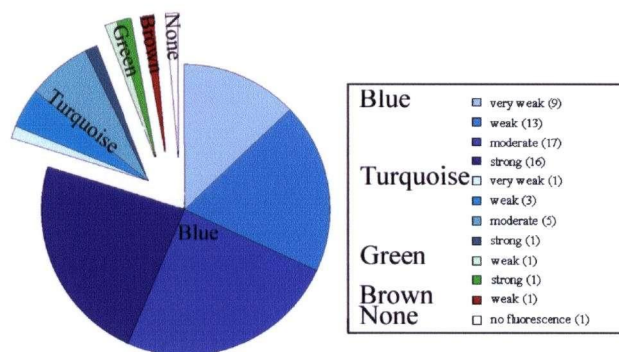
Fig. 4.1. Fluorescence colour and fluorescence colour intensity distribution of Rio Soriso diamonds. (numbers beside colours in legend indicate sample size).

45
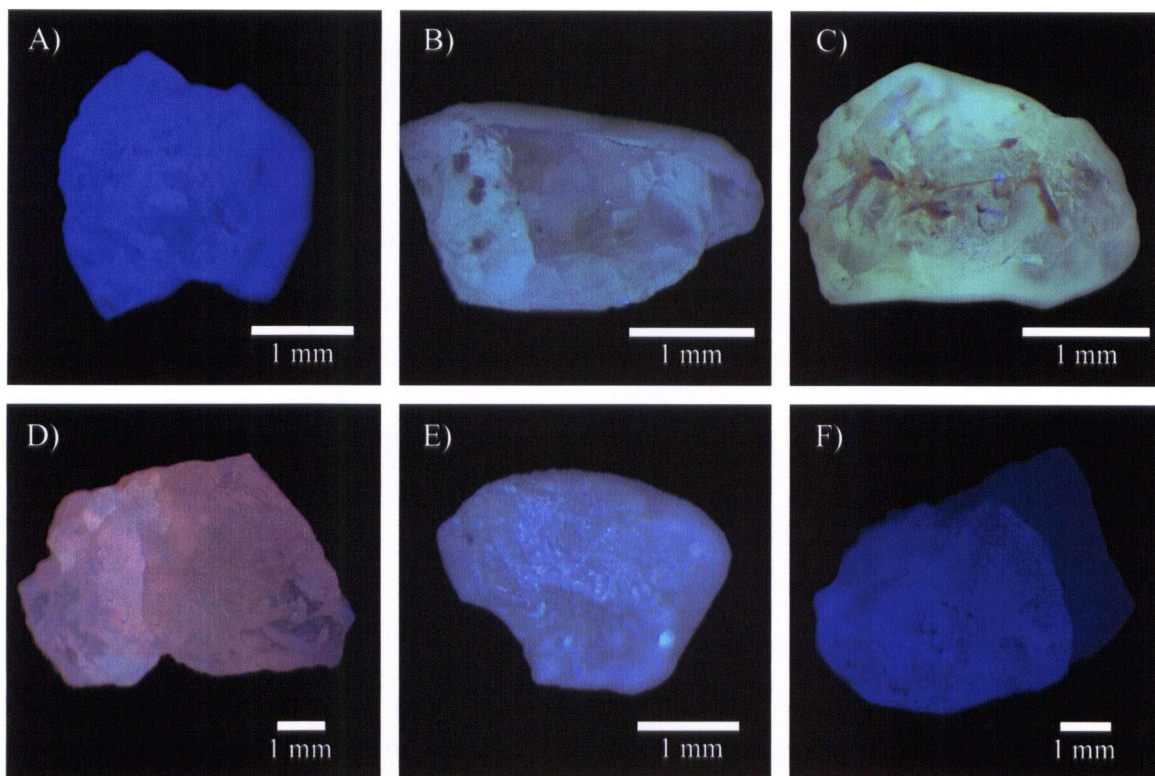
Fig. 4.2. Photographs of various FL colours observed for Rio Soriso diamonds. A) Blue (Diamond 4-3), B) Turquoise (Diamond 6-6), C) Green (Diamond 7-1), D) Brown (Diamond 2-4), E) Non-uniform stone with yellow body and speckled blue overcoat (Diamond 4-7), and F) Non-uniform stone with moderately intense blue FL on left and weakly intense FL on right (Diamond 2-9).

Diamond fluorescence colours are mostly shades of blue (80%) with turquoise (15.5%), green (3%) and brown (1.5%) colours also being observed (Fig. 4.2). One diamond (1.5% of population) did not fluoresce. A photographic compilation of diamond FL for all stones, using the same exposure time, can be seen in Fig. 4.3. The distribution of colours and colour intensity is graphically presented in Fig. 4.1. Colour intensity, although a more arbitrary classification scheme than colour hue, is more evenly divided among the four classes than colour hues. Colour intensity distribution is as follows: moderate (32%), strong (26.5%), weak (26.5%) and very weak (15%). Ten diamonds had non-uniform FL colours (two examples of which can be seen in Figs. 4.2E and F).
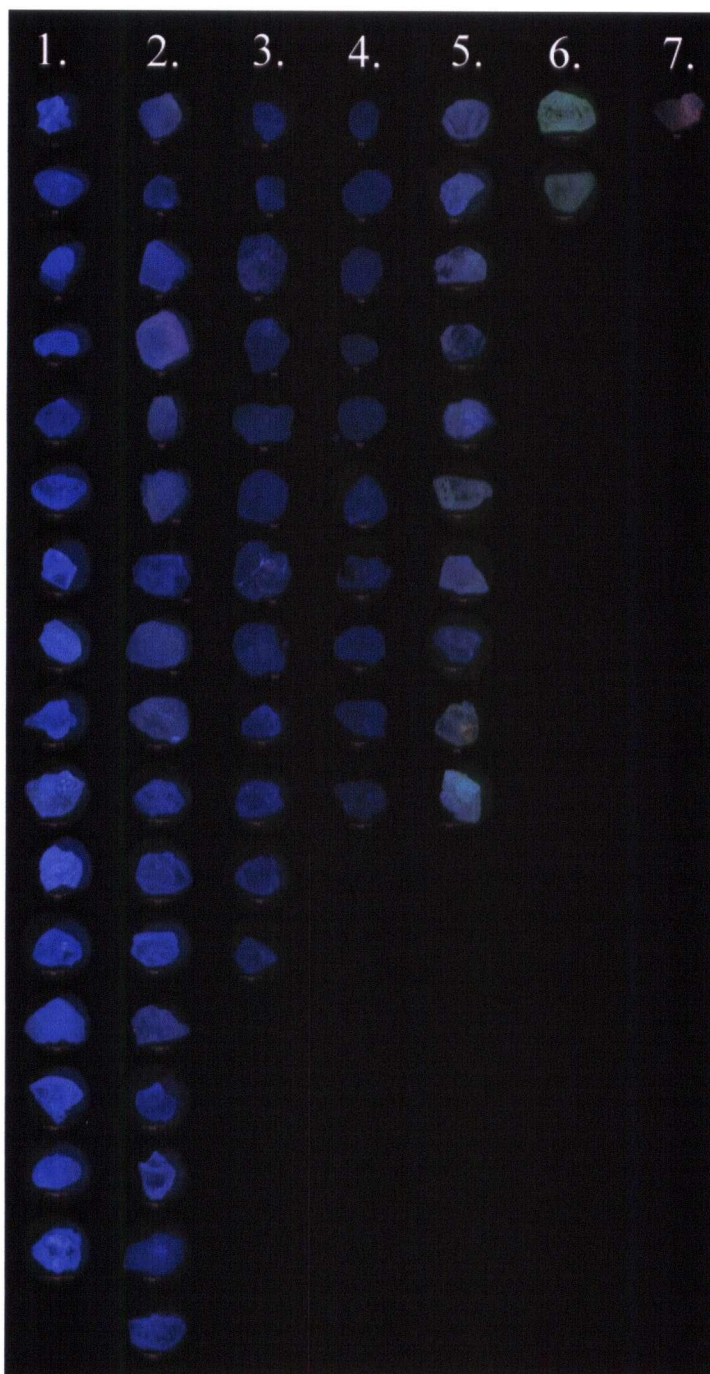
Fig. 4.3. Compilation photograph of FL colours for Rio Soriso diamond suite (using a constant exposure time of 20 seconds). The seven groups are labeled as follows: 1 - strong blue; 2 - moderate blue; 3 - weak blue; 4 - very weak blue; 5 - turquoise (strong, moderate, weak and very weak are all grouped in this column); 6 - green (strong and weak); and 7 - brown (weak). One diamond did not fluoresce at all. (note that for comparative purposes, diamonds are scaled to roughly the same size).

5.0 Cathodoluminescence of Diamonds

5.1 Introduction

Cathodoluminescence (CL), like fluorescenence, is an induced-luminescence property. The difference between the two is the energy source used; FL is caused by exposure to ultraviolet light and CL is caused by the bombardment of electrons. In the same manner that UV-light induces fluorescence in diamond, electron-bombardment excites valence electrons in optical centers to higher energy states and as they fall back to their original energy state, light is emitted. This induced luminescence is what is referred to as CL. The main difference between FL and CL is the depth of penetration of the energy source. Whereas FL excites most if not the whole diamond, CL excites only valence electrons in the uppermost surface of the diamond (~5 μm depth of the diamond surface using a 30 keV electron beam, Hanley et al., 1997).

CL colours of diamond are mostly related to the presence of nitrogen impurities which, when in aggregated forms as is typical for natural diamond (i.e. type Ia), tend to produce a variable sky-blue CL colour. Some of the other more commonly observed colours are yellow, yellow-green, green, canary-yellow, pink, brown and white CL. Yellow CL has been linked to hydrogen impurities that form on (100) faces of diamond (Bulanova, 1995) and to intrinsic defects such as zones around inclusions, along deformation laminations and around radiation spots (Davies, 1998). Yellow-green CL is believed to be caused by N3 centres (three aggregated nitrogen atoms) while green CL is typical for type Ib synthetic diamond (Hutchison, 1997). Radiation damage is thought to induce canary-yellow CL in diamond. Nitrogen-free (type II) diamond containing microscopic CO_2 inclusions produces various shades of pink (including orange and purple) CL and the plastic deformation of these diamonds produces brown CL (Chinn et al., 1995). White CL has been attributed to platelets (Woods, 1986 and Davies, 1998).

CL intensity is dependant on the concentration of defects, and for many diamonds, nitrogen is the main defect. As such, the blue intensity observed is related to the concentration of nitrogen impurities. However, if other defects exist in sufficient quantities, they can alter the colour and produce intermediary CL colours that can be impossible to unambiguously ascribe to a particular defect centre. As a result, the technique of CL examination of diamond is not quantitative.

5.2 Analytical techniques

The CL characteristics of 47 rough diamonds were examined using a Cambridge Instruments Cathode Luminescence (CITL 8200 mK4) system attached to an optical microscope with a 2.5 x lens. The accelerating voltage used was 15kV with an electron beam current of 300 μA and chamber pressure was maintained using a Varian DS 102 pump. Diamonds were washed with ethanol before being placed on a recessed steel tray specially designed to fit in the chamber. Typically, 4 to 5 diamonds were loaded in the tray at a time, being ~1 cm apart. Larger stones were loaded into the machine one at a time. CL images were collected using a Nikon Coolpix 995 digital camera. Exposure times were variable and do not reflect the CL intensity well. Due to an unknown automatic feature on the camera, some photos may not accurately reflect the true CL colour observed, although they certainly are close. It is stressed here that optical CL studies on their own should be used only for non-rigorous, qualitative classification.

5.3 Results

The CL-induced colours of forty-seven rough, unpolished stones were examined. Photographs of diamond CL for these rough diamonds are presented in Appendix A. Diamonds were grouped into seven categories based on observed colours. The colour distribution is graphically illustrated in Fig. 5.1 and some examples of CL colours are presented in Fig. 5.2. There is certainly some ambiguity in assigning stones to particular

colour classes, but in the context of this semi-quantitative study, the divisions are considered satisfactory. These divisions, along with the number of samples are: blue 1 (CL of moderate blue intensity, n=6); blue 2, (strong blue, n=12); turquoise 1, (moderate, n=11); turquoise 2, (strong, n=7); green 1, (moderate, n=4); green 2, (strong, n=2); and
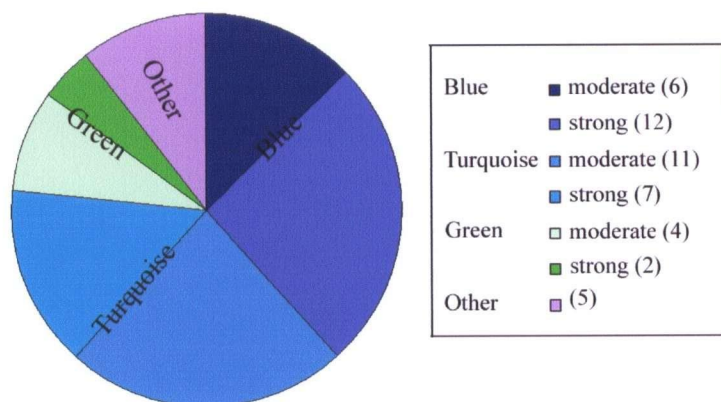
Fig. 5.1. Colour distribution for CL colours. (numbers in brackets in legend indicate sample size).
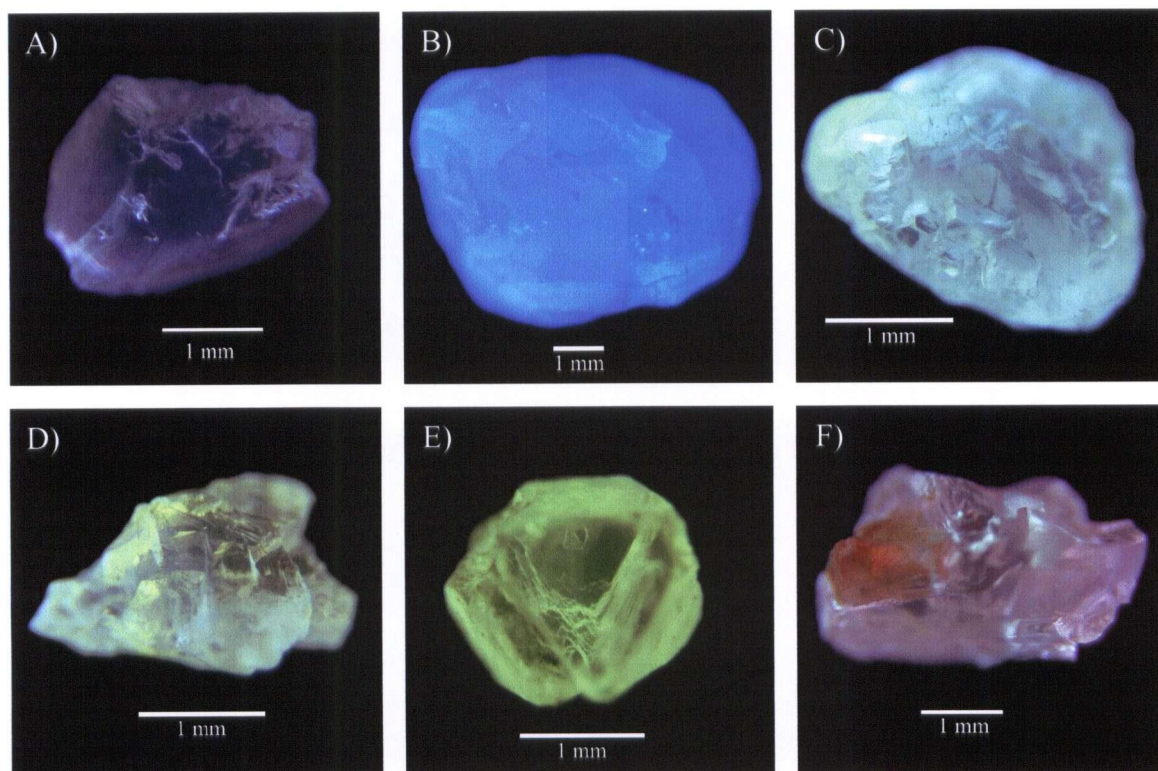
Fig. 5.2. Photographs of representative cathodoluminescence colours of diamonds, this study. A) moderate blue (Diamond 5-1), B) strong blue (Diamond 3-9), C) strong turquoise (Diamond 4-13), D) moderate green (Diamond 4-5), E) strong green (Diamond 4-18), and F) other (Diamond 4-21).

other, (n=5) (Fig. 5.4). If the subgroups are combined, the CL colour proportions are as follows: blue (38.3%), turquoise (42.6%), green (12.8%) and other (10.6%). The CL colours show a gradation from blue to turquoise to green, which is likely an indication that more than one defect centre is responsible for the colouration. Perhaps blue and green CL colours are end-members and they combine in varying proportions to produce intermediate colours.

Blue CL is likely caused by aggregated nitrogen defects of various concentrations, but generally in low abundance. An adequate explanation for the green CL colouration observed is not so clear. Green CL is common for synthetic diamond with disaggregated nitrogen, however, diamond with this nitrogen character is extremely rare in nature (as will be discussed in section 6.1). Yellow-green colouration has been attributed to N3 centres (also an aggregated form of nitrogen, but is different from the aggregated nitrogen that produces blue CL).

Internal growth features are absent for most diamonds, but visible on diamond 4-17 (examined in detail in section 7.3.14) and diamond 3-9 (a macroscopic view of the CL pattern can be seen in Fig. 5.2B and a greyscale close-up in Fig. 5.3). The growth patterns visible on the surface of diamond 3-9 are typical for strongly resorbed surfaces. The pattern is similar in appearance to 'agate' and cannot be deciphered in terms of growth habit based on this image. The CL of internal growth structures is better examined on polished surfaces (Chapter 7.0).
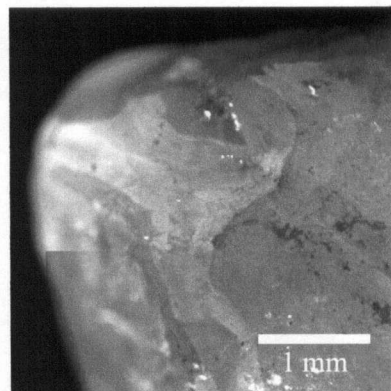
Fig. 5.3. Close-up greyscale photograph of CL of growth features of resorbed diamond. (Diamond 3-9).
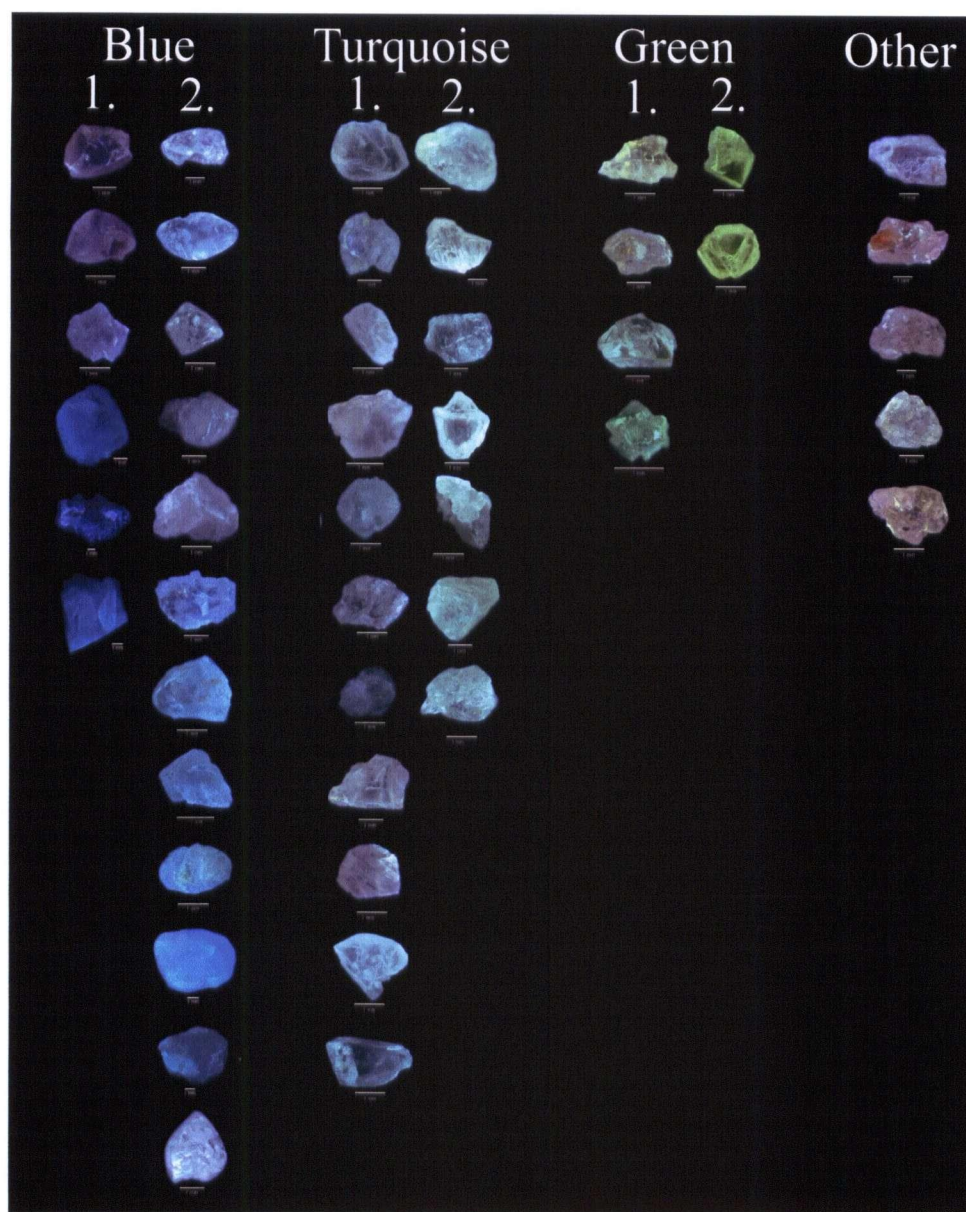
Fig. 5.4. Photographs of CL images of 47 rough, unpolished diamonds from Rio Soriso. Diamonds have been scaled to the same size for comparative purposes.

6.0 Infrared Spectroscopy of rough diamonds

6.1 Introduction

All crystals are made up of atomic bonds which hold atoms together. Some of these bonds can be excited to higher energy levels by infrared (IR) light, which results in the absorption of this light. The bonds detected by IR spectroscopy (termed IR active) are those which have an asymmetric stretch (Fig. 6.1) and thus produce a change in the dipole moment. (IR inactive bonds produce no change in dipole moment during the symmetric stretch vibration). The typical wavelength of IR light used in diamond studies ranges from 900 to 4000 cm^{-1}. Each scan over the crystal records the amount of absorption at each wavelength within this range and absorption is recorded (in arbitrary units), varying from 0, or no absorption, to infinity, or full absorption.

symmetric stretch	asymmetric stretch
1340 cm^{-1}	2350 cm^{-1}
O=C=O	O = C=O
O = C = O $\xleftarrow{\text{equilibrium}}$ $\xrightarrow{\text{position}}$ O = C = O	
O = C = O	O=C = O
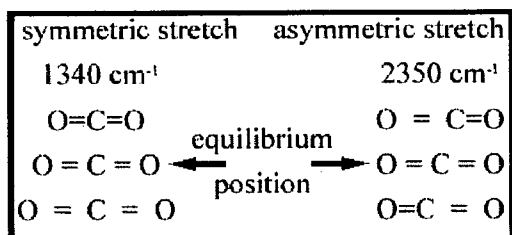
Fig. 6.1. Difference between IR-active and IR-inactive bonds. Bonds which produce a symmetric stretch are IR-inactive and cannot be detected with an FTIR. Bonds which produce an asymmetric stretch are IR-active and can be detected.

The recognition and distinction between diamonds based on their IR absorption patterns was first described by Robertson et al. (1934). They found that most diamonds displayed absorption in the lower frequencies (less than 1500 cm^{-1}) and termed these diamonds type I, and labeled the remaining diamonds that lacked any absorption in this range as type II. Many studies have been performed subsequently, and are summarized by Clark and Davey (1984) and Clark et al. (1992).

The range 900-4000 cm^{-1} used in most diamond studies can be divided into three regions: one, two and three phonon absorptions (Fig. 6.2). After the pioneering work by Robertson et al. (1934), Kaiser and Bond (1959) demonstrated that much of the

53

absorption and its intensity in the one-phonon region (900-1333 cm^{-1}) is due to the presence of nitrogen in diamond. It is now well known that nitrogen is a common impurity in diamond and that most one-phonon absorption is due to its presence. "Perfect" diamond, lacking any impurities or imperfections, does not display any one-phonon absorption. The diamonds which Robertson *et al.* (1934) classified as type I are known as 'nitrogen-bearing' while type II

Fig. 6.2. IR spectrum for a type II diamond from 500-4000 cm^{-1}, illustrating the three regions: the 1-phonon region, where asymmetric bonds produce absorption; the 2-phonon region, which is intrinsic to all diamond; and the 3-phonon region, where most CH complexes produce absorption.

stones are 'nitrogen-free'. Absorption in the two-phonon region is characteristic of all diamond while absorption of hydrocarbons occurs in the three-phonon region.

6.1.1 One-phonon absorption in diamond related to nitrogen impurities

Most studies to date have focused on correlating the absorption in the one-phonon region to nitrogen concentration and form. It was observed that diamond displays many different absorption patterns in the one-phonon region, and studies focused on attempting to elucidate the cause(s) for these different spectra. Davies (1972) was the first to quantitatively decompose the one-phonon spectra of type I diamond into two distinct components, which he termed A and B. He discovered that most one-phonon spectra of natural diamond could be roughly described by linearly combining two end-member spectra (A and B) in different proportions. End-member spectra A and B can be seen in Fig. 6.3A and 6.3B. Since this time there has been the discovery of a third component, labelled D (Fig. 6.3C), and some lesser components (Clark and Davey, 1984).

Davies (1976) showed that the A spectrum is likely a result of two bonded nitrogen atoms incorporated into the crystal structure. Evans and Qi (1982) suggest that the B spectrum is a product of four nitrogen atoms tetrahedrally surrounding a vacancy. Both of these interpretations are agreed upon in most literature. More controversial is the D component produced in the one-phonon region. Woods (1986) attributes this absorption to planar structures called platelets, which are made up of carbon atoms. Platelets are discussed in
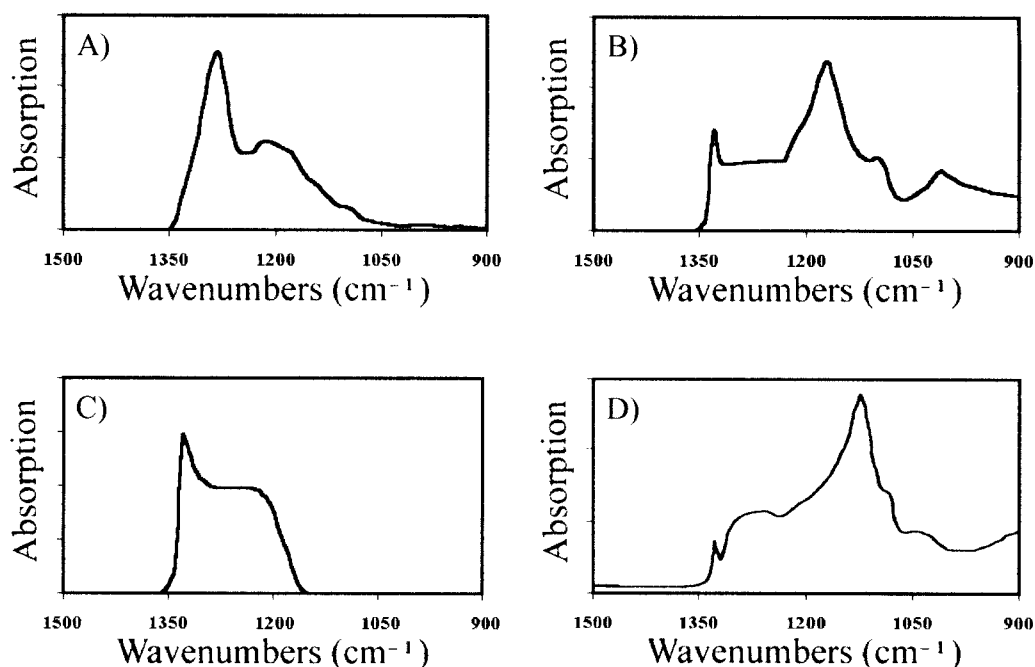
Fig. 6.3. IR spectra for common end-member absorption patterns in diamond from 900-1500 cm^{-1}. A) One-phonon spectrum of pure A centre absorption; B) One-phonon spectrum of pure B absorption; C) One-phonon spectrum of pure D absorption and; D) One-phonon spectrum of pure Ib absorption. Figures A-C from deconvolution software. D) Reproduced from Evans (1992).

greater detail in the following section. Diamonds with A and B centres are classified as type Ia (also termed aggregated forms). The cut-off between type I and type II varies from study to study, but is below 50 ppm total nitrogen. Ninety-eight percent of natural diamonds worldwide are classified as type Ia (Evans, 1992). Diamonds are further subdivided into IaA, IaB, and in most cases, if both A and B centres are observed, as the transitional form IaAB.

IR studies of nitrogen-containing synthetic diamond reveal that they display yet another one-phonon spectrum (Evans, 1992), illustrated in Fig. 6.3D. The characteristic electron paramagnetic resonance (EPR) signal indicates that the nitrogen atoms are singly substituted throughout the crystal structure. These diamonds are classified as type Ib and are extremely rare in nature.

6.1.2 Process of nitrogen aggregation

The history of IR studies in diamond and the connection between nitrogen aggregation and the one-phonon absorption has been discussed in the previous section. After these studies, most work has focused on trying to correlate the intensity of particular IR frequencies with nitrogen aggregation concentrations (most recently Woods *et al.*, 1990; Boyd *et al.*, 1994 and Boyd *et al.*, 1995) and applying this knowledge to geologically significant processes (Taylor *et al.*, 1990; Mendelssohn and Milledge, 1995). In order to decompose the IR spectra and to quantify each component, it is necessary to understand the process of nitrogen aggregation and the causes for the varying one-phonon absorptions.

The degree of nitrogen aggregation depends on the residence time of the diamond in the mantle, the nitrogen content and the temperature history (Evans and Harris, 1989). These parameters have been corroborated by experimental studies of nitrogen aggregation and concentration in diamond at controlled temperature and with time. During diamond crystallisation, nitrogen substitutes for carbon forming point defects and creating type Ib diamond. With time and at the elevated temperatures expected in the mantle, the dispersed nitrogen atoms migrate and form A centres (two bonded nitrogen atoms). This conversion, from type Ib to IaA, depends of kinetics, and is thought to proceed quickly in terms of geologic time at mantle temperatures and requires only 5 ± 0.3 eV to activate the reaction (Evans and Harris, 1986). Experiments on radiogenic minerals included in diamonds by Richardson *et al.*, (1990) and Deines *et al.*, (1991) show that many

diamonds are Archean in age and much older than the intrusive event which brought them to the surface. Evans and Qi, (1982) show that type Ib diamonds of Archean age would only survive in the mantle at low temperatures (<800 °C), which is outside out the diamond stability field for cratons with typical geotherms. These studies illustrate effectively why type Ib diamonds are so rare in nature; only diamonds with short residence times could preserve type Ib character.

More common in nature are diamonds which fall into the IaAB transition. Through longer residence times and higher temperatures, A centres are thought to migrate and form more complex aggregates, B centres. During this process it is suggested that a carbon atom is displaced to make room for the four nitrogen atoms (Woods, 1986). Thus the B centre is interpreted as being four nitrogen atoms tetrahedrally arranged around a vacancy. Many type IaAB diamond IR absorption curves exhibit several local absorption modes, the most prominent peak occurring near 1370 cm^{-1} (Fig. 6.4) and is termed B' (Clark et al., 1992). This peak is thought to be the result of platelet absorption (Taylor et al., 1990). Based on the strong positive correlation between D absorption and the integrated B' absorption area (Fig 6.5, filled circles), Woods (1986) proposed that
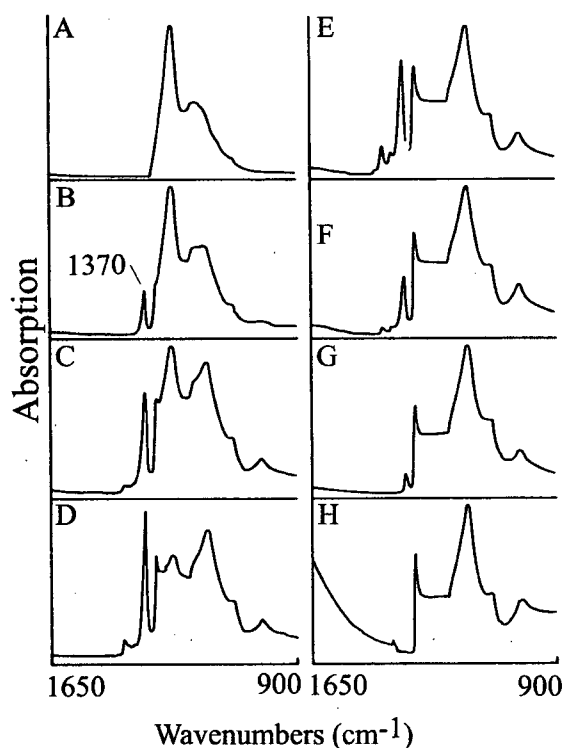
Fig. 6.4. IR absorption spectra of the development and subsequent degradation of the B' peak (at 1370 cm^{-1}). The progression from A-H illustrates the changes in impurity character with increasing time and temperature. The progression is as follows: type IaA (A) through 'regular' transitional IaAB (B-D) to pure IaB with only B and D absorption (E), followed by a departure form regularity (F and G) towards pure IaB with no D absorption (H). Reproduced from Woods (1986).

the D component observed in the one-phonon range is the result of platelet absorption. Thus, the relative absorption produced by D centres is interpreted as a measure of the relative concentration of platelets per unit area.

Woods (1986) proposes that the physical process occurring in diamond during A to B conversion is that the displaced carbon atoms aggregate themselves, to form platelets which in turn are responsible for one-phonon IR-active bands known as D centres and B' peaks. Platelets can be observed by Transmission Electron Microscopy (TEM) and sometimes through CL, and range from a few nanometres to several micrometres in size (Evans and Phall, 1962) as seen in Fig. 6.6.

Matters are complicated by diamonds containing B and D centres which do not correlate positively (open circles, Fig. 6.5). Plots of B/(B+A) versus D centres in these diamonds always fall below the line, indicating that there are less D centres than should be expected for the number of B centres. These diamonds are referred to by Woods (1986) as *irregular* while stones which correlate positively are considered *regular*. Woods (1986) proposes that this non-linearity observed for some diamonds is a product of platelet degradation and the subsequent formation of dislocation loops.
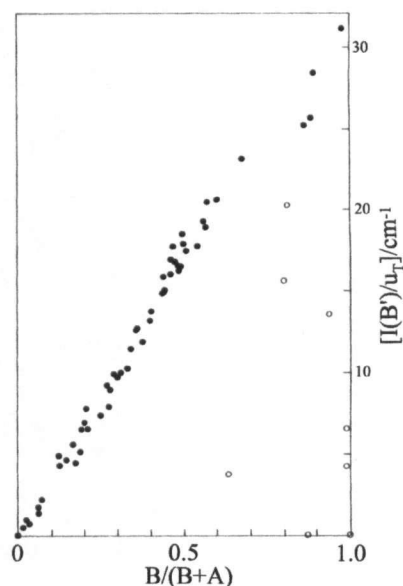
Fig. 6.5. Plot of B/(A+B) centres in diamond versus integrated area under B' absorption peak. Graph illustrates the difference between *regular* (filled circles) and *irregular* (open circles) diamonds. Reproduced from Woods (1986).
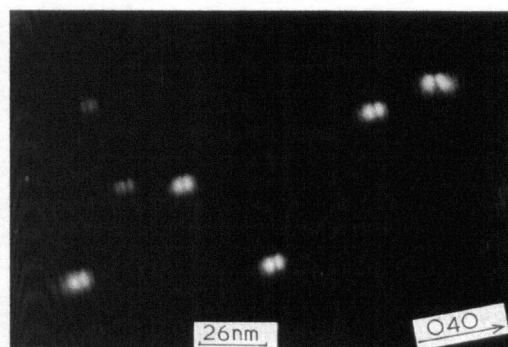
Fig. 6.6. Transmission electron micrograph showing a cross-section view of platelets. Reproduced from Evans (1992).

Sometimes when edge and screw dislocations form they can produce closed dislocation loops which form a complete circle around the segment of the diamond crystal that has slipped. Figs. 6.7A and 6.7B are images of a dislocation loop encircling numerous voidites. Voidites are another defect in diamond and are commonly found in dislocation loops. They are small octahedra, 1-10 nanometers in diameter, bounded by (111) planes (Lang *et al.*, 1992). They produce some one-phonon absorption (Woods, 1986), which makes nitrogen concentrations more difficult to calculate. Also, several studies have found that some IR-

Fig. 6.7. Transmission electron micrograph of A) numerous voidites (small circles) in a dislocation loop (large circle) and B) numerous voidites (small linear features) inside a dislocation loop (one large, discontinuous loop). Reproduced from Field (1992).

inactive form(s) of nitrogen likely occurs in voidites (Barry, 1986; Hirsch *et al.*, 1986). As such, diamonds with a high density of dislocation loops and or voidites may contain a greater concentration of total nitrogen than calculated using IR spectroscopy alone.

The process of nitrogen aggregation is complex and is not fully understood. However, it is quite clear that nitrogen diffuses through diamond with time and the influence of heat, creating more complex forms. Fig. 6.8 is a schematic diagram from Mendelssohn and Milledge (1995) illustrating the process of nitrogen aggregation. The arrows illustrate how initially type Ib diamond converts to type IaA and then IaB as a function of time and temperature. During the conversion of B centres, platelets may form. The final arrow indicates that the IaB character may convert to type IIa diamond; however, the question mark indicates that this conversion is uncertain. It is possible that nitrogen migrates to
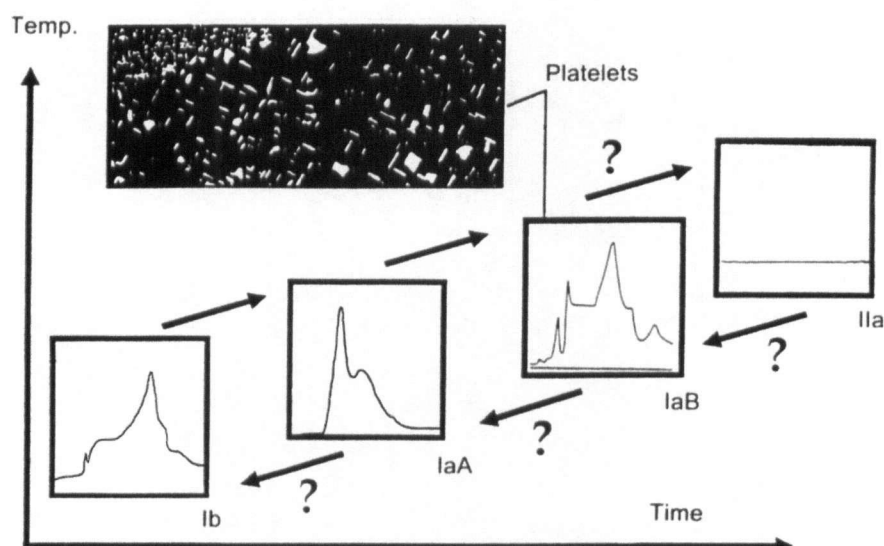
Fig. 6.8. The progression of nitrogen aggregation in diamond. From: Ib, singly substituted nitrogen; to IaA, pairs of nitrogen; to IaB, four nitrogen atoms about a vacancy; to IIa, low nitrogen diamonds with likely numerous platelets and voidites. Reproduced from Mendelssohn and Milledge (1995).

voidites and dislocation loops and may be in an IR-inactive form. By modelling the kinetics of this reaction, we can quantitatively measure nitrogen and its state in diamond and make predictions about the diamonds temperature and/or time history.

6.1.3 Quantitative calculation of nitrogen concentration

Equations relating the concentration for A and B centres in type Ia diamond have been continually improved over the past twenty years. As the causes of IR absorption become better understood, relationships between peak intensity and concentration change. Equations that are commonly used in literature today can be found in Woods *et al.* (1990), Boyd *et al.* (1994) and Boyd *et al.* (1995). D centres are not well understood and no equation exists relating absorption peaks to concentrations.

The equations used to calculate the concentration of nitrogen are typically expressed in terms of absorption units at a particular frequency (μ_{1282}) per unit thickness (cm^{-1}). The formula used to convert A centre absorption into concentration is:

60

$$N_A(\text{ppm}) = 16.5 \pm 1 \text{ x } \mu A_{1282} \text{ (cm}^{-1}), \text{ (Boyd } et \text{ } al., 1994) \tag{6.1}$$

and for the conversion of B centres:

$$N_B(\text{ppm}) = 79.4 \pm 8 \text{ x } \mu B_{1282} \text{ (cm}^{-1}), \text{ (Boyd } et \text{ } al., 1995) \tag{6.2}$$

6.1.4 Time-averaged mantle-residence temperatures

Taylor *et al.* (1996) show that the conversion of singly substituted nitrogen (Ib) to aggregated A centres (IaA) follows second-order kinetics and can be quantitatively expressed by the Arrhenius rate law. However, of more interest to the study of natural diamonds is the conversion of A to B centres. Unfortunately this reaction occurs at much higher temperatures than Ib to IaA conversion and laboratory experiments to accurately model the reaction are difficult. The limited data collected from experiments indicate that the conversion of A to B centres likely follows second-order kinetics as well (Evans and Harris, 1986).

Clark *et al.* (1992) and others have experimentally studied the effects that time and temperature have on the character of nitrogen in diamond by combining the Arrhenius rate law with the second-order reaction rate equation.

The Arrhenius rate law can be expressed by the following equation:

$$K = Ae^{\left[\frac{-Ea}{kT}\right]} \tag{6.3}$$

Where:

K = reaction rate (1/ppm · s)

A = Arrhenius constant (1/ppm · s)

Ea = activation energy (J)

k = Boltzmann constant (J/K)

T = temperature (K)

Ea and A are empirical constants which differ from one reaction to another and are calculated through experimentation. By taking the natural log of both sides and isolating T, equation 6.3 can be rewritten as:

$$T = \left[\frac{-Ea}{k} \right] \left[\ln \frac{K}{A} \right]^{-1}$$

(6.4)

Assuming the conversion of A to B centres follows second-order kinetics, the reaction rate, K, can be related to concentration and time by the following expression:

$$\frac{\partial C}{\partial t} = -KC^2$$

(6.5)

By inverting and integrating equation 6.5 from the initial concentration, C_o, at time = 0 and the final concentration, C, at time = t:

$$K = \left[\frac{1}{C} - \frac{1}{C_o} \right] \Big/ t$$

(6.6)

And by substituting equation 6.6 into 6.4:

$$T = \left[\frac{-Ea}{k} \right] \left[\ln \frac{1/C - 1/C_o}{t \cdot A} \right]^{-1} \qquad (6.7)$$

The empirical constants used for calculating time-averaged mantle residence temperatures in this study are:

$Ea = 1.12633 \times 10^{-18}$ J or 7.03 eV (Taylor et al., 1990)

$A = 2.94181 \times 10^5$ 1/ppm $\cdot$ s (McKenna, 2001), (7.36747×10^5 used by Taylor et al. 1990)

And:

$C_o = N_{(TOT)}$, concentration of nitrogen occurring as A and B aggregates (atomic ppm)

$C = N_{(A)}$, concentration of nitrogen occurring as only A aggregates (atomic ppm)

$k = 1.380658 \times 10^{-23}$ (J/K)

In equation 6.7, both C and C_o can be measured, thus leaving T and t as unknowns.

Diamond mantle residence time is well constrained if two ages can be determined: 1) the age of the diamond, and 2) the age of magmatic emplacement. Mineral inclusions in diamond, such as pyrite, garnet and clinopyroxene, may contain significant quantities of radiogenic isotopes for dating. The difference between the age of the diamond and the age of eruption would represent the mantle residence time.

The average mantle residence temperature is a more difficult variable to estimate using other analytical methods. The main problem is that it is unlikely that the diamonds remained at the same temperature throughout their residency period in the mantle. Lithospheric diamonds may have been forced to shallower depths in the mantle during slab underplating of cratons and thus subjected to lower temperatures and 'sub-

lithospheric' diamonds are likely to have been brought closer to the base of the lithosphere through mantle convection or by the action of a mantle plume before entrainment in a deep-seated magmatic body. It is highly probable that diamonds experience a range of different residence temperatures, and that the simplest way of quantifying this is by calculating a time-averaged value. However, mineral inclusions can be used to provide some constraints on equilibrium temperatures (e.g. Ryan *et al*, 1996; Brey and Kohler, 1990). Temperature constraints can also be estimated based on the pressure-temperature stability field of some minerals, which will be discussed at length in section 8.1. For example, any mineral that is stable only in the transition zone effectively restricts, at least initially, the temperature range at formation (temperatures estimates at the ~410 km and ~660 km seismic discontinuities are 1500°C and 1600°C respectively, Ringwood, 1991). However, in practice, application of this to modelling a diamonds time-temperature history based on nitrogen character does not work because the process of aggregation has either gone to completion, or has resulted in severe platelet degradation.

6.1.5 IR spectra for some other impurities

IR spectroscopy has been used to detect other impurities in diamond. Hydrogen, water, carbon dioxide and carbonate all produce fairly distinctive absorptions between 500 and 4000 cm^{-1} (Navon *et al.*, 1988).

6.1.5.1 CH bonds

The region between 2800-3100 cm^{-1} is known as the CH-stretch region. Absorption in this region forms either sharp peaks or one broad absorption band, and may be attributed to either surface complexes (which, for obvious reasons, are not considered as diamond impurities and therefore not of interest in this study) or *true* lattice defects. *True* hydrogen impurities can produce a variety of absorption bands, depending on the nature

of the complex (i.e. CH, CH_2 or CH_3, among many other possibilities). There is still uncertainty in understanding the true nature of absorption in the CH-stretching region; however, many published reports ascribe the characteristic sharp peak at 3107 cm^{-1} and the smaller accompanying peak at 1405 cm^{-1} to C-H complexes (Fig. 6.9). CH_2 and CH_3 are thought to produce
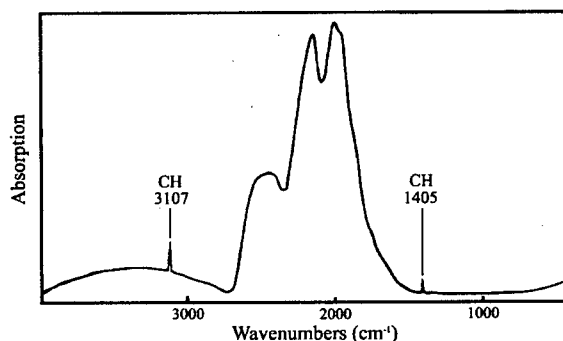
Fig. 6.9. IR spectrum of CH absorption in diamond. Characteristic IR pattern produces a strong absorption peak at 3107 cm^{-1} and a secondary peak at 1405 cm^{-1}.

more complex absorption bands that often overlap, thus requiring spectral deconvolution (Dischler et al., 1993). Furthermore, Sellschop (1992) found no correlation between relative peak height and hydrogen concentration and thus suggested that there may be significant amounts of hydrogen in other bonds, likely in IR-inactive forms.

6.1.5.2 Water (OH and HOH bonds)

A broad peak roughly centred over 3420 cm^{-1} is attributed to OH-stretching while a sharper peak at 1645 cm^{-1} (reported at 1630 cm^{-1} by Navon et al., (1988)) is considered due to H-O-H bending (Koeberl et al., 1997). The presence of either of these absorption bands is considered evidence for the presence of water (Fig. 6.10).
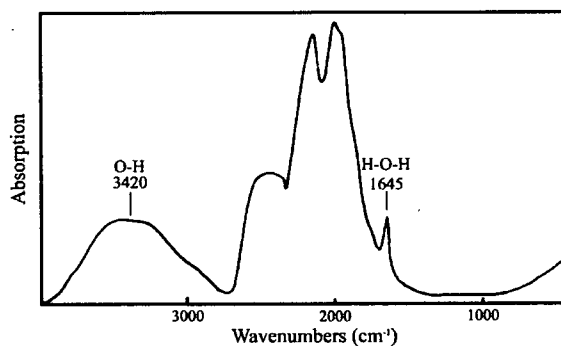
Fig. 6.10. IR spectrum of water in diamond. H_2O produces a broad absorption peak centred approximately at 3420 cm^{-1} and a narrow peak at 1645 cm^{-1}. Reproduced after Koeberl et al. (1997).

65

6.1.5.3 Carbon dioxide (CO_2 bonds)

Carbon dioxide produces a prominent peak at 2383 cm^{-1} (reported at 2350 cm^{-1} by Navon et al., (1988)) and a less obvious peak at 657 cm^{-1}, among others (Schrauder and Navon, 1993). Absorption ~3600 – 3750 cm^{-1} also occurs but is relatively weak compared with the 2383 and 657 cm^{-1} peaks (Fig. 6.11).
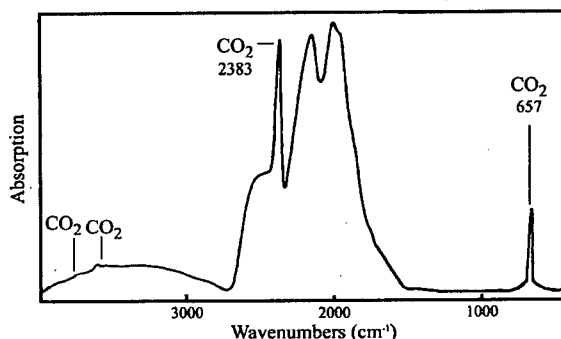
Fig. 6.11. IR spectrum of carbon dioxide in diamond. CO_2 produces strong absorption peaks at 657 and 2383 cm^{-1}. CO_2 also produces less well defined peaks above 3500 cm^{-1} Reproduced after Koeberl et al. (1997).

6.1.5.4 Carbonate (CO_3^{-2} bonds)

The carbonate CO_3^{-2} anion produces absorption bands at 1430 and 876 cm^{-1} (Navon et al., 1988) (Fig. 6.12). The band at 876 cm^{-1} occurs in the same position (± 2 cm^{-1}) for calcite impurities and is distinct from that of dolomite and magnesite (Navon et al., 1988).

6.2 Analytical techniques
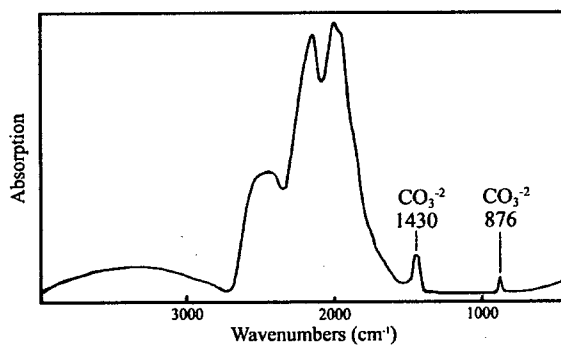
Fig. 6.12. IR spectrum of carbonate in diamond. Carbonate produces absorption bands at 876 and 1430 cm^{-1}. Reproduced after Navon et al. (1988).

IR spectra were collected over the range 650-400 cm^{-1} on a Nicolet Fourier Transform Infrared (FTIR) spectrometer with a liquid-N_2-cooled detector. Spectra were collected in transmission mode using a resolution of 8 cm^{-1} by averaging the signal of 256 scans (similar ranges, resolutions and number of scans were used by Taylor et al., 1990 and

Mendelssohn and Milledge, 1995). Spectra were automatically converted into absorption units, as required for the future manipulation of data, using the equation:

$$absorption = \log(100/\%transmittance) \qquad (6.8)$$

Background spectra were collected at the start of each day and renewed if the experiment lasted more than 2 hours. Spectra were manipulated using Omnic version 6.0a software and interpretation software supplied by T. Stachel.

Rough diamonds were cleaned in an ultrasonic bath of dichloromethane (DCM) for 30 minutes and thoroughly washed with ethanol. They were mounted on glass slides with two-sided scotch tape so that only part of the diamond was on the slide. Smaller diamonds could be fixed to the tape on the edge of the glass slide. If possible, diamonds were mounted in such a way so that a flat face was perpendicular to the IR ray path. By doing this, refraction and dispersion through the diamond is minimized and it was usually possible to collect excellent spectra with minimal noise.

Taylor *et al.* (1990) demonstrate that the effects of diamond refraction on IR path length increase with diamond thickness. They found that refraction effects are only significant for diamonds >1.5 mm thick. Many diamonds in this study were greater than 1.5 mm thick. For these diamonds, the reported nitrogen concentrations will be less than the actual nitrogen concentrations. Mendelssohn and Milledge (1995) find that IR results become increasingly inaccurate for diamonds thicker than 2.0 mm. Thicker diamonds can be analysed if they contain little to no nitrogen.

Absorption intensity is a function of path length, or diamond thickness. To account for diamond thickness variation, a spectrum must be calibrated against a spectrum of known IR path length. An IR spectrum was collected from a 'nitrogen-free' diamond (type II) and calibrated to a thickness of 1 cm using the conversion factor 11.94 absorption

units/cm, measured at 1995 cm^{-1} (T. Stachel, personal communication, 2002). The type II stone (no visible one phonon absorption) was supplied by T. Stachel and is a 0.57 mm thick chip with two reasonably flat, parallel fracture surfaces. The type II spectrum was corrected by taking a linear base line between ~4000 and ~1500 cm^{-1}. All spectra were scaled to match the type II spectrum and base lined following the same procedure as used for the type II diamond. In some cases, more than two points were required to produce an acceptable spectrum for deconvolution. The choice of base line has an effect on the final calculated nitrogen totals, and is explored in more detail below (section 6.2.1.2).

Following this, each sample was deconvoluted into three curves, A, B and D, using software supplied by T. Stachel. In some instances, no curves were fitted to the deconvoluted data curves. In these cases, files were base lined using more points and re-run through the deconvolution software. The program calculates the absorption at 1282 cm^{-1} for the A, B and D curves. Equations relating the absorption measured at 1282 cm^{-1} to A and B centre concentrations have been developed (see section 6.1.3) but no such equations exist yet for D curves. As such, the value quoted for D centres is in absorption units for a diamond of 1 cm thickness. It is best thought of as a dimensionless number which describes the relative concentration of D centres.

The cut-off for type II diamond is arbitrary but in qualitative terms, if absorption attributed to nitrogen defects is visible in the one-phonon range, the diamond is type I. In quantitative terms, in this study, the cut-off of 20 atomic ppm nitrogen as the divide between type I and type II diamond Kaminsky et al., 2001b), was used. In some cases the deconvolution program yielded concentrations greater than 20 ppm nitrogen; however, examination of the IR spectra did not reveal any detectable nitrogen (any one-phonon absorption is likely a result of noise). In these cases, the deconvolution results are recorded, but the diamond is classified as type II. The distinction between type IaAB and the end members IaA and IaB was arbitrarily set using the following divisions: any diamond containing >20 ppm total N with less than 10% B centres is considered type

68

IaA; IaB (>20 ppm total N and >90% B centres); and type IaAB (>20 ppm total N and 10 - 90 %B centres).

Relative hydrogen concentrations were measured after thickness calibration and base lining and recorded by measuring the absorption difference between the base and peak at 3107 cm^{-1}.

6.2.1 Examination of error analysis for infrared studies

Error estimates for nitrogen concentrations are difficult to quantify due to the numerous sources of absorption that may contribute. Most errors in concentrations are produced either during data collection or data processing. The following section examines these errors in attempt to quantify each source.

6.2.1.1 Error from deconvolution software

The deconvolution software uses IR data between the wavenumbers 900-1500 cm^{-1} that have been calibrated for a diamond of 1 cm thickness and base lined. The program calculates a 'best-fit' curve (blue line, Fig. 6.13) which is the sum of theoretical curves for A (green line), B (pink line) and D (turquoise line) curves to the collected data (red line). The black line indicates the difference between the sum of theoretical curves and the collected
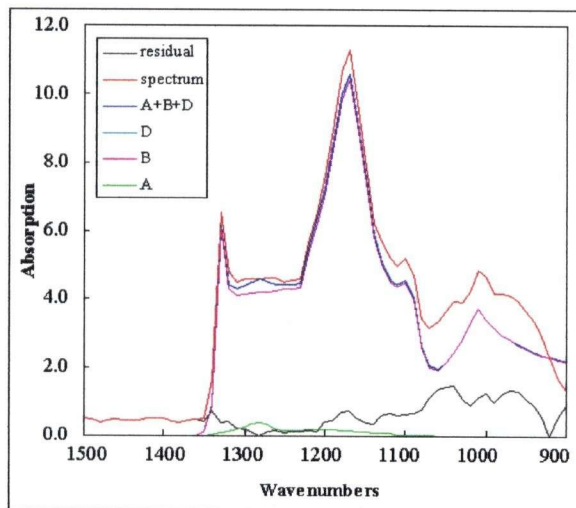
Fig. 6.13. Results from deconvolution software. A,B and D curves represent scaled values for these pure end-member absorption curves (see Fig. 6.3). The other three colours represented are blue (the sum of the three end-members), red (base lined and calibrated data file) and black (the difference between blue and red curves.

69

spectra (red line) and represents the 'degree of fitness'. Based on these curves, the program calculates the absorption units at 1282 cm^{-1} for each of A, B and D curves. The program also calculates a value for the black line, but it is unknown to the author what this term represents; most likely it quantitatively describes the area under the curve. Because of the uncertainty associated with the calculation for determining the error value, no component to the overall error can be quantitatively attributed to the process of spectral deconvolution.

6.2.1.2 Sensitivity to baseline corrections

FTIR spectra in this study are typically sloped so that there is more absorption at higher wave numbers than lower numbers. Reasons for this are numerous, but some of the more common causes include sample scattering, inappropriate choice of background and instrument drift (Smith, 1996). Base line corrections may be straight or curved, however, it is important that regardless of what base line function is used, false peaks are not introduced. A good way to avoid introducing false peaks is to use as few line segments as possible. Mendelssohn and Milledge (1995) suggest fixing the base line at 4000 cm^{-1} and at the minima between 1400-1600 cm^{-1} and extrapolating this backward to 900 cm^{-1}.

Table 6.1. Base line sensitivity study

Base line study no.	A (ppm)	B (ppm)	B/(B+A)	Total N (ppm)
1	11.3	367.5	97.0	378.8
2	6.9	340.6	98.0	347.5

Spectra deconvolution results for two curves in Fig. 6.14. Study 1, one line used for base line, study 2, two line segments used.
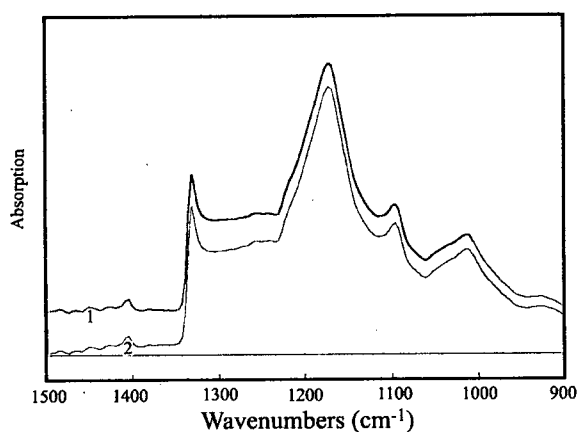
Fig. 6.14. Examination of base line sensitivity. Curve 1 was base lined using one line segment, curve 2 was base lined using two line segments.

In this study most spectra were corrected using one line segment following the approach suggested by Mendelssohn and Milledge (1995). The minima between 1600-1400 cm^{-1} was almost always found at 1558 cm^{-1}. In some cases the spectra between 1558 and 400 cm^{-1} increased in absorption. In these cases two line segments were used, one between 4000 and 1558 cm^{-1} and the other between 1558 and 400 cm^{-1}.

By applying base lines of various slopes to the same raw data file, base line sensitivity was examined. One spectrum was produced by joining a line segment between 4000 and 1558 cm^{-1} and extrapolating backwards (curve 1 on Fig. 6.14) while another spectrum was produced by joining line segments from 4000 and 1558cm^{-1} and 1558 to 400cm^{-1} (curve 2, Fig. 6.14). Nitrogen totals for these two curves are presented in Table 6.1. B/(B+A) is not very sensitive to the choice of base line, however, the total nitrogen concentration varies quite considerably. The difference in total nitrogen between these two spectra is 30 ppm, or 9% relative error.

6.2.1.3 Reproducibility of IR spectra

Reproducibility of IR spectra was estimated by collecting ten spectra from the same point on a crystal with all other parameters remaining constant. Diamond 2-5 was selected for this study because the spectra collected from this crystal did not require any base lining (there was no absorption at 600 and 4000 cm^{-1}) and the diamond contains considerable nitrogen (~300 ppm N). By selecting this crystal for the reproducibility study, any error

Table 6.2. Reproducibility study

Point	A (ppm)	B (ppm)	B/(B+A)	Total N (ppm)
1	36	278	88	315
2	37	277	88	313
3	36	275	88	311
4	36	273	88	309
5	35	271	88	307
6	36	270	88	306
7	35	269	88	304
8	35	267	89	302
9	35	266	88	301
10	34	265	89	299
average	35	271	88	307
stan. dev.	0.8	4.6	0.1	5.4

Columns A (ppm) and B (ppm) are calculated using equations 6.1 and 6.2.

introduced during base lining could be removed. Each spectrum collected was multiplied by the same conversion factor in order to convert the curve to that of diamond of one centimetre thickness and then deconvoluted. The results are presented in Table 6.2.

The average total nitrogen value is 307 ± 5.4 (1σ) while %B averages 88 ± 0.1 (1σ). The apparent reproducibility error is small; however, note that the total nitrogen decreases after each successive analysis. The reason for this is unclear. The relative error between points 1 and 10 at the 95% confidence level is 3.5%.

6.2.2 Precision of IR data

There are other sources of error to consider than just the three sources explored in section 6.2.1; however, the overriding contributor to differences in nitrogen concentration are heterogeneities within the diamond crystal itself. In this study, values within one crystal varied from 30 to 400 ppm nitrogen (1333%).

The error of the method used in this study in estimating nitrogen concentration and aggregation state is a combination of the analytical precision and the error inherent to spectrum calibration, deconvolution, and conversion of results into nitrogen centre concentrations. The analytical precision, calculated through multiple analyses of the same grain is estimated at 3.5% (section 6.2.1.3). The remaining errors are as follows: spectrum calibration, mainly affected by the manual selection of a base line, is estimated at 9% relative (section 6.2.1.2); deconvolution, although certainly a source of error has no absolute quantitative precision attached to the results (discussed in section 6.2.1.1) and hence cannot be included here; and conversion of deconvoluted curves into nitrogen concentrations is calculated as 6% for A centres (Boyd *et al.*, 1994) and 10% for B centres (Boyd *et al.*, 1995) (errors on equations 6.1 and 6.2 in this study). The overall precision of this method is estimated at 19% for A centres and 23% for B centres, which

agrees well with those reported, i.e. 10-20% (Kaminsky *et al.*, 2001b), <25% (Kaminsky *et al.*, 2000), 12-15% (Deines *et al.*, 1991), and 10-20% (Stachel *et al.*, 2002).

Nitrogen concentration errors for this study fall between 19-23%. However, the relative error increases as nitrogen concentrations decrease. The B/(B+A) value (aggregation state) also becomes increasingly imprecise as nitrogen concentrations approach the minimum detection limits.

The precision of relative hydrogen concentrations was examined by measuring the peak height at 3107 cm^{-1} for the same curve several times. From these measurements, an error of 2.6% relative was calculated.

6.2.3 Minimum detection limits

Minimum detection limits (MDL's) were estimated based on visual examination of IR curves and comparison with calculated A, B and D centre concentrations. MDL's are presented in Table 6.3. Examination

Table 6.3. MDL's for IR data

Centre	MDL
A	12 ppm
B	20 ppm
D	1 a.u.
H	0.03 a.u.

a.u. = absorption units for diamond 1 cm thick.

of IR curves in Appendix D show that only a few diamonds have visible peaks from A centre IR absorption. The lowest calculated A centre concentration was 12 ppm. Visual examination of deconvoluted curves show that the MDL for B centres is around 20 ppm. D centre concentrations are so small when compared to suites of *regular* diamonds (i.e. diamonds with abundant platelets, Fig 6.6) and calculated values produce results which appear meaningless. Based on data from *regular* diamonds and diamonds from this study, the MDL for D centres is estimated at ~1 absorption unit measured at 1282 cm^{-1} when calibrated for a diamond of 1 cm thickness (Fig. 6.17). MDL's for hydrogen were calculated based on visual examination of IR curves.

6.3 Results

The results in this section are summarized in table format in Appendix C. A raw spectrum for each diamond, together with deconvolution curves for A, B and D centres, are presented in Appendix D.

6.3.1 Nitrogen concentration and aggregation state measurements

Total nitrogen concentrations in the crystals examined are low, with a mean of 72 ± 72 (1σ) and mode of 36 ppm (the large standard deviation is due to the skewed distribution towards nitrogen-free diamonds) (Fig. 6.15).

Fig. 6.15. Distribution of total nitrogen concentration (ppm) for Rio Soriso diamonds. Diamonds are sorted in order of increasing total nitrogen concentration. MDL = minimum detection limit for nitrogen (20 ppm total nitrogen).

Nitrogen concentration ranges from 0 to 541 ppm for total nitrogen, 0 to 116 for A centres, and 0 to 541 ppm for B centres. There is a gradation in total nitrogen concentration over the complete range, providing no indication of a bimodal character. The mean B/(B+A) centre ratio is 95 ± 22 (1σ) percent, covering the complete range
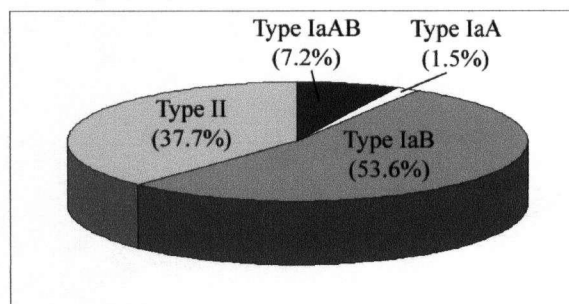
Fig. 6.16. Diamond type distribution for Rio Soriso suite (n=69). Averages were used for heterogeneous samples with multiple analyses points (chapter 7.0 on growth studies).

form 0 to 100 % B centres. The distribution of diamond types are type II (37.7%) and type Ia (62.3%). Type Ia stones are further sub-divided into type IaA (1.5%), IaAB

(7.2%) and IaB (53.6%) (Fig. 6.16). (The cut-off between Type I and II stones used is 20 ppm total nitrogen).

The relative concentration of D centres is very low in comparison with A and B centres (see any deconvoluted curve in Appendix D). When compared with diamonds containing D centres (i.e., *regular* diamonds), it is clear that the measured D centre concentrations are unusually low (Fig. 6.17). On this figure, the open circles (calculated from unpublished work) form a positive linear trend; these diamonds are *regular*. This trend is not observed in Rio Soriso diamonds (filled grey circles) making them *irregular*. Due to

Fig. 6.17. Plot of D centres versus B centres. Small filled circles are from this study and large open circles are from another suite of diamonds that contain roughly equal proportions of A and B centres and are considered *regular* (after Woods, 1986). A straight line through these points and the origin produces a reasonable fit with $R^2=0.859$. a.u. - absorption units for diamond of 1 cm thickness. MDL - minimum detection limit. (Compare with Fig. 6.5 after Woods, 1986).

the high aggregation state of Rio Soriso diamonds, it is not surprising that they are irregular as any platelets (D centres) that existed have likely degraded (see section 6.1.2). Calculated D centres are below the estimated MDL and have not been included in the results of this study.

Six diamonds contain measurable quantities of A centres (diamonds 2-11, 4-10, 4-11, 4-15, 4-17 and 6-8) and, provided that platelet degradation does not begin until nitrogen is mostly aggregated as B centres (such as observed in Fig. 6.5), the type IaAB diamonds would be expected to contain platelets. Although calculated D centre concentrations are low for all diamonds, the B' peak provides another tool for identifying platelets (section 6.1.2, Fig. 6.4). This peak is visible in the IR spectra for 5 of the 6 diamonds, occurring at 1363.7 cm^{-1} and is absent in all other diamonds (types IaB and IIa). Absorption values

75

measured at peak heights are presented in Table 6.4. Comparison with data from *regular* diamonds (diamonds plotted in Fig. 6.17) suggests that all diamonds in this study are *irregular*, even those with A centres. However, note that nitrogen concentrations are extremely low when compared to other studies (average of ~500 ppm total nitrogen for *regular* diamonds which were compared with Rio Soriso diamonds) and that B' peaks and D centre absorption curves would likely be small and possibly below detection. The type IaA and IaAB diamonds may be regular, but the low nitrogen concentrations make any classification difficult.

Table 6.4. B' absorption and D centre concentrations for type IaA and IaAB diamonds

Diamond	B'	uB'	D	A	B	total N	100xB/ (B+A)
2-11(point 19)	1363.75	5.02	1.63	55	428	483	89
4-10	1363.75	0.30	0.00	12	21	33	64
4-11	1363.75	0.84	0.01	48	0	48	0
4-15	1363.75	0.89	0.22	116	22	138	16
4-17 (point A)	1363.75	0.29	0.07	26	27	53	51
6-8	-	-	0.11	23	25	48	52

Multiple points were examined on diamonds 2-11 and 4-17 in Chapter 7.0. Analysis points are indicated on Figs. 7.19 and 7.27 respectively. B' and μB' are measured in cm^{-1}. D, A and B centres represent absorption units (cm^{-1}) measured at 1282 cm^{-1}. Point 19 on diamond 2-11 was not included in Appendix D or Fig. 6.17 because there is considerable noise in the one-phonon range. This IR-data is discussed at greater length in section 7.3.8 (Fig. 7.20).

6.3.2 Other impurities detected by IR spectroscopy

Section 6.1.6.5 outlines typical absorption spectra obtained from diamond due to impurities other than nitrogen. Of these typical absorption spectra, only those pertaining to hydrogen were observed. Water, carbon dioxide and carbonate were not detected in these studies. Two absorption spectra of unknown origin were observed in several different diamonds.

6.3.2.1 C-H bonds

Spectra from seventy-one percent of the diamonds studied showed a hydrogen peak at 3107 cm^{-1}. The intensity of the peak varies from 0 to 6.06 absorption units. Only crystals with large hydrogen peaks at 3107 cm^{-1} ($\sim{>}1.2$ a.u.) had a detectable secondary peak at 1405 cm^{-1}. Peak intensity difference at 3107 cm^{-1} is recorded in Appendix C.

6.3.2.2 CH$_2$ and CH$_3$ bonds

Absorptions in the CH-stretch region of spectra from many of the diamonds occur either as two well defined peaks at 2920 and 2850 cm^{-1}, with a shoulder at 2960 cm^{-1} (Fig. 6.18A), or as one broad peak between 2800–3000 cm^{-1} (Fig. 6.18B). In some cases, an accompanying smaller peak was observed at 1460 cm^{-1}.

Several diamonds that exhibit IR absorption between 2700 and 3100 cm^{-1} were heated to 600 °C for 20 minutes to determine if the CH$_2$ and CH$_3$ complexes were forming only on the diamond surface. Prolonged exposure to these elevated temperatures should remove any CH$_2$ and CH$_3$ surface complexes. In all cases the diamonds heated did not exhibit any absorption in the CH-stretch region or at 1460 cm^{-1} after heating. An IR spectra of
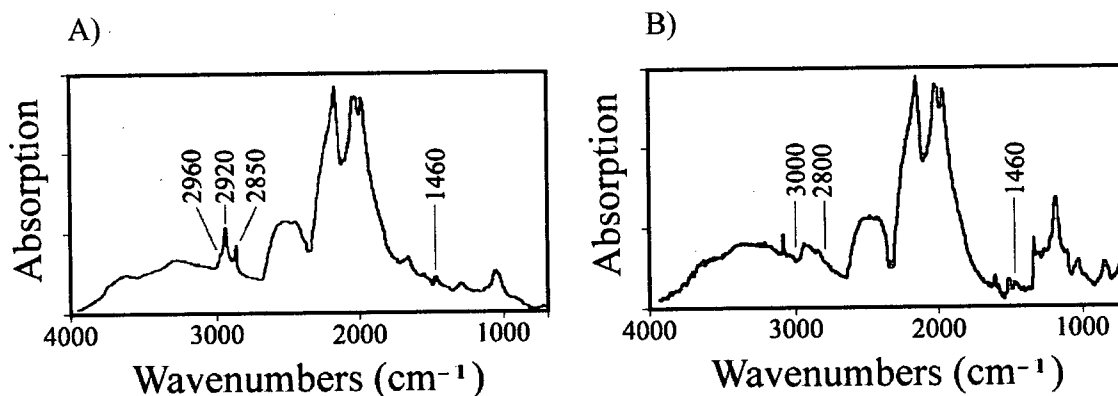
Fig. 6.18. Absorption in the CH stretch region of Rio Soriso diamonds. A) Two sharp peaks at 2850 and 2920 cm^{-1}, B) Broad peak between 2800-3000 cm^{-1}.

two diamonds before and after heating can be seen in Fig. 6.19. Based on these findings, any absorption observed between 2800 and 3000 cm^{-1} was ignored.

6.3.3 Unexplained spectra

There are two IR absorption spectra for which the cause is unknown. To the authors knowledge, they have not been mentioned in diamond literature before. Both spectra create absorption in the one-phonon range, the first will be

Fig. 6.19. IR spectra of diamonds 2-5 and 4-17 before and after heating to ~600°C. 2.5A before heating, and 2.5B after heating, 4.17A, before heating, and 4.17B after heating. Note that in both cases the peaks at 2980, 2850 and 1460 cm^{-1} disappear after heating. Absorption in these regions is thought to be a result of the stretching of CH_2 and CH_3 orbitals. In this case, they are only on the surface of the diamond and are liberated by heating.

referred to as defect 'X' (confirmed in three diamonds, 2-5, 3-10 and 4-17), and the other as defect 'Y' (found in five crystals).

Defect 'X' is characterised by a broad peak with maximum absorption at 1048 cm^{-1}, a smaller peak at 867 cm^{-1} and a small broad absorption band centred on 1419 cm^{-1} (Fig. 6.20 A and B). The defects responsible for this peculiar absorption remain unknown.

Defect 'Y' is observed in several stones, although the broad absorption spectra fails to match up when overlapped (a case may be made to split up defect 'Y' into two or more unknown defect patterns). Defect 'Y' produces the strongest absorption in diamond 2-3. This crystal is unique in this study because it is the only stone with strong yellow colouration. Another unique feature about this crystal are local patches of white/cloudy diamond (Fig. 6.21A). The contact between the white and yellow patches, when viewed under a 35x magnification lens, reveals a rainbow effect of colours. This is interpreted as being a result of stress or internal fractures. IR spectra collected through the yellow diamond, which constitutes the bulk of the crystal, indicates that this part of the diamond
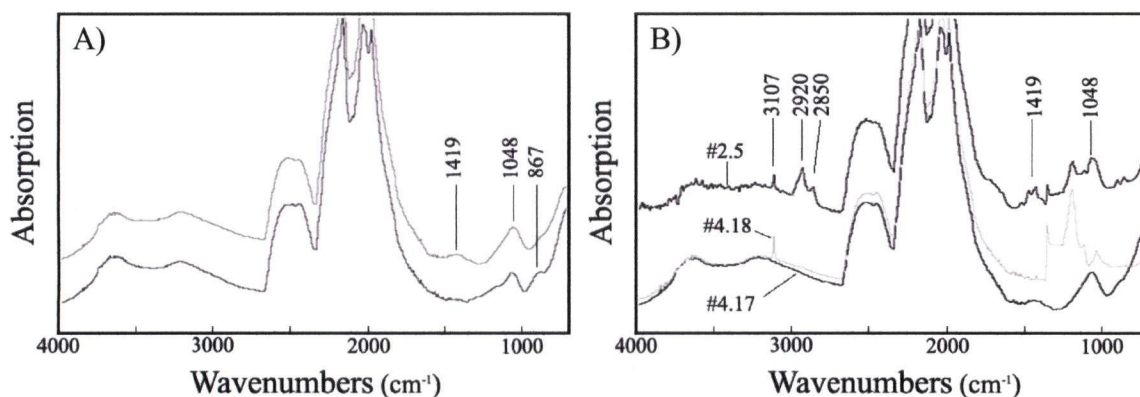
Fig. 6.20. IR spectra of diamond with unexplained defect 'X'. A) Two IR spectra collected from diamond 4.17 after heating to 600 °C for 20 minutes. The most characteristic aspect of the unknown curve is the strong absorption observed at 1048 cm⁻¹. B) IR spectra illustrating the summation of type IaB diamond with impurity "X". Diamond 4.17 contains 'pure' defect 'X' and Diamond 4-18 exhibits pure IaB diamond. Diamond 2-5 (before heating) is interpreted as a combination of B aggregated nitrogen and defect 'X'.

contains no detectable IR-active nitrogen (Fig 6.21B, curve labeled C) and is thus considered type II. IR examination of the white patches contains defect 'Y'. The unexplained curve exhibits a broad asymmetric peak with maximum absorption at 1086 cm⁻¹ and a shoulder at 1230 cm⁻¹. A secondary peak is observed at 815 cm⁻¹ (Fig. 6.21 B). J. Milledge (personal communication, 2003) suggests that defect 'Y' is likely some form of clay, most likely as a secondary mineral in fractures between the white and yellow diamond. No further studies were done to corroborate or refute this hypothesis.
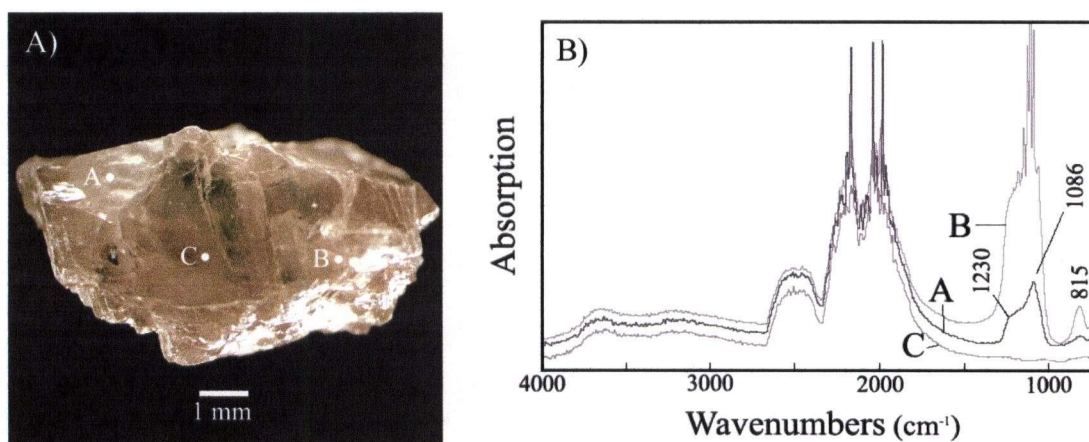
Fig. 6.21. Photograph of diamond 2-3 and IR spectra of defect 'Y'. A) Photograph of IR location points A, B and C on diamond 2-3. B) IR spectra of three points on diamond 2-3. Points A and B are from white patches on diamond while point C is through yellow portion of stone.

79

6.4 Discussion

6.4.1 Relationship between time and temperature

Nitrogen concentration and aggregation state measurements are useful for providing constraints on temperature and residence time the diamonds experienced in the mantle (equation 6.7 from section 6.1.4)., Without further constraints on either of these variables, and assuming the diamonds are from one source in the mantle, we can place them along a curve in time/temperate space (Fig. 6.22). Further constraints for placing these diamonds along this curve come from a variety of sources. Constraints can be placed on the residence time through dating of the magmatic eruption which brought the diamonds to surface and through dating of minerals included in diamond. Further constraints on the residence temperature can be determined after examination of inclusion types, phases and associations (chapter 8.0).

Fig. 6.22 illustrates the estimated minimum time diamonds would need to reside at certain temperatures in the mantle to acquire the observed average nitrogen character measured through IR studies. For example, a diamond at estimated lower mantle temperatures would only need to reside at these depths for ~93,000 years before
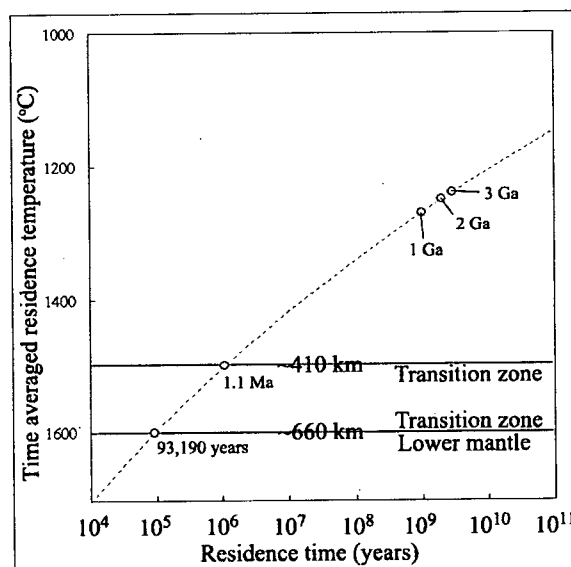
Fig. 6.22. Plot of minimum time averaged mantle residence temperatures versus minimum residence times for Rio Soriso diamonds. The residence time curve is specific to the mean total nitrogen concentration (72 ppm) and mean nitrogen aggregation state (95%) for this study. Diamonds would theoretically only have to reside in the lower mantle for 93,190 years to acquire the average nitrogen character measured. Transition zone diamonds should be less than 1.1 Ma. Temperature estimates for transition zone and lower mantle discontinuities are from Ringwood (1991). Time averaged mantle residence temperatures and times are calculated using A = 736747 1/s·ppm and Ea = 7.03 eV, from Taylor et al. (1990).

converting 95% of A centres to B centres. Conversely, a diamond at temperatures estimated for lithospheric cratons would require a much longer residence time, on the order of 1-3 billion years, to convert 95% of A centres to B centres.

Note, however, that the there are numerous errors associated with equation 6.7 (the equation used to derive the curve in Fig. 6.22). Some of the main errors are: 1) the conversion of A to B centres is still poorly constrained, especially under the effects of deformation, 2) the constants used in equation 6.7 (Ea and A) may not apply to residence temperatures that would be experienced in the transition zone (1500-1600 °C) or lower mantle (>1600 °C), 3) the variable *average residence temperature* is considerably abstract as diamonds most certainly existed in the mantle at varying temperatures, 4) temperature calculations do not work well for irregular diamonds with high aggregation states and may, at best, provide only a minimum estimate, provided the conversion of A to B centres followed the *regular* trend to high aggregation states.

6.4.2 Nitrogen character of Rio Soriso diamonds

The nitrogen character (total concentration of nitrogen and %B aggregation) has been shown to vary between some diamond suites and is a reasonable first-order method for distinguishing between some diamond populations (Kaminsky *et al.*, 2001b). However, because the nitrogen character is strongly controlled by time and temperature, there are many cases where separate populations have
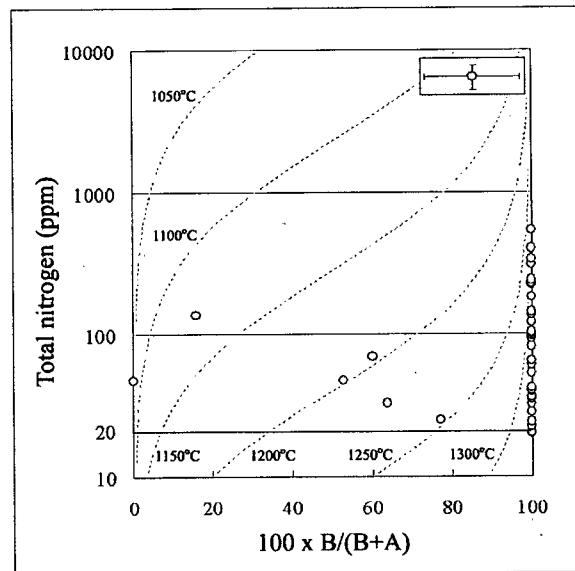
Fig. 6.23. Plot of total nitrogen concentraion versus %B aggregation for Rio Soriso diamonds. Isotherms are calculated using a residence time of 3 Ga. Line at 20 ppm nitrogen marks the MDL for total nitrogen concentraion.

experienced similar histories and hence cannot be unambiguously distinguished based on nitrogen character alone. Nonetheless, the nitrogen character is a useful *fingerprint* to record for a diamond suite. The character for this suite can be examined in Fig. 6.23. From this figure, two separate sub-groups are visible: diamonds that are %100 B aggregated, and diamonds which contain some percentage of A centres. A third sub-group, not depicted, is represented by diamonds which fall below the 20 ppm nitrogen line marking the MDL. Included in this figure are isotherms assuming the diamonds resided in the mantle for 3 Ga. Although there is no data to substantiate this, they are included to illustrate the morphology of isotherms as a function of time.

6.4.3 Comparison of relative hydrogen and total nitrogen concentration

Based on observations of this study and from growth studies (chapter 7.0), there is a positive correlation between hydrogen and nitrogen concentrations (Fig. 6.24). Two possible reasons for this are that: 1) nitrogen and hydrogen impurities in diamond originated as an N-H complex or 2) conditions favorable for the incorporation of nitrogen impurities are also favorable for the incorporation of hydrogen, or visa versa.

The prevalence of hydrogen in diamonds from other deposits is not well recorded. A detailed study by

Fig. 6.24. Plot of relative hydrogen versus total nitrogen concentrations for Rio Soriso diamonds. Relative hydrogen concentration measured as change in absorption units (a.u.) at $3107cm^{-1}$. Error on total nitrogen concentration is 20% relative, and is 2.6% on relative hydrogen concentraion. A straight line of best through the data and the origin yields $R^2=0.788$.

Taylor *et al.* (1990) on several diamond suites from Australasia shows that hydrogen is

not a ubiquitous element in type Ia diamond, as one might conclude from the results of this study. From studies of several diamond suites, Argyle was the only diamond suite found to contain abundant hydrogen bearing diamonds. Argyle diamonds are similar in terms of nitrogen character to the suite in this study (see Fig. 6.25). Total nitrogen concentrations are generally <100 ppm, the aggregation state is high (close to 100% B centres), and platelet degradation is likely advanced (Taylor et al., 1990). Unfortunately there is no information on the relative hydrogen concentrations for Argyle diamonds.

6.4.4 Comparison of nitrogen characteristics with other studies

The nitrogen characteristics (i.e. nitrogen concentration and aggregation state) for Rio Soriso diamonds is essentially the same as recorded by Harte and Harris (1994), Kaminsky et al. (2001b) and Araujo et al. (2003) for Juina diamonds (i.e. low total nitrogen concentrations, mostly in the form of B centres). However, this nitrogen character is not unique to Juina area diamonds (Fig. 6.25).
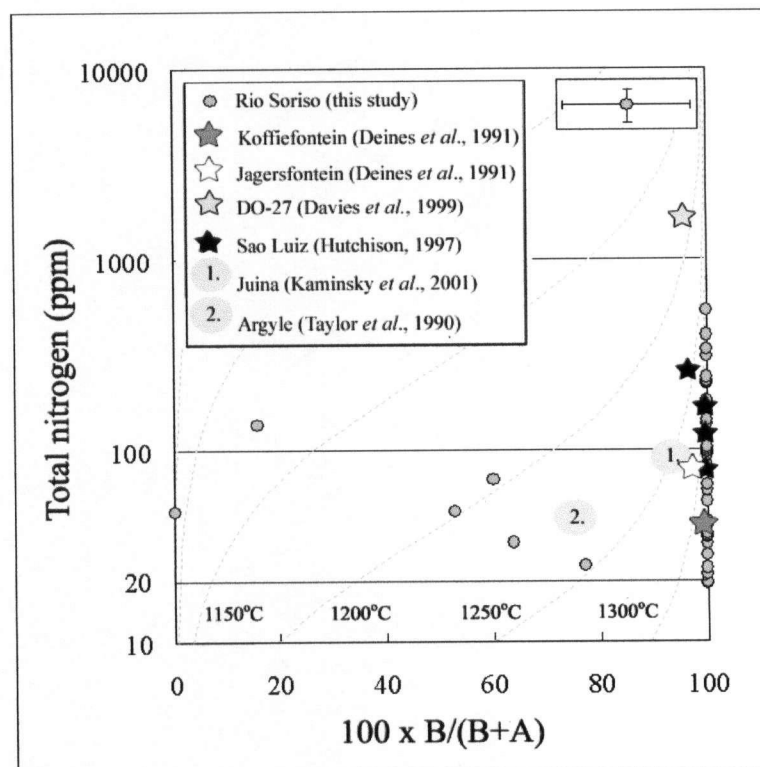
Fig. 6.25. Plot of total nitrogen concentration versus %B aggregation for selected diamonds and diamond suites worldwide. Isotherms are calculated for a mantle residence time of 3 Ga. All data are for single diamonds except points labelled 1. and 2. Point 1 is the average of 98 diamonds from three rivers in the Juina area: Rio Sao Luiz, Rio Vermelho, and Corrigo Chicora, from Kaminsky et al. (2001b). The error on the data point is unclear, although it is likely similar to the error in this study. Point 2 is the average 13 diamonds from Argyle (Taylor et al., 1990). The range in %B is from 60 to 95, and for all but one stone, the total nitrogen concentration is less than 100 ppm.

The combination of 'diamond mineral inclusion' and 'nitrogen character' studies has established that the 'lower mantle' diamond suite is characterized by type II or type IaB diamond with low total nitrogen concentrations (Harte and Harris, 1994; Hutchison, 1999; Davies *et al.*, 1999; and Stachel *et al.*, 2002). There are also isolated occurrences of diamonds with this character from South Africa and Australia, among other places (also plotted on Fig. 6.25), however these diamonds are rarities within their respective diamond suites.

7.0 Growth studies

7.1 Background

Historically, the internal growth morphology of diamond has been examined using a variety of techniques, including birefringence studies (e.g. Tolansky, 1966), X-ray topography of whole diamonds (e.g. Lang, 1964), and etching of diamond plates (e.g. Seal, 1965). However, these techniques have given way more recently to cathodoluminescence (CL) studies of polished diamond sections and plates. A brief background behind the principles of CL is outlined in section 3.1.2. Optical CL is an inexpensive technique which is extremely sensitive to chemical heterogeneities. As such, growth layers with even minute differences in chemistry often exhibit different CL colours or different colour intensities. CL studies of diamond plates (two parallel polished surfaces) and sections (one polished surface) used in conjunction with infrared (IR) and isotopic studies have allowed scientists to map the variations in chemistry during diamond growth (eg. Boyd *et al.*, 1987; Milledge *et al.*, 1989; Mendelssohn *et al.*, 1991). The purpose of this study is to integrate CL studies of diamond plates and sections with IR studies.

7.1.1 Internal structures in diamond

The vast majority of natural single-crystal diamonds grow as octahedrons (eight (111) faces), with cubes (six (100) faces) and cubo-octahedral forms (eight (111) and six (100) faces) generally being less common (previously introduced in section 2.1.1 on diamond growth habits). Other primary growth faces are possible on natural diamonds, but are extremely rare and need not be considered here. The growth history of diamond is inherently more complex than what would be concluded from observation of external morphology alone. Once a suitable site for carbon precipitation exists (from herein referred to as the *seed*), both (111) and (100) faces may grow. The face that will

85

dominate the crystal once growth is complete is the face that grows the slowest - the face that grows the quickest grows to a point and to extinction (Clausing, 1997). Matters are complicated because diamonds often experience multiple events of growth and dissolution; whatever external faces the crystal retains reflects only the last growth event. It is common to observe the 'competition' between the growth of (111) and (100) faces in the core of the crystal.

Fig. 7.1 contains images of opposing sides of an octahedral diamond (in terms of external morphology). In Fig. 7.1A, clearly visible are the seed, the competition zone (where octahedral and cubic faces compete for dominance) and the octahedral outer zone.

Octahedral growth layers are recognised (in two dimensions) because they typically form straight, parallel lines, while cubic growth layers are typically rounded or hummocky. This is likely the main reason why smooth cubic faces are rare in natural stones and octahedral surfaces are often flat (provided the stone has not experienced dissolution). Growth layers developing perpendicular to the (111) are discussed in literature using a variety of names, some of the more common terms are tangential growth (Sunagawa, 1984a and b), flat faces (Harte *et al.*, 1999), faceted
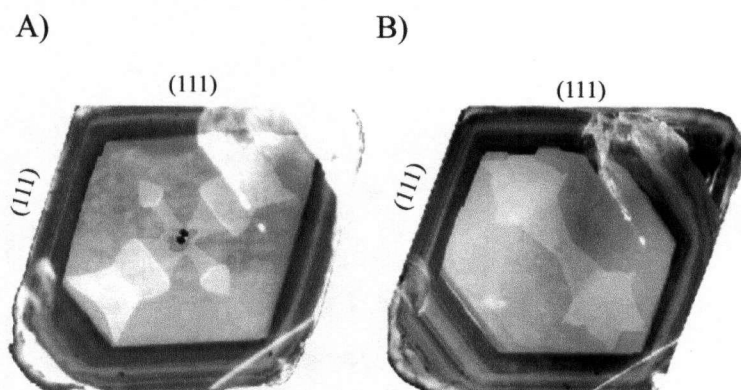
Fig. 7.1. CL images of central plate of diamond (opposite sides). A) The central zone reveals the diamond seed (the two black spots). The lighter grey zones surrounding the seed indicates growth of two types: cuboid (forming perpendicular diagonal arms of two brighter shades of grey) and octahedral (homogeneous darker grey zones in the central region). The fine scale laminations on the outer rim formed on octahedral faces. B) The opposing side of the diamond contains lighter grey zones across the short diagonal (indicating cuboid (100) growth) while the remainder of the central light grey zone is comprised of octahedral growth. Note the fine scale, straight character of the outermost layers. Diamond is cut parallel to the ~(110) plane. Magnification x 40. (image reproduced from Bulanova *et al.*, 2002).
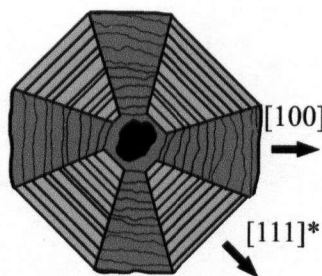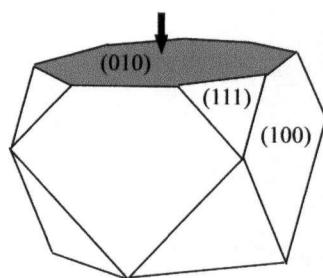
Fig. 7.2. Cartoon of internal morphology for cuboid and octahedral growth where both faces grow evenly. Left image indicates where diamond slice of right image is cut (parallel to the (010) surface). Black spot in middle is crystal seed. * indicates that the growth direction is oblique and not perpendicular to the (111) face when viewed on a surface cut parallel to the (010).

growth (Moore and Lang, 1972), layer by layer growth (Moore and Lang, 1972), or octahedral (111) growth (Davies *et al.*, 1999). For the sake of consistency and simplicity, only the terms octahedral and (111) growth/face will be used in this report. Growth bands that develop roughly perpendicular to the (100) direction are typically irregular and may cross-cut one another. These growth bands are sometimes referred to as normal growth (Khachatryan and Kaminsky, 2002), unfaceted growth (Moore and Lang, 1972), rounded or hummocky growth (Harte *et al.*, 1999) or cuboid (100) growth (Davies *et al.*, 1999). The more irregular the bands the further the growing conditions are considered to be from equilibrium. Cuboid growth of fibrous or columnar habit has also been observed (Lang, 1974b; Sunagawa, 1984b). This report will use the terms cuboid and (100) growth/face for simplicity.

Natural diamonds of solely cuboid growth are not very common (particularly in this study) and thus will not be discussed in isolation, rather, combination cuboid and octahedral forms will be examined. As previously mentioned, cuboid and octahedral growth usually develops once a primary nucleation site exists, e.g. Fig.
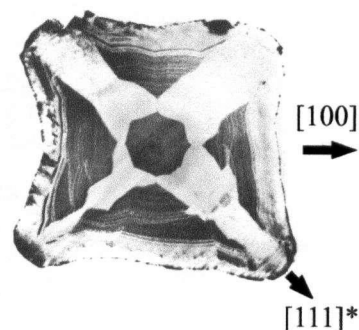
Fig. 7.3. X-ray section image of cubo-octahedral diamond. Note how octahedral (111) sectors are bright while (100) sectors are dark. This is a result of impurity partitioning. Cut parallel to the (010). * indicates that the growth direction is oblique and not perpendicular to the (111) face when viewed on a surface cut parallel to the (010). (image reproduced from Welbourn *et al.*, 1989).

7.1. In this example, in the end, octahedral growth prevailed. In contrast, Figs. 7.2 and 7.3 show examples where both (111) and (100) faces develop without one face growing to extinction (both figures are of slices parallel to the (100)). The difference in CL brightness between cuboid and octahedral growth zones is a result of sector dependence of impurity uptake (e.g. Fig. 7.3).
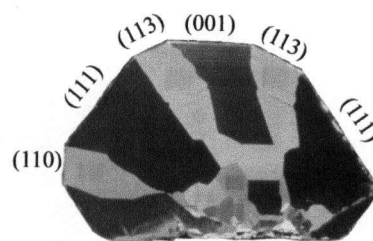
Fig. 7.4. CL image illustrating growth-sectorial dependence in synthetic diamond. (image reproduced from Burns *et al.*, 1990).

Sector dependence of impurity incorporation is perhaps best illustrated in the CL image of a synthetic stone in Fig. 7.4. For this diamond, nitrogen (as disaggregated N centres or type Ib diamond) partitions into different growth zones, from highest to lowest concentration, in the following order: (111), (100), (113) and (110) (Burns *et al.*, 1990). (It is unclear why the most nitrogen rich sector exhibits the faintest CL colour, as the opposite is more often true, that is, zones of higher nitrogen exhibit the brightest CL colours (Davies, 1998)). Pioneering studies by Lang *et al.* (1974) demonstrated the preference for nitrogen impurities to form on (111) faces during growth of natural diamond over (100) faces. However, impurities such as opaque micro-inclusions (<1 µm) or micro-precipitates tend to develop on (100) faces (Lang *et al.*, 1992) (e.g. Fig. 7.3). Burns *et al.* (1990) found that sector dependence is a function of impurity type and temperature, among other variables.

Some other terms commonly used in literature to describe internal growth features are 'agate' structure, 'cellular' structure and sector zoning. Agate (Lang, 1974a; Zezin *et al.*, 1990) and cellular (Davies, 1998) structures are wavy, often finely laminated features. They are interpreted as having grown rapidly under fluctuating conditions and in the presence of fluids (Davies, 1998). Sector zoning (sectorial-growth) forms as a consequence of impurity partitioning between growth faces (Davies *et al.*, 1999; Lang *et al.*, 1992) (described in the preceding paragraph). Contrasting CL colours and/or

intensities for growth faces that formed contemporaneously are an indication of sector zoning. The crystal core in natural diamond is typically rich in impurities and often exhibits brighter CL colours (Harte et al., 1999; Bulanova, 1995). It may be rounded, or in some cases, exhibit a cross or 'X' morphology (commonly referred to as the 'Maltese cross', e.g. Lang et al. (1992) or the 'iron cross', e.g. Shigley et al. (1986)). (Figs. 7.5 and 7.6A). The rounded morphology of a diamond core is typically interpreted as being an indication of resorption. The centre of this core is often comprised of micro-inclusions of graphite (Bulanova, 1995) (e.g. black spots seen in Fig. 3.1A). Bulanova et al. (1996)

Fig. 7.5. SEM-CL image of diamond core. The dark grey sectors indicate growth on the (111) face while the lighter grey, curved and kinked sectors indicate growth developed on the (100) face. (reproduced from Bulanova et al., 2002).

propose that the impurities found at the genetic core lowers the nucleation barrier, thus facilitating diamond crystallization. The irregular morphology of diamond surrounding the growth seed may be cited as evidence for rapid growth under less stable conditions than for subsequent crystal growth (Davies, 1998).

The time it takes for natural diamond crystals to growth remains unclear. However, evidence suggests that diamond growth is a slow process and that it varies depending on which growth layers are developing. Well formed, parallel, fine scale laminations indicating octahedral growth are interpreted as signs of slow growth (Sunagawa, 1984b). Other evidence cited as indicators for slow growth are signs of both growth and resorption in the same diamond and hence fluctuating conditions (Davies, 1998) and variation in mineral inclusion chemistries and types from core to rim, also indicating changing conditions (Bulanova et al., 1995). Cuboid growth, in general, is interpreted as being an indicator of more rapid growth (Sunagawa, 1984b).

It is rather obvious that in order to examine the internal growth structure of diamond, a polished surface must cut through the crystal, thus intersecting different growth layers. And indeed, to examine all stages of growth, a plane must intersect the 'seed' or primary nucleation site. As well, thought should be given to the orientation of the cut, i.e., parallel to the (100), (111), or (110) face. Diamonds that exhibit remnant growth faces in their external morphology can be cut along particular planes. Typically, they are cut parallel to the (110) plane (e.g. Fig. 7.1) or the (100) plane (e.g. Figs. 7.3 and 7.6A-B). However, diamonds that are strongly resorbed (class 1 on the McCallum et al., 1994 resorption scale) or broken, often cannot be oriented in terms of their crystallographic axes. In the case of broken diamonds, it is merely a guess as to where the crystal core is located or if the diamond fragment even still contains the core. Diamonds which have experienced strong resorption and/or have been fragmented, are not the most suitable subjects for growth study. Diamond cuts may only intersect a few growth layers, if any, and will typically not intersect the diamond core.

There is still debate as to whether diamonds are metamorphic or fluid-derived, however, most evidence seems to be in favour of a fluid-derived origin. Sunagawa (1984b) uses the supersaturation level of carbon in a fluid or melt to describe the crystal habit (see section 2.1.1). The concentric oscillatory nature of growth pattern zonation in diamond is considered further evidence for a fluid or melt origin (Bulanova et al., 1995). However, Davies (1998) points out that similar zoning is reported in literature for regional and contact metamorphic minerals (e.g. Yardley et al., 1991). Brittle and plastic deformation is clear evidence that diamonds are surrounded by a solid medium at some time, either during or between episodes of growth. Fractured internal cores with euhedral rims and the truncation of growth structures by other zones indicate brittle fracturing and fine, parallel laminations are evidence for plastic deformation.

A polished surface often reveals the extensive and complex history of events, including multiple stages of growth, resorption, fracturing, deformation and changing

environmental conditions. The interpretation of these events in natural diamond is a difficult task. Examination of a polished surface, even when the diamond can be oriented in terms of crystallographic axes, often reveals very little. Even when internal growth morphology can be observed in CL, often it is too complex to describe, let alone interpret. With this in mind, and using Fig. 7.6 as an example, common internal growth features observed in natural diamond and their possible interpretation are as follows: 1) the seed and immediate core, usually the zone of brightest CL from which features radiate, sometimes in the form of a Maltese cross; 2) the rounded 'outer core', which is conventionally cited as evidence for dissolution, but has also been cited as evidence for cuboid growth (eg. Harte *et al.*, 1999) and non-planar growth in rapidly fluctuating conditions (Davies, 1998); and 3) the outer rim, where typically well-formed octahedral faces develop.

A)   B)
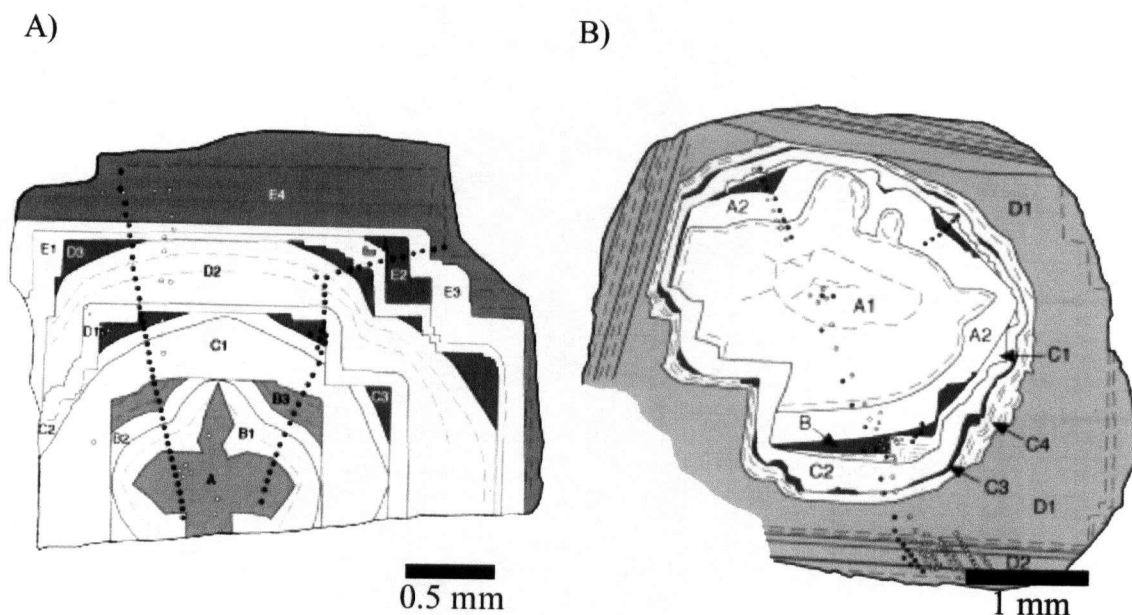
Fig. 7.6. Digitally enhanced CL images highlighting some typical internal structures observed in diamond. A) These regions are: A, the core (centre cross); B, cuboid growth layers; C and D, dominantly cuboid growth but bounded by octahedral faces; and E, dominantly octahedral growth. B) Growth regions are: A, B, and C, dominantly cuboid growth layers; D, dominantly octahedral habit. (black dots are ion microprobe analysis points). (reproduced from Harte *et al.*, 1999).

7.1.2 Infrared spectroscopy of polished diamond

Many CL studies of diamond include IR spectroscopy to measure the abundance of and distributions of impurities present (e.g. Davies *et al.*, 1999a; Davies, 1998; McKenna, 2001). IR data from the diamond core and subsequent growth bands can be used to say something about the diamonds residence temperature and time (discussed in detail in section 6.1.4). For accurate results, it is essential that the IR path through the diamond for each data point only intersect the growth zone of interest. This is accomplished by polishing two parallel, flat faces that are close together. The CL of both sides is examined to determine if and how the patterns match up. From these images it may be possible to select points that will only activate specific zones of interest. However, it is often difficult to polish diamond into thin plates. It is common for IR results to transect more than one growth zone and thus give results that are more qualitative than quantitative. It is important to consider the effects of sampling multiple growth layers when interpreting IR data from diamond plates.

7.2 Analytical techniques

The internal morphology of fourteen diamonds was examined. Thirteen large stones (0.056-0.404 g) were cut and polished and one small stone (0.006 g) with a reasonably flat fracture surface was studied. The selection process used for choosing which diamonds to polish essentially followed four steps. Firstly, all small grains were excluded because it would be difficult to analyse multiple points on the FTIR spectrometer; all diamonds classified as 'large' (Fig. 2.1) became initial candidates for internal growth studies. Secondly, diamonds with large inclusions that could potentially be lost during cutting and polishing were omitted. Thirdly, diamonds with discernable crystal faces were preferentially selected so that polished surfaces could be made parallel to known crystallographic orientations (i.e. polished surfaces parallel to the (100)). However, most grains were strongly resorbed (see section 2.3.3) or broken and irregular

in shape, thus making it difficult to instruct polishers how to orient the grains (for this reason most diamonds were polished in a random orientation). Lastly, a few grains containing abundant 'micro-inclusions' were selected in hopes that polished faces would expose at least some of the inclusions, thus making future inclusion analysis possible. Once cut and polished, the thirteen diamonds were examined under CL and seven of the most interesting grains (in terms of internal morphology) were returned so that a second parallel face could be polished on the opposite side to make diamond plates.

There was initial concern that the internal structures for diamonds polished at a random orientation would be difficult, if not impossible, to decipher. However, it was found that most diamonds revealed something about their growth histories and that orientation was not such a concern. Study of highly deformed diamonds from Eastern Australia by Davies *et al.* (1999b) found that the 'knotting' effect of the deformation seams made it difficult to cut along a preferred crystallographic face. They found that polishing stones in a random orientation was not critical to deciphering the growth morphology. The abundant deformation laminations observed on diamonds in this study (section 2.3.7) suggests that similar problems would likely be encountered if grain orientations were specified for all stones.

The 14 diamonds were examined using a Cambridge Instruments Cathode Luminescence (CITL 8200 mK4) system described in greater detail in section 5.2. Diamonds were thoroughly washed with ethanol before mounting in carbon putty. Grains were embedded in putty so that the polished surface was flush with the putty surface. Carbon putty was used so as to minimize internal luminescence and to avoid charging the outside of the crystal. CL images were collected using a Nikon Coolpix 995 digital camera.

IR data was collected and processed following the procedures outlined in section 6.2. Precision of the method is outlined in section 6.2.2 and MDL's are listed in Table 6.3. The main difference between examination of whole rough stones and polished surfaces is

the need to accurately locate the IR points on the diamond. This was accomplished by taking photographs of diamonds under both a conventional microscope and CL microscope. Images were combined, making it possible to locate points of interest during IR transects. Aperture size varied but was generally less than 200 µm. Diamond thickness (optical path length of transmitted radiation) was determined using the absorption coefficient calculated by Taylor *et al.*, (1990) measured at 2030 cm^{-1} (0.47 ± 0.01 units per mm path length).

7.3 Results

The results of CL and IR examination of seven diamond plates, six polished diamond surfaces, and one fractured stone are presented below. Each diamond is discussed separately in terms of growth mechanisms and how nitrogen and hydrogen character varies across different growth zones. A CL photograph of each diamond is included as well as an IR transect indicating data points. A summary of IR results (total nitrogen concentration, percent aggregation and relative hydrogen concentration) is also included for each stone (diamond 2-11 only includes hydrogen results). The results and interpretations are summarised in Table 7.1 (section 7.4.1).

7.3.1 Diamond 1-2

Diamond 1-2 is a strongly resorbed colourless fragment that possesses weak to moderate blue CL with some evidence for oscillatory zoning (Fig. 7.7). No particular orientation was specified for polishing. The centre of the fragment does not appear to have been intersected with polishing and likely exists towards the top of the image where CL intensity is highest, possibly at depth in the remaining portion of the stone (below points 27-29). Fine growth layers are visible in two places, near the bottom left of the image and near the top. The fine layers near the bottom left are highly irregular, rounded forms

94
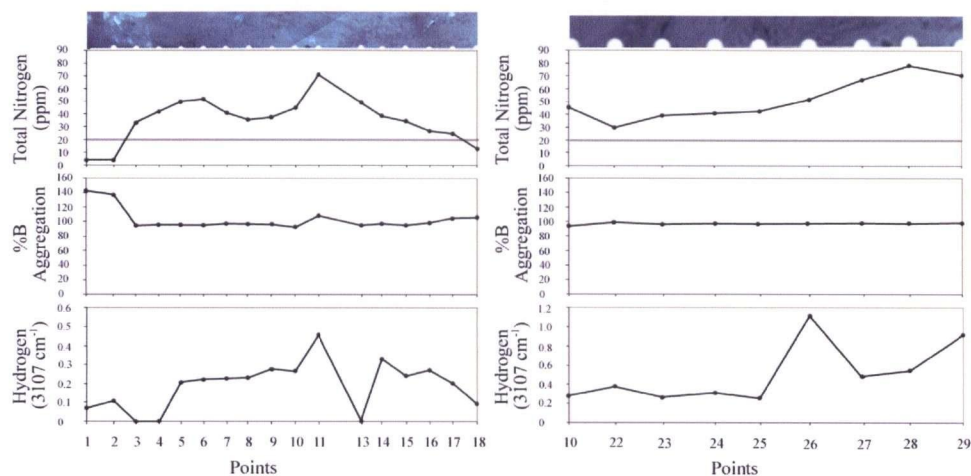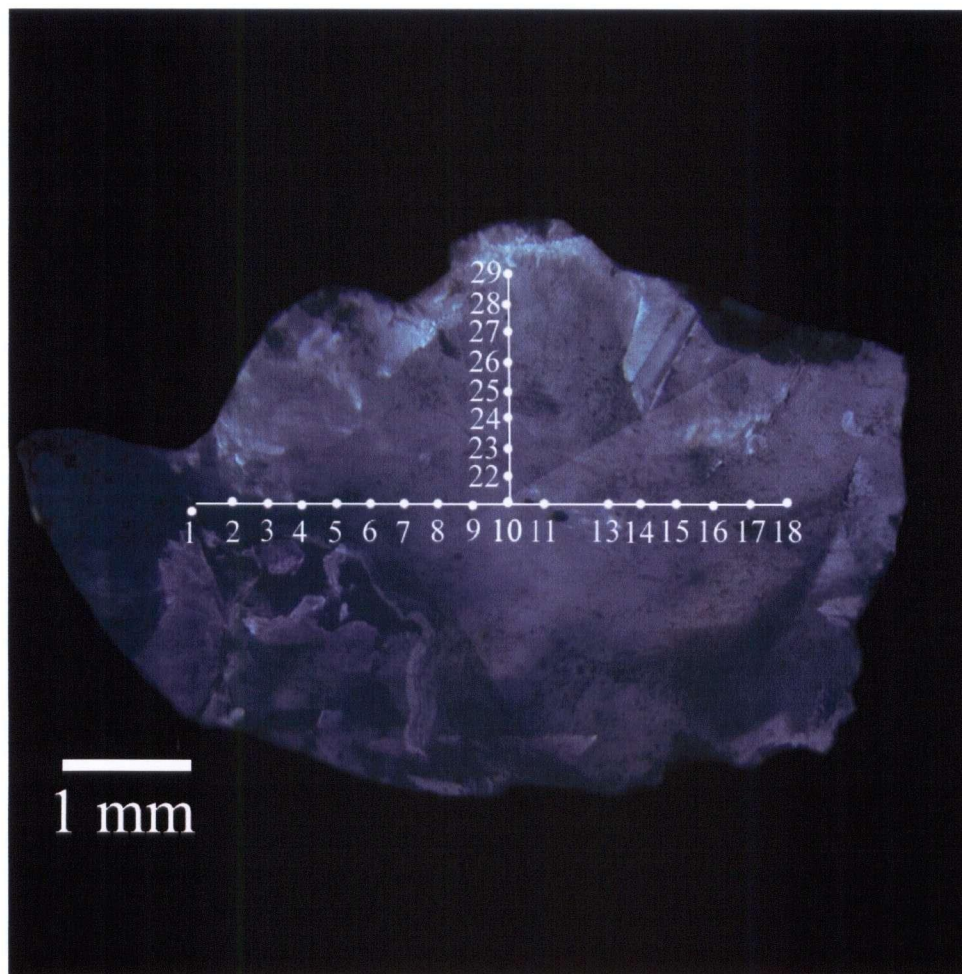
Fig. 7.7. Image of CL of diamond 1-2 with IR data for transects 1 to 18 and 10, 22 to 23. This diamond exhibits weak to moderate blue CL. A fracture surface is visible along the top edge and the crystal core is likely below point 28. Octahedral zoning forms around the bright core while 'agate' zoning forms further from the diamond core (bottom left). Minimum detection limit (MDL) for Total Nitrogen is represented by grey line at 20 ppm. MDL for relative hydrogen concentration is too low to be indicated on graph (listed at 0.03 absorption units in Table 6.3. %B Aggregation for points listed as below MDL for total nitrogen concentration are meaningless.

that appears similar in morphology to 'agate' structure. It is unlikely that these rounded forms be attributed to resorption as dissolution is usually an uneven process which should lead to the formation of cross-cutting structures. They are most likely features of growth, however, their crystallographic nature is unclear.

Flat oscillatory zoning faintly observed near the top of the image is brightened and enlarged in Fig. 7.8. Because of the straight morphology of the bands, this growth pattern is interpreted as indicative of octahedral
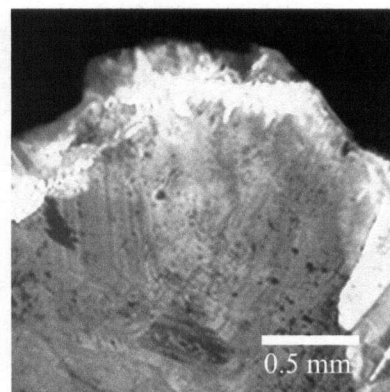
Fig. 7.8. Close-up greyscale CL image of diamond 1-2. Oscillatory zoning with straight boundaries is interpreted as forming on paleo-octahedral faces.

growth. The crystal core appears brighter blue, but is too blurred for a detailed interpretation. Nitrogen concentration, aggregation state and relative hydrogen peak concentration are presented at the bottom of Fig. 7.7 for two traverses, one from points 1 through 18 and the other from 10 and 22 through to point 29. Nitrogen concentrations range from ~0 to 80 ppm while the aggregation state is essentially pure IaB. For the first traverse, nitrogen concentrations generally increase towards the middle, peaking at point 11 (~70 ppm total N) and then decreasing again to point 18 at the edge of the fragment. The impossible totals (130-140 %B) for points 1 and 2 are due to the large error associated with low nitrogen totals. The relative hydrogen concentration peak mimics the total nitrogen curve extremely well, with the exception of points 3, 4 and 13. The second traverse starts close to where the first traverse peaks in total nitrogen. CL intensity increases towards the top of the image where the second traverse terminates. Total nitrogen concentration gradually increases and peaks at point 18 (80 ppm total N). The relative hydrogen concentration curve also mimics the total nitrogen curve well (for traverse 10, 22-29), with the exception of point 26.

The stone is considered type IaB although it gradually becomes void in nitrogen (type II) towards the fragment edges. Total nitrogen concentration gradually decreases from ~80

ppm (type I), likely near the crystal core which is interpreted to be somewhere under the points 27-29, to practically 0 ppm (or type II) at the edges. "A" centres are absent in this crystal, suggesting it experienced either extremely high temperatures or long residence times at moderately high temperatures. The growth structure is interpreted to be octahedral (at least near the core) with 'agate' zoning further away from the growth centre. There is a clear correlation between CL colour and nitrogen concentration as CL colour intensity is strongest where nitrogen concentrations are highest and weakest where nitrogen concentrations are low.

7.3.2 Diamond 1-4

Diamond 1-4 is a non-uniformly coloured stone (brown and colourless) with a peculiar shape, having dimensions 6.0 x 5.5 x 1.25 mm. Both sides were polished (with no particular orientation specified) on this grain, making the plate ~1.3 mm thick, although very little material was removed in the process. CL examination of both sides reveals a very interesting yet complex growth structure (Fig. 7.9). To facilitate comparison between both sides, all images of side B have been flipped horizontally so they could be overlaid. CL colours vary slightly from side A to B however this is only an artefact of the digital camera used to capture the images. The colours are certainly lighter blue (turquoise) than most CL colours observed for Rio Soriso diamonds. There is a remarkable contrast in CL intensity, with some sections of the stone being bright turquoise while others show no evidence of CL. The core of the crystal is likely contained with the remaining polished fragment where the most intense turquoise CL is observed, which is also where the brown colouration is found, as observed under optical microscope. Three or four 'arms' with bright turquoise CL radiate outwards from the crystal core and are separated by diamond that does not CL. There is a rim of diamond that possess bright turquoise CL (best observed at the bottom right of Fig. 7.9 (side B). The cross section A-A' shows a slice orthogonal to the polished surface of one of the arms.
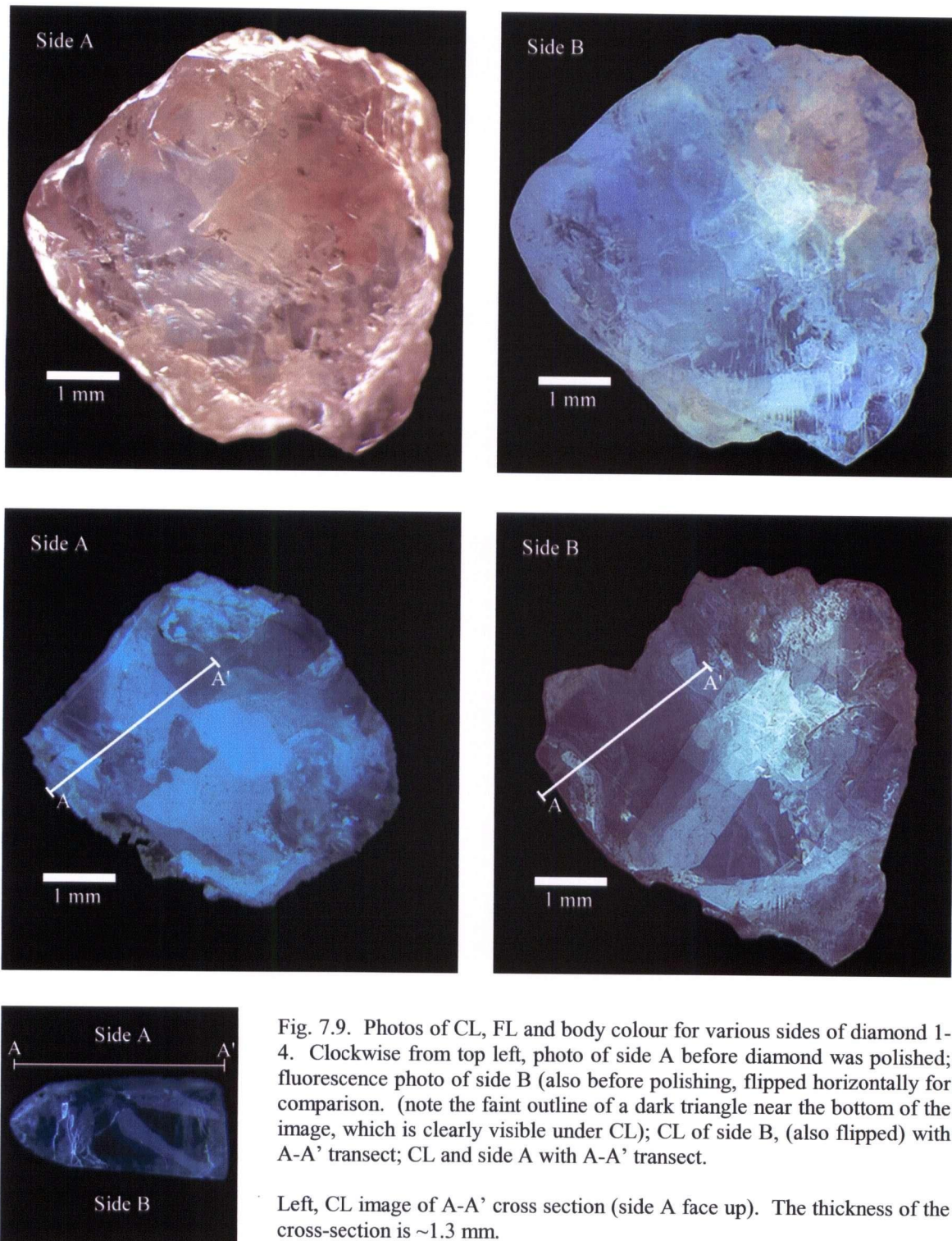
Fig. 7.9. Photos of CL, FL and body colour for various sides of diamond 1-4. Clockwise from top left, photo of side A before diamond was polished; fluorescence photo of side B (also before polishing, flipped horizontally for comparison. (note the faint outline of a dark triangle near the bottom of the image, which is clearly visible under CL); CL of side B, (also flipped) with A-A' transect; CL and side A with A-A' transect.

Left, CL image of A-A' cross section (side A face up). The thickness of the cross-section is ~1.3 mm.

98
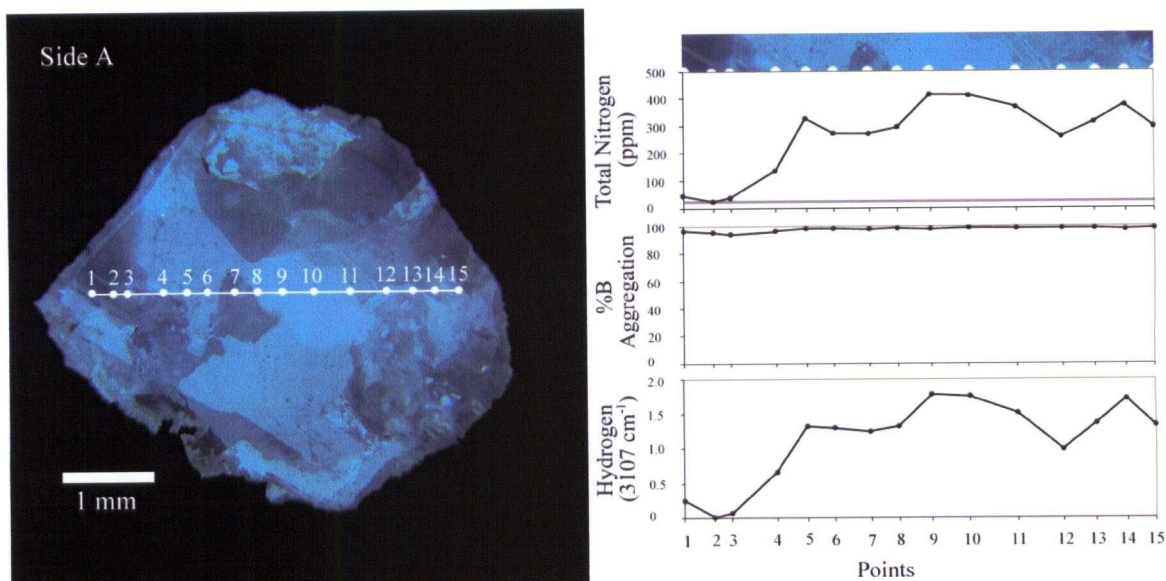
Fig. 7.10. Image of CL of diamond 1-4, side A, with IR data for transect 1-15 across polished surface. Two triangular shaped arms are visible radiating from a bright core, one radiates to the left and the other towards the bottom.

A CL image of side A including transect 1-15 with accompanying IR data can be seen in Fig. 7.10. Nitrogen concentration varies from ~20 to over 400 ppm. This is a considerable range in concentration and highlights the potential errors in collecting 'bulk' IR data from one point in a diamond. There is a clear correlation with total nitrogen concentration and CL intensity, with high nitrogen totals corresponding with the triangular arm and the diamond core. Total nitrogen concentration decreases from core to rim although the 'arms' certainly introduce a complex geometry. When present, nitrogen is only in the form of B aggregates. There is a remarkable positive correlation between the relative hydrogen and total nitrogen concentrations.

The CL pattern observed is complex. There are sections where flat, parallel faces exist, thus indicating octahedral growth. However, most of the stone exhibits either homogenous turquoise CL (the majority of the core and radiating arms), or homogenous dark CL (type II) diamond, revealing little in the way of growth type. It has a similar appearance to sector-dependence growth for cubo-octahedral diamonds, described in section 7.1.1. If this was the growth mechanism, then the turquoise arms would indicate

octahedral growth while the dark zones would indicate cuboid growth. The dissolution seen in the top portion of the image (starting just above point 8) appears to truncate the nitrogen-rich arm.

Deformation laminations were observed on this diamond during characterization of physical features (see SEM image Fig. 2.26B). Plastic deformation is visible in the large triangular shaped arm of side A, recognized by the three sets of intersecting parallel lines (Fig. 7.11).
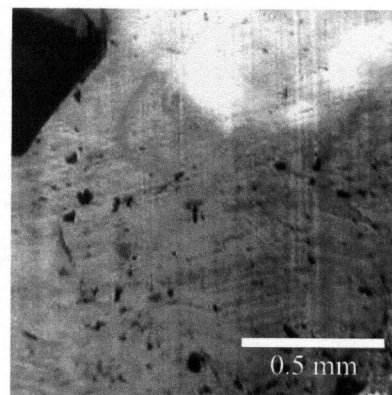
Fig. 7.11. Greyscale photograph of deformation laminations observed under CL. Close-up of Fig. 7.10, side A. (Compare with Fig. 2.24D of SEM image of deformation laminations).

The CL pattern of side B with two accompanying IR data transects can be seen in Fig. 7.12. Transect 1-14 will be discussed in reverse order as it is presented, from left to right, in Fig. 7.12. The transect does not intersect the diamond core and does not reach the highest vales collected for points 9 (side A) and 19 (side B). The maximum value is recorded at point 7 (~375 ppm total N) with minimums at points 3 and 13 (<~75 ppm total N). The aggregation state is pure IaB. The positive correlation between total nitrogen and relative hydrogen is, again, quite remarkable. Transect 15 to 24 follows one arm from the diamond edge to the core. Total nitrogen concentration increases slightly, peaking at point 19 at ~400 ppm N. The same positive correlation between hydrogen and total nitrogen concentration is evident.

Growth patterns with straight, parallel morphology (suggesting octahedral growth) are evident in many parts of the image. The enclosed type II triangle is quite interesting. The CL image of side B suggests sector growth (as did the CL image of side A). There are growth bands on the left side of one 'arm' (at point 8) that appear to grow into the area of type II diamond. This implies that the diamond was hollow and grew inwards. This is in contrast to the direction of growth band laminations that are visible in sector-

100
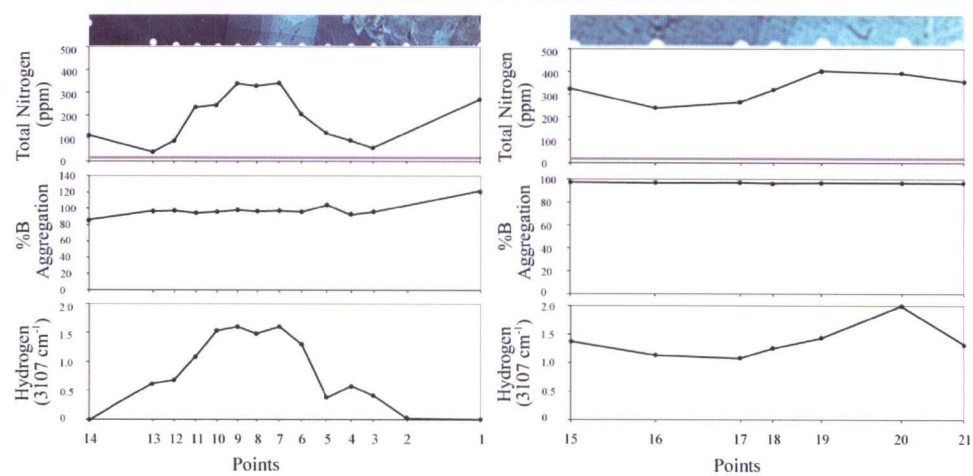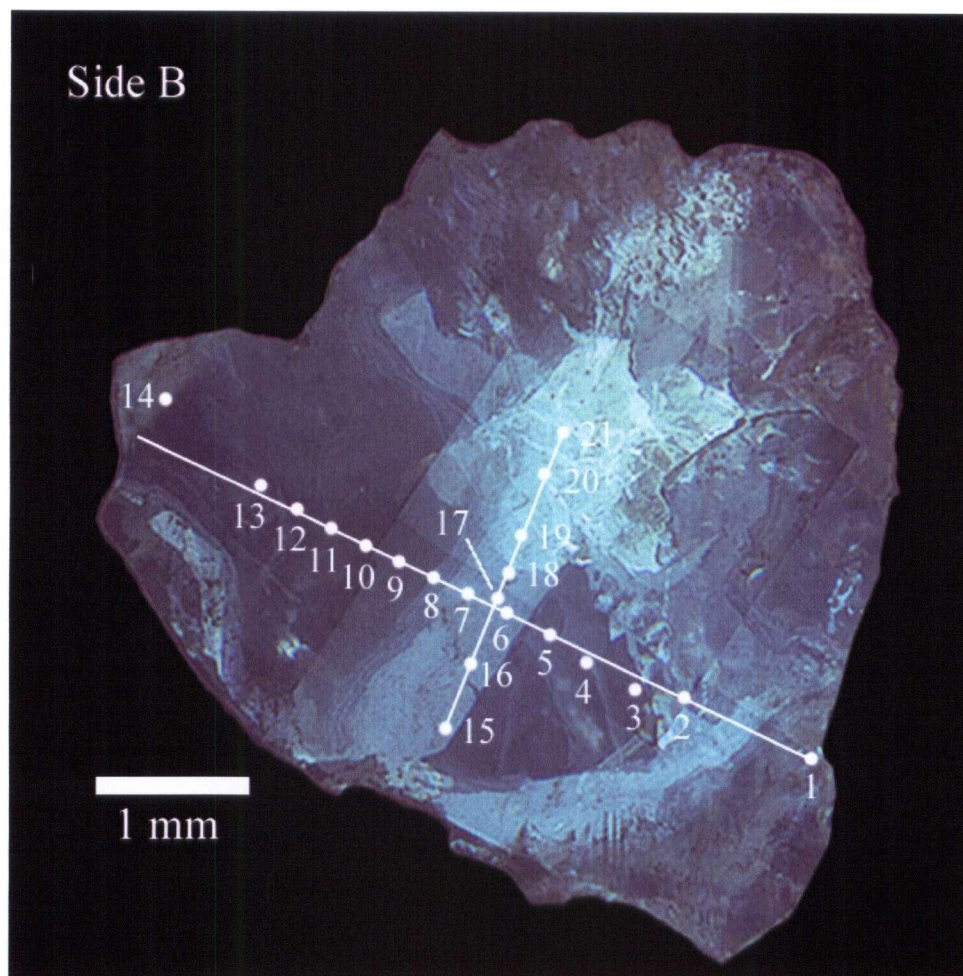
Fig. 7.12. Image of CL of diamond 1-4, side B (flipped horizontally), with IR data from transects 1-14 and 15-21.

101

dependence growth for diamonds in Figs. 7.3-7.4. Dissolution may be visible near the outer margin of the crystal (bottom left and right), truncating a bright turquoise zone. There is a rim of diamond with bright turquoise CL (bottom of Fig. 7.12).

This diamond is considered type IaB but has a marked variation in nitrogen concentration, ranging from 20 to ~400 ppm. Any nitrogen occurs as 100% B centres. The core of the diamond is too blurred and bright to reveal any detailed morphology, however, it is clearly the richest zone in nitrogen and other brownish coloured impurities. Growth development on the core is most likely cubo-octahedral, with octahedral layers soaking up all available nitrogen (the bright turquoise arms) and cuboid layers (dark regions) containing little nitrogen. The enclosed triangle (bottom of Fig. 7.12, side B), formed either cuboid growth as a result of a sudden cessation of growth, or the diamond experienced partial resorption, after which only octahedral growth prevailed. One unresolved matter is that fine growth bands are visible parallel to one growth arm (below point 8 on side B of Fig. 7.12). If cubo-octahedral growth developed, growth bands should be perpendicular (i.e. concentric from the core) as oppose to radiating. At some point in time the diamond experienced deformation (syn or post growth) and brittle fracturing.

7.3.3 Diamond 2-1

Diamond 2-1 is a colourless grain interpreted to be an aggregate of two crystals (Fig. 7.13). The two individual crystals are separated by what appeared to be a fracture (crosses transect at point, Fig. 7.14). It was believed that the diamond was an aggregate before CL examination because etch pits on either side of this fracture were at orientations that could not be explained if they belonged to one crystal. The grain

Fig. 7.13. Photograph of polished surface of diamond aggregate (Diamond 2-1). Note fracture dividing crystal into two (irregular white line).

102

was chosen for growth study because of this hypothesis and was polished into a 2.7 mm thick diamond plate. The diamond contains numerous small, dark inclusions. CL examination of the image reveals that there is a growth centre on the right side of the 'join' but there is no discernable centre on the left side. CL colour is weak to moderate blue (image is brightened for clarity of features), typical of most stones in this study. Brighter green/turquoise CL is visible at the top of the image and is likely late diamond crystallization on the aggregate. There are several fractures with intense CL observed in the stone, one being clearly visible below point 5 (Fig. 7.14). The crystal on the right exhibits three concentric layers, a bright core, a weak shell and then a brighter outer shell. The bright core appears cloudy in Fig. 7.13 and may be comprised of numerous small
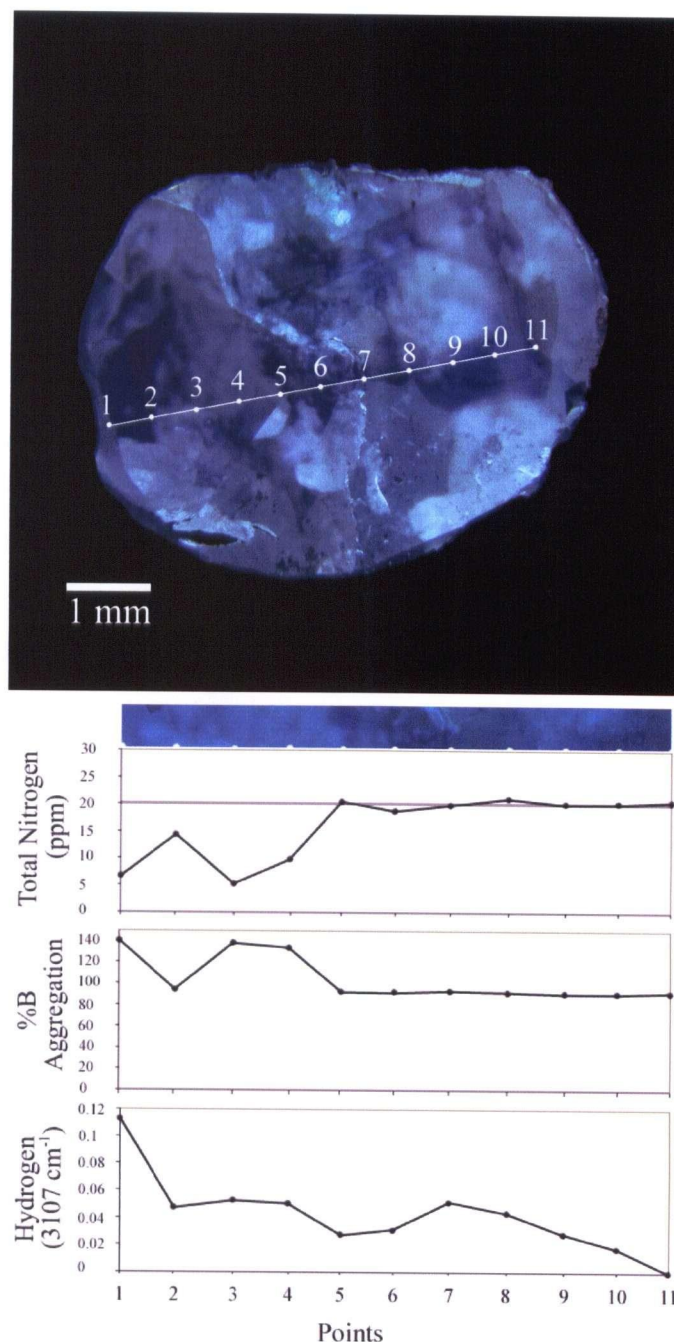
Fig. 7.14. Fig. 7.14. Image of CL of diamond 2-1 with IR data for transect 1 to 11. Diamond is an aggregate of two crystals, core of right crystal is clearly visible above point 9. Growth structures for the crystal on the left are absent. The two crystals are joined along the irregular line that intersects transect near point 7.

103

fluid inclusions (Navon *et al.*, 1988). The boundary between the weak and bright outer shell is irregular in shape. Growth patterns to the left of the join are not so clear. The core of this grain may be near the edge below point 1 where the most intense CL is observed. Irregular growth lines between brighter and darker zones are also visible, although not as well developed as on the right half. It is unknown if the irregular boundaries are a result of growth or dissolution.

IR data for the transect across this aggregate (points 1 through 11), unfortunately, does not intersect the zones of brightest CL, particularly the bright core on the right half. There is effectively no absorption in the one-phonon range, although deconvolution calculates ~5-20 ppm total nitrogen. Detailed examination of IR spectra reveals that there is possibly some nitrogen in the form of B centres, however, this diamond should be classified as type II. It is possible that there are detectable amounts of nitrogen in the crystal core on the right half.

This grain is an aggregate of two crystals, one with probably a more nitrogen-rich core but as a whole, is considered type II and the other crystal, with fewer visible growth structures, is also type II. The mechanism of growth is uncertain. Certainly the diamond experienced an episode of resorption to create the rounded overall rounded morphology, however, it is unclear if the diamond experienced episodic periods of dissolution during growth.

7.3.4 Diamond 2-2

Diamond 2-2 is a large (6 x 5.5 x 2 mm), strongly resorbed, broken, pink crystal that was polished in a random orientation. CL colours are turquoise blue and somewhat brighter than most diamonds in this study. There is one localized section with yellow/green CL found near the top middle of the bright blue CL zone and it is possible that this region is
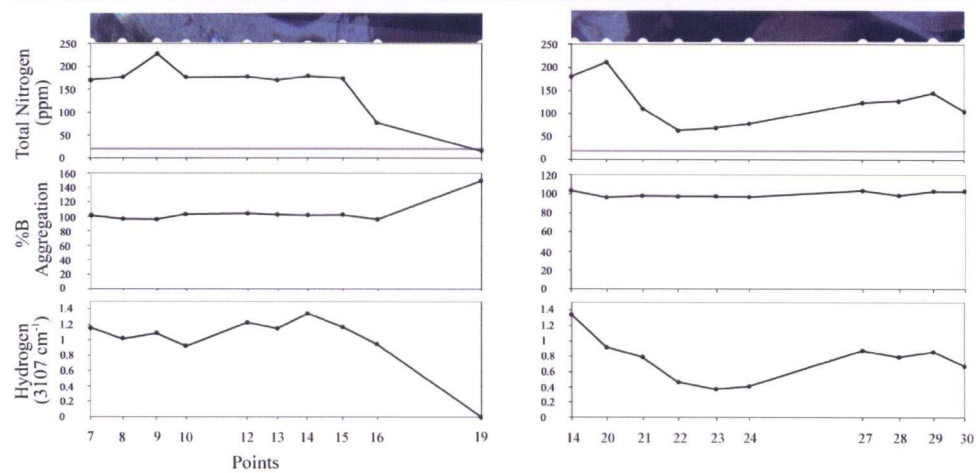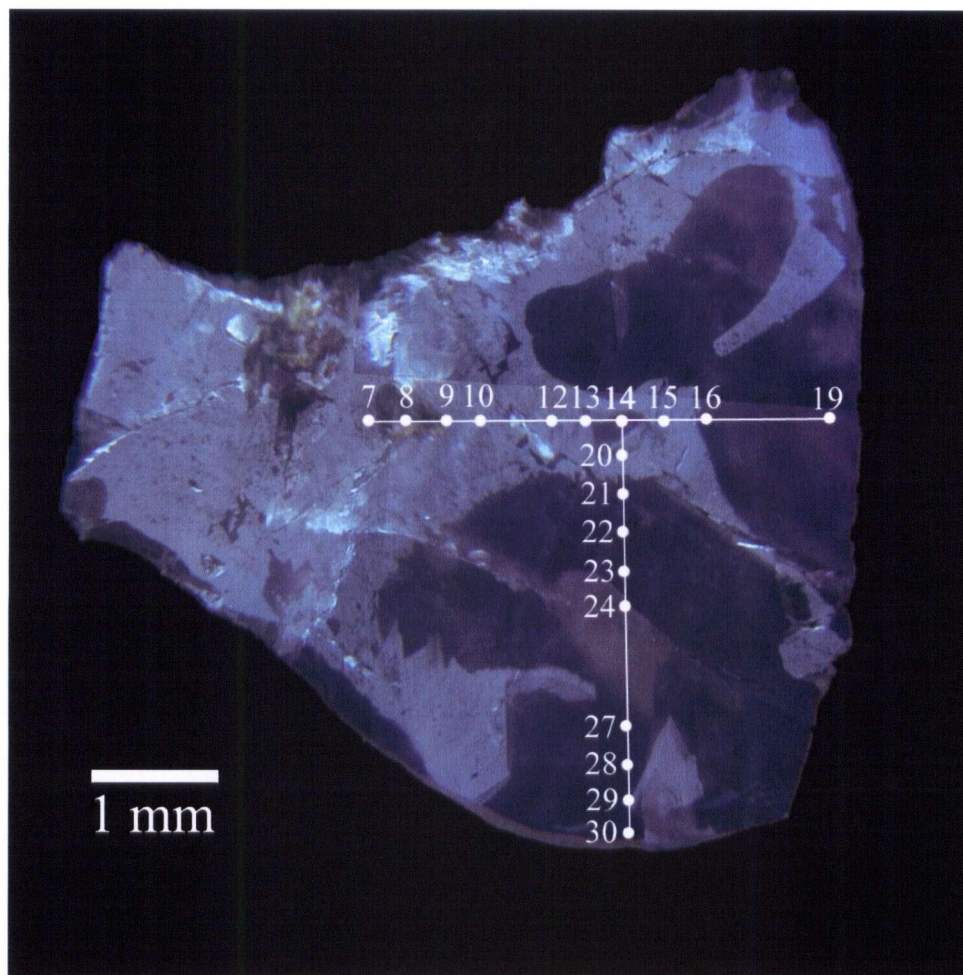
Fig. 7.15. Image of CL of diamond 2-2 with IR data for transects 7 to 19 and 14, 20 to 30.

the core of the crystal (Fig. 7.15). There are essentially only two zones visible, one with bright CL and the other without CL. The bright CL zone is complex in shape and is generally irregular and smooth, but in some places has straight, angular edges (e.g. top right of Fig. 7.15). It is possible that there has been some brittle deformation as is suggested by the 'floating island' of bright CL above points 16 and 19. The contrast in bright and dark zones suggests sectorial dependence of impurity uptake (and thus cubo-octahedral growth), however, the morphology is too complex to conclusively draw this conclusion.

Transect 7-19 follows along an arm, likely starting near the crystal core. Attempts were made to analyse points to the left of 7, but no spectra could be obtained, likely a as result of the large number of fractures in this part of the diamond. Total nitrogen concentrations range from 25 to ~225 ppm and the aggregation state is 100% B centres. Nitrogen concentration remains roughly constant (~175 ppm total N) until points 16 and 19, where the concentration drops considerably (~25 ppm total nitrogen at point 19). There is a positive correlation between relative hydrogen and total nitrogen concentrations. Transect 14, 20-30 starts on the bright blue CL arm and crosses a zone that does not CL. Nitrogen concentrations range from 50 to ~200 ppm total nitrogen, all as B centres. The minimum nitrogen concentration is reached at point 22 and steadily increases towards point 29 (~150 ppm nitrogen). It is possible that the low CL intensity zone that this transect crosses is pseudo-semispherical in shape and that the bright CL arms seen in the middle (along transect 7-19) and the arm seen at the bottom, are joined at depth. The CL of the opposing side of the diamond was examined but was inconclusive towards elucidating the three dimensional morphology of the growth structure. Again, relative hydrogen concentration correlates positively with the total nitrogen concentration.

This diamond has nitrogen free zones, however, the majority of the crystal appears to be relatively nitrogen-rich for the suite of Rio Soriso diamonds. It is a type IaB stone with

zones of type II diamond. The growth structure may indicate sector dependence, and hence cubo-octahedral form. However, there is no clear evidence indicating cubo-octahedral growth, and as such, the internal structure will be classified as complex. The crystal core may exhibit a yellow/green CL, but this is not certain – this zone is more likely contamination of a fracture. The crystal experienced brittle deformation before diamond growth was complete.

7.3.5 Diamond 2-5

This diamond is a large (7 x 6 x 5 mm) grey fragment that has experienced little resorption and contains numerous small dark inclusions of an unknown phase. No particular grain orientation was specified for polishing. CL colours are weak to moderate blue, although there are many short lines of brighter CL centred on these small inclusions (Fig. 7.16). These small bright lines are interpreted as stress fractures around inclusions and should be ignored when interpreting growth zones. The polished surface is essentially homogenous blue, with one exception near points 10 and 11 where crystal CL is absent. The boundary between the CL absent and weak blue CL zones is straight,
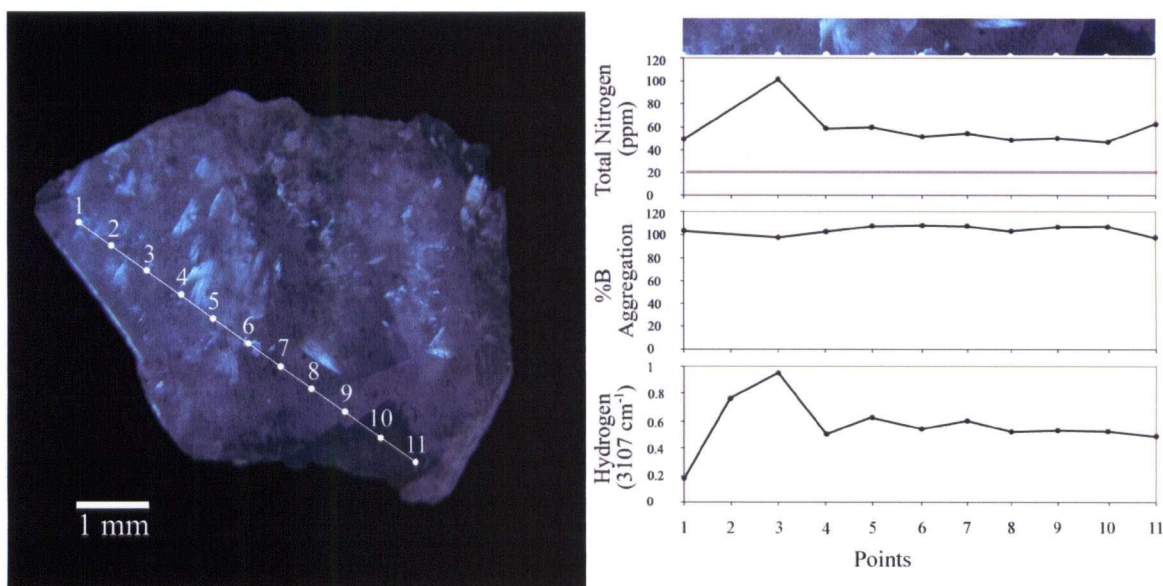
Fig. 7.16. Image of CL of diamond 2-5 with IR data for transect 1 to 11. Note the numerous bright blue CL lines (interpreted to be stress fractures associated with inclusions). Also note the region by points 10 and 11 that has weak CL.

indicating octahedral growth, with orthogonal bends. It is not clear where the crystal core is in relation to the polished surface.

Nitrogen concentration variation along the transect ranges from 50 to ~100 ppm while the aggregation state remains constant at 100% B centres. The nitrogen characters measured at points 10 and 11 in the CL absent zone are essentially the same as for all other points, which likely reflects the thickness of the polished diamond (1.9 mm) and that the results for each data point are more of a bulk IR character. The total relative hydrogen concentration correlates positively with the nitrogen concentration. A peculiar absorption pattern was observed near 1048 cm^{-1} for most of the spectra collected (described in section 6.3.3 and referred to as impurity "X").

Diamond 2-5 is a type IaB crystal which, at least in part, grew by the mechanism of octahedral growth. The absence of numerous growth bands may be a function of the plane of polishing, or, may possibly be an indicator of more rapid crystallization.

7.3.6 Diamond 2-8

Diamond 2-8 is a grey fragment with a complex external morphology that was described as 'unknown'. It contains abundant graphite inclusions and was polished in a random orientation. CL colours for this stone are moderate blue with a thin (less than ~100 μm) coat of bright green/yellow CL (clearly visible on CL image of opposite side, inset top left, Fig. 7.17). There are also several localized zones on bright green/yellow CL but their association is not clear. The diamond contains abundant small inclusions (interpreted as graphite), one large one of which is visible below point 5. The strange pale green appearance of the stone on the top right is an artefact of the CL machine. The only growth zone visible is the thin coat on the stone.
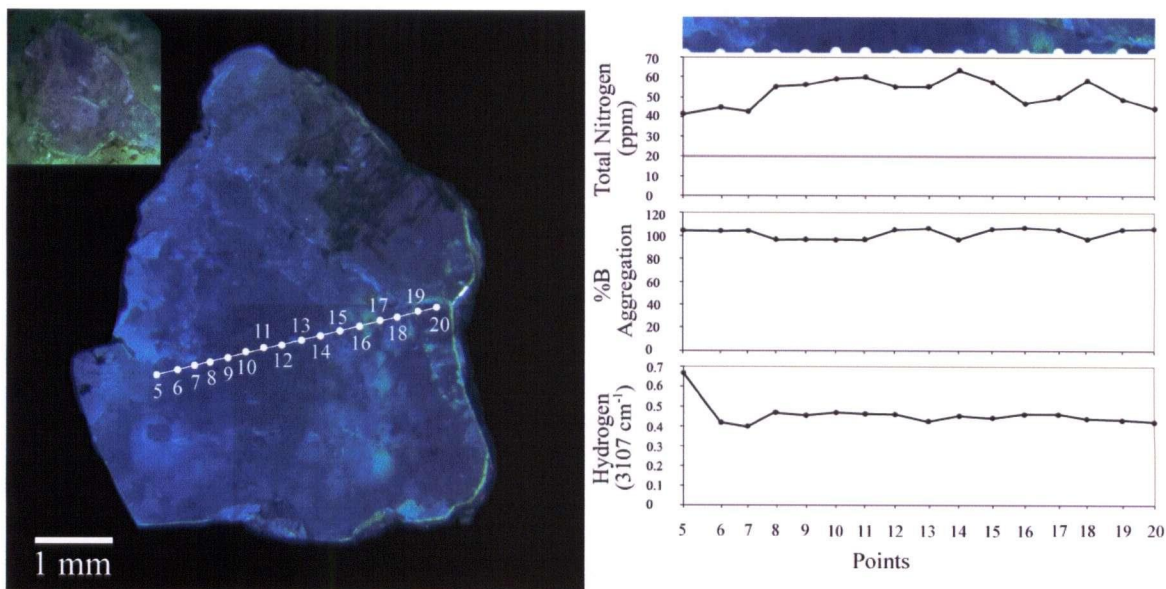
Fig. 7.17. Image of CL of diamond 2-8 with IR data for transect 5 to 20. Inset is CL photo of opposite side (scale of inset is ~2.0 mm across).

Because the CL colours are relatively homogeneous across transect 5-20 it is not surprising that there is little variation in nitrogen character. Total nitrogen concentrations vary from 40 to 65 ppm while the aggregation state is 100% B centres. There is a positive correlation between relative hydrogen and total nitrogen concentrations.

This diamond is type IaB with a thin coat of bright green/yellow diamond that is too thin to analyse with IR but is likely a late stage growth layer on the stone, made up type IaAB or IaA diamond. The growth habit of this stone is unclear.

7.3.7 Diamond 2-9

Diamond 2-9 is a large (6.5 x 5 x 2.5 mm) broken stone that is strongly resorbed. It was polished in a random orientation. The stone is greyish in colour and contained several inclusions, one of which had an orangey-red halo (later revealed during diamond cracking to be an altered inclusion). A fracture crosses the middle of the grain and crosses the transect near point 15. The two sides of the fracture may have different origins as fluorescence of the grain reveals that one half is bright blue while the other half is faintly blue (Fig. 7.18). CL colours are moderate to bright blue with the brightest
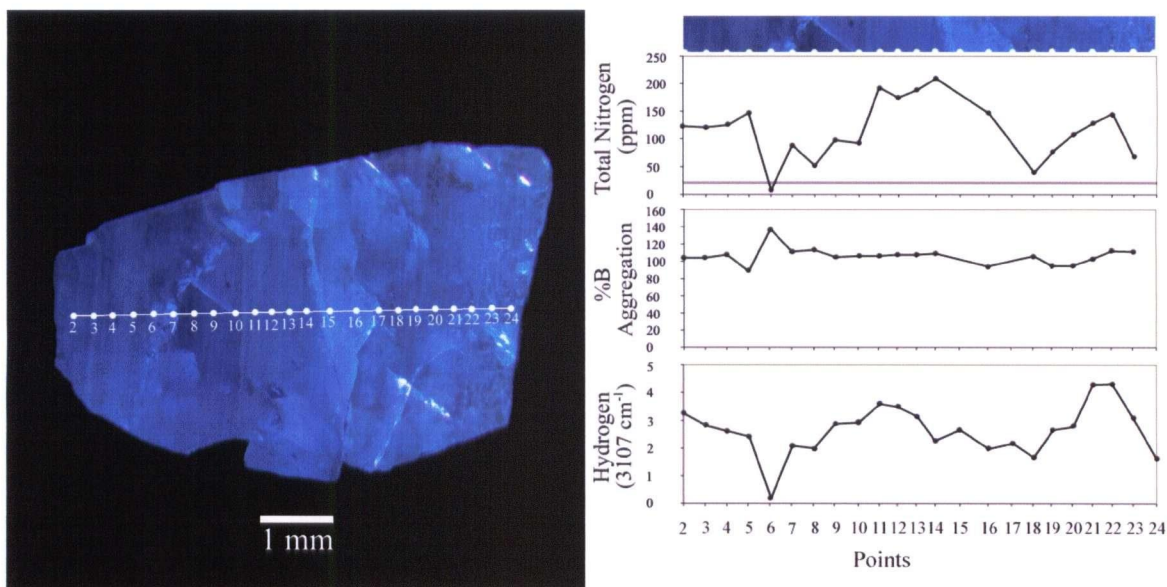
Fig. 7.18. Image of CL of diamond 2-9 with IR data for transect 2 to 24. The bright blue cross-cutting linear features are fractures. One fracture transects the stone completely, crossing at point 15. FL of diamond reveals heterogeneous character of halves bisected by fracture, one half possess bright blue FL while the other does not fluorescence.

sections of the surface being reflections in the many fractures. Deformation laminations occur as numerous parallel lines, seen as sub-vertical lines on Fig. 7.18. Signs of plastic deformation were visible on the resorbed surfaces of the crystal. The relative position of the crystal core to the polished surface is unclear.

IR data collected across transect 2 to 24 was often of poor quality and contained an absorption of unknown origin in the one-phonon range. The abundant fractures are likely the cause for any poor data and perhaps secondary material in fractures is responsible for the anomalous one-phonon absorption. Nitrogen concentration across transect 2 to 24 ranges from ~0 to ~200 ppm with all nitrogen in the form of B centres. There is a positive correlation between relative hydrogen and total nitrogen concentrations.

This diamond is type IaB with an unknown growth habit that experienced plastic deformation. It is unclear how large the original crystal was before fragmentation.

110

7.3.8 Diamond 2-11

This heterogeneous grey/colourless crystal fraction is 5.5 x 5 x 3 mm in size and has an unidentifiable crystal form. It was quite angular in surface topography and contained abundant tiny inclusions which turned out to be sulphides (see section 8.3.1.7). The grain was returned for a second parallel polished surface but was found to be too difficult to polish. As such, the grain was irregularly shaped and had only one polished surface, making it extremely difficult for the collection of decent IR data. The abundant inclusions, the almost opaque dark grey regions, and the grain thickness (~2.7 mm) further complicated matters. A straight transect across the polished surface was not possible, and data was collected for points wherever possible. The CL of this diamond is intriguing, with alternating zones of blue and yellow CL colour (Fig. 7.19).

IR data reveal an unusual absorption pattern in the one-phonon range that looked similar in shape to type IaAB diamond. The deconvolution program was able to fit curves to some of the spectra but the residual curves were large (except in the case of point 23, which clearly has both A and B centres). As such, deconvolution results are not included in Fig. 7.19. The total nitrogen concentration for point 23 is 72 ppm with an aggregation state of 60% B centres. Other points appear to contain significantly more nitrogen (e.g. point 19, Fig. 7.19), but the spectra for these points were very noisy. The calculated total relative hydrogen concentrations are included in Fig. 7.19 as their measurement was not obscured by the noisy one-phonon absorption. Hydrogen concentrations seem to increase from points 22 - 20 (note that points are not in numerical order), but are relatively low.

The growth patterns observed on this polished diamond are complex. Numerous alternating bands of yellow and turquoise CL, generally with straight bounding faces, are cross-cut by both turquoise and yellow CL bands. The straight nature of many bounding surfaces suggests that growth was octahedral, but numerous cross-cutting features are more typical of growth in the (100) direction. Fracturing and re-growth or annealing are
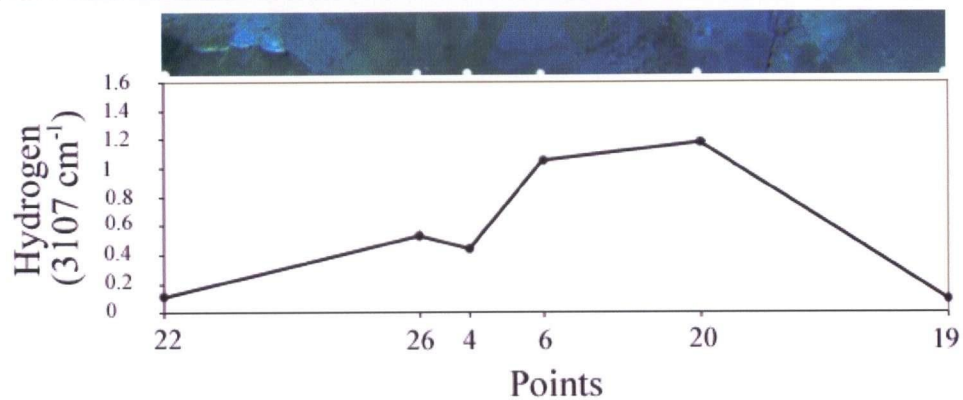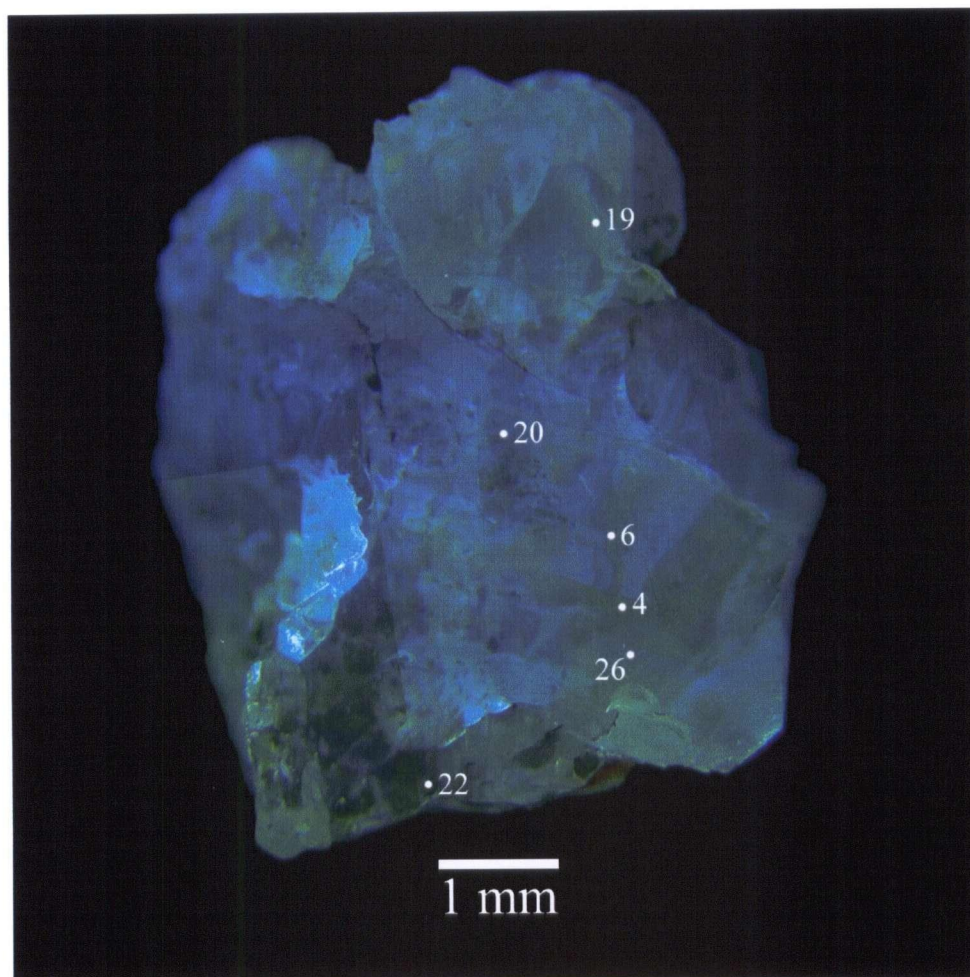
Fig. 7.19. Image of CL of diamond 2-11 with IR data for transect points indicated. Results for the nitrogen character are not included as spectra in the one-phonon range are generally noisy.

possible mechanisms for the generation of such a complex morphology. However, the preferred explanation is that the crystal was initially comprised of diamond with blue CL that was subsequently plastically deformed creating the bands of yellow CL, which are crystallographically controlled. Davies (1998) observed yellow CL in several diamonds from Eastern Australia and interpreted its presence as being a result of plastic deformation.

Diamond 2-11 is the only diamond of the Rio Soriso suite to contain abundant D centres (as calculated by the deconvolution program) and B' absorption at 1360 cm^{-1} (Fig. 7.20). This may be the only *regular* (as defined in section 6.1.2) diamond in this study. However, there is some uncertainty as to the cause of absorption at 1360 cm^{-1} because of the abundant noise. In all likelihood abundant D centres (platelets) are present in this diamond (as oppose to the rest of

Fig. 7.20. IR spectrum from point 19 showing large B' peak (Diamond 2-11). Total nitrogen concentration calculated at ~500 ppm with ~90% B centres. D centre concentration ~1.6 a.u.

the diamonds in this suite that have experienced platelet degradation) making this stone unique. The presence of A centres indicates that at least part of this diamond was not subjected to the extreme temperatures and/or lengths of time that are typical for most diamonds of this suite.

At least part of this diamond is type IaAB (~70 ppm N of which 60% are B centres) with portions that likely contain considerably more nitrogen (i.e. point 19). The reason for the different CL colours is unclear. They may reflect different chemistries (i.e. the yellow CL zones may contain nitrogen of mixed character (type IaAB) while the blue zones may be more highly aggregated (closer to type IaB)) or they may reflect localized plastic deformation. This crystal has experienced some growth on octahedral faces, but the details of its history are certainly more complex.

7.3.9 Diamond 3-1

This diamond is the largest stone for study, weighing 0.404 grams. It is fully intact, strongly resorbed, exhibits a non-uniform colourless/brown hue, and shows signs of plastic deformation. Two surfaces were polished approximately parallel to the (100) face, making a plate ~3.4 mm in thickness. It was possible to orient this diamond for polishing even though the grain was so rounded because of the etching pits visible on the crystal surface. The diamond has moderate blue CL .(Fig. 7.21), typical of many Rio Soriso stones. Oscillatory growth bands are quite remarkable, indicating fluctuations in conditions during growth. The heterogeneous colour (seen when view under an optical microscope (Fig. 7.22)) is caused by both secondary material in fractures and abundant microinclusions in
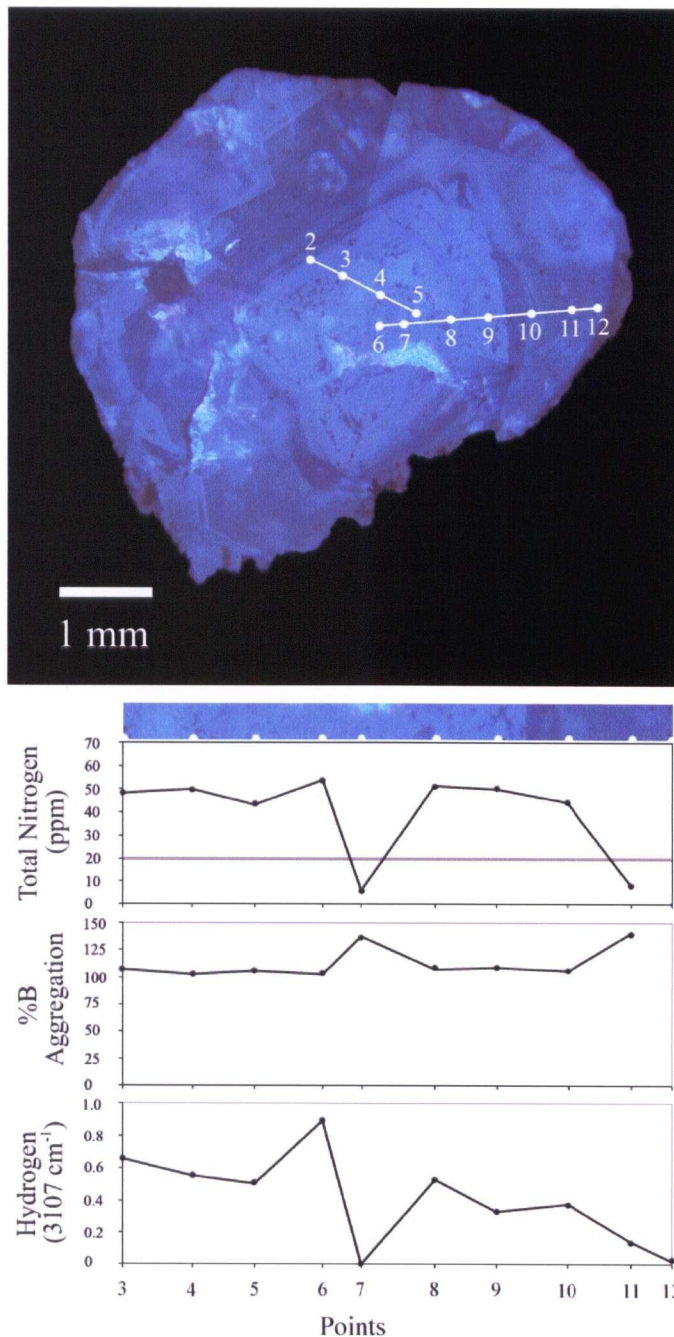
Fig. 7.21. Image of CL of diamond 3-1 side A with IR data for transect 3 to 12. Dark circle to left of point 2 is a large inclusion pit.

114

the centre of the crystal. The cloudy zone with abundant micro-inclusions is also the region of brightest blue CL (points 2 to 6). The morphology of the core suggests that this grain is twinned. The boundary between the core and the next growth zone (points 10-12) is rounded and may be a function of growth or dissolution. After this layer, it appears that growth of the remaining layers continued without disruption, until the final dissolution event responsible for the external morphology occurred. The final growth layer (top left to bottom left) forms on octahedral faces.

IR data (points 3 to 12, Fig. 7.21) reveals that the diamond contains low amounts of nitrogen (<50 ppm). With the exception of point 7, the nitrogen concentration in the core is ~50 ppm and decreases in the next layer, to essentially type II diamond. Unfortunately, IR spectra could not be collected for the brighter CL layer seen on the left of the image. Any nitrogen detected occurs as 100 % B centres. The relative hydrogen concentration roughly mimics the total nitrogen concentration.

Side B (Fig. 7.22) also illustrates the fine oscillatory nature of this diamond: the moderate blue CL core (points 5 and ~4), the darker CL zone (~3 and ~4), and the well formed, octahedral outer zone of variable blue CL (points 6-9). The form of the core and second darker zone are both rounded, likely as a result of dissolution. The nature of growth of these zones is unclear. The final growth zone (points 6-9) is octahedral.

The IR transect, in reverse (points 9 to 2), reveals that the nitrogen concentration increases from rim (type II diamond) to core (~60 ppm) and that the aggregation state is 100% B centres.

This diamond is both type IaB (core) and type II (rim), with any nitrogen in the form of 100% B centres. The nature of growth during the early stages of crystallization are unclear; the diamond may have started off as a twin, may have experienced alternating periods of growth and resorption, or may have grown rounded faces. However, the latter
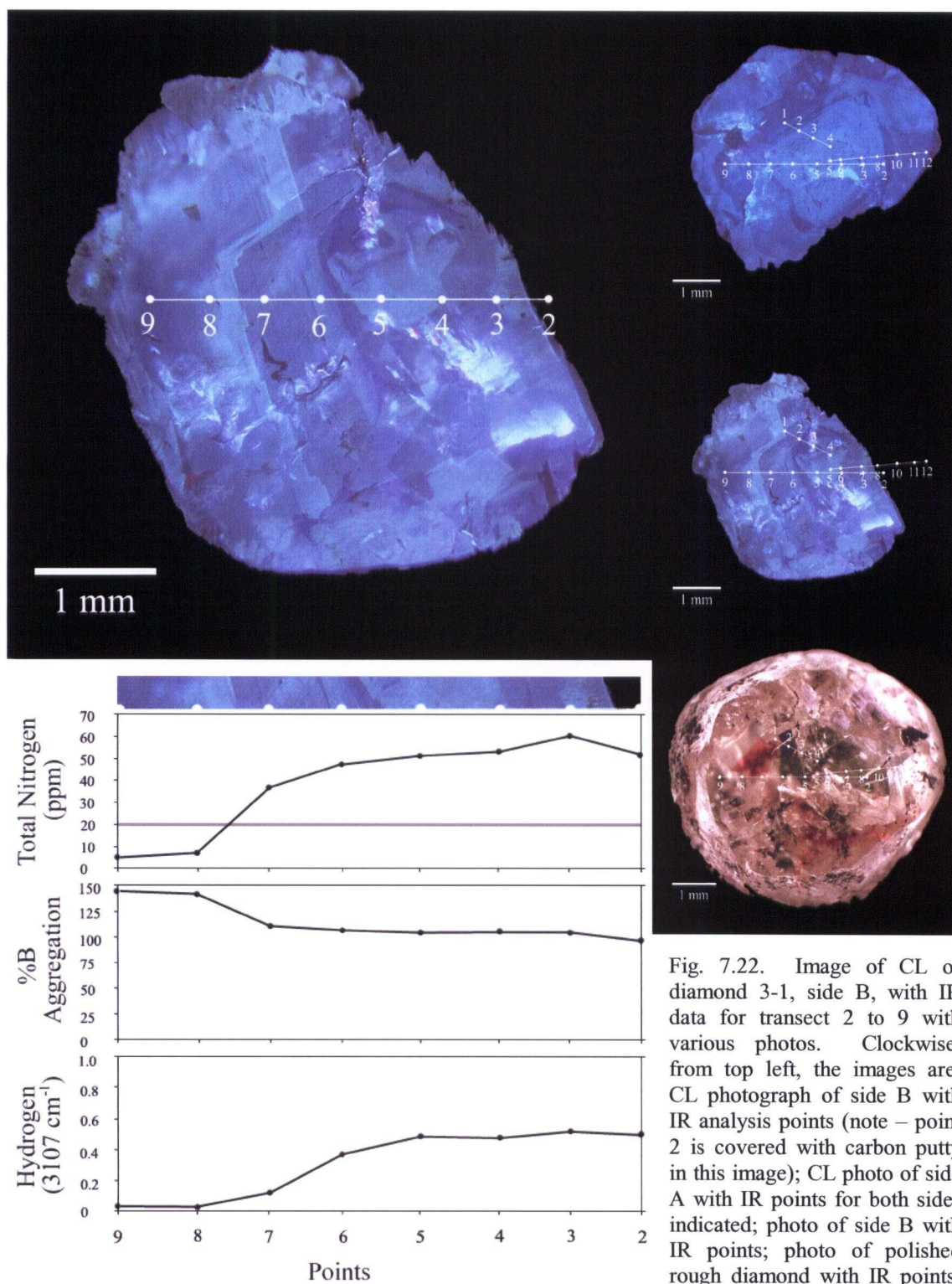
Fig. 7.22. Image of CL of diamond 3-1, side B, with IR data for transect 2 to 9 with various photos. Clockwise, from top left, the images are: CL photograph of side B with IR analysis points (note – point 2 is covered with carbon putty in this image); CL photo of side A with IR points for both sides indicated; photo of side B with IR points; photo of polished rough diamond with IR points; and IR data for points 2 to 9 on side B.

116

stages of growth developed along (111) faces. Finally, the diamond experienced extensive resorption, producing a well rounded external morphology. The crystal experienced deformation during residence in the mantle, although evidence of this is not obvious in CL.

7.3.10 Diamond 3-5

Diamond 3-5 is a moderately well resorbed (class 3), faintly yellow, broken stone. Two parallel surfaces were polished parallel to the (100) surface, creating a plate ~3.6 mm thick. The CL colours observed are moderately intense blue, typical to most stones in this study (Fig. 7.23). The growth morphology recorded under CL is remarkable, and is comprised of essentially three zones: the core, a brighter blue CL zone of possibly two crystals (an aggregate or twin), which has likely experienced resorption (points 5-7 and 13-16); a less intense blue CL zone of octahedral growth surrounds the core (points 1-4, 8-10 and 17-19); and an outer zone of weak blue CL with few discernible growth bands (points 11-12 and 20-21). There may also be a rim of even darker blue CL on this zone (seen on bottom right of image). Two black points are visible in the crystal core (near points 5 and 16), which turned out to be inclusions of ferropericlase (section 8.3.1.1). They are not at the genetic centre, and so are not likely seed crystals, but they were undoubtedly trapped during the early stages of diamond growth. The second growth zone (octahedral layers) warrants further discussion. The zone appears to have symmetry (halves are roughly mirrored on a plan draw through points 6-15) which resembles that of a macle twin.

During data collection, IR light most certainly penetrated more than one growth layer due to diamond thickness, therefore, any results likely do not reflect the absolute IR character of the growth layers observed in Fig. 7.23, but give a good indication of the relative IR changes from core to rim. Both transects (points 1-12 and 13-21) show that total nitrogen concentration is greatest in the core (highest total at point 15 at ~40 ppm) and decreases
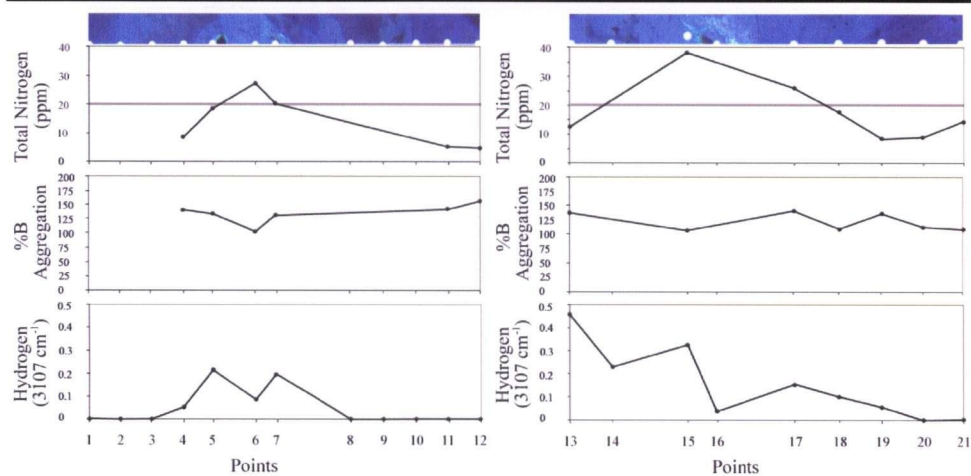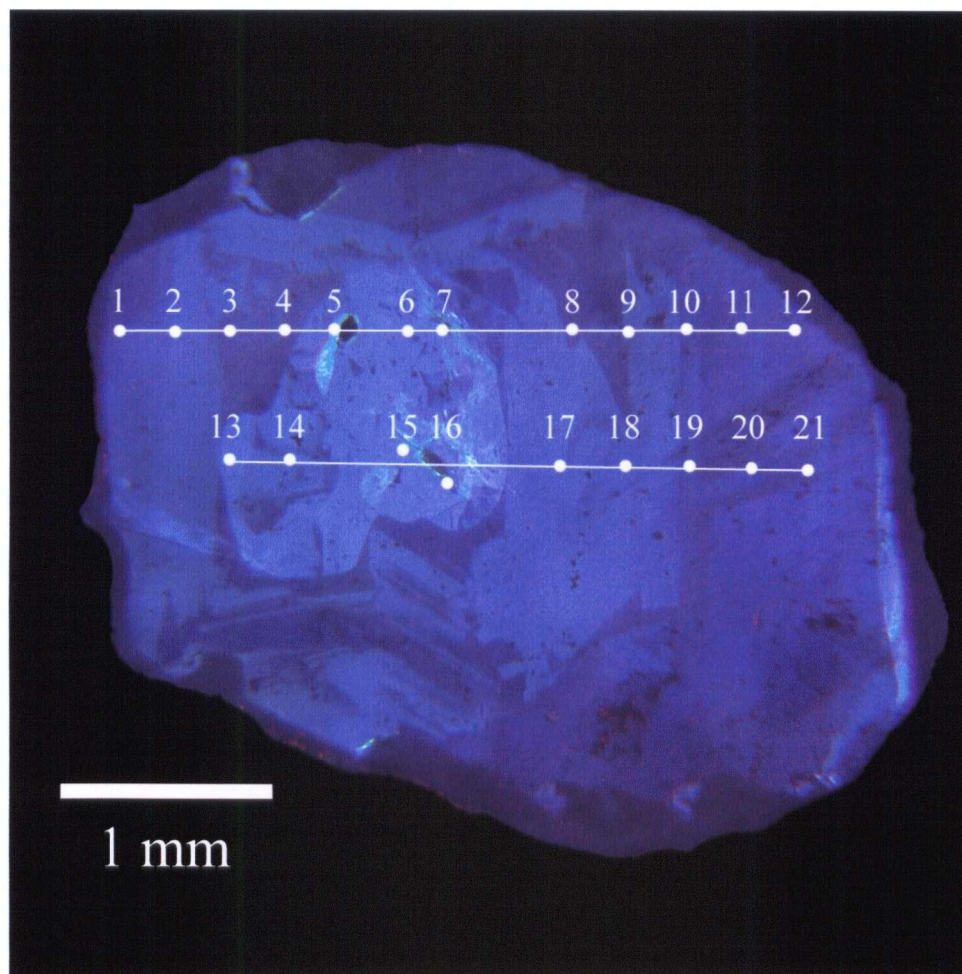
Fig. 7.23. Image of CL of diamond 3-5 with IR data for transects 1-12 and 13-21. This diamond exhibits weak to moderate blue CL. Growth can be divided into at least three zones: 1) the bright core (highest nitrogen totals); intermediate blue, octahedral growth, outer zone (points 1-4, 8-10 and 17-19) with a morphology that suggests twinning; and the darker blue rim with few discernible features.

118

towards the rim where the diamond is type II. The aggregation state calculated is unrealistic (~150% B centres) because IR spectra for most points was unusual in that there was no absorption at ~1280 cm^{-1} (where the prominent absorption for A centres occurs). The negative A centre totals are certainly meaningless (although they may indicate the presence of an unknown impurity). Although many points were noisy in the one-phonon region, it was still possible to measure the hydrogen peak at 3107 cm^{-1} for all spectra collected. This data shows a decrease in relative hydrogen concentration from core to rim in transect 1-12, however, this pattern is not mimicked in the transect 13-21.

This diamond contains very little nitrogen, although the core is type IaB (~40 ppm) with subsequent growth containing little to no nitrogen (type II). Any nitrogen present occurs as 100 %B centres. The growth occurred in at least 3, and potentially 4 stages. The first two zones possibly grew as twins, the second along octahedral faces. The nature of growth of the third (and potential fourth) zone is unclear. Finally, the crystal experienced resorption (class 3).

7.3.11 Diamond 3-8

This brown/colourless stone was polished on one side parallel to the (100) plane. The CL colour of the stone is moderate turquoise (Fig. 7.24), although the image has been brightened for clarity. No growth patterns are observed. The diamond contains numerous small, dark inclusions, which in some instances, are highlighted by lines of brighter CL (likely due to internal stress around the inclusions).

IR data shows that total nitrogen concentration decreases slightly from left to right (~50 to ~20 (9-10) and the aggregation state is 100% B centres. The total relative hydrogen concentrations decreases on either side of point 8, but are generally low.
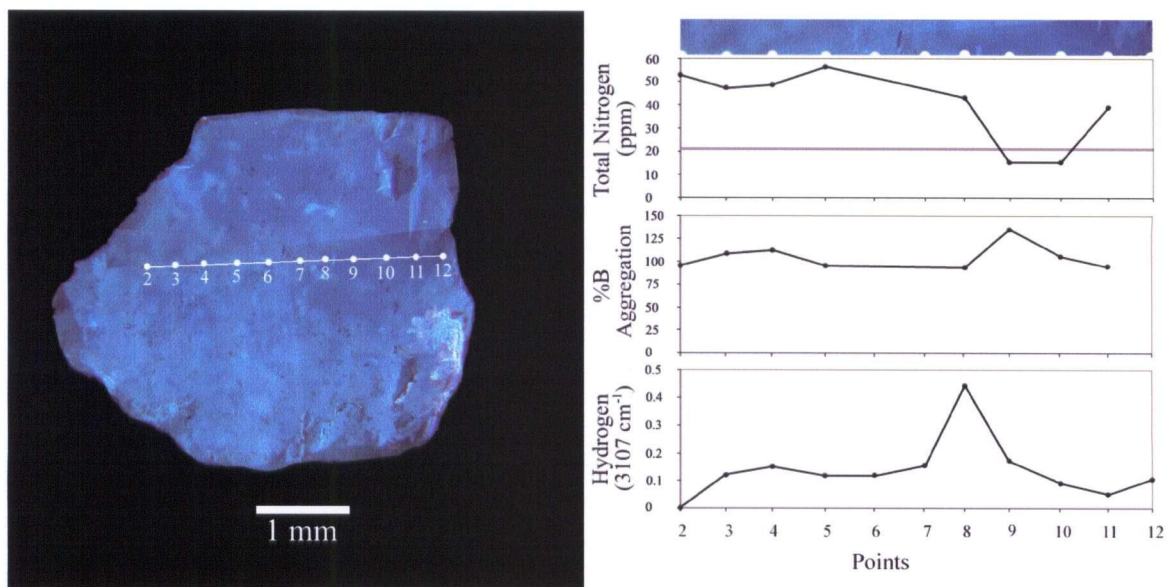
Fig. 7.24. Image of CL of diamond 3-8 with IR data for transect 2 to 12. Diamond exhibits moderate blue CL with no visible growth structures. Bright CL lines form around the abundant mineral inclusions found in this diamond.

This diamond is mostly type IaB (although two points are type II) with 100% B centres. The absence of visible growth structures may be a result of the orientation of polishing (the polished surface does not intersect any growth boundaries) or may indicate that this diamond grew in one episode of crystallization from a medium of homogeneous composition.

7.3.12 Diamond 3-10

This strongly resorbed, colourless diamond fragment was polished in no particular orientation. One half of the stone exhibits moderate blue CL while CL is essentially absent in the other half (Fig. 7.25). Bright green/yellow CL is visible in several places, most notably around a large inclusion pit (below points 3 and 4). The boundary between the two halves is relatively straight and likely a paleo-octahedral face.

IR data across transect 1 to 14 shows that nitrogen concentrations vary from 75-140 ppm for points 1 to 10 and become progressively nitrogen free from points 11 to 14 (IR

120
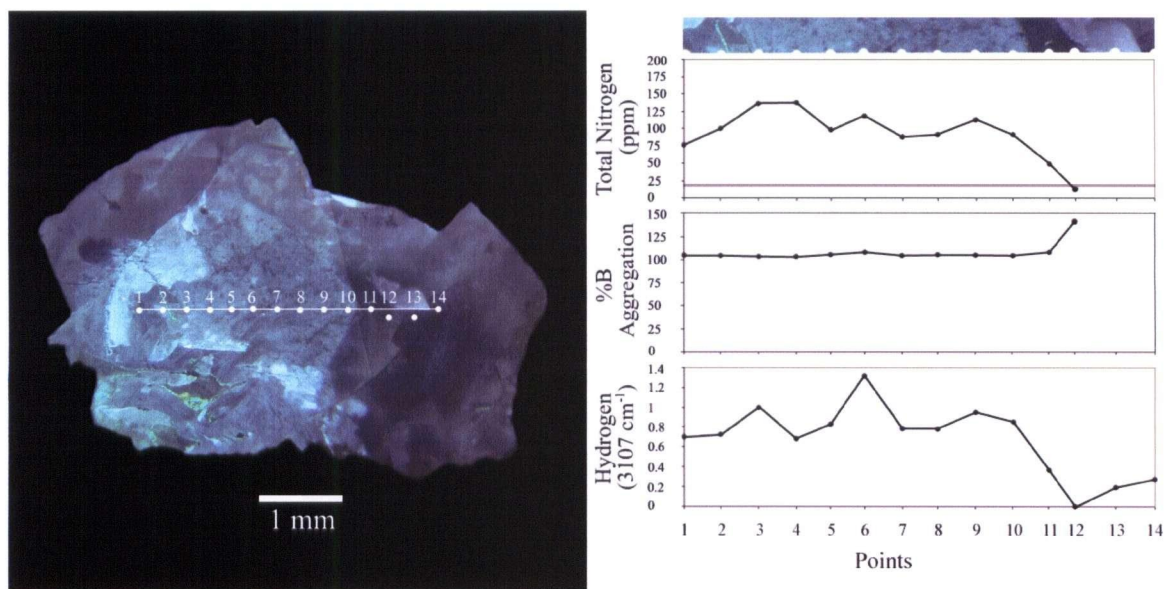
Fig. 7.25. Image of CL of diamond 3-10 with IR data for transect 1-14. Diamond exhibits two zones, one of moderate blue CL on the left while the right half has weak to absent CL. Yellow/green CL is visible around a large inclusions pit and is likely a result of lattice strain.

spectra for points 13 and 14 show no visible nitrogen absorption). Any existing nitrogen occurs as B centres. Relative hydrogen concentrations show a similar pattern to nitrogen, varying across points 1 to 10 and then progressively decreasing towards point 14. There are two unusual absorption patterns observed in IR spectra for most points across the transect. A sharp peak at ~1430 cm^{-1} is visible in spectra collected from points 4 to 11. A broader peak in the one-phonon range centred on ~1048 cm^{-1} (impurity "X") is present in spectra for points 12 to 14. The cause of this absorption remains unknown (see section 6.3.3).

This diamond is mostly type IaB (~60-80 ppm nitrogen, all as B centres) but with a significant type II portion. As there is no visible core, it is unclear if nitrogen concentration decreases from core to rim, as is typical of most stones in this study. The growth of the nitrogen rich zone is likely octahedral. The conspicuous association between yellow/green CL and the inclusion pit suggest a genetic link

7.3.13 Diamond 3-11

Diamond 3-11 is a well resorbed, broken, grey stone with a frosted surface. It was not polished on any particular orientation. The CL pattern of this polished surface shows bizarre patchy bright blue CL zones on a more homogeneous blue background of moderate CL intensity (Fig. 7.26). The nature of these patchy bright blue CL zones in unclear. 'Fingers' of weak yellow/green CL can be seen below points 9 to 13 (Fig. 7.26) and are an artefact of the machine (these 'fingers' were also observed on diamond 2.8). Growth features on this polished surface are not observed.

Transect data for points 2 to 3 reveals a relatively homogeneous distribution (with the exception of point 11) of IR character. Nitrogen concentration is ~60 ppm (all as B centres) and relative hydrogen concentrations are roughly similar at ~0.5 absorption units.

This diamond is type IaB (~60 ppm N), with moderate blue CL, and with no obvious growth features on the polished surface.
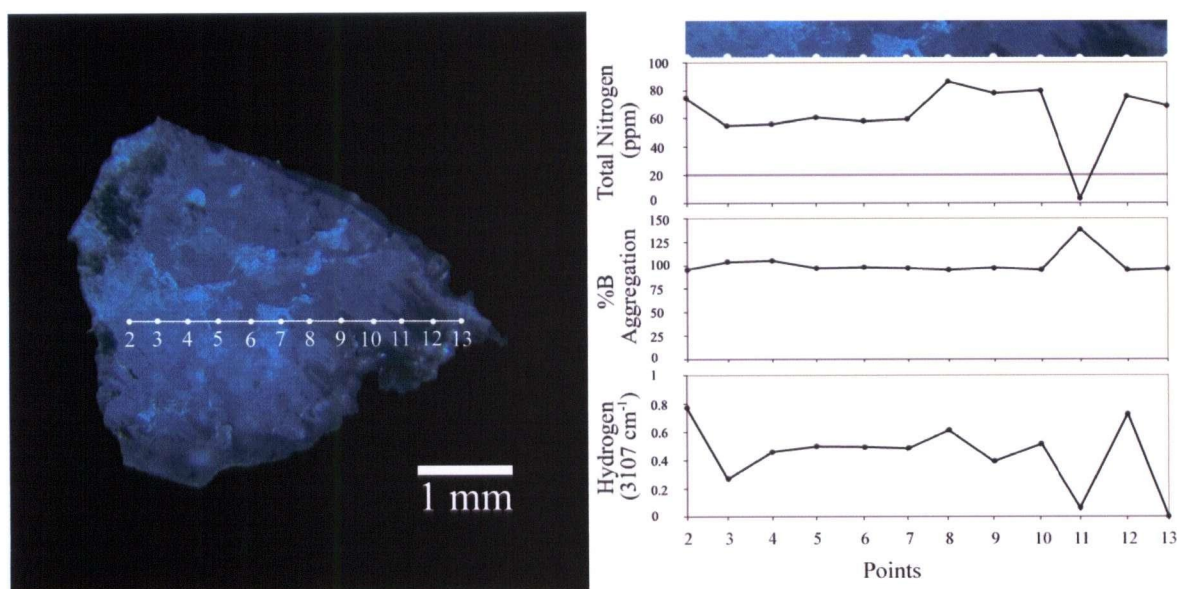
Fig. 7.26. Image of CL of diamond 3-11 with IR data for transect 2 to 13. CL of this diamond is essentially moderate blue (the heterogeneities around points 9 to 13 are an artefact of the CL machine).

7.3.14 Diamond 4-17

This colourless diamond fragment is the only stone that was not polished for growth studies. The fracture surface that was examined for growth morphology was reasonably flat and smooth, although a few steps in the surface are visible in the image (particularly below the transect). However, the CL image turned out remarkably well for an unpolished surface (Fig. 7.27). Most of the stone has weak blue CL but a rim on one half of this fractured diamond exhibits bright yellow/green CL. Three sets of parallel lines (plastic deformation laminations) are visible in the outer growth zone. The boundary between the two zones is remarkably sharp and indicates octahedral growth.

The diamond is ~1.5 mm and the IR path penetrates zones of green CL for all data points (examination of diamond reveals yellow/green CL on most sides, see Appendix A, diamond 4.17). Data from point A likely does not include contamination from the weak blue CL zone. Nitrogen concentration of the yellow CL zone ranges from ~20-50 ppm, possibly decreasing towards the inferred core (within the weak blue CL zone) with an aggregation state of 50% B centres. The weak blue zone is essentially type II. Hydrogen concentrations are also somewhat unusual for this study in that the highest totals do not coincide with the highest total nitrogen concentrations (point A).

This diamond has an inner zone of weak blue CL of type II diamond and a bright yellow/green CL rim of type IaAB (~20-50 ppm total nitrogen). The yellow/green rim grew, on what was likely a flat-faced type II octahedron, by octahedral growth. Subsequent to growth the diamond experienced plastic deformation.
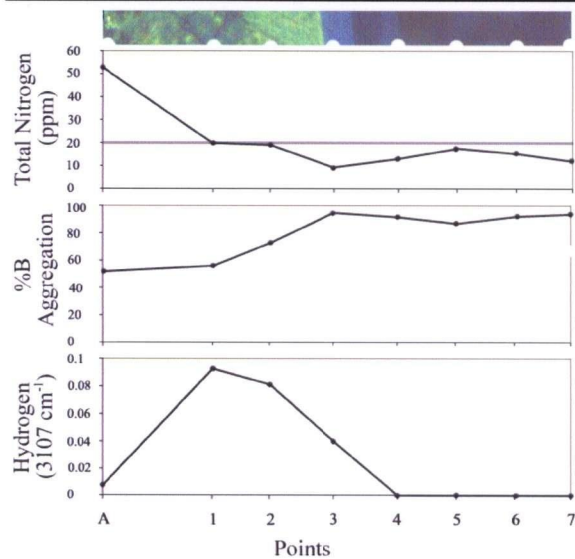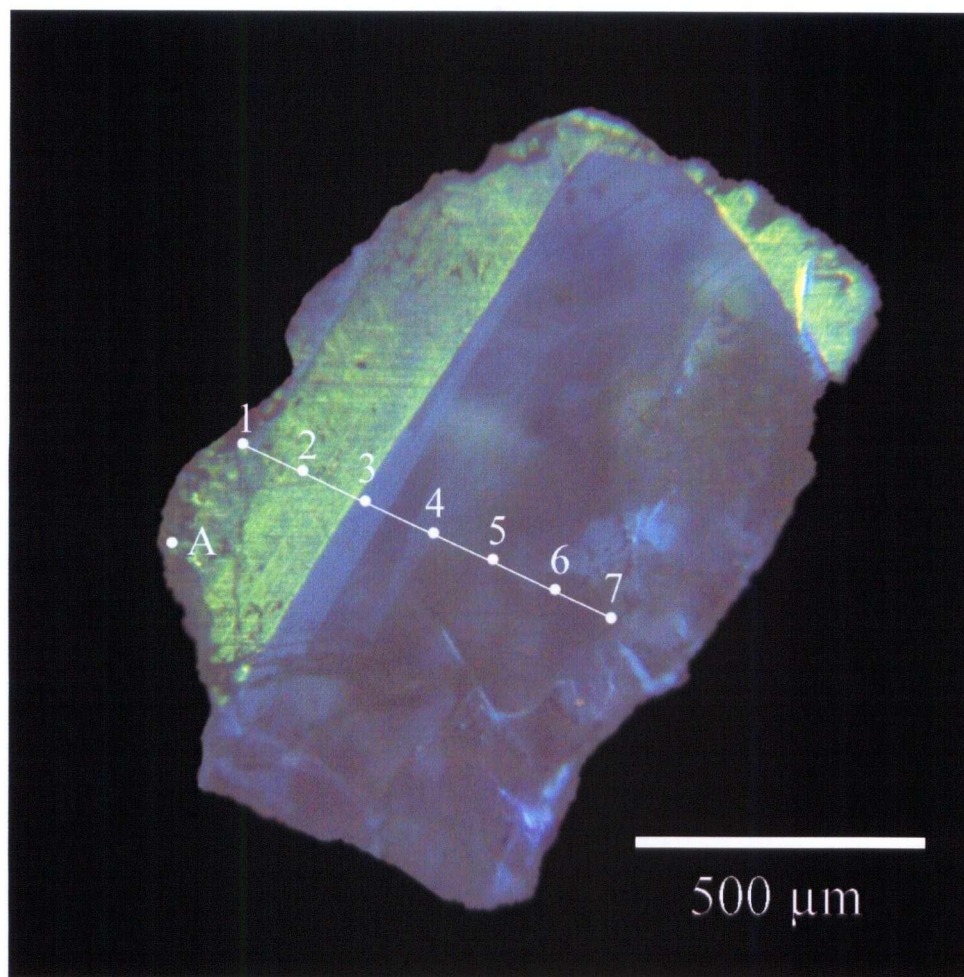
Fig. 7.27. Image of CL of diamond 4-17 with IR data for transect A, 1-7. This diamond exhibits a weak blue CL zone with a bright yellow/green CL rim with extensive deformation laminations (numerous lines that are parallel to the boundary between the blue and yellow/green CL).

124

7.4 Discussion

7.4.1 Summary of growth studies of Rio Soriso diamonds

Examination of the photos in section 7.3 shows that there are a variety of internal structures, some that are relatively simple, others that are extremely complex, and others that exhibit no apparent internal structure. A summary of the results is presented in Table 7.1.

As corroborated by the bulk IR studies on whole diamonds (section 6.3.1), nitrogen concentrations are general low (<100 ppm) and nitrogen occurs mostly as B centres. Diamonds 2-11 and 4-17 are the lone exceptions as they both also contain nitrogen in the form of A centres (diamond 2-8 may also be included in this category because of the bright yellow/green rim). For diamonds with visible concentric internal structures, nitrogen concentrations decrease from core to rim. Relative hydrogen concentrations mimic the relative total nitrogen concentrations, as discussed in section 6.4.3. However, the positive correlation between nitrogen and hydrogen concentrations may be only with nitrogen in the form of B centres as diamond 4-17, with A centres, does not show a correlation.

The more intense CL visible in the core regions of several diamonds is a reflection of the higher impurity concentrations, which are visible in transmitted light using a conventional microscope (e.g. the heterogeneous brown appearance of the core in diamond 1-4 and the cloudy appearance of the cores of diamonds 2-1 and 3-1). The nature of growth in the core is unclear as growth features are not visible. Subsequent growth on the core is often along paleo-octahedral faces (e.g. diamonds 1-2, 3-1 and 3-5) but in most cases growth is unrecognisable. Episodic resorption and growth are visible in several crystals (e.g. diamonds 1-4, 3-1 and 3-5) and most diamonds have experienced an episode of resoption before exhumation. Two diamonds have a yellow CL rim

Table 7.1. Summary of results for growth studies of Rio Soriso diamonds

Sample No.	No.of sides cut	Orientation of polishing	Thickness (mm)	CL colours	Range in total nitrogen (ppm)	Range in B/(B+A) (%)	Type(s) of growth	Direction of nitrogen conc. decrease
1.4	2	random	1.3	strong turquoise to none	20-400	100	sector and agate	?
2.2	1	random	2.4	strong turquoise to none	0-225	100	complex (sector?)	?
2.11	2	random	2.7	mod. turquoise and yellow	72	60	octahedral and complex	?
4.17	0	random	1.5	weak blue with yellow rim	0-52	50-100	octahedral	rim to core
3.1	2	100	3.4	mod. to weak blue	0-60	100	octahedral	core to rim
3.5	2	100	3.6	mod. to weak blue	0-75	100	octahedral	core to rim
1.2	2	random	2.6	mod. blue to none	0-80	100	octahedral and agate	core to rim
2.5	1	random	1.9	mod. to weak blue	50-100	100	octahedral and uncertain	?
2.1	2	random	2.7	mod. to weak blue	0-20	100	uncertain	core to rim
2.8	2	random	2.8	mod. blue with yellow rim	40-65	100	uncertain	?
3.8	1	100	1.6	mod. turquoise	0-60	100	uncertain	?
3.11	1	random	2.5	mod. blue	0-80	100	uncertain	?
2.9	1	random	2.2	strong to mod. blue	0-200	100	uncertain	?
3.10	1	random	1.1	strong blue	0-150	100	uncertain	?

Diamond thickness was calculated using the absorption coefficient calculated by Taylor *et al.*, (1990), measured at 2030 cm^{-1} (0.47 ± 0.01 units per mm path length).

126

(diamonds 2-8 and 4-17), likely of type IaA-IaAB character. Plastic deformation is observed in some diamonds (e.g. diamonds 1-4, 2-9 and 2-11) and brittle deformation is evident in one crystal (diamond 2-2).

Based on the nitrogen concentration, aggregation state and internal morphology, the 14 diamonds are divided into the following subgroups:

1) Strong turquoise CL with a significant episode of combined cubo-octahedral growth. Nitrogen concentrations have a large range (0 to ~225 ppm) and occur only as B centres. Diamond 1-4 (and possibly diamond 2-2) belongs to this subgroup.

2) Alternating bright turquoise and yellow/green CL zones with a complex geometry. Nitrogen concentration likely has a large range (72 to ~500? ppm) and occurs as type IaAB diamond with ~60-90% B centres. Diamond 2-11 is lone crystal to fall into this category.

3) Diamonds with moderate to weak blue CL that exhibit alternating periods of growth and resorption. Nitrogen concentrations are generally low (0 to ~80 ppm), occurring only as B centres, and tend to decrease towards the crystal rim. The majority of the growth for these diamonds (if not all growth) was on octahedral faces. The diamonds that belong to this subgroup are 3-1, 3-5 and possibly 1-2.

4) Weak blue CL (type II diamond) with a reasonably thick rim (up to 250 μm) of bright yellow/green CL (~50 ppm total nitrogen of which ~50% occur as B centres, or type IaAB diamond). Diamond 4-17 is the only diamond in this subgroup.

5) Diamonds that do not appear to have any internal structures that exhibit moderate to strong blue/turquoise CL. Nitrogen concentrations range from 0 to 150 ppm and occur only as B centres (diamonds 2-1, 2-5, 2-8, 2-9, 3-8 and 3-10).

Subgroups 1-3 are likely distinct populations. They are quite different in terms of internal structures and nitrogen character. Subgroup 4 is created for the one diamond with a reasonably thick bright yellow/green CL rim (diamond 4-17). Rims of this CL colour exist on other diamonds and perhaps are not observed because they have broken off the diamond core of type IIa or IaB character. Subgroup 5 likely contains diamonds with internal structures that are not visible on account of the orientation of the polished face. It is likely that at least some diamonds in subgroup 5 could be redistributed between subgroups 1 to 3 (most likely belonging to subgroup 3) if the polished surface was on a more favourable orientation.

7.4.2 Comparisons with other studies

The internal growth morphology and IR character for Juina area diamonds have also been examined by Hutchison (1997) and Araujo *et al.* (2003).

Hutchison (1997) found that most diamonds exhibit weak to moderate blue CL, lack concentric growth features and display internal structures that are truncated at crystal edges, an indication that many stones are broken. The conclusion was that initial growth for at least some stones (as evidenced by step features) was within a reasonably stable growth environment. Following initial growth, all stones were subjected to a period of dissolution followed by precipitation of diamond of lower CL intensity. Many of these stones also exhibit signs of plastic deformation, which may be responsible for the realignment of concentric growth features.

The results from work by Araujo *et al.* (2003) are similar. CL of diamonds is typically homogeneous sky-blue of weak intensity. The rare internal features observed include growth on octahedral faces, step-wise growth, truncated growth zones and fine parallel lines. These observations were interpreted as indicators of octahedral growth, resorption and plastic deformation. Nitrogen concentrations are low (82% of diamonds classified as

type II), but if detected, occur mostly as B centres (>90% B centres). Three stones out of a sample size of 234 diamonds were classified as type IaAB diamond with <90% B centres (bulk analysis). There is no data on the internal morphology of the type IaAB diamonds.

The majority of diamonds found in the Juina area appear to contain internal morphologies that are either complex or absent, exhibit weak to moderate blue CL and typically show evidence for plastic deformation, brittle fracturing and episodes of resorption and reprecipitation. Total nitrogen concentrations are low and occur mostly as B centres (90 to 100% B centres), and in some cases, decreases towards the crystal rim. Other subgroups are likely mixed in with the dominant subgroup just described, however, they are poorly represented. Based on internal growth features and IR character, this study highlights two new subgroups: 1) diamonds with high total nitrogen concentrations that grew, at least in part, as cubo-octahedrons (diamond 1-4 and possibly diamond 2-2), and 2) diamonds with complex internal morphology of alternating turquoise and yellow/green CL that may contain considerable nitrogen (72 - ~500 ppm) of mixed (type IaAB) character and may also contain platelets (D centres) (diamond 2-11).

8.0 Mineral Inclusions

8.1 Introduction

Many diamonds contain mineral inclusions that are syngenetic with their host (Meyer, 1987; Harris, 1992). These inclusions have been trapped by their hosting diamond and have remained in isolation because diamond acts as an impermeable seal around the inclusion, thus preserving a pristine sample of the mantle. An extensive list of minerals which occur as inclusions in diamond is given by Meyer (1987) and Gurney (1989). From this large group of diamond inclusion minerals, only a few have been found in diamonds from the Juina area. Inclusions found in Juina diamonds are also found in diamonds from most continents, but are generally rare occurrences. The Juina area is unique because it has the largest proportion of diamonds which contain these rare inclusions.

Numerous studies have confirmed that mineral inclusions in diamond (and thus diamonds themselves) fall into two broad categories in terms of paragenesis: peridotitic (p-type) and eclogitic (e-type). Inclusions belonging to other paragenetic groups have been found but they are exceedingly rare. Many of the inclusions found in Juina diamonds are considered to represent their own paragenetic group, which has been referred to as both the lower mantle suite (Hutchison, 1997) and the super-deep suite (Kaminsky *et al.*, 2001a). These terms do not indicate the nature of the composition but highlight the extreme depths of formation. A distinction should be made when referring to compositional similarities (i.e. p-type or e-type) and depth of formation. When possible, the minerals and mineral associations in this study will be discussed both in terms of composition (e.g. eclogitic, peridotitic, mafic and ultramafic) and depth of formation.

A brief review follows on the current models of the mantle in terms of composition, phase changes and pressure-temperature (P-T) constraints.

8.1.1 Composition of the mantle

Constraints on models of the mantle come from a variety sources which can be broadly sub-divided into three 'categories': 1) methods of indirect examination (e.g. seismology and tomography), 2) direct examination on materials inferred to be derived from the Earth's interior (e.g. ultramafic massifs, basalts, xenoliths and diamond inclusions) and 3) examination of analogue materials (e.g. lab experiments at high pressures and temperatures on relevant materials, and examination of non-terrestrial materials).

Fig. 8.1. Seismic velocities for P and S waves through the Earth (0-6370km). Compositional subdivisions are listed on the left and rheological subdivisions on the right. Reproduced from Winter (2001) after Kearsey and Vine (1990).

The first data from the 'deep Earth' came from seismic studies. Recognition of sharp changes in wave velocities (and in some cases absences) led to the establishment of several subdivisions in the Earth's interior, which when discussed in a general sense, are widely accepted in literature. These subdivisions are crust, mantle (which is subdivided into upper mantle, transition zone, and lower mantle), outer core, and inner core (Fig. 8.1). Of

Fig. 8.2. Seismic velocities for P and S waves through the Earth (200-800km). Line patterns represent interpretations from different sources. Vs = shear waves, Vp = compressional waves. Modified from Ringwood, 1991.

most interest to this study is the mantle, and in particular, the transition zone (~410-660 km) and lower mantle (~660–2900 km). A more detailed figure of seismic wave velocity

131

variation with depth (between 200 and 800 km) is presented in Fig. 8.2. Seismic profile interpretations generally agree on the depth of the two large discontinuities (~390-420 km and ~650-700 km) and on a less pronounced discontinuity (~500-530 km). For the sake of any future discussion and simplicity in figures, this thesis will consider the upper boundaries of the two major discontinuities at 410 km (transition zone) and 660 km (lower mantle) (Ringwood, 1991).

Direct evidence of mantle minerals comes from a variety of sources found near the Earth's surface, such as ultramafic massifs, xenoliths, basalts and inclusions recovered from diamond. However, there are significant limitations on the interpretations from the studies of these materials. It is important to understand that some materials may be products of partial melting (e.g. basalts) or may not be representative of the bulk mantle (e.g. xenoliths and diamond inclusions). It is unclear if diamonds crystallise in a setting that is chemically distinct and isolated from the bulk mantle, or if diamonds crystallise in rocks that reflect the bulk chemistry of the mantle. Any study of diamond inclusions must consider the possibility that the inclusions in diamond may be sourced from parental rocks that are minor in volume relative to the whole mantle.

The integration of data from geophysics, natural Earth samples and chondrites along with experiments at high pressure and temperature have provided several consistent constraints. Perhaps most notable was the recognition that the depths at which some large seismic discontinuities occur (~410 and ~660 km) correspond well with a phase change in olivine ($(Mg,Fe)_2SiO_4$) at ~410 km, and the breakdown of $(Mg,Fe)_2SiO_4$ into ferropericlase (fPer) and $MgSiO_3$-perovskite (~660 km). Based on this observation among other experimental work, A.E. Ringwood synthesised an analogue material termed 'pyrolite' (composed of dominantly pyroxene-olivine material) to represent the primary composition of the mantle. Fig. 8.3A is a compilation of high pressure and temperature data for material of 'pyrolitic' composition from Ringwood (1991). This figure illustrates very succinctly the range of stability for most mantle phases. Although there is no consensus on the composition of the mantle, the hypothetical mixture of pyrolite is widely accepted (Irifune et al., 1998). Fig. 8.3B shows the range of stability

geothermobarometers. The geothermal gradient below cratonic lithosphere, within the convecting mantle, is constrained by the adiabat, which is the theoretical geothermal gradient for a system where no heat is lost through conduction. Although heat is lost through conduction, the geothermal gradient must be close to the adiabat in the convecting mantle. The geotherm and adiabat included in Figs. 8.4 to 8.7 is an estimated P-T path through the mantle (reproduced from Joswig *et al*, 1999). There is a large error associated with this path (~200 °C), but in the context of this study, the inclusion of the geotherm is considered useful.

8.1.3 Terminology

Mineral terminology is an important matter of discussion because of the numerous polymorphs for the expected dominant mantle minerals. Nomenclature is often confusing in literature and warrants explanation here. Firstly, the minerals introduced in this chapter contain iron (Fe) in their chemical formula, although abbreviations tend to drop Fe and only use Mg. For $(Mg,Fe)SiO_3$-perovskite, *mg* (where *mg* is defined as $Mg^{2+}/(Mg^{2+}+Fe_{tot})$) is generally >0.90 and for the sake of simplicity, the mineral name is abbreviated to MgSi-Prv. Contractions of this nature are common in literature and will be used in this thesis. Also worthy of explanation are terms such as perovskite and ilmenite used to describe certain isomorphs. These terms indicate that the mineral in question has a structure similar to a well-characterised mineral (e.g. $CaSiO_3$-perovskite has the same structure as $CaTiO_3$ (true perovskite), which is orthorhombic, and $MgSiO_3$-ilmenite has the same structure as $FeTiO_3$ (true ilmentite)).

Tables are included for each mineral discussed in section 8.1.4, relating the full mineral name with abbreviations used. When possible, abbreviations are used for minerals from Kretz (1983). However, many of the higher P-T phases do not have widely accepted abbreviations. Abbreviations for these minerals are collected from a variety of sources.

134

for material of initial basaltic composition. In a broad sense, the pyrolite model has withstood many tests, and as such, has widespread appeal.
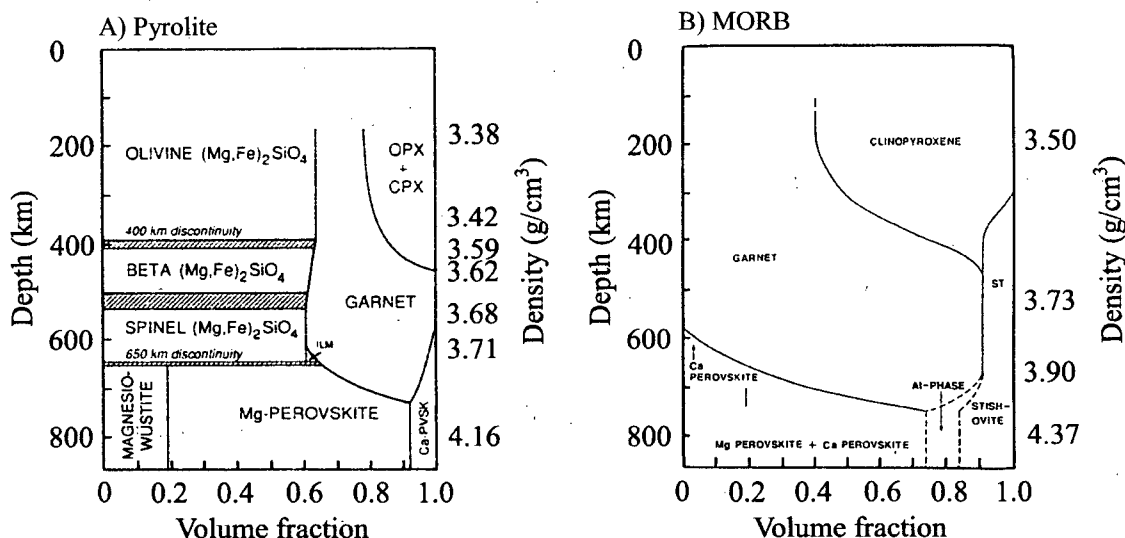
Fig. 8.3. Mineral assemblages and (zero-pressure) densities for A) pyrolite, and B) basaltic (MORB) oceanic crust. Constraints used for temperature are T=1400°C at 400 km and 1600°C at 650 km, from mantle geotherm in Brown and Shankland (1981). Modified from Ringwood, 1991.

8.1.2 Geothermal gradient

The geothermal gradient (geotherm) is important to consider in this study because it provides a possible P-T path that diamonds and their inclusions could follow during exhumation. The number of likely phases represented by a particular composition (see Figs. 8.4-8.7) can be reduced based on an understanding of the geotherm. Geotherms are based on a variety of lines of evidence such as geophysical observation and experimentation as well as high pressure and temperature experimentation on analogue materials. Experiments on the partitioning of elements between phases have led to the development of many geothermometers and geobarometers (e.g. Brey and Kohler, 1990), which can be used on coexisting phases found in xenoliths (e.g. Boyd, 1987) and inclusion pairs in diamond (e.g. Harris, 1992). Using the methods listed above, it is possible to constrain the geotherm in cratonic lithosphere up to 1400 °C and 60 kbar (Brey and Kohler, 1990), or ~200 km. However, the predicted P-T conditions where most of the Juina area diamonds originate are well outside of the experimental limits of

133

8.1.4 Relevant mantle minerals and their stability fields

The minerals considered relevant to this study are essentially the phases depicted in Fig. 8.3A-B. They are: $(Ca,Mg,Fe)SiO_3$ (perovskite and polymorphs), $(Mg,Fe)_2SiO_4$ (olivine and polymorphs), $X_3Y_2Si_3O_{12}$ (various garnets, where X=Mg, Fe and Ca and Y=Al and Cr), $(Mg,Fe)O$ (ferropericlase) and SiO_2 (quartz and polymorphs). Some other phases found as inclusions in Juina diamonds are discussed, but most of these are rare diamond inclusions and likely represent minor mantle phases. In general, the stability fields for these less common phases are poorly constrained.

The most compelling evidence for determining what particular polymorph phase is being represented by a diamond inclusion comes from a combination of chemical and structural analysis. Chemical studies are common practice on diamond inclusions, but crystallographic studies are not. The reason for this is that inclusions are typically too small for most analytical equipment used to determine crystal structure, and, even if analysis is possible, there is a good chance that the inclusion examined has reverted to a more stable, lower P-T, polymorph. Diamond itself is proof that meta-stable minerals can exist at the surface of the Earth, however, the activation energy required to convert diamond to graphite is extremely high. Davies and Evans (1972) determined the activation energy required to induce graphitisation on the (110) surface of diamond is 728 ± 50 kJ/mol. Many of the high P-T polymorphs of inclusions found in diamond have much lower activation energies.

Without crystallographic data, two main lines of evidence are used to determine the identity of the original polymorph before being included in diamond. The first approach is through study of associations, as either composite grains (touching phases) or non-touching phases occurring in the same diamond (that are interpreted as being in equilibrium when included in diamond). The second approach relies on the controls pressure and temperature has on element partitioning. Because the chemical signature for a monomineralic inclusion survives through time, regardless of the P-T conditions

(provided the inclusion remains isolated inside the diamond), chemical studies are not subjected to the same ambiguities as crystallographic studies.

A comprehensive overview of the crystal structure, effects of element substitution and expansion rates is well beyond the scope of this thesis. Instead, information relevant to deciphering clues from the study of diamond mineral inclusions for the Rio Soriso suite will be the focus of the remainder of this section. Inclusion polymorphs along with their stability fields will be discussed with a particular focus on how to recognise relevant polymorphs based on chemistry alone (i.e., in the absence of data on crystal structure). When possible, the inclusion phase and chemistry will be discussed in terms of what it reveals about the composition and the P-T stability field of the parental source rocks.

8.1.4.1 MgSiO₃

Seven polymorphs with MgSiO₃ stoichiometry exist in the P-T range of the upper and lower mantle (Table 8.1). The stability fields for these polymorphs are presented in Fig. 8.4. The polymorphs of most interest to this study are MgSi-Prv and enstatite. However, it is noted that throughout this report, enstatite inclusions in diamond will be referred to as orthopyroxene (Opx), to account for the substitution of Fe.

Table 8.1. MgSiO₃ polymorphs

Mineral	Abbreviation
MgSi-perovskite	MgSi-Prv
MgSi-ilmenite	MgSi-Ilm
MgSi-tetragonal garnet	MgSi-TGar
Enstatite	En
High-temperature clinoenstatite	HCen
Low-temperature clinoenstatite	LCen
Protoenstatite	Pen

MgSi-Prv is generally accepted as the dominant phase found in the lower mantle (660 to 2900 km's depth) (Fiquet *et al.*, 1998) and constitutes ~70% of a lower mantle of pyrolitic composition (Fig. 8.3A). It is considered to be a highly unstable phase outside of the lower mantle. Studies on the activation energy required for the back-transformation of MgSi-Prv (*mg* = 0.90) to enstatite by Knittle and Jeanloz (1987) find that only 70±20 kJ/mol are needed, compared to 728±50 kJ/mol required to convert

diamond to graphite (Davies and Evans, 1972). Knittle and Jeanloz (1987) suggest that MgSi-Prv brought to the Earth's surface would likely survive less than 3-100 years. Other authors, such as Sharp *et al.* (1997), Wang *et al.* (1992) and McCammon *et al.* (1992) have drawn similar conclusions. Kesson *et al.* (1991) report the retrogressive transformation of MgSi-Prv to En (as an inclusion in diamond)

Fig. 8.4. Phase transformations for $MgSiO_3$. Stability fields for liquid, Pen, MgSi-TGrt, MgSi-Ilm, MgSi-Prv, Sti and wadsleyite (β-Ol) and Sti and ringwoodite (γ-Ol) are from Fei and Bertka (1999). Stability fields for LCen, En and HCen are from Ulmer and Stadler (2001). Horizontal lines at ~14.5 GPa and 23.5 GPa mark the approximate upper limits of the transition zone and lower mantle respectively and the thick bent curve indicates an approximate geotherm (from Joswig *et al.*, 1999)

is accompanied by an expansion of ~20%. Because of the relative ease at which MgSi-Prv reverts to lower P-T phases and the substantial volume increase, it is no surprise that MgSi-Prv has not been directly confirmed through crystallographic studies as an inclusion in diamond.

MgSi-Prv diamond inclusions may be distinguished from Opx inclusions based on Al and Ni content. At shallow levels (~<250 km) garnet is the main host for Al and examination of Opx inclusions from diamonds of shallow origin find Al contents <1.00 wt% Al_2O_3 (Meyer, 1987). However, at depth (~600 km, see Fig. 8.3) garnet begins to dissolve into MgSi-Prv and CaSi-Prv. Experiments at high P-T conditions find that MgSi-Prv can accommodate the complete budget of Al_2O_3 predicted in the lower mantle for a pyrolitic composition (~4 mole %) (Kesson *et al.*, 1995; Irifune *et al.*, 1996) and can accommodate as much as ~25 mol % Al_2O_3 at pressures between 55-70 GPa (Kesson *et al.*, 1995). Inferred former MgSi-Prv inclusions from Kankan, Guinea contain 1.1-1.7 wt% Al_2O_3 (Stachel *et al*, 2000b) and inclusions from Juina contain even higher Al contents, up to 12.6 wt% Al_2O_3 (Hutchison, 1997). Lower Al_2O_3 contents (~1.1-1.7 wt%) are thought to suggest crystallization within the top 10-20 km of the lower mantle (Stachel *et al.*,

137

2000b). Al content in MgSiO$_3$ (~>1.00 wt% Al$_2$O$_3$) is not an indicator of former MgSi-Prv on its own, indeed Al contents can be considerable for MgSiO$_3$ in both spinel-facies peridotites (1-6 wt% Al$_2$O$_3$) and garnet-facies peridotites (<2 wt% Al$_2$O$_3$). However, low Al content is a signature of depleted harzburgites, which are the parental rocks for most peridotitic diamonds (Pearson *et al.*, in print). As an inclusion in diamond with Al$_2$O$_3$ >~1.00 wt% is reasonable grounds to suggest a deep origin. NiO content is another useful discriminating tool because in a system of MgSi-Prv and fPer, NiO is always strongly partitioned into fPer (Kesson *et al.*, 1991). Upper mantle Opx grains typically contain >0.1 NiO wt% (Meyer, 1987) while inferred former MgSi-Prv inclusions typically contain ≤0.03 wt% NiO (Hutchison, 1997; Stachel *et al.*, 2000b).

MgSi-Prv is stable in both mafic and ultramafic rocks at lower mantle P-T conditions, however, it is the expected dominant phase in ultramafic rocks (~70%) and would be the second or third most abundant phase in mafic rocks after CaSi-Prv and SiO$_2$, depending on the Ca:Mg ratio.

8.1.4.2 CaSiO$_3$

CaSiO$_3$ has three polymorphs in the P-T range of the mantle (wollastonite, CaSi-walstromite, and CaSi-perovskite) as well as a stability field where it occurs as two minerals (Ca$_2$SiO$_4$ and CaSi$_2$O$_5$) (Table 8.2 and Fig. 8.5A). However, unlike MgSiO$_3$, CaSiO$_3$ does not have any stable polymorphs in an open system in the upper mantle.

Table 8.2. CaSiO$_3$ polymorphs

Mineral	Abbreviation
CaSi-perovskite	CaSi-Prv
CaSi-walstromite	CaSi-Wal
CaSi-wollatonite	Wo

As such, the presence of CaSiO$_3$ is a likely indicator of depths ~>580 km.

Above ~580 km, calcium occurs in either garnet or clinopyroxene. Below ~580 km, calcium, in both eclogitic and peridotititc source rocks, begins to form a new high-pressure species, CaSi-Prv (Fig. 8.3A-B). Experiments by Irifune and Ringwood (1987) and Wood (2000) show that CaSi-Prv exsolves from majorite garnet at pressures

exceeding 20-21 GPa. In the lower mantle, CaSi-Prv is predicted to be the third most abundant phase in pyrolite (~10 vol %) and the second most abundant phase in eclogite (~30 vol %) (Irifune et al., 1993). In terms of chemistry, there is little substitution of other elements in CaSi-Prv, even in a chemically complex mantle (Gasparik, 1989, 1990). As such, there are no geothermobarometers yet established that can be used for even a crude estimation of the depth of formation.

Trace element geochemistry is likely the only method available to determine the nature of the parental material for CaSi-Prv inclusions (in the absence of mineral associations) and has been used by several authors (e.g. Stachel et al., 2000b; Harte et al., 1999; Hutchison, 1997). The Eu anomaly observed in $CaSiO_3$ grains by Harte et al. (1999) has been interpreted as a possible indicator of a crustal source.
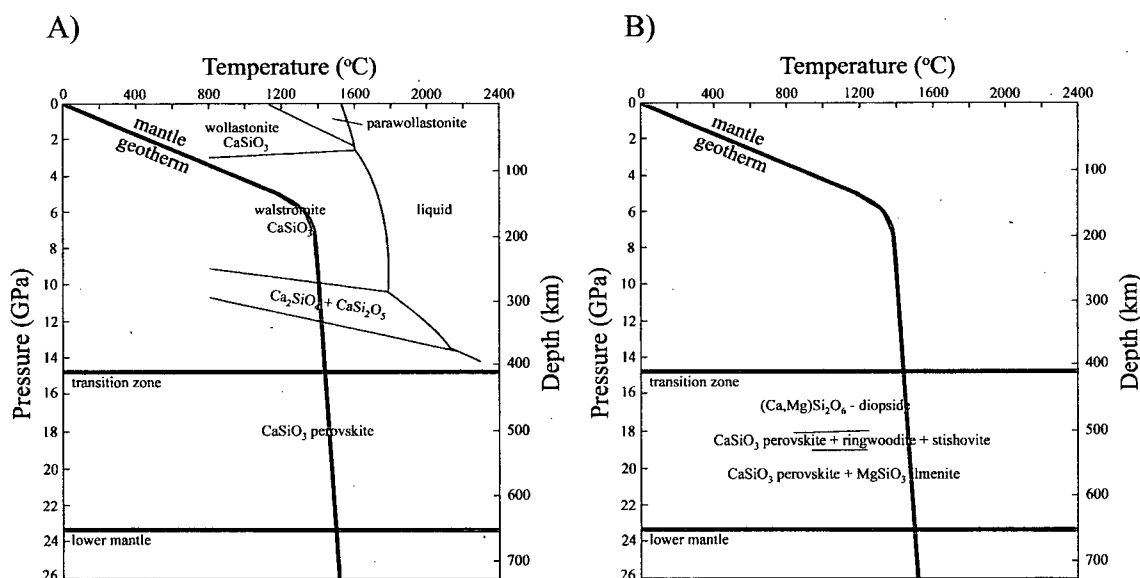
Fig. 8.5. Phase transformations for the predicted dominant Ca phases in the mantle. A) Phase transformations for $CaSiO_3$ (modified after Gasparik et al., 1994), and B) Phase transformations for $(Ca,Mg)Si_2O_6$, (modified after Koito et al., 2000).

8.1.4.3 Garnets and highly aluminous silicates

Garnets inclusions in diamond typically fall into one of two broad compositional divisions: eclogitic and peridotitic. With the discovery of non-stoichiometric garnets included in diamonds from Sloan, Colorado (Otter and Gurney, 1989), a third category of

139

garnet was included, termed majorite. A fourth mineral, tetragonal-almandine-pyrope phase (TAPP) will be included here, although this mineral in not really a garnet. The sole reason for grouping these fours phases (e-type, p-type, majoritic and TAPP) is that they all contain abundant Al_2O_3 (~>18 wt%). In this report, in the absence of supporting data, any highly aluminous silicate will be referred to as garnet (Grt). More specific abbreviations are listed in Table 8.3.

Table 8.3. Aluminous silicates

Mineral	Abbreviation
Highly aluminous silicate (general)	Grt
Tetragonal almandine-pyrope phase	TAPP
Eclogitic garnet	eGrt
Peridotitic garnet	pGrt
Majoritic garnet	Maj

The garnet group covers a large number of minerals with the general chemical formula $X_3Y_2Si_3O_{12}$, where $X=Ca$, Fe^{2+}, Mg and Mn, and $Y=Al$, Cr and Fe^{3+}. Peridotitic garnets are characterised by high chromium content (>2.00 wt% Cr_2O_3, Gurney, 1989) while eclogitic garnets are typically void of chromium (<2.00 wt % Cr_2O_3, Gurney, 1989). As well, pGrt's are Mg-rich while eGrt's contain more Fe and Ca (Meyer, 1987). Garnets are generally isotropic, however this property tends to change with depth as the garnet structure begins to accommodate elements in non-stoichiometric proportions. Ringwood (1967) first reported the solubility of pyroxene in garnet at high pressures. Based mainly on studies by Akaogi and Akimoto (1977 and 1979) and Lui (1977), it was concluded that pyroxenes gradually dissolve into garnet with increasing pressures until the transition zone (~410 km depth), at which point only one 'garnet' phase exists. This 'garnet' phase is called majorite and any garnet containing a dissolved pyroxene component is considered a majoritic garnet. By calculating the number of silica cations (as a ratio of oxygen anions), it is possible to differentiate between majoritic and non-majoritic garnets; any grain with greater than 3.075 Si^{4+} cations per 12 oxygens has a majoritic component (Stachel *et al.*, 2000a). Both eclogitic and peridotitic garnets can contain a majoritic component. Experimental work by Irifune (1987) shows that the amount of Si^{4+} in majoritic garnets can be used to determine the pressure at formation.

A fourth phase is considered here on account of the large amount of aluminium accommodated in the structure. Examination of mineral inclusions from Juina diamonds by Harris *et al.* (1997) found a new aluminous silicate which they termed tetragonal-almandine-pyrope phase (TAPP). They concluded that TAPP is a stable phase in the uppermost part of the lower mantle. TAPP grains contain the normal garnet Si:Al ratio without evidence of a majoritic component. Some characteristics of TAPP are: unusually low CaO contents (<0.12 wt%); relatively restricted chromium values between 1.39 and 2.80 wt% Cr_2O_3; and *mg* between 0.82 and 0.91. The composition of parental rocks for TAPP is unclear.

8.1.4.4 Mg_2SiO_4

Mg_2SiO_4 is the main phase predicted for a pyrolitic upper mantle and transition zone (Fig. 8.3A) and exists in the form of three polymorphs (Table 8.4). The three changes that Mg_2SiO_4 undergoes from the upper mantle to base of the transition zone are from orthorhombic (referred to as α-Ol), to a modified spinel structure (β-Ol or Wadsleyite) and finally to a true spinel structure (γ-Ol or Ringwoodite), as has been demonstrated by numerous experiments (Ringwood, 1991 and references therein) (Fig. 8.6). The transformation of α-Ol to β-Ol occurs over a depth interval of 4-35 km, depending on the mantle temperature and water content (Frost, 2003) and results in a ~8.0 % decrease in volume (Lui, 1975). The next transformation (to γ-Ol) occurs over a depth interval of

Table 8.4. Mg_2SiO_4 polymorphs.

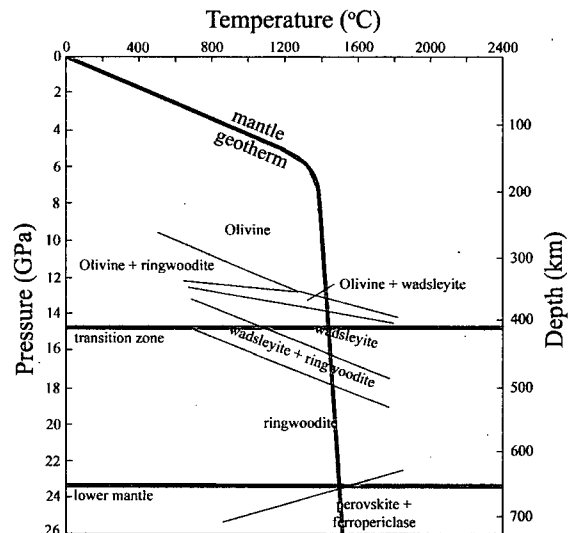| Mineral	Abbreviation
Olivine	α-Ol
Wadsleyite	β-Ol
Ringwoodite	γ-Ol

Fig. 8.6. Phase transformation for $(Mg_{0.89}Fe_{0.11})_2SiO_4$. Modified from Akaogi *et al.*, 1989.

20 km (Frost, 2003), which results in a ~2.0 % decrease in volume (Lui, 1975). Eventually γ-Ol breaks down into two phases, MgSi-Prv and ferropericlase (fPer) (Ito and Takahashi, 1998) occurring over a depth interval of 5-12 km (Yamazaki *et al.*, 1994).

Olivine inclusions in diamond (depths of origin ~<250 km) are typically Mg-rich (*mg* = 0.91 – 0.95), contain ~0.05 wt% Cr_2O_3 and nickel concentrations of ~0.40 wt% NiO (Meyer, 1987). The sparse data for Mg_2SiO_4 of deeper origin (depths >250 km) suggests that *mg* is typically lower (i.e. 0.87 to 0.91, Hutchison, 1997), which is in part corroborated by experimental studies. High-pressure experiments at $1400°C$ on pyrolite (*mg* = 0.89) reveal that the *mg* of α-Ol increases with depth towards the transition zone to *mg* = ~0.925, after which the structural change to β-Ol results in an immediate decrease in *mg* to 0.885, which then steadily increases with greater pressure (Irifune *et al.*, 1998). Although data on the partitioning behaviour of the three polymorphs of Mg_2SiO_4 are sparse, there may be some distinguishing chemical features to determine what initial polymorph formed when the inclusion crystallised. γ-Ol has the ability to incorporate trivalent cations better than β-Ol, which in turn incorporates trivalent cations better then α-Ol (Brey *et al.*, 2003). The partitioning of divalent cations also changes between polymorphs (Brey *et al.*, 2003). These authors conclude that Mg_2SiO_4 with high *mg*-values and low Ni, Co and Cr indicates an upper mantle origin (and equilibrium with ferropericlase), whereas Mg_2SiO_4 with high Ni, Co and Cr contents at intermediate to low *mg*-values are indicative of an origin in the transition zone or at the ~660 km boundary with the lower mantle. Note that the stability of ferropericlase in the upper mantle is debatable, although traditionally, it is considered stable only in the lower mantle.

8.1.4.5 SiO₂

SiO_2 is not predicted to be an abundant phase in the mantle and is not in equilibrium with a mantle of pyrolitic composition of *mg* = 0.89. More Fe-rich material, however, is in equilibrium with SiO_2 (Fei *et al.*, 1996) as is mafic material

Table 8.5. SiO_2 polymorphs

Mineral	Abbreviation
α-quartz	α-Qtz
β-quartz	β-Qtz
coesite	Coe
stishovite	Sti

(similar to MORB in composition) at ~>300 km depth (Fig. 8.3B). SiO_2 exhibits four polymorphs at P-T conditions that are relevant for the mantle (Table 8.4 and Fig. 8.7).

The distinction between SiO_2 polymorphs based on chemistry alone is difficult because of the lack of element substitution into SiO_2. Polymorph determination can be determined based on phase association, or by varying CL properties (Sobolev *et al.*, 1999), which will be expanded upon in section 8.3.2.1.
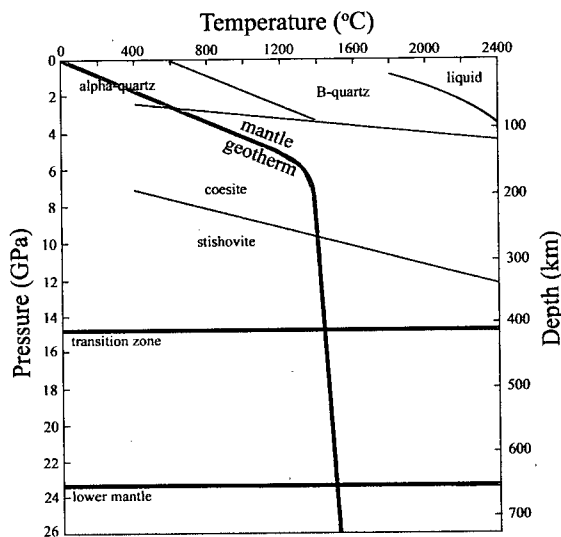
Fig. 8.7. Phase transformations for SiO_2. Modified from Fei and Bertka (1999).

8.1.4.6 Ferropericlase

Ferropericlase has the chemical formula (Mg,Fe)O and forms a solid-solution mineral in the lower mantle, with end-members MgO (periclase) and FeO (wustite). Because of the high *mg* (0.50<*mg*<1.00) for most (Mg,Fe)O grains, they are most accurately described as ferropericlase (fPer); grains with more Fe (0.00<*mg*<.50) are most accurately described as magnesiowustite. FPer forms, along with MgSi-Prv, as a result of the decomposition of γ-Ol (Ito and Takahashi, 1998) and is considered to be the second most abundant phase, ~19 vol %, (16% by weight, Wood, 2000) in the lower mantle (Ringwood, 1991). As previously discussed, this transformation is likely responsible for the strong seismic discontinuity observed at ~660 km and is what distinguishes the upper mantle from the lower mantle (Figs. 8.1 and 8.2). For a pyrolitic lower mantle of *mg* = 0.90, fPer (*mg* = 0.84-0.80) and MgSi-Prv (*mg* = 0.95-0.96) would be in equilibrium (Wood, 2000). Although fPer is considered to form only in the lower mantle, it is not restricted to lower mantle pressures; it is also stable in an upper mantle with sufficiently low Si activity (Stachel *et al.*, 2000b). Ferropericlase does not undergo any phase changes for P-T conditions experienced in the upper and lower mantle, although

preliminary experimental work by Dubrovinsky *et al.*, (2003) find that fPer may dissociate into MgO and FeO at 85 GPa, corresponding to a depth of 1900 to 2000 km. The parental source rocks for fPer are likely pyrolitic or magnesian in bulk composition; fPer is not a predicted phase in a lower mantle of mafic composition.

8.1.4.7 Stability of other phases

$CaTiO_3$, magnetite and sulphides are minor phases that have previously been found in Juina diamonds (Hutchison, 1997; Kaminsky *et al.*, 2001a) and warrant consideration here. As there are little data on the high P-T stability of these minerals little can be said, particularly on the stability of these minerals in an open system of predicted mantle compositions. The pyrolitic and basaltic models do not predict any of these three phases which is likely a result of them either not being in equilibrium with a pyrolitic or eclogitic mantle, or that they only make a small overall proportion of the mantle.

Magnetite (Mag) has the chemical formula $Fe^{2+}Fe^{3+}_2O_4$, and has two polymorphs between temperatures (0 to $1000^{\circ}C$) and pressures (0 to 30 GPa or ~800 km depth) (Haavik *et al.*, 2000). Structural transformation likely takes place somewhere between 200 to 400 km depths (from extrapolation of data from Haavik *et al.*, 2000). Sobolev (1983) finds Mag in association with eclogitic source rocks, although this mineral is rare as an inclusion in diamond. The stability of Mag within eclogite and peridotite as a function of pressure and temperature is unclear.

Perovskite (Prv) has the chemical formula $CaTiO_3$ and is a common mineral in kimberlites and some other deep-sourced magmatic rocks (Mitchell, 1995). It is a relatively rare inclusion in diamond and the stability of this mineral in an open mantle system is unclear.

Sulphides are often cited as being the most common mineral inclusion in diamond, although this may only be true for diamonds from South African kimberlites (Harris and Gurney, 1979) and Yakutian diamonds (Bulanova *et al.*, 1990). Sulphide inclusions are

thought to have formed by the trapping of a primary liquid sulphide melt that crystallises into monosulphide solid solution (MSS) during diamond growth (Bulanova et al., 1996). The P-T stability of sulphides and distribution coefficients as a function of P-T is unclear. Sulphide inclusions from peridotitic diamonds contain 22-36 wt.% Ni, whereas eclogitic diamond inclusion sulphides contain 0-12 wt.% Ni (Bulanova et al., 1996). An intermediate class of sulphides contains 11-18 wt.% Ni and may be sourced from pyroxenitic material (Bulanova et al., 1996).

8.2 Analytical Techniques

8.2.1 Extraction and mounting of inclusions

Inclusions were extracted by mechanical crushing of diamond in an enclosed steel cracker (Fig. 8.8). Diamonds were oriented inside the cell under microscope, lid height was adjusted to ensure it rested on the diamond and then the lid was struck with a hammer. The lid was removed and the contents of the cell were examined under microscope. Often the diamond did not break and the procedure described was repeated, but by applying greater force on the hammer. The goal
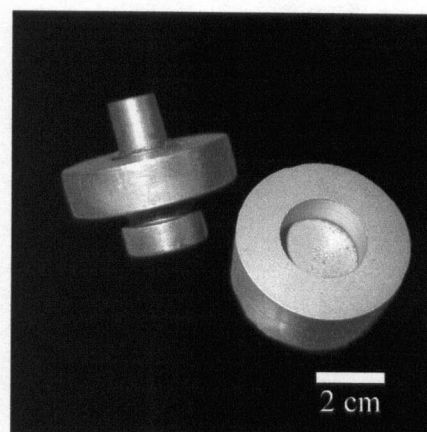
Fig. 8.8. Photograph of diamond cracker.

of this method was to use the minimum force required to induce brittle fracturing so as to cause minimum breakage of the inclusion and to avoid separating the inclusion from its hosting diamond chip. The benefits of this procedure are twofold: 1) smaller inclusions can be examined because of the tendency for inclusions to remain partially embedded in diamond chips, therefore making it possible to pick up and move inclusions of any size; and 2) it is easier to distinguish lab contaminants from diamond inclusions when inclusions are partially embedded in diamond host (e.g. Fig. 8.9A and B).

Once inclusions were exposed, they were moved using fine tweezers to stubs for examination on the SEM. For the case of colourless inclusions, it was often difficult to keep track of which newly produced diamond chips actually contained the

Fig. 8.9. SEM image of inclusions embedded in diamond. A) 4.3 C, D and E. (one Ol and two $MgSiO_3$ grains) and B) 4.3A (fPer).

colourless mineral. Examination of diamond chips under cross-polarised light did not prove helpful in finding inclusions. In many cases where the inclusion could not be located under the microscope, diamond chips were placed on stubs in hope that the inclusion would be located using the SEM. In several cases this approach proved successful. The material remaining in the cell after prospective diamond fragments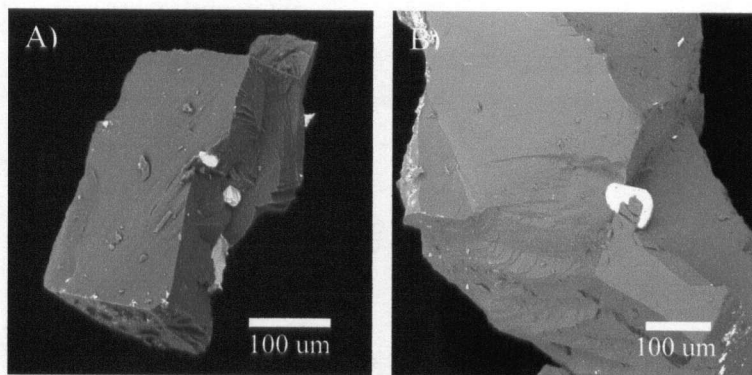 were removed and mounted was dumped into a petri dish and the cell was cleaned with compressed air. Once all prospective fragments had been mounted the 'diamond dust' in the petri dish was examined under polarized and cross-polarized light. Rarely was anything found as it was uncommon for the 'diamond dust' to be isotropic (likely due to extensive crystal deformation as is inferred from the abundant deformation lamellae observed (section 2.3.7)). Diamond dust was placed on a clean sheet of paper and funneled into a vial for reference and future work. Several procedures were followed in order to minimize the possibility of contamination or mixing of samples. Firstly, the cracker (including lid) was examined before breaking any new diamond. As well, the cell was cleaned with a sandblaster roughly twice a week, however, the frequency of sandblasting was motivated more by the oxidation of the cracker than by diamond chip contamination. The petri dish in which the 'diamond dust' was collected was cleaned with compressed air and washed twice with ethanol after all the inclusions had been extracted from each diamond. In most cases diamond chips from different diamonds were stored on separate stubs. Photographs of each stub were collected as a 'map' for future reference.

146

8.2.2 Qualitative identification of inclusions (EDS)

Diamond fragments and inclusions were examined in back scattered electron (BSE) mode on the SEM. As inclusions are typically made up of elements with higher atomic number than that of diamond, they appear bright under BSE and are thus easily identified (Fig. 8.9). Energy dispersion spectrometry (EDS) was used to qualitatively identify inclusions and multi-phase inclusions. Prospective inclusions for EPMA were located and marked on the reference maps.

8.2.3 Quantitative identification of inclusions (EMPA)

The methodology employed in this study to quantitatively examine mineral inclusions was somewhat unusual and warrants description here. The procedure followed in most diamond inclusion studies involves: extraction of individual inclusions, mounting inclusions in small stubs in epoxy and then finely polishing inclusions before electron-probe microanalyses (EPMA). This arduous procedure is followed because the analytical equipment requires a near horizontal surface to produce acceptable results. However, in the case of this study, it was considered too risky or impossible to separate inclusions from their hosting diamond, to mount the separated grains in glue and then to polish the sample.

Table 8.6. Statistics on oxide analyses

Diamond No.	Total number of analyses	Number of analyses between 98-102 wt%	Percent success
1.2	90	29	32.2
1.4	38	5	13.2
1.5	52	21	40.4
2.2	11	3	27.3
2.6	27	3	11.1
2.7	45	5	11.1
2.8	39	3	7.7
2.10	7		0.0
2.11	6		0.0
3.1	28	8	28.6
3.2	97	21	21.6
3.4	21	4	19.0
3.5	58	17	29.3
3.6	41	12	29.3
3.7	30		0.0
3.8	4		0.0
3.9	11	9	81.8
3.10	64	15	23.4
4.3	56	15	26.8
4.7	28	2	7.1
4.10	12	8	66.7
4.11	15		0.0
4.16	6		0.0
5.10	19	3	15.8
6.1	13	5	38.5
6.2	11	2	18.2
6.6	3		0.0
6.8	9		0.0
6.9	11	5	45.5
7.1	4	3	75.0
total	856	198	23.1

147

Instead, inclusions exposed on cleavage surfaces were examined in their unpolished state. Some larger inclusions (>100 microns) were separated from their hosting diamond, however, even these inclusions were examined without polishing. Inclusions were mounted on stubs on double-sided black tape. Because the microprobe has limited vertical range for focusing, it was necessary to ensure that all inclusions were at roughly the same height on the stub. Although every effort was made to orient inclusions in such a way as to create a near

Table 8.7. Statistics on sulphide analyses

Diamond No.	Total number of analyses	Number of analyses between 98-102 wt%	Percent success
2.11	24	6	25.0
4.11	4	2	50.0
6.8	3	3	100.0
total	31	11	35.5

Table 8.8. List of standards used in electron microprobe analyses

Anion	Element	Synthetic/ Natural	Standard	Chemical formula	X-ray lines	Crystal
oxide	Mg	natural	olivine	$Mg_{1.8}Fe_{0.2}SiO_4$	MgK	TAP
	Si	natural	olivine	$Mg_{1.8}Fe_{0.2}SiO_4$	SiK	TAP
	Fe	synthetic	fayalite	Fe_2SiO_4	FeK	LIF
	Mn	synthetic	rhodonite	$MnSiO_3$	MnK	LIF
	Na	natural	albite	$NaAlSi_3O_8$	NaK	TAP
	Al	natural	kaersutite	$NaCa(Fe,Mg)_4TiSi_6Al_2O_{22}(OH)_2$	AlK	TAP
	P	natural	apatite	$Ca_5(PO_4)_3(OH)$	PK	PET
	K	natural	orthoclase	$KAlSi_3O_8$	KK	PET
	Ca	natural	diopside	$CaMgSi_2O_6$	CaK	PET
	Ti	natural	rutile	TiO_2	TiK	PET
	Cr	synthetic	Mg-chromite	$MgCr_2O_4$	CrK	LIF
	Ni	synthetic	Ni-olivine	Ni_2SiO_4	NiK	LIF
	Y		YAG	$Y_3Al_5O_{12}$	YL	TAP
	Zr		zircon	$ZrSiO_4$	ZrL	PET
	Ce		cerium dioxide	CeO_2	CeL	LIF
	La	synthetic	La element	Ca-Al-Si-REE glass	La$L\beta$	LIF
	Pr	synthetic	Pr element	Ca-Al-Si-REE glass	Pr$L\beta$	LIF
	Nd	synthetic	Nd element	Ca-Al-Si-REE glass	NdL	LIF
	Sm	synthetic	Sm element	Ca-Al-Si-REE glass	SmL	LIF
	Gd	synthetic	Gd element	Ca-Al-Si-REE glass	GdL	LIF
sulphide	Fe		pyrite	FeS_2	FeK	LIF
	Co		Co metal		CoK	LIF
	Ni		Ni metal		NiK	LIF
	Cu		tetrahedrite	$(Cu,Fe)_{12}Sb_4S_{13}$	CuK	LIF
	Zn		sphalerite	ZnS	ZnK	LIF
	Mn		Mn metal		MnK	LIF
	S		pyrite	FeS_2	SK	PET

Ca-Al-Si glass standard is from (Drake and Weill 1972).

horizontal surface, many totals collected were poor. Analyses success rates for each diamond are presented in Table 8.6 (for silicates) and Table 8.7 for sulphides.

EPMA of inclusions were done on a fully-automated CAMECA SX-50 microprobe, operating in the wavelength-dispersion mode with the following operating conditions: excitation voltage, 15 kV; beam current, 20 nA; peak count time, 20 s; background count time, 10 s; beam diameter, 1 μm. For elements Y, Zr, Ce, La, Pr, Nd, Sm and Gd, peak count time was 40 s and background count time was 20 s. Data reduction was performed using the 'PAP' $\phi(\rho Z)$ method (Pouchou and Pichoir 1985). Table 8.8 lists the standards, X-ray lines and crystals used for the elements analysed. Minimum detection limits (MDL's) for all data listed as weight percent oxides is found in Table 8.9. MDL's for sulphides are listed as element weight percent. Table 8.10 lists the MDL's for all cation calculations. Error limits for EPMA analyses are listed in Table 8.11 (wt% totals) and Table 8.12 (cation totals) at the 95% confidence level (2σ).

Table 8.9. Minimum detection limits for weight percent values

mineral	P_2O_5	SiO_2	TiO_2	Al_2O_3	Cr_2O_3	FeO	MnO	NiO	MgO	CaO	Na_2O	K_2O
fPer	0.06	0.03	0.05	0.04	0.13	0.65	0.07	0.10	0.38	0.04	0.03	0.03
Grt	0.09	0.32	0.06	0.22	0.13	0.36	0.07	0.06	0.13	0.17	0.03	0.03
Mag	-	0.04	0.07	0.06	0.10	1.01	0.07	0.06	0.05	0.03	0.03	0.04
Ol	0.05	0.33	0.04	0.02	0.11	0.28	0.06	0.09	0.33	0.03	0.02	0.03
$MgSiO_3$	0.06	0.42	0.04	0.06	0.15	0.17	0.06	0.05	0.27	0.03	0.02	0.02
$CaSiO_3$	0.07	0.38	0.04	0.03	0.09	0.06	0.05	0.06	0.02	0.56	0.04	0.03

	Y_2O_3	ZrO_4	Nb_2O_5	La_2O_3	Ce_2O_3	Pr_2O_3	Nd_2O_3	Sm_2O_3	Gd_2O_3	ThO_4
Prv	0.03	0.09	0.06	0.06	0.07	0.17	0.10	0.13	0.07	0.03

	S	Mn	Fe	Co	Ni	Cu	Zn	As	Ag	Cd	Sb	Pb
Sul	0.31	0.03	0.40	0.05	0.19	0.05	0.03	0.02	0.06	0.06	0.05	0.00

MDL's of weight percent results listed for each mineral type identified. Table is subdivided into three sections: major oxides, LREE's for Prv, and sulphides. MDL's for the major oxides in Prv are the same as those for $CaSiO_3$.

Table 8.10. Minimum detection limits for cation values

mineral	P^{5+}	Si^{4+}	Ti^{4+}	Al^{3+}	Cr^{3+}	Fe^{2+}	Mn^{2+}	Ni^{2+}	Mg^{2+}	Ca^{2+}	Na^+	K^+
fPer	0.008	0.005	0.003	0.006	0.010	0.007	0.006	0.007	0.007	0.004	0.011	0.004
Grt	0.007	0.005	0.003	0.005	0.010	0.005	0.005	0.006	0.004	0.003	0.009	0.004
Mag	-	0.003	0.002	0.003	0.006	0.005	0.004	0.005	0.004	0.002	0.008	0.003
Ol	0.002	0.002	0.001	0.001	0.003	0.002	0.002	0.002	0.002	0.001	0.003	0.001
$MgSiO_3$	0.001	0.001	0.001	0.001	0.002	0.001	0.001	0.001	0.001	0.001	0.002	0.001
$CaSiO_3$	0.002	0.001	0.001	0.001	0.003	0.001	0.001	0.002	0.001	0.001	0.002	0.001

	Y^{+3}	Zr^{+4}	Nb^{+5}	La^{+3}	Ce^{+3}	Pr^{+3}	Nd^{+3}	Sm^{+3}	Gd^{+3}	Th^{+4}
Prv	0.001	0.001	0.001	0.001	0.001	0.003	0.001	0.002	0.001	0.000

	S^-	Mn^{+2}	Fe^{+2}	Co^{+2}	Ni^{+2}	Cu^{+2}	Zn^+	As	Ag^{+2}	Cd	Sb	Pb^+
Sul	0.001	0.001	0.001	0.001	0.001	0.001	0.001	0.002	0.001	0.001	0.001	0.001

MDL's of cation values listed for each mineral type identified. Table is subdivided into three sections: major oxides, LREE's for Prv, and sulphides. MDL's for the major oxides in Prv are the same as those for $CaSiO_3$. The general formula units with cation totals (R) are as follows: 10RO for fPer; R_8O_{12} for Grt; R_3O_4 for Mag and Ol and; R_2O_3 for $MgSiO_3$ and $CaSiO_3$.

Table 8.11. Precision for weight percent values at 95% confidence level

mineral	P_2O_5	SiO_2	TiO_2	Al_2O_3	Cr_2O_3	FeO	MnO	NiO	MgO	CaO	Na_2O	K_2O
fPer	0.11	0.06	0.05	0.06	0.16	0.10	0.08	0.11	0.05	0.04	0.07	0.04
Grt	0.11	0.07	0.06	0.05	0.16	0.08	0.08	0.10	0.04	0.04	0.06	0.04
Mag	-	0.06	0.06	0.06	0.15	0.11	0.09	0.12	0.05	0.04	0.08	0.04
Ol	0.11	0.07	0.05	0.05	0.16	0.08	0.07	0.10	0.04	0.04	0.05	0.04
$MgSiO_3$	0.10	0.08	0.05	0.05	0.16	0.08	0.08	0.10	0.04	0.04	0.05	0.03
$CaSiO_3$	0.12	0.07	0.06	0.04	0.18	0.08	0.08	0.11	0.04	0.05	0.06	0.04

	Y_2O_3	ZrO_4	Nb_2O_5	La_2O_3	Ce_2O_3	Pr_2O_3	Nd_2O_3	Sm_2O_3	Gd_2O_3	ThO_4
Prv	0.05	0.12	0.08	0.10	0.09	0.29	0.14	0.25	0.12	0.09

	S	Mn	Fe	Co	Ni	Cu	Zn	As	Ag	Cd	Sb	Pb
Sul	0.03	0.04	0.05	0.05	0.05	0.04	0.08	0.14	0.10	0.10	0.09	0.32

Precision for weight percent errors listed at the 95% confidence level for each mineral type identified. Table is subdivided into three sections: major oxides, LREE's for Prv, and sulphides. Error for the major oxides found in Prv are the same as those for $CaSiO_3$.

Table 8.12. Precision for cation calculations at 95% confidence level

mineral	P^{5+}	Si^{4+}	Ti^{4+}	Al^{3+}	Cr^{3+}	Fe^{2+}	Mn^{2+}	Ni^{2+}	Mg^{2+}	Ca^{2+}	Na^+	K^+
fPer	0.004	0.003	0.003	0.004	0.009	0.045	0.005	0.007	0.048	0.004	0.005	0.003
Grt	0.006	0.024	0.003	0.019	0.008	0.023	0.005	0.003	0.015	0.013	0.005	0.003
Mag	-	0.002	0.003	0.004	0.004	0.043	0.003	0.003	0.004	0.002	0.003	0.003
Ol	0.001	0.008	0.001	0.001	0.002	0.006	0.001	0.002	0.012	0.001	0.001	0.001
$MgSiO_3$	0.001	0.007	0.001	0.001	0.002	0.003	0.001	0.001	0.007	0.001	0.001	0.000
$CaSiO_3$	0.001	0.007	0.001	0.001	0.001	0.001	0.001	0.001	0.001	0.012	0.001	0.001

	Y^{+3}	Zr^{+4}	Nb^{+5}	La^{+3}	Ce^{+3}	Pr^{+3}	Nd^{+3}	Sm^{+3}	Gd^{+3}	Th^{+4}
Prv	0.000	0.001	0.001	0.001	0.001	0.001	0.001	0.001	0.001	0.000

	S^-	Mn^{+2}	Fe^{+2}	Co^{+2}	Ni^{+2}	Cu^{+2}	Zn^+	As	Ag^{+2}	Cd	Sb	Pb^+
Sul	0.009	0.001	0.007	0.001	0.003	0.001	0.000	0.000	0.001	0.000	0.000	0.000

Cation errors listed at the 95% confidence level for each mineral type identified. Table is subdivided into three sections: major oxides, LREE's for Prv, and sulphides. Error for the major oxides found in Prv are the same as those for $CaSiO_3$.

8.3 Results

The following section contains the results of EPMA and EDS analysis for mineral inclusions as well as SEM images for the majority of grains analysed in this study. EPMA data was preferred over EDS data, however, due to the small grain size and inclusion heterogeneity, it was often not possible to collect decent EPMA data (see Tables 8.6 and 8.7 for analysis success rates). When acceptable EPMA data is not available, EDS spectra are generally included. The mineral phases and frequency of phases that occur in each diamond (i.e. mineral associations) that were analysed using EPMA and produced acceptable results (i.e. wt% totals between 98 and 102) are listed in table format in Appendix E. Appendix F lists all the inclusions identified in each diamond through EDS.

This section is divided into five subsections: inclusions of primary origin, inclusions of uncertain origin, touching phases and inclusions of secondary origin. The fifth section, a somewhat special category, has been created for Fe-Ni blebs on ferropericlase grains. Assigning inclusions to either a primary or secondary origin is not a trivial matter and is responsible for much debate, and hence the motivation for the 'inclusions of uncertain origin' category. When resources and time permit, some scientists polish 'windows' on diamonds to determine if any cracks lead from the diamond surface to the inclusion (e.g. Harris *et al.*, 1997), however, this technique was not used in this study. Instead, grains were examined using a conventional microscope and any diamond with extensive fractures was noted. During mechanical fracturing, diamonds with extensive fractures (previously noted) typically fragmented easily. A more detailed description of the criteria used to distinguish the origin of inclusions (i.e. primary vs. secondary) is presented in the preamble to each subsection.

## 8.3.1 Inclusions of primary origin

Primary grains are inclusions that have remained isolated inside the diamond since encapsulation during diamond crystallization. They are pristine samples from the mantle. These inclusions are typically competent (i.e. they do not break easily), subhedral to euhedral in crystal form and homogeneous (in terms of chemistry). Eight phases comprise primary inclusions. They are: ferropericlase, $MgSiO_3$, $CaSiO_3$, Mg_2SiO_4, pyrope-almandine-grossular garnet, tetragonal-almandine-pyrope phase, pyrrhotite and magnetite.

8.3.1.1 Ferropericlase

Ferropericlase (fPer) is the most abundant inclusion found during this study. Approximately 100 individual crystals have been extracted from 16 diamonds (36% of diamonds broken or 23% of the total diamonds in this study). FPer belongs to the isometric crystal system, with cubes and octahedrons being the most common forms to develop (Nesse, 1991). Grains in this study are typically euhedral and exhibit either an equant cubo-octahedral form (e.g. Figs. 8.10, 3.10C, O and 5.10E) or a cubo-octahedral form with elongation in one or two directions (e.g. Figs. 8.10, 1.2AJ, 1.5G, 3.2A, F, and G, 3.5D, E, and M and 4.3J). In some cases there is minor development of a (110) face (e.g Fig. 8.10, 3.10W). Because diamond also forms octahedra and cubo-octahedra (section 2.1.1.1), it is unclear if the euhedral morphology is being imposed by the host diamond or is in fact an expression of the primary growth faces of fPer grains. Regardless of whether or not the cubo-octahedral morphology of fPer is a result of fPer growth or imposed diamond growth, the large percentage of euhedral crystals is mostly uncommon for other phases in this study. Euhedral crystals may be more common because the fPer structure is likely stable from the time of entrapment in diamond until extraction in the laboratory, whereas most of the other phases likely undergo a number of structural changes.
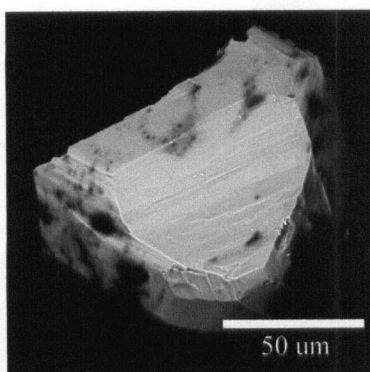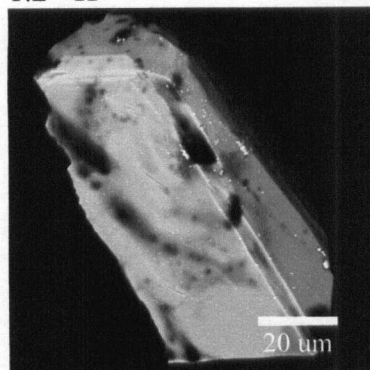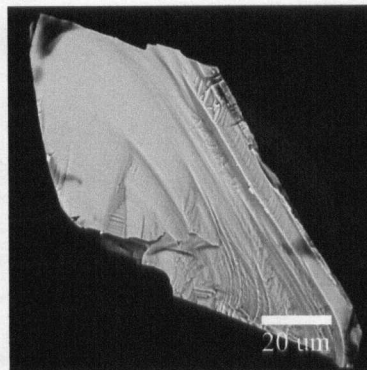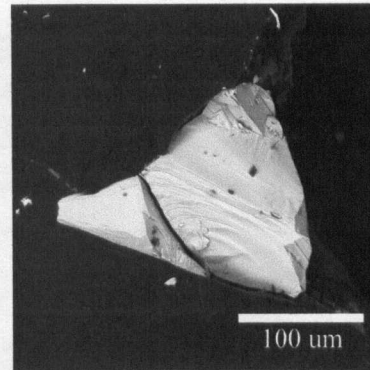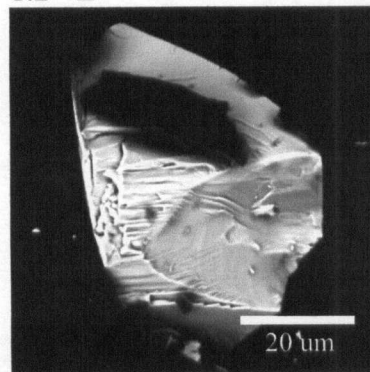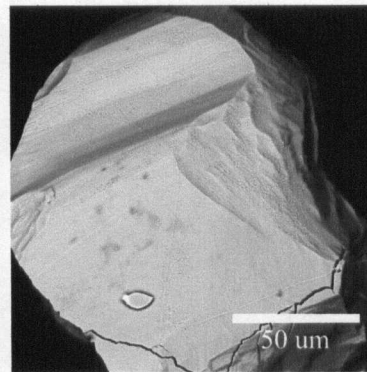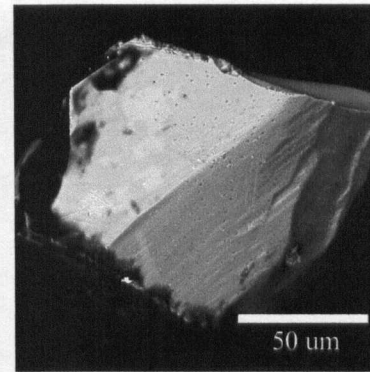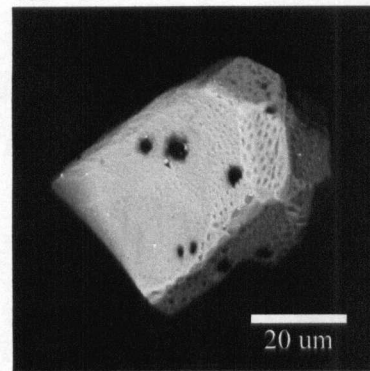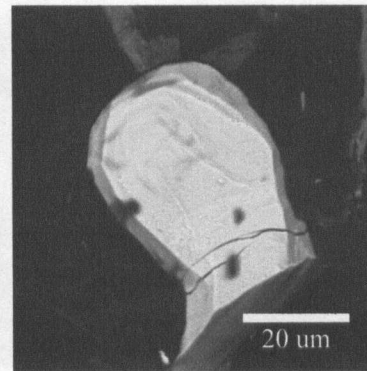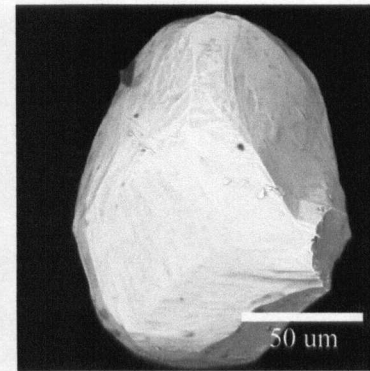
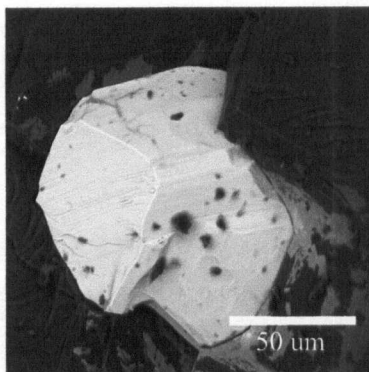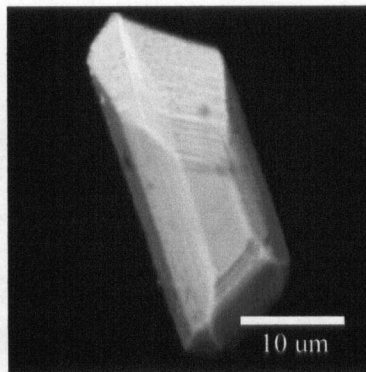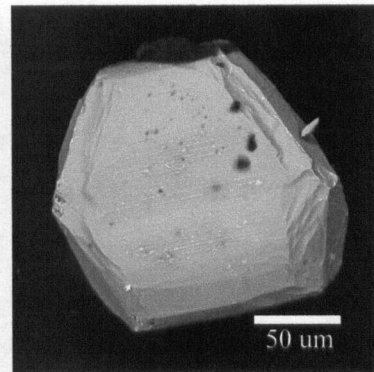1.2 - H
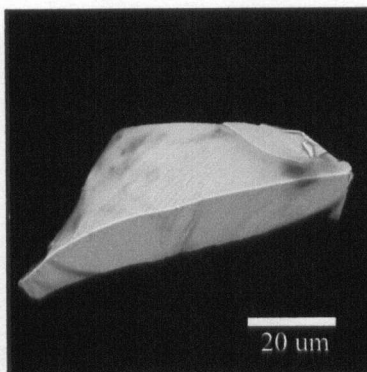
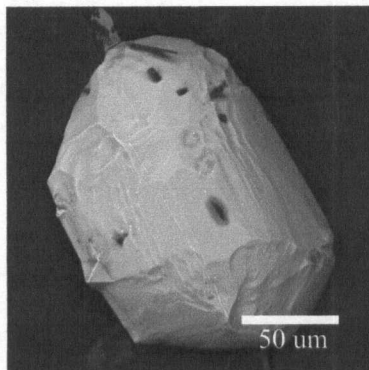1.2 - I
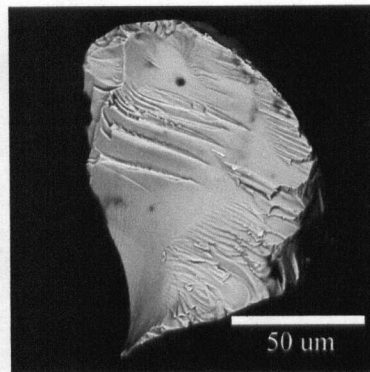
1.2 - J

1.2 - L
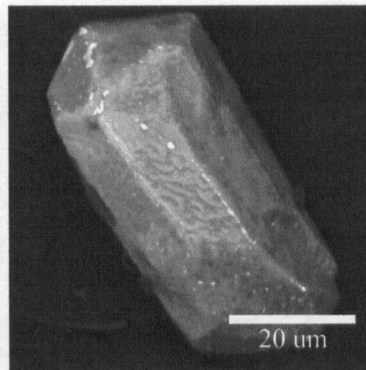
1.2 - M

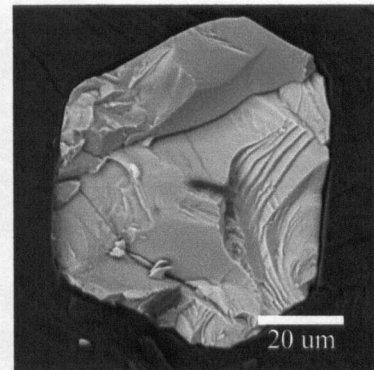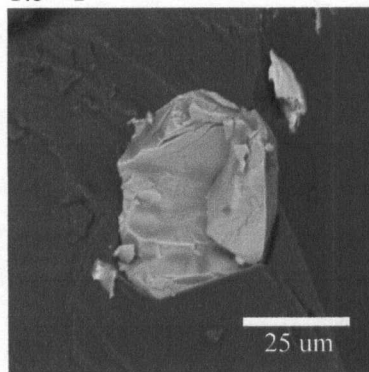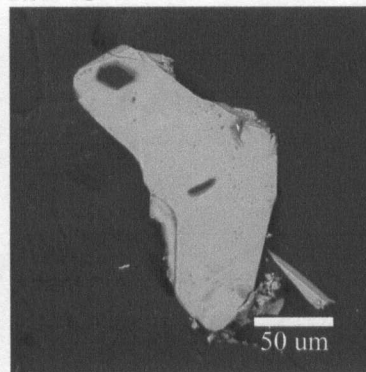1.2 - P

1.2 - R

1.2 - V

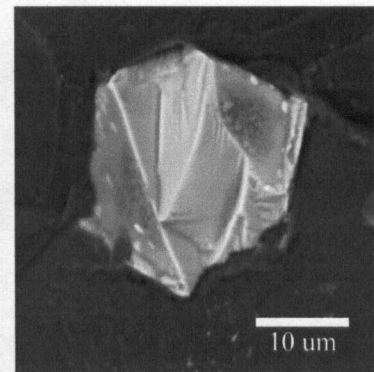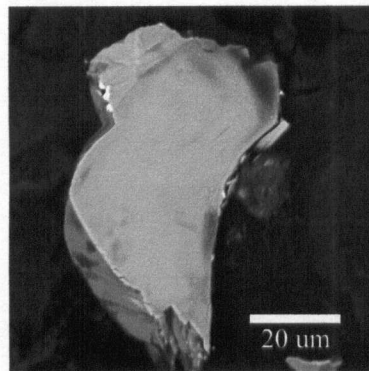1.2 - W

1.2 – Y

1.2 - AE

1.2 - AF

1.2 - AI

1.2 – AJ

1.5 - D

1.5 - F

1.5 – G

1.5 - K

2.2 – E

2.7 – A

2.7 – C

2.7 – E
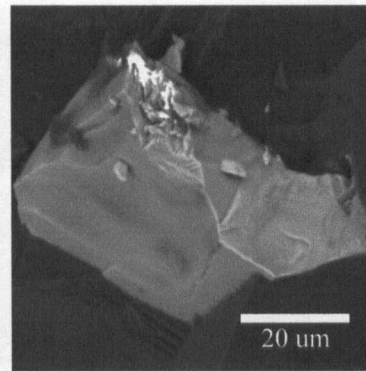
2.7 – O
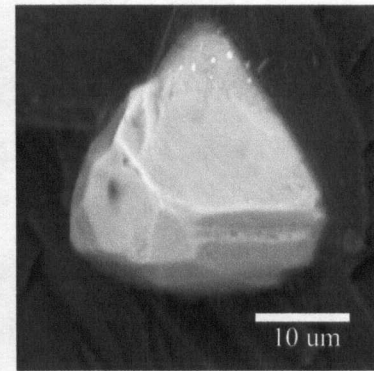
3.1 - B
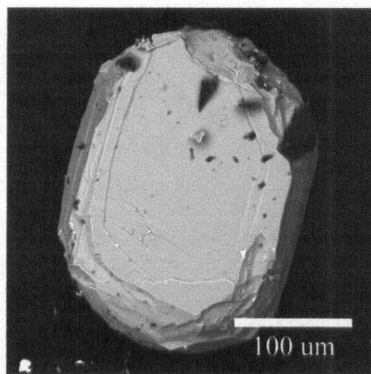
3.2 – A
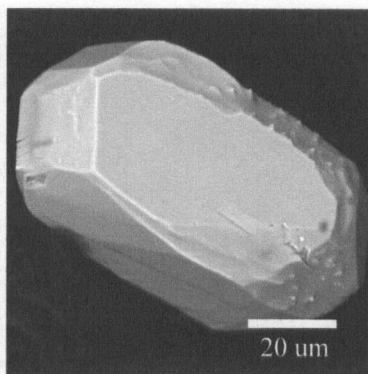
3.2 – F
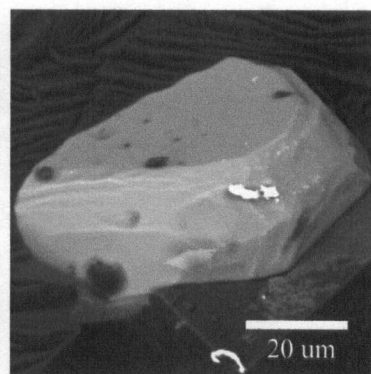
3.2 – G
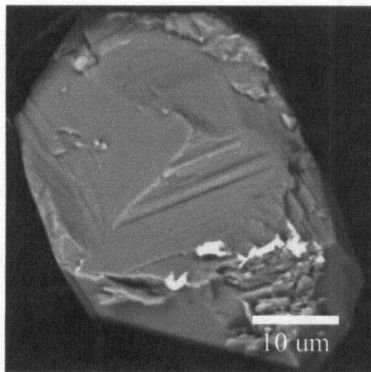
3.2 J
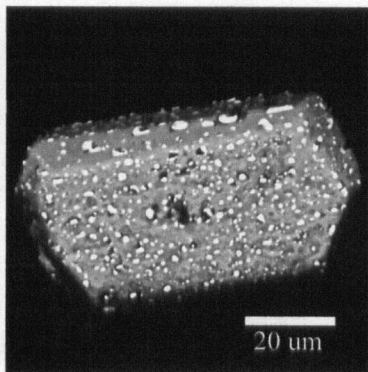
3.5 – D
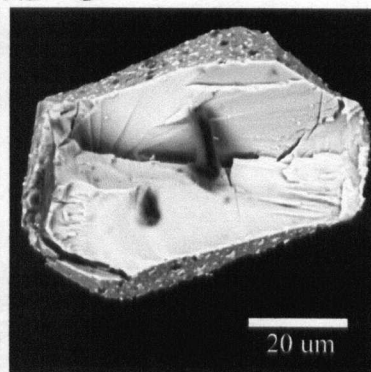
3.5 – E
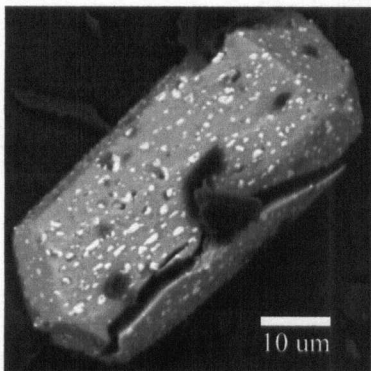
3.5 - M
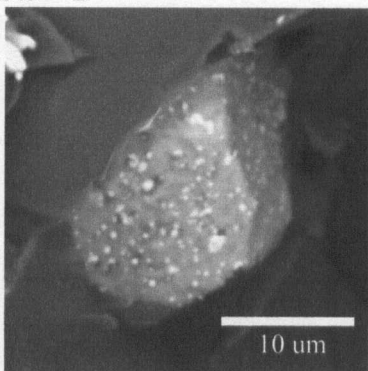
3.5 – P
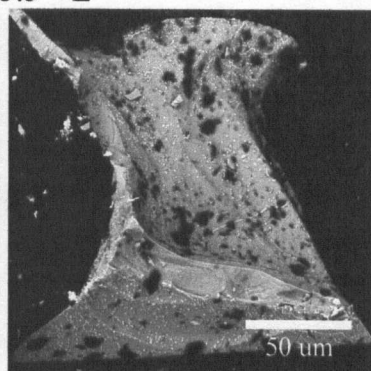
3.6 - D
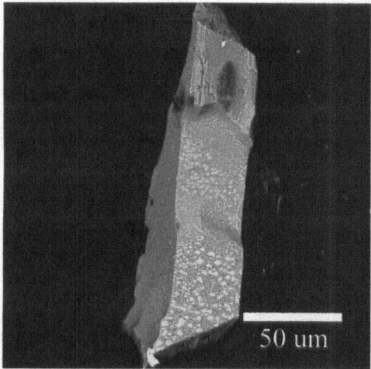
3.6 – J
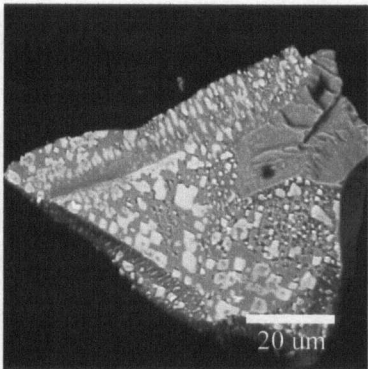
3.6 - K
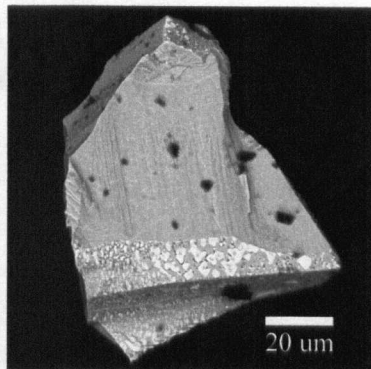
3.6 – L
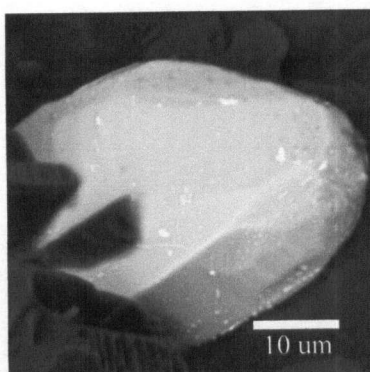
3.9 - H
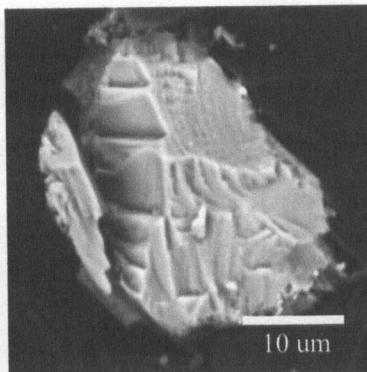
3.9 – I
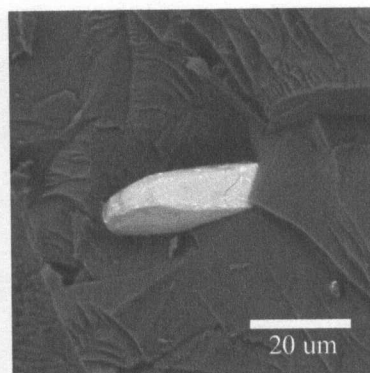
3.9 – J
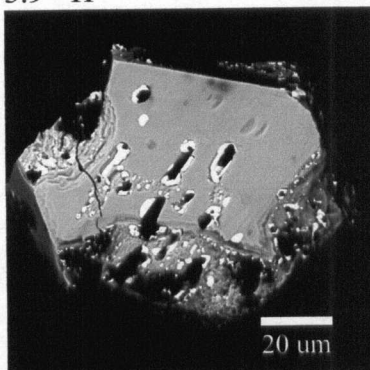
3.10 – C
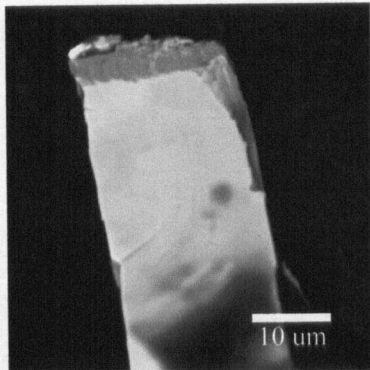
3-10 – H
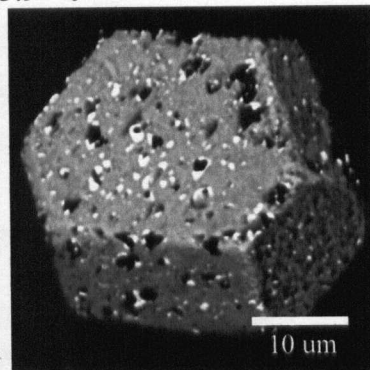
3.10 – O
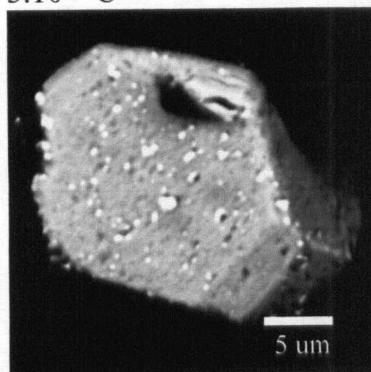
3.10 – W
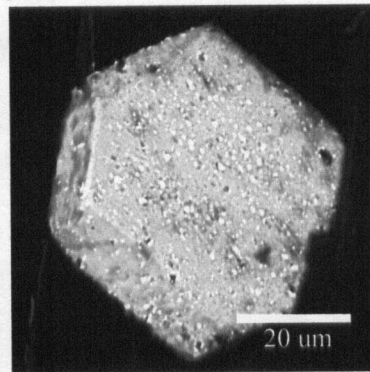
3.10 – Z
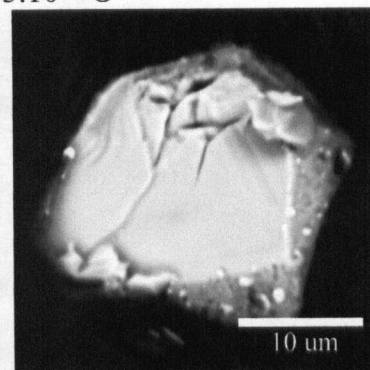
3.10 – AA
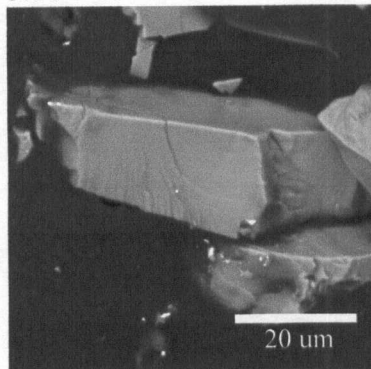
4.3 – B
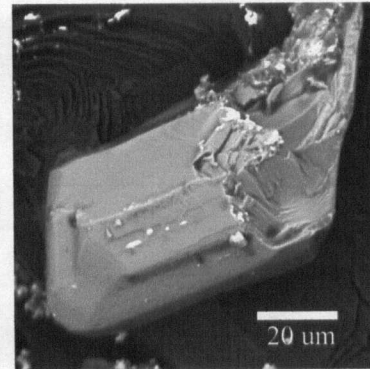
4.3 – J
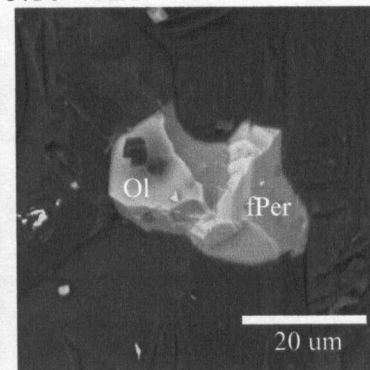
4.3 – K2
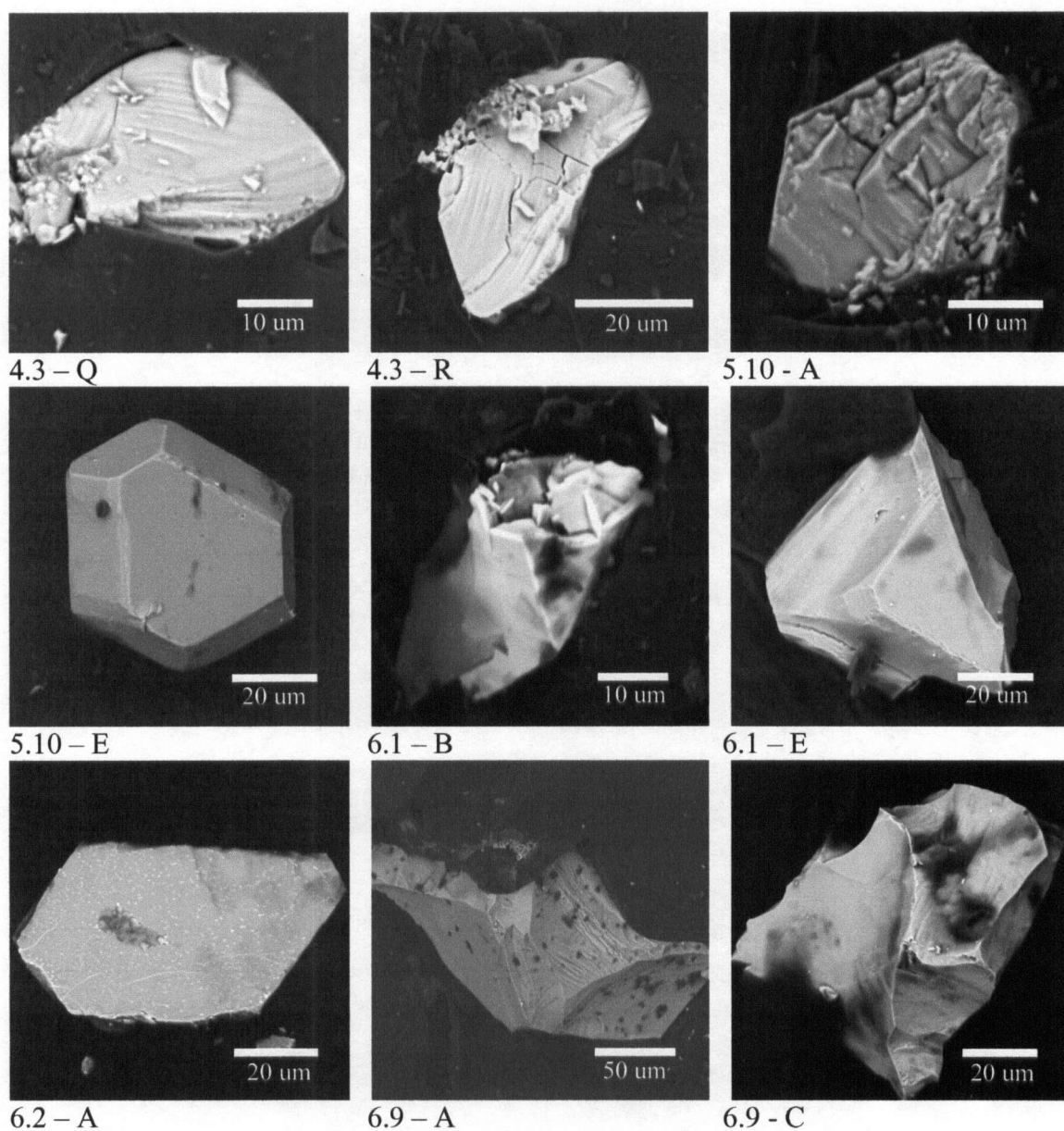
Fig. 8.10. SEM images of ferropericlase grains. Number refers to diamond which hosted the inclusion while the letter refers to the inclusion sample code. Major oxide chemistry and cation calculations for each inclusion are found in Tables 8.13 and 8.14 respectively.

Ferropericlase grains are typically black and opaque; however, some grains are pale orange (Diamond 2.7, inclusion A) while others are pale purple (Diamond 3.2, inclusions F, G, and J). Inclusion colour is likely both a function of grain thickness and chemistry, although chemical data does not seem to support the latter hypothesis. Inclusions range in size from 20 to 250 microns.

Major oxide chemical data for 57 grains from 15 diamonds are presented in Table 8.13, with accompanying cation calculations in Table 8.14. Grains fall along the periclase-wustite (MgO-FeO) solid-solution series and are skewed towards the more magnesium-rich end-member. There is considerable range in *mg* (herein defined as $Mg^{2+}/(Mg^{2+}+Fe^{2+})$, where all iron is calculated as Fe^{2+}) from 45.1 to 88.9 with an average of 66.9 ± 13.0 (1σ). However, it is important to note that this average is skewed towards diamonds containing more ferropericlase grains.

Analyses for grains 3-5D, M and P are likely a combination of two phases (fPer and Fe-Ni blebs) and will be removed for the following generalisations (Fe-Ni blebs are discussed in section 8.3.4). Mg^{2+} and Fe^{2+} fill 92.8 to 99.6% of the cation site, with the remainder of site being filled by NiO (0.11-1.46 with an average 0.72 wt%), Cr_2O_3 (0.00-1.30 wt%, average 0.47 wt%), MnO (0.12-1.46 wt%, average 0.41 wt%) and Na_2O (0.00-2.31 wt%, average 0.39 wt%). There is a positive correlation between Ni and Mg content.

Fig. 8.11 illustrates the general similarities in FeO and MgO wt% between fPer inclusions liberated from the same diamond. Diamond 3-9 is the main exception, hosting three fPer inclusions with *mg* ranging from 0.74 to 0.89. A linear fit to data in Fig. 8.11 yields the

Fig. 8.11. Plot of FeO versus MgO of fPer grains by diamond. Legend refers to diamond sample number. Substitution between FeO and MgO is almost 1:1. (Diamond 3-5 (purple squares) is a combination of two phases (fPer and Fe-Ni blebs)).

equation FeO = -0.9905MgO + 96.814 with an R^2 value of 0.9813.

Table 8.13. Major oxide chemistry for ferropericlase grains (wt%)

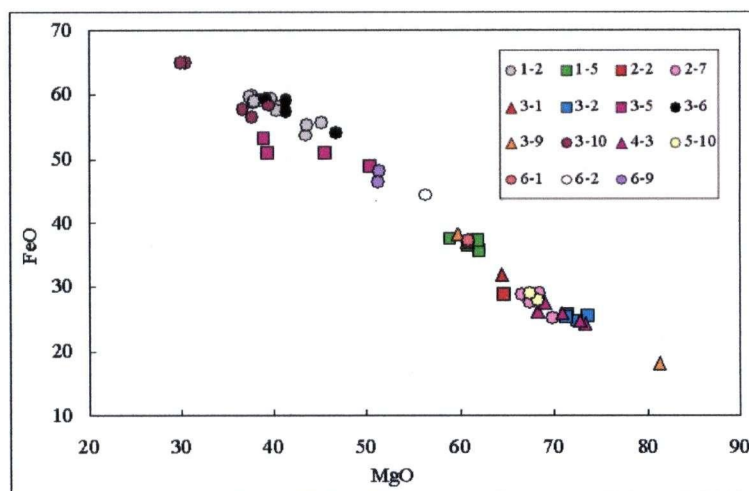| Inclusion No.	No.	Inclusion assemblage	No. of analyses averaged	P_2O_5	SiO_2	TiO_2	Al_2O_3	Cr_2O_3	FeO	MnO	NiO	MgO	CaO	Na_2O	K_2O	Total
1-2H	1		3	na	0.00	0.00	0.00	0.17	59.93	0.31	0.22	37.63	0.00	0.12	0.00	98.37
1-2I	2		3	na	0.09	0.00	0.00	0.00	58.38	0.29	0.20	39.94	0.00	0.14	0.00	99.05
1-2J	3		2	na	0.06	0.00	0.00	0.20	58.49	0.30	0.20	40.42	0.00	0.11	0.00	99.80
1-2L	4		1	na	0.08	0.00	0.00	0.16	55.67	0.38	0.18	45.19	0.00	0.00	0.00	101.68
1-2M	5		3	na	0.10	0.00	0.00	0.17	59.51	0.32	0.21	39.38	0.00	0.13	0.00	99.82
1-2P	6		3	na	0.08	0.00	0.00	0.19	59.54	0.27	0.20	39.75	0.00	0.11	0.00	100.13
1-2R	7		1	na	0.12	0.00	0.00	0.17	53.56	0.24	0.21	43.54	0.00	0.11	0.00	97.96
1-2V	8		1	na	0.09	0.00	0.00	0.18	59.56	0.38	0.30	37.38	0.00	0.16	0.00	98.04
1-2W	9		1	na	0.11	0.00	0.07	0.23	58.92	0.33	0.27	37.88	0.00	0.14	0.00	97.94
1-2Y	10		3	na	0.22	0.00	0.00	0.22	57.59	0.43	0.17	40.44	0.00	0.48	0.00	99.55
1-2AE	11		1	na	0.11	0.00	0.00	0.19	59.18	0.37	0.23	38.34	0.00	1.15	0.00	99.56
1-2AF	12		3	na	0.10	0.00	0.00	0.17	59.22	0.37	0.26	38.70	0.00	0.45	0.00	99.28
1-2AI	13		2	na	0.09	0.00	0.08	0.21	59.07	0.35	0.26	37.99	0.00	0.42	0.00	98.46
1-2AJ	14		2	na	0.24	0.00	0.06	0.16	55.28	0.37	0.23	43.70	0.00	0.10	0.00	100.14
1-5D	15	Ol-MgSiO$_3$-TAPP	3	0.00	0.07	0.00	0.00	0.35	37.56	0.30	1.18	58.97	0.00	0.11	0.00	98.55
1-5F	16	Ol-MgSiO$_3$-TAPP	3	0.00	0.09	0.00	0.00	0.39	36.42	0.32	1.20	60.94	0.00	0.00	0.00	99.35
1-5G	17	Ol-MgSiO$_3$-TAPP	3	0.00	0.08	0.00	0.00	0.41	35.58	0.28	1.14	62.13	0.00	0.49	0.00	100.11
1-5K	18	Ol-MgSiO$_3$-TAPP	1	0.00	0.09	0.00	0.00	0.32	37.25	0.23	1.13	61.86	0.00	0.23	0.00	101.11
2-2E	19	CaSiO$_3$	3	na	0.15	0.00	0.11	0.50	33.90	0.26	1.35	64.63	0.00	0.49	0.00	101.40
2-7A	20		1	0.00	0.06	0.00	0.00	0.47	28.86	0.36	1.32	66.68	0.00	0.19	0.00	97.95
2-7C	21		1	0.00	0.12	0.00	0.00	0.42	27.56	0.43	1.07	67.49	0.27	0.41	0.28	98.05
2-7E	22		2	0.00	0.72	0.00	0.50	0.47	25.12	0.41	1.11	69.95	0.26	0.57	0.19	99.30
2-7O	23		1	0.00	0.00	0.00	0.00	0.57	28.94	0.38	1.28	68.45	0.00	0.29	0.06	99.97
3-1B	24	CaSiO$_3$	2	na	0.18	0.00	0.18	0.87	31.86	0.49	1.01	64.54	0.00	1.50	0.00	100.63
3-2A	25	Ol-MgSiO$_3$-CaSiO$_3$-TAPP?	2	na	0.14	0.00	0.00	0.36	25.69	0.25	1.39	71.45	0.00	0.00	0.00	99.28
3-2F	26	Ol-MgSiO$_3$-CaSiO$_3$-TAPP?	1	na	0.00	0.00	0.00	0.40	25.43	0.24	1.17	73.67	0.00	0.67	0.00	101.58
3-2G	27	Ol-MgSiO$_3$-CaSiO$_3$-TAPP?	3	na	0.08	0.00	0.00	0.35	24.67	0.22	1.36	72.41	0.00	0.18	0.00	99.26
3-2J	28	Ol-MgSiO$_3$-CaSiO$_3$-TAPP?	2	na	0.11	0.00	0.00	0.38	25.27	0.27	1.34	71.30	0.00	0.18	0.00	98.86
3-5D	29	Ol-MgSiO$_3$	3	na	0.08	0.00	0.08	0.91	53.24	0.78	2.69	38.96	0.00	2.20	0.00	98.93
3-5E	30	Ol-MgSiO$_3$	1	na	0.11	0.00	0.06	0.76	48.97	0.79	0.31	50.34	0.00	0.34	0.00	101.68
3-5M	31	Ol-MgSiO$_3$	2	na	0.07	0.00	0.12	0.73	51.02	0.69	6.40	39.34	0.00	0.61	0.00	98.98
3-5P	32	Ol-MgSiO$_3$	2	na	0.06	0.00	0.11	0.86	51.01	0.66	2.46	45.48	0.00	0.09	0.00	100.73
3-6D	33		2	na	0.12	0.00	0.00	0.00	53.97	0.23	0.24	46.84	0.00	0.00	0.00	101.41
3-6J	34		3	na	0.00	0.00	0.08	0.00	57.35	0.18	0.30	41.39	0.00	0.00	0.00	99.29
3-6K	35		3	na	0.06	0.00	0.13	0.00	59.38	0.20	0.22	39.17	0.00	0.00	0.00	99.17
3-6L	36		3	na	0.10	0.00	0.10	0.00	59.28	0.19	0.15	41.34	0.00	0.00	0.00	101.15
3-9H	37		3	na	0.11	0.00	0.00	0.35	38.37	0.34	1.01	59.77	0.00	0.14	0.00	100.10
3-9I	38		3	na	0.25	0.00	0.08	0.22	18.00	0.16	0.92	81.24	0.04	0.00	0.00	100.91
3-9J	39		3	na	0.20	0.00	0.06	0.33	37.05	0.30	0.97	60.77	0.00	0.73	0.00	100.41
3-10C	40		3	na	0.00	0.00	0.18	1.30	64.97	1.46	0.13	30.35	0.00	0.64	0.00	99.02
3-10H	41		2	na	0.13	0.00	0.20	1.27	58.39	1.35	0.11	39.59	0.00	0.56	0.00	101.60
3-10O	42		3	na	0.10	0.00	0.20	1.24	57.71	1.29	0.16	36.68	0.00	1.52	0.00	98.89
3-10Z	43		1	na	0.00	0.00	0.18	1.20	65.00	1.38	0.75	30.42	0.00	1.58	0.00	100.53
3-10AA	44		2	na	0.00	0.00	0.17	1.24	65.09	1.33	0.12	30.02	0.00	1.20	0.00	99.18
3-10W	45		3	na	0.14	0.00	0.25	0.95	56.59	1.11	1.31	37.64	0.00	2.31	0.00	100.31
4-3B	46	Ol-MgSiO$_3$	1	na	0.06	0.00	0.11	0.83	24.21	0.22	1.28	73.29	0.00	0.49	0.00	100.50
4-3J	47	Ol-MgSiO$_3$	2	na	0.14	0.00	0.10	0.98	24.71	0.23	1.41	72.82	0.00	0.89	0.00	101.30
4-3K2	48	Ol-MgSiO$_3$	2	na	0.26	0.00	0.42	1.01	25.96	0.26	1.35	70.83	0.00	0.00	0.00	100.08
4-3Q	49	Ol-MgSiO$_3$	1	na	0.12	0.00	0.10	1.01	26.19	0.20	1.46	68.35	0.00	0.92	0.00	98.35
4-3R	50	Ol-MgSiO$_3$	2	na	0.07	0.00	0.08	1.18	27.57	0.23	1.26	68.98	0.00	0.57	0.00	99.96

Table 8.13. Major oxide chemistry for ferropericlase grains (wt%) (continued)

Inclusion No.	No.	Inclusion assemblage	No. of analyses averaged	P$_2$O$_5$	SiO$_2$	TiO$_2$	Al$_2$O$_3$	Cr$_2$O$_3$	FeO	MnO	NiO	MgO	CaO	Na$_2$O	K$_2$O	Total
5-10A	51		1	0.00	0.14	0.00	0.08	0.54	28.09	0.28	1.07	68.33	0.00	0.00	0.00	98.55
5-10E	52		2	0.00	0.34	0.00	0.07	0.51	28.94	0.36	1.21	67.52	0.00	0.08	0.00	99.02
6-1B	53		2	na	0.13	0.00	0.22	0.44	36.95	0.40	0.91	60.93	0.00	0.00	0.00	99.99
6-1E	54		3	na	0.08	0.00	0.41	0.40	37.21	0.38	0.93	60.97	0.00	0.23	0.00	100.61
6-2A	55		2	na	0.16	0.00	0.00	0.29	44.39	0.12	0.39	56.34	0.00	0.00	0.00	101.69
6-9A	56		3	0.00	0.08	0.00	0.00	0.25	48.03	0.12	0.26	51.35	0.00	0.08	0.00	100.19
6-9C	57		2	na	0.11	0.00	0.00	0.21	46.38	0.12	0.24	51.22	0.00	0.00	0.00	98.29

Inclusion assemblage - refers to the other confirmed phases in the diamond (blank entries indicate that only fPer was found); No. of analyses averaged - the number of analyses with acceptable results (generally between 98-102) that were averaged. na - not analysed. Values below MDL (see Table 8.9) are replaced by 0.00.

Table 8.14. Cation calculations for ferropericlase

Inclusion No.	Inclusion assemblage	P^{5+}	Si^{4+}	Ti^{4+}	Al^{3+}	Cr^{3+}	Fe^{2+}	Mn^{2+}	Ni^{2+}	Mg^{2+}	Ca^{2+}	Na$^+$	K$^+$	Total	mg
1-2H		na	0.000	0.000	0.000	0.012	4.686	0.024	0.016	5.244	0.000	0.023	0.000	10.005	0.53
1-2I		na	0.008	0.000	0.000	0.000	4.475	0.023	0.015	5.458	0.000	0.025	0.000	10.004	0.55
1-2J		na	0.005	0.000	0.000	0.015	4.444	0.023	0.015	5.475	0.000	0.020	0.000	9.998	0.55
1-2L		na	0.007	0.000	0.000	0.011	4.057	0.028	0.013	5.870	0.000	0.000	0.000	9.987	0.59
1-2M		na	0.009	0.000	0.000	0.012	4.548	0.024	0.015	5.364	0.000	0.022	0.000	9.996	0.54
1-2P		na	0.007	0.000	0.000	0.014	4.530	0.021	0.014	5.390	0.000	0.019	0.000	9.995	0.54
1-2R		na	0.011	0.000	0.000	0.012	4.049	0.019	0.015	5.867	0.000	0.020	0.000	9.993	0.59
1-2V		na	0.008	0.000	0.000	0.013	4.671	0.030	0.022	5.225	0.000	0.030	0.000	10.000	0.53
1-2W		na	0.010	0.000	0.007	0.017	4.606	0.027	0.020	5.278	0.000	0.025	0.000	9.990	0.53
1-2Y		na	0.020	0.000	0.000	0.015	4.374	0.033	0.012	5.475	0.000	0.085	0.000	10.015	0.56
1-2AE		na	0.010	0.000	0.000	0.014	4.553	0.029	0.017	5.258	0.000	0.204	0.000	10.086	0.54
1-2AF		na	0.009	0.000	0.000	0.013	4.561	0.029	0.020	5.314	0.000	0.080	0.000	10.025	0.54
1-2AI		na	0.008	0.000	0.008	0.015	4.596	0.028	0.019	5.268	0.000	0.075	0.000	10.018	0.53
1-2AJ		na	0.022	0.000	0.006	0.012	4.100	0.028	0.017	5.777	0.000	0.018	0.000	9.978	0.58
1-5D	Ol-MgSiO$_3$-TAPP	0.000	0.006	0.000	0.000	0.023	2.592	0.021	0.078	7.253	0.000	0.017	0.000	9.991	0.74
1-5F	Ol-MgSiO$_3$-TAPP	0.000	0.007	0.000	0.000	0.025	2.473	0.022	0.078	7.375	0.000	0.000	0.000	9.980	0.75
1-5G	Ol-MgSiO$_3$-TAPP	0.000	0.007	0.000	0.000	0.026	2.387	0.019	0.074	7.430	0.000	0.076	0.000	10.018	0.76
1-5K	Ol-MgSiO$_3$-TAPP	0.000	0.007	0.000	0.000	0.020	2.487	0.016	0.073	7.362	0.000	0.035	0.000	10.000	0.75
2-2E	CaSiO$_3$	na	0.012	0.000	0.010	0.031	2.223	0.018	0.085	7.552	0.000	0.074	0.000	10.005	0.77
2-7A		0.000	0.005	0.000	0.000	0.029	1.919	0.024	0.085	7.903	0.000	0.029	0.000	9.995	0.80
2-7C		0.000	0.010	0.000	0.000	0.026	1.822	0.029	0.068	7.954	0.023	0.062	0.028	10.023	0.81
2-7E		0.000	0.056	0.000	0.045	0.029	1.611	0.026	0.068	7.999	0.022	0.084	0.019	9.959	0.83
2-7O		0.000	0.000	0.000	0.000	0.035	1.882	0.025	0.080	7.935	0.000	0.044	0.006	10.007	0.81
3-1B	CaSiO$_3$	na	0.014	0.000	0.017	0.054	2.094	0.033	0.064	7.561	0.000	0.228	0.000	10.065	0.78
3-2A	Ol-MgSiO$_3$-CaSiO$_3$-TAPP?	na	0.011	0.000	0.000	0.022	1.652	0.016	0.086	8.191	0.000	0.000	0.000	9.978	0.83
3-2F	Ol-MgSiO$_3$-CaSiO$_3$-TAPP?	na	0.000	0.000	0.000	0.024	1.595	0.015	0.071	8.235	0.000	0.098	0.000	10.037	0.84
3-2G	Ol-MgSiO$_3$-CaSiO$_3$-TAPP?	na	0.006	0.000	0.000	0.021	1.580	0.014	0.084	8.265	0.000	0.027	0.000	9.997	0.84
3-2J	Ol-MgSiO$_3$-CaSiO$_3$-TAPP?	na	0.008	0.000	0.000	0.023	1.631	0.018	0.083	8.203	0.000	0.028	0.000	9.994	0.83

Table 8.14. Cation calculations for ferropericlase (continued)

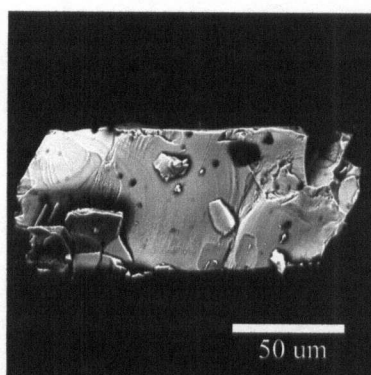| Inclusion No.	Inclusion assemblage	P^{5+}	Si^{4+}	Ti^{4+}	Al^{3+}	Cr^{3+}	Fe^{2+}	Mn^{2+}	Ni^{2+}	Mg^{2+}	Ca^{2+}	Na^+	K^+	Total	mg
3-5D	Ol-MgSiO$_3$	na	0.007	0.000	0.008	0.066	4.087	0.061	0.198	5.332	0.000	0.391	0.000	10.151	0.57
3-5E	Ol-MgSiO$_3$	na	0.010	0.000	0.006	0.051	3.457	0.057	0.021	6.334	0.000	0.055	0.000	9.990	0.65
3-5M	Ol-MgSiO$_3$	na	0.006	0.000	0.013	0.053	3.920	0.054	0.473	5.387	0.000	0.108	0.000	10.015	0.58
3-5P	Ol-MgSiO$_3$	na	0.005	0.000	0.011	0.060	3.728	0.049	0.173	5.925	0.000	0.016	0.000	9.967	0.61
3-6D		na	0.011	0.000	0.000	0.000	3.904	0.017	0.017	6.041	0.000	0.000	0.000	9.990	0.61
3-6J		na	0.000	0.000	0.009	0.000	4.352	0.013	0.022	5.599	0.000	0.000	0.000	9.996	0.56
3-6K		na	0.006	0.000	0.014	0.000	4.566	0.016	0.016	5.369	0.000	0.000	0.000	9.987	0.54
3-6L		na	0.009	0.000	0.010	0.000	4.432	0.014	0.011	5.510	0.000	0.000	0.000	9.987	0.55
3-9H		na	0.009	0.000	0.000	0.022	2.607	0.023	0.066	7.240	0.000	0.022	0.000	9.991	0.74
3-9I		na	0.018	0.000	0.006	0.012	1.091	0.010	0.054	8.780	0.000	0.000	0.000	9.972	0.89
3-9J		na	0.016	0.000	0.006	0.021	2.495	0.020	0.063	7.293	0.000	0.114	0.000	10.028	0.75
3-10C		na	0.000	0.000	0.020	0.099	5.255	0.120	0.010	4.376	0.000	0.119	0.000	10.000	0.45
3-10H		na	0.012	0.000	0.021	0.090	4.370	0.102	0.008	5.282	0.000	0.097	0.000	9.981	0.55
3-10O		na	0.009	0.000	0.022	0.091	4.483	0.101	0.012	5.079	0.000	0.274	0.000	10.071	0.53
3-10Z		na	0.000	0.000	0.021	0.091	5.189	0.112	0.058	4.328	0.000	0.292	0.000	10.091	0.45
3-10AA		na	0.000	0.000	0.019	0.095	5.268	0.109	0.009	4.330	0.000	0.226	0.000	10.056	0.45
3-10W		na	0.013	0.000	0.027	0.069	4.321	0.086	0.096	5.124	0.000	0.408	0.000	10.144	0.54
4-3B	Ol-MgSiO$_3$	na	0.005	0.000	0.010	0.049	1.528	0.014	0.078	8.245	0.000	0.072	0.000	10.002	0.84
4-3J	Ol-MgSiO$_3$	na	0.011	0.000	0.009	0.058	1.554	0.015	0.085	8.158	0.000	0.130	0.000	10.021	0.84
4-3K2	Ol-MgSiO$_3$	na	0.020	0.000	0.038	0.061	1.656	0.017	0.083	8.056	0.000	0.000	0.000	9.931	0.83
4-3Q	Ol-MgSiO$_3$	na	0.010	0.000	0.009	0.063	1.716	0.013	0.092	7.982	0.000	0.139	0.000	10.024	0.82
4-3R	Ol-MgSiO$_3$	na	0.006	0.000	0.008	0.072	1.782	0.015	0.078	7.950	0.000	0.086	0.000	9.997	0.82
5-10A		0.000	0.011	0.000	0.008	0.034	1.842	0.019	0.068	7.987	0.000	0.000	0.000	9.969	0.81
5-10E		0.000	0.026	0.000	0.006	0.031	1.897	0.024	0.076	7.887	0.000	0.012	0.000	9.961	0.81
6-1B		na	0.011	0.000	0.021	0.028	2.492	0.027	0.059	7.326	0.000	0.000	0.000	9.965	0.75
6-1E		na	0.006	0.000	0.039	0.025	2.497	0.026	0.060	7.291	0.000	0.036	0.000	9.980	0.74
6-2A		na	0.013	0.000	0.000	0.019	3.038	0.008	0.026	6.874	0.000	0.000	0.000	9.978	0.69
6-9A		0.000	0.007	0.000	0.000	0.017	3.417	0.009	0.018	6.511	0.000	0.014	0.000	9.992	0.66
6-9C		na	0.010	0.000	0.000	0.014	3.346	0.009	0.017	6.587	0.000	0.000	0.000	9.983	0.66

Cation totals are calculated on the basis of 10 anions. Inclusion assemblage - refers to the other confirmed phases in the diamond (blank entries indicate that only fPer was found); na - not analysed; mg - $Mg^{2+}/(Mg^{2+}+Fe^{2+})$ with typical errors of 0.010 at the 95% confidence level. Any values below MDL (see Table 8.10) are replaced by 0.00.
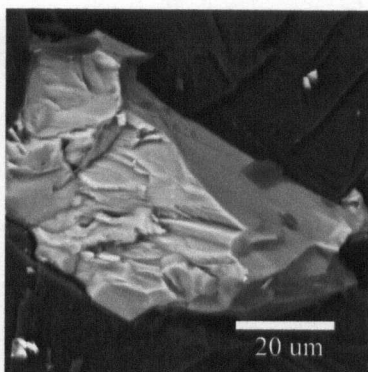
8.3.1.2 MgSiO$_3$

Fifteen distinct inclusions of MgSiO$_3$ are confirmed in 5 diamonds (diamonds 1-5, 3-2, 3-5, 4-3 and 6-8), representing only 11% of diamonds cracked and 7% of the diamond population. They are not referred to as MgSiO$_3$ *perovskites* as there is no supporting crystallographic data suggesting they are indeed perovskites. However, there is a high

probability that these grains at one time possessed (and perhaps still possess) the perovskite structure, as will be discussed in section 8.4.1.2.
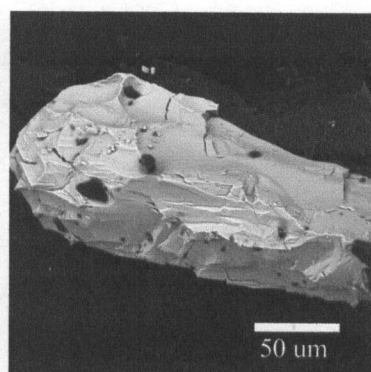
Grains are colourless and break easily once removed from their hosting diamond. MgSiO$_3$ inclusions tend not to exhibit crystal faces as commonly as fPer grains. They may have an elongated ellipsoid shape (Figs. 8.12, 3.2AD1, 3.2I1, and 4.3E), moderately well-formed euhedral shape but undistinguishable overall form (Figs. 8.12, 1.5A1, 3.5G1, 3.5Q and 4.3D), or no discernable form at all (Figs. 8.12, 1.5J1). There is evidence for imposed octahedral shape on a few grains (Figs. 8.12 1.5A1 and 3.5G1). Grain size ranges from 15 to 150 µm.
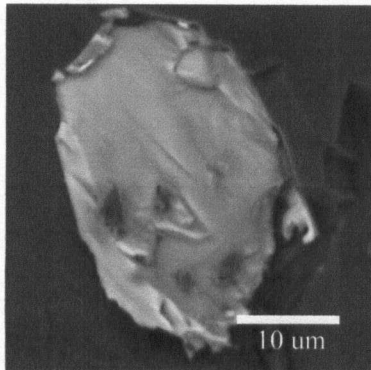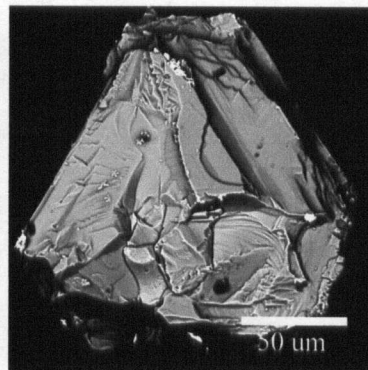

1.5 – A1   1.5 – J1   3.2 – I1
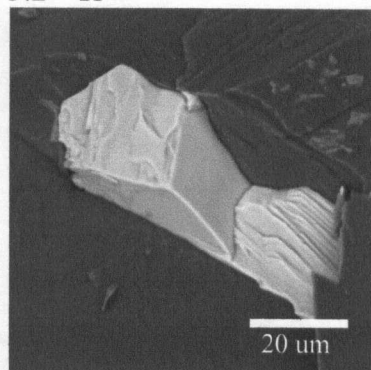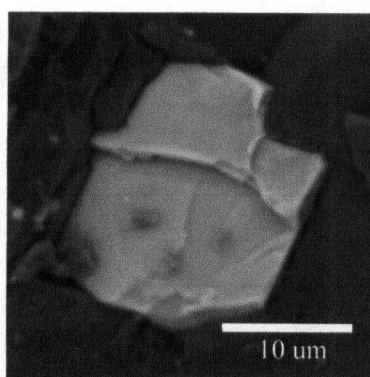
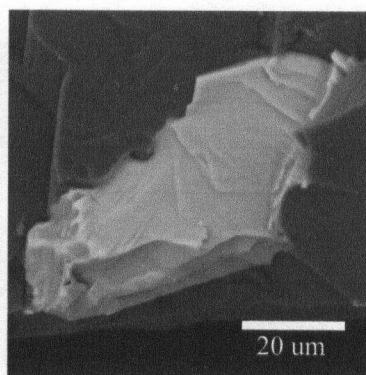3.2 – AD1   3.5 – G1   3.5 – Q

Fig. 8.12. SEM images of MgSiO₃ grains. Number refers to diamond which hosted the inclusion while the letter refers to the inclusion code. Major oxide chemistry and cation calculations for each inclusion are found in Tables 8.15 and 8.16 respectively.

4.3 – D   4.3 – E

Table 8.15. Major oxide data for MgSiO₃ grains (wt%)

Inclusion No.	No.	Inclusion assemblage	No. of analyses averaged	P_2O_5	SiO_2	TiO_2	Al_2O_3	Cr_2O_3	FeO	MnO	NiO	MgO	CaO	Na_2O	K_2O	Total
1-5A1	1	Ol-fPer-TAPP	3	0.00	57.31	0.16	1.91	0.21	6.34	0.13	0.00	33.91	0.06	0.00	0.00	100.04
1-5J1	2	Ol-fPer-TAPP	3	0.00	54.92	0.17	2.22	0.20	6.15	0.13	0.00	35.68	0.04	0.00	0.00	99.52
3-2I1	3	Ol-fPer-CaSiO₃-TAPP?	2	na	58.19	0.20	1.60	0.22	4.21	0.14	0.00	33.43	0.04	0.00	0.00	98.02
3-2AD1	4	Ol-fPer-CaSiO₃-TAPP?	2	na	51.87	0.16	1.94	0.29	4.23	0.14	0.00	39.37	0.04	0.00	0.00	98.04
3-5G1	5	Ol-fPer	3	na	51.60	0.14	3.37	0.20	6.66	0.27	0.00	35.91	0.00	0.10	0.00	98.26
3-5Q	6	Ol-fPer	3	na	59.88	0.15	2.73	0.19	6.58	0.26	0.00	30.54	0.01	0.00	0.00	100.34
4-3D	7	Ol-fPer	3	0.00	55.36	0.21	2.54	0.20	4.29	0.10	0.00	36.30	0.00	0.07	0.00	99.08
4-3E	8	Ol-fPer	2	na	56.73	0.21	2.36	0.20	4.25	0.10	0.00	34.41	0.00	0.08	0.00	98.35

Any values below MDL (see Table 8.9) are replaced by 0.00.

Table 8.16. Cation calculations for MgSiO₃.

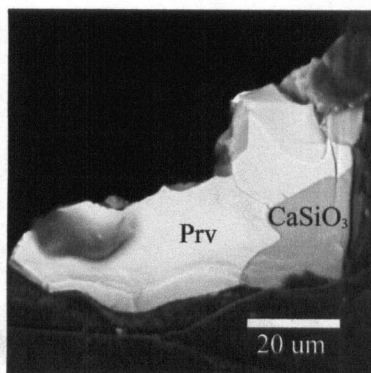| Inclusion No.	Inclusion assemblage	P^{5+}	Si^{4+}	Ti^{4+}	Al^{3+}	Cr^{3+}	Fe^{2+}	Mn^{2+}	Ni^{2+}	Mg^{2+}	Ca^{2+}	Na^+	K^+	Total	mg
1-5A1	Ol-fPer-TAPP	0.000	0.985	0.002	0.039	0.003	0.091	0.002	0.000	0.869	0.001	0.000	0.000	1.992	0.91
1-5J1	Ol-fPer-TAPP	0.000	0.954	0.002	0.045	0.003	0.089	0.002	0.000	0.924	0.001	0.000	0.000	2.020	0.91
3-2I1	Ol-fPer-CaSiO₃-TAPP?	na	1.008	0.003	0.033	0.003	0.061	0.002	0.000	0.863	0.001	0.000	0.000	1.972	0.93
3-2AD1	Ol-fPer-CaSiO₃-TAPP?	na	0.915	0.002	0.040	0.004	0.062	0.002	0.000	1.035	0.001	0.000	0.000	2.061	0.94
3-5G1	Ol-fPer	na	0.916	0.002	0.071	0.003	0.099	0.004	0.000	0.950	0.000	0.003	0.000	2.047	0.91
3-5Q	Ol-fPer	na	1.019	0.002	0.055	0.003	0.094	0.004	0.000	0.775	0.000	0.000	0.000	1.950	0.89
4-3D	Ol-fPer	0.000	0.957	0.003	0.052	0.003	0.062	0.001	0.000	0.935	0.000	0.002	0.000	2.015	0.94
4-3E	Ol-fPer	na	0.983	0.003	0.048	0.003	0.062	0.002	0.000	0.888	0.000	0.003	0.000	1.990	0.94

Cation totals are calculated on the basis of 3 anions. $mg = Mg^{2+}/(Mg^{2+}+Fe^{2+})$ with typical errors of 0.012 at the 95% confidence level. Any values below MDL (see Table 8.10) are replaced by 0.00.

164

Major oxide data for eight MgSiO$_3$ grains from four diamonds are presented in Table 8.15 and cation calculations in Table 8.16. *Mg* ranges from 89.2 to 94.3 with an average of 92.1. The main substitutional elements are Al$_2$O$_3$ (1.60 – 3.37 wt%, average 2.33 wt%), TiO$_2$ (0.14 – 0.21 wt %, average 0.17 wt%), Cr$_2$O$_3$ (0.19 - 0.29 wt%, average 0.21 wt%) and MnO (0.10 – 0.27 wt%, average 0.16 wt%). NiO is below detection (<0.05 wt%) and CaO contents are low (0.00 – 0.06 wt%).
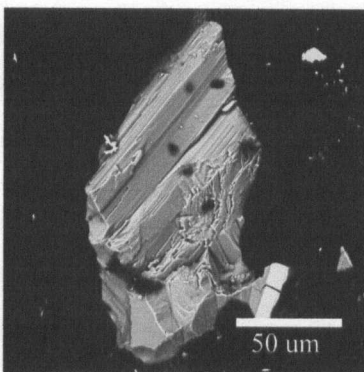
8.3.1.3 CaSiO$_3$

Twenty-seven grains of CaSiO$_3$ are found in 12 separate diamonds (27% of diamonds cracked and 17% of the whole population). In the absence of crystallographic data, these grains cannot be classified as CaSiO$_3$ *perovskites*; they will be simply referred to as CaSiO$_3$ inclusions. However, the presence of these minerals as inclusions in diamond strongly supports the interpretation that they had, at least initially, the perovskite structure. Any lower P-T polymorph of CaSiO$_3$, other than CaSi-Prv, is not stable in the mantle (such as wollastonite).
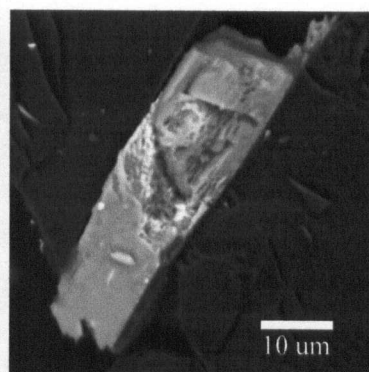
They are colourless to milky and range in size from 10 to 120 microns. Grains tend to fragment once removed or exposed (Fig. 8.13, 4.7C), and cleavage tends to control fragmentation (Figs. 8.13, 3.2L and 4.7C). About one half of the crystals are anhedral (e.g. Figs. 8.13, 2.8L1, 3.1A1 and 7.1A) while the other half are euhedral (e.g. Figs. 8.13,

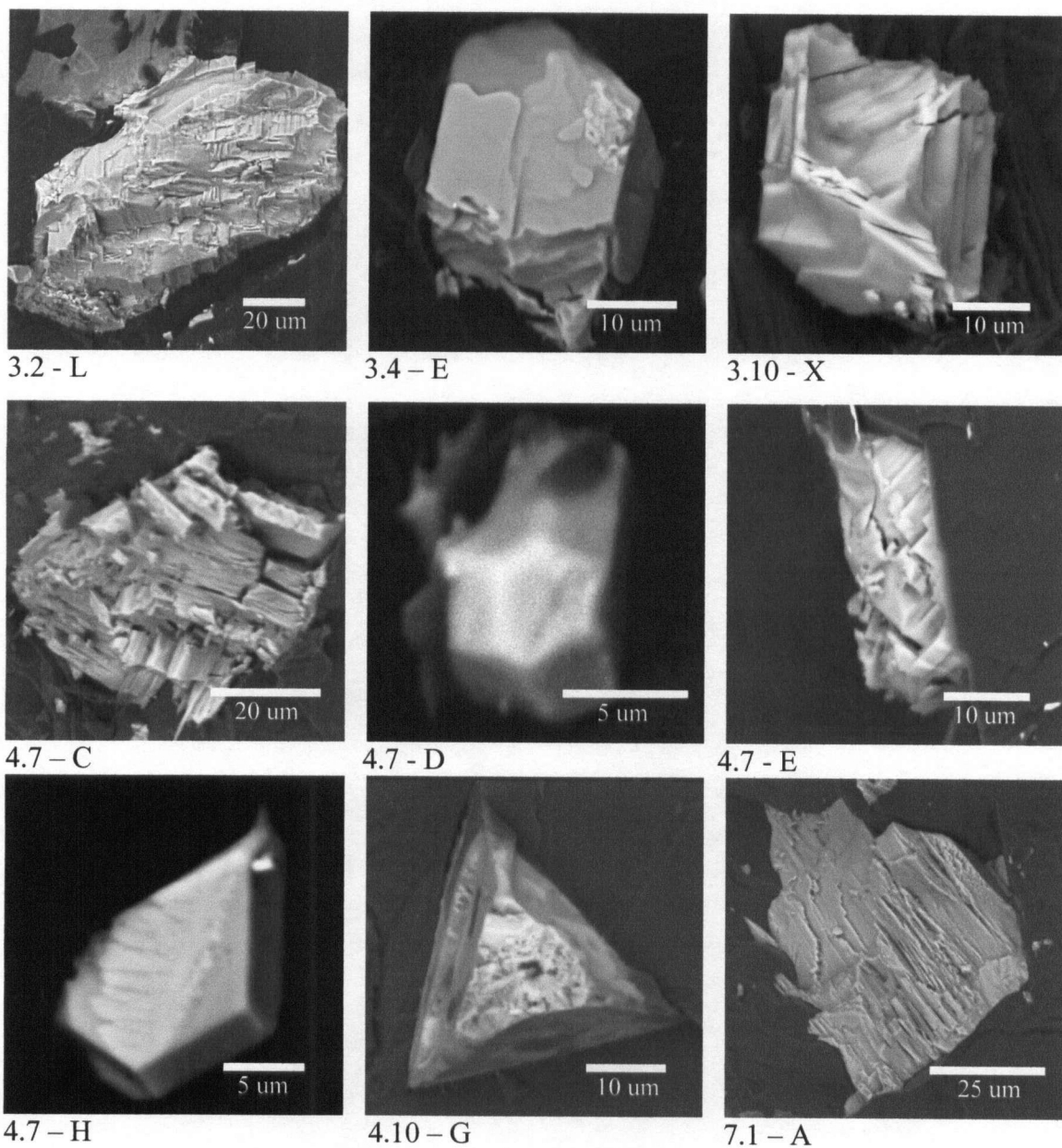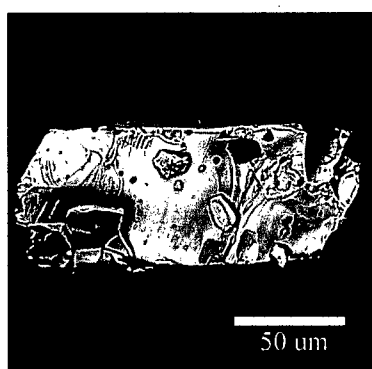2.8 – L1   3.1 – A1   3.1 – E1
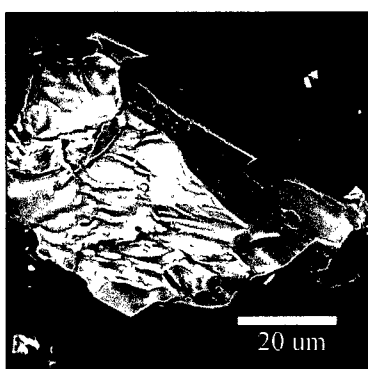
Fig. 8.13. SEM images of CaSiO₃ grains.

3.1E1, 3.4E, 4.7D and H). Euhedral grains may exhibit faces that are a negative shape imposed on the inclusion by the octahedral diamond host, however the friable nature of the inclusions tend to obscure or not preserve primary habit.

probability that these grains at one time possessed (and perhaps still possess) the perovskite structure, as will be discussed in section 8.4.1.2.
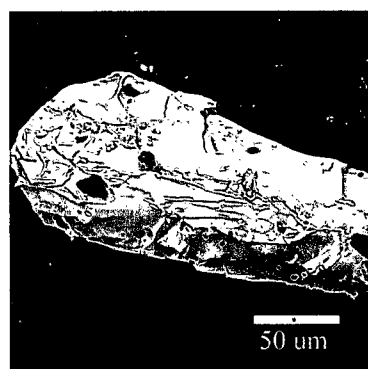
Grains are colourless and break easily once removed from their hosting diamond. $MgSiO_3$ inclusions tend not to exhibit crystal faces as commonly as fPer grains. They may have an elongated ellipsoid shape (Figs. 8.12, 3.2AD1, 3.2I1, and 4.3E), moderately well-formed euhedral shape but undistinguishable overall form (Figs. 8.12, 1.5A1, 3.5G1, 3.5Q and 4.3D), or no discernable form at all (Figs. 8.12, 1.5J1). There is evidence for imposed octahedral shape on a few grains (Figs. 8.12 1.5A1 and 3.5G1). Grain size ranges from 15 to 150 μm.
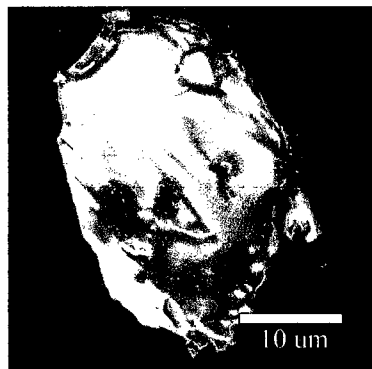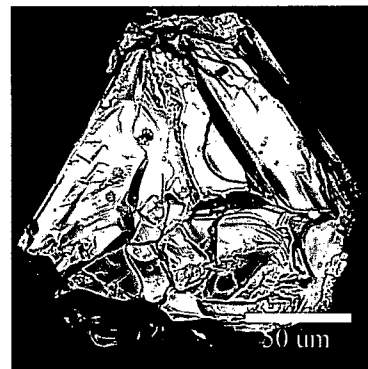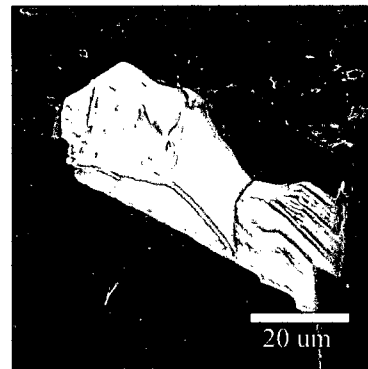

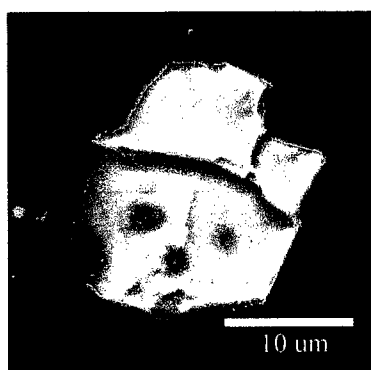1.5 – A1   1.5 – J1   3.2 – I1

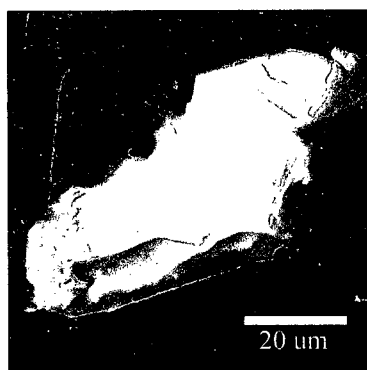3.2 – AD1   3.5 – G1   3.5 – Q

Fig. 8.12. SEM images of $MgSiO_3$ grains. Number refers to diamond which hosted the inclusion while the letter refers to the inclusion code. Major oxide chemistry and cation calculations for each inclusion are found in Tables 8.15 and 8.16 respectively.

4.3 – D   4.3 – E

Table 8.15. Major oxide data for $MgSiO_3$ grains (wt%)

Inclusion No.	No.	Inclusion assemblage	No. of analyses averaged	P_2O_5	SiO_2	TiO_2	Al_2O_3	Cr_2O_3	FeO	MnO	NiO	MgO	CaO	Na_2O	K_2O	Total
1-5A1	1	Ol-fPer-TAPP	3	0.00	57.31	0.16	1.91	0.21	6.34	0.13	0.00	33.91	0.06	0.00	0.00	100.04
1-5J1	2	Ol-fPer-TAPP	3	0.00	54.92	0.17	2.22	0.20	6.15	0.13	0.00	35.68	0.04	0.00	0.00	99.52
3-2I1	3	Ol-fPer-CaSiO₃-TAPP?	2	na	58.19	0.20	1.60	0.22	4.21	0.14	0.00	33.43	0.04	0.00	0.00	98.02
3-2AD1	4	Ol-fPer-CaSiO₃-TAPP?	2	na	51.87	0.16	1.94	0.29	4.23	0.14	0.00	39.37	0.04	0.00	0.00	98.04
3-5G1	5	Ol-fPer	3	na	51.60	0.14	3.37	0.20	6.66	0.27	0.00	35.91	0.00	0.10	0.00	98.26
3-5Q	6	Ol-fPer	3	na	59.88	0.15	2.73	0.19	6.58	0.26	0.00	30.54	0.01	0.00	0.00	100.34
4-3D	7	Ol-fPer	3	0.00	55.36	0.21	2.54	0.20	4.29	0.10	0.00	36.30	0.00	0.07	0.00	99.08
4-3E	8	Ol-fPer	2	na	56.73	0.21	2.36	0.20	4.25	0.10	0.00	34.41	0.00	0.08	0.00	98.35

Any values below MDL (see Table 8.9) are replaced by 0.00.

Table 8.16. Cation calculations for $MgSiO_3$.

Inclusion No.	Inclusion assemblage	P^{5+}	Si^{4+}	Ti^{4+}	Al^{3+}	Cr^{3+}	Fe^{2+}	Mn^{2+}	Ni^{2+}	Mg^{2+}	Ca^{2+}	Na^+	K^+	Total	mg
1-5A1	Ol-fPer-TAPP	0.000	0.985	0.002	0.039	0.003	0.091	0.002	0.000	0.869	0.001	0.000	0.000	1.992	0.91
1-5J1	Ol-fPer-TAPP	0.000	0.954	0.002	0.045	0.003	0.089	0.002	0.000	0.924	0.001	0.000	0.000	2.020	0.91
3-2I1	Ol-fPer-CaSiO₃-TAPP?	na	1.008	0.003	0.033	0.003	0.061	0.002	0.000	0.863	0.001	0.000	0.000	1.972	0.93
3-2AD1	Ol-fPer-CaSiO₃-TAPP?	na	0.915	0.002	0.040	0.004	0.062	0.002	0.000	1.035	0.001	0.000	0.000	2.061	0.94
3-5G1	Ol-fPer	na	0.916	0.002	0.071	0.003	0.099	0.004	0.000	0.950	0.000	0.003	0.000	2.047	0.91
3-5Q	Ol-fPer	na	1.019	0.002	0.055	0.003	0.094	0.004	0.000	0.775	0.000	0.000	0.000	1.950	0.89
4-3D	Ol-fPer	0.000	0.957	0.003	0.052	0.003	0.062	0.001	0.000	0.935	0.000	0.002	0.000	2.015	0.94
4-3E	Ol-fPer	na	0.983	0.003	0.048	0.003	0.062	0.002	0.000	0.888	0.000	0.003	0.000	1.990	0.94

Cation totals are calculated on the basis of 3 anions. $mg = Mg^{2+}/(Mg^{2+}+Fe^{2+})$ with typical errors of 0.012 at the 95% confidence level. Any values below MDL (see Table 8.10) are replaced by 0.00.
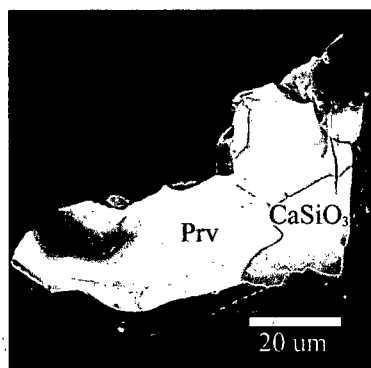
164

Major oxide data for eight MgSiO$_3$ grains from four diamonds are presented in Table 8.15 and cation calculations in Table 8.16. *Mg* ranges from 89.2 to 94.3 with an average of 92.1. The main substitutional elements are Al$_2$O$_3$ (1.60 – 3.37 wt%, average 2.33 wt%), TiO$_2$ (0.14 – 0.21 wt %, average 0.17 wt%), Cr$_2$O$_3$ (0.19 - 0.29 wt%, average 0.21 wt%) and MnO (0.10 – 0.27 wt%, average 0.16 wt%). NiO is below detection (<0.05 wt%) and CaO contents are low (0.00 – 0.06 wt%).
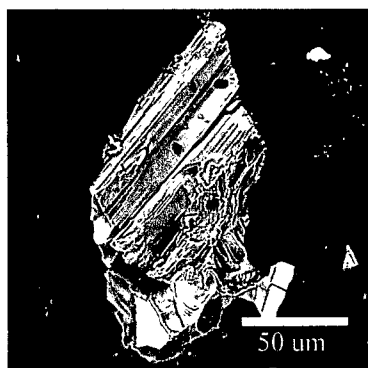
8.3.1.3 CaSiO$_3$

Twenty-seven grains of CaSiO$_3$ are found in 12 separate diamonds (27% of diamonds cracked and 17% of the whole population). In the absence of crystallographic data, these grains cannot be classified as CaSiO$_3$ *perovskites*; they will be simply referred to as CaSiO$_3$ inclusions. However, the presence of these minerals as inclusions in diamond strongly supports the interpretation that they had, at least initially, the perovskite structure. Any lower P-T polymorph of CaSiO$_3$, other than CaSi-Prv, is not stable in the mantle (such as wollastonite).
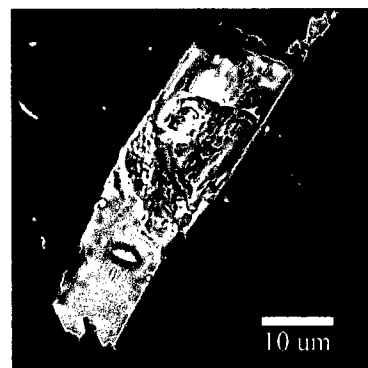
They are colourless to milky and range in size from 10 to 120 microns. Grains tend to fragment once removed or exposed (Fig. 8.13, 4.7C), and cleavage tends to control fragmentation (Figs. 8.13, 3.2L and 4.7C). About one half of the crystals are anhedral (e.g. Figs. 8.13, 2.8L1, 3.1A1 and 7.1A) while the other half are euhedral (e.g. Figs. 8.13,

2.8 – L1   3.1 – A1   3.1 – E1

3.2 - L 3.4 – E 3.10 - X

4.7 – C 4.7 - D 4.7 - E

4.7 – H 4.10 – G 7.1 – A
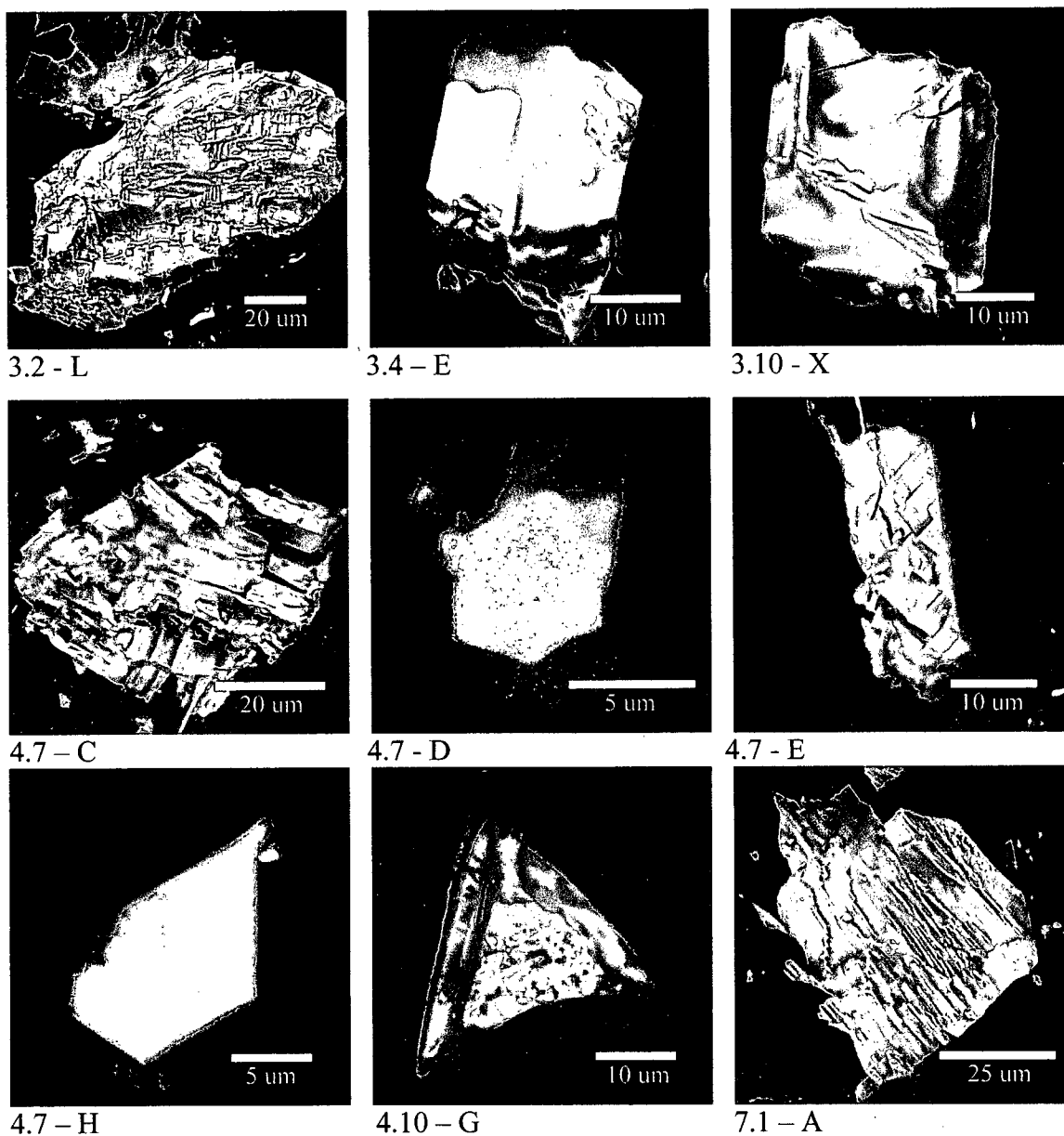
Fig. 8.13. SEM images of CaSiO₃ grains.

3.1E1, 3.4E, 4.7D and H). Euhedral grains may exhibit faces that are a negative shape imposed on the inclusion by the octahedral diamond host, however the friable nature of the inclusions tend to obscure or not preserve primary habit.

166

Table 8.17. Major oxide chemistry for $CaSiO_3$ grains (wt%)

Inclusion No.	No.	Inclusion assemblage	No. of analyses averaged	P_2O_5	SiO_2	TiO_2	Al_2O_3	Cr_2O_3	FeO	MnO	NiO	MgO	CaO	Na_2O	K_2O	Total
2-8L1	1	fPer	3	na	52.59	0.07	0.00	0.00	0.42	0.00	0.00	0.00	46.61	0.16	0.14	99.98
3-1A	2	fPer	3	na	50.31	0.00	0.00	0.00	0.00	0.00	0.00	0.12	47.94	0.00	0.04	98.42
3-1E	3	fPer	3	0.00	52.11	0.21	0.21	0.00	0.28	0.29	0.00	0.08	45.50	0.10	0.00	98.79
3-2L	4	Ol-fPer-MgSiO₃-TAPP?	3	na	52.18	0.00	0.00	0.00	0.00	0.00	0.00	0.05	46.97	0.09	0.00	99.30
3-4E	5		4	0.00	49.15	2.13	0.26	0.00	0.00	0.00	0.00	0.05	47.15	0.00	0.00	98.74
4-7E	6		2	na	52.40	0.00	0.00	0.00	0.12	0.00	0.00	0.00	47.74	0.00	0.00	100.27
4-10G1	7	eGrt	1	na	52.05	0.10	0.00	0.00	1.14	0.17	0.00	0.35	46.32	0.48	0.08	100.69
7-1A	8		3	0.00	51.91	0.00	0.00	0.00	0.08	0.00	0.00	0.00	47.94	0.00	0.00	99.93

Any values below MDL (see Table 8.9) are replaced by 0.00.

Table 8.18. Cation calculations for $CaSiO_3$ grains

Inclusion No.	Inclusion assemblage	P^{5+}	Si^{4+}	Ti^{4+}	Al^{3+}	Cr^{3+}	Fe^{2+}	Mn^{2+}	Ni^{2+}	Mg^{2+}	Ca^{2+}	Na^+	K^+	Total
2-8L1	fPer	na	1.012	0.001	0.000	0.000	0.007	0.000	0.000	0.000	0.961	0.006	0.005	1.992
3-1A	fPer	na	0.992	0.000	0.000	0.000	0.000	0.000	0.000	0.004	1.012	0.000	0.002	2.009
3-1E	fPer	0.000	1.013	0.003	0.005	0.000	0.005	0.005	0.000	0.002	0.947	0.004	0.000	1.984
3-2L	Ol-fPer-MgSiO₃-TAPP?	na	1.011	0.000	0.000	0.000	0.000	0.000	0.000	0.001	0.975	0.003	0.000	1.991
3-4E		0.000	0.967	0.032	0.006	0.000	0.000	0.000	0.000	0.001	0.994	0.000	0.000	1.999
4-7E		na	1.007	0.000	0.000	0.000	0.002	0.000	0.000	0.000	0.983	0.000	0.000	1.993
4-10G1	eGrt	na	1.001	0.001	0.000	0.000	0.018	0.003	0.000	0.010	0.954	0.018	0.003	2.008
7-1A		0.000	1.003	0.000	0.000	0.000	0.001	0.000	0.000	0.000	0.993	0.000	0.000	1.997

Cation totals are calculated on the basis of 3 anions. Any values below MDL (see Table 8.10) are replaced by 0.00.

Chemical data of eight $CaSiO_3$ grains from seven diamonds are presented in Table 8.17, with accompanying cation calculations in Table 8.18. Grains are essentially pure $CaSiO_3$, with Ca and Si occupying 97.3 - 99.9% of the cation sites (average of 99.1%).

In order of decreasing average weight percent, substitutional elements are: TiO_2 (0.00 – 2.13 wt%, average 0.31 wt%), FeO (0.00 – 1.14 wt%, average 0.26 wt%), Na_2O (0.00 – 0.48 wt%, average 0.10 wt%), MgO (0.00 – 0.35 wt%, average 0.08 wt%), MnO (0.00 – 0.29 wt%, average 0.06 wt%), Al_2O_3 (0.0 – 0.26 wt%, average 0.06 wt%), and K_2O (0.0 – 0.14 wt%, average 0.03 wt%).

8.3.1.4 Mg_2SiO_4

Ten grains of Mg_2SiO_4 have been identified by EDS analysis in 6 diamonds (13% of diamonds cracked and 9% of population). In the absence of crystallographic data and supporting experimental data, these grains are difficult to further subdivide into α-Ol, β-Ol or γ-Ol based on chemistry alone. For the sake of conciseness, Mg-Si oxides with a cation:anion ratio of 3:4 will be called 'olivine' (Ol), but the reader is reminded that these grains could have initially crystallised as one of the three structures mentioned, or be the result of a retrograde reaction.

Grains are colourless and generally small, ranging in size from 10–100 microns. Crystal form is evident in some grains (e.g. Figs. 8.14, 3.2S and 4.3C), but is typically poorly developed. Four grains of olivine are in direct contact with $MgSiO_3$ inclusions.

Major oxide data are presented for seven olivine grains in Table 8.19 with cation calculations in Table 8.20 and images in Fig. 8.14. Si, Mg and Fe fill 98.8 to 99.7% of the cation sites available. The main substitutional elements are: Al_2O_3 (0.00 – 0.80 wt%, average 0.26 wt%), NiO (0.00 – 0.40 wt%, average 0.17 wt%), MnO (0.08 – 0.29 wt%, average 0.14 wt%) and Cr_2O_3 (0.00 – 0.28 wt%, average 0.04 wt%). Grains are Mg-rich but have a reasonably wide variation in *mg*, ranging between 0.88 and 0.95 (average of 0.91). Five Ol grains from three diamonds cluster around *mg* = ~0.89 while two Ol grains liberated from only one diamond have *mg* = ~0.945.
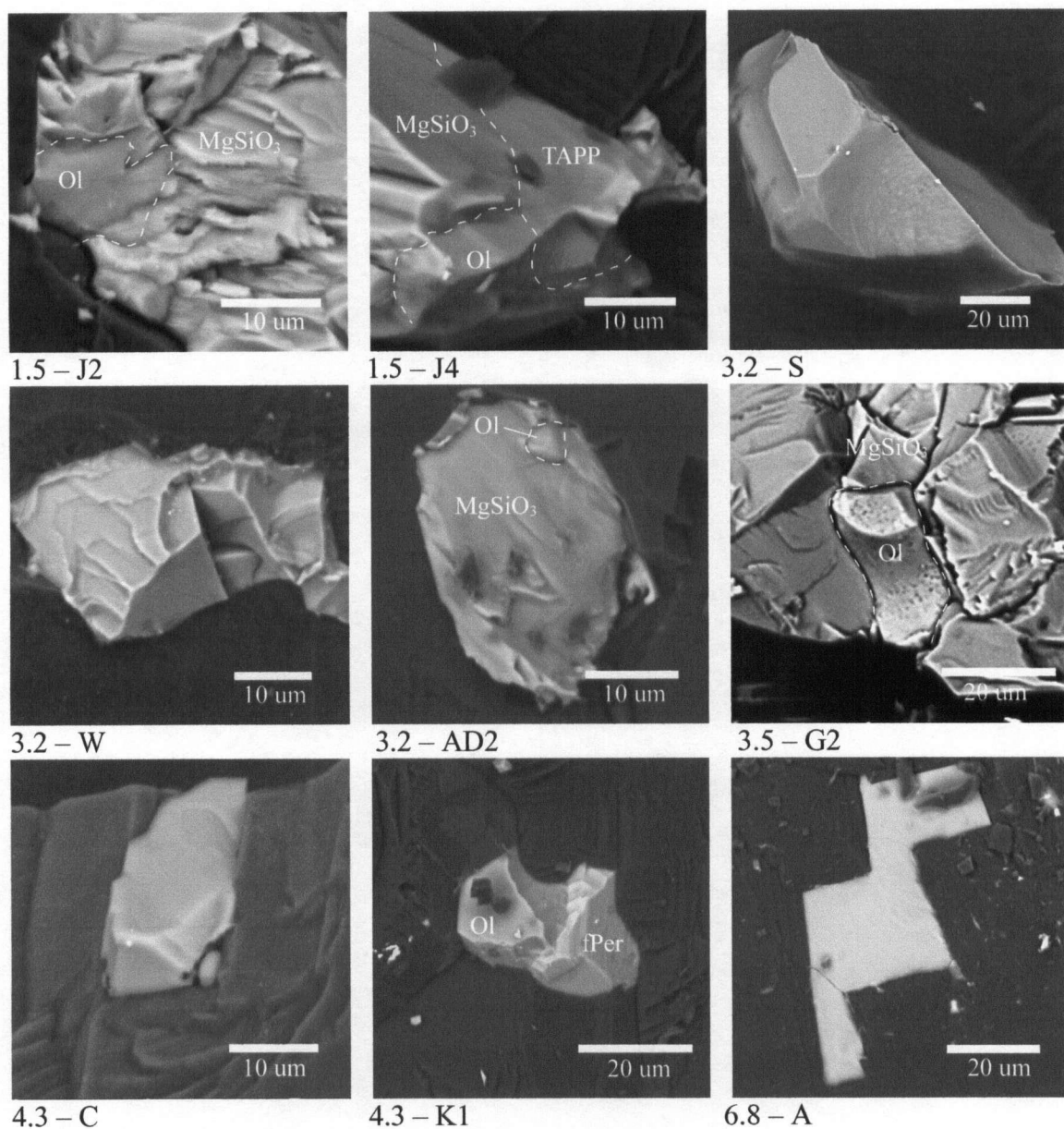
Fig. 8.14. SEM images of Ol grains.

All grains but one are in association with fPer and MgSiO$_3$. The *mg* of olivine does not seem to vary in accord with inclusion associations, rather, it varies between diamonds; olivine grains in diamond 4-3 have an elevated *mg* (0.95) while the olivine grain in diamond 3-5 has a lower *mg* (0.89), even though both diamonds have the same MgSiO$_3$-fPer-Ol association.

Table 8.19. Major oxide data for olivine grains (wt%)

Inclusion No.	No.	Inclusion assemblage	No. of analyses averaged	P_2O_5	SiO_2	TiO_2	Al_2O_3	Cr_2O_3	FeO	MnO	NiO	MgO	CaO	Na_2O	K_2O	Total
1-5J2	1	fPer-MgSiO$_3$-TAPP	2	0.00	38.03	0.05	0.12	0.00	10.24	0.12	0.00	48.46	0.00	0.00	0.00	97.02
3-2S	2	Ol-fPer-CaSiO$_3$-TAPP?	3	na	39.42	0.00	0.00	0.00	11.15	0.12	0.31	48.85	0.07	0.00	0.00	99.93
3-2W	3	Ol-fPer-CaSiO$_3$-TAPP?	3	na	41.38	0.00	0.00	0.00	10.90	0.08	0.40	45.22	0.00	0.06	0.00	98.05
3-5G2	4	fPer-MgSiO$_3$	3	na	37.45	0.00	0.20	0.00	11.05	0.29	0.00	50.54	0.00	0.07	0.00	99.61
4-3C	5	fPer-MgSiO$_3$	2	na	42.74	0.07	0.80	0.00	4.61	0.15	0.00	51.96	0.00	0.00	0.00	100.33
4-3K1	6	fPer-MgSiO$_3$	1	na	36.97	0.14	0.72	0.28	5.83	0.14	0.19	55.73	0.00	0.05	0.00	100.05
6-8A	7		1	0.00	43.43	0.00	0.00	0.00	8.85	0.12	0.25	43.29	0.06	0.05	0.00	96.07

Any values below MDL (see Table 8.9) are replaced by 0.00.

Table 8.20. Cation calculations for olivine grains

Inclusion No.	Inclusion assemblage	P^{5+}	Si^{4+}	Ti^{4+}	Al^{3+}	Cr^{3+}	Fe^{2+}	Mn^{2+}	Ni^{2+}	Mg^{2+}	Ca^{2+}	Na^+	K^+	Total	mg
1-5J2	fPer-MgSiO$_3$-TAPP	0.000	0.967	0.001	0.004	0.000	0.218	0.003	0.000	1.837	0.000	0.000	0.000	3.030	0.89
3-2S	Ol-fPer-CaSiO$_3$-TAPP?	na	0.977	0.000	0.000	0.000	0.231	0.003	0.006	1.805	0.002	0.000	0.000	3.023	0.89
3-2W	Ol-fPer-CaSiO$_3$-TAPP?	na	1.036	0.000	0.000	0.000	0.228	0.002	0.008	1.688	0.000	0.003	0.000	2.965	0.88
3-5G2	fPer-MgSiO$_3$	na	0.935	0.000	0.006	0.000	0.231	0.006	0.000	1.882	0.000	0.003	0.000	3.063	0.89
4-3C	fPer-MgSiO$_3$	na	1.015	0.001	0.023	0.000	0.091	0.003	0.000	1.839	0.000	0.000	0.000	2.973	0.95
4-3K1	fPer-MgSiO$_3$	na	0.902	0.003	0.021	0.005	0.119	0.003	0.004	2.026	0.000	0.002	0.000	3.084	0.94
6-8A		0.000	1.091	0.000	0.000	0.000	0.186	0.003	0.005	1.621	0.002	0.002	0.000	2.910	0.90

Cation totals are calculated on the basis of 3 anions. $mg = Mg^{2+}/(Mg^{2+}+Fe^{2+})$ with typical errors of 0.012 at the 95% confidence level. Any values below MDL (see Table 8.10) are replaced by 0.00.

8.3.1.5 Garnet and TAPP

Six highly aluminous silicates were identified by EDS analysis from four diamonds. Only two of these grains were found before examination on SEM as they exhibited a distinctive pale orange hue (diamond 4-10, inclusions A and B). Two of the grains show evidence of crystal form (Figs. 8.15, 3.212, and 4.16E) (which again, may be a result of
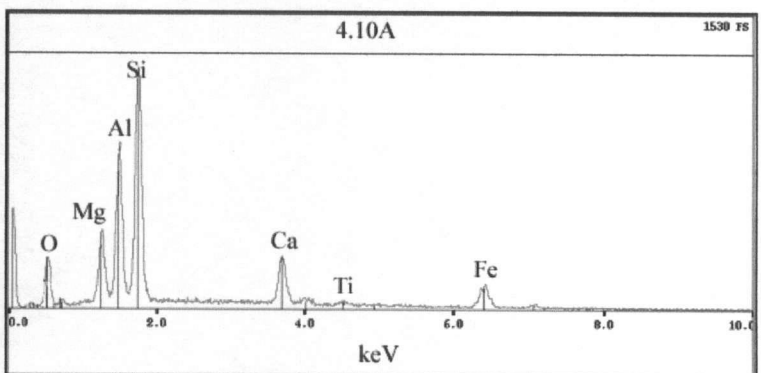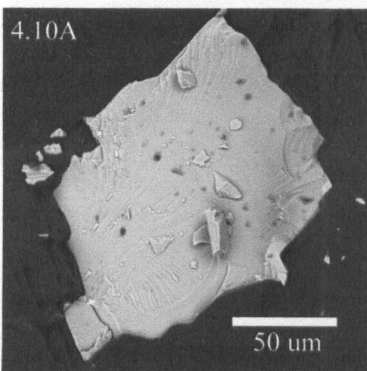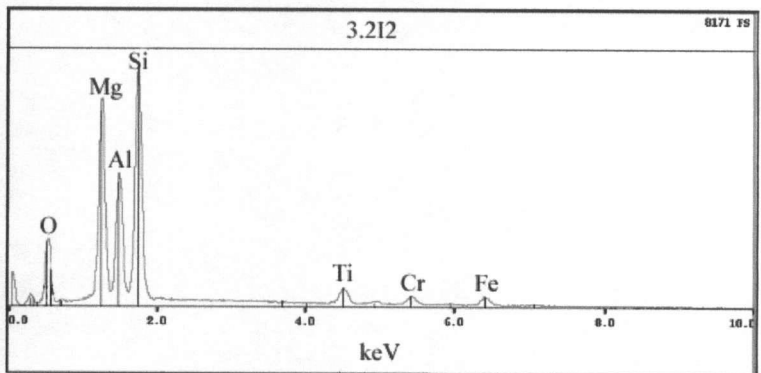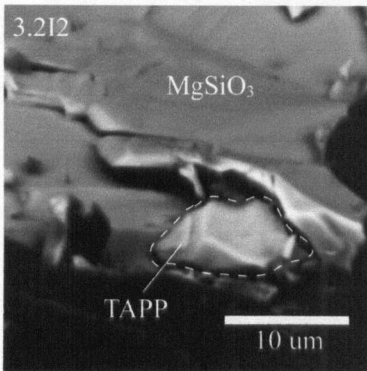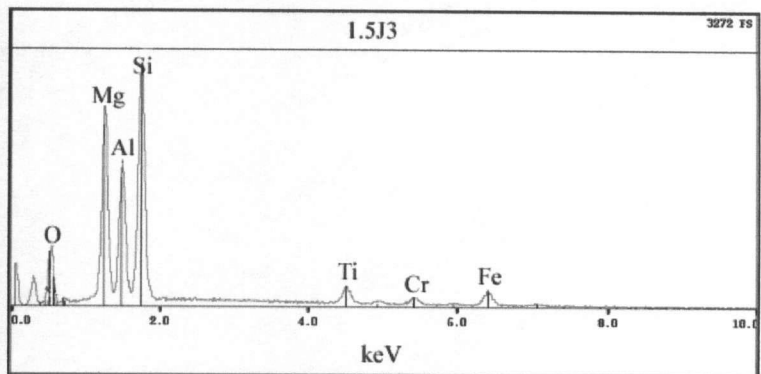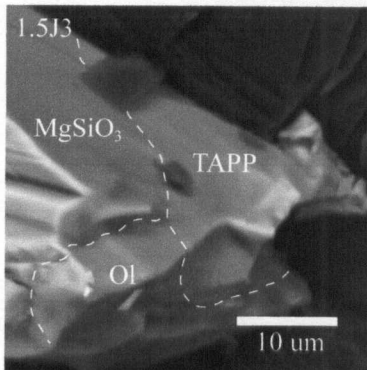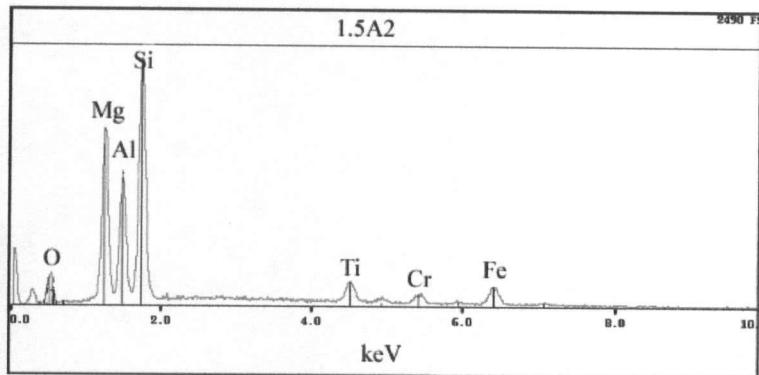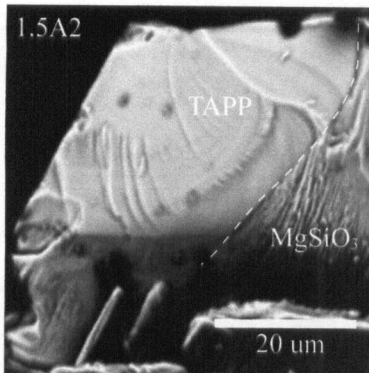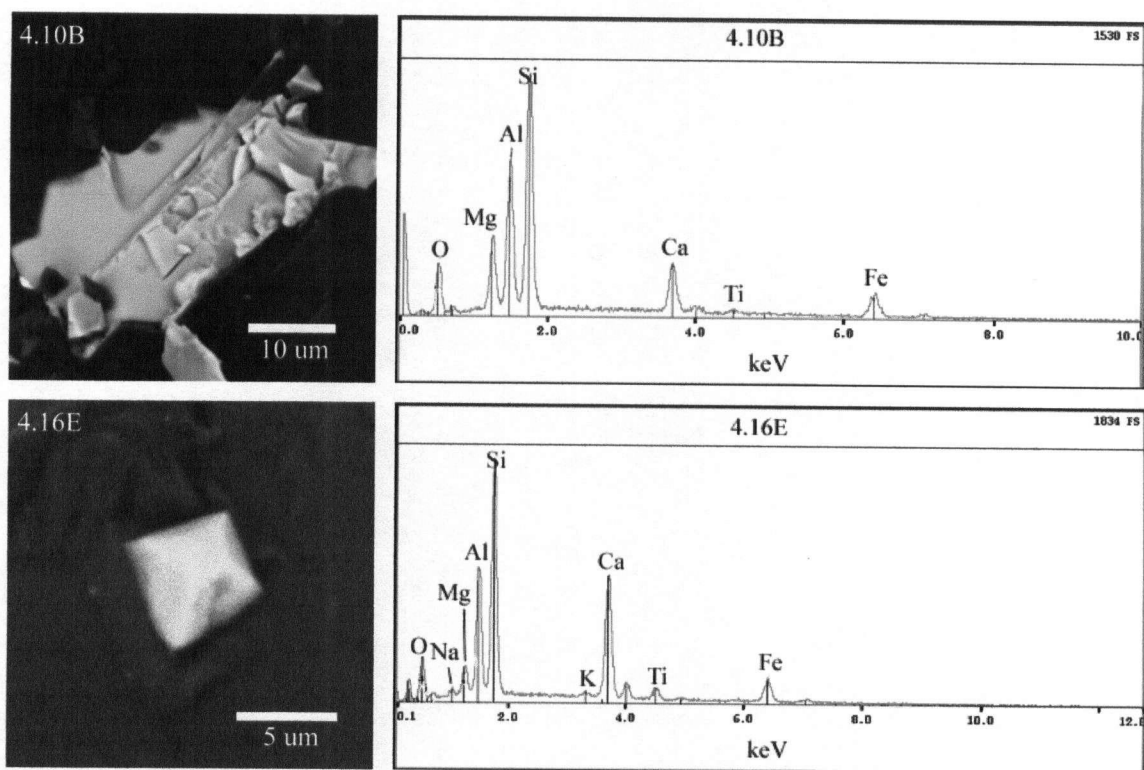
Fig. 8.15. SEM images and accompanying EDS spectra of aluminous silicate grains. Inclusions are likely either: TAPP (1.5A2, 1.5J2 and 3.2I2) or eclogitic garnet (4.10A, 4.10B and 4.16E).

diamond imposed morphology) while the remaining grains appear anhedral to subhedral. Grains range in size from 5 to 120 microns. Two of the six grains are found in contact with $MgSiO_3$ (Figs. 8.15. 1.5A2 and 3.2 I2) and one is in contact with both $MgSiO_3$ and Ol (1.5J3).

Major oxide chemical data for three of these grains are presented in Table 8.21 along with cation calculations in Table 8.22. As there are several different types of garnets or

Table 8.21. Major oxide data for TAPP and eGrt grains (wt%)

Inclusion No.	No.	Inclusion assemblage	No. of analyses averaged	P_2O_5	SiO_2	TiO_2	Al_2O_3	Cr_2O_3	FeO	MnO	NiO	MgO	CaO	Na_2O	K_2O	Total
1-5A2	1	Ol-MgSiO₃-fPer	3	0.00	39.99	4.71	19.03	2.74	6.87	0.14	0.00	25.75	0.04	0.00	0.00	99.26
4-10A	2	CaSiO₃	4	na	40.04	0.92	21.52	0.00	17.15	0.32	0.00	10.39	8.87	0.17	0.00	99.38
4-10B	3	CaSiO₃	2	na	36.98	0.91	23.04	0.00	16.65	0.30	0.00	11.30	9.02	0.14	0.00	98.35

Any values below MDL (see Table 8.9) are replaced by 0.00.

172

Table 8.22. Cation calculations for TAPP and eGrt grains

Inclusion No.	Inclusion assemblage	P^{5+}	Si^{4+}	Ti^{4+}	Al^{3+}	Cr^{3+}	Fe^{2+}	Mn^{2+}	Ni^{2+}	Mg^{2+}	Ca^{2+}	Na^+	K^+	Total	mg
1-5A2	Ol-MgSiO₃-fPer	0.000	2.852	0.252	1.600	0.155	0.410	0.009	0.000	2.738	0.003	0.000	0.000	8.018	0.87
4-10A	CaSiO₃	na	3.016	0.052	1.911	0.000	1.080	0.021	0.000	1.167	0.716	0.025	0.000	7.988	0.52
4-10B	CaSiO₃	na	2.829	0.053	2.077	0.000	1.065	0.019	0.000	1.289	0.740	0.020	0.000	8.091	0.55

Cation totals are calculated on the basis of 12 anions. $mg = Mg^{2+}/(Mg^{2+}+Fe^{2+})$ with typical errors of 0.02 at the 95% confidence level. Any values below MDL (see Table 8.10) are replaced by 0.00.

aluminum-rich silicates, it is necessary to further classify these grains. There are a variety of mantle garnets and aluminium-rich silicates, each with specific chemistries (previously introduced in section 8.1.4.3). As well, the possibility that these grains are aluminous pyroxenes must also be considered.

Hutchison (1997) reports several pyroxenes with as much as 12.5 wt% Al_2O_3 (which he termed type III). The lowest Al_2O_3 total of any of these grains is 19.0 wt%; it is unlikely that these are aluminous pyroxenes.

A Cr_2O_3-CaO plot used to differentiate peridotitic from eclogitic garnets (Fig. 8.16). Inclusion 1.5A2 plots in the peridotitic, or, more specifically, the harzburgitic field, while inclusions 4.10A and B plot in the eclogitic field. It should be noted here that mantle garnets found in diamonds are rarely void of calcium. One highly aluminous silicate void in calcium is TAPP, a rare inclusion that so far has only been reported in Juina diamonds (Harris *et al.*, 1997; Hutchison, 1997; Kaminsky
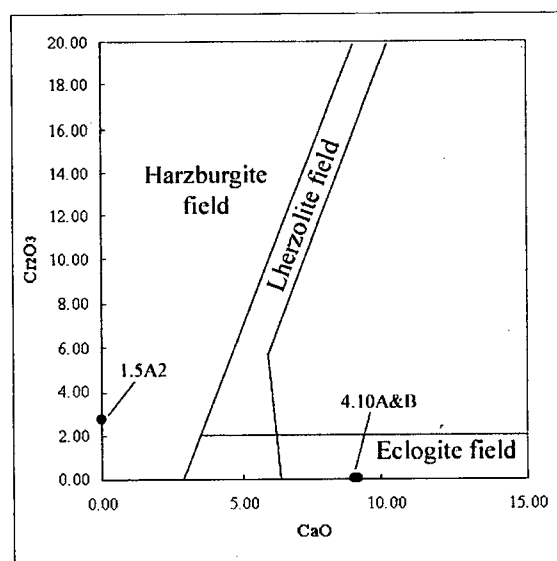

Fig. 8.16. Plot of CaO versus Cr_2O_3 (wt%) for aluminous silicates in this study. The lherzolitic field is from Sobolev *et al.* (1973) the 2% Cr_2O_3 cutoff for the eclogitic field is from Gurney (1984).

173

et al., 2001a). Based on EPMA and EDS analyses shared between inclusions without EMPA results, the aluminous silicates likely represent two phases: TAPP (1.5A2, 1.5J3 and 3.2I2) and eclogitic garnet (4.10A, 4.10B and 4.16E), or, more specifically, pyrope-grossular-almandine garnet.

Pyroxene begins to dissolve into garnet at depths ~250 km and is complete at ~410 km (for both a pyrolitic and eclogitic mantle), as discussed in detail in section 8.1.4.3. A dissolved pyroxene component can be recognised by determining the $Si^{4+}:O^{2-}$ ratio; any garnet with a ratio $>3.075{:}12$ is considered majoritic. Fig. 8.17 shows that there is no dissolved pyroxene component in the grains analysed.

Fig. 8.17. Plot of Al^{3+}+ Cr^{3+} versus Si^{4+} for aluminous silicates in this study. Cations calculated on basis of 12 oxygen atoms. The line at 3.075 cations Si^{4+} is used to separate majoritic and non-majoritic garnets.

The TAPP grain (1.5A2) is deficient in Si^{4+} (2.852 cations per 12 oxygens) and contains modest amounts of TiO_2 (4.71 wt%) and Cr_2O_3 (2.74 wt%). NiO, CaO, Na_2O and K_2O are essentially absent. There are similarities and differences between the two pyrope-grossular-almandine garnets analysed. The main differences are in Al^{3+} and Si^{4+} (i.e. Fig. 8.17). The remaining major oxide constituents are similar: TiO_2 (0.91 - 0.92 wt%), MnO (0.30 – 0.32 wt%) and Na_2O (0.14 – 0.17 wt%). Cr_2O_3, NiO and K_2O are absent in both grains. The differences in Si and Al content between the grains bring into question the quality of analyses. The large grain size coupled with better data for inclusion 4-10A (99.38 versus 99.31 wt% and 7.988 versus 8.091 cations per 12 oxygens) suggests that the data for inclusion B may be of poor quality.
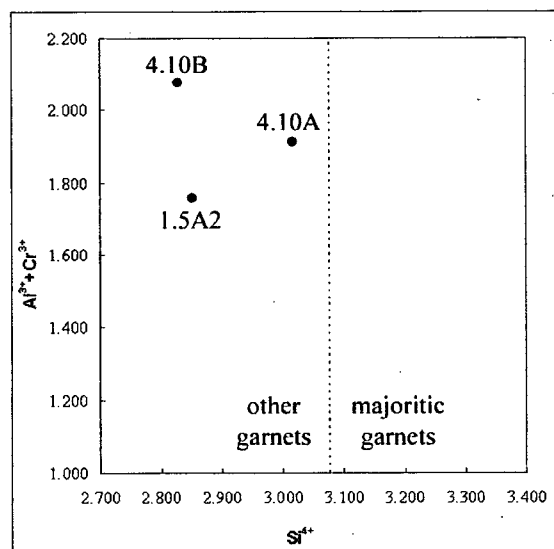
8.3.1.6 Magnetite

Magnetite grains have been confirmed in two diamonds, 1-4, and 2-6 (Fig. 8.18) and may also occur in diamond 2-10. Twenty-two individual inclusions were identified by EDS analysis. They are typically euhedral and dark brown/black in colour and range in size from 10 to 60 microns. Magnetite belongs to the isometric crystal system and generally forms octahedral crystals. Thus, the euhedral morphology of inclusions in this study cannot be used to deduce whether or not the euhedral nature is a result of diamond growth imposition, or is a growth feature.

Major oxide data are presented in Table 8.23 and cation calculations in Table 8.24. Grains comprise of Fe_2O_3 (51.74 – 60.11 wt%, average 56.74 wt%) and FeO (28.33 – 30.80 wt%, average 29.69 wt%). $Fe^{3+}/(Fe^{3+}+Fe^{2+})$ ranges from 0.612 to 0.656 (average 0.632) and was calculated using *Formula* (Ercit, T.S., 1996). Minor constituents include:
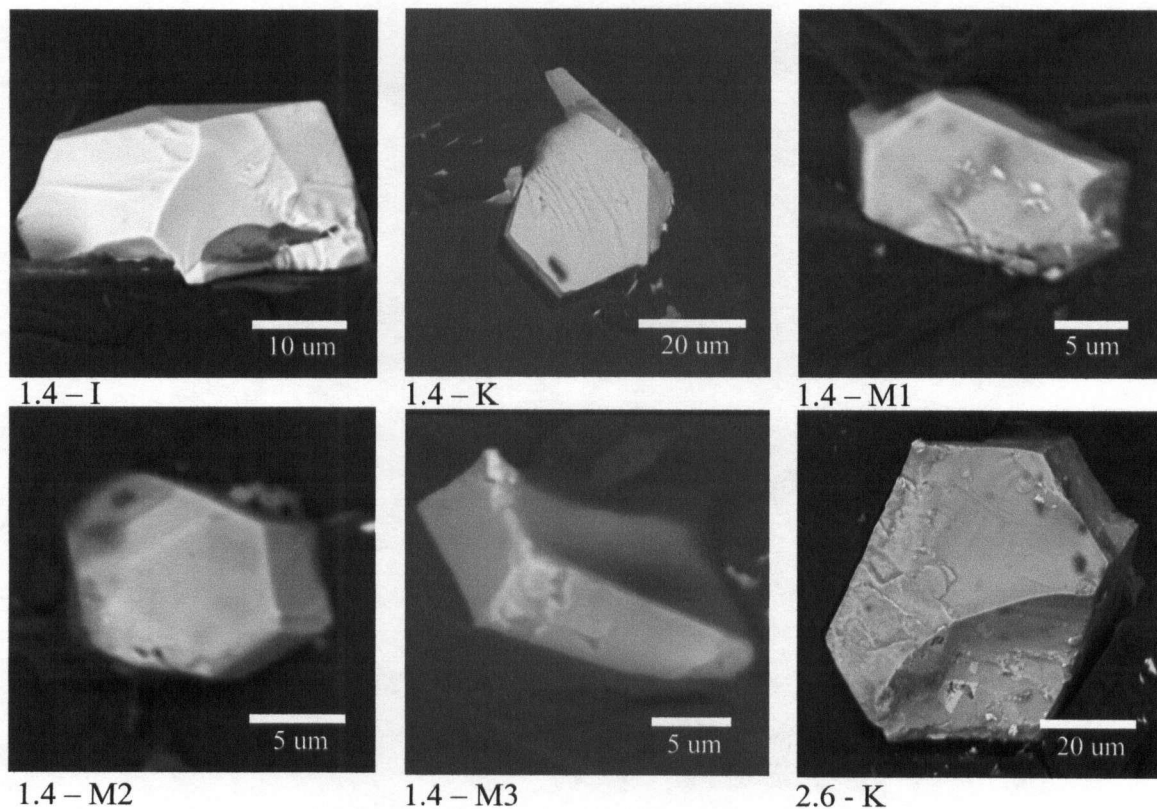

1.4 – I   1.4 – K   1.4 – M1

1.4 – M2   1.4 – M3   2.6 - K

Fig. 8.18. SEM images of magnetite grains.

Table 8.23. Major oxide data for magnetite grains (wt%)

Inclusion No.	No.	Inclusion assemblage	No. of analyses averaged	SiO_2	TiO_2	Al_2O_3	Cr_2O_3	Fe_2O_3	FeO	MnO	NiO	MgO	CaO	Na_2O	K_2O	Total
1-4I	1	SiO_2	3	0.16	1.50	5.56	0.00	60.11	28.33	0.61	0.00	2.85	0.00	0.00	0.00	99.13
1-4K	2	SiO_2	2	0.16	2.36	4.75	0.00	58.21	30.80	0.58	0.00	1.46	0.15	0.00	0.00	98.46
2-6B	3		1	0.17	3.61	6.92	3.03	51.74	29.48	0.62	0.00	3.58	0.00	0.00	0.00	99.15
2-6K	4		4	0.28	2.97	3.44	2.10	56.91	30.16	0.53	0.00	2.04	0.00	0.11	0.00	98.53

Any values below MDL (see Table 8.9) are replaced by 0.00. Fe_2O_3 and FeO contents calculated using using *Formula* (Ercit, T.S., 1996).

Table 8.24. Cation calculations for magnetite grains

Inclusion No.	Inclusion assemblage	Si^{4+}	Ti^{4+}	Al^{3+}	Cr^{3+}	Fe^{3+}	Fe^{2+}	Mn^{2+}	Ni^{2+}	Mg^{2+}	Ca^{2+}	Na^+	K^+	Total	*mg*
1-4I	SiO_2	0.006	0.042	0.241	0.000	1.664	0.872	0.019	0.000	0.156	0.000	0.000	0.000	3.000	0.06
1-4K	SiO_2	0.006	0.067	0.210	0.000	1.645	0.967	0.018	0.000	0.082	0.006	0.000	0.000	3.000	0.03
2-6B		0.006	0.098	0.295	0.087	1.409	0.892	0.019	0.000	0.193	0.000	0.000	0.000	3.000	0.08
2-6K		0.011	0.084	0.152	0.062	1.606	0.946	0.017	0.000	0.114	0.000	0.008	0.000	2.999	0.04

Cations are calculated on the basis of 4 anions. $mg = Mg^{2+}/(Mg^{2+}+Fe_{tot})$ with typical errors of 0.01 at the 95% confidence level. Any totals below MDL (see Table 8.10) are replaced by 0.00. Fe^{2+} and Fe^{3+} calculated using *Formula* (Ercit, T.S., 1996).

TiO_2 (1.50 – 3.61 wt%, average 2.61 wt%), MgO (1.46 – 3.58 wt%, average 2.48 wt%) and Cr_2O_3 (0.00 – 3.03 wt%, average 1.28 wt%).

8.3.1.7 Sulphides

Twelve inclusions of sulphide were found in three diamonds (6.8% of diamonds cracked or 4.3% of whole population). Grains are dark/black, very small (<30 microns in size) and typically anhedral (with the exception of one inclusion, 2.11G) (Fig. 8.19). Inclusion 6.8A2 was determined to be secondary after SEM examination, which revealed a fracture filled with sulphides leading up to the inclusion. EPMA data for five sulphide grains are presented in Table 8.25 with accompanying cation totals in Table 8.26. However, weight percent totals are generally poor, falling between 93.48 and 95.67. Poor totals are likely a consequence of the heterogeneous nature of the grains.
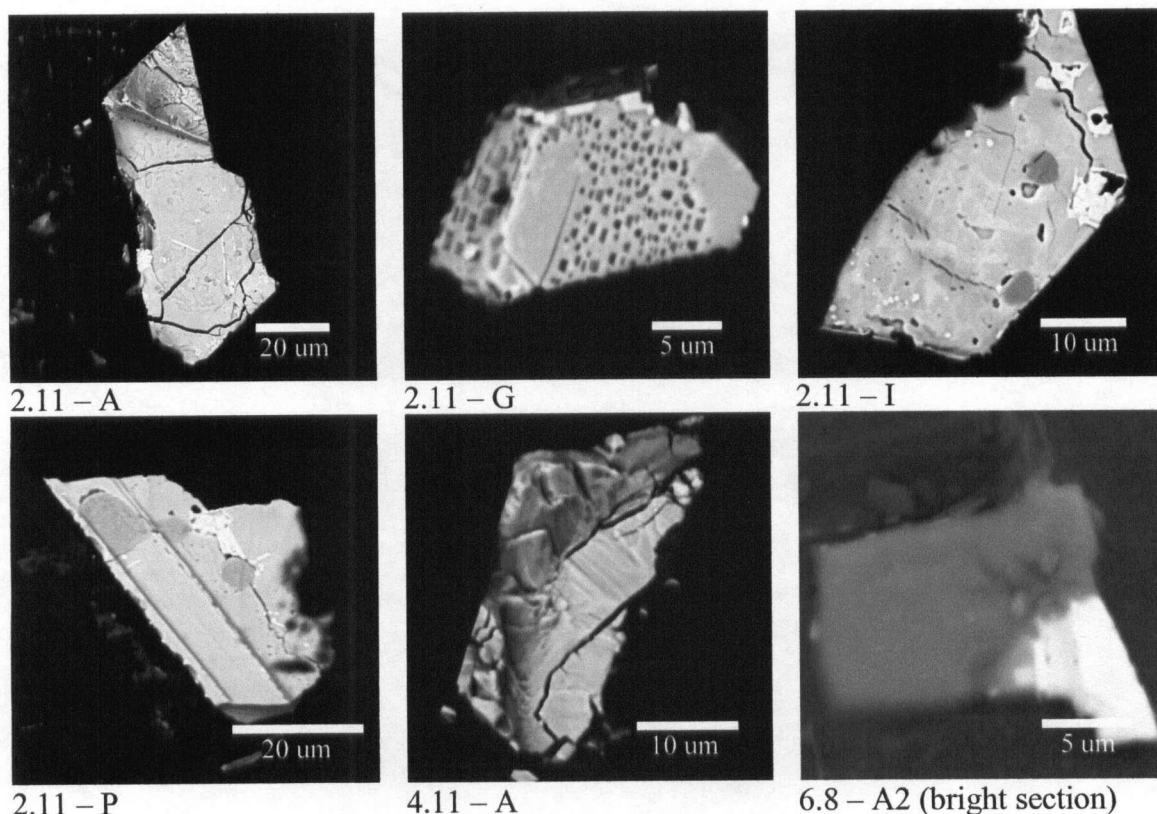
Fig. 8.19. SEM images of sulphide grains.

Grains are comprised of essentially five elements (Fe, Ni, Cu, Co and S). The heterogeneous character of the grains makes it difficult to describe them in terms of one mineral (they are likely monsulphide solid solution minerals). Nonetheless, a description of the grains is warranted. For three of the grains, Fe and S combine to make up between 95.7 and 100.0% of the total mineral. Based on the Fe:S for these three sulphide grains

Table 8.25. Chemical data for sulphide grains listed as weight percent for each element (wt%).

Inclusion No.	No.	Inclusion type	Inclusion assemblage	No. of analyses averaged	Fe	Co	Ni	Cu	Zn	Mn	S	Total
2-11A	1	pyrrhotite	SiO_2	4	55.87	0.23	3.58	0.21	0.00	0.00	35.53	95.42
2-11I	2	pyrrhotite?	SiO_2	1	43.48	0.28	14.34	6.18	0.00	0.00	30.93	95.21
2-11P	3	pyrrhotite	SiO_2	1	56.01	0.19	2.68	1.19	0.00	0.00	35.03	95.10
4-11A	4	pyrrhotite	$CaSiO_3$	2	59.90	0.00	0.00	0.01	0.00	0.00	33.58	93.48
6-8A2	5	pentlandite	Ol	3	25.16	0.38	35.06	0.04	0.00	0.00	35.02	95.67

MDL's and precision are listed in Table 8.9.

Table 8.26. Cation calculations for sulphide grains

Inclusion No.	Inclusion type	Inclusion assemblage	Fe	Co	Ni	Cu	Zn	Mn	S	Total
2-11A	pyrrhotite	SiO_2	0.903	0.004	0.055	0.003	0.000	0.000	1.000	1.964
2-11I	pyrrhotite?	SiO_2	0.807	0.005	0.253	0.101	0.000	0.000	1.000	2.166
2-11P	pyrrhotite	SiO_2	0.918	0.003	0.042	0.017	0.000	0.000	1.000	1.980
4-11A	pyrrhotite	$CaSiO_3$	1.024	0.000	0.000	0.000	0.000	0.000	1.000	2.024
6-8A2	pentlandite	Ol	0.412	0.006	0.547	0.001	0.000	0.000	1.000	1.966

MDL's and precision are listed in Table 8.10.

(between 0.90 and 1.02), they should be classified as pyrrhotite. The secondary sulphide (6.8A2) contains abundant Fe and Ni, where Fe + Ni is slightly less than S. This grain should be classified as pentlandite. The remaining grain, inclusion 2.11I, is trickier to categorise. The Fe:S ratio is too far from unity and contains too much Ni (14.34 wt%) and Cu (6.18 wt%) to be considered pyrrhotite. Inclusion 2.11I remains unclassified although it is likely close to pyrrhotite in composition as two other inclusions from diamond 2.11 (2.11I and P) are pyrrhotite.

8.3.2 Inclusions of uncertain origin

There are several inclusions that fail to meet the criteria used in this study for syngenesis. An amorphous flaky, fine-grained appearance, anhedral form, and heterogeneous composition are common characteristics used to distinguish inclusions of secondary origin. Grains in this section tend to exhibit one or more of these characteristics, however, they also have some features which suggest they are primary. As well, most of the grains have been reported as inclusions in diamonds from other localities worldwide. Inclusions described here are not necessarily secondary, but there is an added element of uncertainty to their primary origin. The inclusions are SiO_2, several Ca-rich minerals, perovskite ($CaTiO_3$) and metallic iron.

8.3.2.1 SiO₂

Twelve grains of SiO_2 have been identified, found in 11% of diamonds cracked or 7% of the total diamond population. When examined under SEM, all grains are polycrystalline and fine-grained, which is typical of secondary minerals (Fig. 8.20). However, this appearance may be a result of crystal expansion due to phase changes from stishovite to any or all of coesite, β-quartz or α-quartz (e.g. Fig. 8.7). Another reason for the uncertainty of the origin for these grains is the abundance of SiO_2 found on fracture surfaces of several cracked diamonds (Fig. 8.20 2.3-C). SiO_2 in fractures is clearly secondary and demonstrates the existence of secondary SiO_2 in at least some of the diamonds studied. Although the twelve SiO_2 grains reported under are discrete inclusions with no obvious connection to fractures or the diamond surface, there certainly is potential for silica-rich fluids to alter inclusions through unrecognised fractures.

There is no EPMA data for the SiO_2 grains found in this study although EDS spectra suggest they are essentially pure SiO_2. SiO_2 has several polymorphs which can provide constraints on P-T. In the absence of

2.11 – C   2.7 – K

1.4 - C   2.3 - C
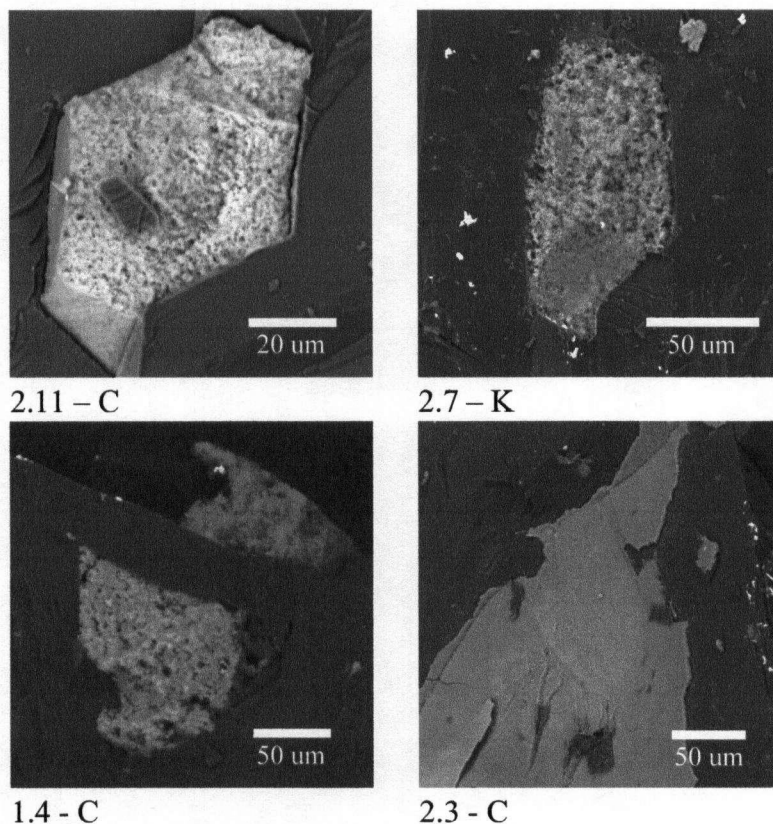
Fig. 8.20. SEM images of SiO_2. Images 2.11-C, 2.7-K and 1.4-C are discrete inclusions while 2.3-C is secondary SiO_2 deposited on fracture surface.

179

crystallographic data, cathodoluminescence (CL) was found to be an effective tool for discriminating quartz from coesite (Sobolev *et al.*, 1984). They found that quartz (it is unclear if this is α-quartz or β-quartz) exhibits a pink or greyish yellow CL colour while coesite exhibits a bright blue CL colour.

CL of inclusion 2.11C shows moderate yellow green colours suggesting the grain is quartz (Fig. 8.21C). Inclusion 2.7K, however, does not exhibit any CL colours (Fig. 8.21F) and could not be classified (it likely is not flush with the diamond surface and was thus not excited by electrons). The reader is reminded that even if these grains were shown to be quartz, this does not exclude the possibility that they were coesite or stishovite at one time.
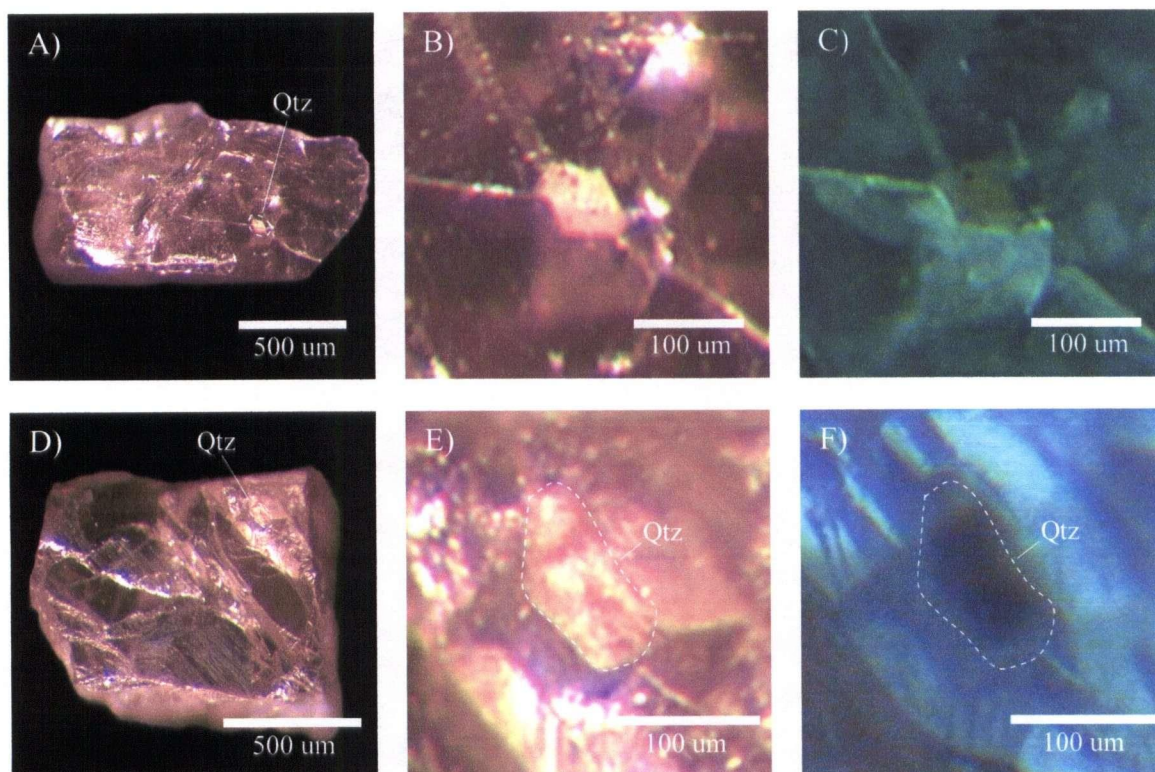
Fig. 8.21. Photographs of SiO_2 grains under UV light and in the absence of UV light. A-C - Inclusion 2.11C and D-F - Inclusion 2.7K. Photographs A, B, D and E show cloudy colour of SiO_2 inclusions. Photo C shows the greyish/yellow cathodoluminescence that is typical of quartz while in photo F, SiO_2 inclusion shows no CL, which is likely a result of the inclusion being somewhat recessed in the diamond host and thus not being activated by electrons.

8.3.2.2 Perovskite

Four separate grains of perovskite (Prv) have been released from two diamonds. Grains are dark grey/black and do not appear to exhibit crystal form (except in the case of inclusion 3.7D2). They range in size from 80 to less than 10 microns. All four grains found are touching $CaSiO_3$ inclusions (Fig. 8.22).

EDS spectra are included for all four grains (Fig. 8.22) while major oxide data are available for two grains (2.8L2 and 3-7A2, Table 8.27) and light rare earth element chemistry for only one grain (2.8L2). Cation calculations are included in Table 8.28. CaO and TiO_2 make up 92-95% of the total weight percent (although there may be some elements missing from the totals for 3.7A2). Substitutional oxides include SiO_2 (1.92 – 2.06 wt%), Al_2O_3 (1.11 – 1.48 wt%) and FeO (0.17 – 1.13 wt%). Rare earth elements (REE's) and high field strength elements (HFSE's) make up the remainder of the impurities present. EDS spectra confirm the substantial amounts of REE's that are common in perovskites. Peaks indicating the presence of cerium are present in three EDS spectra (Fig. 8.22) (cerium is present although not so clearly discerned in 2.8L2,

Table 8.27. Major oxide data for perovskite grains (wt%)

Inclusion No.	No.	Inclusion assemblage	No. of analyses averaged	SiO_2	TiO_2	Al_2O_3	Cr_2O_3	FeO	CaO	Y_2O_3	ZrO_2	La_2O_3	Ce_2O_3	Pr_2O_3	Nd_2O_3	Sm_2O_3	Gd_2O_3	Total
2-8L2	1	$CaSiO_3$	3	2.06	52.41	1.48	0.00	0.17	38.78	0.13	0.60	0.49	1.33	0.29	0.72	0.00	0.21	98.67
3-7A2	2	$CaSiO_3$	1	1.92	51.17	1.11	0.29	1.13	36.15	na	na	na	na	na	na	na	na	91.78

Any values below MDL (see Table 8.9) are replaced by 0.00. P, Mn, Ni, Mg, Na and K were analysed for both inclusions but were below MDL's and removed. Th, and Nb were below the MDL's in 2.8L2.

Table 8.28. Cation calculations for perovskite grains

Inclusion No.	Inclusion assemblage	Si^{4+}	Ti^{4+}	Al^{3+}	Cr^{3+}	Fe^{2+}	Ca^{2+}	Y^{2+}	Zr^{2+}	La^{2+}	Ce^{2+}	Pr^{2+}	Nd^{2+}	Sm^{2+}	Gd^{2+}	Total
2-8L2	$CaSiO_3$	0.048	0.911	0.040	0.000	0.003	0.959	0.002	0.005	0.004	0.011	0.002	0.006	0.000	0.001	1.993
3-7A2	$CaSiO_3$	0.047	0.940	0.032	0.006	0.023	0.946	na	na	na	na	na	na	na	na	1.994

Any values below MDL (see Table 8.10) are replaced by 0.00. P, Mn, Ni, Mg, Na and K were analysed for both inclusions but were below MDL's and removed. Th, and Nb were below the MDL's in 2.8L2.
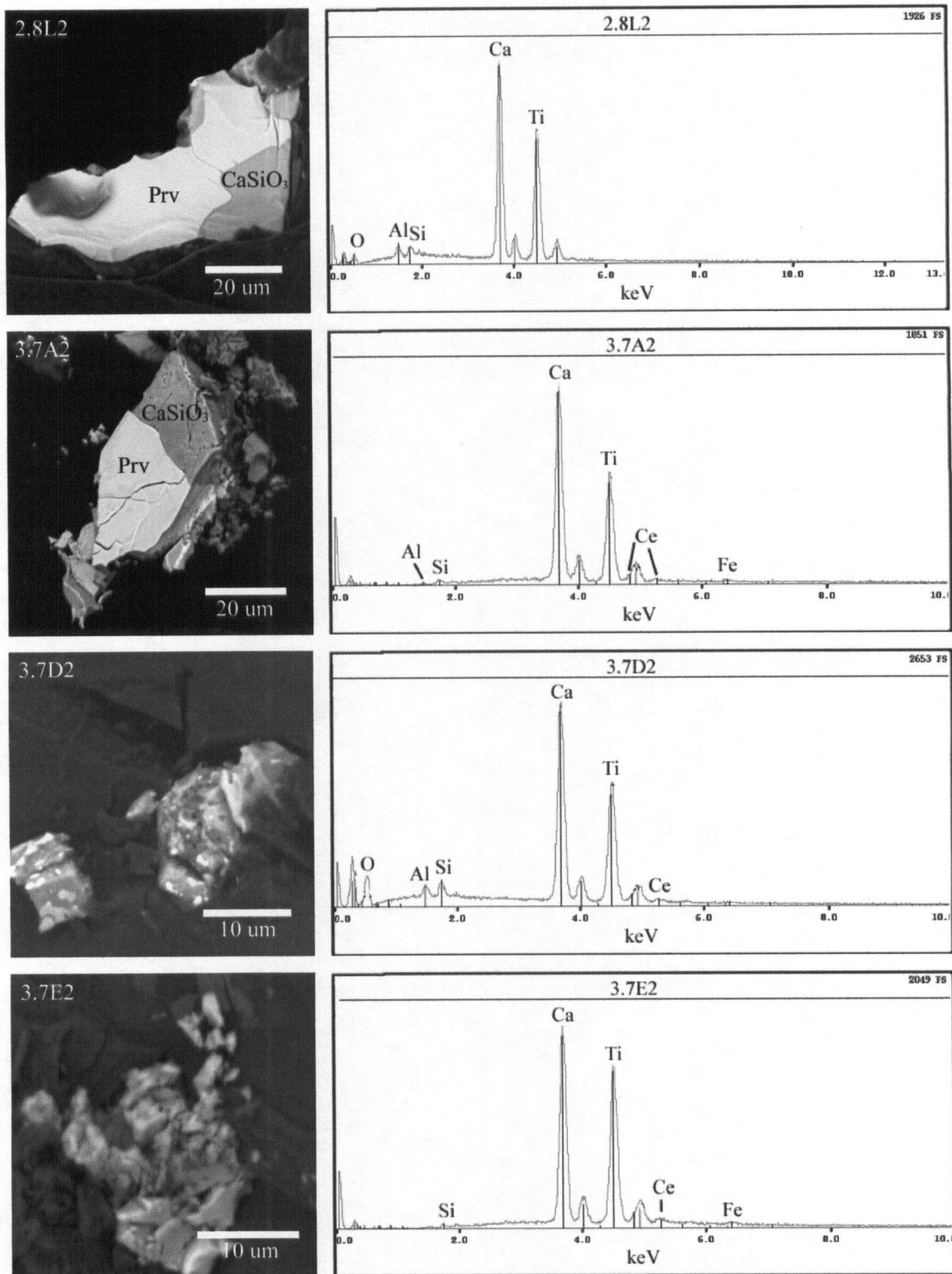
Fig. 8.22. SEM images and EDS spectra of perovskite grains. EPMA data is available for inclusions 2.8L2 and 3.7A2.

which suggests other REE's are also present). Using EMPA, inclusion 2.8L2 was analysed and found to contain ~4.0 wt% of various REE and HFSE's. In decreasing order of abundance, the top three oxides present are: Ce_2O_3 (1.33 wt%), Nd_2O_3 (0.72) and ZrO_2 (0.60 wt%). Although 3.7A2 was not analysed for REE's or HFSE's, it likely contains at least the same amount (and likely more, based on the larger Ce peak), which would considerably increase the wt% oxide total from 91.78 (Table 8.27).

8.3.2.3 Other calcium-bearing minerals

Four Ca-Si oxides with 'exotic' elements were found in two diamonds, and can be sub-divided into two groups. The first group is Ca-Si-P oxides (two grains in diamond 3.1A) and the second is Ca-Si-Ti-Al oxides (two grains found in diamond 3-4, although it is possible that they are two halves of the same inclusion). It is possible that these gains are altered $CaSiO_3$ inclusions, however, their homogenous appearance suggests they may be primary. Inclusion 3.1E2 is likely secondary. Grains are small (<20 microns), thus making EPMA analysis difficult. SEM images of all grains, including EDS spectra, are presented in Fig. 8.23.

Table 8.29. Major oxide data for 'exotic' Ca-Si-O grains (wt%)

Inclusion No.	Inclusion assemblage	P_2O_5	SiO_2	TiO_2	Al_2O_3	Cr_2O_3	FeO	MnO	NiO	MgO	CaO	Na_2O	K_2O	Total
3-1A2	fPer-$CaSiO_3$	10.85	9.58	0.02	0.00	0.00	0.00	0.00	0.00	0.00	46.63	0.00	0.00	67.09
3-1E2	fPer-$CaSiO_3$	0.10	27.85	5.35	12.03	0.46	4.52	0.69	0.03	5.56	25.51	0.33	0.00	82.44
3-4D	$CaSiO_3$	0.02	32.14	25.01	8.82	0.04	0.02	0.00	0.00	0.00	28.57	0.00	0.01	94.64

MDL's and precisions were not calculated for these inclusions.

Table 8.30. Cation calculations for 'exotic' Ca-Si-O grains

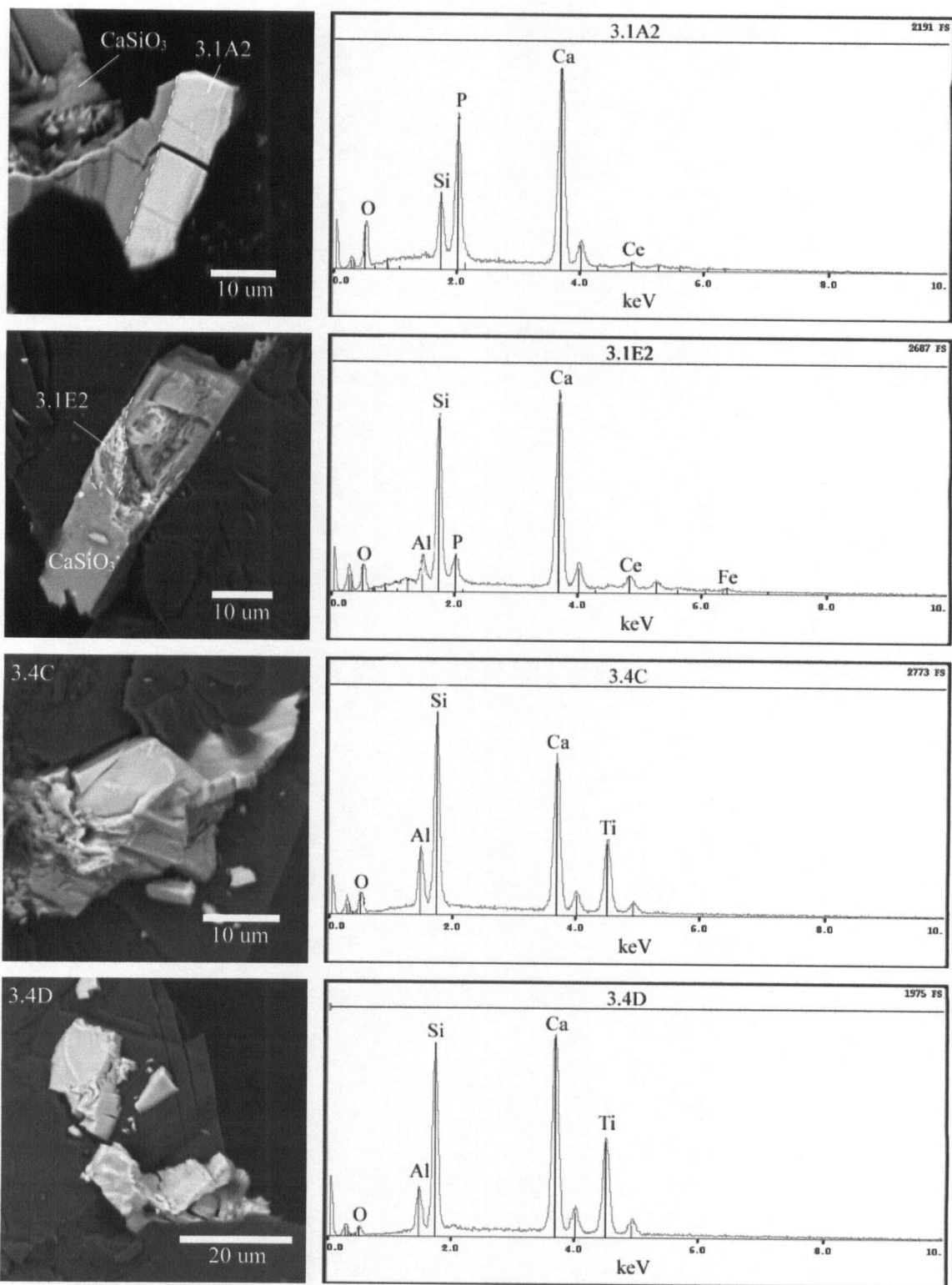| Inclusion No.	Inclusion assemblage	P^{5+}	Si^{4+}	Ti^{4+}	Al^{3+}	Cr^{3+}	Fe^{2+}	Mn^{2+}	Ni^{2+}	Mg^{2+}	Ca^{2+}	Na^+	K^+	Total
3-1A2	fPer-$CaSiO_3$	0.304	0.139	0.000	0.000	0.000	0.000	0.000	0.000	0.000	0.722	0.000	0.000	1.166
3-1E2	fPer-$CaSiO_3$	0.002	0.221	0.032	0.113	0.003	0.030	0.005	0.000	0.066	0.217	0.005	0.000	0.693
3-4D	$CaSiO_3$	0.000	0.217	0.127	0.070	0.000	0.000	0.000	0.000	0.000	0.207	0.000	0.000	0.621

Cations calculated on basis of 1 oxygen anion.

Fig. 8.23. SEM images and EDS spectra of exotic Ca-Si-O grains. EPMA data is available for 3.1A2, 3.1E2 and 3.4D.

EPMA data for the four grains are poor (totals ranging from 67-94 wt%). However, the results are included here as diamond inclusions of this composition have not yet been recorded (Table 8.29). EPMA Results for the two Ca-Si-P minerals are poor and will not be considered further, however, the results for a Ca-Si-Ti-Al inclusion (3-4D), given the inclusion size, are acceptable and warrant further discussion. Koito *et al.* (2000) synthesized minerals in the $CaSiO_3$ - $CaTiO_3$ solid-solution series and found that intermediate compositions were stable at pressures greater than 12 GPa (~400 km). Stoichiometry for this inclusion is close to the 2:3 cation:anion ratio for minerals of this solid-solution series (1.864:3) (Table 8.30). Experimental work mentioned does not examine the effects of aluminum, which make up a significant proportion of inclusion 3.4D (8.82 wt%). Inclusions 3.1A2 and 3.1E2 can only be discussed in terms of EDS analysis. These Ca-Si-P oxides also include Al, Ce and Fe. The presence of Ce suggests that other rare earth elements likely exist (as was observed in perovskites, section 8.3.2.2).

8.3.2.4 Metallic iron

One large grain (150 x 200 μm) of native iron was found in diamond 2-11 (Fig. 8.24). It appears dark black/metallic when viewed under the microscope. EDS analysis shows that the grain in comprised of essentially pure iron, with no complexing anions, such as
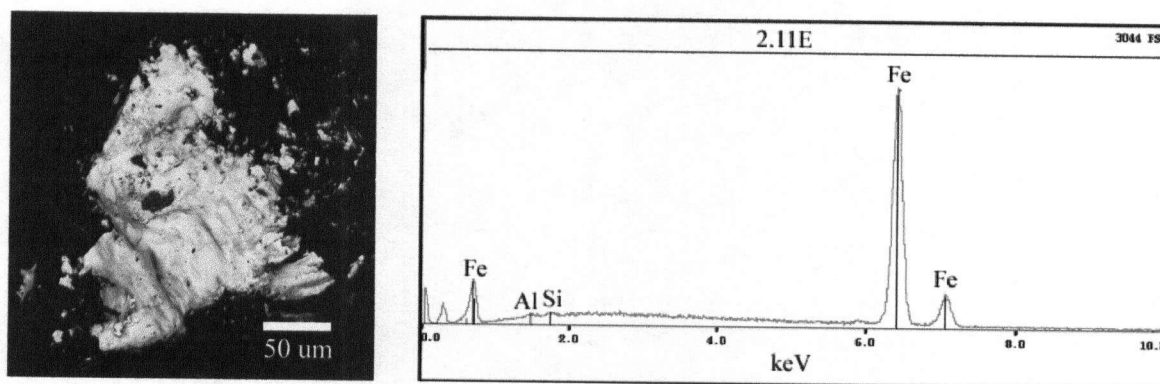
Fig. 8.24. SEM image and EDS spectrum of native iron grain (Diamond 2.11E). Peaks on EDS spectra on the far left (not labelled) correspond to Li (noise peak) and C (from the carbon coat).

oxygen or sulphur (EDS spectrum in Fig. 8.24). SEM examination also shows that the grain is homogeneous in composition.

8.3.3 Touching phases

The term 'assemblage' as applied to diamond studies is used to indicate a collection of minerals that coexisted in equilibrium under certain pressure, temperature and compositional conditions. Unless there is evidence to suggest otherwise, primary inclusions occurring in the same diamond are considered to represent an assemblage. The assumption that a single diamond traps all of its inclusions under the same conditions may or may not be valid; there are certainly instances indicating both scenarios occur. The difference in chemistry from inclusions of the same phase liberated from one diamond is evidence that dis-equilibrium exits. As well, cathodoluminescence images (e.g. chapter 7.0) show that most diamonds do not grow during a single event.

Primary (pristine) touching inclusions remove the uncertainty of equilibrium, however, unlike isolated monocrystalline inclusions, touching phases have the opportunity to re-equilibrate with changing P-T conditions and to re-distribute elements between touching phases. As such, the composite grain as a whole represents 'pristine' mantle material, but the individual phases may not reflect the chemical subtleties acquired during initial crystallization. Table 8.31 summarises the touching phases observed in this study, which

Table 8.31. Touching phases and their associations for Rio Soriso diamonds

Assemblage	No. of occurrences	Diamond(s) #	Touching inclusions				
			Ol-MgSiO$_3$	Ol-fPer	MgSiO$_3$-TAPP	CaSiO$_3$-Prv	MgSiO$_3$-Ol-TAPP
CaSiO$_3$-Prv	2	2.8, 3.7				2.8, 3.7	
fPer-Ol-MgSiO$_3$	2	3.5, 4.3	3.5, 4.3	4.3			
fPer-Ol-MgSiO$_3$-TAPP	1	1.5			1.5		1.5
fPer-Ol-MgSiO$_3$-CaSiO$_3$-TAPP?	1	3.2	3.2		3.2		

'Assemblage' refers to all inclusion phases in diamond (touching and non-touching).

will be the focus of the remainder of this section; non-touching phases will be considered further in the discussion on paragenesis.

Touching inclusions are divided into five subgroups:

1. Large $MgSiO_3$ grains hosting small Ol inclusions. (3 occurrences)
2. Large $MgSiO_3$ grains in contact with likely TAPP. (3 occurrences)
3. Ol-fPer (1 occurrence)
4. $CaSiO_3$ inclusions in contact with exotic calcium-rich minerals. (~2 occurrences)
5. Large $MgSiO_3$ grain in contact with both likely TAPP and two inclusions of Ol. (1 occurrence)

8.3.3.1 $MgSiO_3$ and Mg_2SiO_4 composites

Three occurrences of small Ol grains hosted in large $MgSiO_3$ inclusions were observed. The inclusions are 1.5J2 (Ol on left) and 1.5J4 (Ol on right) in 1.5-J1 ($MgSiO_3$) (Fig. 8.25, 1.5-J), 3.5G2 (Ol) in 3.5G1 ($MgSiO_3$) and 3.5AD2 (Ol) in 3.5AD1 ($MgSiO_3$). Chemical data are available for two olivine inclusions (1.5J2 and 3.5G2) and all three $MgSiO_3$ grains and accompanying photos are found in Fig. 8.25. Chemical data and cation totals are presented in Tables 8.32 and 8.33 respectively. The *mg's* for Ol and
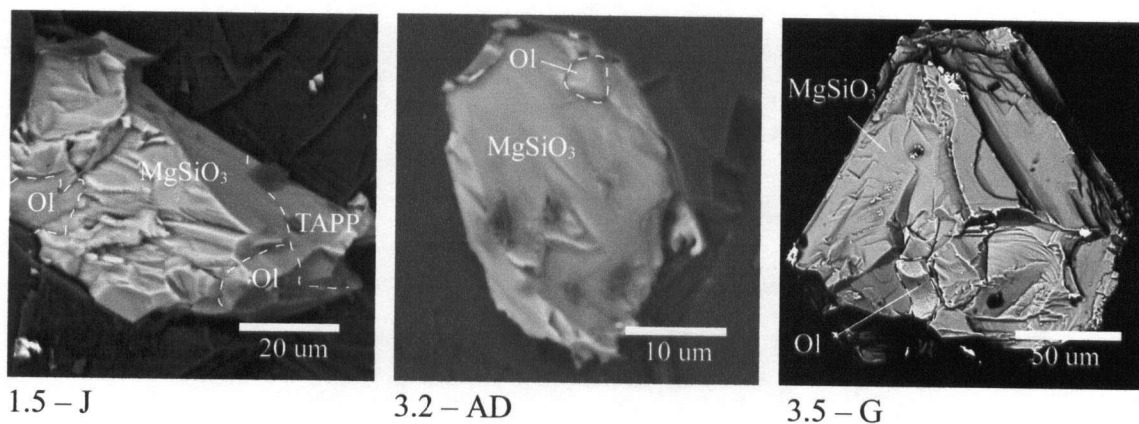
Fig. 8.25. SEM images of touching olivine and $MgSiO_3$ inclusions.

187

Table 8.32. Major oxide data for touching inclusions of $MgSiO_3$ and olivine (wt%)

Inclusion No.	Inclusion Type	Inclusion assemblage	No. of analyses averaged	P_2O_5	SiO_2	TiO_2	Al_2O_3	Cr_2O_3	FeO	MnO	NiO	MgO	CaO	Na_2O	K_2O	Total
1-5J1	$MgSiO_3$	Ol-fPer-TAPP-$MgSiO_3$	3	0.00	54.92	0.17	2.22	0.20	6.15	0.13	0.00	35.68	0.04	0.00	0.00	99.52
1-5J2	Ol	Ol-fPer-TAPP-$MgSiO_3$	2	0.00	38.03	0.05	0.12	0.00	10.24	0.12	0.00	48.46	0.00	0.00	0.00	97.02
3-5G1	$MgSiO_3$	Ol-fPer-$MgSiO_3$	3	na	51.60	0.14	3.37	0.20	6.66	0.27	0.00	35.91	0.00	0.10	0.00	98.26
3-5G2	Ol	Ol-fPer-$MgSiO_3$	3	na	37.45	0.00	0.20	0.00	11.05	0.29	0.00	50.54	0.00	0.07	0.00	99.61
3-2AD1	$MgSiO_3$	Ol-fPer-$CaSiO_3$-TAPP?-$MgSiO_3$	2	na	51.87	0.16	1.94	0.29	4.23	0.14	0.00	39.37	0.04	0.00	0.00	98.04

Chemical data for the touching olivine inclusion 3-2AD2 does not exist.

Table 8.33. Cation calculations for touching inclusions of $MgSiO_3$ and olivine

Inclusion No.	Inclusion Type	Inclusion assemblage	P^{5+}	Si^{4+}	Ti^{4+}	Al^{3+}	Cr^{3+}	Fe^{2+}	Mn^{2+}	Ni^{2+}	Mg^{2+}	Ca^{2+}	Na^+	K^+	Total	mg
1-5J1	$MgSiO_3$	Ol-fPer-TAPP-$MgSiO_3$	0.000	0.954	0.002	0.045	0.003	0.089	0.002	0.000	0.924	0.001	0.000	0.000	2.020	0.91
1-5J2	Ol	Ol-fPer-TAPP-$MgSiO_3$	0.000	0.967	0.001	0.004	0.000	0.218	0.003	0.000	1.837	0.000	0.000	0.000	3.030	0.89
3-5G1	$MgSiO_3$	Ol-fPer-$MgSiO_3$	na	0.916	0.002	0.071	0.003	0.099	0.004	0.000	0.950	0.000	0.003	0.000	2.047	0.91
3-5G2	Ol	Ol-fPer-$MgSiO_3$	na	0.935	0.000	0.006	0.000	0.231	0.006	0.000	1.882	0.000	0.003	0.000	3.063	0.89
3-2AD1	$MgSiO_3$	Ol-fPer-$CaSiO_3$-TAPP?-$MgSiO_3$	na	0.915	0.002	0.040	0.004	0.062	0.002	0.000	1.035	0.001	0.000	0.000	2.061	0.94

$MgSiO_3$ cations are calculated on the basis of 3 anions while olivine cations are calculated on basis of four anions.

$MgSiO_3$ are 0.89 and 0.91 respectively (in both composite inclusions 1.5-J and 3.5-G). The mg for the composite 3.2-AD is only available for $MgSiO_3$, and is considerably higher at 0.94. All three $MgSiO_3$ grains contain elevated amounts of Al_2O_3 (1. 94 – 3.37 wt%), but this is within the range for the results of other grains analysed in this study.

The *mg* values reported for these two 'olivines' are the lowest recorded for Ol's in this study, but are not unique to grains touching $MgSiO_3$ inclusions (the isolated Ol inclusion 3.2S also has *mg*=0.89). In all other respects, the Ol grains are similar to the five other grains analysed. The prevalence of Ol inclusions inside $MgSiO_3$ grains, coupled with the relative size difference between grains, may be an indication that these Ol grains are the products of a retrograde reaction between fPer and MgSi-Prv.

8.3.3.2 $MgSiO_3$ and TAPP composites

There are two occurrences of TAPP in contact with $MgSiO_3$ (inclusions 1.5A and 3.2I) and one occurrence of $MgSiO_3$ in contact with TAPP and two Ol grains (inclusion 1.5J) (Fig. 8.26). Major oxide data and cation calculations for these composites are presented in Tables 8.34 and 8.35 respectively.

The *mg* for both $MgSiO_3$ inclusions in diamond 1-5 (inclusions 1.5A and J) is 0.91, while the TAPP grain (1.5A2) has *mg*=0.87. There is no EPMA data for TAPP inclusion 1.5J3. The $MgSiO_3$ inclusion in diamond 3-2 has a higher *mg* (=0.93) and there are no EPMA data for the suspected touching TAPP phase. The chemistry data for the three $MgSiO_3$ grains are similar in all other respects. Inclusion 1.5J2 is the only TAPP grain with

1.5 - A   1.5 – J   3.2 – I
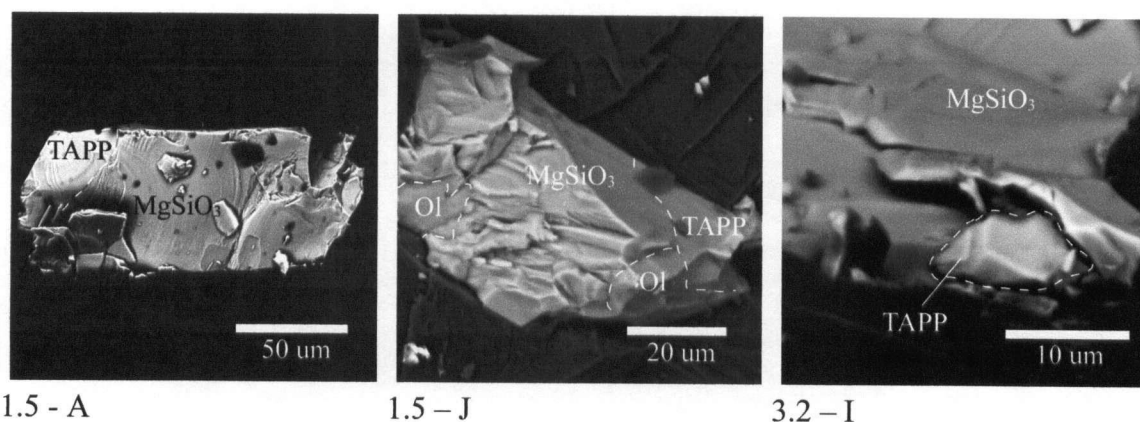
Fig. 8.26. SEM images of touching $MgSiO_3$ and TAPP inclusions.

189

Table 8.34. Major oxide data for touching $MgSiO_3$ and TAPP inclusions (wt%)

Inclusion No.	Inclusion Type	Inclusion assemblage	No. of analyses averaged	P_2O_5	SiO_2	TiO_2	Al_2O_3	Cr_2O_3	FeO	MnO	NiO	MgO	CaO	Na_2O	K_2O	Total
1-5A1	$MgSiO_3$	Ol-$MgSiO_3$-fPer-TAPP	3	0.00	57.31	0.16	1.91	0.21	6.34	0.13	0.00	33.91	0.06	0.00	0.00	100.04
1-5A2	TAPP	Ol-$MgSiO_3$-fPer-TAPP	3	0.00	39.99	4.71	19.03	2.74	6.87	0.14	0.00	25.75	0.04	0.00	0.00	99.26
1-5J1	$MgSiO_3$	Ol-$MgSiO_3$-fPer-TAPP	3	0.00	54.92	0.17	2.22	0.20	6.15	0.13	0.00	35.68	0.04	0.00	0.00	99.52
3-2I1	$MgSiO_3$	Ol-fPer-$CaSiO_3$-$MgSiO_3$-TAPP?	2	na	58.19	0.20	1.60	0.22	4.21	0.14	0.00	33.43	0.04	0.00	0.00	98.02

There is no supporting chemical data for the TAPP inclusions touching grains 1-5J1 and 3-2I1

Table 8.35. Cation calculations for touching $MgSiO_3$ and TAPP inclusions

Inclusion No.	Inclusion Type	Inclusion assemblage	P^{5+}	Si^{4+}	Ti^{4+}	Al^{3+}	Cr^{3+}	Fe^{2+}	Mn^{2+}	Ni^{2+}	Mg^{2+}	Ca^{2+}	Na^+	K^+	Total	mg
1-5A1	$MgSiO_3$	Ol-$MgSiO_3$-fPer-TAPP	0.000	0.985	0.002	0.039	0.003	0.091	0.002	0.000	0.869	0.001	0.000	0.000	1.992	0.91
1-5A2	TAPP	Ol-$MgSiO_3$-fPer-TAPP	0.000	2.852	0.252	1.600	0.155	0.410	0.009	0.000	2.738	0.003	0.000	0.000	8.018	0.87
1-5J1	$MgSiO_3$	Ol-$MgSiO_3$-fPer-TAPP	0.000	0.954	0.002	0.045	0.003	0.089	0.002	0.000	0.924	0.001	0.000	0.000	2.020	0.91
3-2I1	$MgSiO_3$	Ol-fPer-$CaSiO_3$-$MgSiO_3$-TAPP?	na	1.008	0.003	0.033	0.003	0.061	0.002	0.000	0.863	0.001	0.000	0.000	1.972	0.93

$MgSiO_3$ and TAPP cations are calculated on the basis of three and twelve anions respectively.

acceptable EPMA data, thus excluding the possibility of comparison with other grains in this study.

8.3.3.3 Mg_2SiO_4 and ferropericlase composite

Diamond 4-3 contains one occurrence of a small composite (~30 microns in size) of olivine and ferropericlase (inclusion K) (Fig. 8.27). Only one acceptable EPMA result was collected from the Ol (K1) and two were collected for the fPer (K2) grain (Tables 8.36 and 8.37). The mg of the fPer and Ol grains is 0.83 and 0.94 respectively. The Ol inclusion is similar in most respects to another olivine, which was in isolation, liberated from diamond 4-3 (inclusion 4-3C). The main differences being inclusion 4-3K1

190

Table 8.36. Major oxide data for touching grains of ferropericlase and olivine (wt%)

Inclusion No.	Inclusion Type	Inclusion assemblage	No. of analyses averaged	P_2O_5	SiO_2	TiO_2	Al_2O_3	Cr_2O_3	FeO	MnO	NiO	MgO	CaO	Na_2O	K_2O	Total
4-3K1	Ol	Ol-fPer-MgSiO$_3$	1	na	36.97	0.14	0.72	0.28	5.83	0.14	0.19	55.73	0.00	0.05	0.00	100.05
4-3K2	fPer	Ol-fPer-MgSiO$_3$	2	na	0.26	0.00	0.42	1.01	25.96	0.26	1.35	70.83	0.00	0.00	0.00	100.08

Table 8.37. Cation calculations for touching grains of ferropericlase and olivine

Inclusion No.	Inclusion Type	Inclusion assemblage	P^{5+}	Si^{4+}	Ti^{4+}	Al^{3+}	Cr^{3+}	Fe^{2+}	Mn^{2+}	Ni^{2+}	Mg^{2+}	Ca^{2+}	Na^+	K^+	Total	mg
4-3K1	Ol	Ol-fPer-MgSiO$_3$	na	0.902	0.003	0.021	0.005	0.119	0.003	0.004	2.026	0.000	0.002	0.000	3.084	0.94
4-3K2	fPer	Ol-fPer-MgSiO$_3$	na	0.020	0.000	0.038	0.061	1.656	0.017	0.083	8.056	0.000	0.000	0.000	9.931	0.83

contains 0.19 wt% NiO and 0.28 wt% Cr_2O_3, which are absent or below detection in inclusion 4-3C. Compared to the remaining olivines in this study, 4-3K1 is the only Ol grain to contain detectable chromium and it also contains elevated amounts of titanium (0.14 wt% TiO_2). Compared to the rest of the population, both olivines liberated from diamond 4-3 contain elevated amount of aluminium (0.72 – 0.80 wt% Al_2O_3). The mg of Ol does not represent the most extreme value, but is close to the upper limit of mg's for 'olivines' in this study. The

Fig. 8.27. SEM image of touching olivine and ferropericlase inclusion (Diamond 4.3 – K).

chemistry of the fPer is unremarkable, with mg and all wt% totals falling within the ranges for all fPer grains analysed. The possibility of the Ol being the result of a retrograde reaction between fPer and MgSi-Prv must be considered, but the similarity in chemistry with the isolated Ol in diamond 4-3 makes this conclusion less likely.

8.3.3.4 MgSiO₃, Mg₂SiO₄ and TAPP composite

Inclusion 1.5J is the only composite with more than two touching phases found. This composite is composed of TAPP (J3), MgSiO$_3$ (J1) and two Ol grains (J2 and J4) (Fig. 8.28). There appears to be a triple junction between one of the Ol grains and the MgSiO$_3$ and TAPP. Tables 8.38 and 8.39 contain chemical data for inclusions J1 (MgSiO$_3$) and J2 (Ol), as well as A1 (MgSiO$_3$) and A2 (TAPP). Chemical data are available only for MgSiO$_3$ and the Ol grain (J2) not in contact with TAPP. *Mg*'s for MgSiO$_3$ and Ol are 0.91 and 0.89 respectively. Both Ol (J2) and MgSiO$_3$ (J1) are

Fig. 8.28. SEM images of three-phase composite (Inclusion 1.5-J) Individual phases are: Ol (J2 on left, J4 on right), MgSiO$_3$ (J1) and TAPP (J3).

unremarkable in terms of chemistry, with all EPMA wt% totals falling within the ranges measured for the complete sets of inclusions. Although there is chemical data for another TAPP grain hosted in the same diamond (inclusion 1.5A2), its chemistry may not reflect that of 1.5J3. As both TAPP grains are in contact with MgSiO$_3$, a comparison between

Table 8.38. Major oxide data for inclusions in diamond 1-5 (wt%)

Inclusion No.	Inclusion Type	Inclusion assemblage	No. of analyses averaged	P$_2$O$_5$	SiO$_2$	TiO$_2$	Al$_2$O$_3$	Cr$_2$O$_3$	FeO	MnO	NiO	MgO	CaO	Na$_2$O	K$_2$O	Total
1-5A2	TAPP	Ol-fPer-TAPP-MgSiO$_3$	3	0.00	39.99	4.71	19.03	2.74	6.87	0.14	0.00	25.75	0.04	0.00	0.00	99.26
1-5A1	MgSiO$_3$	Ol-fPer-TAPP-MgSiO$_3$	3	0.00	57.31	0.16	1.91	0.21	6.34	0.13	0.00	33.91	0.06	0.00	0.00	100.04
1-5J1*	MgSiO$_3$	Ol-fPer-TAPP-MgSiO$_3$	3	0.00	54.92	0.17	2.22	0.20	6.15	0.13	0.00	35.68	0.04	0.00	0.00	99.52
1-5J2*	Ol	Ol-fPer-TAPP-MgSiO$_3$	2	0.00	38.03	0.05	0.12	0.00	10.24	0.12	0.00	48.46	0.00	0.00	0.00	97.02

The three-phase touching inclusion 1.5J contains Ol (2 grains), TAPP and MgSiO$_3$. Only chemical data for the MgSiO$_3$ and one Ol exist (1-5J1 and 1.5J2 respectively). Chemical data for the two-phase touching inclusion 1.5A of MgSiO$_3$ and TAPP that is found in the same diamond is included for comparison.

Table 8.39. Cation calculations for inclusions in diamond 1-5

Inclusion No.	Inclusion Type	Inclusion assemblage	P^{5+}	Si^{4+}	Ti^{4+}	Al^{3+}	Cr^{3+}	Fe^{2+}	Mn^{2+}	Ni^{2+}	Mg^{2+}	Ca^{2+}	Na^+	K^+	Total	*mg*
1-5A2	TAPP	Ol-fPer-TAPP-MgSiO3	0.000	2.852	0.252	1.600	0.155	0.410	0.009	0.000	2.738	0.003	0.000	0.000	8.018	0.87
1-5A1	MgSiO3	Ol-fPer-TAPP-MgSiO3	0.000	0.985	0.002	0.039	0.003	0.091	0.002	0.000	0.869	0.001	0.000	0.000	1.992	0.91
1-5J1	MgSiO3	Ol-fPer-TAPP-MgSiO3	0.000	0.954	0.002	0.045	0.003	0.089	0.002	0.000	0.924	0.001	0.000	0.000	2.020	0.91
1-5J2	Ol	Ol-fPer-TAPP-MgSiO3	0.000	0.967	0.001	0.004	0.000	0.218	0.003	0.000	1.837	0.000	0.000	0.000	3.030	0.89

these two $MgSiO_3$ inclusions is warranted. 1.5J1 contains more Al_2O_3 (2.22 vs. 1.91), less SiO_2 (54.92 vs. 57.31) and more MgO (35.68 vs. 33.91) than inclusion 1.5A1. Because of these differences in chemistry, the chemical data for TAPP inclusion 1.5A2 may be different from the chemical data for the TAPP inclusion 1.5J3 despite the similarities in EDS spectra (Fig. 8.15). The *mg* of TAPP 1.5A2 is 0.87.

8.3.3.5 $CaSiO_3$ and Ca-rich mineral composites

There are six occurrences of composite grains in contact with $CaSiO_3$. They can be subdivided into three groups:

1. $CaSiO_3$ and $CaTiO_3$. (4 occurrences, 2.8L, 3.7A, D and E)
2. $CaSiO_3$ and a Ca, Si, Al, P Ce, Fe oxide. (1 occurrence, 3.1E)
3. $CaSiO_3$ and a Ca, P, Si, Ce oxide. (1 occurrence, 3.1A)

These composite grains have a high degree of uncertainty attached to their pristine nature. They are small, in some case heterogeneous, and typically anhedral (and therefore fail to meet some of the criteria for primary inclusions). However, they are included here because some pass all the criteria and there is merit in presenting them together. Group 1 occurs in two diamonds and appears most likely to be primary. Two grains are quite
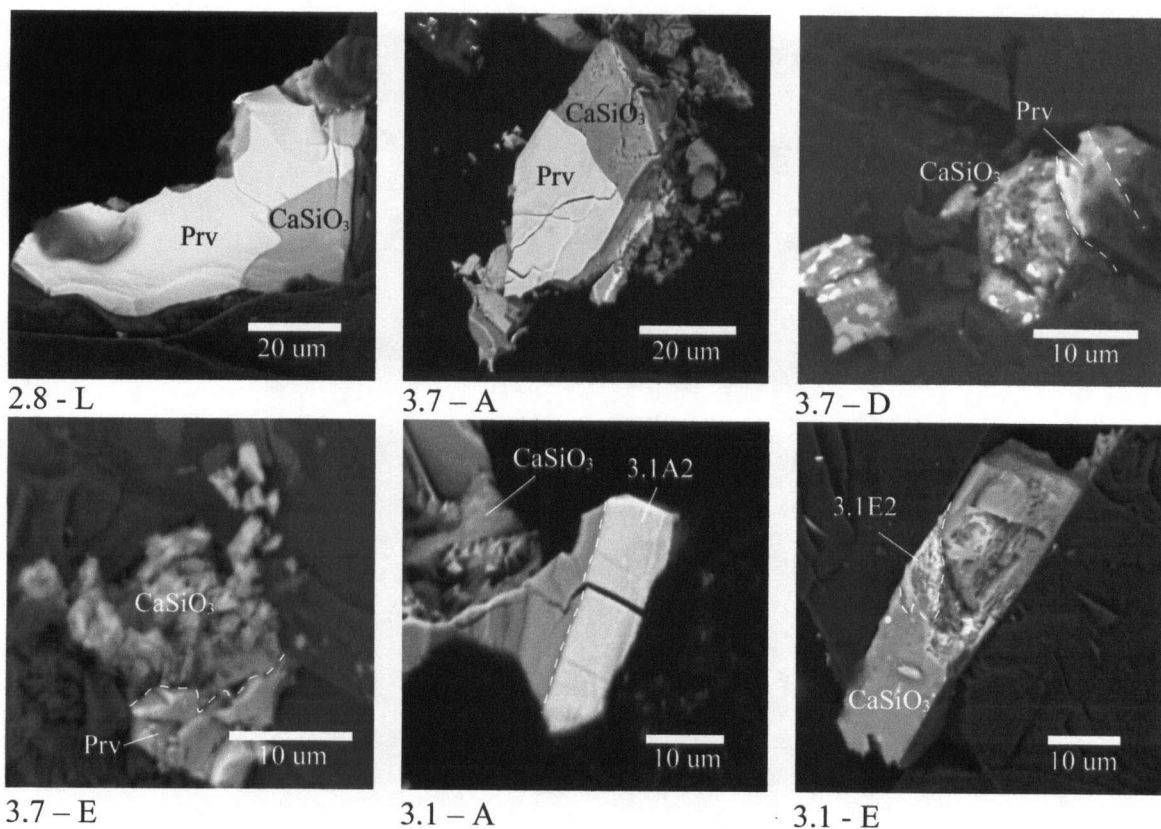
Fig. 8.29. SEM images of composite grains of CaSiO$_3$ and 'exotic' Ca-rich phases. Inclusions 3.1A2 and 3.1E2 were analysed using EDS and are a Ca,P,Si oxide and a Ca,Si,P,Al oxide respectively.

large and each phase is homogeneous (2.8L and 3.7A). In the case of inclusion 3.7A, the grains did not separate easily as is common for grains which have experienced alteration. Group 2 is most likely secondary, as EPMA results were poor for the 'exotic' phase and the SEM image shows that it is heterogeneous (Fig. 8.29 3.1E). Table 8.40 is a summary of EDS and EPMA results.

Table 8.40. EMPA and EDS data for composite grains of $CaSiO_3$ and other Ca phases

Inclusion No.	Inclusion type	No. of analyses averaged	P_2O_5	SiO_2	TiO_2	Al_2O_3	Cr_2O_3	FeO	CaO	Y_2O_3	ZrO_2	La_2O_3	Ce_2O_3	Pr_2O_3	Nd_2O_3	Sm_2O_3	Gd_2O_3	Total
2-8L1	$CaSiO_3$	3	na	52.59	0.07	0.01	0.00	0.42	46.61									99.70
2-8L2	$CaTiO_3$	3	na	2.06	52.41	1.48	0.07	0.17	38.78	0.13	0.60	0.49	1.33	0.29	0.72	0.11	0.21	98.98
3-1A1	$CaSiO_3$	3	na	50.31	0.03	0.09	0.02	0.08	47.94									98.47
3-1A2	Ca,P,Si,O?	1	10.85	9.58	0.02	0.00	0.00	0.00	46.63				+					67.08
3-1E1	$CaSiO_3$	3	0.14	52.11	0.21	0.21	0.01	0.28	45.50									98.47
3-1E2	Ca,Si,P,Al?	1	0.05	47.58	1.43	3.80	0.10	2.35	38.66				+					93.97
3-7A1	$CaSiO_3$	1	0.00	49.19	0.05	0.01	0.03	0.50	36.15									85.92
3-7A2	$CaTiO_3$	1	na	1.92	51.17	1.11	0.29	1.13	36.15				+					91.78
3-7D1	$CaSiO_3$			+					+									
3-7D2	$CaTiO_3$				+	+			+				+					
3-7E1	$CaSiO_3$	1	0.02	45.41	0.08	0.02	0.00	0.42	44.41									90.37
3-7E2	$CaTiO_3$				+	+			+				+					

'+' indicates the element was detected using EDS. Blank entries for major oxides (P_2O_5 through CaO) indicate phase was not analysed using EPMA. Blank entries for oxides Y_2O_5 through Gd_2O_3 indicate they were not detected using EDS.

8.3.4 Fe-Ni blebs on ferropericlase

Blebs of Fe-Ni alloy were observed on the surfaces of several ferropericlase grains released from two diamonds (3-5 and 3-10). The blebs are small, generally less than 2 microns in size, have an elliptical morphology, and tend to form in lines. EDS analysis shows that they consist essentially of iron and nickel alloy. However, most analyses are likely contaminated to varying degrees by their ferropericlase hosts, thus introducing Mg and O, among other elements, into the results. The EDS analysis for inclusion 3-10W2 (Fig. 8.30) is considered to be the most representative of the blebs. Fractured ferropericlase grains in diamonds 3-5 and 3-10 show that the blebs only develop on the crystal surface (it is also possible that they are too small to resolve on fractured surfaces, however, if they do exist on fracture surfaces, they are proportionally minor compared to surface blebs). Ferropericlase grains released from several other diamonds appear to have small (<1 μm) blebs as well, however they were too small to analyse with EDS (e.g.
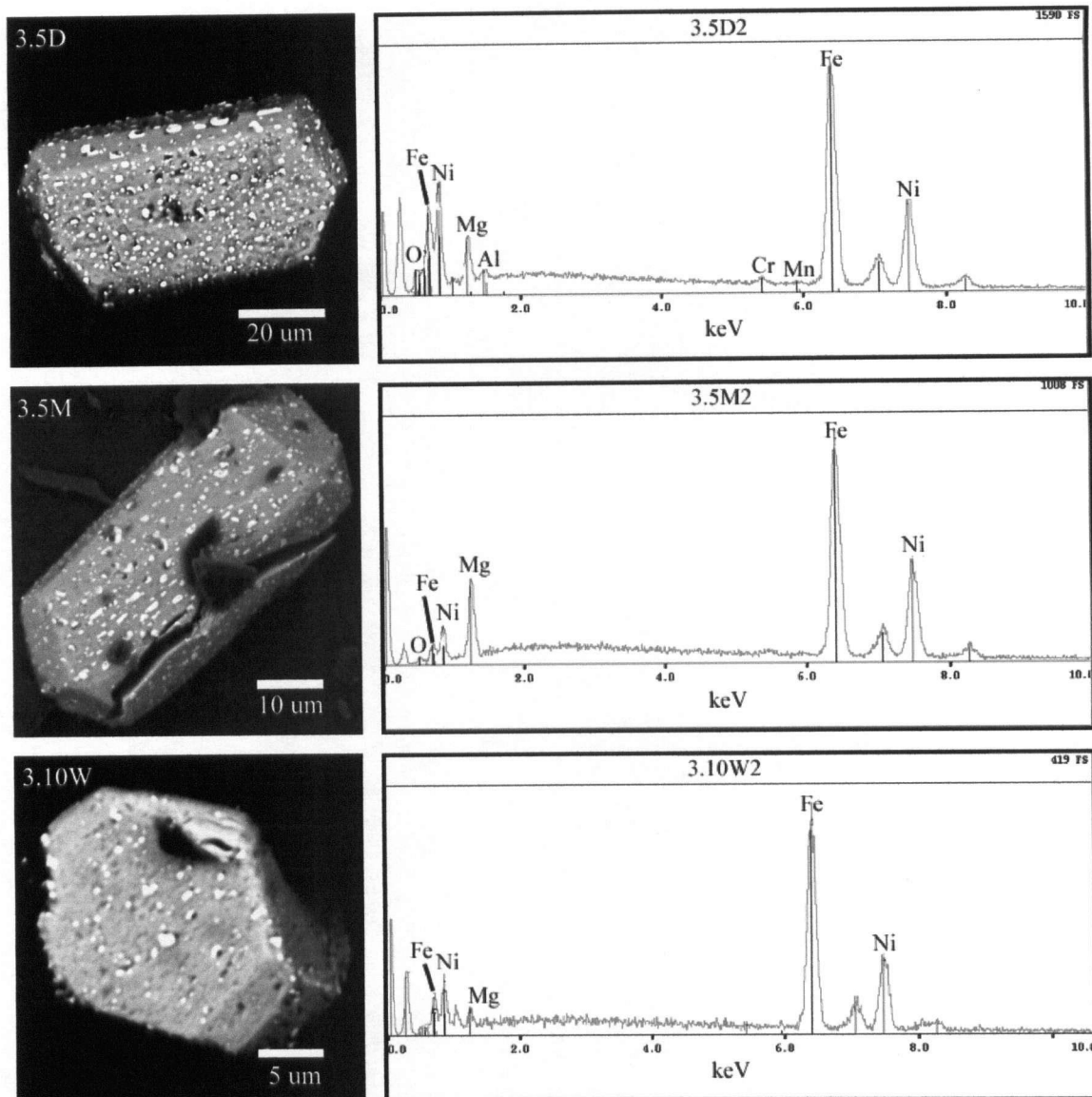
Fig. 8.30. SEM images and EDS spectra for Fe-Ni blebs on ferropericlase gains. Blebs are Fe-Ni-rich and occur as moderately aligned elliptical blebs, only on the inclusion surface.

Figs. 8.31 1-2H, 1-5F and 6-2A). All blebs were too small for EPMA, however, several results from ferropericalse grains released from diamond 3-5 contain anomalously high iron and nickel contents as a result of overlap with Fe-Ni blebs (Tables 8.13 and 8.14).
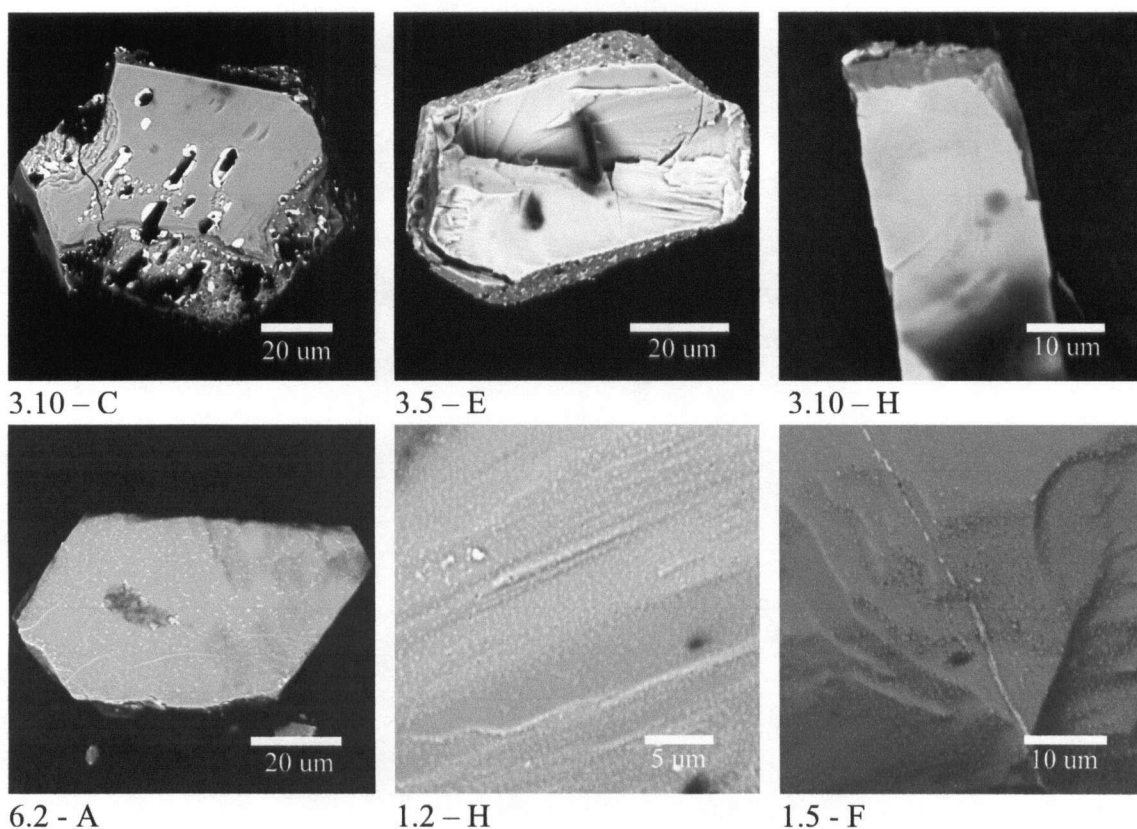
Fig. 8.31. SEM images of Fe-Ni blebs and linear features on ferropericlase grains. Linear feature on inclusion 1.5F were too small for EDS analysis.

8.3.5 Inclusions of secondary origin

Inclusions were classified as secondary based on several criteria. The possibility of a secondary origin was suspected during inclusion extraction and mounting when the inclusion appeared amorphous when released from the diamond host, was flaky, had a tendency to crumble, or was reddish in colour. There is certainly uncertainty as to whether an inclusions' amorphous nature is a result of crystal structure inversion (as was hypothesized for SiO_2 inclusions, section 8.3.2.1) or as a result of alteration. However, after further examination using the SEM, it was usually possible to resolve this issue. Under the SEM, secondary inclusions typically appear heterogeneous (with the exception of primary sulphides, section 8.3.1.7), have rough crystal faces with irregular 'holes' or pits or have no crystal faces at all.

8.3.5.1 Altered ferropericlase grains

Altered ferropericlase grains were observed in a few diamonds. Once inclusions were released from diamond, they were easy to recognize as they were difficult to move without destroying and they were typically reddish in colour (Fig. 8.32). Diamond 3-10 contained a number of altered fPer grains (Fig. 8.33). From this figure, the general progression from primary to secondary can be seen. EPMA data is not available for the highly altered grain in Fig. 8.33, but based on the EDS spectra (and EPMA data for the pristine fPer's from

Fig. 8.32. Photo of altered ferropericlase grain (Inclusion 3-9A).

diamond 3-10) it appears that alteration increases the Fe, Si, Al and Cr content of fPer gains while lowering the Mg content.
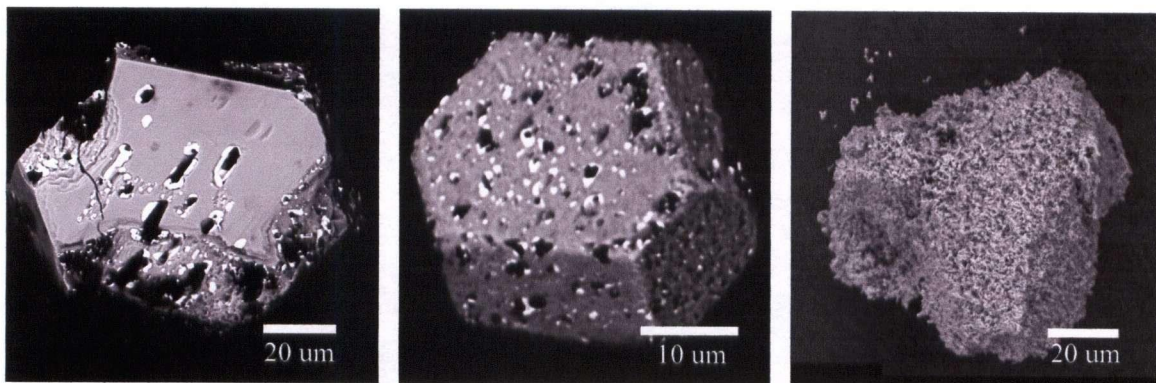
Fig. 8.33. SEM images of weathered ferropericlase grains. These images illustrate the progression of alteration of fPer grains, from least altered on the left, to most altered on the right. (inclusions released from diamond 3-10).

8.3.5.2 Local oxidation of ferropericlase grains

Twelve grains of fPer were found in diamond 3-6, of which several grains contained small (<5 um) spots that appeared bright under SEM and were restricted to particular domains on the inclusion surface (Fig. 8.34). EDS analysis of these spots indicate that

they are mainly Fe-oxide with minor Mg. EPMA of several fPer grains from this diamond yielded *mg* values ranging from 0.54-0.61. One Fe-rich value was poor (90.92 wt%) and was recalculated assuming the presence of both ferric and ferrous iron. Table 8.41 lists the reassigned major oxide values and Table 8.42 lists the calculated cation values for this analysis. When calculated on the basis of four oxygen anions, the sum of calculated cations

3.6 - K   3.6 – L

Fig. 8.34. SEM images and EDS spectrum of secondary magnesioferrite spots on ferropericlase (from Diamond 3.6). EDS spectra of spot from inclusion 3-6P.

is three. The iron-rich spots are thus interpreted to fall along the magnetite-magnesioferrite solid solution series in the spinel group. The formula of these blebs would be: $(Fe_{0.43}Mg_{0.49}Ca_{0.06}Na_{0.01})$ $(Fe_{1.99}Al_{0.01})O_4$. These features will be referred to as magnesioferrite spots.

Magnesioferrite spots are different from the primary inclusions of magnetite identified in section 8.3.1.6 as they contain significantly more magnesium (8.96 wt% MgO compared to 1.46-3.58 wt% MgO for the primary magnetite grains). As well, these secondary spots contain little or no TiO_2, Al_2O_3, Cr_2O_3, or MnO.

Table 8.41. Major oxide data for secondary magnesioferrite spots on ferropericlase grain 3-6P (wt%)

Inclusion No.	Inclusion assemblage	No. of analyses averaged	SiO_2	TiO_2	Al_2O_3	Cr_2O_3	Fe_2O_3	FeO	MnO	NiO	MgO	CaO	Na_2O	K_2O	Total
3-6P	fPer	1	0.18	0.00	0.24	0.00	72.68	14.17	0.12	0.00	8.96	1.55	0.18	0.00	98.08

Fe_2O_3 and FeO values determined using *Formula* (Ercit, T.S., 1996).

Table 8.42. Cation calculations for secondary magnesioferrite spots on ferropericlase grain 3-6P

Inclusion No.	Inclusion assemblage	Si^{4+}	Ti^{4+}	Al^{3+}	Cr^{3+}	Fe^{3+}	Fe^{2+}	Mn^{2+}	Ni^{2+}	Mg^{2+}	Ca^{2+}	Na^+	K^+	Total	*mg*
3-6P	fPer	0.007	0.000	0.010	0.000	1.989	0.431	0.004	0.000	0.486	0.060	0.013	0.000	3.000	0.53

Fe^{2+} and Fe^{3+} values determined using *Formula* (Ercit, T.S., 1996).

8.3.5.3 Altered Ca-rich grains

Heterogeneous grains are generally interpreted as being secondary in origin, although this is not necessarily true for sulphides (see section 4.3.1.7). SEM images of two grains clearly reveal their secondary nature
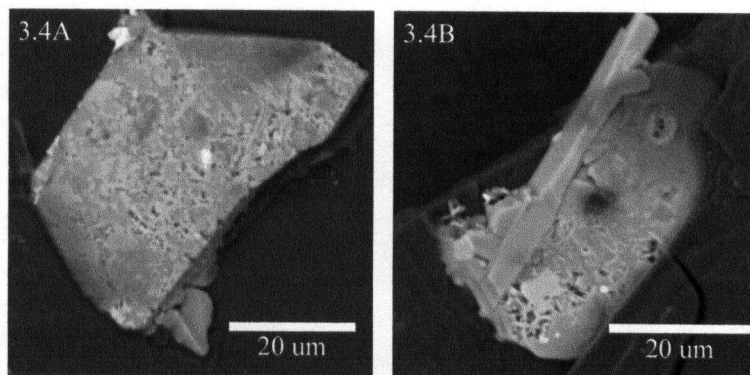
Fig. 8.35. SEM images of weathered Ca-rich grains. Inclusion 3.4A (left) and inclusions 3.4B (right).

(Fig. 8.35). Although little can be said about these grains, they are included here for the purpose of illustration. They were likely $CaSiO_3$ grains (one grain of $CaSiO_3$ was identified in diamond 3-4) before they were exposed to external fluids, likely through a small fracture in the diamond. The relative timing of alteration is unknown, it could have occurred in the mantle, during transport to the surface, or in the secondary collector at surface. Because of the uncertainty surrounding secondary inclusions (i.e. what they say about their primary compositions and the relative timing of alteration), they are generally ignored in diamond studies.

8.4 Discussion

8.4.1 Comparison with diamond inclusions from other studies

In order to properly evaluate the results from examination of mineral inclusions in this study, an in depth comparison with other diamond inclusions is warranted. More specifically, comparison with other diamond inclusions should further help differentiate 'typical' upper mantle peridotitic and eclogitic phases from inclusions with a deeper origin.

8.4.1.1 Ferropericlase

There is an increasing amount of published data on ferropericlase inclusions from localities all over the world (Table 8.43). From this table, it is striking that fPer grains from Juina, Central South America (including Sao Luiz) have a distinctly different mg range and average (Fig. 8.36). Juina fPer grains cover essentially the complete range in mg from 0.36-0.89 with an average of 0.68. The range of mg's from all other localities is 0.75-0.94 with an average of 0.86 (although it is important to note that the vast majority of data for all other localities is from Guinea, Western Africa). Using Mossbauer spectroscopy, McCammon et $al.$ (1997) found that Fe^{3+} is low ($Fe^{3+}/\Sigma Fe_{tot} \leq 7\%$) for ferropericlase grains extracted from Juina diamonds. Although no quantitative analytical technique to specifically analyse Fe^{3+} has been used on ferropericlase in this study, weight percent oxide values are close to 100.00 (97.94-101.69 wt%, average 99.75 wt%), thus suggesting iron occurs mostly as Fe^{2+}. Stachel et $al.$ (2000b) observed a positive correlation between Na_2O and Cr_2O_3 and explained this correlation as being due to coupled substitution. This coupled substitution is not observed in this study as there is considerable scatter when Na_2O wt% is plotted against Cr_2O_3 wt%. Aside from the few analyses in this study that include Fe-Ni contamination (section 8.3.5), the chemistry of fPer grains recovered in this study is similar to that previously reported.

Table 8.43. Published data on ferropericlase diamond inclusions

General region	Author	Locality	No. of grains	Range of mg	Average mg
Central South America	Hutchison (1997)	Sao Luiz, Brazil	36	0.36-0.85	0.71
	Kaminsky et al., (2001a)	Juina, Brazil	28	0.49-0.83	0.66
	this study	Rio Soriso, Brazil	57	0.45-0.89	0.67
			121	0.36-0.89	0.68
Northern South America	Kaminsky et al., (2000)	Guaniamo, Venizuela	1		0.88
Certral North America	Otter and Gurney (1989)	Sloan, USA	1		0.88
Northern North America	Davies et al., (1999)	DO-27, Canada	7	0.80 - 0.87	0.85
West Africa	Hutchison (1997)	Guinea	2	0.87	0.87
	Stachel et al., (2000b)	Guinea	44	0.75-0.94	0.86
			46	0.75-0.94	0.86
East Africa	Stachel et al., (1998)	Mwadui, Tanzania,	1		0.86
Southern Africa	McDade and Harris (1999)	Letseng-la-Teria, Lesotho	1		0.89
	Scott-Smith et al., (1984)	Koffiefontein, South Africa	2	0.86-0.87	0.87
	Kopylova et al., (1997)	River Ranch, Zimbabwe	1		0.85
			4	0.85-0.89	0.87
Australia	Scott-Smith et al., (1984)	Orroroo, Australia	2	0.86-0.87	0.87
total			183	0.36-0.94	0.74

8.4.1.2 MgSiO3

Table 8.44 is a compilation of sources for data on MgSiO3 diamond inclusions that are interpreted as having initially crystallized as MgSi-Prv. Other data may exist, but because grains can be confused for upper mantle Opx, they may have been overlooked (e.g. a grain from Mwadui, Tanzania, as discussed in Stachel et al., 2000b).

As previously introduced in section 8.1.4.1, there are usually three chemical differences between MgSiO3 grains that crystallized in the lower and upper mantle: Ni and Al contents, and mg.
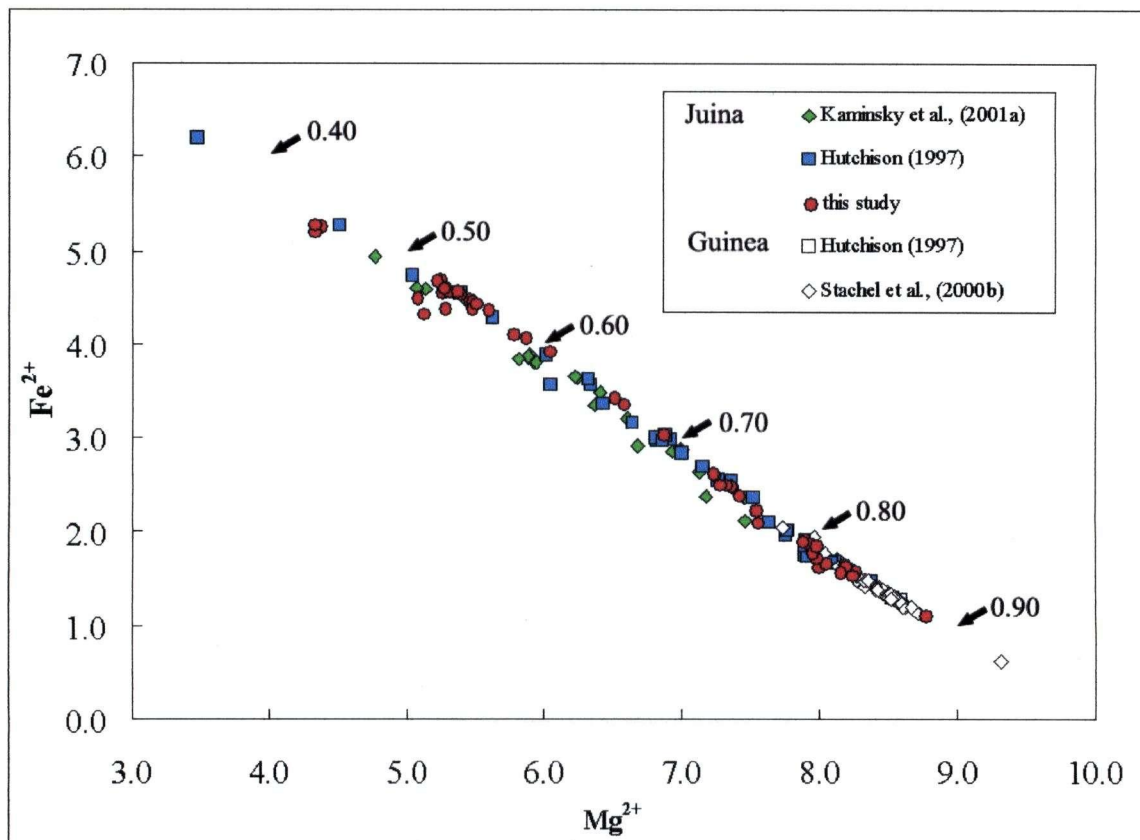
Fig. 8.36. Plot of Fe^{2+} versus Mg^{2+} for ferropericlase grains from Juina, Brazil and Guinea, West Africa. Cation totals are calculated on basis of ten oxygens. Fe calculated all as Fe^{2+} (cation totals were recalculated for all published data for consistency). Numbers 0.40 to 0.90 on the upper right side of the data indicate *mg*. Rare data from other locales not included (Table 8.43) plot between *mg* 0.80 and 0.89.

Table 8.44. Published data on $MgSiO_3$ grains with a probable deep origin (>660 km)

General region	Author	Locality	No. of grains	Range of *mg*	Average *mg*
Central South America	Hutchison (1997)	Sao Luiz, Brazil	10	0.86-0.94	0.90
	Kaminsky *et al.*, (2001a)	Juina, Brazil	1		0.87
	this study	Rio Soriso, Brazil	8	0.89-0.94	0.92
			19	0.86-0.94	0.91
Northern North America	Davies *et al.*, (1999)	DO-27, Canada	1		0.94
West Africa	Stachel *et al.*, (2000b)	Guinea	7	0.93-0.95	0.94
Southern Africa	Scott-Smith *et al.*, (1984)	Koffiefontein	1		0.95
total			28	0.86-0.95	0.92

Nickel content for all $MgSiO_3$ grains listed in Table 8.44 is less than 0.06 wt%. $MgSiO_3$ inclusions in diamonds from more shallow sources typically contain ~>0.1 wt% NiO (Meyer, 1987) and $MgSiO_3$ grains in mantle xenoliths contain 0.03-0.11 wt% NiO (Pearson *et al.*, in print).

Although the aluminium content in mantle xenolith $MgSiO_3$ grains may be relatively high (up to 6 wt%, Pearson et al., in print), typical $MgSiO_3$ diamond inclusions (of lithospheric origins at depths ~<250 km) contain little aluminium (<1.00 wt% Al_2O_3, Meyer, 1987). Al_2O_3 is generally >1.00 wt% for lower mantle MgSi-Prv's, with a few exceptions (two inclusions from Guinea (Stachel *et al.*, 2000b) and one each from South Africa (Scott-Smith *et al.*, 1984) and Australia (Scott-Smith *et al.*, 1984)). Hutchison (1997) found several grains of $MgSiO_3$ with significant Al_2O_3, which he termed type II (~10 wt% Al_2O_3) and type III (~10 wt% Al_2O_3 and ~5 wt% CaO and 6 wt% Na_2O). $MgSiO_3$ grains liberated from Juina area diamonds all have Al_2O_3 values above 1 wt%. Thirteen type I inclusions have been found in Juina (with Al_2O_3 wt% range of 1.23-3.37 and average of 2.19). The seven grains identified in Hutchison (1997) and classified as either type II or III contain an average of 10.46 wt% Al_2O_3 with a range of 8.34-12.58 wt% Al_2O_3. The sole grain found by Davies *et al.*, (1999) falls into the type I classification. Stachel *et al.*, (2000b) and Scott-Smith *et al.*, (1984) found seven grains in association with ferropericlase. These $MgSiO_3$ grains have a more restricted range (0.55-1.68 wt% Al_2O_3) and lower average (1.15 wt% Al_2O_3). The reason for the gap in Al_2O_3 wt% between type I and II $MgSiO_3$ grains is unclear.

The *mg* distribution is different from upper mantle Opx's only for Juina area inclusions (Fig. 8.37), although data from other locales is sparse. *Mg*'s for upper mantle diamond inclusion Opx's are generally restricted between 0.91-0.95 (with very few exceptions) and are skewed to the more Mg-rich end of the range. The Orapa mine in Botswana appears to be an exception in that diamond inclusion Opx's found there are more Fe-rich, ranging from 0.77 to 0.93 (Meyer, 1987). $MgSiO_3$ grains found from Junia tend to be more Fe-rich, although not nearly as extreme as those found in Orapa. Hutchison's (1997) type II and III $MgSiO_3$ grains average 0.89 *mg* and range from 0.87 to 0.91 *mg*.

The thirteen type I grains from Hutchison (1997), Kaminsky *et al.*, (2001a), and this study average 0.92 *mg* and range from 0.86 to 0.94 *mg*. The lone $MgSiO_3$ grains found in association with fPer by Davies *et al.* (1999) and Scott-Smith *et al.*, (1984) are more Mg-rich, at
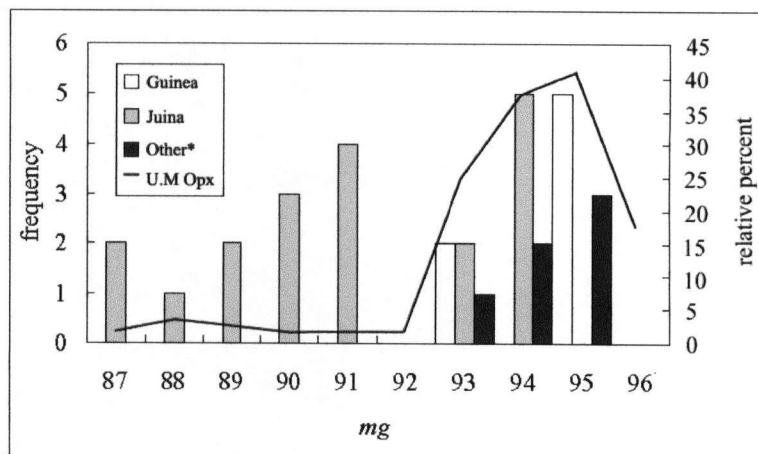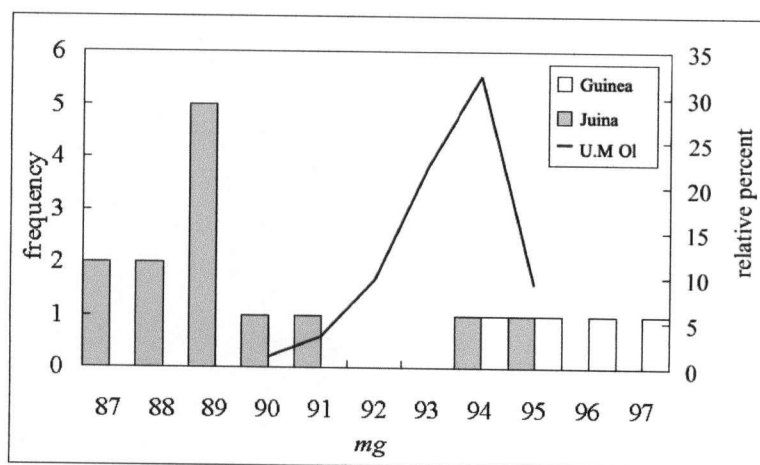

Fig. 8.37. Plot of *mg* vs. frequency for $MgSiO_3$ inclusions worldwide. U.M. Opx = upper mantle Opx from Meyer (1987) (plotted against relative percent, n=82). Juina, Guinea and Other* are plotted against frequency. Other* are $MgSiO_3$ data from locales other than Juina and Guinea listed in Table 8.44.

0.94 and 0.95 *mg* respectively. There are seven grains from Stachel *et al.*, (2000b), of which all but one occur in association with fPer. They have a more restricted range closer to the Mg-rich end-member, lying between 0.93 to 0.94 *mg* and averaging 0.94 *mg*. In terms of *mg*, there is considerable overlap between upper mantle Opx and possible lower mantle type I $MgSiO_3$ perovskite.

It appears that upper mantle $MgSiO_3$ grains can be distinguished from lower mantle $MgSiO_3$ grains based on chemistry alone, however, all criteria should be used in unison. Low Ni content appears to be the most unambiguous indicator of a lower mantle origin while *mg* has a considerable overlap between the two fields, and may not be such a useful indicator on its own. Provided diamonds are only stable in a depleted harzburgite source, then the aluminium content is also a useful indicator. However, if diamond can remain stable in a less depleted harzburgite or lherzolite, there is no reason why an aluminous $MgSiO_3$ (>1.00 wt% Al_2O_3) could not be included in diamond in the upper mantle.

Chemistry of the $MgSiO_3$ inclusions is consistent with grains of a lower mantle origin. They are similar in composition with all other lower mantle MgSiO3 grains, with the exception of the exceptionally aluminium-rich grains (types II and III) reported by Hutchison (1997).

8.4.1.3 CaSiO₃

Roughly 20 grains of $CaSiO_3$ have been reported as inclusions in diamond prior to this study from three localities: Juina, Brazil (Hutchison, 1997 and Kaminsky et al., 2001a), Kankan, Guinea (Stachel et al., 2000b) and Sloan, Colorado, USA (Otter and Gurney, 1989) (Table 8.45). All grains are essentially pure $CaSiO_3$ which makes any comparison between major oxide chemistry data difficult. Unlike $MgSiO_3$, there is no $CaSiO_3$ polymorph found in equilibrium with typical inferred mantle compositions at shallow levels and hence no need to weed out lower P-T polymorphs; they are all deep ($\sim$>580 km's depth).

Table 8.45. Published data on $CaSiO_3$ diamond inclusions

General region	Author	Locality	No. of grains
Central South America	Hutchison (1997)	Sao Luiz, Brazil	3
	Kaminsky et al., (2001a)	Juina, Brazil	6
	this study	Rio Soriso, Brazil	8
			17
Central North America	Otter and Gurney (1989)	Sloan, USA	1
West Africa	Stachel et al., (2000b)	Guinea	6*
total			24

* Stachel et al. (2000b) found some Ca-silicates that do not have $CaSiO_3$ stoichiometry. They interpreted these grains as retrograde phases of $CaSiO_3$.

8.4.1.4 'Olivine'

Because olivine is the major constituent of the upper mantle, it is one of the most common inclusions found in peridotitic upper mantle diamonds, as reported by Harris and Gurney (1979) and Meyer (1987). This is not the case, however, for diamonds which originate from a deeper source, such as those found in Juina and Guinea. Olivine inclusions are relatively rare in Juina and most of those which are reported from Guinea (Stachel et al., 2000b) are likely sourced from shallower depths ($\sim$<410 km) in the upper mantle. Table 8.46 is a compilation of all 'olivine' grains reported from Guinea and Juina that are interpreted as having a deep origin. For Guinea, where shallow upper

Table 8.46. Published data on olivine grains with a probable deep origin (>400 km)

General region	Author	Locality	No. of grains	Range of mg	Average mg
Central South America	Hutchison (1997)	Sao Luiz, Brazil	3	0.87-0.91	0.89
	Kaminsky *et al.*, (2001a)	Juina, Brazil	3	0.87-0.89	0.88
	this study	Rio Soriso, Brazil	7	0.88-0.95	0.91
			13	0.87-0.95	0.90
West Africa	Stachel *et al.*, (2000b)	Kankan, Guinea	4	0.94-0.97	0.95
total			17	0.87-0.97	0.91

mantle diamonds are also abundant, the only 'olivines' reported are those that occur in association with ferropericalse. Data from Juina, where there is no evidence for a large source of shallow contamination, contain all 'olivine' grains reported from Hutchison (1997), Kaminsky *et al.*, (2001a) and this study.

The separation of 'olivines' into α-Ol, β-Ol, γ-Ol and retrograde olivine from MgSi-Prv + fPer based on chemistry alone is difficult. Although Brey *et al.*, (2003) suggest that γ-Ol incorporates trivalent cations more easily than either α-Ol or β-Ol, there are no known published works on laboratory experiments corroborating this hypothesis. 'Olivine' inclusions in this study contain little or not trivalent cations (Ol inclusions in diamond 4-3 are the lone exception). The only striking difference between upper mantle Ol (α-Ol) and 'olivines' associated with fPer is the variation in mg (Fig . 8.38). 'Olivines' in association with fPer are either mg-rich (mg=0.94-0.97) or mg-poor (mg=0.87-0.91), whereas the mg

Fig. 8.38. Plot of mg vs. frequency for 'olivine' inclusions worldwide. U.M. Ol = upper mantle olivines from Meyer (1987) (plotted against relative percent on right, n=154) Guinea and Juina inclusions are plotted against frequency on left.

for upper mantle olivine inclusions is restricted between 0.90-0.95 (Meyer, 1987). The *mg* for olivines from off-craton xenoliths range from 0.88-0.92 and from 0.91-0.94 for on craton xenoliths (Pearson *et al.*, in print). The low *mg* for diamond inclusion 'olivines' in this study is consistent for a non-cratonic source, such as transition zone. There is no apparent explanation for the small population of 'high-*mg* olivines' in Juina, which is similar to the 'olivine' in association with fPer form Kankan.

At present, there is not enough experimental work demonstrating the partitioning behavior of Mg_2SiO_4 polymorphs. At the very least, the low-*mg* 'olivines' recovered indicates an off craton source. Although this says nothing about their depth of formation, it is consistent for a deep source, such as the transition zone.

8.4.1.5 Garnet and TAPP

Two different highly aluminous silicates were recovered from diamonds in this study, eclogitic garnet and TAPP. Because no majoritic garnets were found in this study, these deep inclusions (>250 km) will not be considered further in this section, however, it is

Table 8.47. Aluminous silicates and TAPP data from select localities with a deep origin

General region	Author	Locality	No. of TAPP grains	No. of majoitic garnet grains	No. of Eclogitic garnets	No. of Peridotitic garnets
Central South America	Hutchison (1997)	Sao Luiz, Brazil	9	6	0	1
	Wilding (1990)	Sao Luiz, Brazil	0*	14*	20*	0*
	Kaminsky *et al.*, (2001a)	Juina, Brazil	1	3	0	0
	this study	Rio Soriso, Brazil	1	0	2	0
			11	23	22	1
Northern North America	Davies *et al.*, (1999)	DO-27, Canada	0	1	11	1
West Africa	Stachel *et al.*, (2000a)	Kankan, Guinea	0	6	6	6
	Hutchison (1997)	Kankan, Guinea	0	1	-	-
				7	6	6
Southern Africa	Moore & Gurney (1985)	Monastery, S. A.	0	4	-	-
total			11	35	39	8

* = data is referenced through Hutchison (1997).

important to point out that numerous majoritic garnets have been recovered from the Juina area (Table 8.47).
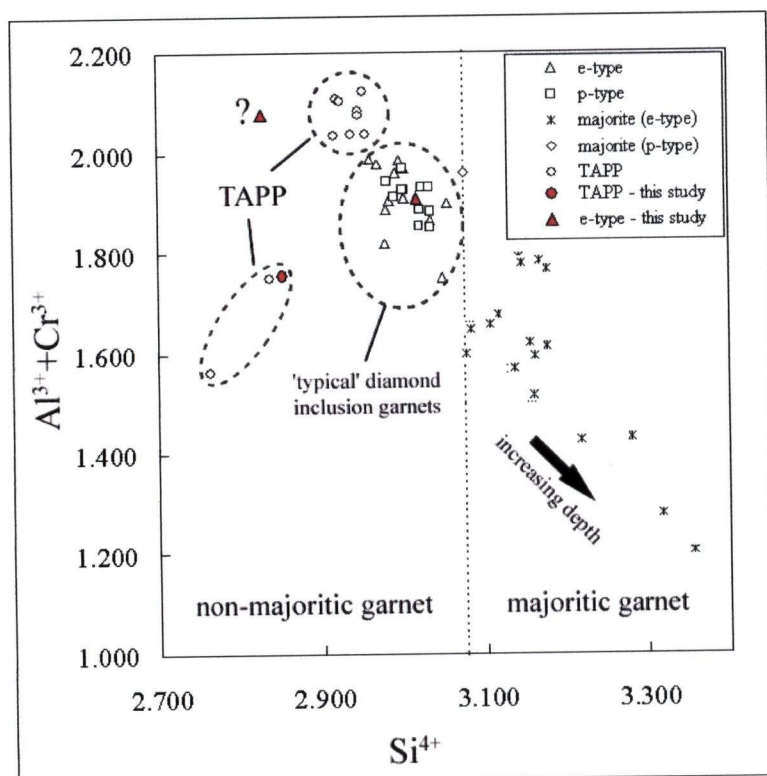
Fig. 8.39. Plot of $Al^{3+}+ Cr^{3+}$ versus Si^{4+} for aluminous silicates worldwide. Cations calculated on the basis of 12 oxygen anions. The line at 3.075 Si^{4+} is used to sepate majoritic from non-majoritic garnets (from Stachel *et al.*, 2000a). Data compiled from Stachel *et al.* (2000a), Stachel *et al.* (2000b), Mayer (1987), Hutchison (1997), Kaminsky *et al.*, (2001a) and Moore and Gurney (1985). Question mark (?) indicates anomalous value from this study which may be a result of poor quality data. Arrow indicating increasing depth only applies to majoritic garnets.

It appears that it may be possible to discriminate between TAPP and other aluminous silicate minerals based solely on chemical data, although criteria are based on a very limited number of TAPP inclusions and in the absence of supporting experimental work. The deficiency in silica and the low calcium content are the two characteristic features of TAPP. Fig. 8.39 is a plot that highlights the division between majoritic and non-majoritic garnets.

However, it may also prove useful in separating TAPP from other mantle garnets as TAPP grains contain less Si^{4+} per 12 oxygens than typical mantle garnets (both eclogitic and peridotitic). Based on empirical observation, a TAPP/garnet divide may be placed at ~2.95 Si^{4+} per 12 oxygens. Silica deficiency may be a reflection of elevated Fe^{3+} and Ti^{4+} contents, however, elevated amounts of titanium are only found in three TAPP grains (titanium is absent in the remaining eight), while Fe^{3+} has not been accurately determined for the complete database. TAPP grains also are markedly different from all other garnets (majoritic included) in that they contain no calcium (Fig. 8.40). Using these two

209

criteria, the current data seems to be relatively easy to separate into the three types: normal garnets, majoritic garnets and TAPP. The conventional discriminating factor used to distinguish peridotitic from eclogitic garnets using Cr_2O_3 wt% may not apply to TAPP grains. The compositional paragenesis of TAPP grains is unclear (Harris et al., 1997), although it has been found in

Fig. 8.40. CaO versus Cr_2O_3 (wt%) in garnets from Juina, Guinea, and around the world. The outline of the lherzolitic field is taken from Sobolev et al., (1973) and the cutoff at 2.00 wt% Cr_2O_3 for the eclogitic paragenesisis from Gurney (1984). Data compiled from Stachel et al. (2000a), Stachel et al. (2000b), Mayer (1987), Hutchison (1997), Kaminsky et al., (2001a) and Moore and Gurney (1985).

association with material that is equilibrium with a peridotitic bulk composition.

Grain 4-10A plots in the same field as 'normal garnets' (Fig. 8.39) and is likely sourced from no deeper than 250 km. Although inclusion 4-10B had the same orange colour and was recovered from the same diamond as 4.10A, its chemistry is markedly different. It plots in a field of its own (Fig. 8.39) and thus brings into question the reliability of the chemical data for this small (20-40μm) grain. The chemistry for eGrt (inclusion 4-10A) is typical for eclogitic garnets with an origin less than 8 GPa ($\sim$<250 km).

8.4.1.6 Perovskite

To the authors' knowledge, there have only been three published reports of perovskite occurring as an inclusion in diamond: one from Juina (Kaminsky et al., 2001a), another

from River Ranch, Zimbabwe (Kopylova *et al.*, 1997), and a third from Sloan, Colorado, USA (Meyer and McCallum, 1986). The grain reported by Kaminsky *et al.* (2001a) is found in association with ilmenite, majorite and an unidentified Si-Mg phase, thus indicating a deep origin (>~250 km). The grain reported by Meyer and McCallum (1986) occurs as a polyphase inclusion of perovskite, ilmenite and phlogopite and the grain reported by Kopylova *et al.* (1997) occurs in association with chromite. The four perovskites in this study occur as composite grains with $CaSiO_3$.

Perovskites reported are divided here into two groups, those containing REE and HFSE and those void in these elements. The grain reported by Kaminsky *et al.* (2001a) is the lone example of a diamond inclusion perovskite void in REE's and HFSE's. It has almost a stoichiometric composition with minor SiO_2 (1.05 wt%), Al_2O_3 (0.64 wt%), and Na_2O (0.22 wt%). The grains from River Ranch and this study contain appreciable amount of REE's and HFSE's (7.00 wt% and ~>4.00 wt% respectively), and while these elements were not analysed for in the grain reported from Colorado, the low values reported (93.3 wt%) suggest appreciable amounts are also present. In all cases where REE's were analysed, Ce contents are greater than La. There are some similarities between grains in this study and those reported in Kaminsky *et al.* (2001a), particularly in the abundance of silica (~2.00 wt% SiO_2) and aluminium (~1.30 wt% Al_2O_3), although these is no detectable sodium.

Perovskites inclusions found in diamond are traditionally considered secondary because perovskite is not considered stable in the deep upper mantle in the diamond stability field and perovskite is a common primary phase in kimberlite. Elevated content of Ce over La is a distinguishing feature of kimberlitic perovskites (Mitchell *et al.*, 1988). Because of the similarities in chemistry between diamond inclusion perovskites and kimberlitic perovskites, grains reported from Sloan and River Ranch were interpreted as secondary in origin.

Experiments have shown that $CaTiO_3$ (in isolation) is stable at high pressures and temperatures, and that complete solid-solution between $CaSiO_3$ perovskite is possible

211

(Koito et al., 2000), however, its stability in mafic and ultramafic rocks at high pressures and temperatures is poorly constrained. It is possible that in the absence of pyroxene (such as in the lower mantle), $CaTiO_3$ may be the main reservoir for titanium, REE's and HFSE's. The association of $CaTiO_3$ with $CaSiO_3$ in this study suggests a deep ($\sim$>580 km) origin, possibly in the lower mantle. High Si and Al may be indicators of deep (lower mantle) perovskites.

8.4.1.7 SiO_2

SiO_2 is a relatively common inclusion in diamond (Table 8.48). Although this table is not a comprehensive list of all localities where SiO_2 has been recovered, it does illustrate that SiO_2 has been found in most localities where fPer has also been reported. There are three instances where it has been reported in association with fPer (two from Juina and

Table 8.48. SiO_2 data from select localities worldwide

General region	Author	Locality	No. of grains	phases in association
Central South America	Hutchison (1997)	Sao Luiz, Brazil	5	(1) moissanite?, (1) fPer, biotite and plagioclase
	Kaminsky et al., (2001a)	Juina, Brazil	3	(1) fPer
	this study	Rio Soriso, Brazil	12	
Northern South America	Sobolev et al., (1998)	Guaniamo, Venezuela	27	(6) eGrt, (8) Cpx, (3) eGrt and Cpx, (1) eGrt and sanadine, (1) Cpx and rutile, (1) Cpx and Mag, (1) rutile and ilmenite, (1) eGrt, Cpx and Ti-Mag, (1) eGrt, rutile and Mag
West Africa	Stachel et al., (2000b)	Kankan, Guinea	2	(1) fPer
Eastern Africa	Stachel et al., (1998)	Mwadui, Tanzania	1	Harzburgitic garnet
Southern Africa	Kopylova et al., (1997)	River Ranch, Zimbabwe	1	(Mg,Fe)SiO4-pGrt (not majoritic)
	Gurney et al., (1984)	Orapa, Botswana	?	
	McKenna (2001)	Helam, S.A.	12	eGrt, (2) corundum
Russia	Sobolev (1984)	Siberia platform	?	Mag, metallic Fe, eGrt, Cpx and rutile
	Sobolev et al., (1976)	Siberia platform		eGrt and omphacite
Australia	Sobolev et al., (1984)	Southeastern Aus.	?	
	Hall and Smith (1984)	lamproite in W. Aus.	?	
	Jaques et al., (1989)	Argyle		
	Meyer et al., (1997)	New South Wales	12	

one from Kankan). There are several reports of SiO_2 and magnetite in association (e.g. Siberian platform, Sobolev, 1984; and Guaniamo, Sobolev et al., 1998). The uncertainty in the primary origin of SiO_2 grains has already been discussed (section 8.3.2.1). However, there are two grains which are reasonable candidates for a primary origin, occurring in diamond 2-7 (SiO_2 and fPer) and diamond 2-11 (SiO_2 and eclogitic pyrrhotite).

SiO_2 and fPer are not in equilibrium in a peridotitic mantle of mg=0.89, however, they are stable in a more iron-rich peridotite, where mg<~0.78, depending on the specific P-T conditions (Ito and Takahashi, 1989). The mg's for fPer grains in association with SiO_2 are 0.69 (Hutchison, 1997), 0.78 (Kaminsky et al., 2001a), 0.86 (Stachel et al., 2000b) and 0.81 (this study).

8.4.1.8 Pyrrhotite, magnetite and native iron

Pyrrhotite, magnetite and native iron were also recovered from diamonds in this study. The chemical subtleties for these inclusions are unremarkable in comparison to grains recovered from other locations.

In the case of pyrrhotite, there are abundant data from localities all over the world and the four grains reported in this study are similar to all pyrrhotites of eclogitic paragenesis. Six grains have been previously reported from Juina, one of which was in association with a majoritic eGrt (Hutchison, 1997). Other locations where both pyrrhotite and fPer have been reported (but not in the same diamond) include DO-27, NWT (Davies et al., 1999) and Guaniamo (Kaminsky et al., 2000). No grains have yet been reported from Kankan, Guinea.

Magnetite ($Fe^{2+}Fe^{3+}_2O_4$) is a rare inclusion in diamond. It has previously been observed in diamonds from Juina (Hutchison, 1997), Guaniamo, Venezuela (Sobolev at al., 1998), Sloan, USA (Meyer and McCallum, 1986) and several localities on the Siberan plateau (Sobolev et al., 1981). It has been found in association with SiO_2, among other

inclusions, in Guaniamo (Sobolev *et al.*, 1998) and the Siberian platform (Sobolev, 1984). It is mostly found in association with inclusions of eclogitic paragenesis. Magnetite has never been found in cratonic peridotite, but can occur in cratonic eclogite (Pearson *et al.*, in print).

To the author's knowledge, there are only a few published occurrences of native iron as an inclusion in diamond. One has been recovered from Sloan (Meyer and McCallum, 1986) and two from Siberia (Sobolev *et al.*, 1981). Native iron from Siberia was found in association with pGrt, chromite and sulphides. The inclusion in this study was found in association with pyrrhotite (eclogitic) and SiO_2, which is in contrast to the peridotitic association found for Siberian diamonds containing native iron.

8.4.1.9 Fe-Ni blebs and magnesioferrite spots on ferropericlase

Hutchison (1997) distinguishes between two types of *blebs* found on several fPer grains. Transmission electron microscopy (TEM) of one type of bleb finds they are comprised of magnesioferrite $(Mg^{2+}Fe^{3+})_2O_4$, while EDS of the other type of bleb finds that they are Fe-Ni alloy. Both types of features were observed in this study. Fe-Ni blebs were best developed on fPer grains from diamonds 3-5 and 3-10 (section 8.3.5.1) and magnesioferrite was observed only on fPer grains from diamond 3-6 (section 8.3.5.2).

Characterisation and interpretation of these features was more difficult in previous studies because of the differences between the procedures followed. In previous studies, inclusions were mounted in epoxy and polished before examination, whereas in this study, inclusions were mounted on stubs and not polished. SEM images of both types of features on fPer show that they develop on the grain surface and are not pervasive with depth. Any polishing of fPer inclusions would result in the reduction of bleb size available for examination.

The observation that magnesioferrite spots are restricted to particular domains on ferropericlase inclusions was interpreted as an indication that these features are secondary. As, such , they are of less interest than the Fe-Ni blebs.

In contrast, the Fe-Ni blebs are found covering the complete surface of the ferropericlase inclusions. The regularity to their formation suggests that they are likely a product of exsolution. The *mg's* for fPer grains with blebs in this study are low, but not unique (*mg*=0.65 for fPers from diamonds 3-5, and *mg*=0.45-0.55 for fPers from diamond 3-10). Several grains released from other diamonds have similar *mg's* without Fe-Ni blebs. Hutchison (1997) proposed a possible link between blebs and the core-mantle-boundary (CMB). At present, little can be concluded regarding these peculiar blebs. Experiments on the ability of fPer grains (of varying *mg*) to incorporate varying amounts of nickel at P-T conditions up to the CMB are likely required to better understand this phenomena.

8.4.2 Inclusion paragenesis

The separation of diamonds into subgroups based on the predicted composition of the parental material is common practice in any diamond study (e.g. Davies *et al.*, 1999; Stachel *et al.*, 2000a and b). The stability of relevant minerals has been introduced in section 8.1. Using the results from section 8.3, this discussion will divide the inclusion-bearing diamonds into subgroups based on paragenetic associations. Subgroups will include diamonds of similar parental material, as well as diamonds of similar origin of depth.

A number of problems and uncertainties were encountered when trying to subdivide the diamond suite into paragenetic groups. 1) As highlighted throughout section 8.3, it is difficult to unambiguously classify an inclusion as primary. Chemical homogeneity (except in the case of sulphides) and euhedral form were considered the most convincing evidence for a primary origin. 2) It is also important to bear in mind that material from a variety of regions has the potential of being included in diamond, from depths where diamond began crystallization to depths where the diamond was (presumably) entrained

in a magmatic eruption. Disequilibrium between phases is certainly a possibility. 3) As inclusions are accidental material in diamond, it is unlikely that all phases from one source rock will be represented in one diamond. 4) The variation in phase stability between different inclusions, along with variations in partitioning, make it easier to place some phases in P-T space (e.g. majoritic garnet and TAPP) while others are difficult to place (e.g. olivine). When combined with the scenario highlighted in point 3, this becomes a more serious problem. For example, in this study, the association Ol-fPer-$MgSiO_3$ is considered to have formed at the lower mantle/upper mantle boundary. However, when only Ol is found, it is difficult to determine if it has a similar paragenesis (i.e. lower mantle/upper mantle), or whether it truly represents its own subgroup.

In order to avoid any assumptions, diamonds will only be placed in a paragenetic group that the chemistry of the extracted inclusions permit. For example, diamonds containing fPer-$CaSiO_3$ are considered as belonging to lower mantle paragenesis, however, $CaSiO_3$ in the absence of fPer (and $MgSiO_3$ and TAPP) will be considered as having formed at depths $\sim$>580 km. In all likelihood, many diamonds containing $CaSiO_3$ in the absence of fPer have a lower mantle paragenesis, but such a classification requires more evidence.

8.4.2.1 Lower mantle

Although the ferropericlase stability field is not restricted to the lower mantle, it is generally used as an indicator of the lower mantle paragesesis. In general, the transformation of fPer in an open system (i.e. in the presence of silicates) is considered to take place at the 660 km discontinuity (Akaogi *et al.*, 1998). Many argue that this seismic discontinuity is a result of the breakdown of γ-Ol to fPer and MgSi-Prv.

Twelve diamonds, or 27% of the diamonds cracked, contain fPer in the absence of Ol and are thus grouped in the lower mantle paragenesis (the importance of this will become clear in section 8.4.1.2). Of these 12 diamonds, the number of grains in the particular association, along with the average *mg* for fPer grains in that association are: fPer as the only phase (found in 7 diamonds, with average *mg*=69), fPer + $CaSiO_3$ (3 diamonds,

average mg=68), fPer + SiO_2 (1 diamond, average mg=81), and fPer + eGrt? (1 diamond, no EPMA data for fPer grain). There is a wide spread in mg for fPer grains in this paragenetic group (0.45-0.83).

In terms of bulk composition of the mantle, the inclusion associations are mostly in equilibrium with a peridotitic or pyrolitic lower mantle. $CaSiO_3$ is found in association with fPer in three diamonds, which is consistent for a mantle of pyrolitic composition at lower-mantle P-T conditions. Phase associations in two diamonds (2-7 and 4-16) are either not in equilibrium, or have different protoliths. Diamond 2-7 also contains an inclusion of SiO_2 (Fig 8.21, 2.7K), which if indeed primary and syngenetic, would suggest the source region was iron-rich peridotite (Ito and Takahashi, 1989). Diamond 4-16 contains two euhedral grains that leave little doubt in their primary origin, however, both grains are too small for EPMA analysis (<10 μm). The garnet is unlikely to be TAPP as it contains too much calcium (see section 8.3.1.5), and as it is found with fPer, it should either have a large majoritic component, or not be in equilibrium with fPer. The similarities in EDS spectra between the aluminous silicate in diamond 4-16 and a non-majoritic garnet (confirmed by EPMA) is a first approximation that the garnet does not have a majoritic component, and is thus sourced from depths <250 km.

8.4.2.2 Lower mantle/upper mantle

Many authors have demonstrated experimentally that olivine is not stable in the lower mantle (e.g. Ito and Takahashi, 1998; Yamazaki *et al.*, 1994). Therefore, its presence in association with fPer has implications on the origin of the diamond. Four different scenarios where diamond could include fPer and Ol are considered here:

1. fPer formed at depths <660 km where silica activity was low enough for it to form in the presence of γ-Ol.
2. Ol is a retrograde phase of MgSi-Prv plus fPer.
3. fPer and Ol were not trapped at the same time and are thus not in equilibrium.

4. Inclusions were trapped at the lower mantle/upper mantle (LM/UM) boundary at the predicted conditions where fPer, Ol and MgSi-Prv are in equilibrium.

There are four grains containing fPer and Ol (diamonds 1-5, 3-2, 3-5 and 4-3), or 9% of diamonds cracked. All four grains also contain $MgSiO_3$, one of which also contains TAPP while another contains both TAPP (based only on EDS analysis) and $CaSiO_3$. The $MgSiO_3$ inclusions contain elevated amount of Al_2O_3, consistent with that of grains which initially crystallized with the perovskite structure and formed in the upper ~10-20 km of the lower mantle (Stachel *et al.*, 2000b), thus excluding scenario #1 for all diamonds (provided that the fPer and $MgSiO_3$ inclusions are in equilibrium). Further corroborating an origin of depth below 660 km is the presence of TAPP, which has been interpreted as being sourced from the uppermost part of the lower mantle (Harris *et al.*, 1997; Gasparik *et al.*, 2000). The similarity in chemistry of the touching (4-3K2) and the non-touching (4-3C) Ol inclusions excludes the possibility of a retrograde origin from touching fPer and MgSi-Prv inclusions for diamond 4-3. In any case, scenario #2 is unlikely for olivine inclusions that are not in direct contact with other phases because it requires diamond to trap the perfect proportion of fPer and MgSi-Prv to make Ol, without any leftover components. A strong case for a retrograde origin for Ol grains in diamonds 1-5 (inclusions J2 and J4) and 3-5 (inclusion G2) could be made. In the absence of convincing experimental data demonstrating the chemical differences between α-Ol, β-Ol and γ-Ol, scenario #3 is difficult to corroborate or refute. The variation in *mg* for Ol in this study does suggest there are some differences in parental material for diamond 4-3. It is difficult to exclude the first three scenarios for all four diamonds, however, scenario four is the most probable origin for the associations found in diamonds 3-2 and 4-3. Olivine inclusions in diamonds 1-5 and 3-5 may be retrograde phases and the diamonds may have origins deeper than ~660 km.

The associations in these diamonds provide a rare opportunity to examine the partitioning of elements between various phases. The variation in *mg* for fPer, Ol, $MgSiO_3$ and TAPP grain(s) is recorded in Table 8.49 and depicted graphically in Fig. 8.41. Diamond 3-2 is the only sample where Ol, fPer and $MgSiO_3$ fall along a straight line (Fig 8.41); the

Table 8.49. *Mg* for olivine-ferroperliclase-MgSiO₃ associations (this study)

Diamond	fPer		Ol		MgSiO₃		TAPP	
	range	ave	range	ave	range	ave	ave	range
1.5	0.74-0.76(4)	0.75	0.89(1)	0.89	0.91(2)	0.91	0.87(1)	0.87
3.2	0.83-0.84(4)	0.84	0.88-0.89(2)	0.89	0.93-0.94(2)	0.94	-	-
3.5	0.57-0.65(4)	0.60	0.89(1)	0.89	0.89-0.91(2)	0.90	-	-
4.3	0.82-0.84(5)	0.83	0.94-0.95(2)	0.95	0.94(2)	0.94	-	-

Mg calculated as $Mg^{2+}/(Mg^{2+}+Fe^{2+})$ where all Fe was calculated as Fe^{2+}. Numbers in brackets represent the numbers of inclusions.

remaining three diamonds contain Ol with *mg* that is shifted to elevated magnesium contents. This suggests that the parental material is likely not the same for the four grains. Experimental work on olivine (*mg*=0.90) at high P-T conditions find that the MgSiO₃ (*mg*=0.93±0.006) is in equilibrium with fPer (*mg*=0.82±0.009) at predicted P-T conditions at the upper mantle-lower mantle boundary (~660 km) and MgSiO₃ (*mg*=0.919±0.004) is in

Fig. 8.41. Plot of Mg^{2+} versus Fe^{2+} versus Si^{4+} for MgSiO₃, Ol and fPer grains in association in this study.

equilibrium with fPer (*mg*=0.84.9±0.008) at predicted P-T conditions at the upper core-mantle boundary (~2650 km) (Fig 8.42A, Kesson *et al.*, 2002). These results are plotted with data from this study in Fig. 8.42B. The fPer grains in diamonds 3-2 and 4-3 contain magnesium contents that are predicted for a mantle of *mg*=0.90, however, the olivine data from diamond 4-3 is curious. The fPer inclusions in diamonds 1-5 and 3-5 contain low magnesium contents, suggesting the parental material also contains considerably less magnesium. FPer grains from diamond 3-5 were also anomalous in that they contain small blebs of Fe-Ni alloy on their surfaces (section 8.3.4).

219

Fig. 8.42. Plot of Mg^{2+} versus Fe^{2+} versus Si^{4+} for $MgSiO_3$ and fPer grains from experimental studies and associations in this study. A) Experimental data on olivine (mg=0.90) at predicted P-T conditions at the upper mantle-lower mantle boundary (~660 km) and the core-mantle boundary (~2650 km) (Kesson $et\ al.$, 2002). B) Comparison between four diamonds from this study with fPer and $MgSiO_3$ in association with results from experimental data.

8.4.2.3 Deep transition zone/lower mantle (>~580 km)

Although $CaSiO_3$ is considered the dominant calcium host in the lower mantle, it is likely the second most dominant calcium-bearing phase in the deeper reaches of the transition zone where it begins to exsolve from garnet. As such, the presence of $CaSiO_3$ as a mineral inclusion, in the absence of fPer, TAPP or aluminous $MgSiO_3$, cannot be considered an indicator of the lower mantle paragenetic association without neglecting the possibility of a deep transition zone origin. As well, unlike fPer, $CaSiO_3$ is stable in both eclogitic and peridotitic rocks. For these reasons, $CaSiO_3$ in the absence of the three minerals discussed, will not be considered as an indicator of a lower mantle paragenesis; it will be considered an indicator of the deep transition zone/lower mantle (DTZ/LM), or depths >~580 km.

There are seven grains (16% of cracked stones) that belong to this paragenesis (diamonds 2-8, 3-4, 3-7, 4-7, 6-6, 7-1, 4-10). EPMA data exists for four $CaSiO_3$ grains from four diamonds and for three $CaSiO_3$ grains from two diamonds that also contain fPer. There does not appear to be any chemical distinction between $CaSiO_3$ grains whether or not

they are in association with fPer. However, the purity of all $CaSiO_3$ grains makes any such comparison difficult.

$CaSiO_3$ grains from two diamonds are in contact with $CaTiO_3$ (diamonds 2-8 and 3-7) and another is in association with non-majoritic eclogitic garnet (diamond 4-10). The composition of the parental material which crystallised $CaTiO_3$ is unclear. The non-majoritic garnet in association with $CaSiO_3$ cannot be in equilibrium. As such, this diamond either belongs to two different paragenetic associations, or one or both phases are secondary.

The parental material for most diamonds in this paragenetic group could be sourced from either eclogitic or peridotitic rocks. Diamond 4-10 has an eclogitic inclusion, but it cannot be in equilibrium with $CaSiO_3$.

8.4.2.4 Peridotitic

Diamonds 4-18 and 6-8 both contain olivine in the absence of fPer (comprising 5% of the diamonds cracked). Unfortunately, the EPMA data for the olivine inclusion in 6-8 are poor (wt% value of 96.07) and there are no chemical data for the accompanying $MgSiO_3$ (identified by EDS analysis) nor are there chemical data for the olivine grain (identified by both Raman and EDS analysis) extracted from diamond 4-18 (grain was lost during polishing). The *mg* for the olivine inclusion 6.8A is 0.90, which falls slightly below the typical range for 'lithospheric' olivines (0.91-0.95, Meyer, 1987). To suggest that these inclusions belong to a different paragenesis than the olivines found in association with ferropericlase based solely on the inability to find fPer in the diamond is tenuous: it is certainly possible to not include fPer even if these diamonds did originate at the UM/LM boundary, as well, it is possible that fPer was included but not found. The chemistry is poor or non-existent and therefore assigning these inclusions to the lower mantle paragenesis can not be justified. The depth of formation of these diamonds is unclear, however, the composition of the parental rocks certainly was peridotitic.

8.4.2.5 Eclogitic

Six diamonds have been classified as belonging to the eclogitic paragenesis: diamond 2-11, 4-10, 4-11, 2-6, 1-4 and 2-10. Diamonds in this paragenesis are recognised by the presence of low-Ni sulphides, Ca-rich garnets or magnetite.

Diamond 4-10 contains two garnet grains with abundant calcium and no chromium, as well as a small inclusion of $CaSiO_3$ (previously discussed in section 8.4.1.3). The garnets plot in the eclogitic field delineated by Gurney (1984) and are considered pyrope-grossular-almandine in composition. They do not have a majoritic component and thus likely formed at depths shallower than ~250 km. $CaSiO_3$ and non-majoritic garnet is a 'forbidden' assemblage in both pyrolite and eclogite. The chemistry of the $CaSiO_3$ grain (Fig. 8.13 and Table 8.17) is markedly different from the seven other grains with chemical data; it contains more FeO (1.14 wt%, average of 7 other grains is 0.13 wt%), MgO (0.35 wt%, average of 7 other grains is 0.04 wt%) and Na_2O (0.48 wt%, average of 7 other grains is 0.05 wt%) than the other grains studied. There appears to be something unique about the $CaSiO_3$ grain found in this diamond. This diamond may have began crystallization at depths >580 km where the $CaSiO_3$ grain was included, and later, after the diamond had been exhumed to shallower levels (<250 km), included eGrt. This diamond belongs to two paragenetic associations, one deep (>580 km) of either eclogitic or peridotitic material, and one that is relatively shallow from eclogite source material.

Diamond 2-11 contains abundant SiO_2 (7 grains) and sulphides (9 grains), as well as an inclusion of native iron. Out of all the SiO_2 grains observed in diamonds from Rio Soriso, the only SiO_2 grain with crystal faces (Fig. 8.20, 2.11-C) was found in diamond 2-11. SiO_2 is also found in several fractures which places some doubt on the primary origin of inclusions recovered (certainly in the case of SiO_2). The wt% of NiO in the three sulphide grains analysed ranges from 2.68 to 14.34. Two of the sulphides would be considered to be in equilibrium with eclogite (Gurney, 1989; Bulanova *et al.*, 1996) while the third is in equilibrium with pyroxenitic source material (Bulanova *et al.*, 1996). This diamond will be classified as eclogitic based on the abundance of SiO_2 and the low NiO

wt% values of two out of three sulphide inclusions, but it is recognized that the there is secondary material present in the diamond which could have overprinted an eclogitic paragenesis. The depth of origin of this grain is unclear.

Three diamonds were found to contain euhedral crystals of magnetite. Chemical data are only available for grains from two of the diamonds (2-6 and 1-4) and it is possible that the grains originally identified as magnetite by EDS in diamond 2-10 are some other Fe-O phase or are secondary in origin. Diamond 1-4 also contains an inclusion of SiO_2 (Fig. 8.20 in section 8.3.2.1). The primary nature of this SiO_2 inclusion is certainly questionable, although primary silica is common in eclogitic rocks. Magnetite is stable in cratonic eclogite and has not been reported from any cratonic peridodite (Pearson et al., in print). However, the stability of this inclusion at higher P-T conclusions is unclear. As there are no other inclusions in association with magnetite, the depth of formation is unknown.

8.4.2.6 Paragenesis summary

Although the sample size is small (44 diamonds cracked, 30 diamonds containing identifiable inclusions) comments about the number of different source regions where diamonds grew as well as the frequency of sampling of these different sources are warranted. Three distinct associations are recognized (LM/UM, lower mantle and eclogitic) as well as two associations which may represent their own distinct groups, or may appear unique only on account of other phases not being included in diamond (>580 km and peridotitic). The relative proportions of each subgroup are presented in Fig. 8.43.
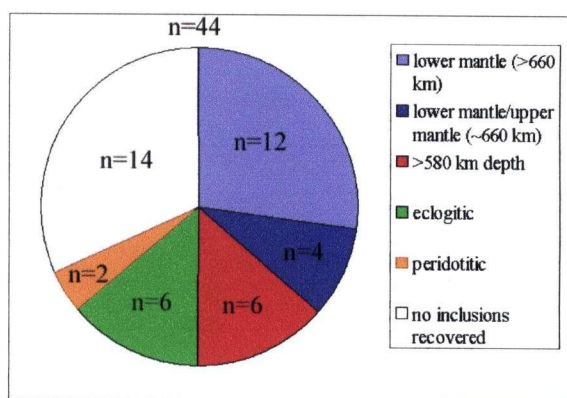
Fig. 8.43. Distribution of diamond paragenetic groupings based on mineral inclusion data. Diamond 4-10 is in equilibrium with two groups (>580 km and eclogitic) but has been grouped with the eclogitic paragenesis.

9.0 Discussion

9.1 Correlations between diamond body colour, FL, CL and IR

One goal of this thesis was to identify correlations between diamond body colour, fluorescence, cathodoluminescence and its infrared absorption, with a particular emphasis on understanding the effects that impurities (revealed through IR analysis) have on diamond body colour, FL and CL.

Fluorescence colours for most diamonds worldwide are various shades of blue and are generally interpreted as being a result of nitrogen impurities. The defects responsible for other FL colours, however, are poorly understood, or are a result of several combined defects. In this study, where diamond body colours are compared with FL colours, it becomes apparent that most of the FL colours other than blue are found in diamonds that are coloured (with the exception of grey diamonds) (Fig. 9.1). This is strong evidence for a correlation between diamond body colour and diamond FL colour. Therefore, centres that are responsible for variations in diamond body colour also have a strong control on diamond FL. Fig. 9.1 also highlights the similarities in FL colour distribution between grey and colourless diamond. These similar distribution patterns are evidence for the interpretation that grey
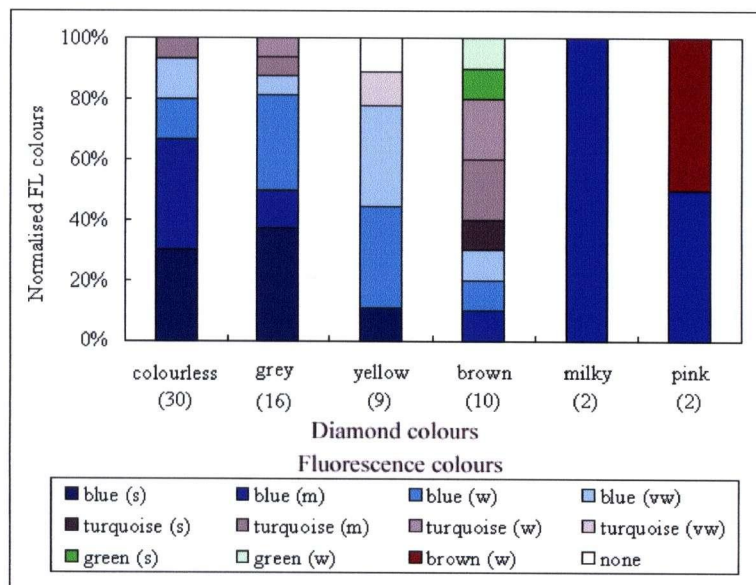
Fig. 9.1. Comparison of FL colour distribution by diamond body colour. Number in brackets below each diamond body colour represents sample size.

diamond is not a true body colour, but results from incorporation of numerous dark inclusions (section 3.3.1).

Although both cathode-induced and ultraviolet-induced luminescence are caused by crystal defects and impurities, their resultant colours and patterns may be quite different (Fig. 9.2). Most diamonds exhibit CL and FL colours of various shades of blue, but there are some marked differences which are likely a combination of both the volume of diamond and the optical centre that is activated by each technique. As illustrated in Fig. 9.1, diamond FL is strongly controlled by the same defect centres
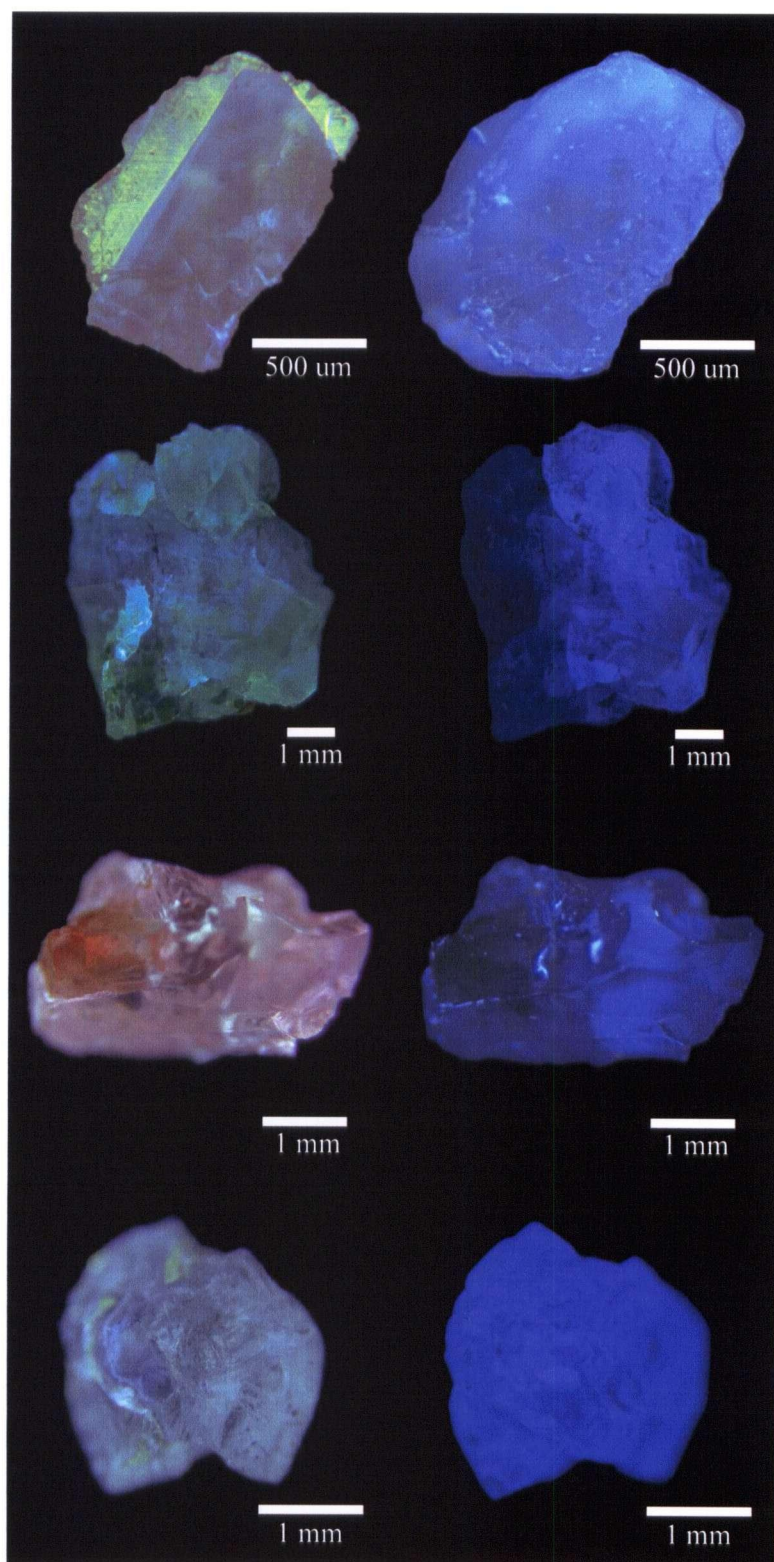
Fig. 9.2. Photos comparing diamond CL (on left) and diamond FL (on right). From top to bottom, 4-17, 2-11, 4-21, and 4-3.

225

responsible for diamond body colour, and as such, is a bulk crystal property. CL, however, only activates a small volume of diamond (provided certain precautions are taken, such as those outlined in sections 5.2 and 7.2), and thus any resultant colours reflect only local defects. Whereas diamond FL generally appears homogeneous, diamond CL can be extremely heterogeneous (e.g. images of internal structures in diamonds in section 7.3).

Comparisons between nitrogen character and diamond FL, and CL reveal several correlations. Firstly, the intensity of diamond FL and CL generally reflects the nitrogen concentration; diamonds with high total nitrogen concentrations tend to have brighter FL (Fig 9.3) and CL (e.g. Figs. 7.12 and 7.15). This correlation is particularly true for CL colour intensity, but not so strong for FL intensity. There does not appear to be any correlation between nitrogen
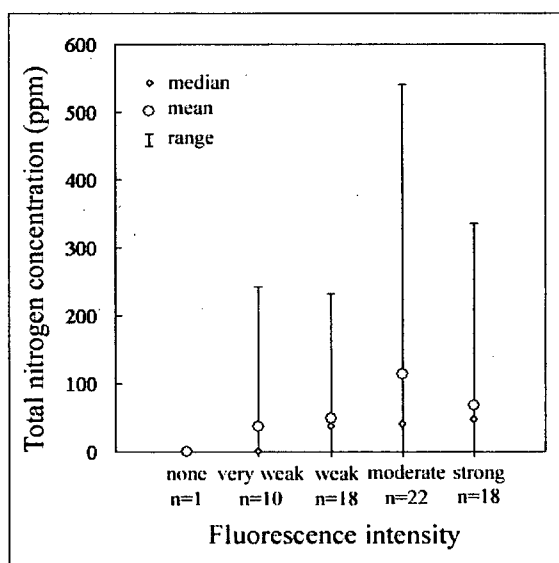
Fig. 9.3. Plot of nitrogen concentration versus fluorescence intensity.

aggregation state and FL intensity or colour. There may be a correlation between CL colour and aggregation state in some instances, but there are not enough transitional (type IaAB) diamonds to test this hypothesis. Diamond 4-17 has a rim with yellow-green CL (type IaAB), which becomes more aggregated towards the core, but also decreases in nitrogen concentration to below detection. Not all type IaAB diamonds have yellow-green CL, and not all yellow-green CL colours should be considered type IaAB diamond. Yellow-green CL colours observed in some diamonds (i.e. diamond 2-11, section 7.3.8) are interpreted as being a result of plastic deformation. Because plastic deformation

226

cannot focus slip on only the diamond rim, this mechanism of formation was ruled out for diamond 4-17.

The three main causes of body colouration in diamond (impurity defects, dislocations and irradiation) have been discussed in section 3.1.1. The defect centres revealed through IR spectroscopy should reflect diamond colouration, however, few correlations were observed. Yellow colouration in diamond is usually found in type Ib diamond or in diamonds with N3 centres. No diamonds in this study contain nitrogen in a disaggregated form (type Ib) and N3 centres are not IR-active and thus could not be detected. It is possible that the yellow stones contain N3 centres. Brown and pink colouration is a result of plastic deformation, which does not produce IR-active defects. The two milky diamonds contain high concentrations of both nitrogen (all as B centres) and hydrogen. With the exception of milky diamonds, bulk diamond body colour reveals nothing about the nitrogen character. The internal morphology of several diamonds examined in chapter 7.0 reveals that some crystal cores may be recognised, without the aid of CL or FL, by either a local brownish body colour (i.e. diamond 1-4) or by a local cloudy aggregate (i.e. diamond 2-1). These recognisable cores contain the highest nitrogen concentrations.

9.2 Diamond subpopulations

Diamond paragenesis has been discussed based solely on inclusion chemistry in detail in section 8.4.1. In this section, diamond paragenesis will be discussed using an integrated approach by including all methods of diamond *fingerprinting* described in Chapters 2 through 7.

9.2.1 Upper mantle diamonds

The term 'upper mantle' diamonds, as used here, applies to the typical assemblage of mineral inclusions for both peridotitic and eclogitic sourced diamonds, as described by Meyer (1987) and Gurney (1989). Diamonds are assigned to this subgroup based mainly on two upper-mantle 'indicators': 1) diamond type (either IaA or IaAB) and 2) mineral inclusion chemistry and associations.

Six diamonds in this study still contain nitrogen in the form of A centres and are considered either type IaA or IaAB. Most diamonds in Juina contain relatively low nitrogen concentrations, with all nitrogen in the form of B centres. No diamond assigned to the lower mantle paragenesis (in this study or in any other) has ever been found to contain A centres. This observation has been cited as evidence that these diamonds have been exposed to high mantle residence temperatures and/or long mantle residence times. As well, diamonds from lithospheric sources with only B centres are relatively rare.

Certainly there is a high probability that these diamonds are old as most studies on the age of diamond find that they are >1 Ga (e.g. Pearson *et al.*, 1999), however, without further constraints, we cannot rule out the possibility that type IaA and IaAB diamonds are young and that although they were subjected to high mantle residence temperatures, they were not subject to long residency periods, thus preserving A centres. Fig. 6.22 demonstrates the short duration of time required to achieve 95% B centres with total nitrogen concentrations less than 100 ppm. The short duration of time to achieve 95% aggregation (1.1 Ma) for temperatures predicted at ~410 km makes a deep but young origin highly improbable. As well, there are no known processes that slow down aggregation, only those that enhance the rate of aggregation, such as plastic deformation, which would result in shifting the curve in Fig. 6.22 to the left.

Constraints on the age and equilibrium temperatures of peridotitic and eclogitic xenoliths recovered from kimbelites in Juina could explain the aggregation states observed in four of the type IaA and IaAB diamonds. The xenoliths, dated at 1166-1884 Ma (Costa *et al.*, 2003), are brought by 95 Ma kimberlites (Heaman *et al.*, 1998), thus indicating a mantle residence time of ~1100 to 1800 Ma. Five different types of xenoliths recovered are plotted in time-temperature space, along with the aggregation pathways for diamonds containing 10 and 100 ppm total

Fig. 9.4. Plot of mantle residence time versus mantle residence temperature for xenoliths and diamond nitrogen character. Xenoliths are recovered from kimberlites in Juina (Costa *et al.*, 2003) and nitrogen character curves are calculated using equation 6.7. Note that the time scale is logarithmic.

nitrogen with 5 and 95% B centres. In 1.1 Ga, 95% of A centres will be converted to B centres at a temperature of ~1325 °C (Fig. 9.4). In other words, diamonds with 10-100 ppm total nitrogen exposed to temperatures greater than ~1325 °C would have >95% B centres. Assuming these diamonds have similar ages (or greater) than the xenoliths recovered, they likely have origins in the upper mantle, possibly in the cratonic lithosphere.

9.2.1.1 Upper mantle peridotitic diamonds

This subpopulation includes diamonds that have crystallised in a peridotitic source in the upper mantle.

Two diamonds were classified into this subgroup based on mineral inclusions as they contained Ol in the absence of fPer (diamonds 4-18 and 6-8). EPMA chemical data is

only available for the Ol inclusion in diamond 6-8 and is dissimilar to both UM/LM Ol's and shallow olivines (α-Ol) (Meyer, 1987; Gurney, 1989). In this case, however, comparisons based on chemistry are subject to errors as the analysis is poor. Diamond 6-8 contains the only sulphide with abundant nickel (inclusion 6.8A2, section 8.3.1.7), and is consistent for sulphides of peridotitic origin of lithosperic depths (although the sulphide is clearly secondary). These two diamonds have many shared characteristics and are different in several respects from the majority of the population. The most obvious difference is the bright green CL

Fig. 9.5. Photos of diamond body colour (left), FL (middle) and CL (right) for upper mantle diamonds of peridotitic paragenesis. From top to bottom, diamonds are: 4-17, 4-18 and 6-8.

colour, which has not been found on eclogitic or deep Rio Soriso diamonds (Fig. 9.5). Based on the green CL colour and low aggregation state (~75% B centres), a third diamond (4-17) is tentatively assigned to this paragenesis, although it contained no inclusions.

Comparison of morphology, FL, CL and body colour of the three diamonds reveals more similarities than differences. The diamonds are generally intact (relatively small amounts of diamond have been lost from brittle fracturing) and two grains show no signs of resorption while one shows strong resorption (class 2). One of the diamonds is an aggregate of many octahedral diamonds. Two diamonds exhibit strong blue FL and one exhibits moderate turquoise FL (4-18). All three stones exhibit moderate to strong yellow-green CL and clearly stand out among the whole population of diamonds. Diamonds 4-17 and 4-18 have the brightest green CL colours (diamonds in Fig. 5.3 in category 'Green 2') while diamond 6-8 is the next brightest green CL diamond in the suite. Two diamonds are colourless while one is classified as grey.

Two diamonds are type IaAB (53 and 75% B centres with ~50 total ppm nitrogen) while one diamond (4-18) contains 144 ppm total N all as B centres. Assuming these diamonds have similar ages to the peridotitic xenoliths recovered from Juina kimberlitres, the two type IaAB diamonds can be plotted on Fig. 9.6 to determine their time-averaged mantle residence temperatures (~1200 °C). Estimated temperatures of nitrogen aggregation are consistent with those calculated for both sheared peridotite and granular peridotite xenoliths (Costa *et al.*, 2003) (Fig. 9.6). If diamonds are sourced from granular peridotite, they

Fig. 9.6. Plot of temperature versus pressure for peridotitic xenoliths and diamonds. Grey P-T fields are estimates for xenoliths from Juina kimberlites (Costa *et al.*, 2003). The lower pressure estimates for sheared peridotites are unusual in the woldwide context. Diamond/graphite stability is from Kennedy et al. (1976). The estimated temperatures for diamonds 6-8 and 4-17 represent time-averaged mantle residence temperatures for ~1.1 Ga diamonds.

are likely lithospheric in origin. The low *mg* (0.90) of olivine in diamond 6-8 is consistent with composition of olivines from sheared asthenospheric peridotite (Boyd, 1989) and may indicate that the diamond is sourced from the sublithopheric mantle. This is highly unusual as diamonds have never been reported in sheared peridotites or having olivine inclusions with fertile asthenospheric mantle compositions (Meyer, 1987; Gurney, 1989).

Information on the internal structure is available from two diamonds, 4-17 and 6-8. Diamond 4-17 has a rim of bright green CL (type IaAB) that forms on a core of weaker blue CL (type IIa) (section 7.3.14). The aggregation state of the rim increases towards the crystal centre, but is below detection in the blue CL interior. Although the cross-section of diamond 4-17 does not reveal the complete growth history, the growth of the

outer rim likely formed on a flat-faced octahedron. It is certainly possible that the type IaAB diamond formed on a core that initially crystallised in the deep mantle (the type II core may attest to such a history). Chips from diamond 6-8 (produced from cracking of diamond for mineral inclusion extraction) also reveal a blue CL interior, however the core appears bright turquoise and is surrounded by a zone of weaker blue CL and a thin rim of bright yellow-green CL diamond. There are no IR data for specific CL zones for this diamond.

The bright green CL rim is perhaps the hallmark of this subgroup. The relatively intact nature of crystals, the general absence of resorption, the tendency for grains to be IaAB, and the presence of Ol in the absence of fPer are other distinguishing features.

9.2.1.2 Upper mantle eclogitic diamonds (type IaA and IaAB)

This subpopulation includes type IaA and IaAB diamonds that have crystallised in an eclogitic source in the upper mantle. However, if the diamonds experienced short mantle residence times (<1 Ma), than a deeper origin for some grains cannot be ruled out.

Three grains were classified as having an eclogitic origin based on inclusion studies alone (diamonds 2-11, 4-10 and 4-11). They are considered eclogitic based on the low nickel content of sulphides (2-11 and 4-11) and the calcium-rich, chromium-poor garnets (with no majoritic component) found in diamond 4-10 (indicating a depth of formation of less than 250 km). Diamond 4-10 contains two forbidden phases, $CaSiO_3$

Fig. 9.7. Photos of diamond body colour (left), FL (middle) and CL (right) for upper mantle eclogitic diamonds. From top to bottom, diamonds are: 2-11, 4-10, 4-11 and 4-15.

232

and non-majoritic garnet, and as such, can be placed in two paragenetic subgroups. SiO_2 was found in diamond 2-11 and is likely primary on account of its euhedral form (it occurs in association with low-NiO pyrrhotite). A fourth grain is tentatively included (diamond 4-15) based of its nitrogen character (type IaAB) and similarities in FL, CL and crystal form to diamond 4-10.

Like the peridotitic diamonds of upper mantle origin, this subpopulation tends to be less resorbed than most diamonds, although they are slightly more resorbed than the p-type diamonds (resorption scale 2,3 and 4 and one stone is classified as 'unknown'). Diamonds are mostly intact crystals of various shades of colourless to grey. Two of the stones are aggregates. The FL of all diamonds is blue, and the intensity is strong in all but one (Fig. 9.7). CL colour of the exterior of three diamonds occurs as shades of blue of various intensities (Fig. 9.7).

All four diamonds contain A centres, one is type IaA (48 ppm N) while the other three are type IaAB (16-64 %B, 33-138 ppm total N). Assuming that these diamonds have similar ages as eclogitic xenoliths recovered from Junia kimberlites, we can place some constraints on temperatures and pressures of formation for the diamonds in this subgroup. Three types of eclogitic xenoliths have been recovered, they are: orthopyroxene-rutile eclogites (1648 Ma), sanidine-coesite eclogites (1166 Ma) and coarse-grained eclogites (1593 Ma) (Costa *et al*., 2003). The
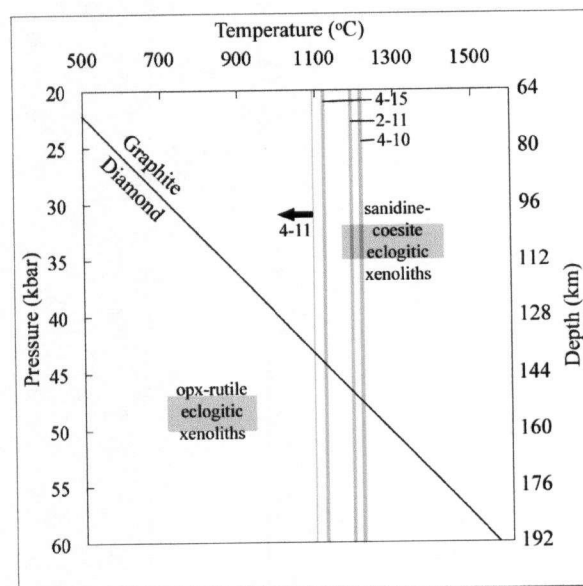
Fig. 9.8. Plot of temperature versus pressure for eclogitic xenoliths and diamonds. Grey P-T fields are estimates for xenoliths from Juina kimberlites (Costa *et al*., 2003). Diamond/graphite stability field is from Kennedy *et al*. (1976). The estimated temperatures for diamonds 2-11, 4-10, 4-11 and 4-15 represent time-averaged mantle residence temperatures for ~1.1 Ga diamonds. Diamond 4-11 contains 100% A centres, which is outside the limits of equation 6.7.

time-averaged mantle residence temperatures for minimum residence times of 1.1 Ga for each diamond are shown in Fig. 9.8. Note that the estimated temperature for diamond 4-11 falls somewhere to the left of the line indicated. Although the estimated temperatures are consistent with those predicted for the sanidine-coesite xenoliths, the estimated pressures fall outside of the diamond stability field (Kennedy *et al.*, 1976). Only diamond 4-11 could be sourced from the opx-rutile eclogite for these residence times. Temperatures of formation for the course-grained eclogites were estimated between 1182 – 1287 °C, however no pressure estimates were determined (Costa *et al.*, 2003). These temperatures are consistent for two eclogitic diamonds recovered, however it is unknown whether or not these xenoliths are sourced within the diamond stability field.

Only one diamond (2-11) from this subgroup was polished for growth studies, which revealed an internal morphology unique to this study (section 7.3.8). CL studies reveal a complex, mostly alternating pattern of turquoise blue and yellow-green CL bands. The yellow-green zones were interpreted as being the result of plastic deformation. Growth, at least in part, was on octahedral faces.

Eclogitic diamonds from the upper mantle are characterised by their lower aggregation states (<100% B centres) and by the presence of mineral inclusions that are commonly found in eclogitic diamonds from cratonic sources (e.g. non-majoritic pyrope-almandine-grossular garnets, low-Ni pyrrhotites and possibly SiO_2). They tend to be colourless to grey and exhibit FL and CL colours or various shades of blue of moderate to strong intensity. Aggregated forms may be more common than in other subgroups identified.

9.2.2 Eclogitic diamonds (type IaB)

Diamonds in this subgroup are type IaB and contain inclusions of eclogitic paragenesis. Three diamonds were grouped into the eclogitic paragenesis in section 8.4.3.2 based on the presence of inclusions of magnetite (diamonds 1-4, 2-6 and 2-10). Three other

diamonds were also grouped into the eclogitic parogenesis based on inclusions, however examination of nitrogen character separated these six diamonds into two subgroups within the eclogitic paragenesis, those with A centres, types IaA and IaAB (which defines the subgroup of likely upper mantle origins described in section 9.2.1.2) and those with only B centres, or type IaB (the three diamonds in this subgroup). Diamond 1-4 also contains an inclusion of SiO_2 (the primary nature of which is questionable) and the magnetite in diamond 2-10 was determined based only on EDS analysis.
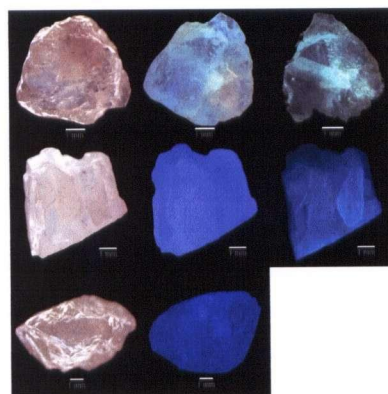
Fig. 9.9. Photos of diamond body colour (left), FL (middle) and CL (right) for eclogitic type IaB diamonds. From top to bottom, diamonds are: 1-4, 2-6 and 2-10.

The three diamonds are mostly intact, appear strongly resorbed and are yellow, milky and non-uniform brown/colourless. FL and CL colours range from blue to turquoise of moderate to strong intensity (Fig. 9.9).

All three grains are classified as type IaB. Two grains contain unusually high concentrations of nitrogen for this study (maximum recorded values of 233 and 541 ppm) while diamond 2-10 contains low concentrations of total nitrogen (24 ppm). It should be noted that IR analysis of this diamond was performed on a diamond chip, which may contain unusually low amounts of nitrogen. Examination of Figs. 7.9 - 7.12 illustrates that that nitrogen concentrations are highly variable. One IR analysis of a diamond chip will clearly give no indication of a heterogeneous nitrogen character. The less intense FL colours of diamond 2-10, compared to the colours in diamonds 1-4 and 2-6, suggest that the total nitrogen concentrations are low, but likely higher than the suite average of 72 ppm N. The IR results for diamond 2-10 are questionable, and a large range in nitrogen concentration may a characteristic of this subgroup. The high aggregation state indicates

that the diamonds have likely resided in the mantle at temperatures higher than is typical for cratons.

Internal growth studies reveal that diamond 1-4 has a complex and unique pattern (although there are similarities with the internal structure of diamond 2-2). There is a core of bright turquoise CL, which has what appears to be combined cubic and octahedral faces growing on the core (Figs. 7.10 and 7.12). Nitrogen concentrations range from 20 to 400 ppm and occur only as B centres.

This paragenesis is characterised by the presence of magneite inclusions, type IaB character, and possibly high nitrogen concentrations. Diamonds exhibit variable FL, CL and body colours. Growth of diamond, in part, may occur on both cubic and octahedral faces, which is unique to this study.

9.2.3 Eclogitic and/or peridotitic diamonds from depths greater than ~580 km

Six diamonds have been included in this subgroup based on the presence of $CaSiO_3$ grains in the absence of fPer (diamonds 2-8, 3-4, 3-7, 4-7, 6-6, 7-1). This subdivision is based purely on inclusion assemblage. Two diamonds contain touching inclusions of $CaSiO_3$ and $CaTiO_3$ (although the perovskite may be secondary). Diamond 4-10 could also be included in this subgroup because of its $CaSiO_3$-eGrt disequilibrium association.

The prevalence of $CaSiO_3$ compared to $MgSiO_3$ inclusions in this study is somewhat curious considering that a lower mantle of peridotitic bulk composition should contain, by weight, 79% $MgSiO_3$ and only 5% $CaSiO_3$ (Wood, 2000). The $MgSiO_3$/$CaSiO_3$ ratio in mafic material at lower mantle depths should be much closer to unity. Particularly striking are the number of $CaSiO_3$ inclusions occurring in the absence of fPer, while no diamonds are found with $MgSiO_3$ in the absence of fPer. The most plausible explanation for this observation is that $CaSiO_3$ inclusions are sourced from mafic material from the

transition zone where $CaSiO_3$ is stable but $MgSiO_3$ and fPer are not (e.g. Figs. 8.3A and B). It is suggested that this paragenetic group is sourced from eclogitic rocks from the relatively restricted depth interval between 580 and 660 km. An alternate model for the origin of these diamonds would place them in the lower mantle, where $CaSiO_3$ is also stable. The observed high $CaSiO_3/MgSiO_3$ ratio is unlikely to occur by chance alone, unless a process can be proposed whereby $MgSiO_3$ is selectively removed over $CaSiO_3$. One such process could be a preferential fracturing of diamond that contains $MgSiO_3$ because of its higher thermal expansion rate compared to $CaSiO_3$. To account for both models, diamonds with $CaSiO_3$ inclusions in the absence of fPer are classified as having either a mafic or ultramafic source, from depths greater than 580 km.

Out of the six diamonds, two have moderately resorbed forms and one is strongly resorbed. Diamonds occur as either fragments or broken stones. FL colours and intensity are variable, from blue (3 diamonds), turquoise (2) and green (1), while CL colours are either yellow or turquoise (Fig. 9.10). Four grains are type IaB and two are type IIa. Nitrogen concentration ranges from ~40-225 ppm and averages 105 ppm. The internal morphology of one diamond was examined (2-8, section 7.3.6), however results show either that the diamond lacked any internal structure, or that the polished surface does not intersect any growth zones. This diamond may have a green CL rim (Fig. 7.17) similar to those seen on upper mantle peridotitic diamonds (Fig. 9.5).

This subgroup is characterised by the presence of $CaSiO_3$ in the absence of fPer. Diamonds are either

Fig. 9.10. Photos of diamond body colour (left), FL (middle) and CL (right) for diamonds classified to the >580 km paragenesis. From top to bottom, diamonds are: 2-8, 3-4, 3-7, 4-7, 6-6 and 7-1.

type IIa or IaB with nitrogen concentrations less than 225 ppm. They exhibit a variety of FL and CL colours and tend to show moderate signs of resorption and tend not to occur as intact crystals.

9.2.4 Upper mantle/lower mantle (~660 km) diamonds

Four diamonds have been grouped into the upper mantle/lower mantle (LM/UM) subgroup based on the association of Ol and fPer, which can only be in equilibrium at a narrow depth range straddling the upper mantle/lower mantle boundary (diamonds 1-5, 3-2, 3-5 and 4-3). Olivines in diamonds 1-5 and 3-5 may be retrograde, which would place these two diamonds in the lower mantle paragenesis. All diamonds contain fPer-Ol-$MgSiO_3$, while two also contain TAPP and one contains $CaSiO_3$. In comparison to other inclusions of the same phases in this study, the chemistries are unremarkable. The $MgSiO_3$ grains contain Al_2O_3 contents that are consistent for MgSi-Prv near the top of the lower mantle and are not

Fig. 9.11. Photos of diamond body colour (left), FL (middle) and CL (right) for diamonds classified to the UM/LM peridotitic paragenesis. From top to bottom, diamonds are: 1-5, 3-2, 3-5 and 4-3.

consistent for diamond inclusion $MgSiO_3$ grains from cratonic sources. The average mg of the fPer grains is somewhat higher in comparison to most grains in this study for three diamonds (75, 83 and 84 – the average in this study 66.9 ± 13 (1σ)) and is low for the third (average $mg = 60$ for fPer's in diamond 3-5).

Diamonds are moderately resorbed and occur as fragments, broken stones or fractions of stones. The FL colours of this subgroup are variable, from shades of blue to turquoise and green. FL intensity is also variable. CL colours were only examined for two diamonds (3-5 and 4-3) and appear moderate blue and turquoise (Fig. 9.11).

238

All four diamonds are type IaB, however there is considerable range in the nitrogen concentrations. Diamond 3-5 contains 32 ppm N, 4-3 (82 ppm N), 3-2 (228 ppm total N) and 1-5 (311 ppm N). The high aggregation state is consistent with diamonds that have resided in the mantle at high temperatures, such as temperatures predicted near the 660 km seismic discontinuity.

The internal growth habit of diamond 3-5 was examined. It was one of only two diamonds in this study to exhibit a reasonably simple pattern of concentric growth layers with some intermittent episodes of resorption. It has a brighter blue CL core and nitrogen concentration (all as B centres) decreases from core to rim.

This subgroup is characterised by the presence of fPer and Ol inclusions. Diamonds are type IaB with concentrations ranging from 32-211 ppm total nitrogen. Diamonds fluoresce blue and are generally well resorbed.

9.2.5 Lower mantle diamonds

Twelve diamonds were classified into the lower mantle (LM) subgroup based on mineral inclusions alone (diamonds 1-2, 2-2, 2-7, 3-1, 3-6, 3-9, 3-10, 4-16, 5-1, 6-1, 6-2 and 6-9). All diamonds contain fPer in the absence of Ol (and are thus not restricted to the upper mantle/lower mantle boundary). Four diamonds also contain $CaSiO_3$ (2-2, 3-1, 3-10 and 4-16), one of which may also contain an eclogitic garnet (diamond 4-16), which was determined based on EDS alone (in the absence of supporting EPMA data and considering the small grain size, the identification of eGrt cannot be considered conclusive). Another diamond (2-7) also contains SiO_2 (although it is of questionable origin). The variation in mg for fPer does not appear to be controlled by inclusion association. The Mg-number for fPer grains that occur alone are $mg = 55, 57, 66, 69, 75, 79, 81$ (seven diamonds), for fPer grains in association with $CaSiO_3$, $mg = 50, 77, 78$

(three diamonds), fPer in association with eGrt (no EPMA results for the fPer) and fPer in association with SiO_2 (*mg* = 81).

Diamonds are more resorbed than in any of the previous subgroups (mostly resorption categories 1 and 2, or tetrahexahedroids and dodecahedroids). Diamonds are mostly colourless (7 grains) with yellow (3), pink (1), and non-uniform brown/colourless (1) making up the remainder of the subgroup. Plastic deformation laminations are observed on half of the diamonds, which is significantly higher than the percentage observed on the population as a whole (20%, section 2.3.7). FL colours for all twelve diamonds are blue and moderate to very weak in intensity (Fig. 9.12). Although these FL colours are not unique to this subgroup, a preliminary subdivision of diamonds based on this criteria alone may be valid.

Diamonds are either type IIa or IaB, with nitrogen concentrations ranging from 0 to 400 and averaging ~60 ppm.

The internal structures were examined for four of the diamonds in this subgroup. Three diamonds exhibit blue CL of variable intensity while one diamond exhibits turquoise CL (diamond 2-2). The internal structure in diamond 2-2 was different from the others (it is similar in internal morphology to diamond 1-4) and was interpreted as being complex, but likely showing signs of sector

Fig. 9.12. Photos of diamond body colour (left), FL (middle) and CL (right) for diamonds classified to the LM peridotitic paragenesis. From top to bottom, diamonds are: 1-2, 2-2, 2-7, 3-1, 3-6, 3-9, 3-10, 4-16, 5-1, 6-1, 6-2 and 6-9.

dependence of impurity incorporation. Some domains of the diamond were rich in nitrogen (225 ppm total nitrogen) while others were essentially type IIa diamond. Diamonds 1-2 and 3-1 exhibit typical diamond growth features, i.e. concentric pattern of growth with episodic events of resorption. Nitrogen concentration for both of these diamonds decreases towards the crystal rim.

This subgroup is characterised by the presence of fPer inclusions in the absence of olivine. $CaSiO_3$ and TAPP (as well as $MgSiO_3$) may also be present. Diamonds are type IIa or IaB with generally low total nitrogen concentrations (~<60 ppm N). FL colours are blue of weak to moderate intensity. CL colours are more variable, exhibiting a variety of shades of blue of weak to strong intensity. Diamonds often exhibit signs of plastic deformation, are colourless to various shades of brown and pink, and are strongly resorbed (classes 1 or 2).

9.2.6 Diamonds of unknown paragenesis

There are 37 diamonds that cannot be assigned to a source rock subgroup, however the high aggregation state suggests that these diamonds are not sourced from lithospheric mantle. A few diamonds contain elevated concentrations of total nitrogen (e.g. diamond 4-4, 335 ppm N; diamond 1-3, 243 ppm N; and diamond 3-3, 226 ppm N), however, the nitrogen concentrations for the 37 diamonds cover the complete spectrum from <20 to 336 ppm N, with no indication of bimodal character. Sixteen diamonds contain <20 ppm nitrogen, thus making impossible the time/temperature estimates based on nitrogen aggregation. However, low nitrogen concentrations are uncommon for most diamond suites and are considered to be an indicator of a deep source (Kaminsky *et al.*, 2001b).

In terms of morphology, colour, FL and CL characteristics, these diamonds exhibit a range of features compatible with those for all other paragenetic groups defined. There are a couple of diamonds that are peculiar and may represent their own paragenetic

groups. Diamond 2-3 is unique in that it possesses the most intense yellow body colour and is the only diamond which does not fluorescence. No inclusions were recovered after cracking this type IIa diamond. Diamond 2-4 has an intense pink colour (one other diamond was classified as pink), contains moderate amounts of nitrogen (94 ppm), all as B centres.

9.3 Distribution of paragenetic groups

The distribution of paragenetic groups (Fig. 9.13) does not vary much from the distribution determined in section 8.4.1.7. However, integration of all studies helps to reinforce divisions based on mineral inclusion studies. In particular, nitrogen aggregation
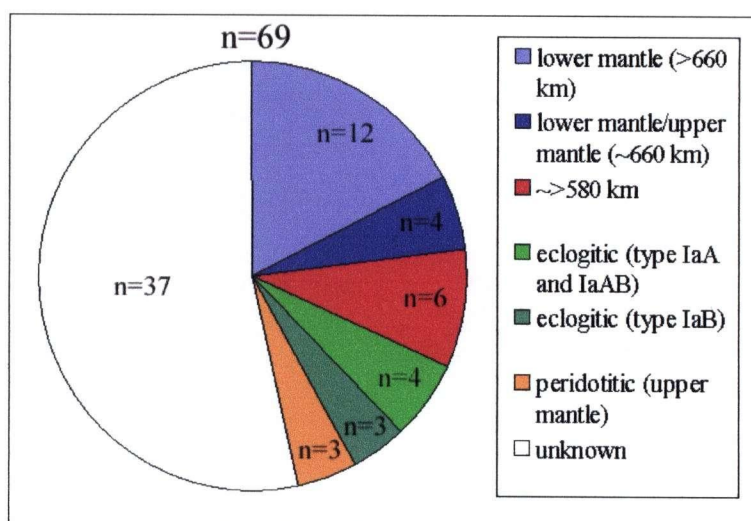
Fig. 9.13. Distribution of paragenetic groups for Rio Soriso diamonds based on diamond morphology, colour, FL, CL, internal morphology, nitrogen character and mineral inclusions. n – represents sample size.

state helps to separate diamonds of upper mantle origin from deeper sourced stones. Six diamonds contained at least some A centres (~9% of the population) and one diamond was added to this subgroup, increasing the proportion of diamonds that likely resided in the upper mantle to 7 diamonds (10% of the population). The remaining 62 diamonds (90%) are likely sourced from greater depths, as suggested by either the 100% aggregation to B centres or the type IIa character. No diamonds can be placed, with any certainty, to depths between ~250 and 660 km. However, any diamonds containing $CaSiO_3$ in the absence of fPer, TAPP or $MgSiO_3$, could be sourced from depths below 580 km. Four diamonds of peridotitic origin (6% of population), are likely sourced from

242

somewhere near the upper mantle/lower mantle divide at ~660 km (assuming all phases are in equilibrium, which may not be justified in all cases). At least twelve diamonds (17%) are likely sourced from the lower mantle (660 – 2900 km depth), however, as of yet, there are no constraints to place the diamonds within a more restricted depth interval in the lower mantle. Three diamonds containing magnetite are sourced from eclogitic material, likely of deeper origins than the type IaA and IaAB eclogitic diamonds.

The 37 diamonds of unknown origin likely belong to either the lower mantle, the LM/UM or the ~>580 km subgroup based on similar nitrogen character (they are all either type IIa and IaB) and they are generally well resorbed, broken crystals with variable FL colours and CL colours of various shades of blue and turquoise. However, in the absence of supporting data, they will remain unclassified.

9.4 Plume origin of Rio Soriso diamonds

The discovery of several subpopulations in a diamond suite is typical for most studies (e.g. McKenna, 2001; Gurney et al., in print). However, in the case of most studies, the variation in depth of origin between subgroups is not so markedly different; most diamond suites represent subgroups sourced from only the cratonic mantle between ~150 – 250 km depths, whereas the diamonds in this study are interpreted as having origins spanning depths from ~200 to >660 km. Certainly an explanation is required describing how material spanning such a large depth interval in the mantle could be sampled.

The simplest explanation invokes entrainment in a mantle plume as it rises from depths within the lower mantle to the base of the craton. This model has been proposed by several authors to explain the occurrence of fPer as an inclusion in diamond (e.g. Haggerty, 1994; Hutchison, 1997; Griffin et al., 1999; Kaminsky et al., 2001a).

Based on evidence from xenoliths and the presence of lower mantle diamonds, Griffin *et al.* (1999) conclude that the Slave craton is comprised of two layers: a shallow ultra-depleted upper layer and a less depleted lower layer, with a boundary at 140-150 km. They concluded that the less depleted lower layer represents the head of a plume or diapir that incorporated both moderately depleted mantle and subducted crustal material during ascent from >660 km depth and eventually accreted onto the base of the craton.

The theory of superplumes was first proposed by Larson (1991) to explain the voluminous mid-Cretaceous basaltic lavas at Ontong Java. Haggery (1994; 1999) used this superplume model to relate the periodicity of kimberlite eruptions with superchron events. It has been shown that the Earth's polarity reverses every few million years, with the exception of several extended periods where no reversals are observed. These periods are referred to as superchrons and occur every ~200 Ma (Haggery, 1999). The recognition that kimberlite ages are restricted to time intervals that tend to match those of superchrons is strong support that there is a link between the outer core and the generation and eruption of kimberlite magma. Superplumes originate at the core-mantle boundary and have potential to sample material at any depth during ascent, including lower mantle diamonds. The age of emplacement for Juina kimberlites is 95 Ma (Heaman *et al.*, 1998), which places them in the middle of the 80-120 superchron. It is suggested that the Rio Soriso suite was entrained in an ascending superplume from the mid-Cretaceous superchron and were subsequently exhumed to shallow crustal levels in a kimberlitic magma generated from this superplume.

This model explains how any sublithospheric material can be brought to upper mantle levels. The advected material was picked up by Group 1 Juina kimberlites (H. Cookenboo, personal communication) at ~250-300 km depths in the upper asthenospheric mantle. Group 1 kimberlitic magmas must have asthenospheric origins based on the Sr-Nd isotopic compositions similar to the Bulk Silicate Earth (Mitchell, 1995). The maximum depth where Group 1 kimberlites can form is not constrained, but

general consensus is that it becomes increasingly difficult to generate and propagate magma through mantle at greater depths. During magma ascent to the surface, the kimberlite must have sampled the cratonic lithosphere containing diamondiferous peridotite and eclogite. In the proposed scenario, the plume material from the lower mantle (superplume) was neither underplated to the Amazonian craton nor became part of the cratonic root. Equally possible, however, is the alternate scenario, where the plume was frozen to the cratonic keel before being sampled by a kimberlite.

9.5 Origin and distribution of eclogitic diamonds

A significant proportion of Rio Soriso diamonds may have been sourced from rocks of mafic composition from sub-lithospheric depths up to ~660 km.

Eclogites in the cratonic mantle can be produced either by high-pressure crystallization from peridotite-generated magmas (Barth, *et al.*, 2001) or by the subduction of oceanic lithosphere (Helmstaedt *et al.*, 1989). Tassinari *et al.* (1999) suggest that subduction was occurring under the Amazonian craton in the Proterozoic (1.2 - 1.95 Ga), forming a magmatic arc that becomes progressively younger to the west. This subduction event encompasses the dates from eclogitic xenoliths recovered from Juina kimberlites (1116 – 1648 Ma, Costa *et al.*, 2003). Thus, subduction of oceanic crust provides a potential source for eclogitic diamonds in this study.

In general, eclogite has a higher potential than peridotite to host diamonds in the sublithospheric mantle. Experimental studies show that the fO_2 stability field of diamond is larger in eclogite than in peridotite (Luth, 1993). Also, in a worldwide context, almost all mineral inclusions sourced from the sublithospheric upper mantle and transition zone are eclogitic (Stachel, 2001). Furthermore, diamonds are never recovered from sheared peridotites (Gurney and Zweistra, 1995) that are interpreted as having deep asthenospheric origins (e.g. Boyd, 1989). One possible explanation for the absence of

diamonds is that oxygen fugacity is too low in these rocks for diamond to be stable. Evidence from mossbauer spectroscopic studies of garnet in cratonic peridotites shows that the fO_2 is equal to ~QFM-4 at ~220 km (i.e. 4 log units below the quartz-fayalite-magnetite reference oxygen buffer) and that it likely decreases with further depth, reaching conditions of metal saturation near the 410 km discontinuity (Woodland *et al.*, 2003). Under such reducing conditions, carbon is no longer stable in the form of diamond and forms complexes with hydrogen, such as methane (Haggerty, 1986). The combination of these experiments and observations provide compelling evidence that there is an 'eclogite-only-diamond-window' in the sub-lithospheric mantle up to 660 km.

The 'eclogite-only-diamond-window' is consistent with observations of this study. Based on mineral phase stabilities, there are two mafic subgroups in this study that could be sourced from sub-lithospheric upper mantle to depths of ~660 km while no ultramafic or peridotitic subgroups are stable at these depths. Furthermore, previous studies have established a sub-lithospheric eclogitic source in Juina by the discovery of numerous eclogitic-majoritic garnets (Wilding, 1991). The presence of eclogites at all mantle depths, as evidenced by tomography (e.g. Davies *et al.*, 2002), is consistent with a subduction origin. Furthermore, the possibility of some eclogitic material building up at the boundary between the upper and the lower mantle provides a large eclogitic reservoir at the precise depth interval from where these diamonds may be sourced.

9.6 Implications for exploration

Lower mantle and other diamonds with deep origins may represent only a small proportion of the worldwide population of diamonds at shallow crustal levels. However, their presence has some serious implications for both regional and local exploration.

The observation that all primary economic diamond deposits occur on Archean and Proterozoic cratons (Clifford's rule) has focussed exploration to these areas in the past.

Cratons form the cores of most continents and often contain lithospheric roots up to 250 km thick. Most diamonds found in kimberlites crystallise within certain domains in these lithospheric roots. A model that invokes mantle plumes to concentrate diamonds, however, is not restricted to cratonic environments. In fact, mantle plumes are more common in non-cratonic settings, particularly below continental and oceanic rift zones. However, the stability field of diamond and the fundamental differences in geologic settings makes rift zones poor targets for primary diamond deposits. Cratons act as a barrier, stopping the vertical ascent and thus keeping the subcratonic diamonds in the diamond stability field before they are quickly brought up to the Earth's surface by kimberlitic magma. No such barrier exists to stop the continued ascent of off-craton superplumes. Furthermore, the higher geotherm in rift zones results in a higher degree of decompression partial melting that accompanies plume ascent, which would further reduce the diamond preservation potential. If there is no eruptive event that can tap an off-craton superplume before its diamond has reverted to graphite and bring it quickly to surface, Clifford's rule is still valid.

Kimberlite indicator mineral tracing is common practise for many diamond exploration programs, and it is likely that through the use of well established exploration techniques, kimberlites in the Juina area may be found. Once a kimberlite has been located, the next step in most exploration programs is to evaluate its diamond potential. The diamond potential is estimated based on the amount of eclogitic and peridotitic xenocrystic material sourced from the diamond stability field that has been incorporated into the kimberlite. Thus, the established algorithm to assess the diamond potential would give an incorrect estimate for Juina kimberlites. Clearly, the algorithm should be modified to account for possible lower mantle diamonds.

Indicator minerals for lower mantle diamonds should be chosen from phases found in equilibrium with the Rio Soriso diamonds, i.e. fPer, $MgSiO_3$, $CaSiO_3$ and TAPP. These minerals are certainly more abundant in the lower mantle than diamond, but they likely

revert and re-equilibrate to upper mantle minerals relatively quickly unless they are protected in some manner. Thus, their potential as indicator minerals is questionable. Further research on the possibility of the metastable existence of lower mantle minerals in kimberlites and in the upper mantle is needed before the diamond potential of Juina kimberlites can be properly evaluated through similar petrological techniques.

10. Conclusions

1. The examined suite of Rio Soriso diamonds contains several subpopulations of diamonds that originated in the upper and lower mantle. The subgroups are: 1) lower mantle diamonds (>660 km) of ultramafic paragenesis, 2) diamonds generally restricted to the upper mantle/lower mantle boundary ~660 km, also of ultramafic paragenesis, 3) diamonds of mafic paragenesis that formed at depths between ~580-660 km, 4) diamonds of mafic paragenesis that formed at sublithospheric depths, 5) upper mantle eclogitic diamonds, and 6) upper mantle peridotitic diamonds. The large range in depth of origin for the Rio Soriso suite is a result of their ascent in a plume originating at the core-mantle boundary.

2. Diamonds of the lower mantle paragenesis are characterised by i) the presence of ferropericlase inclusions in the absence of olivine, ii) the abundance of deformation laminations, iii) the strongly resorbed forms, iv) weak blue FL colours, and v) their type IaB or IIa character.

3. Diamonds that formed are the boundary between the upper and lower mantle are characterised by i) the association of ferropericlase and olivine inclusions, and ii) their type IaB character.

4. Diamonds that formed at depths between ~580-660 km of mafic paragenesis are characterised by i) the presence of $CaSiO_3$ in the absence of ferropericlase, ii) the large variety of CL and FL colours, and iii) their type IaB or IIa character.

5. Sublithospheric mafic diamonds are characterised by i) the presence of magnetite inclusions, ii) the intense blue to turquoise FL and CL colours, iii) the episode of combined cubo-octahedral growth, and iv) their type IaB character with higher nitrogen concentrations than typical.

6. Upper mantle eclogitic diamonds are characterised by: i) their type IaA or IaAB character, ii) the presence of garnet and low-Ni pyrrhotite, iii) their strong blue FL and turquoise to blue CL, and iv) the prevalence of aggregated crystals.

7. Upper mantle peridotitic diamonds are characterised by: i) the presence of olivine in the absence of fPer and other deeply-sourced phases, ii) their bright green CL rims, iii) unresorbed, intact crystals, and iv) the prevalence of type IaAB diamond.

8. The paucity of radiation damage of Rio Soriso diamonds suggests they did not spend a long time in a secondary collector. Furthermore, the paucity of mechanical abrasion on crystal surfaces indicates that they have not travelled far from their primary source.

9. There is a strong correlation between diamond body colour and FL colour for Rio Soriso diamonds. Brown diamonds are more likely to fluorescence of various shades of turquoise and green.

10. There is a positive correlation between CL intensity and nitrogen concentration. Diamonds with bright CL colours tend to have higher concentrations of nitrogen.

11. There is a strong positive correlation between nitrogen and hydrogen concentrations in Rio Soriso diamonds.

References

Akaogi, M., and Akimoto, S. 1977. Pyroxene – garnet solid solution equilibria in the systems $Mg_4Si_4O_{12} - Mg_3Al_2Si_4O_{12}$ and $Fe_4Si_4O_{12} - Fe_3Al_2Si_4O_{12}$ at high pressures and temperatures. Physics of the Earth and Planetary Interiors, **15**, 90-106.

Akaogi, M., and Akimoto, S. 1979. High-pressure phase equilibria in a garnet lherzolite, with special reference to $Mg^{2+}-Fe^{2+}$ partitioning among constituent minerals. Physics of the Earth and Planetary Interiors, **19**, 31-51.

Akaogi, M., Ito, E., and Navrotsky, A. 1989. Olivine-modified spinel-spinel transitions in the system $Mg_2SiO_4 - Fe_2SiO_4$: Calorimetric measurements, thermochemical calculation, and geophysical application. Journal of Geophysical Research, **94**, 15,671-15,685.

Araujo, D.P., Gaspar, J.C., Yingwei, F., Hauri, E.H., Hemley, R., and Bulanova, G. 2003. Mineralogy of diamonds from the Juina province, Brazil. Extended Abstracts, Proceedings of the 8th International Kimberlite Conference, Victoria, Canada.

Bardet, M.G. 1977. Geologie du Diamant. Bureau Recherches Geol. Min. Memoire, **83**, 169.

Barry, A.C. 1986. Voidites in diamond - do they contain nitrogen? Ultramicroscopy, **20**, 169-176.

Barth, M.G., Rudnick, R.L., Horn, I., McDonough, W.F., Spicuzza, M.J., Valley, J.W. and Haggerty, S.E. 2001. Geochemistry of xenolithic eclogites from West Africa; Part I, A link between low MgO eclogites and Archean crust formation. Geochimica et Cosmochimica Acta, **65**, 1499-1527.

Bibby, D.M. 1982. Impurities in natural diamond. Chemistry and Physics of Carbon, **18**, 1-91.

Boggs, S. 1987. Principles of Sedimentology and Stratigraphy. Merril Publishing Company, Columbus, Ohio, U.S.A.

Bovenkerk, H.P. 1961. Some observations on the morphology and physical characteristics of synthetic diamond. The American Mineralogist, **46**, 952-963.

Boyd, S.R., Kiflawi, I., and Woods, G.S. 1994. The relationship between infrared absorption and the A defect concentration in diamond. Philosophical Magazine B, **69**(6), 1149-1153.

Boyd, S.R., Kiflawi, I., and Woods, G.S. 1995. Infrared absorption by the B nitrogen aggregate in diamond. Philosophical Magazine B, **72**(3), 351-361.

Boyd, F.R. 1989. Compositional distinction between oceanic and cratonic lithosphere. Earth and Planetary Science Letters, **96**, 15-26.

Boyd, S., Mattey, D., Pillinger, C., Milledge, H., Mendelssohn, M. and Seal., M. 1987. Multiple growth events during diamond genesis: an integrated study of carbon and nitrogen isotopes and nitrogen aggregation state in coated stones. Earth and Planetary Science Letters, **86**, 341-353.

Brey, G.P., Bulatov, V., Girnis, A., Harris, J.W. and Stachel, T. 2003. Ferropericlase – a lower mantle mineral phase in the upper mantle. 8th International Kimberlite Conference, Extended Abstracts, Victoria, Canada.

Brey, G.P. and Kohler, T. 1990. Geothermobarometry in four-phase lherzolites II. New thermobarometers, and practical assessment of existing thermobarometers. Journal of Petrology, **31**(6) 1353-1378.

Brown, J. and Shankland, T. 1981. Thermodynamic parameters in the earth as determined from seismic profiles. Geophysical Journal of the Royal Astronomical Society, **6**, 579-596.

Brunton, E. 1978. Diamonds. N.A.G. Press, London.

Bulanova, G.P. 1995. The formation of diamond. *In*: W.L. Griffin (ed.), Diamond exploration into the 21st century. Journal of Geochemical Exploration, **53**(1-3), 1-23.

Bulanova, G.P., Griffin, W.L., Ryan, C.G., Shestakova, O.Y., Barnes, S.J. 1996. Trace elements in sulfide inclusions from Yakutia diamonds. Contributions to Mineralogy and Petrology, **124**(2), 111-125.

Bulanova, G.P., Pearson, D.G., Hauri, E.H., and Griffin, B.J. 2002. Carbon and nitrogen systematics within a sector-growth diamond from the Mir kimberlite, Yakutia. Chemical Geology, **188**, 105-123.

Bulanova, G.P., Spetsius, Z.V. and Leskova, N.V. 1990. Sulfides in diamonds and mantle xenoliths from kimberlite pipes of Yakutia, Nauka, Novosibirsk, 118 pages (in Russian).

Burns, R.C., Cvetkovic, V., and Dodge, C.N. 1990. Growth-sector dependence of optical features in large synthetic diamonds. Journal of Crystal Growth, **104**, 257-279.

Chinn, I.L., Gurney, J.J, Milledge, H.J., Taylor, W.R., and Woods, P.A. 1995. Cathodoluminescence properties of CO_2 -bearing and CO_2 -free diamonds from the George Creek K1 kimberlite dike. International Geology Review, 37(3), 254-258.

Clark, C.D., Collins, A.T. and Woods, G.S. 1992. Optical spectroscopy of diamond. *In*: J.E. Field (ed.), The properties of natural and synthetic diamond, Academic Press: 35-69.

Clark, C.D. and Davies, S.T. 1984. One-phonon infrared absorption in diamond. Journal of Physics C: Solid State Physics, 17, 1127-1140.

Clausing, R.E. 1997. Diamond Morphology. *In*: M.A. Prelas, G. Popovici and L.K. Bigelow (eds.), Handbook of Industrial Diamonds and Diamond Films, New York, Marcel Dekker Inc., 19-48.

Davies, G. 1972. The effect of nitrogen impurity on the annealing of radiation damage in diamond. Journal of Physics C: Solid State Physics, 5, 2534-2542.

Davies, G. 1976. The A nitrogen aggregate in diamond – its symmetry and possible structure. Journal of Physics C: Solid State Physics, 9, L537-L542.

Davies, G. and Evans, T. 1972. Graphitization of diamond at zero pressure and at high pressure. Proceedings of the Royal Society of London, A328, 413-427.

Davies, J.H., Brodholt, J.P. and Wood, B.J. 2002. Introduction. Philosophical Transactions of the Royal Society of London, Series A: Mathematical and Physical Sciences, 360, 2361-2369.

Davies, R.M. 1998. The characteristics and origins of alluvial diamonds from Eastern Australia. Unpublished PhD Thesis, Macquarie University, Sydney, Australia.

Davies, R.M., Griffin, W.L., Pearson, N.J., Andrew, A.S., Doyle, B.J. and O'Reilly, S.Y. 1999. Diamonds from the deep: pipe DO-27, Slave craton, Canada. *In*: Gurney, J.J., Gurney, J.L., Pascoe, M.D. and Richardson, S.H. (eds.). Proceedings of the VIIth International Kimberlite Conference, 1, 148-155.

Davies, R.M., O'Reilly, S.Y., and Griffin, W.L. 1999b. Growth structures and nitrogen characteristics of Group B alluvial diamonds from Bingara and Wellington, eastern Australia. *In*: Gurney, J.J., Gurney, J.L., Pascoe, M.D. and Richardson, S.H. (eds.). Proceedings of the VIIth International Kimberlite Conference, 1, 156-163.

Deines, P., Harris, J.W. and Gurney, J.J. 1991. The carbon isotopic composition and nitrogen content of lithospheric and asthenospheric diamonds from the

Jagersfontein and Koffiefontein kimberlite, South Africa. Geochemica et Cosmochimica Acta, **55**, 2615-2625.

DeVries, R.C. 1975. Plastic deformation and "work-hardening" of diamond. Materials Research Bulletin, **10**, 1193-1200.

Dischler, B., Wild, C., Muller-Sebert, W. and Koidl, P. 1993. Hydrogen in polycrystalline diamond. Physica B, **185**, 217-221.

Drake, M.J. and Weill, D.F. 1972. New rare earth element standards for electron microprobe analysis. Chemical Geology, **10**(2), 179-181.

Dubrovinsky, L.S., Dubrovinskaia, N.A., Saxena, S.K., Annersten, H., Halenius, E., Harryson, H., Tutti, F., Rekhi, S. and Le Bihan, T. 2003. Stability of ferropericlase in the lower mantle. Science, **289**(5478), 430-432.

Ellis, D. and Green, D. 1979. An experimental study of the effect of Ca upon garnet-clinopyroxene Fe-Mg exchange equilibria. Contributions to Mineralogy and Petrology, **71**, 13-22.

Ercit, T.S. 1996. *Formula* Microsoft DOS-based program.

Evans, T. 1976. Diamonds. Contemporary Physics, **17**, 45-70.

Evans, T. 1992. Aggregation of nitrogen in diamond. *In*: J.E. Field (ed.), The properties of natural and synthetic diamond. Academic Press: 259-290.

Evans, T. and Harris, J.W. 1986. Nitrogen aggregation, inclusion equilibration temperatures and the age of diamonds. Proceedings of the 4th International Kimberlite Conference, Perth, 11-16 August, 1986, Blackwell Scientific Publications, Carlton, Victoria, Australia, **2**, 1001-1006.

Evans, T. and Phall, C. 1962. Imperfections in Type I and Type II diamonds. Proceedings of the Royal Society of London, **A270**, 538-552.

Evans, T.and Qi, Z. 1982. The kinetics of the aggregation of nitrogen atoms in diamond. Proceedings of the Royal Society of London, **A381**, 159-178.

Evans, T. and Sauter, D.H. 1961. Etching of diamond surfaces with gases. Philosophy Magazine, **6**, 429-440.

Fei, Y. and Bertka, C.M. 1999. Phase transitions in the Earth's mantle and mantle mineralogy, *In*: Y. Fei, C.M. Bertka and B.O. Mysen (eds.), Mantle petrology; field

observations and high-pressure experimentation; a tribute to Francis R. (Joe) Boyd, Special Publication - Geochemical Society, **6**, 189-207.

Fei, Y., Wang, Y. and Finger, L.W. 1996. Maximum solubility of FeO in $(Mg,Fe)SiO_3$-perovskite as a function of temperature at 26 GPa; implication for FeO content in the lower mantle. Journal of Geophysical Research, B, Solid Earth and Planets, **101**(5), 11,525-11,530.

Fipke, C.E., Gurney, J.J. and Moore, R.O. 1995. Diamond exploration techniques emphasising indicator mineral geochemistry and Canadian examples. Geological Survey of Canada, Report, No. 423, 86 pages.

Fritsch, E. 1998. The nature of colour in diamonds. *In*: G.E. Harlow (ed.) The Nature of Diamonds, Cambridge University Press. 23-47.

Frost, D.J. 2003. The structure and sharpness of $(Mg,Fe)_2SiO_4$ phase transformations in the transition zone. Earth and Planetary Science Letters, **216**, 313-328.

Gasparik, T. 1989. Transformations of enstatite-diopside-jadeite pyroxenes to garnet. Contributions to Mineralogy and Petrology, **102**, 389-405.

Gasparik, T. 1990. Phase relations in the transition zone, Journal of Geophysical Research, B, Solid Earth and Planets, **95**(10), 15,751-15,769.

Gasparik, T. and Hutchison, M.T. 2000. Experimental evidence for the origin of two kinds of inclusions in diamonds from the deep mantle. Earth and Planetary Science Letters, **181**, 103-114.

Gasparik, T. and Wolf K. 1994. Experimental determination of the phase relations in the $CaSiO_3$ system from 8 to 15 Gpa. American Mineralogist, **79**, 1219-1222.

Grantham, D.R. 1974. Observations on diamonds and their morphologies. (compiled by J.W. Harris). Consolidated African Selection Trust Ltd., London.

Griffin, W.L., Doyle, B.J., Ryan, C.G., Pearson, N.J., O'Reilly, S.Y., Natapov, L., Kivi, K., Kretshchmar, U. and Ward, J. 1999. Lithospheric structure and mantle terranes: Slave craton, Canada. *In*: Gurney, J.J., Gurney, J.L., Pascoe, M.D. and Richardson, S.H. (eds.). Proceedings of the 7th International Kimberlite Conference, **1**. 299--306.

Gurney, J.J. 1984. A correlation between garnets and diamonds. *In*: J.E. Glover, P.G. Harris (eds.), Kimberlite occurrence and origins: a Basis for Conceptual Models in Exploration, Geology Department and University Extension, University of Western Australia, Publication No. 8, 143-166.

Gurney, J.J. 1989. Diamonds. *In*: J. Ross, A.L. Jaques, J. Ferguson, D.H. Green, S.Y. O'Reilly, R.V. Danchin and A.J.A. Janse, (eds.), Kimberlites and Related Rocks, **2**. Blackwell Science Publications, Carlton, Australia, No. 14, 935-965.

Gurney, J.J., Hildebrande, P.R., Carlson, J.A., Fedortchouk, Y., and Dyck, D.R. in print. The morphological characteristics of diamonds from the Ekati property, North West Territories, Canada.

Gurney, J.J. and Zweistra, P. 1995. The interpretation of the major element compositions of mantle minerals in diamond exploration. Journal of Geochemical Exploration, **53**, 293-309.

Haavik, C., Stolen, S., Fjellvag, H., Hanfland, M. and Hausermann, D. 2000. Equation of state of magnetite and its high-pressure modification: Theromodynamics of the Fe-O system at high pressure. American Mineralogist, **85**, 514-523.

Haggerty, S. E. 1986. Diamond genesis in a multiply-constrained model. Nature, **320**, 34-38.

Haggerty, S.E. 1994. Superkimberlites: a geodynamic diamond window to the Earth's core. Earth and Planetary Science Letters, **122**, 57-69.

Haggerty, S.E. 1999. A diamond trilogy: superplumes, supercontinents, and supernovae. Science, **285**, 851-860.

Hall, A.E. and Smith, C.B. 1984. Lamproite Diamonds: Are They Different? *In*: J.E. Glover and P.G. Harris (eds.), Kimberlite Occurrence and Origin: A Basis for Conceptual Models in Exploration, Geology Department and University Extension, University of Western Australia, Publication No. 8, 167-212.

Hanley, P.L., Kiflawi, I. And Lang, A.R. 1977. On topographically identifiable sources of cathodoluminescence in natural diamonds. Philosophical Transactions of the Royal Society of London, Series A: Mathematical and Physical Sciences, **284**(1324), 329-368.

Harris, J.W. 1987. Recent physical, chemical, and isotopic research of diamond. *In*: P.H. Nixon (ed.) Mantle Xenoliths. Toronto, John Wiley and Sons. 477-500.

Harris, J.W. 1992. Diamond geology. *In*: J.E. Field (ed.), The properties of natural and synthetic diamond. Academic Press: 345-394.

Harris, J.W. and Gurney, J.J. 1979. Inclusions in diamond. *In*: J.E. Field (ed.), Properties of diamond, Academic Press, London, 555-594.

Harris, J.W., Hawthorne, J.B., Oosterveld, M.M., and Wehmeyer, E. 1975. A classification scheme for diamond and a comparative study of South African diamond. Physics and Chemistry of the Earth, **9**, 765-783.

Harris, J.W., Hutchison, M.T., Hursthouse, M., Light, M. and Harte, B. 1997. A new tetragonal silicate mineral occurring as inclusions in lower-mantle diamonds. Nature, **387**, 486-488.

Harris, J.W. and Vance, E.R. 1974. Studies of the reaction between diamond and heated kimberlite. Contribution to Mineral Petrology, **47**, 237-244.

Harte, B., Fitzsimons, C.W., Harris, J.W., and Otter, M.L. 1999. Carbon isotope ratios and nitrogen abundances in relation to cathodoluminescence characteristics for some diamonds from the Kaapvaal province, South Africa. Mineralogical Magazine, **63**(3), 829-856.

Harte, B. and Harris, J.H. 1994. Lower mantle mineral associations preserved in diamonds. Mineralogial Magazine, **58A**, 384-385.

Harte, B., Harris, J.W., Hutchison, M.T., Watt, G.R. and Wilding, M.C. 1999. Lower mantle mineral associations in diamonds from Sao Luiz, Brazil. *In*: Y. Fei, C.M. Bertka and B.O. Mysen (eds.), Mantle petrology; field observations and high-pressure experimentation; a tribute to Francis R. (Joe) Boyd, Special Publication - Geochemical Society, **6**, 125-153.

Hartman, L.A., Silva, L.C. da, Daitx, E., and Girardi, V. 1980. O complexo granulitico da Santa Catarina, a bacia de Campo Alegre e o complexo basico-ultrabasico de Pien. 31st Congresso Brasileiro de Geologia, Buletim No. 3, roteiro de excursoes, 60-68.

Heaman, L., Teixeira, N.A., Gobbo, L., and Gaspar, J.C. 1998. U-Pb mantle zircon ages for kimberlites from the Juina and Paranatinga provinces, Brazil. Final Proceedings 7th International Kimberlite Conference, Extended Abstracts, Cape Town, South Africa, 322-342.

Helmstaedt, H.H. and Schulze, D.J., 1989. South African kimberlites and their mantle sample: Implications for Archean tectonics and lithosphere evolution. *In*: J. Ross (ed.), Kimberlites and Related Rocks, **1**. Blackwell Science Publications, Carlton, Australia, No. 14, 358-368.

Hirsch, P.B., Hutchinson, J.L. and Titchmarsh, J. 1986. Voidites in diamond: Evidence for a crystalline phase containing nitrogen. Philosophical Magazine, **54**, L49-L54.

Hutchison, M.T. 1999. Constitution of the deep transition zone and lower mantle shown by diamonds and their inclusions. Unpublished PhD Thesis, University of Edinburgh.

Irifune, T. 1987. An experimental investigation of the pyroxene–garnet transformation in a pyrolite composition and its bearing on the constitution of the mantle. Physics of the Earth and Planetary Interiors, **45**, 324-336.

Irifune, T. and Isshiki, M. 1998. Iron partitioning in a pyrolite mantle and the nature of the 410-km discontinuity. Nature, **392**(6677), 702-705.

Irifune, T., Koizumi, T. and Ando, J.I. 1996. An experimental study on the garnet-perovskite transformation in the system $MgSiO_3 - Mg_3Al_2Si_3O_{12}$. Physics of the Earth and Planetary Interiors, **96**, 147-157.

Irifune, T. and Ringwood, A.E. 1987. Phase transformation in primitive MORB and pyrolite compositions to 25 Gpa and some geophysical implications. *In*: M. Manghnani and Y. Syono (eds.), High Pressure Research in Geophysics, American Geophysical Union, Washington, DC, 231-242.

Irifune, T, and Ringwood, A.E. 1993. Phase transformations in subducted oceanic crust and buoyancy relationships at depths of 600-800 km in the mantle, Earth and Planetary Science Letters, **117**(1-2), 101-110.

Ito, E. and Takahashi, E. 1989. Postspinel transformation in the system $Mg_2SiO_4 - Fe_2SiO_4$ and some geophysical implications, Journal of geophysical Research, **94**, 10,637-10,646.

Jaques, A.L., Hall, A.E., Sheraton, J.W., Smith, C.B., Sun, S.S., Drew, R.M., Foudoulis, C. and Ellingsen, K. 1989. Composition of crystalline inclusions and C-isotopic composition of Argyle and Ellendale diamonds. *In*: J. Ross, A.L. Jaques, J. Ferguson, D.H. Green, S.Y. O'Reilly, R.V. Danchin and A.J.A. Janse, (eds.), Kimberlites and Related Rocks, **2**, Blackwell Science Publications, Carlton, No. 14, 966-989.

Joswig, W., Stachel, T., Harris, J.W., Baur, W.H. and Brey G.P. 1999. New Ca-silicate inclusions in diamonds – tracers from the lower mantle. Earth and Planetary Science Letters, **173**, 1-6.

Juina Mining website, http://www.juinamining.com/ (February 23rd, 2004).

Kaiser, W. and Bond, W.L. 1959. Nitrogen, a major impurity in common type I diamond. Physical Review, **115**, 857-863.

Kaminsky, F.V. 1992. Carbonado and yakutite: properties and possible genesis. *In*: H.O.A Meyer and O.H. Leonardos, (eds), Diamonds: Characterisation, Genesis and Exploration. GPRM Spec. Publ. No 1/B, CPRM, Brasilia, 136-143.

Kaminsky, F.V., and Khachatryan, G.K. 2001b. Characteristics of nitrogen and other impurities in diamond, as revealed by infrared absorption data. The Canadian Mineralogist, **29**, 1733-1745.

Kaminsky, F.V., Zakharchenko, O.D., Griffin, W.L., DeR. Channer, D.M., and Khachatryan-Bilnova, G.K. 2000. Diamond from the Guaniamo area, Venezuela. The Canadian Mineralogist, **38**, 1347-1370.

Kaminsky, F.V., Zakharchenko, O.D., Davies, R., Griffin, W.L., Khachatryan-Bilnova, G.K. and Shiryaev, A.A. 2001a. Superdeep diamonds from the Juina area, Mato Grosso State, Brazil. Contributions to Mineralogy and Petrology, **140**, 734-753.

Kanda, H. and Yamaoka, S. 1993. Inhomogeneous distribution of nitrogen impurities in {111} growth sectors of high pressure synthetic diamond. Diamond and Related Materials. **2**, 1420-1423.

Kanda, H., Yamaoka, S. and Setaka, N., 1977. Etching of diamond octahedrons by high pressure water. Journal of Crystal Growth, **38**, 1-7.

Katsura, T. and Ito, E. 1989. The system $Mg_2SiO_4 - Fe_2SiO_4$ at high pressures and temperatures. Precise determination of stabilities of olivine, modified spinel and spinel. Journal of Geophysical Research, **94**, 15,663-15,670.

Kearsey, P. and Vine, F.J. 1990. Global Tectonics, Blackwell Scientific, Oxford.

Kennedy, C.S. and Kennedy, G.C. 1976. The equilibrium boundary between graphite and diamond. Journal of Geophysical Research, **81**(14), 2467-2470.

Kesson, S.E. and Fitz Gerld, J.D. 1991. Partitioning of MgO, FeO, NiO, MnO and Cr_2O_3 between magnesian silicate perovskite and magnesiowustite: implications for the origin of inclusions in diamond and the composition of the lower mantle. Earth and Planetary Science Letters, **111**, 229-240.

Kesson, S.E., Fitz Gerald, J.D., O'Neill, H.St.C. and Shelley, J.M.G. 2002. Partitioning of iron between magnesian silicate perovskite and magnesiowustite at about 1 Mbar. Physics of the Earth and Planetary Interiors, **131**, 395-310.

Kesson, S.E., Fitz Gerald, J.D., Shelley, J.M.G. and Withers, R.L. 1995. Phase relations, structure and crystal chemistry of some aluminous silicate perovskites. Earth and Planetary Science Letters, **134**(1-2), 187-201.

Khachatryan, G.K., and Kaminsky, F.V. in print. 'Equilibrium' and 'non-equilibrium' diamond crystals from deposits in the East European Platform as revealed by infrared absorption data.

Klein, C. and Hurlbut, C.S. 1985. Manual of Mineralogy, John Wiley and Sons Inc.

Knittle, E. and Jeanloz, R. 1987. Synthesis and equation of state of $(Mg,Fe)SiO_3$ perovskite to over 100 gigapascals. Science, **235**, 668-670.

Koeberl, C., Masaitis, V.L., Shafranovsky, G.I., Gilmour, I., Langenhorst, F. and Schrauder, M. 1997. Diamonds from the Popigai impact structure, Russia. Geology, **25**, 697-970.

Koito, S., Akaogi, M., Kubota, O. and Suzuki, T. 2000. Calorimetric measurements of perovskites in the system $CaTiO_3$ -$CaSiO_3$ and experimental and calculated phase equilibria for high-pressure dissociation of diopside. Physics of the Earth and Planetary Interiors, **120**(1-2), 1-10.

Kopylova, M.G., Rickard, R.S., Kleyenstueber, A., Taylor, W.R., Gurney, J.J., and Daniels, L.R.M. 1997. First occurrence of strontium K-Cr Loparite and Cr-Chevkinite in diamonds. Russian Geology and Geophysics, **38**(2), 405-420.

Krajick, K. 2001. Barren Lands. Times Books, New York, U.S.A.

Kramers, J.D. 1979. Lead, uranium, strontium, potassium and rubidium in inclusion-bearing diamond and mantle-derived xenoliths from southern Africa. Earth and Planetary Science Letters, **42**, 58-70.

Kretz, R., 1983. Symbols for rock-forming minerals. American Mineralogist, **68**(1-2), 277-279.

Lang, A.R. 1964. A proposed structure for nitrogen impurity platelets found in diamond. Proceedings of the Royal Society of London, **84**, 871-876.

Lang, A.R. 1974b. Space-filling by branching columnar single-crystal growth: an example from crystallization of diamond. Journal of Crystal Growth, **23**, 151-153.

Lang, A.R. 1974a. On the growth-sectorial dependence of defects in natural diamonds. Proceedings of the Royal Society of London, **340A**, 233-248.

Lang, A.R. and Moore, M. 1972. On the internal structure of natural diamonds of cubic habit. Philosophy Magazine, **26**, 1313-1325.

Lang, A.R., Moore, M. and Walmsley, J.C. 1992. Diffraction and imaging studies of diamond. *In*: J.E. Field (ed.), The properties of natural and synthetic diamond. Academic Press, 215-258.

Larson, R.L. 1991. Geological consequences of superplumes. Geology, **19**, 963-966.

Lui, L-G. 1975. Post-oxide phases of forsterite and enstatite. Geophysical Research Letters, **2**(10), 417, 419.

Lui, L.-G. 1977. The system enstatite-pyrope at high pressures and temperatures and the mineralogy of the Earth's mantle. Earth and Planetary Science Letters, **41**, 398-404.

Luth, R.W. 1993. Diamond, eclogites, and the oxidation-state of the Earth's mantle. Science, **261**, 66-68.

McCallum, M.E., Huntley, P.M., Falk, R.W., and Otter, M.L. 1994. Morphological, resorption and etch feature trends of diamonds from kimberlite populations within Colorodo-Wyoming State Line District, USA. *In*: H.O.A Meyer and O.H. Leonardos, (eds.). Diamonds: Characterisation, Genesis and Exploration. GPRM Spec. Publ. No 1/B, CPRM, Brasilia: 32-50.

McCammon, C.A., Rubie, D.C., Ross, C.R. II, Seifert, F. and O'Neill, H. St. C. 1992. Moessbauer spectra of $^{57}Fe_{0.05}Mg_{0.95}SiO_3$ perovskite at 80 and 298 K. American Mineralogist, **77**, 894-897.

McCammon, C., Hutchison, M.T. and Harris, J.W. 1997. Oxidation of mineral inclusions in diamonds form Sao Luiz: A view into the lower mantle. Science, **278**, 434-436.

McDade, P. and Harris, J.W. 1999. Syngenetic inclusion bearing diamonds from Letseng-la-Terai, Lesotho, *In*: Gurney, J.J., Gurney, J.L., Pascoe, M.D. and Richardson, S.H. (eds.). Proceedings of the 7th International Kimberlite Conference, **2**, 557-565.

McKenna, N., 2001. A study of the diamonds, diamond inclusion minerals and other mantle minerals from the Swartruggens kimberlite, South Africa. Unpublished MSc. thesis, University of Cape Town.

Mendelssohn, M.J. and Milledge, H.J. 1995. Geologically significant information from routine analysis of the mid-infrared spectra of diamonds. International Geology Review, **37**, 95-110.

Meyer, H.O.A. 1987. Inclusions in diamonds. *In*: P. Nixon (ed.), Mantle Xenoliths, Wiley Winchester, 501-522.

Meyer, H.O.A. and McCallum, M.E. 1986. Mineral inclusions in diamonds from the Sloan kimberlites, Colorado. Journal of Geology, **94**(4), 600-612.

Meyer, H.O.A., Milledge, H.J., Sutherland, F.L. and Kennewell, P. 1997. Unusual diamonds and unique inclusions from New South Wales, Australia, Proceedings of the 6th international kimberlite conference; Volume 2, Diamonds; characterization, genesis, and exploration, Russian Geology and Geophysics, **38**(2), 305-331, 1997

Milledge, H.J., Mendelssohn, M.J., Boyd, S.R., Pillinger, C.T., and Seal, M. 1989. Infrared topography and carbon and nitrogen isotope distribution in natural and synthetic diamonds in relation to mantle processes. *In*: F.R. Boyd, H.O.A. Meyer, and N.V. Sobolev (eds.), Extended abstracts; Workshop on Diamonds, Geophysics Laboratory, Washington, DC, USA.

Mining Journal, London, Aug 23, 2003

Mitchell, R.H. 1995. Petrology of Kimberlites, Orangeites and Related Rocks Plenum Publishing Company, New York, 410 pages.

Mitchell, R.H. and Reed, S.J. 1988. Ion microprobe determination of rare earth elements in perovskite from kimberlites and alnoites. Mineralogical Magazine, **52**, 331-339.

Moore, M. and Lang, A.R. 1974. On the origin of the rounded dodecahedral habit of natural diamond. Journal of Crystal Growth, **26**, 133-139.

Moore, M., and Lang, A.R. 1972. On the internal structure of natural diamonds of cubic habit. Philosophical Magazine, **26**, 1313-1325.

Navon, O., Hutcheon, I.D., Rossman, G.R. and Wassweburg, G.J. 1988. Mantle-derived fluids in diamond micro-inclusions. Nature, **335**, 784-789.

Nesse, W.D. 1991. Introduction to optical mineralogy. Oxford University Press, New York.

Orlov, Y.L. 1977. Mineralogy of the Diamonds. New York, Izdatel'stva Nauka, John Wiley and Sons.

Otter, M.L. and Gurney, J.J. 1989. Mineral inclusions in diamonds from the Sloan diatremes of Colorado-Wyoming State line kimberlite district, North America. Kimberlite and Related Rocks, Vol. 2. Geological Society of Australia Special Publication No. 14: 1042-1053.

Pattison, D. R. M. and Levinson, A.A. 1995. Are euhedral microdiamonds formed during ascent and decompression of kimberlite magma: Implications for use of microdiamonds in diamond grade estimation. Applied Geochemisty, **10**, 725-738.

Pearson, D.G., Canil, D. and Shirey, S.B. in print. Chapter 7: Mantle samples included in volcanic rocks: xenoliths and diamonds. In: Carlson, R. (ed.), Volume 2, Treatise of Geochemistry, Elsevier Publishing, 191 pages.

Pearson, D.G., Shirey, S.B., Bulanova, G.P., Carlson, R.W. and Milledge, H.J. 1999. Dating and paragenetic distinction of diamonds using the Re-Os isotope system; application to some Siberian diamonds, In: Gurney, J.J., Gurney, J.L., Pascoe, M.D. and Richardson, S.H. (eds.). Proceedings of the 7th International Kimberlite Conference, 2, 637-643.

Phaal, C. 1965. Surface studies of diamond. Industrial Diamond Review, 25, 486-489 and 591-595.

Richardson, S.H., Erlank, A.J., Harris, J.H. and Hart, S.R. 1990. Eclogitic diamonds of Proterozoic age from Cretaceous kimberlites. Nature, 346, 54-56.

Ringwood, A.E. 1967. The pyroxene-garnet transformation in the Earth's mantle. Earth and Planetary Science Letters, 2, 255-263.

Ringwood, A.E. 1991. Inaugural ingerson lecture. Geochemica et Cosmochimica Acta, 55, 2083-2110.

Robertson, R., Fox, J.J. and Martin, A.E. 1934. Two types of diamond. Philosophical Transactions of the Royal Society of London, A232, 463.

Robinson, D.N. 1978. The characteristics of natural diamond and their interpretation. Minerals Science and Engineering, 10(2), 55-72.

Robinson, D.N. 1979. Surface textures and other features of diamonds. Unpublished PhD thesis, University of Cape Town.

Robinson, D.N., Scott, J.A., Van Niekerk, A., and Anderson, V.G. 1989. The sequence of events reflected in the diamonds of some southern African kimberlites. Kimberlite and Related Rocks, Vol. 2. Geological Society of Australia Special Publication No. 14: 990-1000.

Ryan, C.G., Griffin, W.L. and Pearson, N.J. 1996. Garnet geotherms: a technique for derivation of P-T data from Cr-pyrope garnets. Journal of Geophysical Research, 101, 5611-5625.

Schobbenhaus, C., and Campos, D. de A. 1984. A evolucao da plataforma Sul-Americana no Brasil e suas principais concentracoes minerais. In: C. Schobbenhaus, D. de A.

Campos, G.R. Derza, and H.E. Asmus (eds.), Geologia do Brasil, Departamentao Nacional da Producao Mineral, Brasilia, 9-53.

Schrauder, M. and Navon, O.D. 1993. Solid carbon dioxide in a natural diamond. Nature, **365**, 42-44.

Scott-Smith, B.H., Danchin, R.V., Harris, J.W., and Stracke, K.J. 1984. Kimberlites near Orroroo, South Australia. *In*: J. Kornprobst (ed.), Kimberlites I: kimberlites and related rocks. Elsivier, Amsterdam, 121-142.

Seal, M. 1963. The growth history of natural diamonds as revealed by etching experiments. American Mineralogist, **50**, 105-123.

Seal, M. 1965. Structure in diamonds as revealed by etching. American Mineralogist, **50**, 105-131.

Sellschop, J.P.F. 1992. Nuclear probes in the study of diamond. *In*: J.E. Field (ed.), The properties of natural and synthetic diamond. Academic Press: 81-179.

Sharp, T.G., Lingemann, C.M., Dupas, C. and Stoffler, D. 1997. Natural occurrence of $MgSiO_3$-ilmenite and evidence for $MgSiO_3$-perovskite in a shocked L chondrite. Science, **277**, 352-355.

Shigley, J.E., Fritsch, E., Stockton, C.M., Koivula, J.I., Frwyer, C.W., and Kane, R.E. 1986. The gemological properties of the Sumitomo gem-quality synthetic yellow diamonds. Gems and Gemmology, **22**, 192-208

Smith, B.C. 1996. Fundamentals of Fourier transform infrared spectroscopy. Boca Raton pp. 202.

Sobolev, N.V. 1983. Parageneses of the diamonds and the problem of mineral formation in deep seated conditions. Zapiski Vsesoyuznogo Mineralogicheskogo Obshchestva, **112**, 389-397.

Sobolev, N.V. 1984. Kimberlites of the Siberian Platform: their geological and mineralogical features. *In*: J.E. Glover and P.G. Harris (eds.), Kimberlite Occurrence and Origin: a basis for conceptual models in exploration. Geology Department and University Extension, University of Western Australia, Publication No. 8, 275-287.

Sobolev, N.V., Botkunov, A.I., Lavrent'yev, Y.G. and Usova, L.V. 1976. New data on mineral compositions coexisting with diamond in the Mir kimberlite pipe. Geologiya i Geofizika, No.12, 3-15.

Sobolev, N.V., Snyder, G.A., Yefimova, E.S. and Taylor, L.A. 1999. Significance of eclogitic and related parageneses of natural diamonds. International Geology Review, **41**, 129-140.

Sobolev, N.V., Yefimova, E.S., Channer, D.M.D., Anderson, P.F.N. and Barron, K.M. 1998. Unusual upper mantle beneath Guaniamo, Guyana Shield, Venezuela; evidence from diamond inclusions. Geology, **26**(11), 971-974.

Sobolev, N.V., Yefimova, E.S., Lavrent'yev, Y.G. and Sobolev, V.S. 1984. Dominant calcsilicate assemblage of crystalline inclusions in diamonds from alluvial deposits of southeastern Australia. Doklady Akademii Nauk SSSR, **274**(6), 130-135 (in Russian).

Sobolev, N.V., Yefimova, E.S. and Pospelova, L.N. 1981. Native iron in Yakutian diamonds and its paragenesis. Geologika I Geofizica, **12**, 25-29.

Stachel, T. 2001. Diamonds from the asthenosphere and the transition zone. European Journal of Mineralogy, **13**, 883-892.

Stachel, T., Brey, G.P., and Harris, J.H. 2000a. Kankan diamonds (Guinea) I: from the lithosphere down to the transition zone. Contributions to Mineralogy and Petrology, **140**, 1-15.

Stachel, T., Harris, J.H., Aulbauch, S. and Deines, P. 2002. Kankan diamonds (Guinea) III: $\delta^{13}C$ and nitrogen characteristics of deep diamonds. Contributions to Mineralogy and Petrology, **142**, 465-475.

Stachel, T., Harris, J.W. and Brey, G.P. 1998. Rare and unusual mineral inclusions in diamonds from Mwadui, Tanzania. Contributions to Mineralogy and Petrology, **132**, 34-47.

Stachel, T., Harris, J.H., Brey, G.P., and Joswig, W. 2000b. Kankan diamonds (Guinea) II: lower mantle inclusion parageneses. Contributions to Mineralogy and Petrology, **140**, 16-27.

Sunagawa, I. 1984a. Growth of crystals in nature. *In*: I. Sunagawa (ed.). Mineral Science of the Earth's Interior, Tokyo, Terra Scientific Publishing Company, 63-105.

Sunagawa, I. 1984b. Morphology of natural and synthetic diamond. *In*: I. Sunagawa (ed.). Mineral Science of the Earth's Interior, Tokyo, Terra Scientific Publishing Company, 303-330.

Sunagawa, I., Tsukamoto, K. and Yasuda, T. 1984. Surface microtopographic and x-ray topographic study octahedral crystal of natural diamond from Siberia. In: I.

Sunagawa (ed.). Mineral Science of the Earth's Interior, Tokyo, Terra Scientific Publishing Company, 331-349.

Svisero, D.P. 1995. Distribution and origin of diamonds in Brazil; an overview. Journal of Geodynamics, **20**(4), 493-514.

Tassinari, C.C.G, Macambira, M.J.B. 1999. Geochronological provinces of the Amazonian craton. Episodes, **22**(3), 174-182.

Taylor, W.R., Canil, D. and Milledge, H.J. (1996). Kinetics of Ib to IaA nitrogen aggregation in diamond. Geochemica et Cosmochimica Acta, **60**, 4725-4733.

Taylor, W.R., Jaques, A.L., and Ridd, M. 1990. Nitrogen-defect aggregation characteristics of some Australasian diamonds: Time-temperature constraints on the source regions of pipe and alluvial diamonds. American Mineralogist, **75**, 1290-1320.

Tolansky, S. 1955. The Microstructure of Diamond Surfaces. N.A.G. Press, London.

Tolansky, S. 1966. Birefringence of diamond. Nature, **211**(5045), 158-160.

Tompkins, L.A. 1992. Tectono-structural environments of primary diamond source rocks in Brazil: A review. Diamonds: Characterization, Genesis and Exploration. 259-267.

Ulmer, P. and Stadler, R. 2001. The $Mg(Fe)SiO_3$ orthoenstatite-clinoenstatite transitions at high pressures and temperatures determined by Raman-spectroscopy on quenched samples. American Mineralogist, **86**, 1267-1274.

Tompkins, L.A. 1992. Kimberlite structural environments and diamond productivity of Brasil. Russian Geology and Geophysics, **33**(10), 91-98.

Urusovskaya, A.A and Orlov, Y.L. 1964. Nature of plastic deformation of diamond crystals. Doklady Akademii Nauk USSR, **154**, 112-115.

Vance, E.R. and Milledge, H.J. 1972. Natural and laboratory alpha -particle irradiation of diamond. Mineralogical Magazine and Journal of the Mineralogical Society, **38** (299), 878-881.

Wang, Y., Guyot, F. and Liebermann, R.C. 1992. Electron microscopy of $(Mg,Fe)SiO_3$ perovskite; evidence for structural phase transitions and implications for the lower mantle. Journal of Geophysical Research, B, Solid Earth and Planets, **97**, 12,327-12,347.

Welbourn, C.M., Rooney, M., and Evans, D.J.F. 1989. A study of diamonds of cube and cube-related shape from the Jwaneng Mine. Journal of Crystal Growth, **94**, 229-252.

Wilding, M.C. 1990. Untitled, Unpublished PhD Thesis, University of Edinburgh.

Wilding, M.C., Harte, B., and Harris, J.W. 1991. Evidence for a deep origin for Sao Luiz diamonds. Proceedings 5th International Kimberlite Conference Extended Abstracts, 456-458.

Winter, J.D. 2001. An Introduction to Igneous and Metamorphic Petrology. Prentice-Hall Inc., New Jersey, USA.

Wood, B.J. 2000. Phase transformations and partitioning relations in peridotite under lower mantle conditions. Earth and Planetary Science Letters, **174**(3-4), 341-354.

Woodland, A.B. and Koch, M. 2003. Variation in oxygen fugacity with depth in the upper mantle beneath the Kapvaal craton, Southern Africa. Earth and Planetary Science Letters, **6760**, 1-16.

Woods, G.S. 1986. Platelets and the infrared absorption of type Ia diamonds. Proceedings of the Royal Society of London, **A407**, 219-238.

Woods, G.S., and Collins, A.T. 1983. Infrared-absorption spectra of hydrogen complexes in Type I diamonds. Journal of Physical and Chemistry of Solids, **44**, 471-475.

Woods, G.S., Purser, G.C., Mtimkulu, A.S.S. and Collins, A.T. 1990. The nitrogen content of Type Ia natural diamonds. Journal of Physical and Chemistry of Solids, **51**, 1191-1197.

Yamazaki, A. and Hirahara, K. 1994. The thickness of upper mantle discontinuities, as inferred from short-period J-Array data, Geophysical Research Letters, **21**(17), 1811-1814.

Yardley, B.W.D. 1991. *In*: An introduction to Metamorphic Petrology. Longman Scientific and Technical, 248 pages.

Zezin, R.B., Saparin, G.V., Smirnova, E.P., Obyden, S.K. and Chukichev, M.V. 1990. Cathodoluminescence of natural diamonds from Jakutian deposits, Scanning, **12**, 326-333.

Appendix A – Images of diamond body colour, fluorescence and cathodoluminescence

Photos for diamond colour and diamond fluorescence (FL) have been collected for all rough diamonds. Cathodoluminescence (CL) images have been collected for 47 rough diamonds and 13 cut diamonds (denoted by '*'). Photographs for diamond colour and FL were collected following the procedures outlines in sections 3.2 and 4.2 respectively, and CL images were collected following the procedures outlined in section 5.2 (for rough diamonds) and 7.2 (for cut diamonds).

Diamond colour   Fluorescence   Cathodoluminescence

Diamond 1.1
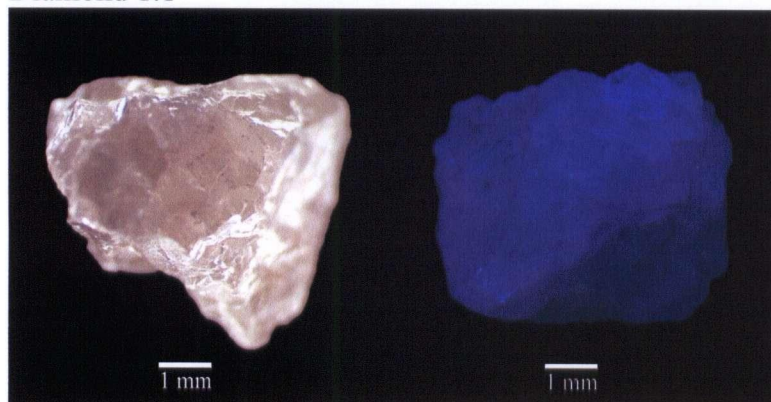
Diamond 1.2*
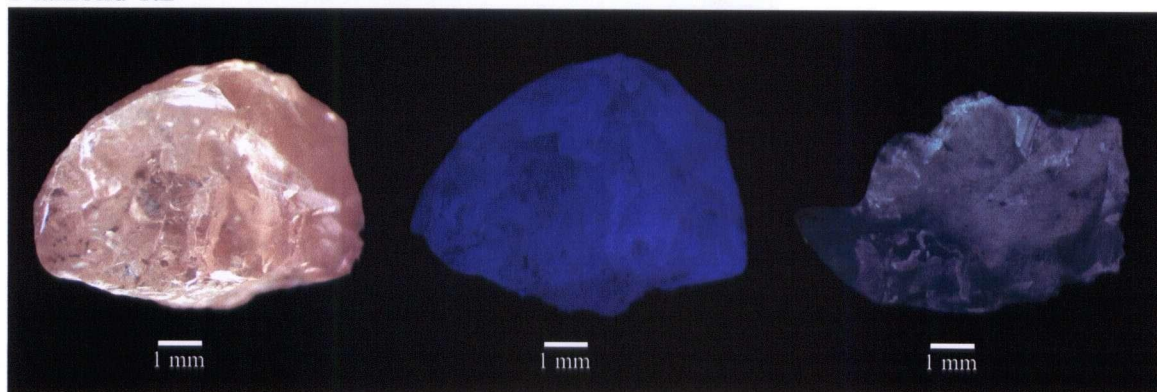
Diamond 1.3
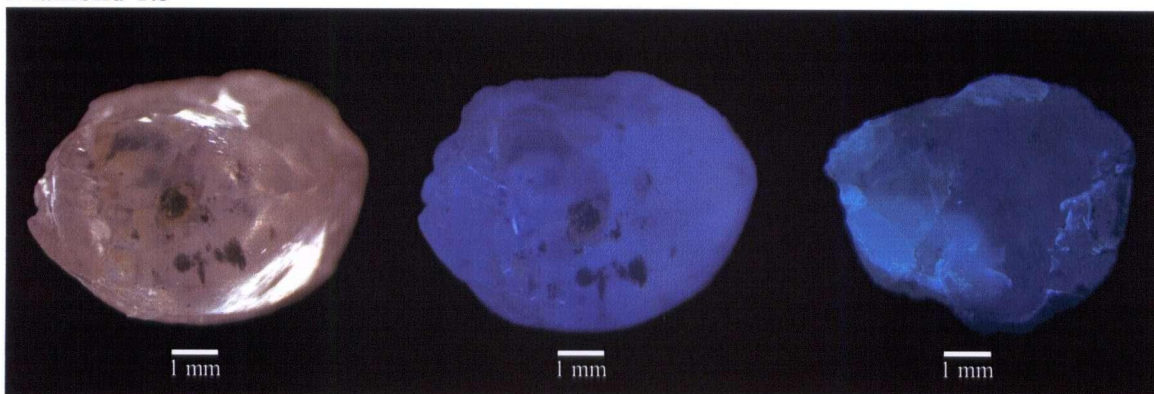
Diamond 1.4*
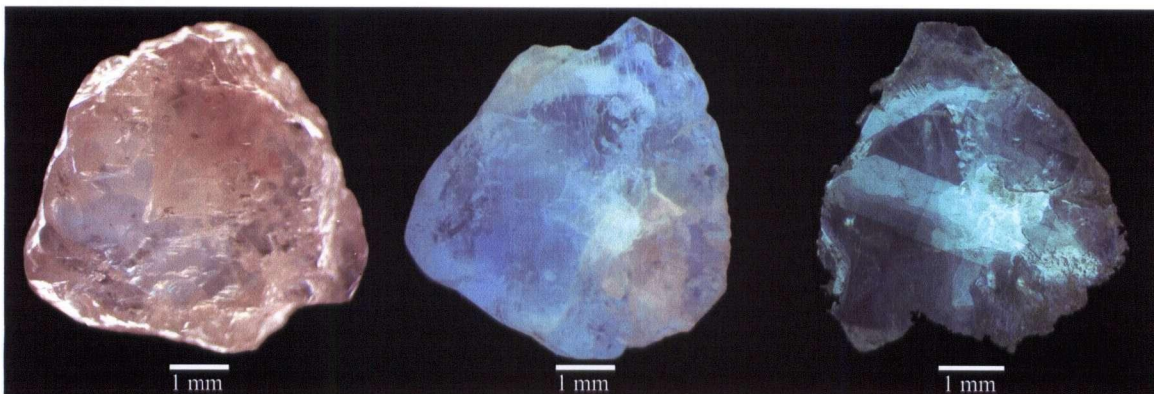
Diamond 1.5
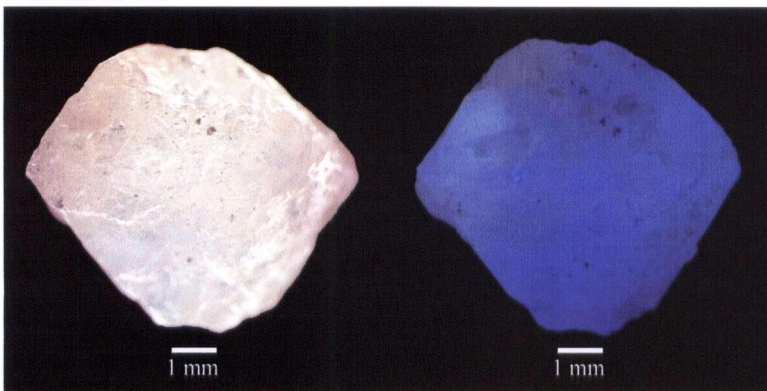
Diamond 2.1*
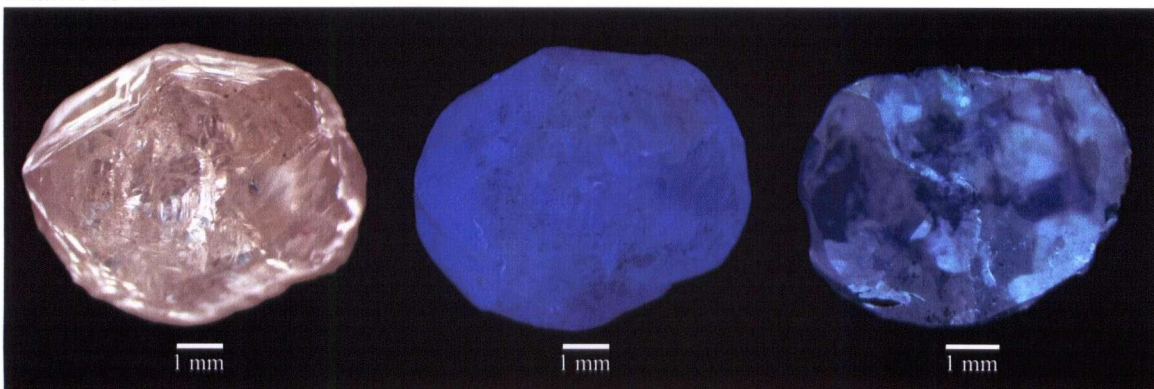
Diamond 2.2*
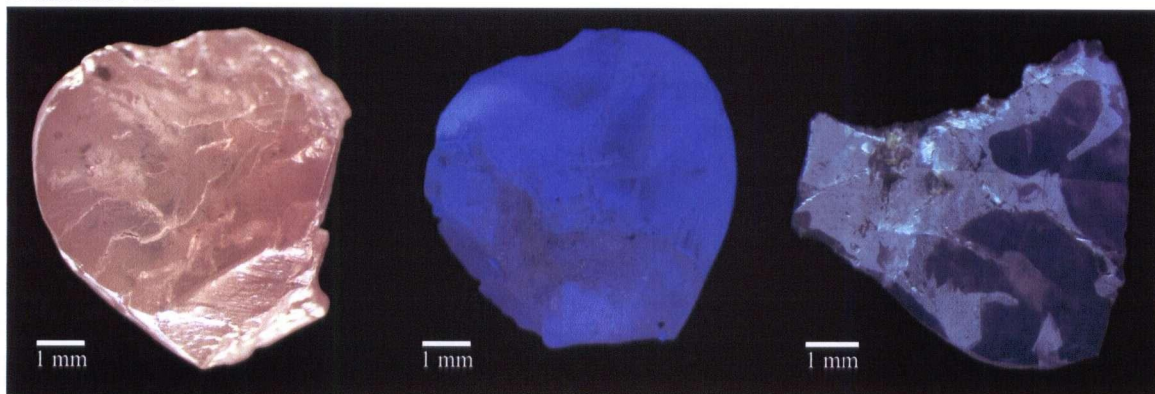
Diamond 2.3
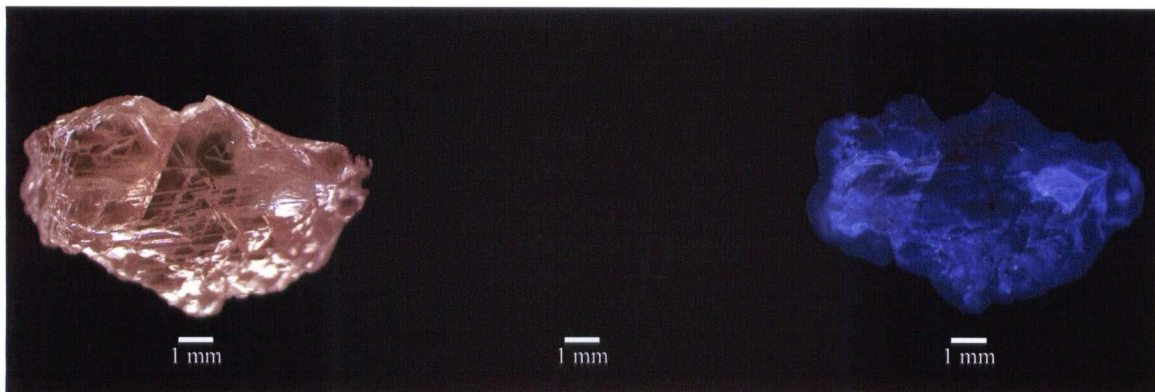
Diamond 2.4
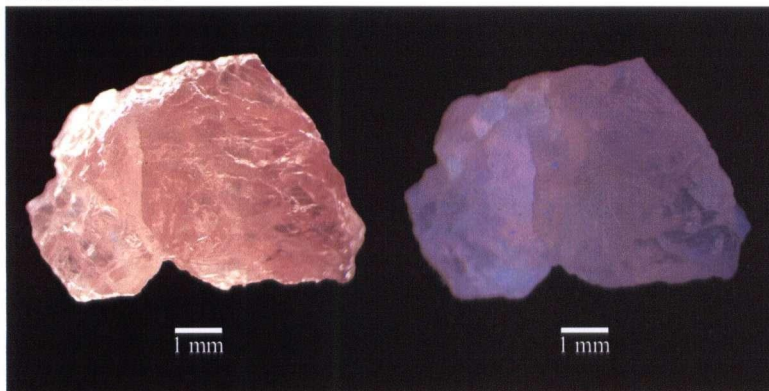
Diamond 2.5*
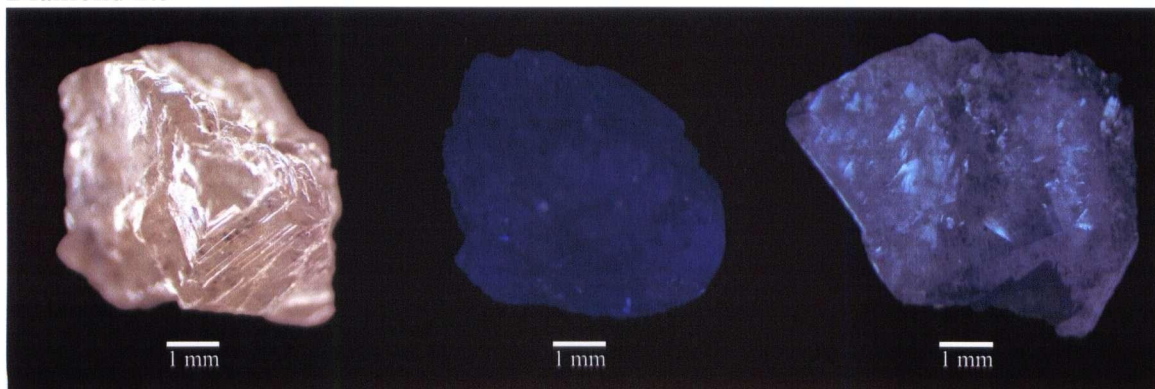
Diamond 2.6
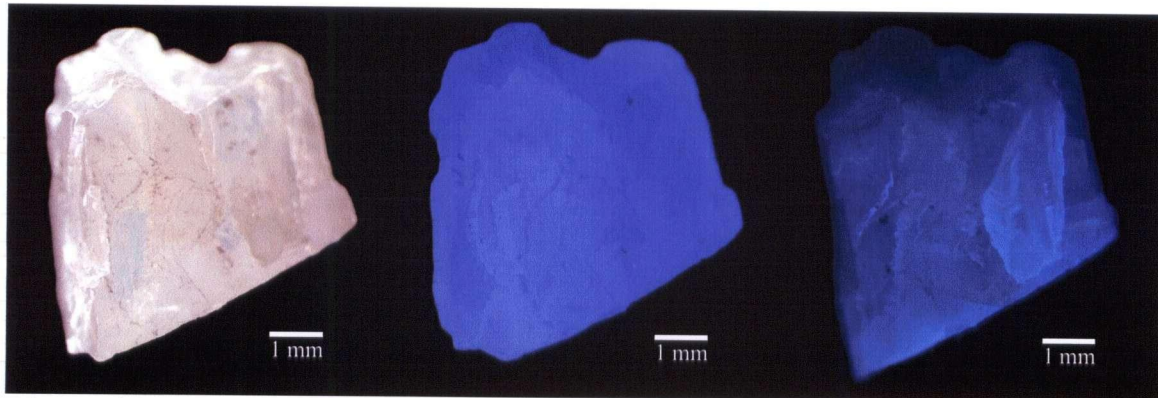
Diamond 2.7
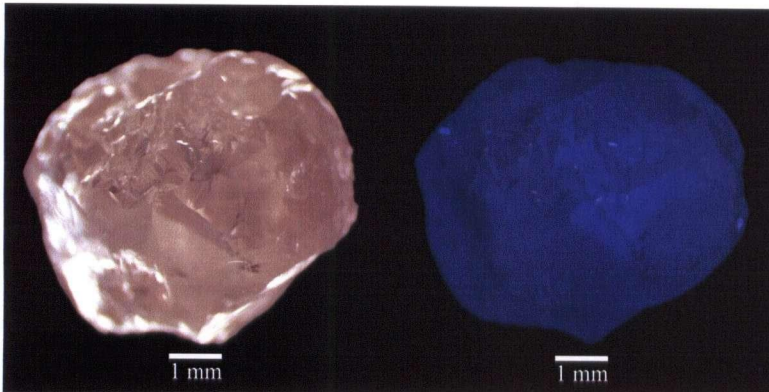
Diamond 2.8*

Diamond 2.9*

271
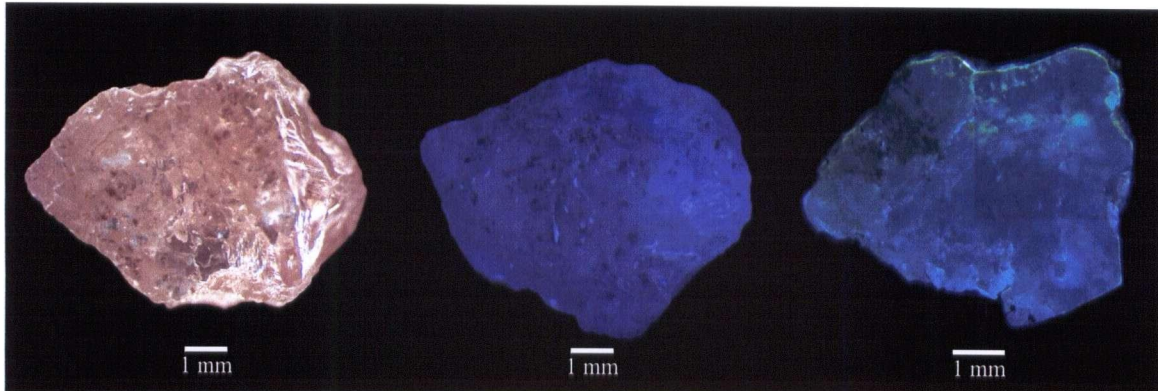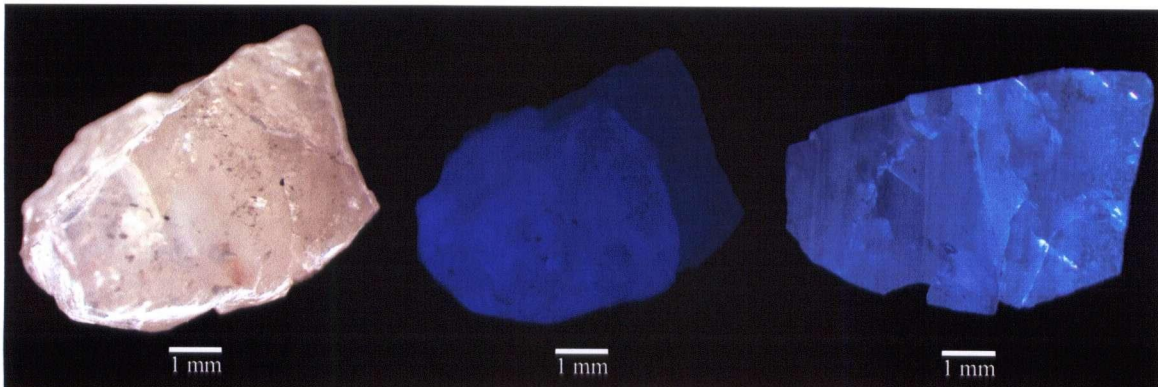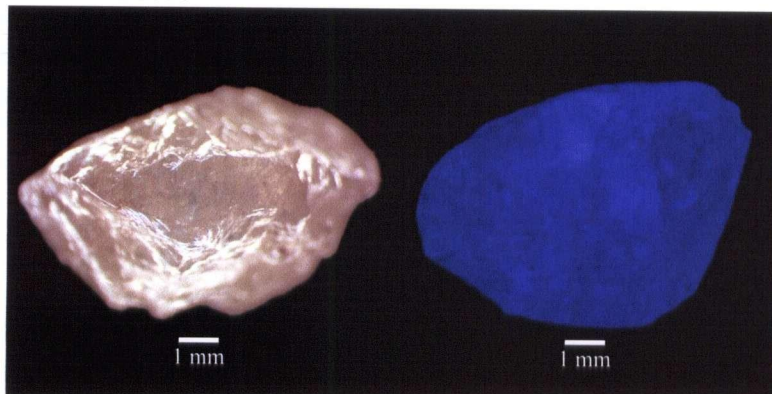
Diamond 2.10

Diamond 2.11*
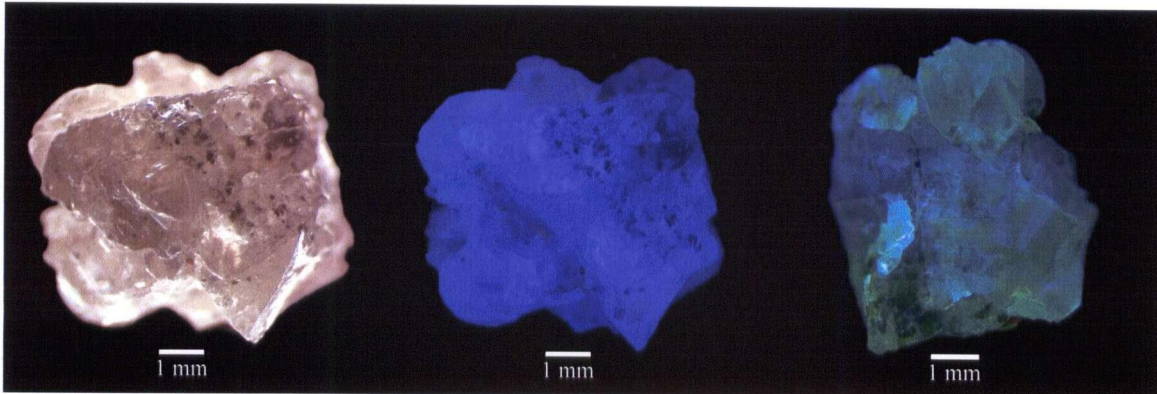
Diamond 3.1*

Diamond 3.2

272
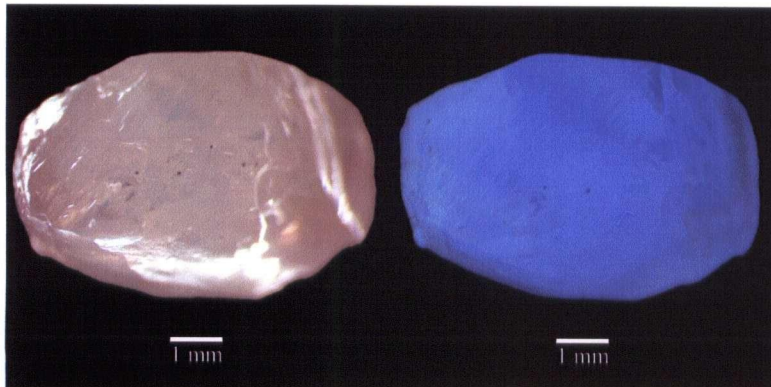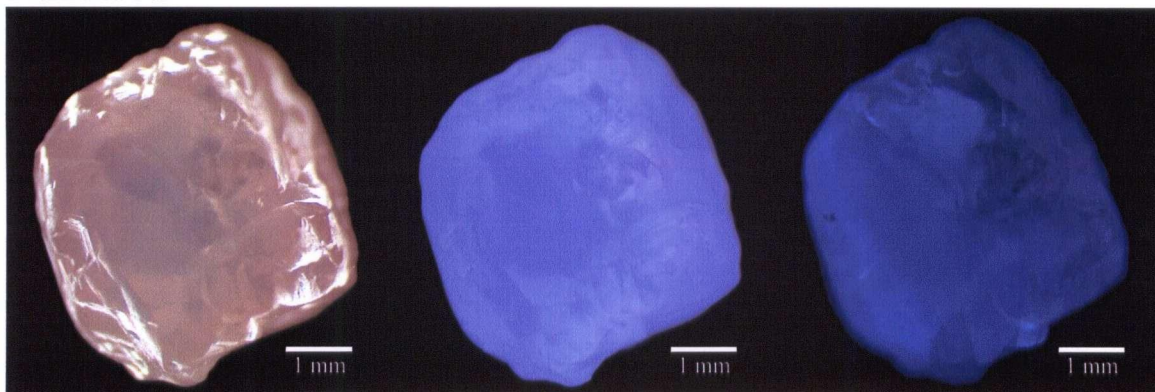
Diamond 3.3

Diamond 3.4
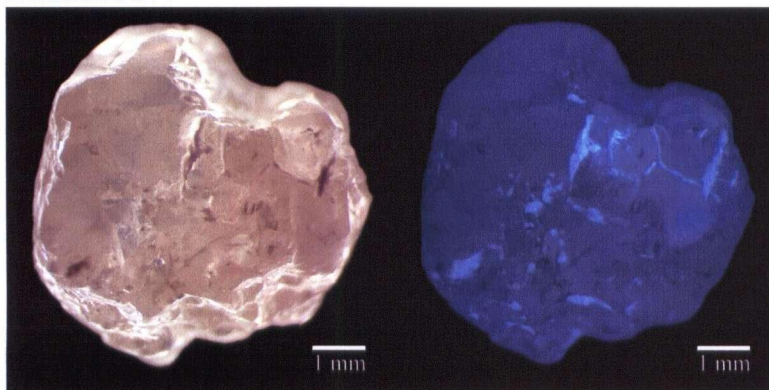
Diamond 3.5*
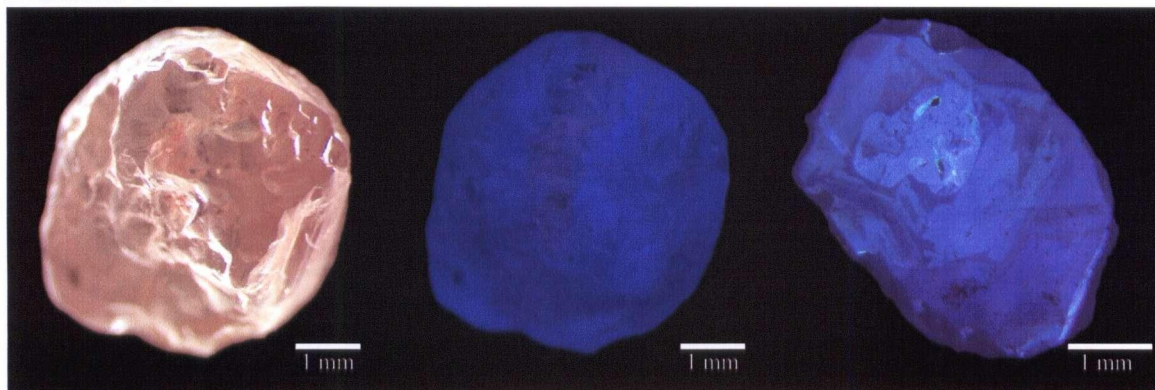
Diamond 3.6
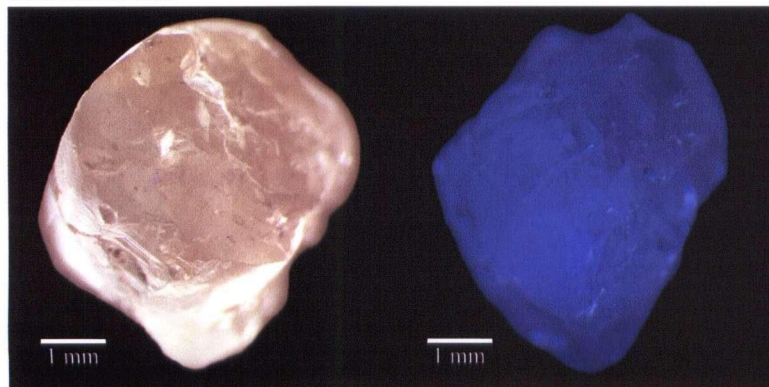
Diamond 3.7
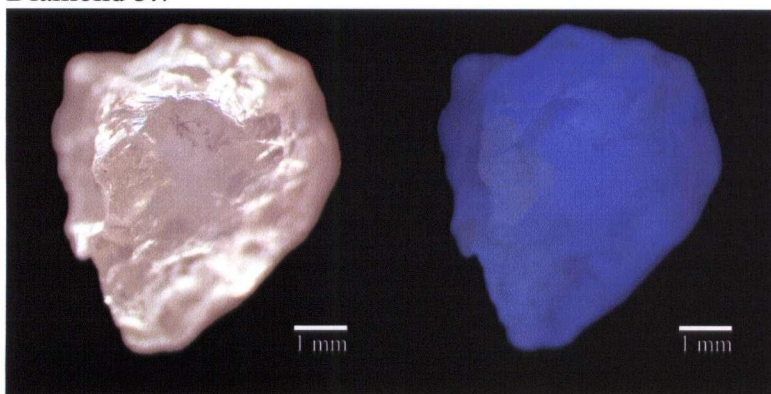
Diamond 3.8*
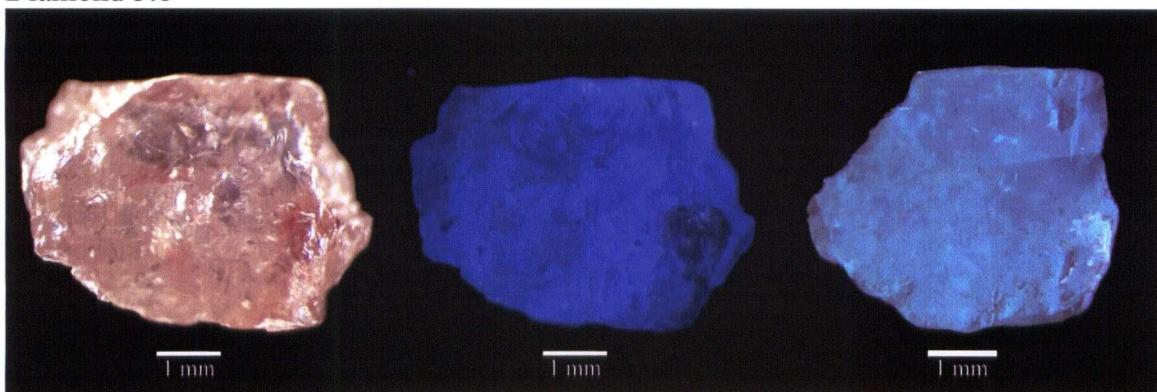
Diamond 3.9

Diamond 3.10*

274
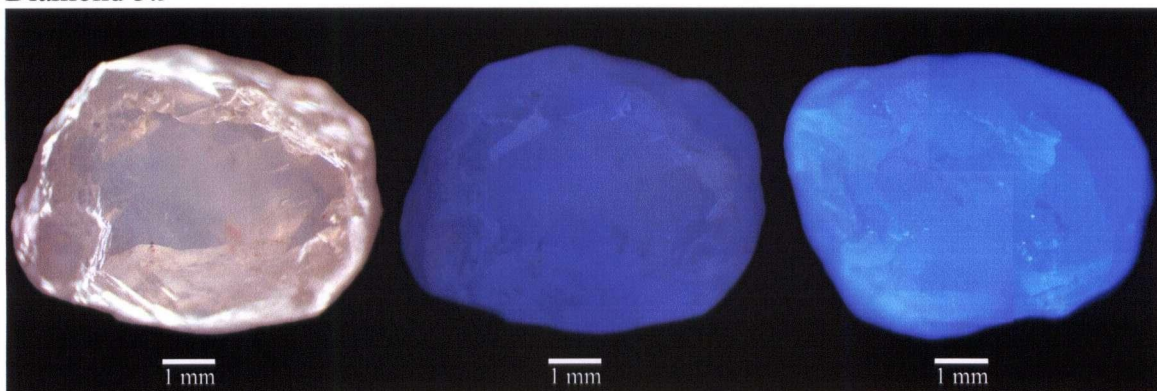
Diamond 3.11*
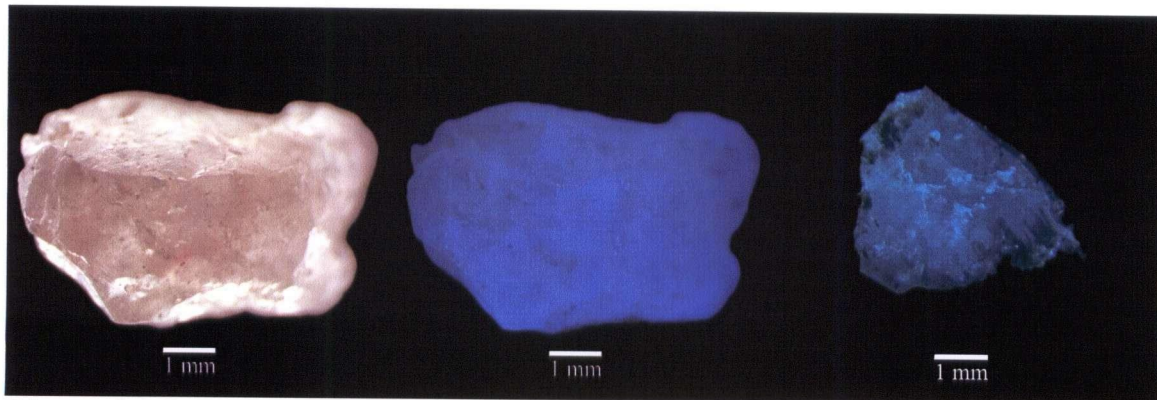
Diamond 4.1
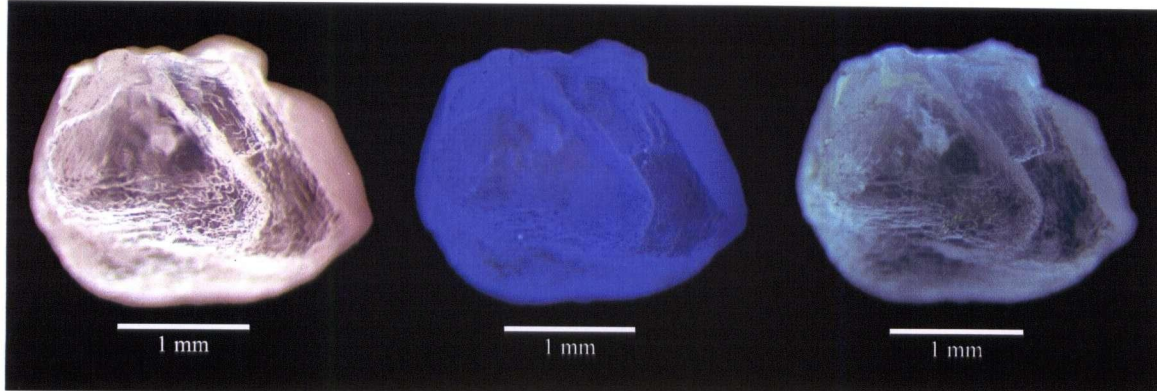
Diamond 4.3
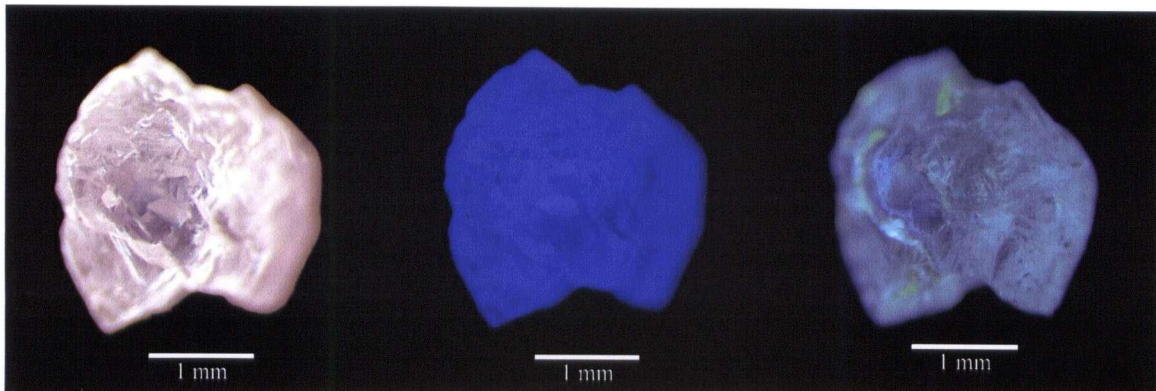
Diamond 4.4
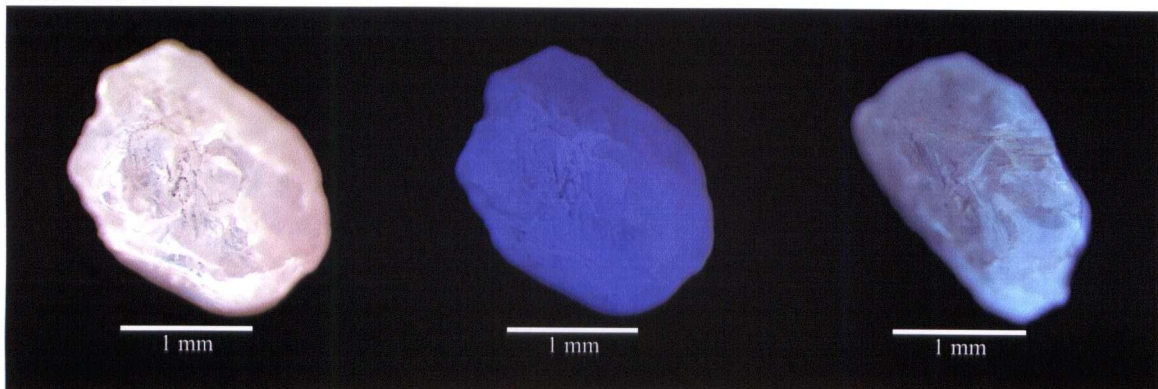
Diamond 4.5
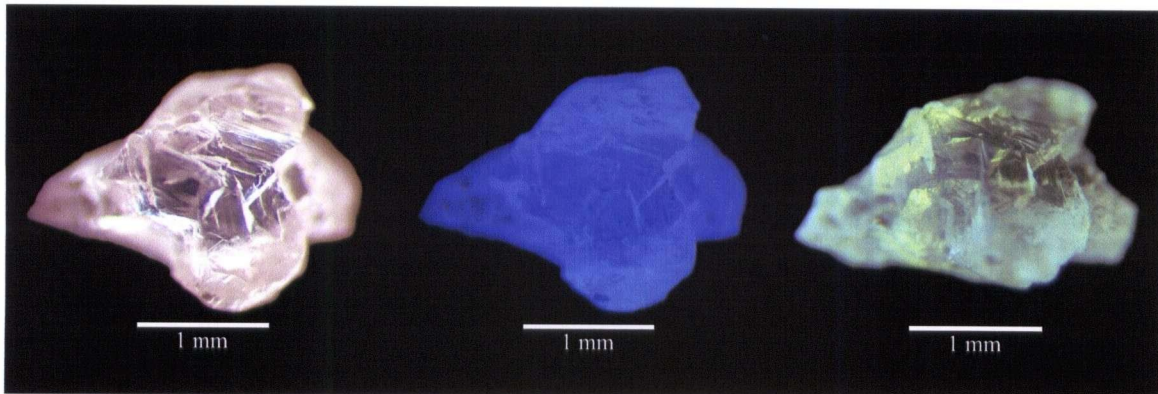
Diamond 4.6
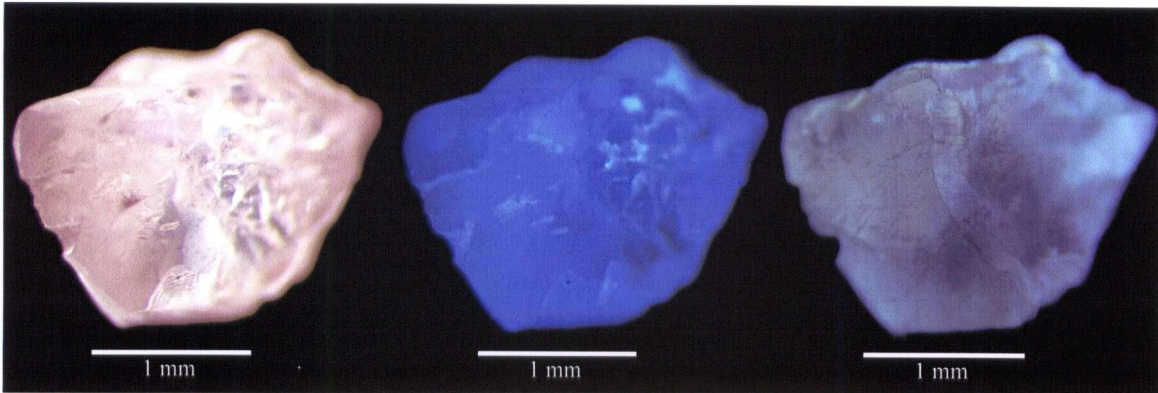
Diamond 4.7
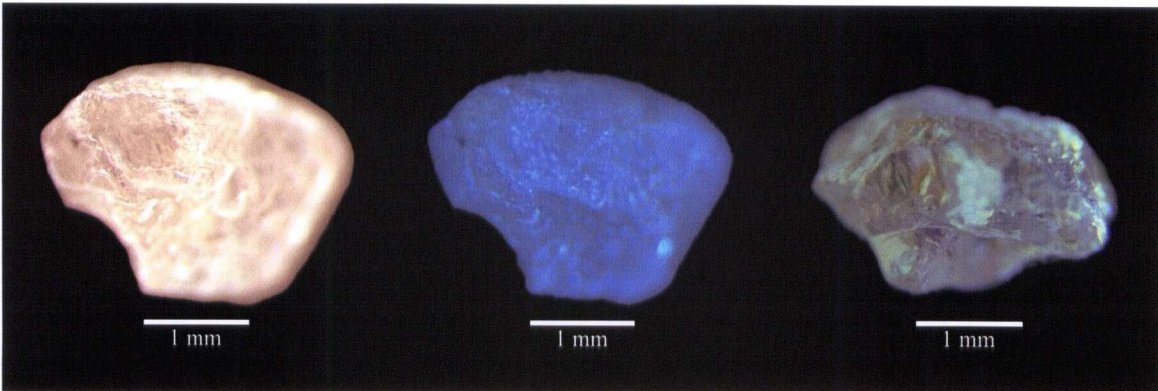
Diamond 4.8
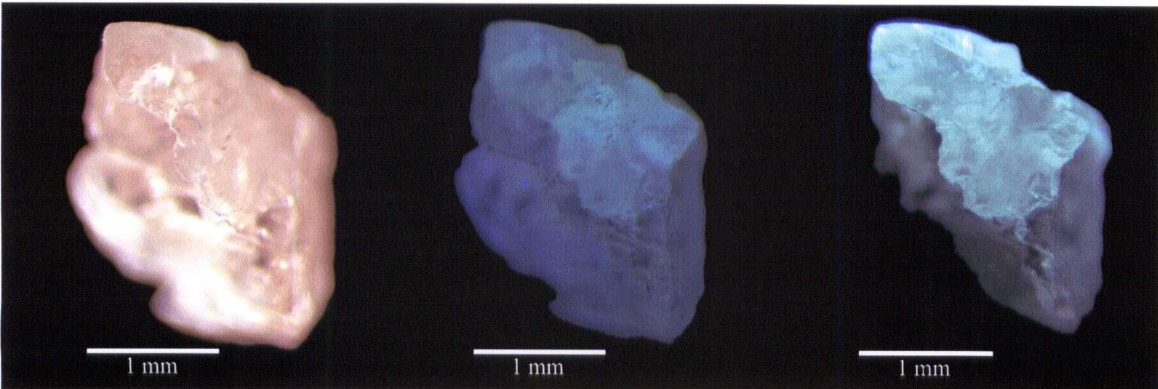
Diamond 4.9
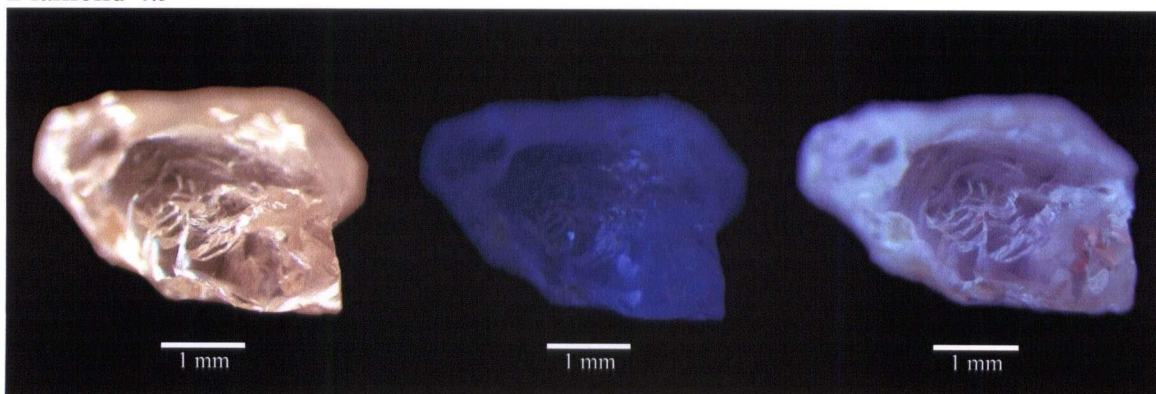
Diamond 4.10
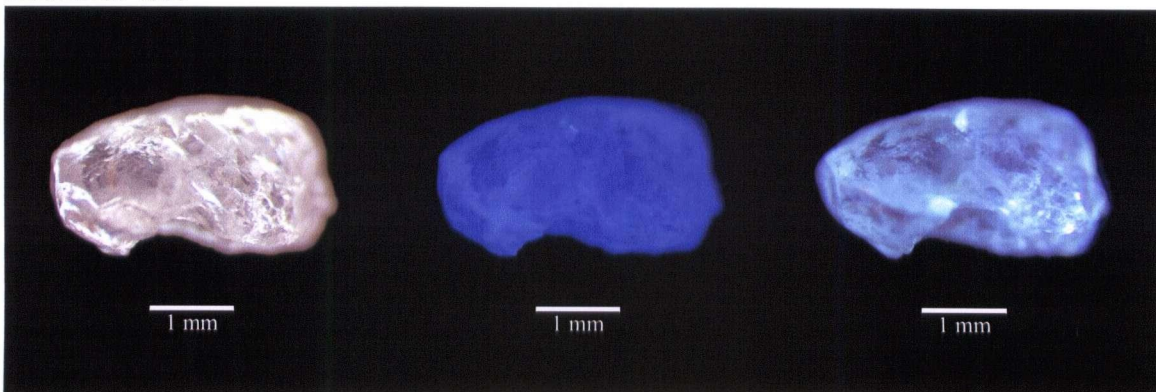
Diamond 4.11
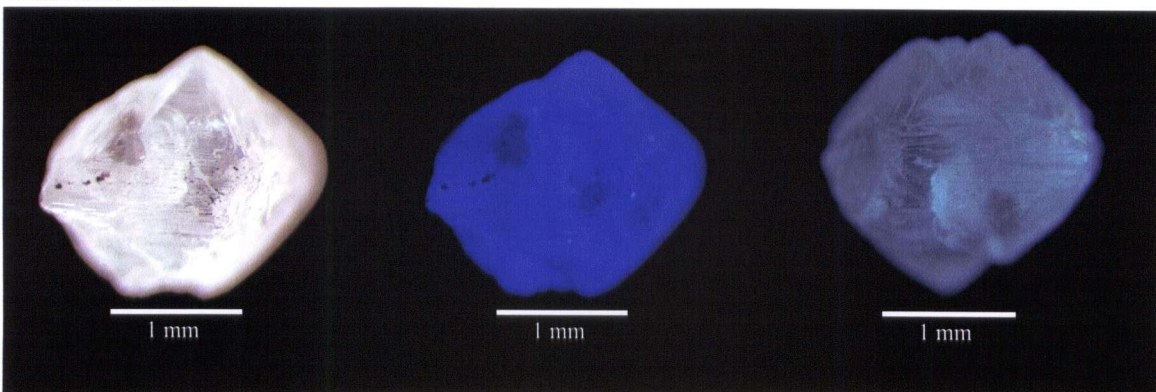
Diamond 4.12
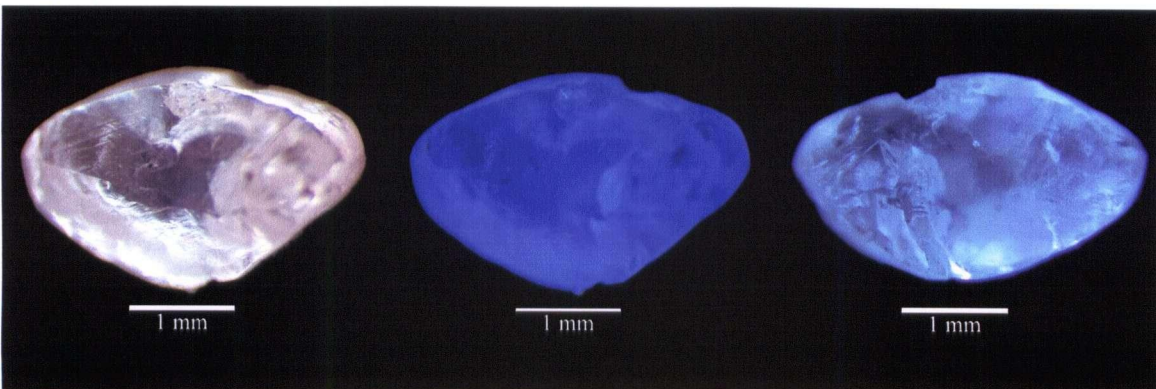
Diamond 4.13
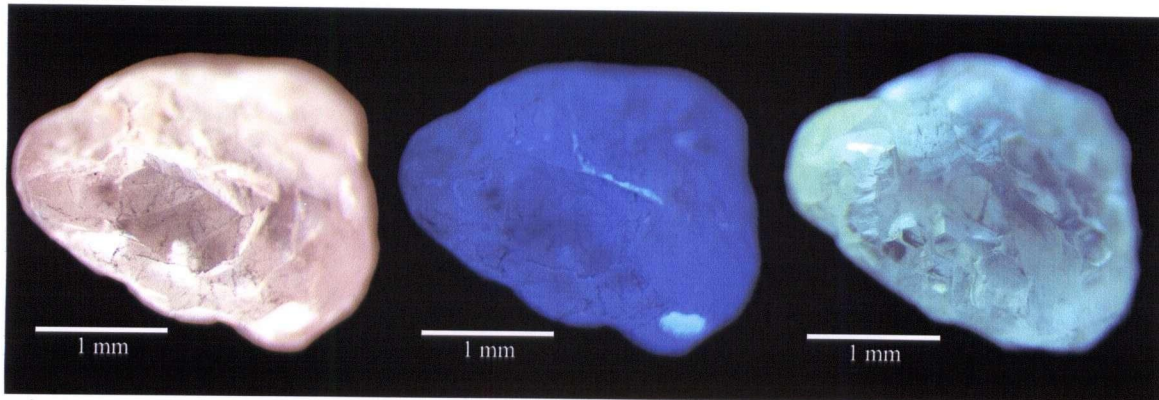
Diamond 4.14

Diamond 4.15

Diamond 4.16

278

Diamond 4.17*

1 mm   1 mm   1 mm

Diamond 4.18

1 mm   1 mm   1 mm

Diamond 4.19

1 mm   1 mm   1 mm

Diamond 4.21

1 mm   1 mm   1 mm
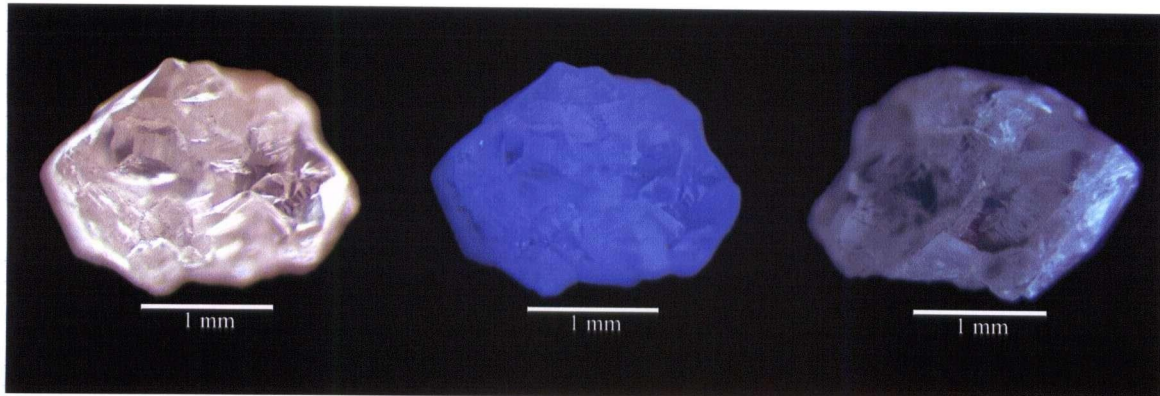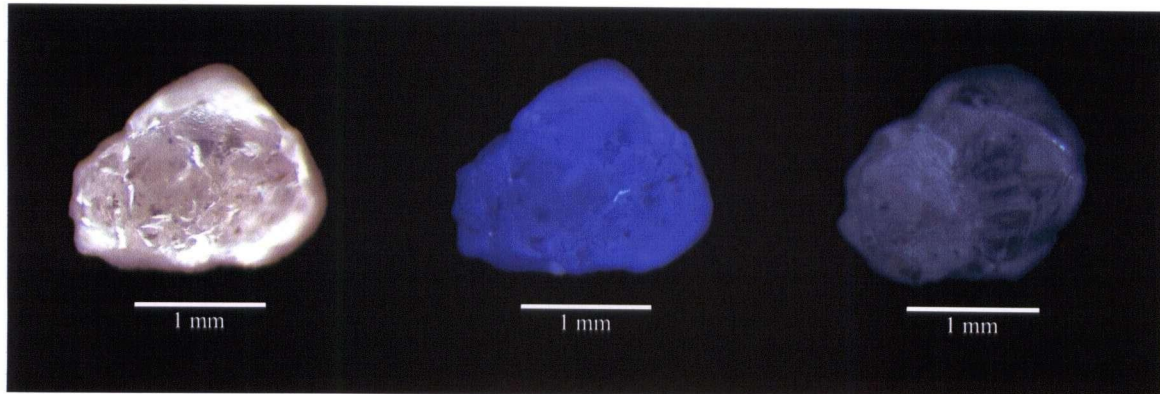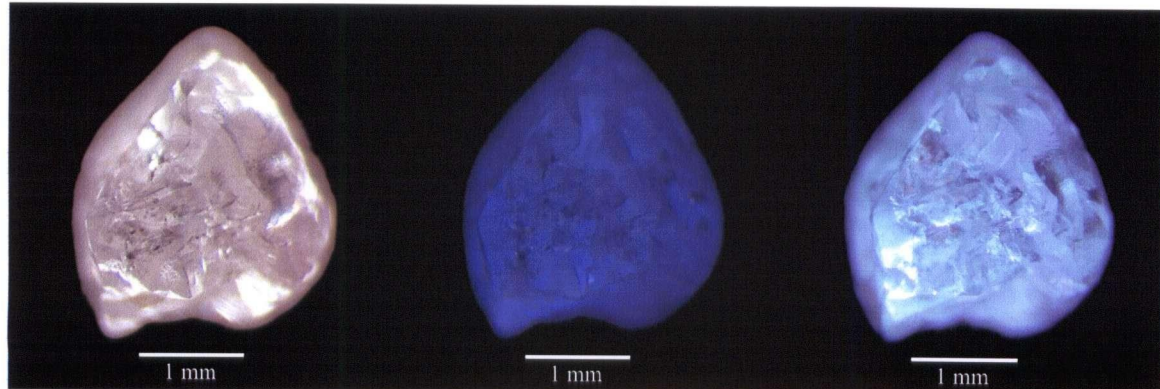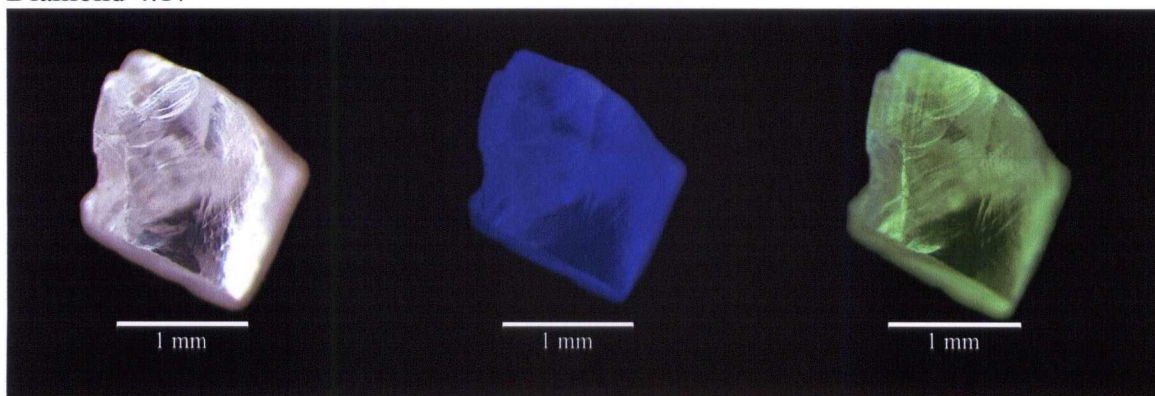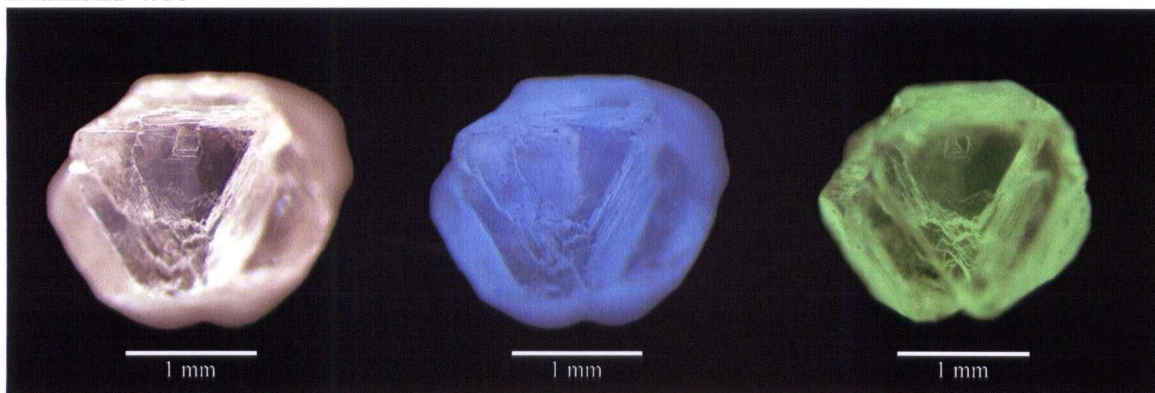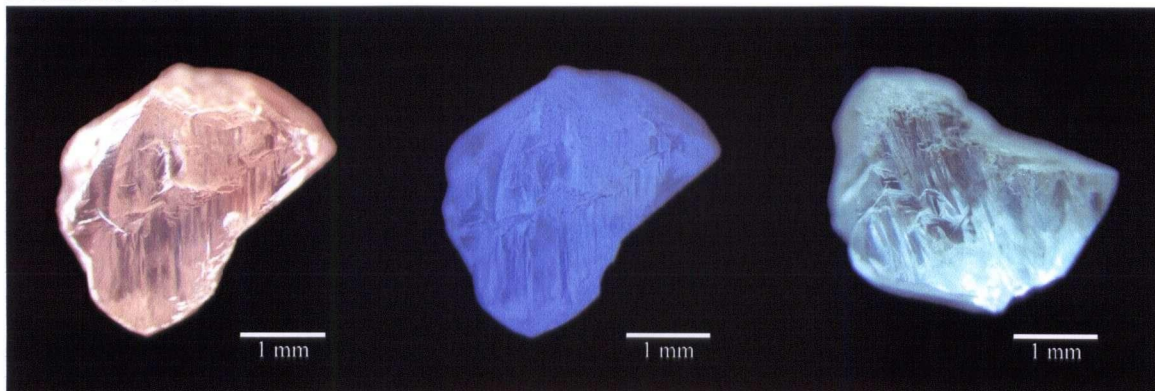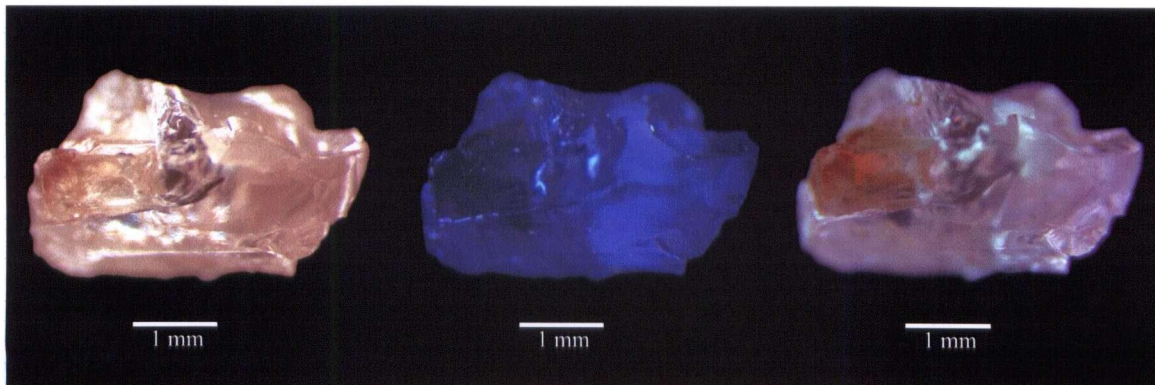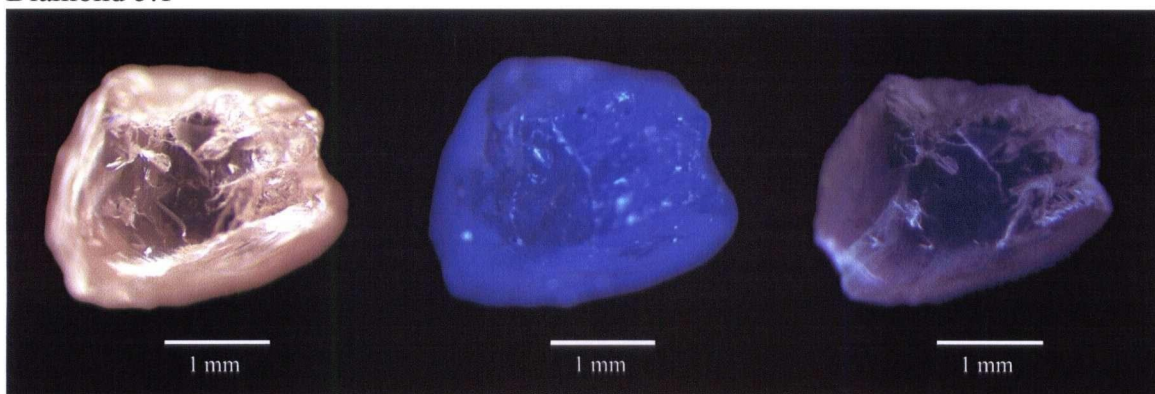
Diamond 5.1
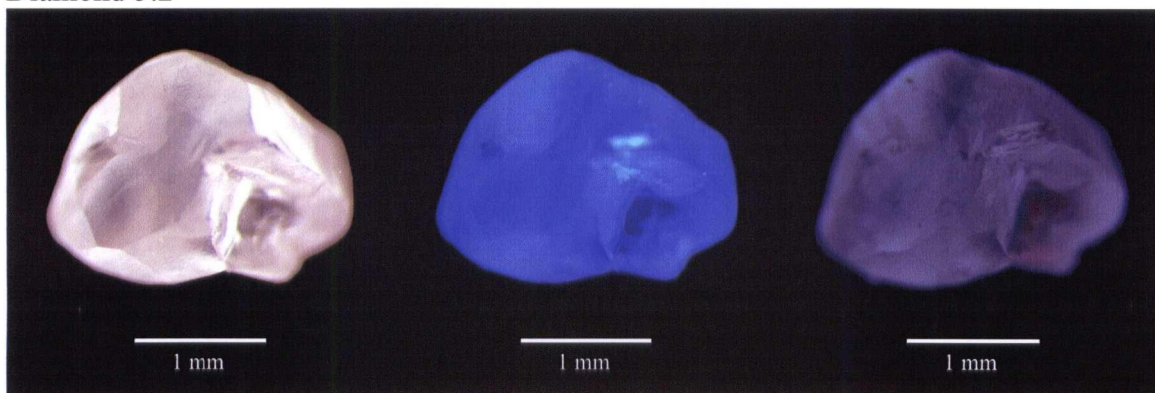
Diamond 5.2

Diamond 5.3
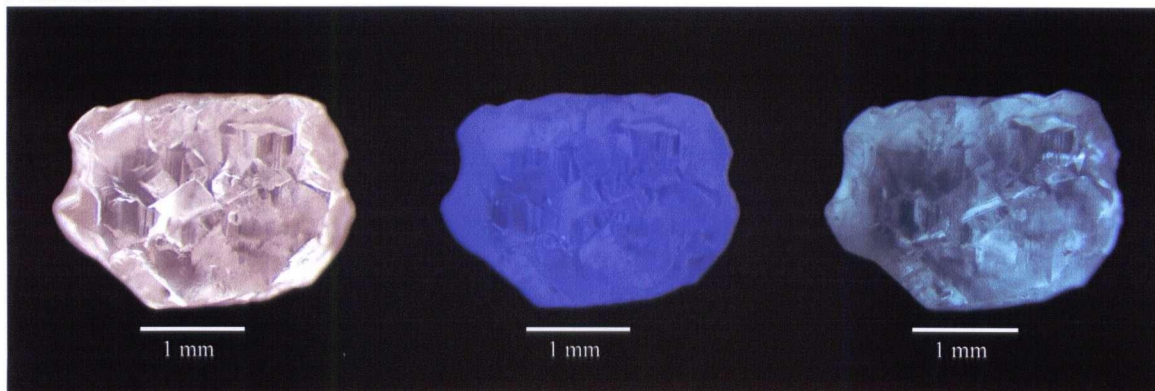
Diamond 5.4
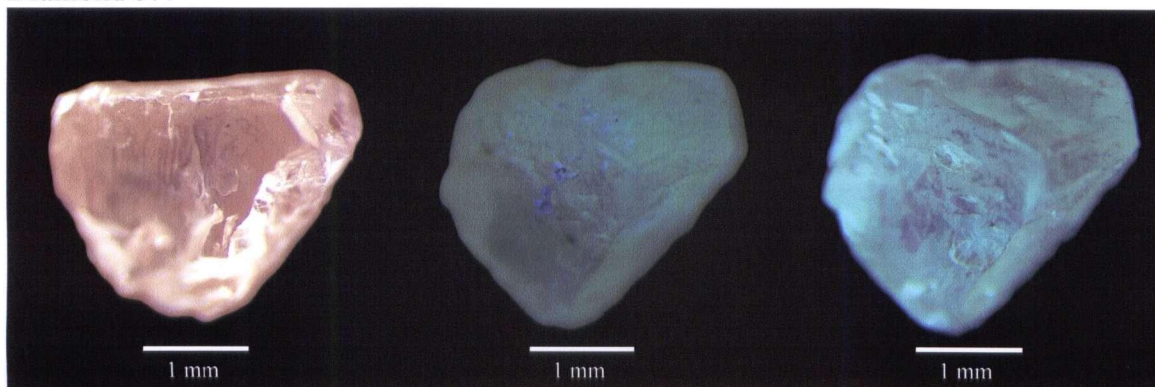
Diamond 5.5
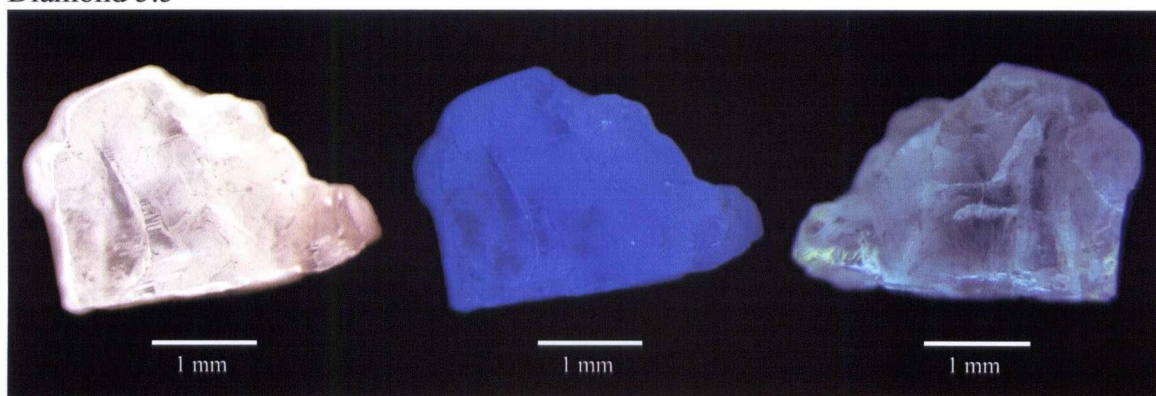
Diamond 5.6
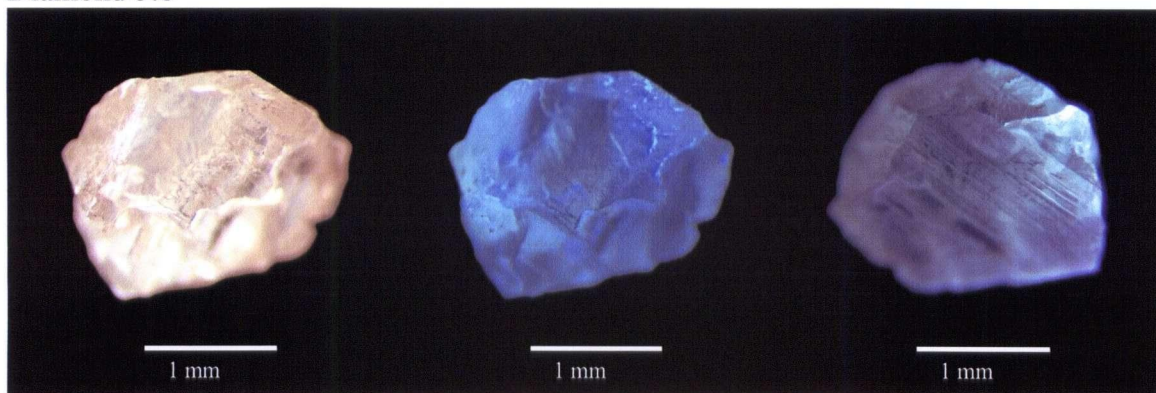
Diamond 5.7
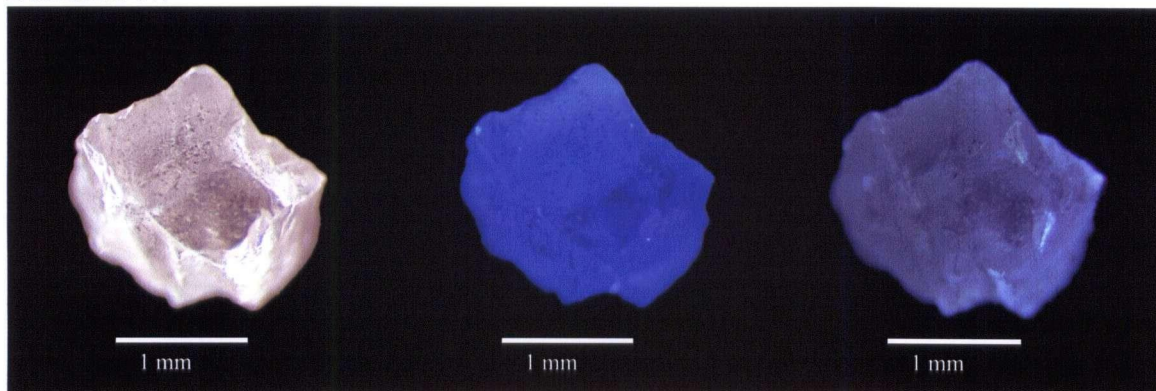
Diamond 5.8
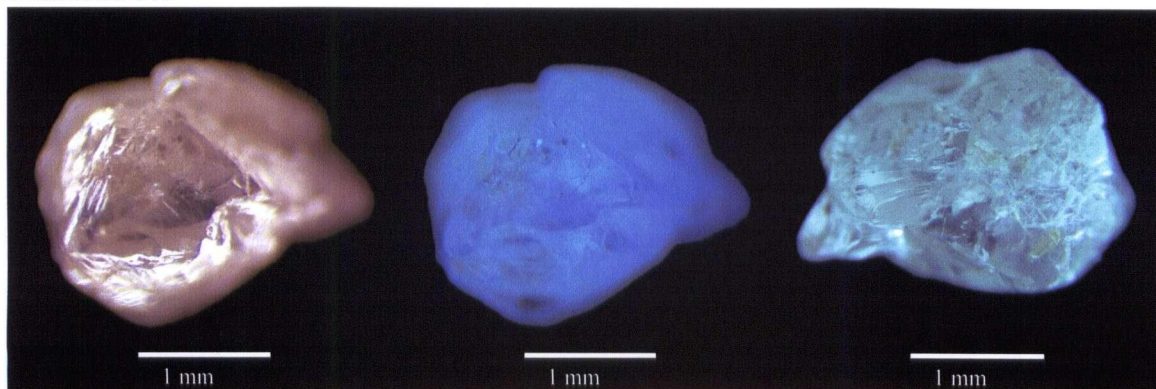
Diamond 5.9
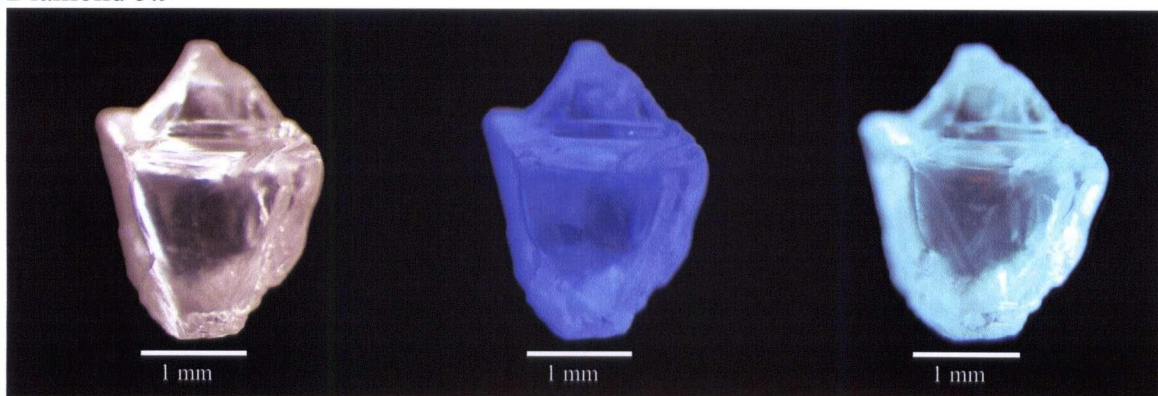
Diamond 5.10
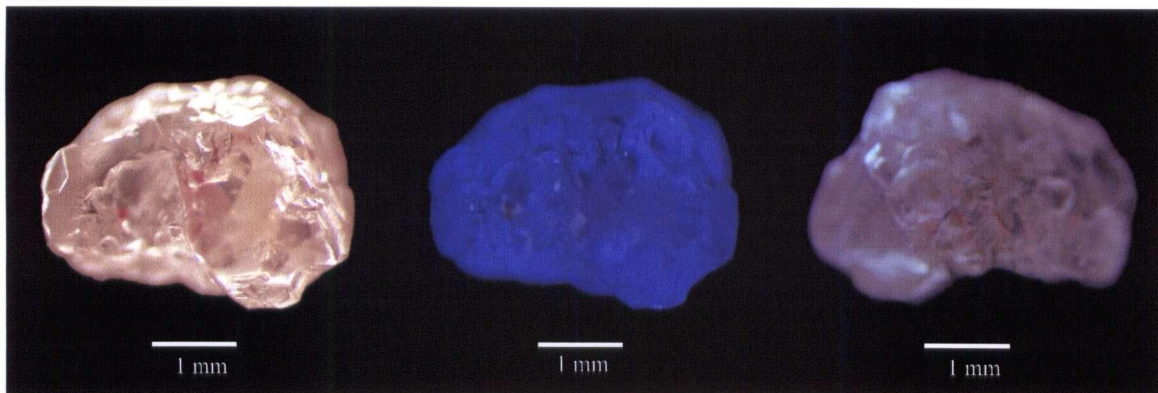
Diamond 5.11
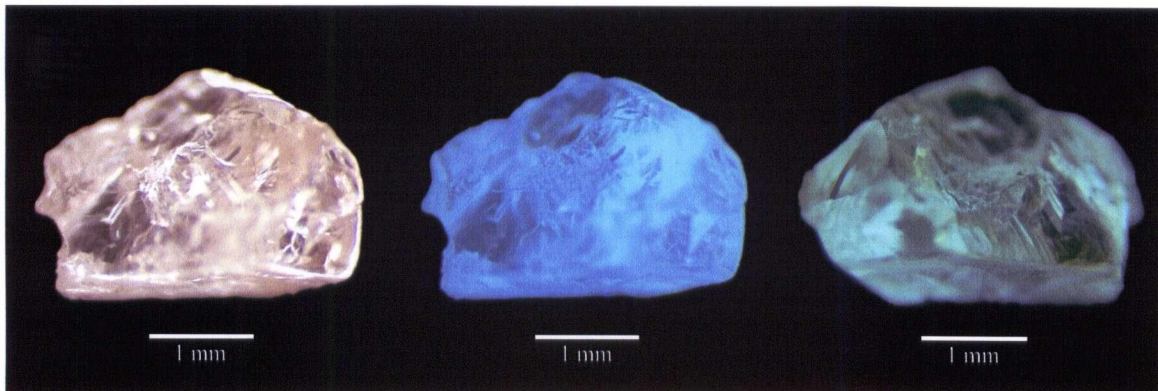
Diamond 6.1
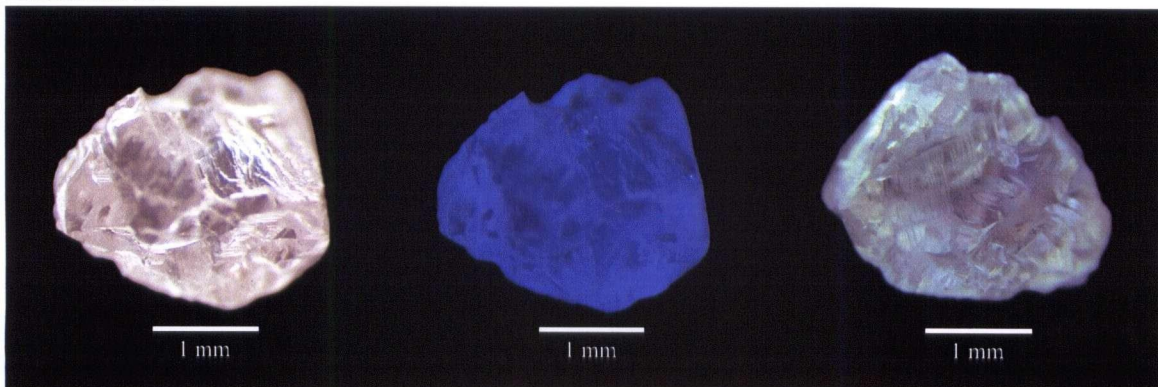
Diamond 6.2
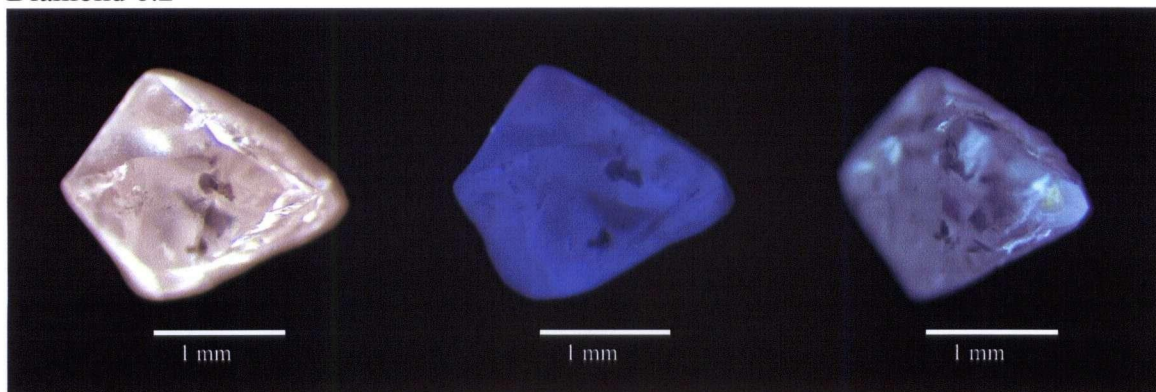
Diamond 6.3
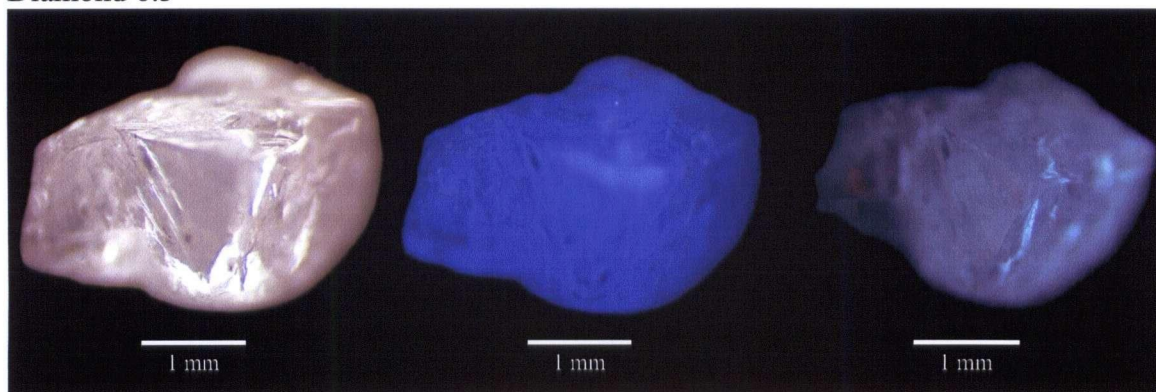
Diamond 6.4
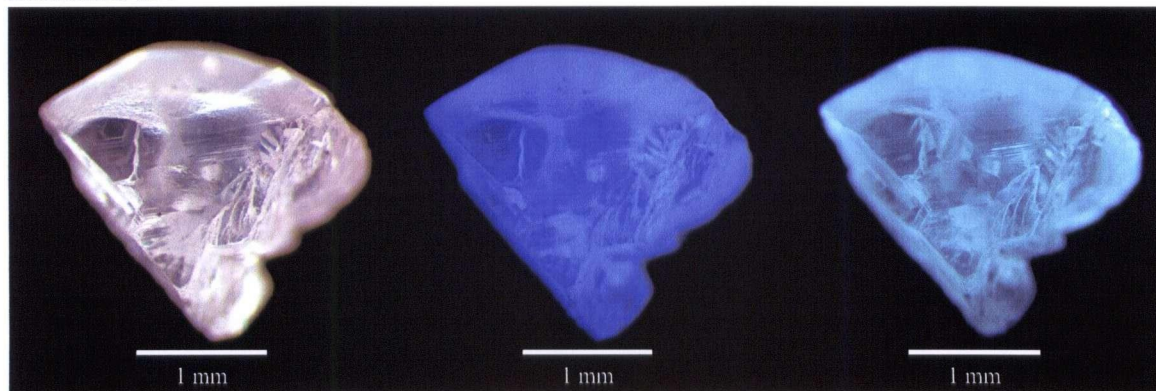
Diamond 6.5
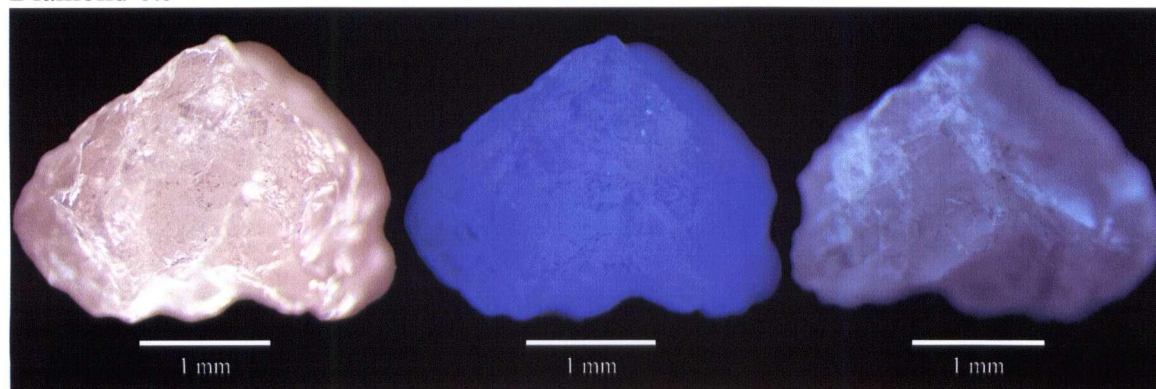
Diamond 6.6
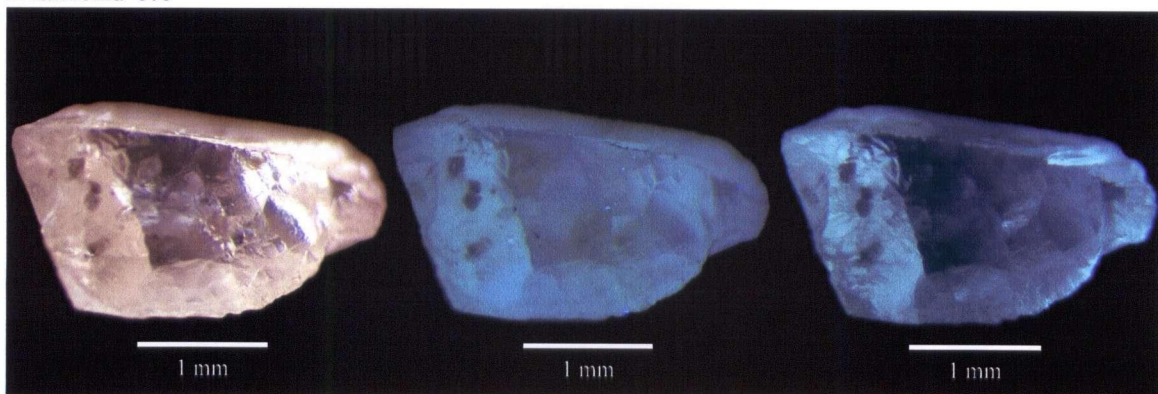
Diamond 6.7
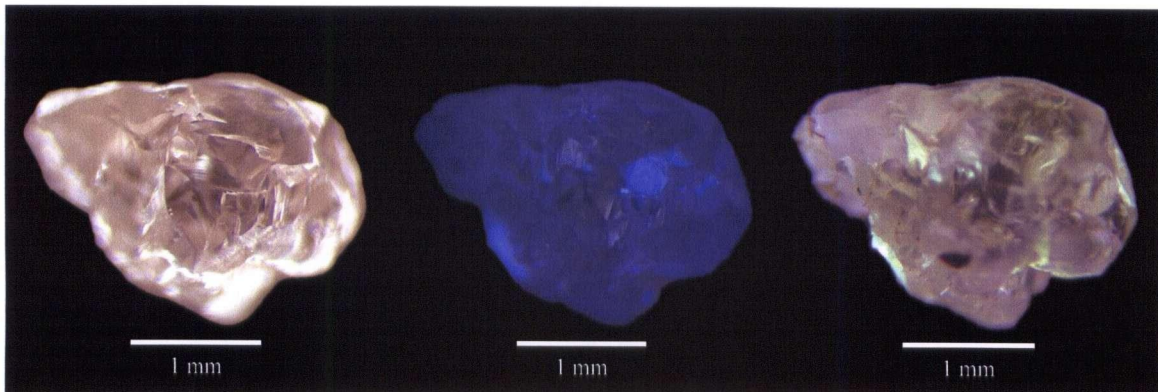
Diamond 6.8
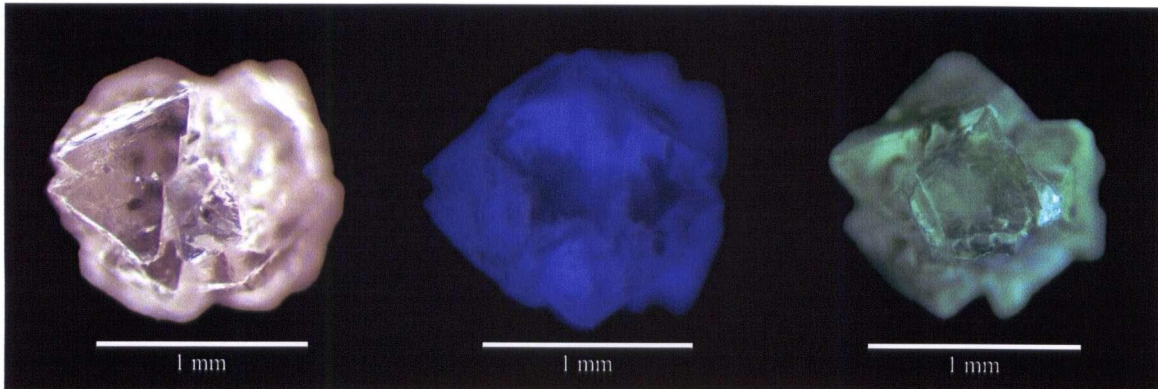
Diamond 6.9
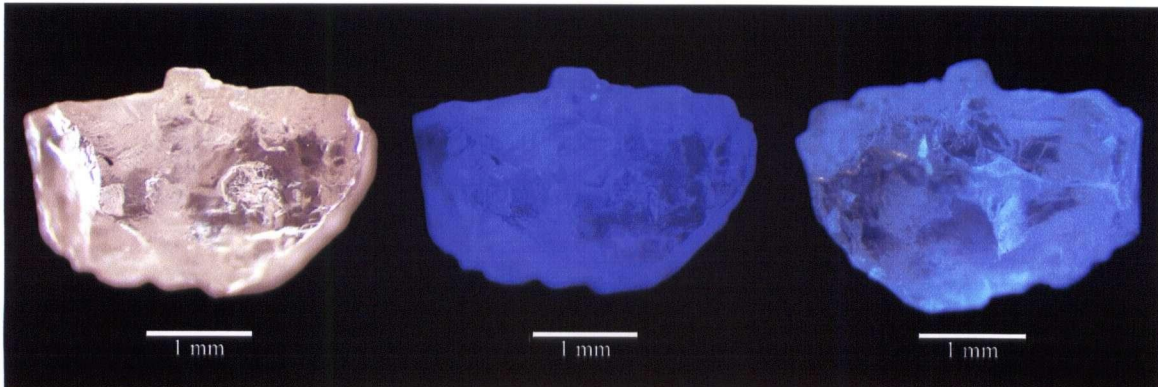
Diamond 6.10
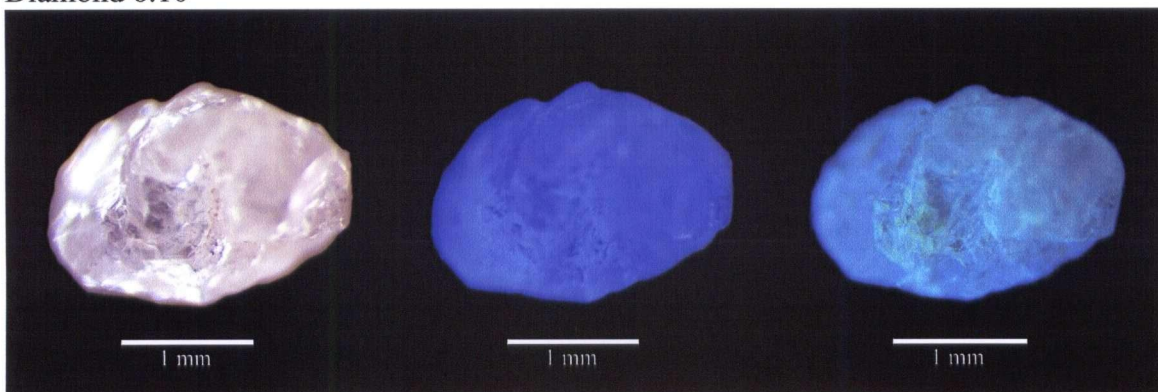
Diamond 7.1
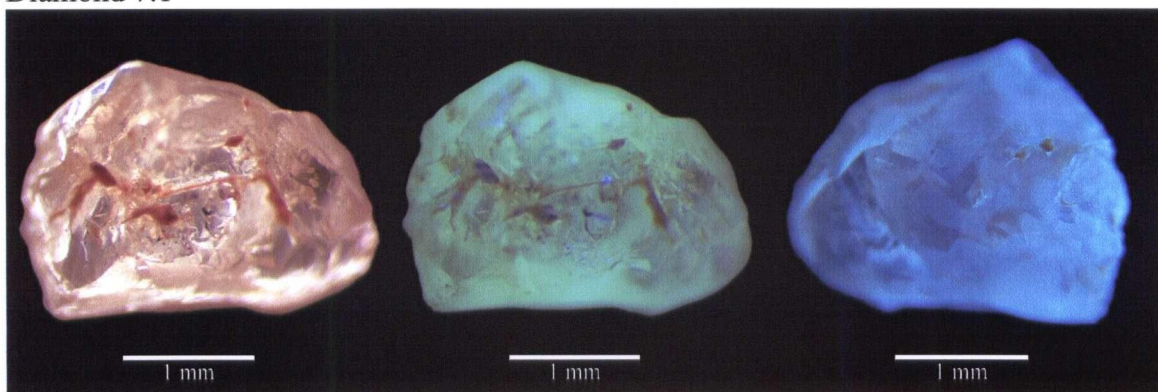
Diamond 7.2
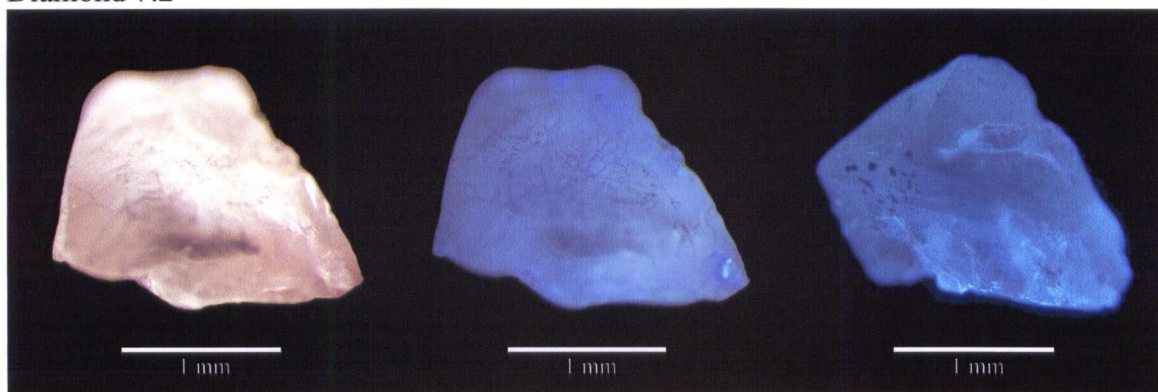
285

Appendix B – Catalogue of morphological features and diamond fluorescence (explanation of abbreviations used)

Morph. = Morphology of crystal:
O = octahedron
D = dodecahedroid
O-D = octahedron-dodecahedroid transition
THH = tetrahexahedroid
A = aggregate
U = unknown

Res. Cat. = Resorption category, after McCallum *et al.* (1994) (Fig. 2.7):
1 = >45% of crystal lost to resorption
2 = 56-70% preservation
3 = 71-80% preservation
4 = 81-90% preservation
5 = 90-99% preservation
6 = <99% of crystal lost to resorption
U = Unknown class.

Colour:
b = brown
c = colourless
g = grey
m = milky white
p = pink
y = yellow
slash indicates non-uniform colour

Transparency:
t = transparent
s-t = semi-transparent
n-t = non-transparent (opaque)

Fluorescence: format: colour-intensity-uniform/non-uniform.
m = moderate
s = strong
u = uniform fluorescence
n = non-uniform fluorescence

Intactness:
intact = no crystal lost to fragmentation
broken = >2/3's of original grain present
fragment = <2/3's but >1/3 of original grain
fraction = <1/3 of original grain present

Def. Lam. = Deformation Laminations.

Hill. = Hillocks.

Appendix B (continued) - Catalogue of morphological features and diamond fluorescence (explanation of abbreviations used)

Pre-erupt. = Pre-eruption fractures.

Brittle fract. = Brittle fractures.

Etching: '+' symbol indicates positive orientation, '-' symbol indicates negative orientation and 'x' denotes unknown orientation

Tri. = Trigons,
Hex. = Hexagons
Tetr. = Tetragons
Chan. = Etch channels

Frost. = Frosting.

Appendix B - Catalogue of morphological features and diamond fluorescence

Sample No.	Weight (grams)	Dim. 1	Dim. 2	Dim. 3	Morph.	Res. Cat.	Colour	Trans-parency	Fluore-scence	Intactness	Def. Lam.	Hill.	Pre-eru. fract.	Brittle fract.	Tri.	Hex.	Tetr.	Cha.	Frost.
1.1	0.187	5.5	5.0	3.5	O-D	4	g/c	n-t	b-w-nu	fragment		x	x	x	-				
1.2	0.196	7.0	4.0	3.0	D	2	c	s-t	b-w-nu	fragment			x	x	x	x			
1.3	0.172	6.0	4.5	2.5	THH	1	c	s-t	b-vw-u	broken	x		x	x					
1.4	0.165	6.0	5.5	1.3	D	2	b/c	s-t	t-w-nu	broken	x		x		-	x	+		
1.5	0.082	6.5	5.5	2.0	O-D	5	m	s-t	b-m-u	broken			x	x	-	x	x		
2.1	0.331	7.0	5.0	3.0	A-O-D	3	c	s-t	b-vw-u	intact					-	x			
2.2	0.203	6.0	5.5	2.0	THH	1	p	s-t	b-m-u	broken	x		x	x	+	x	+	x	x
2.3	0.313	8.5	4.0	4.0	O-D	5	y	n-t	none	broken			x	x					x
2.4	0.149	6.0	5.0	2.0	U	U	p	n-t	br-w-u	fraction			x		-				
2.5	0.315	7.0	6.0	5.0	U	5	g	s-t	b-vw-u	fragment	x		x	x			+		
2.6	0.222	6.0	5.0	2.5	U	U	m	n-t	b-m-u	fraction			x	x	x				
2.7	0.316	7.0	5.5	4.5	D	2	y	s-t	b-vw-u	broken			x	x	+/-	x	+		
2.8	0.185	7.5	6.0	2.0	U	U	g	s-t	b-w-u	fragment			x	x			+		
2.9	0.224	6.5	5.0	2.5	THH	1	g	s-t	b-s-nu	broken	x		x	x	x	x		x	
2.10	0.357	7.0	5.5	3.5	U	5/2	y	s-t	b-s-u	fragment	x		x		-	x	+		
2.11	0.189	5.5	5.0	3.0	U	U	g/c	n-t	b-s-nu	fraction	x		x	x	x	x		x	
3.1	0.404	6.3	6.0	3.0	THH	1	b/c	s-t	b-vw-nu	intact	x		x	x	-	x	+		
3.2	0.187	6.0	3.0	3.0	D	2	c	n-t	b-m-u	broken		x	x	x	-	x	+		
3.3	0.153	5.0	4.0	2.5	O-D	3	c	s-t	b-m-u	intact			x		-	x	+		
3.4	0.205	6.0	5.5	3.0	U	3	g	s-t	b-w-u	broken	x		x		-	x	+		x
3.5	0.154	5.0	4.5	3.0	O-D	3	y	s-t	b-w-u	broken			x			x	+		x
3.6	0.176	4.5	4.0	3.5	THH	1	y	s-t	b-w-u	broken			x	x	x	x	+	x	x
3.7	0.169	6.0	6.0	3.0	U	1/5	c	n-t	b-m-u	fragment			x	x	-				
3.8	0.056	4.5	3.8	2.0	O-D	5	b/c	s-t	b-m-nu	broken			x	x		x	+	x	
3.9	0.266	6.5	5.0	3.0	D	2	c	s-t	b-m-u	broken			x		x	x			
3.10	0.080	6.0	4.5	1.5	D	2	c	s-t	b-w-u	fragment			x					x	x
3.11	0.164	6.5	4.5	2.3	THH	1	g	s-t	b-w-u	broken			x					x	x
4.1	0.008	2.5	2.0	1.0	O	6	c	t	b-m-u	broken			x	x	-				
4.3	0.016	2.5	2.5	1.5	O-D	3/6	c	s-t	b-s-u	broken			x		-	x	+		
4.4	0.006	2.3	1.8	1.0	U	4	g	n-t	b-s-u	fragment			x		-		+		
4.5	0.004	2.0	1.8	1.3	U	3/6	c	s-t	b-s-u	fragment	x		x					x	x
4.6	0.006	2.5	2.0	1.0	U	5/1	c	s-t	b-s-u	fraction			x	x		x	+	x	
4.7	0.015	2.5	2.0	1.8	O-D	5	y	s-t	t-vw-nu	broken			x	x			+		
4.8	0.008	2.8	1.8	1.0	U	1/6	b	s-t	t-s-nu	fragment	x	x	x	x	-				

Appendix B (continued) - Catalogue of morphological features and diamond fluorescence

Sample No.	Weight (grams)	Dimensions (mm) 1	2	3	Morph.	Res. Cat.	Colour	Trans-parency	Fluore-scence	Intactness	Def. Lam.	Hill.	Pre-eru. fract.	Brittle fract.	Tri.	Etching Hex.	Tetr.	Cha.	Frost.
4.9	0.036	4.3	3.0	2.0	O-D	3	y	t	b-w-u	fragment	x		x	x	-	x	+		
4.10	0.017	3.0	2.0	1.5	O-D	3	c	s-t	b-s-u	fragment			x	x	-	x	+		
4.11	0.011	2.0	2.0	1.3	A-O-D	4	c	s-t	b-s-u	intact								x	
4.12	0.009	3.0	1.8	1.0	THH	1	c	s-t	b-s-u	intact	x	x							
4.13	0.019	3.0	2.5	1.5	THH	1	g	s-t	b-m-u	intact						x	+	x	x
4.14	0.006	2.0	1.5	1.0	U	2	c	s-t	b-m-u	broken			x		-	x	+	x	
4.15	0.007	2.0	1.8	1.5	A-O-D	2/5	g	s-t	b-w-u	intact						x			
4.16	0.016	2.5	2.0	1.5	THH	1	c	s-t	b-vw-u	broken			x	x	-	x	+	x	
4.17	0.006	1.8	1.3	1.0	D	2	c	t	b-s-u	fragment	x	x	x	x	+/-				
4.18	0.010	2.0	2.0	1.3	O	6	g	t	t-m-u	intact					-				
4.19	0.021	3.0	2.5	1.5	O-D	1/5	b	s-t	t-m-u	broken			x	x	-	x	+	x	
4.21	0.040	4.0	2.5	2.0	U	1/5	y	t	b-vw-nu	broken			x	x		x		x	
5.1	0.014	2.5	2.0	1.5	D	2	b	t	b-w-u	broken	x	x	x	x	x	x			x
5.2	0.007	2.5	2.0	1.0	THH	1	c	s-t	b-s-u	broken			x			x	+		x
5.3	0.011	2.3	1.8	1.0	U	2	c	s-t	b-m-u	intact					+	x	+	x	x
5.4	0.016	3.0	2.0	1.3	O-D	3	b	s-t	g-w-u	broken			x	x			x	x	x
5.5	0.011	3.0	2.0	1.0	U	2	c	s-t	b-m-u	fragment			x		x	x	+		x
5.6	0.004	2.0	1.5	1.0	O-D	5	b	s-t	t-w-nu	fraction			x	x					x
5.7	0.005	2.0	1.8	1.0	U	4	c	s-t	b-m-u	fraction			x	x			+		x
5.8	0.013	2.5	1.5	1.5	A-O-D	2/5	g	s-t	t-w-u	broken			x						
5.9	0.012	2.5	2.5	1.3	O-D	5	c	t	b-m-u	fragment		x	x	x	-	x	+		
5.10	0.029	3.0	2.3	1.8	THH	1	y	s-t	b-vw-u	broken			x	x	+/-	x	+		
5.11	0.013	2.8	2.0	1.5	O-D	4	c	t	t-m-u	fragment			x	x		x	+		
6.1	0.013	2.5	2.0	1.0	U	4	c	s-t	b-w-u	broken			x	x		x	+		
6.2	0.006	2.0	1.5	1.0	THH	1	c	s-t	b-w-u	broken	x		x	x		x			
6.3	0.025	3.5	2.0	1.5	O-D	3	g	s-t	b-m-u	broken			x		-	x			
6.4	0.005	2.5	2.0	1.0	O-D	3	c	t	b-s-u	fragment	x		x	x	-	x	+		
6.5	0.015	3.0	2.5	1.5	U	5	g	n-t	b-s-u	fraction			x						
6.6	0.009	3.0	1.5	1.0	O-D	2/5	c	t	t-m-u	fragment			x						
6.7	0.009	2.5	1.5	1.0	D	2	c	s-t	b-vw-u	broken			x	x		x	+		
6.8	0.003	1.0	1.0	1.0	A-O	6	g	s-t	b-s-u	intact			x		-				
6.9	0.012	3.0	2.0	1.0	U	5	c	s-t	b-m-u	fraction			x	x	-	x	+	x	
6.10	0.007	2.0	1.3	1.3	D	2	g	s-t	b-s-u	fragment		x	x	x	x	x		x	
7.1	0.011	3.0	2.0	1.0	THH	1	b	s-t	g-s-u	broken	x	x	x	x	x	x		x	
7.2	0.006	1.5	1.3	1.0	THH	1	b	n-t	t-m-u	fragment			x	x	x				x

Appendix C - Nitrogen concentration, aggregation state and relative hydrogen concentration

Sample No.	A centres (ppm)	B centres (ppm)	Total nitrogen (A + B, in ppm)	%B (100xB/(B+A))	Diamond type	Hydrogen (Δ3107 cm-1)
1.1	0	37	37	100	IaB	0.03
1.2*	0	40	40	100	IaB	0.30
1.3	0	243	243	100	IaB	2.24
1.4*	0	233	233	100	IaB	1.07
1.5**	0	311	311	100	IaB	2.20
2.1*	0	<20	<20	100	IIa	0.04
2.2*	0	137	137	100	IaB	0.86
2.3	0	0	0	-	IIa	0.00
2.4	0	94	94	100	IaB	0.90
2.5*	0	66	66	100	IaB	0.55
2.6**	0	541	541	100	IaB	6.06
2.7	0	0	0	-	IIa	0.00
2.8*	0	54	54	100	IaB	0.46
2.9*	0	122	122	100	IaB	2.65
2.10**	0	24	24	100	IaB	0.00
2.11*	28	42	70	60	IaAB	0.54
3.1*	0	40	40	100	IaB	0.35
3.2	0	228	228	100	IaB	1.46
3.3	0	226	226	100	IaB	1.36
3.4**	0	40	40	100	IaB	0.35
3.5*	0	32	32	100	IaB	0.09
3.6**	0	0	0	-	IIa	0.03
3.7	0	225	225	100	IaB	1.07
3.8*	0	41	41	100	IaB	0.14
3.9	0	400	400	100	IaB	1.59
3.10*	0	98	98	100	IaB	0.68
3.11*	0	61	61	100	IaB	0.44
4.1	0	41	41	100	IaB	0.43
4.3	0	82	82	100	IaB	0.58
4.4	0	335	335	100	IaB	2.22
4.5	0	0	0	-	IIa	0.00
4.6	0	0	0	-	IIa	0.00
4.7	0	0	0	-	IIa	0.00
4.8	0	0	0	-	IIa	0.14
4.9	0	0	0	-	IIa	0.00
4.10	12	21	33	64	IaAB	0.21
4.11	48	0	48	0	IaA	0.16
4.12	0	20	20	100	IaB	0.22
4.13	0	0	0	-	IIa	0.00
4.14	0	22	22	100	IaB	0.29

Appendix C (continued) - Nitrogen concentration, aggregation state and relative hydrogen concentration

Sample No.	A centres (ppm)	B centres (ppm)	Total nitrogen (A + B, in ppm)	%B (100xB/(B+A))	Diamond type	Hydrogen (Δ3107 cm-1)
4.15	116	22	138	16	IaAB	0.67
4.16	0	0	0	-	IIa	0.11
4.17*	<26	<32	<53	75	IaAB	0.03
4.18	0	144	144	100	IaB	1.03
4.19	0	35	35	100	IaB	0.47
4.21	0	0	0	-	IIa	0.00
5.1	0	0	0	-	IIa	0.00
5.2	0	0	0	-	IIa	0.00
5.3	0	42	42	100	IaB	0.46
5.4	0	0	0	-	IIa	0.22
5.5	0	0	0	-	IIa	0.00
5.6	0	0	0	-	IIa	0.00
5.7	0	0	0	-	IIa	0.00
5.8	0	54	54	100	IaB	0.45
5.9	0	36	36	100	IaB	0.43
5.10	0	0	0	-	IIa	0.00
5.11	0	0	0	-	IIa	0.14
6.1	0	0	0	-	IIa	0.00
6.2	0	0	0	-	IIa	0.00
6.3	0	28	28	100	IaB	0.48
6.4	0	182	182	100	IaB	1.20
6.5	0	105	105	100	IaB	1.23
6.6	0	0	0	-	IIa	0.04
6.7	0	0	0	-	IIa	0.00
6.8	23	25	48	53	IaAB	1.28
6.9	0	0	0	-	IIa	0.00
6.10	0	0	0	-	IIa	0.17
7.1	0	101	101	100	IaB	0.65
7.2	0	35	35	100	IaB	0.41

Precision and minimum detection limits are listed in sections 6.2.2 and 6.2.3 respectively.

A, B, and D centres are calculated using deconvolution software (section 3.2.3). %B and diamond type are calculated from these numbers.

Hydrogen (Δ3107 cm^{-1}) represents the relative concentration, measured as the difference in peak height and base at 3107 cm^{-1}.

The cut-off between type I and II stones is 20 ppm nitrogen

" - "indicates that although nitrogen was calculated using deconvolution software, qualitative examination of IR spectra revealed no nitrogen absorption.

" * " results represent an average as diamond was examined for growth studies in Chapter 7.0.

" ** " diamonds were analysed as chips (not whole rough stones)

For a more detailed explanation of headings, see Chapter 6.0.

Appendix D – Infrared spectra and deconvolution curves

The following appendix contains infrared spectra, respective deconvoluted curves, and calculated nitrogen character for all whole rough diamonds analysed (n=55). The remaining 14 diamonds in this study are marked with a '*', indicating detailed IR examinations was performed (see growth studies in Chapter 7.0). Numerous points were analysed for these diamonds, and as such, the numbers presented reflect the average nitrogen character. The raw spectra included for these diamonds are somewhat representative (although many diamonds are extremely heterogeneous in impurity content). Diamonds marked with '**' were analysed as chips. The procedures for spectral deconvolution are described in section 6.2.

Diamond 1.1

A   = -9.39
B   = 36.87
%B   = 134
N   = 27.48
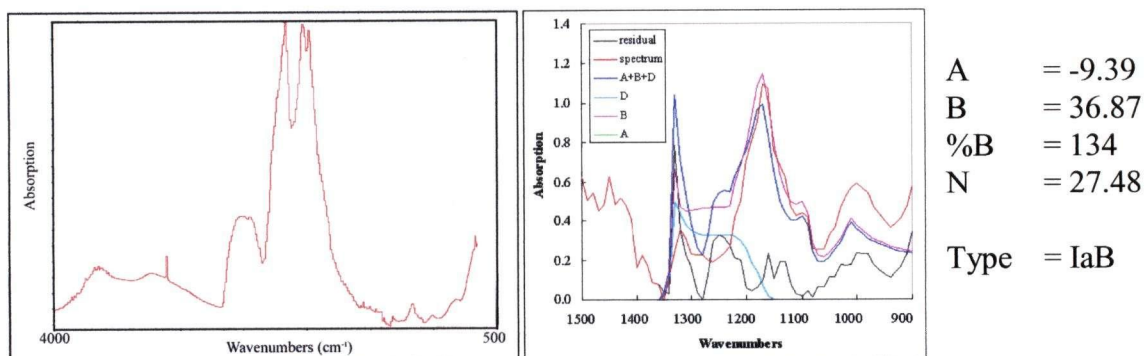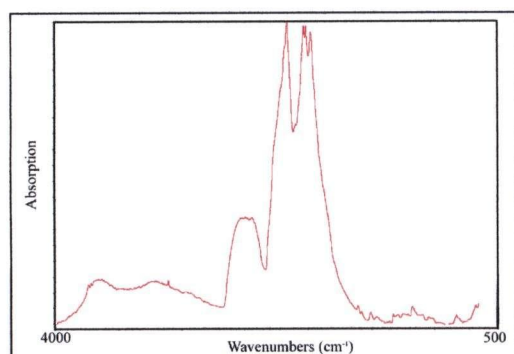
Type = IaB

Diamond 1.2*

25 points on polished surface were examined

A   = 0.88   (-5.98 – 2.94)
B   = 39.87   (4.47 – 76.97)
%B   = 98   (93-108)
N   = 40.75   (3.27 – 78.67)

Type = IaB   (3 points IIa)

Diamond 1.3
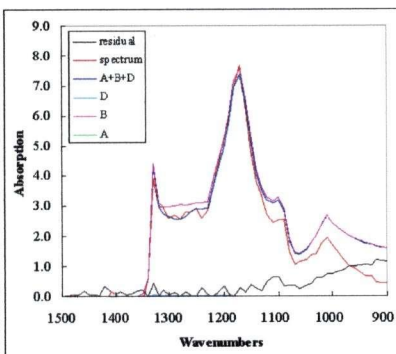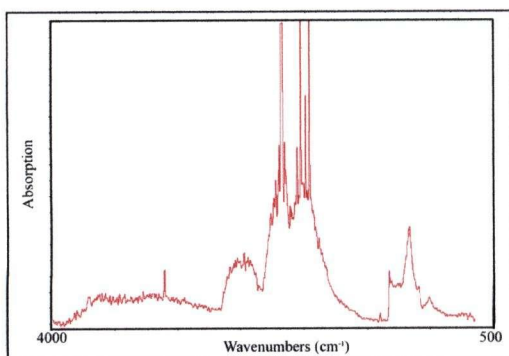
A = -8.52
B = 243.1
%B = 104
N = 234.5

Type = IaB

Diamond 1.4*
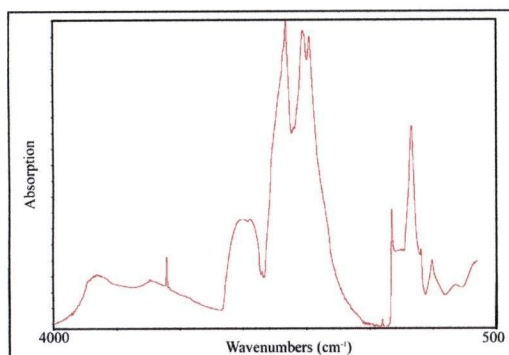
35 points on polished surface were examined

A = 6.5 (-56.96 – 16.34)
B = 232.6 (23.28 – 403.94)
%B = 97 (85-121)
N = 239.1 (24.50 – 412.33)

Type = IaB

Diamond 1.5**
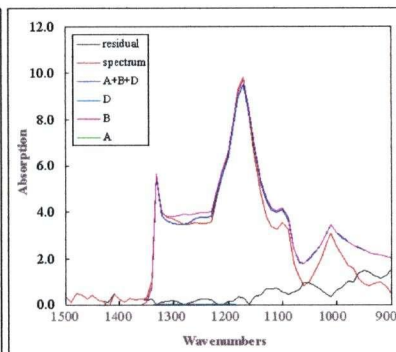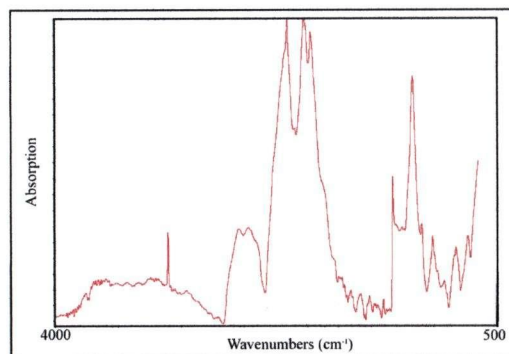
A = -7.7
B = 311.4
%B = 103
N = 303.7

Type = IaB

Diamond 2.1*
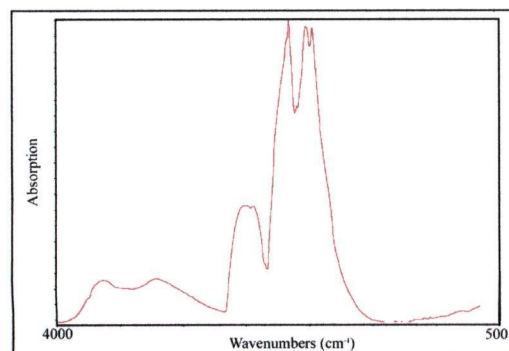
11 points on polished surface were examined

A = 0.4 (-3.37 – 1.92)
B = 15.81 (7.38 – 19.46)
%B = 98 (91 - 141)
N = 16.18 (5.34 – 21.11)

Type = IIa

293
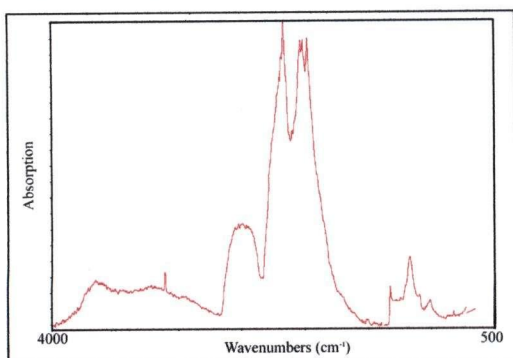
Diamond 2.2*

19 points on polished surface were examined

A	= -0.98	(-8.66 – 9.26)
B	= 137.14	(26.00 – 218.85)
%B	= 101	(69-150)
N	= 136.16	(17.33 – 227.30)

Type = IaB   (one poor spectra)

Diamond 2.3
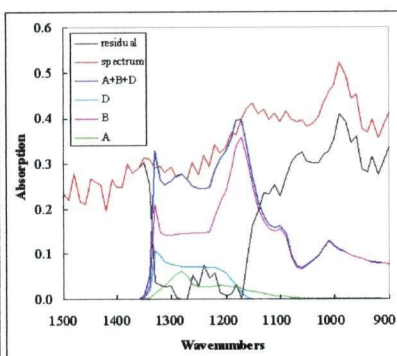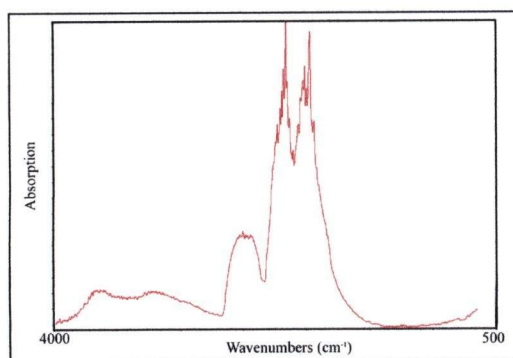
A	= 1.01
B	= 11.54
%B	= 92
N	= 12.55

Type = IIa

Diamond 2.4
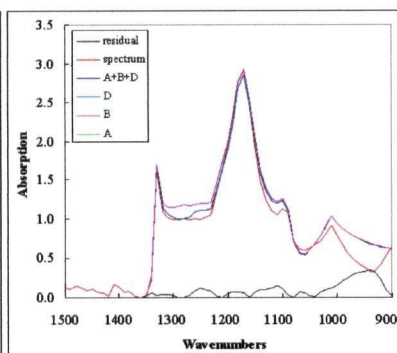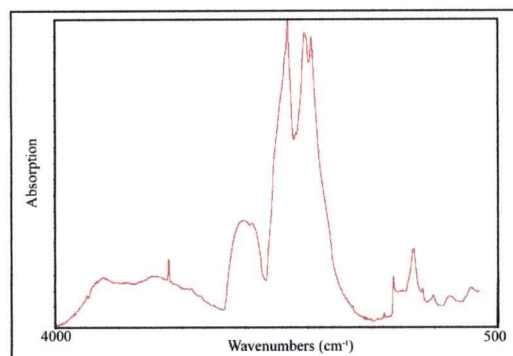
A	= -2.97
B	= 93.96
%B	= 103
N	= 90.99

Type = IaB

Diamond 2.5*
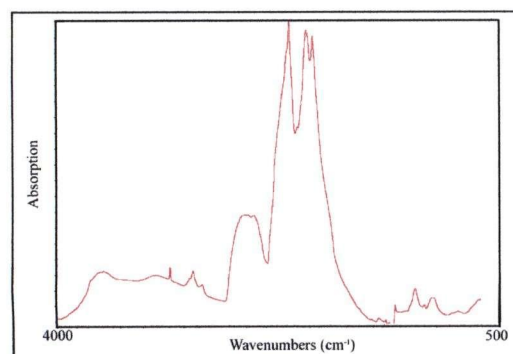
11 points on polished surface were examined

A	= -2.1	(-4.5 – 1.2)
B	= 60.6	(50.5 – 99.3)
%B	= 104	(98 - 108)
N	= 58.5	(49.3 – 101.4)

Type = IaB

Diamond 2.6**
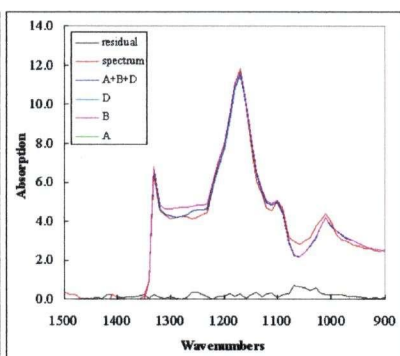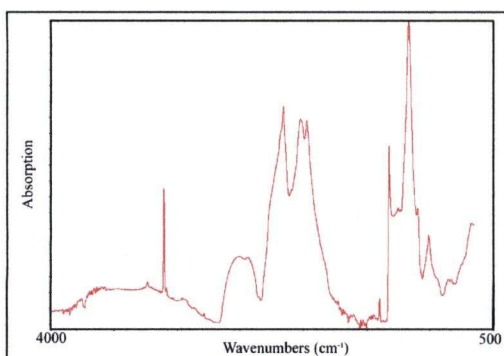
A	= -13.0
B	= 540.8
%B	= 103
N	= 527.8
Type	= IaB

Diamond 2.7
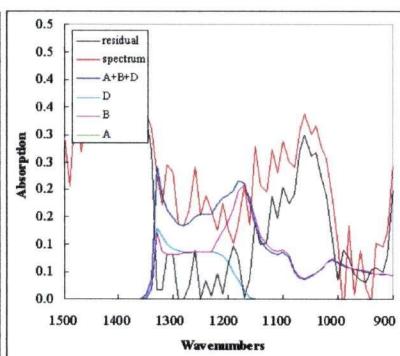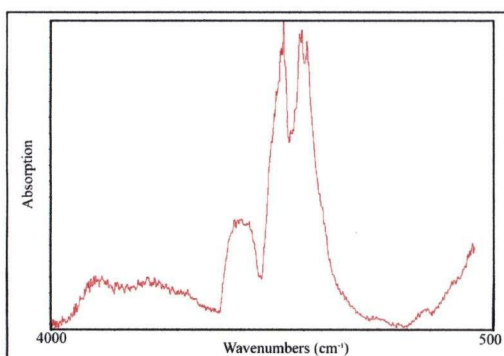
A	= -0.61
B	= 6.71
%B	= 110
N	= 6.10
Type	= IIa

Diamond 2.8*
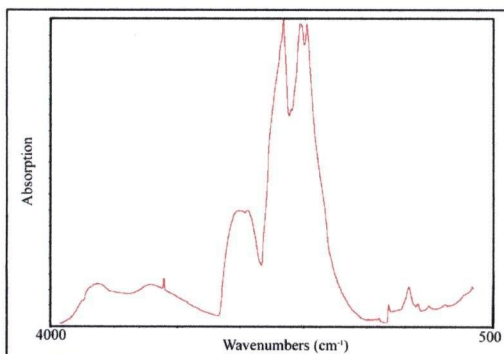
16 points on polished surface were examined

A	= -1.03	(-3.75 – 2.02)
B	= 53.61	(43.21 – 61.73)
%B	= 102	(97 - 107)
N	= 52.58	(41.36 – 63.75)
Type	= IaB	

Diamond 2.9*
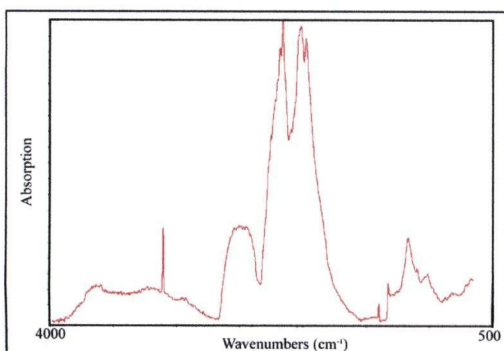
20 points on polished surface were examined

A	= -5.47	(-19.51 – 14.66)
B	= 122.00	(11.14 – 228.77)
%B	= 105	(90 - 136)
N	= 116.53	(8.18 – 209.26)
Type	= IaB	(2 points IIa)

Diamond 2.10**
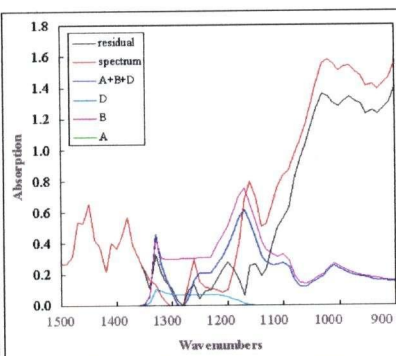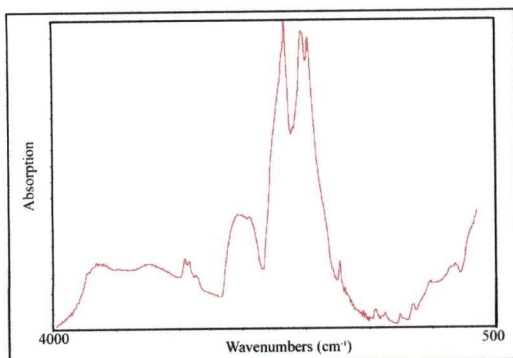
A = -6.4
B = 24.1
%B = 136
N = 17.7

Type = IaB

Diamond 2.11*
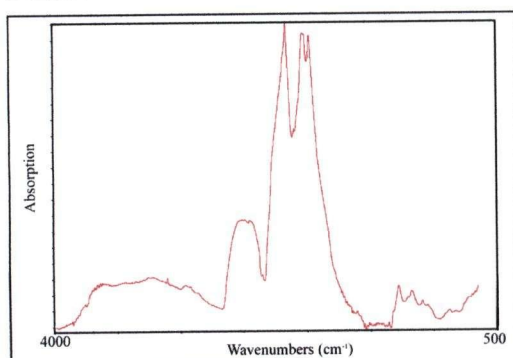
1 decent point on polished surface examined

A = 28
B = 42
%B = 60
N = 72

Type = IaAB

Diamond 3.1*
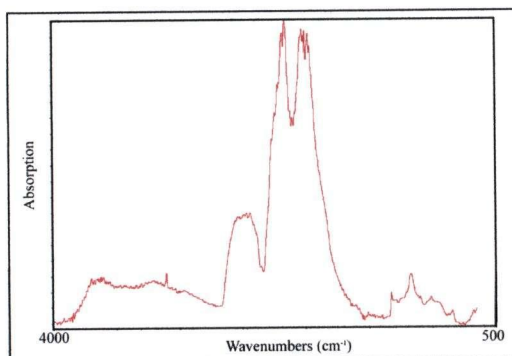
18 points on polished surface were examined

A = -2.54   (-4.65 – 1.92)
B = 39.59   (0.00- 63.51)
%B = 98   (96-111)
N = 37.04   (0 – 60.40)

Type = IaB   (5 points are IIa)

Diamond 3.2
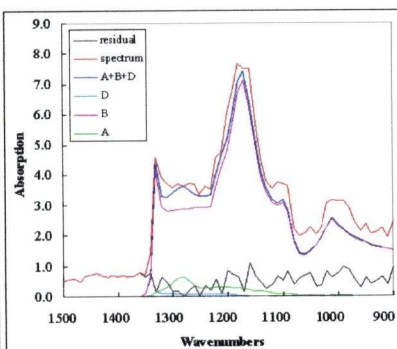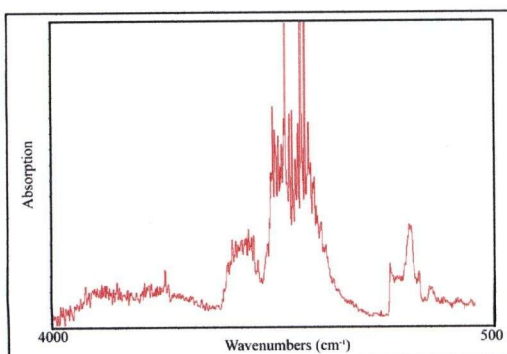
A = 10.69
B = 228.5
%B = 96
N = 239.2

Type = IaB

Diamond 3.3
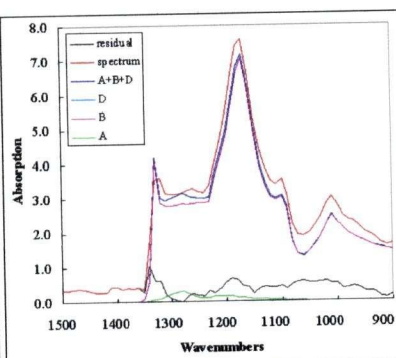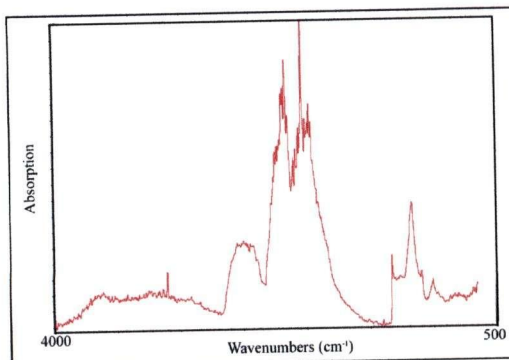
A	= 5.21
B	= 225.9
%B	= 98
N	= 231.1
Type	= IaB

Diamond 3.4**
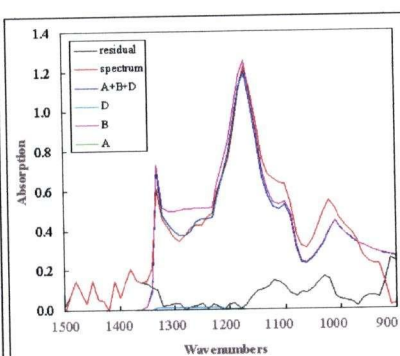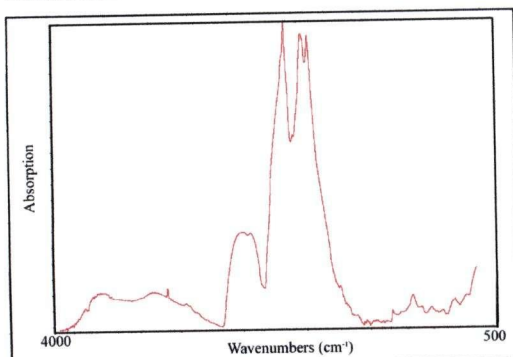
A	= -2.3
B	= 40.1
%B	= 106
N	= 37.8
Type	= IaB

Diamond 3.5*
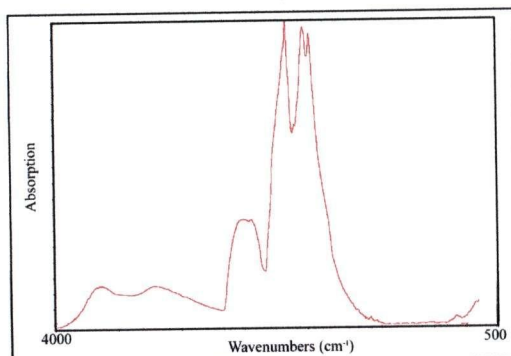
14 points on polished surface were examined

A	= 0.43	(-5.05 – 2.09)
B	= 25.65	(8.52 – 53.19)
%B	= 102	(92 - 139)
N	= 26.08	(8.07 – 54.84)

Type   = IaB (8 points) and IIa (6 points)

Diamond 3.6**
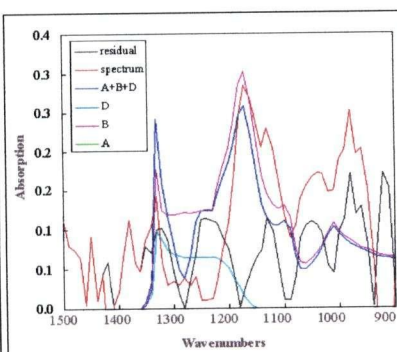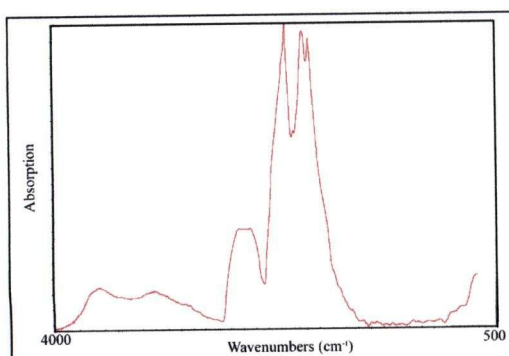
A	= -2.4
B	= 9.7
%B	= 1.34
N	= 7.3
Type	= IIa

Diamond 3.7
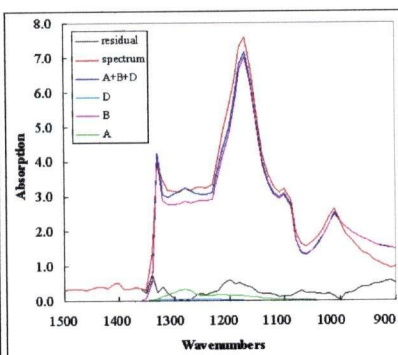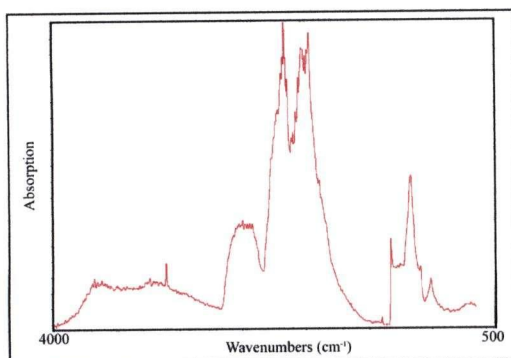
A = 5.63
B = 225.5
%B = 98
N = 231.1

Type = IaB

Diamond 3.8*
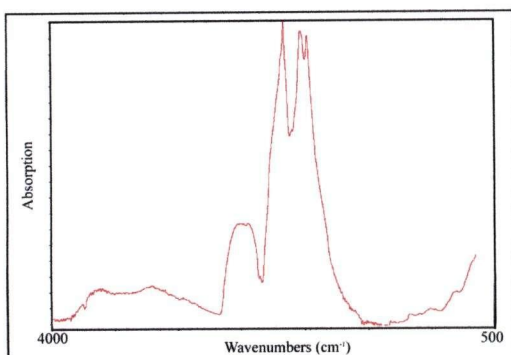
10 points on polished surface were examined

A = -0.97   (-5.4 – 2.7)
B = 40.78   (16.32 – 54.13)
%B = 105   (94 - 136)
N = 39.9   (15.1 – 56.7)

Type = IaB

Diamond 3.9
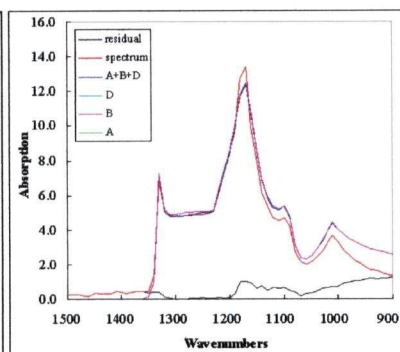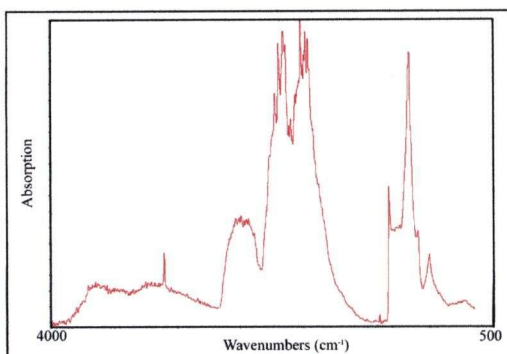
A = -3.14
B = 399.6
%B = 101
N = 396.4

Type = IaB

Diamond 3.10*
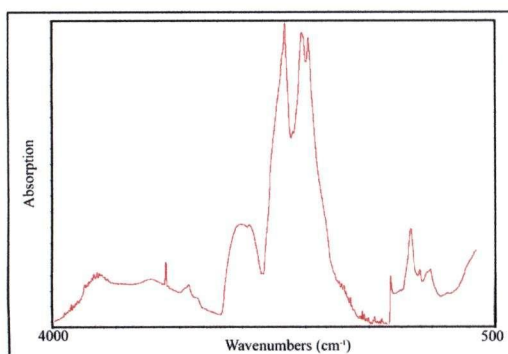
14 points on polished surface were examined

A = -3.00   (-9.34 – 15.12)
B = 98.00   (18.74 – 148.84)
%B = 106   (91-141)
N = 95.04   (13.29 – 163.96)

Type = IaB   (1 point IIa)

298

Diamond 3.11*
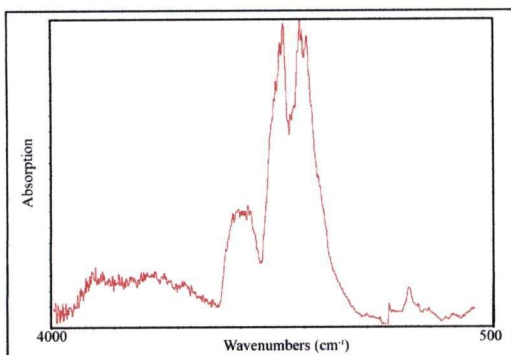
13 points on polished surface were examined

A	= 1.61	(-2.91 – 3.96)
B	= 61.47	(4.28 – 82.60)
%B	= 102	(95 - 138)
N	= 56.23	(3.09 – 86.55)

Type = IaB

Diamond 4.1
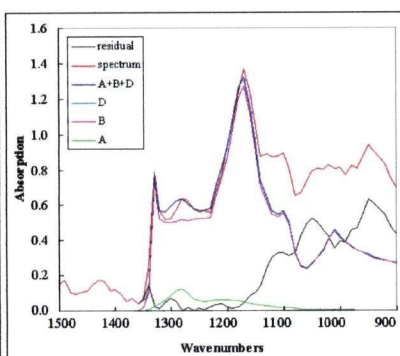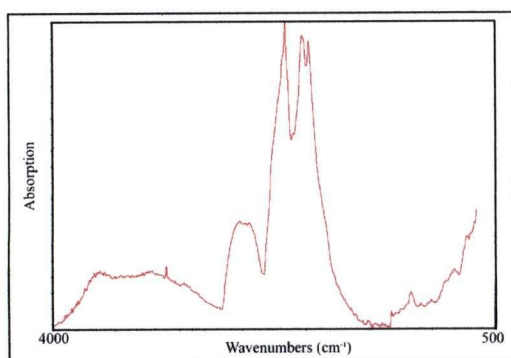
A	= 1.98
B	= 40.93
%B	= 95
N	= 42.91

Type = IaB

Diamond 4.3
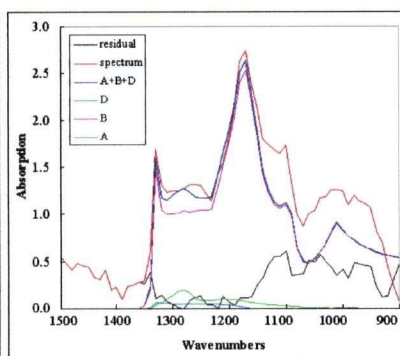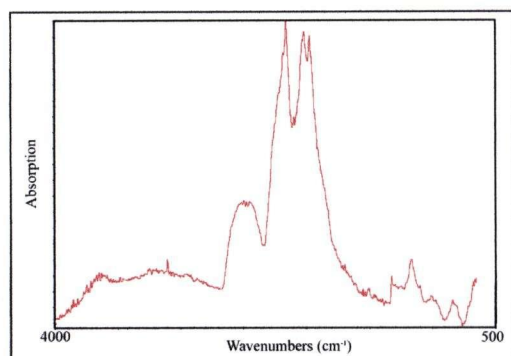
A	= 3.27
B	= 81.65
%B	= 96
N	= 84.91

Type = IaB

Diamond 4.4
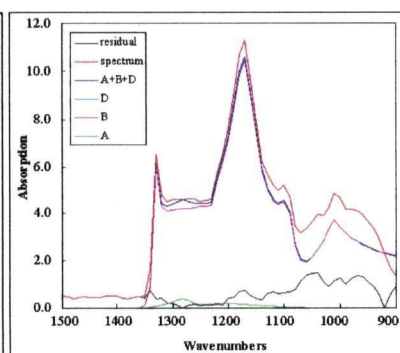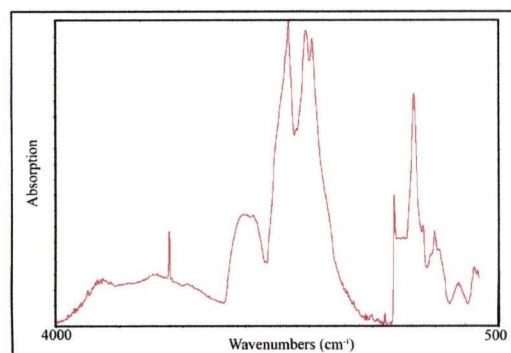
A	= 6.18
B	= 334.6
%B	= 98
N	= 340.7

Type = IaB

Diamond 4.5
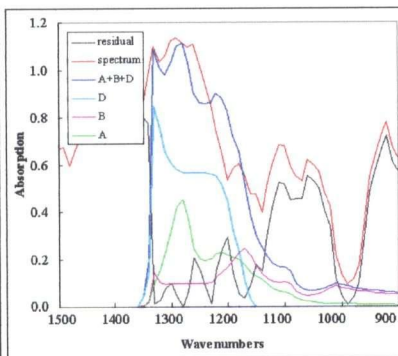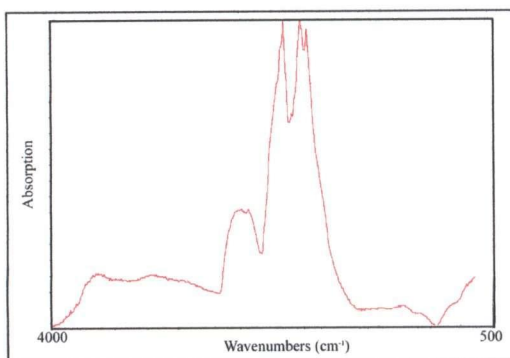
A = 7.47
B = 7.78
%B = 51
N = 15.26

Type = IIa

Diamond 4.6
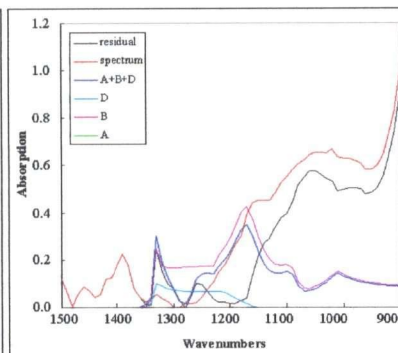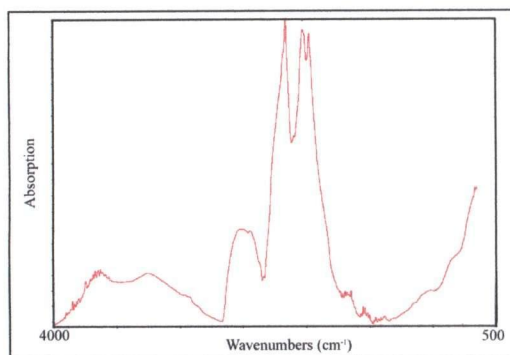
A = -3.74
B = 13.7
%B = 138
N = 9.96

Type = IIa

Diamond 4.7
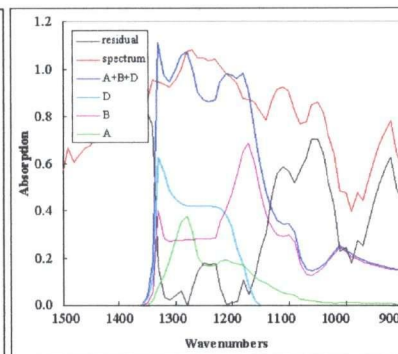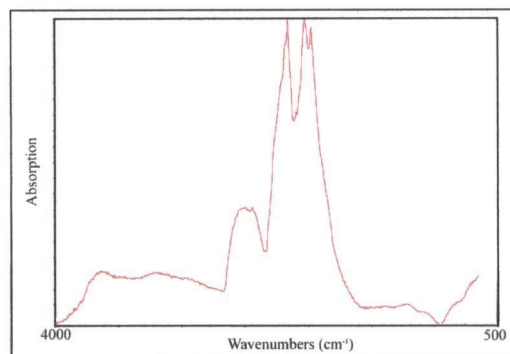
A = 6.24
B = 22.07
%B = 78
N = 28.30

Type = IIa

Diamond 4.8
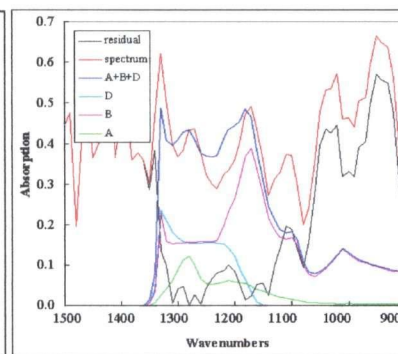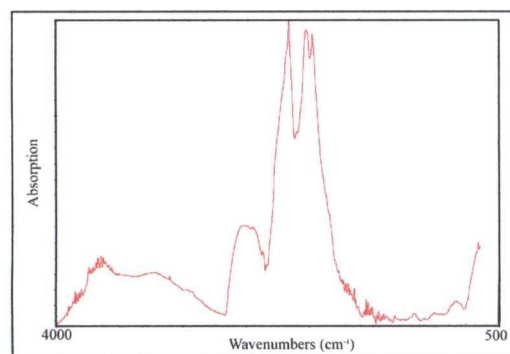
A = 2.00
B = 12.49
%B = 86
N = 14.49

Type = IIa

Diamond 4.9
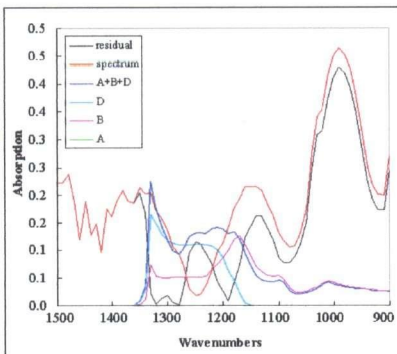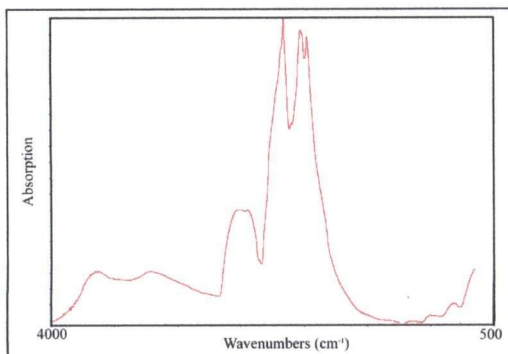
A	= -1.15
B	= 4.07
%B	= 139
N	= 2.92
Type	= IIa

Diamond 4.10
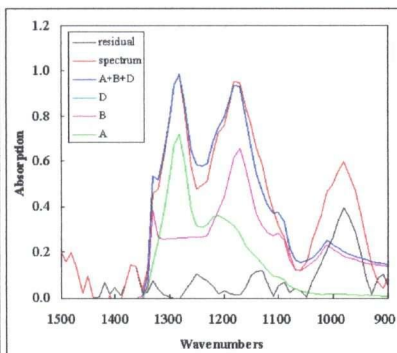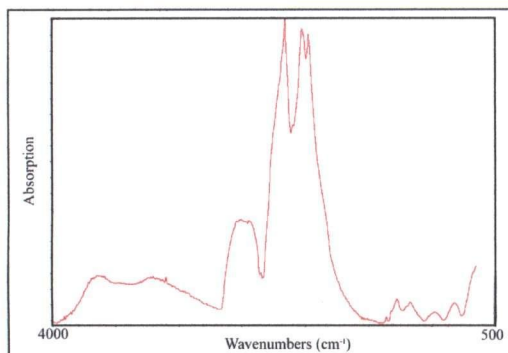
A	= 11.93
B	= 21.03
%B	= 64
N	= 32.96
Type	= IaAB

Diamond 4.11
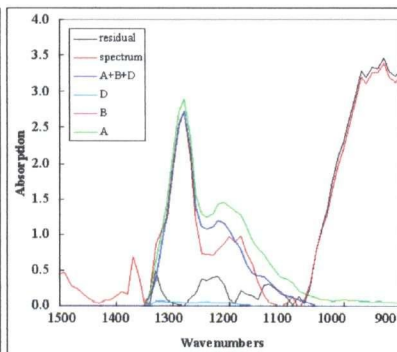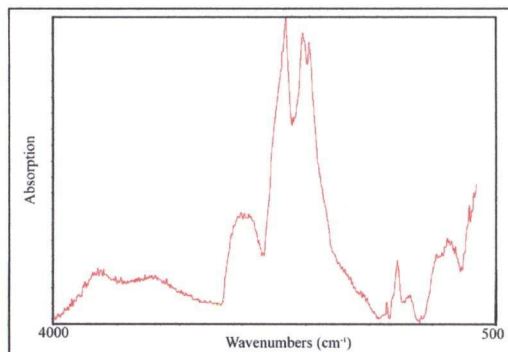
A	= 48.42
B	= -17.1
%B	= 0
N	= 48.42
Type	= IaA

Diamond 4.12
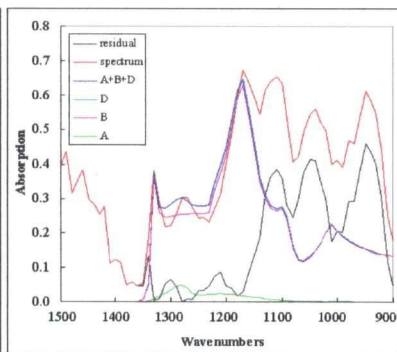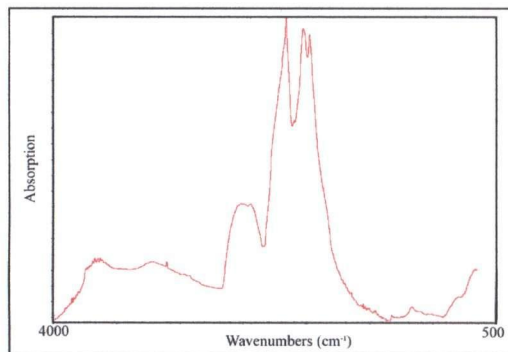
A	= 0.81
B	= 20.14
%B	= 96
N	= 20.95
Type	= IaB

Diamond 4.13
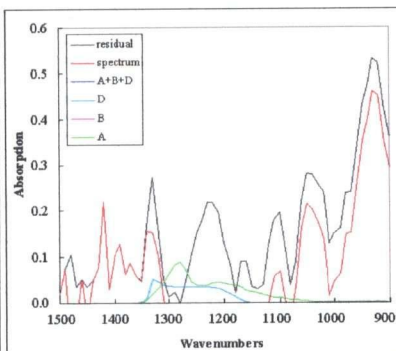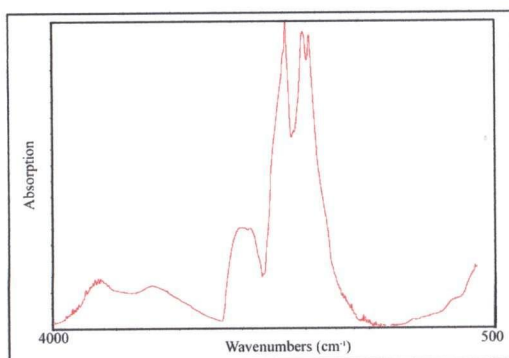
A = 2.48
B = 1.57
%B = 39
N = 4.05

Type = IIa

Diamond 4.14
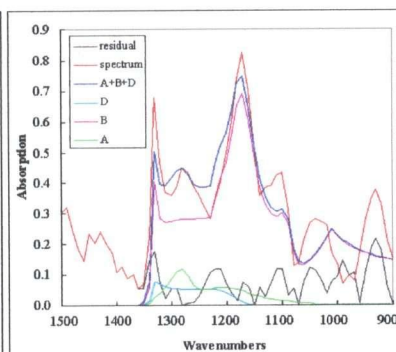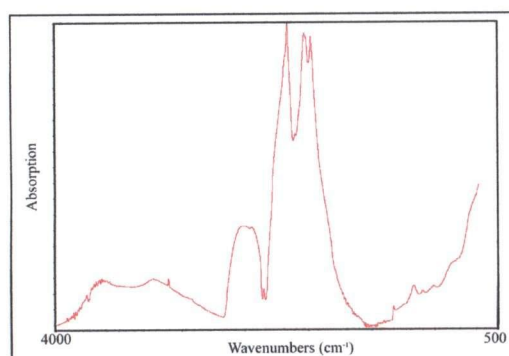
A = 1.93
B = 22.21
%B = 92
N = 24.15

Type = IaB

Diamond 4.15
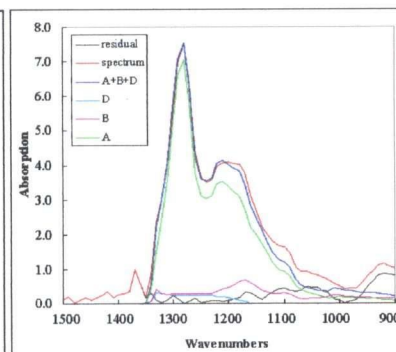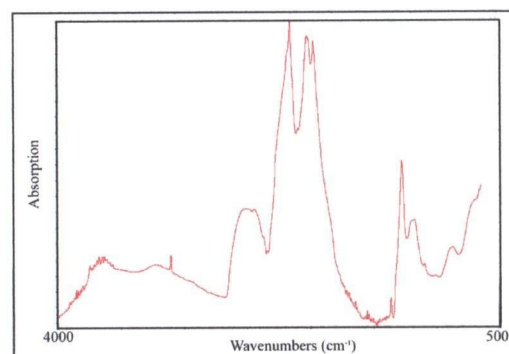
A = 116.3
B = 21.90
%B = 15.85
N = 138.2

Type = IaAB

Diamond 4.16
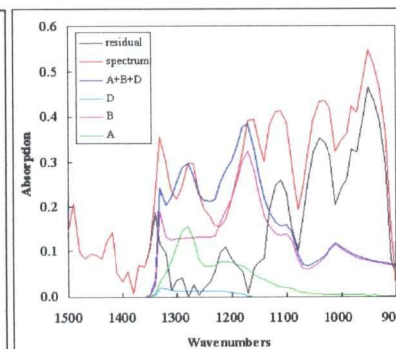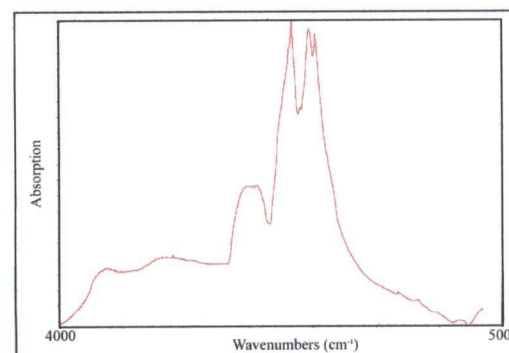
A = 2.56
B = 10.35
%B = 80
N = 12.91

Type = IIa

Diamond 4.17*
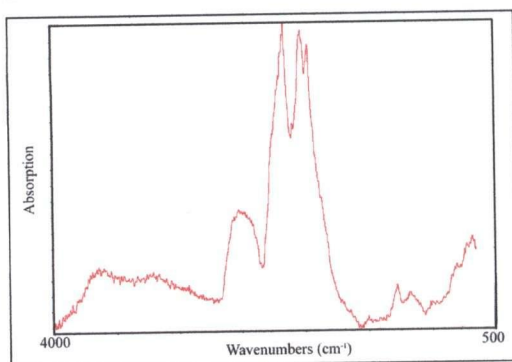
8 points on polished surface were examined

A	= 5.7	(-3.1 – 25.7)
B	= 19.2	(11.2 – 31.6)
%B	= 84	(51 - 131)
N	= 24.9	(9.1 – 52.7)

Type = IaAB

Diamond 4.18
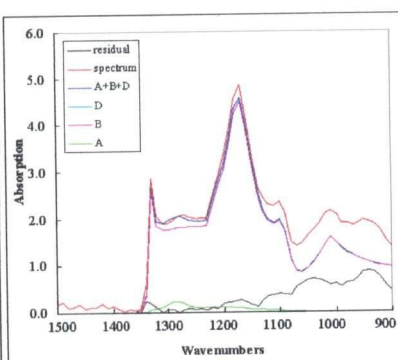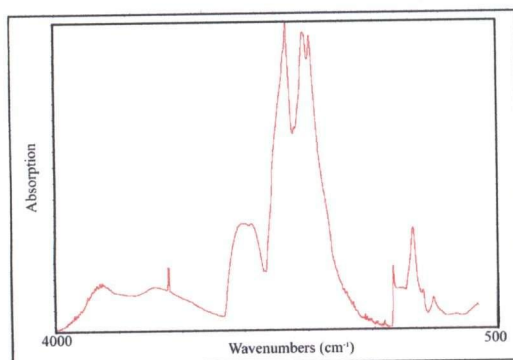
A	= 3.91
B	= 143.9
%B	= 97
N	= 147.8

Type = IaB

Diamond 4.19
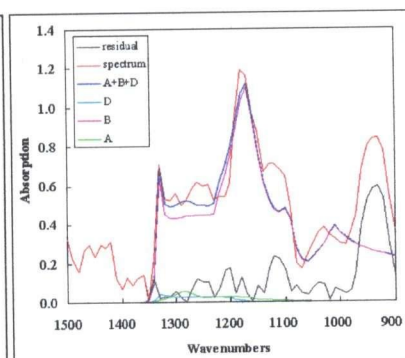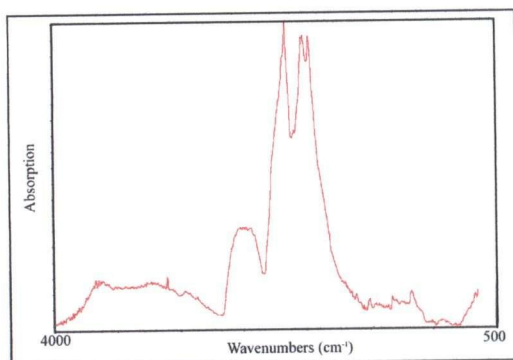
A	= 0.92
B	= 35.16
%B	= 97
N	= 36.08

Type = IaB

Diamond 4.21
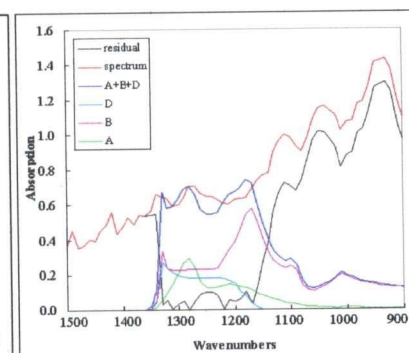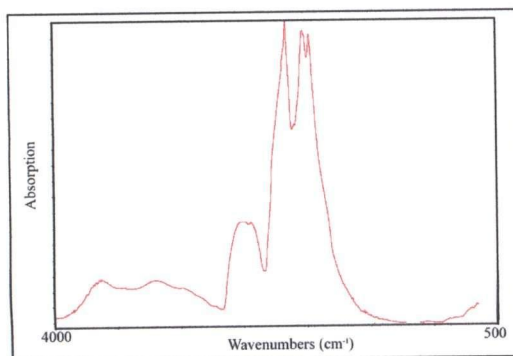
A	= 4.78
B	= 18.36
%B	= 79
N	= 0

Type = IIa

Diamond 5.1
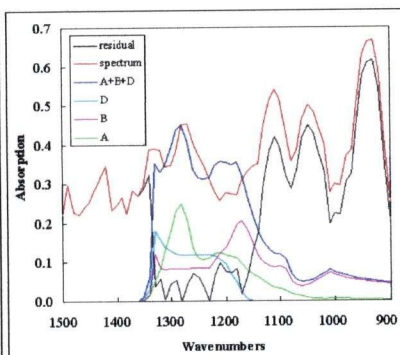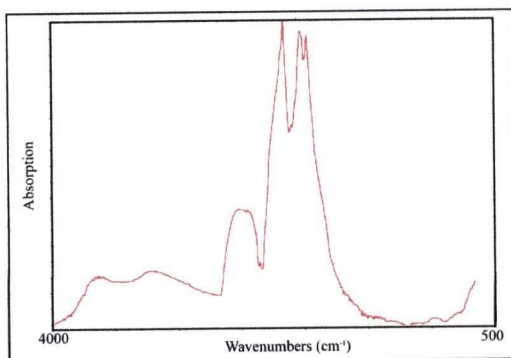
A = 4.11
B = 6.65
%B = 62
N = 10.76

Type = IIa

Diamond 5.2
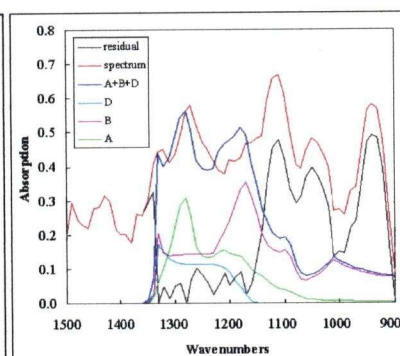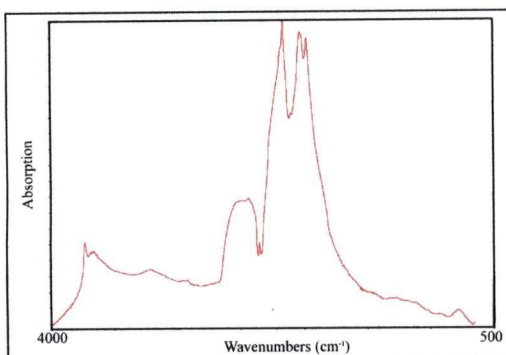
A = 5.04
B = 11.34
%B = 69
N = 16.38

Type = IIa

Diamond 5.3
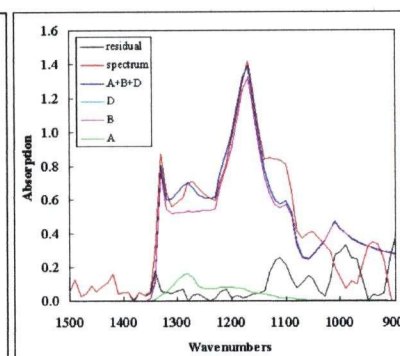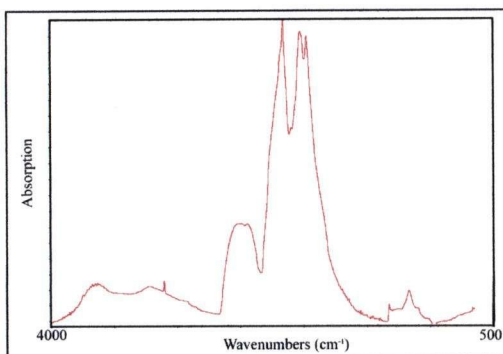
A = 2.75
B = 42.46
%B = 94
N = 45.21

Type = IaB

Diamond 5.4
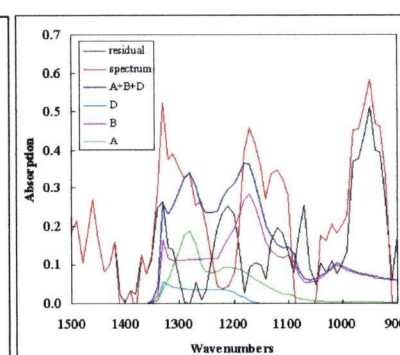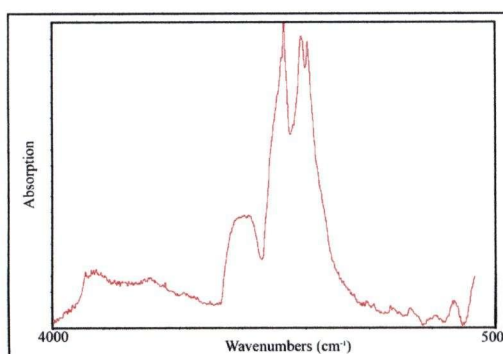
A = 3.12
B = 9.10
%B = 74
N = 12.22

Type = IIa

Diamond 5.5
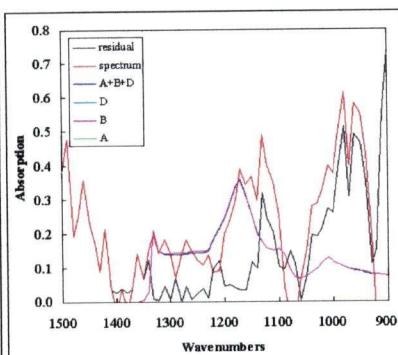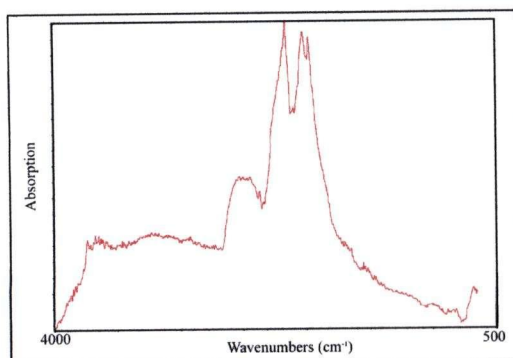
A = -0.08
B = 11.45
%B = 101
N = 11.37

Type = IIa

Diamond 5.6
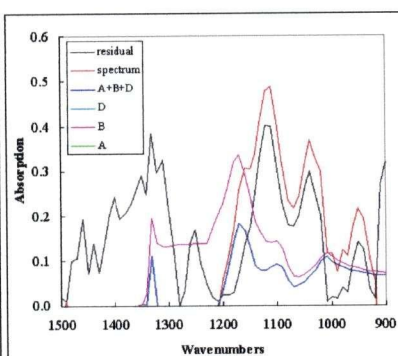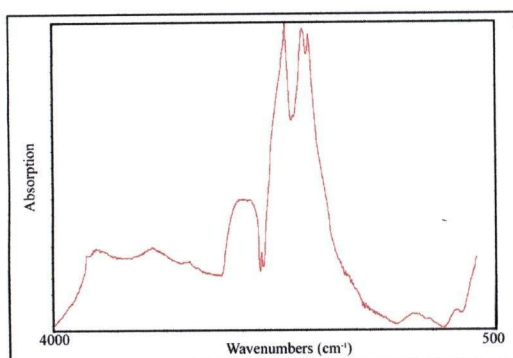
A = -6.60
B = 10.82
%B = 257
N = 4.22

Type = IIa

Diamond 5.7
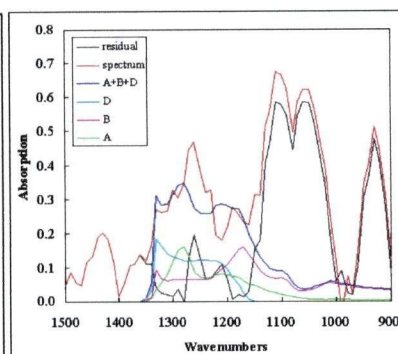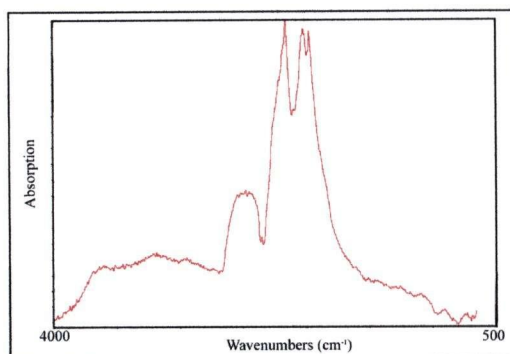
A = 2.68
B = 5.11
%B = 66
N = 7.79

Type = IIa

Diamond 5.8
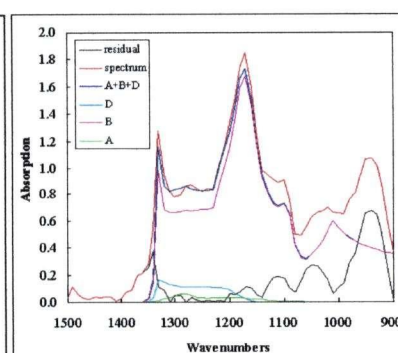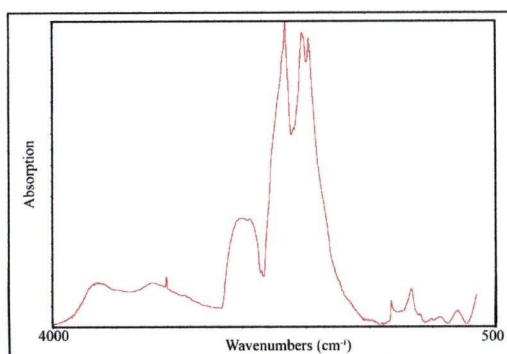
A = 1.08
B = 54.04
%B = 98
N = 55.12

Type = IaB

305
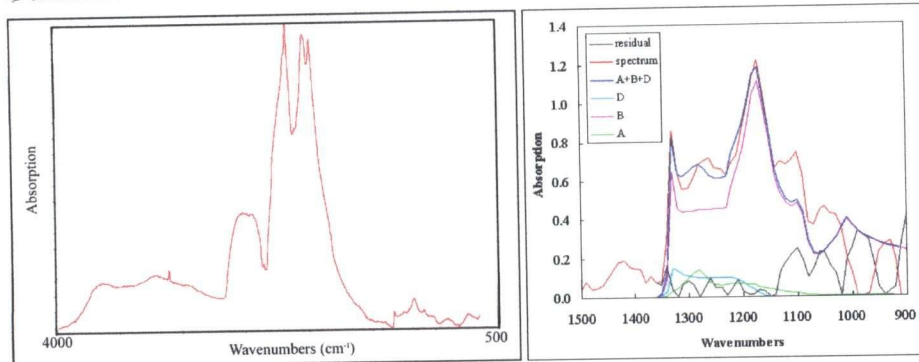
Diamond 5.9

A   = 2.26
B   = 35.62
%B   = 94
N   = 37.88

Type = IaB

Diamond 5.10
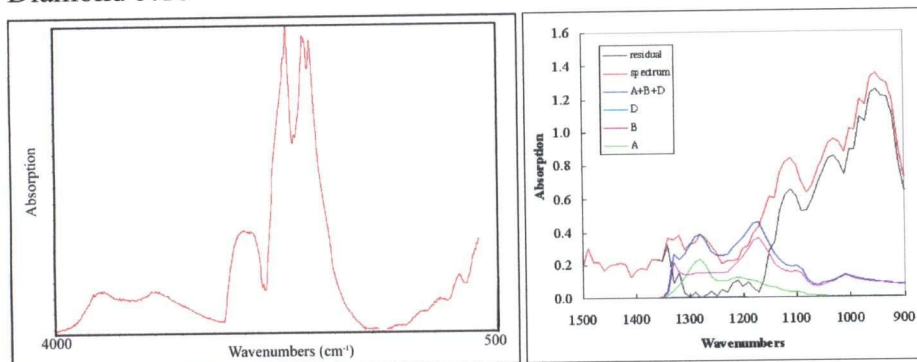
A   = 3.89
B   = 11.71
%B   = 75
N   = 15.60

Type = IIa

Diamond 5.11
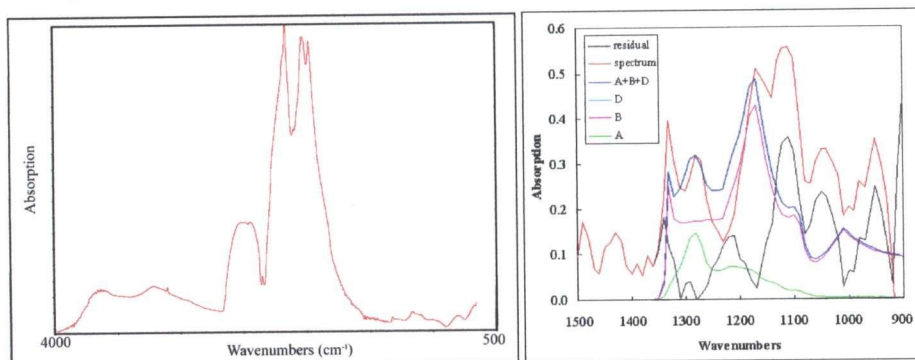
A   = 2.41
B   = 13.77
%B   = 85
N   = 16.18

Type = IIa

Diamond 6.1
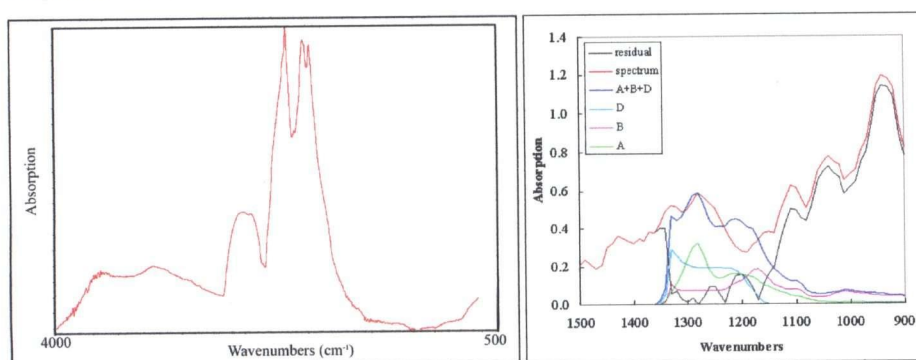
A   = 5.33
B   = 5.96
%B   = 53
N   = 11.28

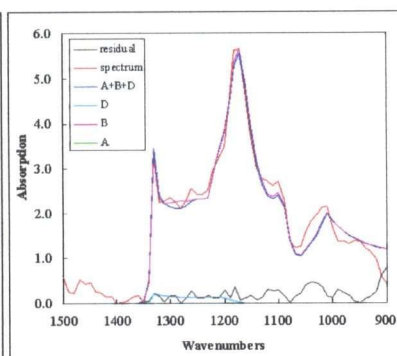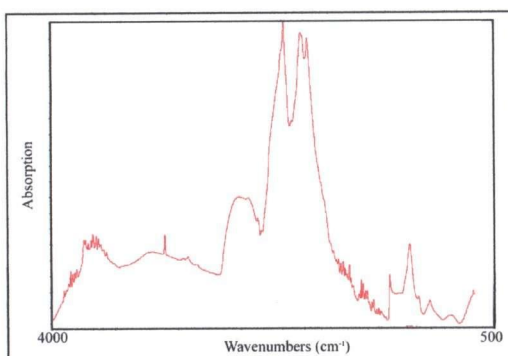Type = IIa

Diamond 6.2
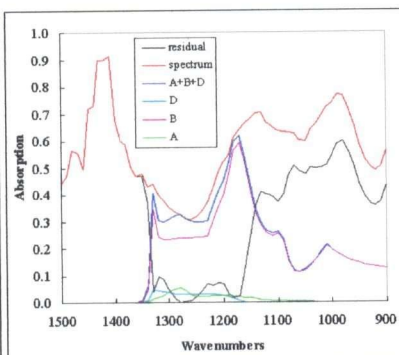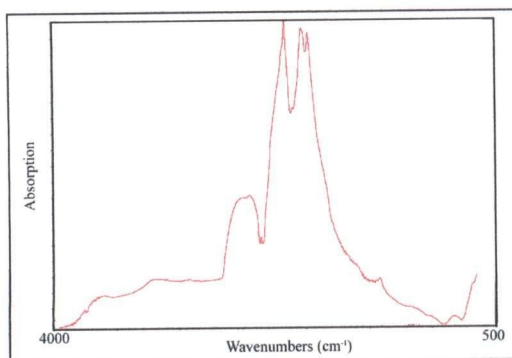
A	= 0.90
B	= 19.02
%B	= 96
N	= 19.92
Type	= IIa

Diamond 6.3
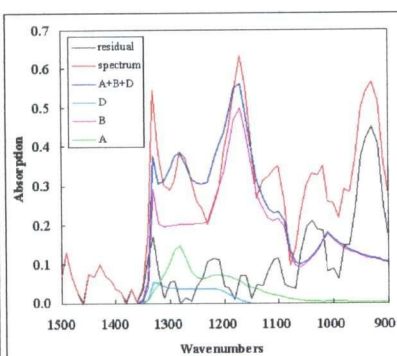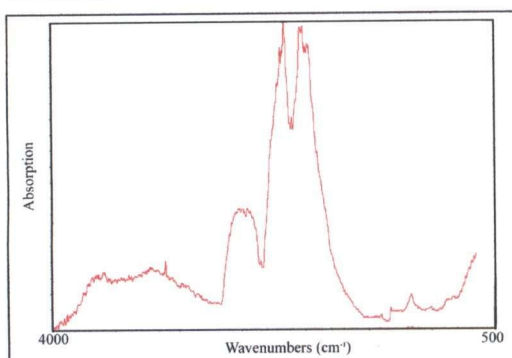
A	= 3.6
B	= 28.2
%B	= 89
N	= 31.8
Type	= IaB

Diamond 6.4

A	= -5.17
B	= 181.8
%B	= 103
N	= 176.6
Type	= IaB

Diamond 6.5
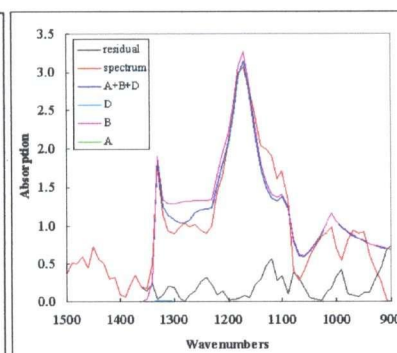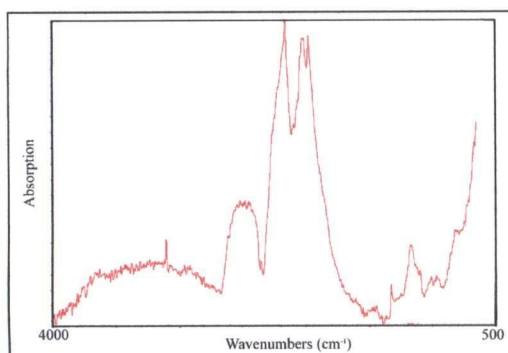
A	= -4.79
B	= 104.5
%B	= 105
N	= 99.72
Type	= IaB

Diamond 6.6
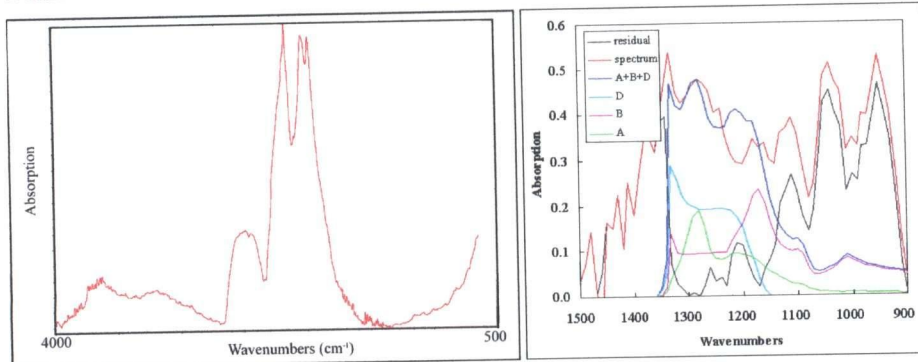
A = 3.13
B = 7.54
%B = 71
N = 10.67

Type = IIa

Diamond 6.7

A = 3.08
B = 6.38
%B = 67
N = 9.46

Type = IIa

Diamond 6.8

A = 22.68
B = 25.45
%B = 53
N = 48.13

Type = IaAB

Diamond 6.9

A = -0.39
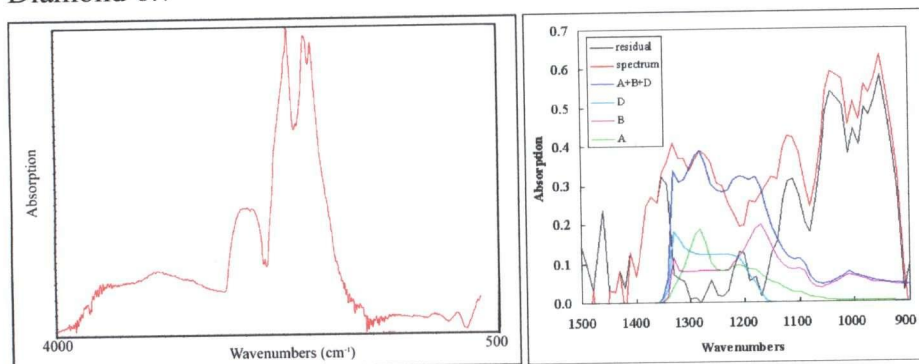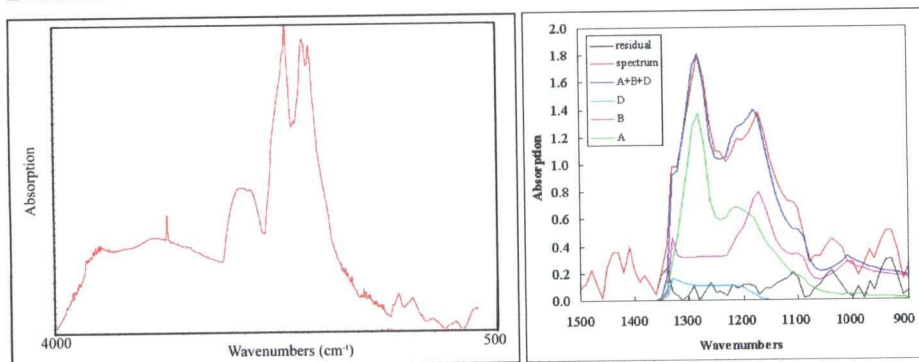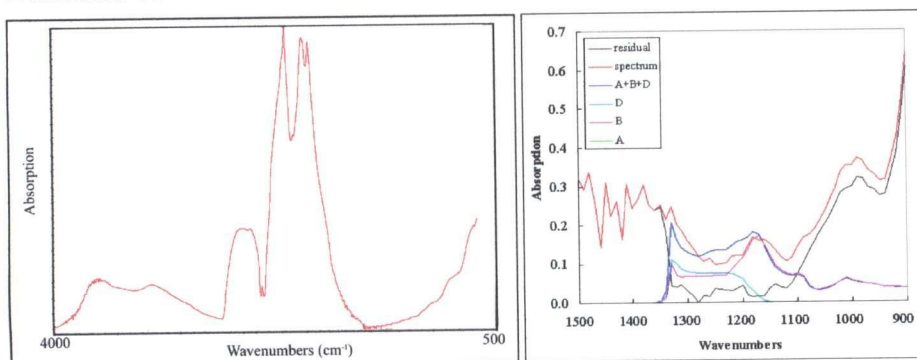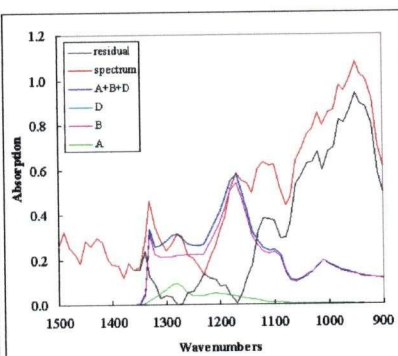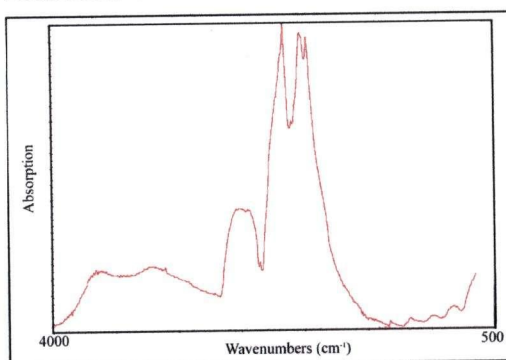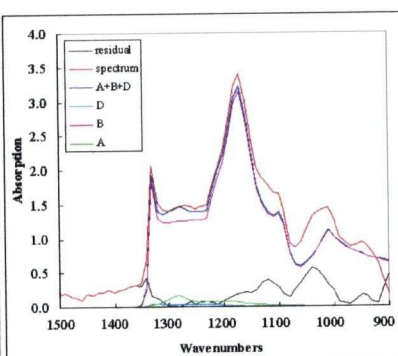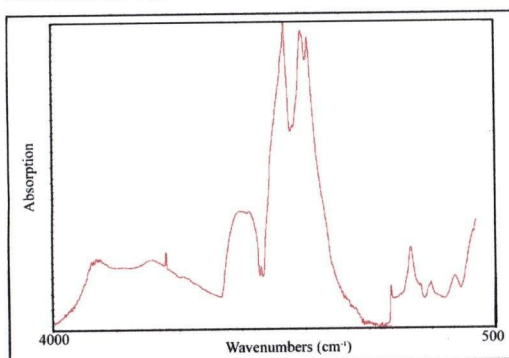B = 5.45
%B = 108
N = 5.06

Type = IIa

Diamond 6.10
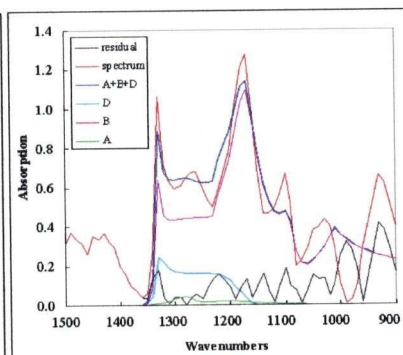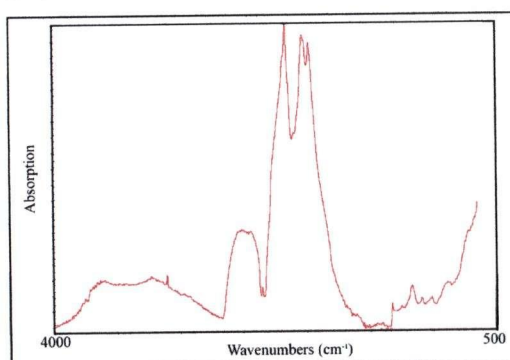

A = 1.60
B = 17.36
%B = 92
N = 18.96

Type = IIa

Diamond 7.1

A = 2.68
B = 100.7
%B = 97
N = 103.4

Type = IaB

Diamond 7.2

A = 0.74
B = 35.12
%B = 98
N = 35.86

Type = IaB

Appendix E - Frequency of inclusion phases analysed from each diamond by EPMA method

Sample No.	Inclusion assemblage	Inclusion phases								
		fPer	Ol	MgSiO$_3$	eGrt	TAPP	CaSiO$_3$	Prv	Sul	Mag
1.2*	fPer	14								
1.4*	SiO$_2$-Mag									2
1.5	fPer-Ol-MgSiO$_3$-TAPP	4	1	2		1				
2.2*	fPer-CaSiO$_3$	1								
2.6	Mag									﹢2
2.7	fPer-SiO$_2$	4								
2.8*	CaSiO$_3$-Prv						1	1		
2.10	Mag									
2.11*	SiO$_2$-Pyr								3	
3.1*	fPer-CaSiO$_3$	1					2			
3.2	fPer-Ol-MgSiO$_3$-CaSiO$_3$-TAPP?	4	2	2			1			
3.4	CaSiO$_3$						1			
3.5*	fPer-Ol-MgSiO$_3$	4	1	2						
3.6	fPer	4								
3.7	CaSiO$_3$-Prv									
3.9	fPer	3								
3.10*	fPer-CaSiO$_3$	6								
4.10	CaSiO$_3$-eGrt				2		1			
4.11	Pyr								1	
4.16	fPer-eGrt?									
4.18	Ol									
4.3	fPer-Ol-MgSiO$_3$	5	2	2						
4.7	CaSiO$_3$						1			
5.10	fPer	2								
6.1	fPer	2								
6.2	fPer	1								
6.6	CaSiO$_3$									
6.8	Ol-MgSiO$_3$		1						1s	
6.9	fPer	2								
7.1	CaSiO$_3$						1			
Subtotal		57	7	8	2	1	8	1	5	4
TOTAL	30 diamonds									93

Inclusion assemblage refers to primary minerals occurring in the same diamond, regardless of whether or not they are touching phases. s – secondary. * - internal morphology of diamond is examined in Chapter 7.0.

310

Appendix F - Frequency of inclusion phases analysed from each diamond by EDS method

Sample No.	Inclusion assemblage	fPer	Ol	MgSiO₃	eGrt	TAPP	CaSiO₃	Prv	Sul	SiO₂	Mag	Other
1.2*	fPer	22										
1.4*	SiO₂-Mag									1	13	
1.5	fPer-Ol-MgSiO₃-TAPP	7	2	2		2						
2.2*	fPer-CaSiO₃	1					2					
2.6	Mag										8	
2.7	fPer-SiO₂	12								1s?		
2.8*	CaSiO₃-Prv						1	1				
2.10	Mag										1	Si,Ca,Na,O
2.11*	SiO₂-Pyr								9	7		Fe
3.1*	fPer-CaSiO₃	1					2			1s?		Ca,P,Si,Ce,O
3.2	fPer-Ol-MgSiO₃-CaSiO₃-TAPP?	12	3	4		1	1					
3.4	CaSiO₃						5			2s?		Ca,Si,Al,O
3.5*	fPer-Ol-MgSiO₃	5	1	2								
3.6	fPer	12										
3.7	CaSiO₃-Prv						3	3				
3.9	fPer	5										
3.10*	fPer-CaSiO₃	10					2					
4.3	CaSiO₃-eGrt	7	2	6								
4.7	Pyr						6					
4.10	fPer-eGrt?				2		1					
4.11	Ol						2		2			
4.16	fPer-Ol-MgSiO₃	1			1?				1s			
4.18	CaSiO₃		1									
5.10	fPer	2										
6.1	fPer	3										
6.2	fPer	1										
6.6	CaSiO₃						1					
6.8	Ol-MgSiO₃		1	1					2s			
6.9	fPer	3										
7.1	CaSiO₃						1					
Subtotal		104	10	15	3	3	27	4	14	8	22	4
TOTAL	30 diamonds											214

Inclusion assemblage refers to minerals occurring in the same diamond, regardless of whether or not they are touching phases. s – secondary. ? – uncertain if observed phase is indeed an inclusion. * - internal morphology of diamond is examined in Chapter 7.0.